Third Edition

METAL FORMING

MECHANICS AND METALLURGY

William F. Hosford
Robert M. Caddell

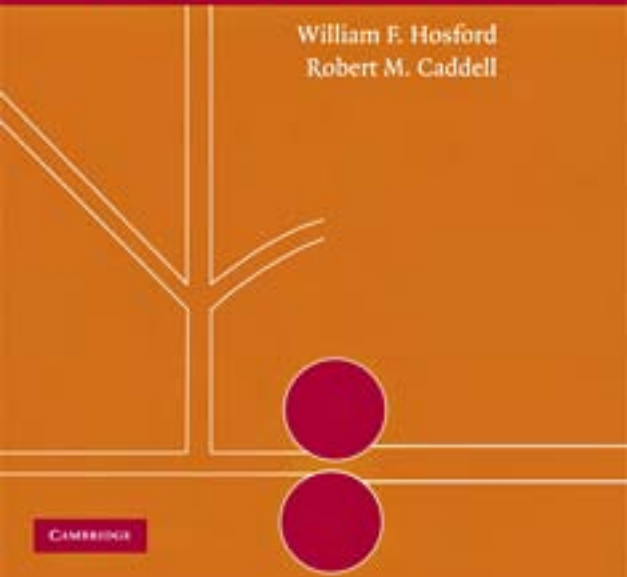

CAMBRIDGE www.cambridge.org/9780521881210

This page intentionally left blank

METAL FORMING, THIRD EDITION

This book is designed to help the engineer understand the principles of metal forming and analyze forming problems – both the mechanics of forming processes and how the properties of metals interact with the processes. The first third of the book is devoted to fundamentals of mechanics and materials; the middle to analyses of bulk forming processes such as drawing, extrusion, and rolling; and the last third covers sheet forming processes. In this new third edition, an entire chapter has been devoted to forming limit diagrams; another to various aspects of stamping, including the use of tailor-welded blanks; and another to other sheet forming operations, including hydroforming of tubes. Sheet testing is covered in a later chapter. Coverage of sheet metal properties has been expanded to include new materials and more on aluminum alloys. Interesting end-of-chapter notes and references have been added throughout. More than 200 end-of-chapter problems are also included.

William F. Hosford is a Professor Emeritus of Materials Science and Engineering at the University of Michigan. Professor Hosford is the author of more than 80 technical articles and a number of books, including the leading selling *Mechanics of Crystals and Textured Polycrystals*, *Physical Metallurgy*, *Mechanical Behavior of Materials*, and *Materials Science: An Intermediate Text*.

Robert M. Caddell was a professor of mechanical engineering at the University of Michigan, Ann Arbor.

METAL FORMING

Mechanics and Metallurgy

THIRD EDITION

WILLIAM F. HOSFORD

University of Michigan, Ann Arbor

ROBERT M. CADDELL

Late of University of Michigan, Ann Arbor

CAMBRIDGE
UNIVERSITY PRESS

CAMBRIDGE UNIVERSITY PRESS
Cambridge, New York, Melbourne, Madrid, Cape Town, Singapore, São Paulo

Cambridge University Press
The Edinburgh Building, Cambridge CB2 8RU, UK
Published in the United States of America by Cambridge University Press, New York

www.cambridge.org
Information on this title: www.cambridge.org/9780521881210

First published in print format 2007

ISBN-13 978-0-511-35453-3 eBook (EBL)
ISBN-10 0-511-35453-3 eBook (EBL)

ISBN-13 978-0-521-88121-0 hardback
ISBN-10 0-521-88121-8 hardback

Contents

Preface to Third Edition

My coauthor Robert Caddell died in 1990. I have greatly missed interacting with him.

The biggest changes from the second edition are an enlargement and reorganization of the last third of the book, which deals with sheet metal forming. Changes have been made to the chapters on bending, plastic anisotropy, and cup drawing. An entire chapter has been devoted to forming limit diagrams. There is one chapter on various aspects of stampings, including the use of tailor-welded blanks, and another on other sheet-forming operations, including hydroforming of tubes. Sheet testing is covered in a separate chapter. The chapter on sheet metal properties has been expanded to include newer materials and more depth on aluminum alloys.

In addition, some changes have been made to the chapter on strain-rate sensitivity. A treatment of friction and lubrication has been added. A short treatment of swaging has been added. End-of-chapter notes have been added for interest and additional end-of-chapter references have been added.

No attempt has been made in this book to introduce numerical methods such as finite element analyses. The book *Metal Forming Analysis* by R. H. Wagoner and J. L. Chenot (Cambridge University Press, 2001) covers the latest numerical techniques. We feel that one should have a thorough understanding of a process before attempting numerical techniques. It is vital to understand what constitutive relations are imbedded in a program before using it. For example, the use of Hill's 1948 anisotropic yield criterion can lead to significant errors.

Joining techniques such as laser welding and friction welding are not covered.

I wish to acknowledge the membership in the North American Deep Drawing Group from which I have learned much about sheet metal forming. Particular thanks are given to Alejandro Graf of ALCAN, Robert Wagoner of the Ohio State University, John Duncan of the University of Auckland, Thomas Stoughton and David Meuleman of General Motors, and Edmund Herman of Creative Concepts.

1 Stress and Strain

An understanding of stress and strain is essential for analyzing metal forming operations. Often the words *stress* and *strain* are used synonymously by the nonscientific public. In engineering, however, stress is the intensity of force and strain is a measure of the amount of deformation.

1.1 STRESS

Stress is defined as the intensity of force, F, at a point.

$$\sigma = \partial F / \partial A \quad \text{as} \quad \partial A \to 0, \tag{1.1}$$

where A is the area on which the force acts.

If the stress is the same everywhere,

$$\sigma = F/A. \tag{1.2}$$

There are nine components of stress as shown in Figure 1.1. A normal stress component is one in which the force is acting normal to the plane. It may be tensile or compressive. A shear stress component is one in which the force acts parallel to the plane.

Stress components are defined with two subscripts. The first denotes the normal to the plane on which the force acts and the second is the direction of the force.* For example, σ_{xx} is a tensile stress in the x-direction. A shear stress acting on the x-plane in the y-direction is denoted σ_{xy}.

Repeated subscripts (e.g., σ_{xx}, σ_{yy}, σ_{zz}) indicate normal stresses. They are tensile if both subscripts are positive or both are negative. If one is positive and the other is negative, they are compressive. Mixed subscripts (e.g., σ_{zx}, σ_{xy}, σ_{yz}) denote shear stresses. A state of stress in tensor notation is expressed as

$$\sigma_{ij} = \begin{vmatrix} \sigma_{xx} & \sigma_{yx} & \sigma_{zx} \\ \sigma_{xy} & \sigma_{yy} & \sigma_{zy} \\ \sigma_{xz} & \sigma_{yz} & \sigma_{zz} \end{vmatrix}, \tag{1.3}$$

* The use of the opposite convention should cause no problem because $\sigma_{ij} = \sigma_{ji}$.

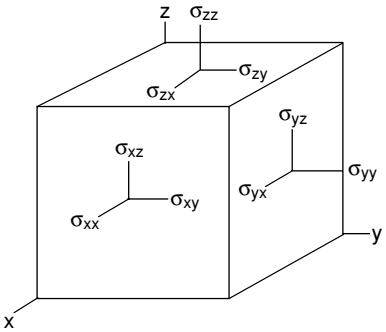

1.1. Nine components of stress acting on an infinitesimal element.

where i and j are iterated over x, y, and z. Except where tensor notation is required, it is simpler to use a single subscript for a normal stress and denote a shear stress by τ. For example, $\sigma_x \equiv \sigma_{xx}$ and $\tau_{xy} \equiv \sigma_{xy}$.

1.2 STRESS TRANSFORMATION

Stress components expressed along one set of axes may be expressed along any other set of axes. Consider resolving the stress component $\sigma_y = F_y/A_y$ onto the x' and y' axes as shown in Figure 1.2.

The force F'_y in the y' direction is $F'_y = F_y \cos\theta$ and the area normal to y' is $A_{y'} = A_y/\cos\theta$, so

$$\sigma_{y'} = F_{y'}/A_{y'} = F_y \cos\theta/(A_y/\cos\theta) = \sigma_y \cos^2\theta. \tag{1.4a}$$

Similarly

$$\tau_{y'x'} = F_{x'}/A_{y'} = F_y \sin\theta/(A_y/\cos\theta) = \sigma_y \cos\theta \sin\theta. \tag{1.4b}$$

Note that transformation of stresses requires two sine and/or cosine terms.

Pairs of shear stresses with the same subscripts in reverse order are always equal (e.g., $\tau_{ij} = \tau_{ji}$). This is illustrated in Figure 1.3 by a simple moment balance on an

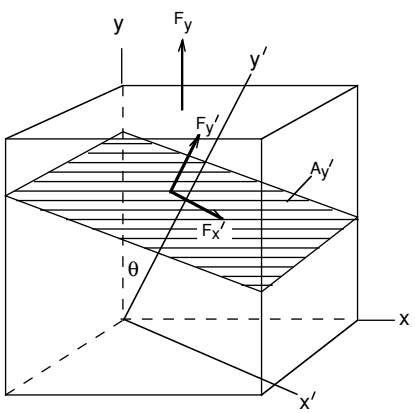

1.2. The stresses acting on a plane, A', under a normal stress, σ_y.

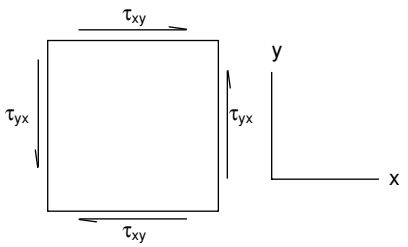

1.3. Unless $\tau_{xy} = \tau_{yx}$, there would not be a moment balance.

infinitesimal element. Unless $\tau_{ij} = \tau_{ji}$, there would be an infinite rotational acceleration. Therefore

$$\tau_{ij} = \tau_{ji}. \tag{1.5}$$

The general equation for transforming the stresses from one set of axes (e.g., n, m, p) to another set of axes (e.g., i, j, k) is

$$\sigma_{ij} = \sum_{n=1}^{3}\sum_{m=1}^{3} \ell_{im}\ell_{jn}\sigma_{mn}. \tag{1.6}$$

Here, the term ℓ_{im} is the cosine of the angle between the i and m axes and the term ℓ_{jn} is the cosine of the angle between the j and n axes. This is often written as

$$\sigma_{ij} = \ell_{im}\ell_{jn}\sigma_{mn}, \tag{1.7}$$

with the summation implied. Consider transforming stresses from the x, y, z axis system to the x', y', z' system shown in Figure 1.4.

Using equation 1.6,

$$\begin{aligned}\sigma_{x'x'} = {} & \ell_{x'x}\ell_{x'x}\sigma_{xx} + \ell_{x'x}\ell_{x'y}\sigma_{xy} + \ell_{x'x}\ell_{x'z}\sigma_{xz} \\ & + \ell_{x'y}\ell_{x'x}\sigma_{yx} + \ell_{x'y}\ell_{x'y}\sigma_{yy} + \ell_{x'y}\ell_{x'z}\sigma_{yz} \\ & + \ell_{x'z}\ell_{x'x}\sigma_{zx} + \ell_{x'z}\ell_{x'y}\sigma_{yz} + \ell_{x'z}\ell_{x'z}\sigma_{zz}\end{aligned} \tag{1.8a}$$

and

$$\begin{aligned}\sigma_{x'y'} = {} & \ell_{x'x}\ell_{y'x}\sigma_{xx} + \ell_{x'x}\ell_{y'y}\sigma_{xy} + \ell_{x'x}\ell_{y'z}\sigma_{xz} \\ & + \ell_{x'y}\ell_{y'x}\sigma_{yx} + \ell_{x'y}\ell_{y'y}\sigma_{yy} + \ell_{x'y}\ell_{y'z}\sigma_{yz} \\ & + \ell_{x'z}\ell_{y'x}\sigma_{zx} + \ell_{x'z}\ell_{y'y}\sigma_{yz} + \ell_{x'z}\ell_{y'z}\sigma_{zz}\end{aligned} \tag{1.8b}$$

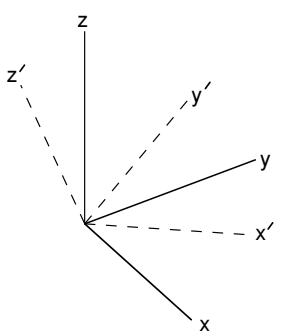

1.4. Two orthogonal coordinate systems.

These can be simplified to

$$\sigma_{x'} = \ell_{x'x}^2\sigma_x + \ell_{x'y}^2\sigma_y + \ell_{x'z}^2\sigma_z + 2\ell_{x'y}\ell_{x'z}\tau_{yz} + 2\ell_{x'z}\ell_{x'x}\tau_{zx} + 2\ell_{x'x}\ell_{x'y}\tau_{xy} \tag{1.9a}$$

and

$$\begin{aligned}\tau_{x'y'} = {} & \ell_{x'x}\ell_{y'x}\sigma_x + \ell_{x'y}\ell_{y'y}\sigma_y + \ell_{x'z}\ell_{y'z}\sigma_z + (\ell_{x'y}\ell_{y'z} + \ell_{x'z}\ell_{y'y})\tau_{yz} \\ & + (\ell_{x'z}\ell_{y'x} + \ell_{x'x}\ell_{y'z})\tau_{zx} + (\ell_{x'x}\ell_{y'y} + \ell_{x'y}\ell_{y'x})\tau_{xy}.\end{aligned} \tag{1.9b}$$

1.3 PRINCIPAL STRESSES

It is always possible to find a set of axes along which the shear stress terms vanish. In this case σ_1, σ_2, and σ_3 are called the principal stresses. The magnitudes of the principal stresses, σ_p, are the roots of

$$\sigma_p^3 - I_1\sigma_p^2 - I_2\sigma_p - I_3 = 0, \tag{1.10}$$

where I_1, I_2, and I_3 are called the *invariants* of the stress tensor. They are

$$\begin{aligned}I_1 &= \sigma_{xx} + \sigma_{yy} + \sigma_{zz}, \\ I_2 &= \sigma_{yz}^2 + \sigma_{zx}^2 + \sigma_{xy}^2 - \sigma_{yy}\sigma_{zz} - \sigma_{zz}\sigma_{xx} - \sigma_{xx}\sigma_{yy}, \quad \text{and} \\ I_3 &= \sigma_{xx}\sigma_{yy}\sigma_{zz} + 2\sigma_{yz}\sigma_{zx}\sigma_{xy} - \sigma_{xx}\sigma_{yz}^2 - \sigma_{yy}\sigma_{zx}^2 - \sigma_{zz}\sigma_{xy}^2.\end{aligned} \tag{1.11}$$

The first invariant $I_1 = -p/3$ where p is the pressure. I_1, I_2, and I_3 are independent of the orientation of the axes. Expressed in terms of the principal stresses, they are

$$\begin{aligned}I_1 &= \sigma_1 + \sigma_2 + \sigma_3, \\ I_2 &= -\sigma_2\sigma_3 - \sigma_3\sigma_1 - \sigma_1\sigma_2, \quad \text{and} \\ I_3 &= \sigma_1\sigma_2\sigma_3.\end{aligned} \tag{1.12}$$

EXAMPLE 1.1: Consider a stress state with $\sigma_x = 70\,\text{MPa}$, $\sigma_y = 35\,\text{MPa}$, $\tau_{xy} = 20$, $\sigma_z = \tau_{zx} = \tau_{yz} = 0$. Find the principal stresses using equations 1.10 and 1.11.

SOLUTION: Using equations 1.11, $I_1 = 105$ MPa, $I_2 = -2050$ MPa, $I_3 = 0$. From equation 1.10, $\sigma_p^3 - 105\sigma_p^2 + 2050\sigma_p + 0 = 0$, so

$$\sigma_p^2 - 105\sigma_p + 2{,}050 = 0.$$

The principal stresses are the roots $\sigma_1 = 79.1\,\text{MPa}$, $\sigma_2 = 25.9\,\text{MPa}$, and $\sigma_3 = \sigma_z = 0$.

EXAMPLE 1.2: Repeat Example 1.1 with $I_3 = 170{,}700$.

SOLUTION: The principal stresses are the roots of $\sigma_p^3 - 105\sigma_p^2 + 2050\sigma_p + 170{,}700 = 0$. Since one of the roots is $\sigma_z = \sigma_3 = -40$, $\sigma_p + 40 = 0$ can be factored out. This gives $\sigma_p^2 - 105\sigma_p + 2050 = 0$, so the other two principal stresses are $\sigma_1 = 79.1\,\text{MPa}$, $\sigma_2 = 25.9\,\text{MPa}$. This shows that when σ_z is one of the principal stresses, the other two principal stresses are independent of σ_z.

1.4 MOHR'S CIRCLE EQUATIONS

In the special cases where two of the three shear stress terms vanish (e.g., $\tau_{yx} = \tau_{zx} = 0$), the stress σ_z normal to the xy plane is a principal stress and the other two principal stresses lie in the xy plane. This is illustrated in Figure 1.5.

For these conditions $\ell_{x'z} = \ell_{y'z} = 0$, $\tau_{yz} = \tau_{zx} = 0$, $\ell_{x'x} = \ell_{y'y} = \cos\phi$, and $\ell_{x'y} = -\ell_{y'x} = \sin\phi$. Substituting these relations into equations 1.9 results in

$$\begin{aligned}
\tau_{x'y'} &= \cos\phi \sin\phi(-\sigma_x + \sigma_y) + (\cos^2\phi - \sin^2\phi)\tau_{xy}, \\
\sigma_{x'} &= (\cos^2\phi)\sigma_x + (\sin^2\phi)\sigma_y + 2(\cos\phi \sin\phi)\tau_{xy}, \quad \text{and} \\
\sigma_{y'} &= (\sin^2\phi)\sigma_x + (\cos^2\phi)\sigma_y + 2(\cos\phi \sin\phi)\tau_{xy}.
\end{aligned} \tag{1.13}$$

These can be simplified with the trigonometric relations

$$\sin 2\phi = 2\sin\phi\cos\phi \quad \text{and} \quad \cos 2\phi = \cos^2\phi - \sin^2\phi \quad \text{to obtain}$$

$$\tau_{x'y'} = -\sin 2\phi(\sigma_x - \sigma_y)/2 + (\cos 2\phi)\tau_{xy}, \tag{1.14a}$$

$$\sigma_{x'} = (\sigma_x + \sigma_y)/2 + \cos 2\phi(\sigma_x - \sigma_y)/2 + \tau_{xy}\sin 2\phi, \quad \text{and} \tag{1.14b}$$

$$\sigma_{y'} = (\sigma_x + \sigma_y)/2 - \cos 2\phi(\sigma_x - \sigma_y)/2 + \tau_{xy}\sin 2\phi. \tag{1.14c}$$

If $\tau_{x'y'}$ is set to zero in equation 1.14a, ϕ becomes the angle θ between the principal axes and the x and y axes. Then

$$\tan 2\theta = \tau_{xy}/[(\sigma_x - \sigma_y)/2]. \tag{1.15}$$

The principal stresses, σ_1 and σ_2, are then the values of $\sigma_{x'}$ and $\sigma_{y'}$

$$\begin{aligned}
\sigma_{1,2} &= (\sigma_x + \sigma_y)/2 \pm (1/2)[(\sigma_x - \sigma_y)\cos 2\theta] + \tau_{xy}\sin 2\theta \quad \text{or} \\
\sigma_{1,2} &= (\sigma_x + \sigma_y)/2 \pm (1/2)\left[(\sigma_x - \sigma_y)^2 + 4\tau_{xy}^2\right]^{1/2}.
\end{aligned} \tag{1.16}$$

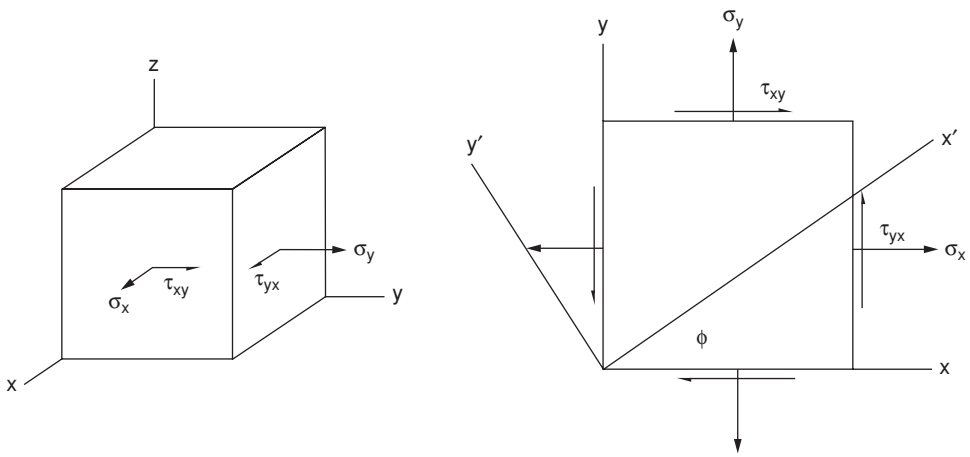

1.5. Stress state for which the Mohr's circle equations apply.

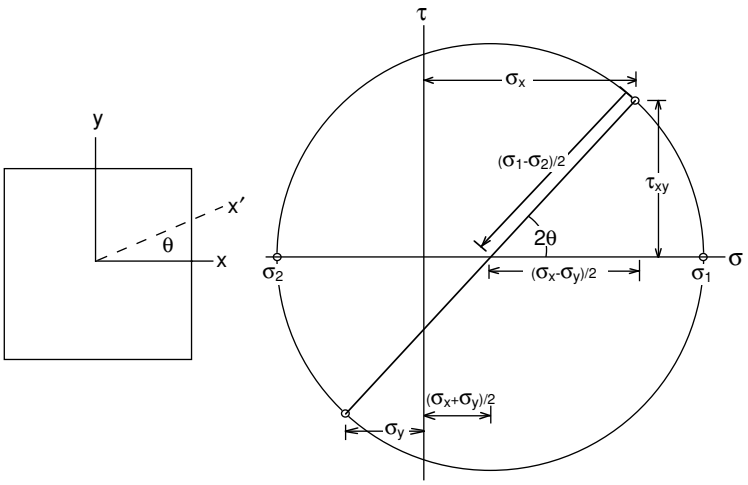

1.6. Mohr's circle diagram for stress.

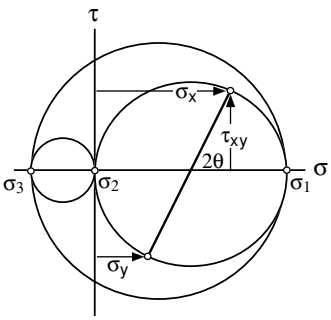

1.7. Three-dimensional Mohr's circles for stresses.

A Mohr's* circle diagram is a graphical representation of equations 1.16 and 1.17. They form a circle of radius $(\sigma_1 - \sigma_2)/2$ with the center at $(\sigma_1 + \sigma_2)/2$ as shown in Figure 1.6. The normal stress components are plotted on the ordinate and the shear stress components are plotted on the abscissa.

Using the Pythagorean theorem on the triangle in Figure 1.6,

$$(\sigma_1 - \sigma_2)/2 = \left\{[(\sigma_x - \sigma_y)/2]^2 + \tau_{xy}^2\right\}^{1/2} \tag{1.17}$$

and

$$\tan 2\theta = \tau_{xy}/[(\sigma_x - \sigma_y)/2]. \tag{1.18}$$

A three-dimensional stress state can be represented by three Mohr's circles as shown in Figure 1.7. The three principal stresses σ_1, σ_2, and σ_3 are plotted on the ordinate. The circles represent the stress state in the 1–2, 2–3, and 3–1 planes.

EXAMPLE 1.3: Construct the Mohr's circle for the stress state in Example 1.2 and determine the largest shear stress.

* O. Mohr, *Zivilingeneur* (1882), p. 113.

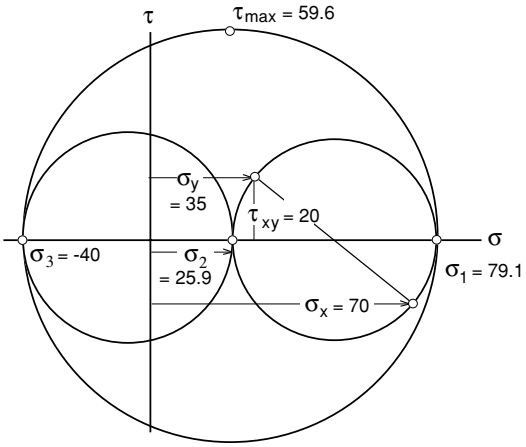

1.8. Mohr's circle for stress state in Example 1.2.

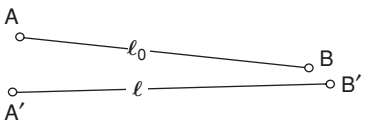

1.9. Deformation, translation, and rotation of a line in a material.

SOLUTION: The Mohr's circle is plotted in Figure 1.8. The largest shear stress is $\tau_{\max} = (\sigma_1 - \sigma_3)/2 = [79.1 - (-40)]/2 = 59.6\,\text{MPa}$.

1.5 STRAIN

Strain describes the amount of deformation in a body. When a body is deformed, points in that body are displaced. Strain must be defined in such a way that it excludes effects of rotation and translation. Figure 1.9 shows a line in a material that has been that has been deformed. The line has been translated, rotated, and deformed. The deformation is characterized by the *engineering* or *nominal strain*, e:

$$e = (\ell - \ell_0)/\ell_0 = \Delta\ell/\ell_0. \tag{1.19}$$

An alternative definition* is that of *true* or *logarithmic strain*, ε, defined by

$$d\varepsilon = d\ell/\ell, \tag{1.20}$$

which on integrating gives

$$\varepsilon = \ln(\ell/\ell_0) = \ln(1 + e). \tag{1.21}$$

The true and engineering strains are almost equal when they are small. Expressing ε as $\varepsilon = \ln(\ell/\ell_0) = \ln(1 + e)$ and expanding,

$$\varepsilon = e - e^2/2 + e^3/3! - \cdots, \text{ so as } e \to 0, \varepsilon \to e.$$

There are several reasons why true strains are more convenient than engineering strains. The following examples indicate why.

* First defined by P. Ludwig, *Elemente der Technishe Mechanik*, Springer, 1909.

EXAMPLE 1.4:

(a) A bar of length ℓ_0 is uniformly extended until its length $\ell = 2\ell_0$. Compute the values of the engineering and true strains.
(b) To what final length must a bar of length ℓ_0 be compressed if the strains are the same (except sign) as in part (a)?

SOLUTION:

(a) $e = \Delta\ell/\ell_0 = 1.0$, $\varepsilon = \ln(\ell/\ell_0) = \ln 2 = 0.693$.
(b) $e = -1 = (\ell - \ell_0)/\ell_0$, so $\ell = 0$. This is clearly impossible to achieve.

$$\varepsilon = -0.693 = \ln(\ell/\ell_0), \text{ so } \ell = \ell_0 \exp(0.693) = \ell_0/2.$$

EXAMPLE 1.5: A bar 10 cm long is elongated to 20 cm by rolling in three steps: 10 cm to 12 cm, 12 cm to 15 cm, and 15 cm to 20 cm.

(a) Calculate the engineering strain for each step and compare the sum of these with the overall engineering strain.
(b) Repeat for true strains.

SOLUTION:

(a) $e_1 = 2/10 = 0.20$, $e_2 = 3/12 = 0.25$, $e_3 = 5/15 = 0.333$, $e_{\text{tot}} = 0.20 + .25 + .333 = 0.783$. $e_{\text{overall}} = 10/10 = 1$.
(b) $\varepsilon_1 = \ln(12/10) = 0.182$, $\varepsilon_2 = \ln(15/12) = 0.223$, $\varepsilon_3 = \ln(20/15) = 0.288$, $\varepsilon_{\text{tot}} = 0.693$, $\varepsilon_{\text{overall}} = \ln(20/10) = 0.693$.

With true strains, the sum of the increments equals the overall strain, but this is not so with engineering strains.

EXAMPLE 1.6: A block of initial dimensions ℓ_0, w_0, t_0 is deformed to dimensions of ℓ, w, t.

(a) Calculate the volume strain, $\varepsilon_{\text{v}} = \ln(v/v_0)$ in terms of the three normal strains, ε_ℓ, ε_w and ε_t.
(b) Plastic deformation causes no volume change. With no volume change, what is the sum of the three normal strains?

SOLUTION:

(a) $\varepsilon_{\text{v}} = \ln[(\ell wt)/(\ell_0 w_0 t_0)] = \ln(\ell/\ell_0) + \ln(w/w_0) + \ln(t/t_0) = \varepsilon_\ell + \varepsilon_w + \varepsilon_t$.
(b) If $\varepsilon_{\text{v}} = 0$, $\varepsilon_\ell + \varepsilon_w + \varepsilon_t = 0$.

Examples 1.4, 1.5, and 1.6 illustrate why true strains are more convenient than engineering strains.

1. True strains for an equivalent amount of tensile and compressive deformation are equal except for sign.
2. True strains are additive.
3. The volume strain is the sum of the three normal strains.

EXAMPLE 1.7: Calculate the ratio of ε/e for $e = 0.001, 0.01, 0.02, 0.05, 0.1$, and 0.2.

SOLUTION:

For $e = 0.001$, $\varepsilon/e = \ln(1.001)/0.001 = 0.0009995/0.001 = 0.9995$.
For $e = 0.01$, $\varepsilon/e = \ln(1.01)/0.01 = 0.00995/0.01 = 0.995$.
For $e = 0.02$, $\varepsilon/e = \ln(1.02)/0.02 = 0.0198/0.02 = 0.990$.
For $e = 0.05$, $\varepsilon/e = \ln(1.05)/0.05 = 0.04879/0.05 = 0.9758$.
For $e = 0.1$, $\varepsilon/e = \ln(1.1)/0.1 = 0.0953/0.1 = 0.953$.
For $e = 0.2$, $\varepsilon/e = \ln(1.2)/0.2 = 0.1823/0.2 = 0.9116$.

As e gets larger the difference between ε and e become greater.

1.6 SMALL STRAINS

Figure 1.10 shows a small two-dimensional element, $ABCD$, deformed into $A'B'C'D'$ where the displacements are u and v. The normal strain, e_{xx}, is defined as

$$e_{xx} = (A'D' - AD)/AD = A'D'/AD - 1. \tag{1.22}$$

Neglecting the rotation

$$e_{xx} = A'D'/AD - 1 = \frac{dx - u + u + (\partial u/\partial x)\,dx}{dx} - 1 \quad \text{or}$$
$$e_{xx} = \partial u/\partial x. \tag{1.23}$$

Similarly, $e_{yy} = \partial v/\partial y$ and $e_{zz} = \partial w/\partial z$ for a three-dimensional case.

The shear strains are associated with the angles between AD and $A'D'$ and between AB and $A'B'$. For small deformations

$$\angle^{AD}_{A'D'} \approx \partial v/\partial x \quad \text{and} \quad \angle^{AB}_{A'B'} = \partial u/\partial y. \tag{1.24}$$

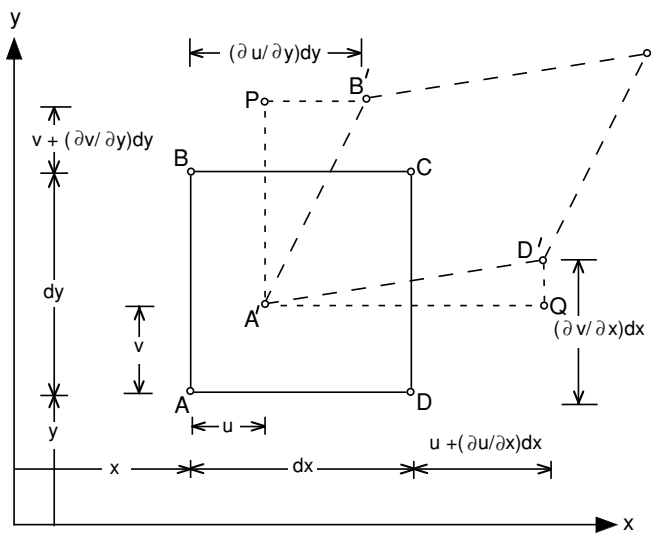

1.10. Distortion of a two-dimensional element.

The total shear strain is the sum of these two angles,

$$\gamma_{xy} = \gamma_{yx} = \frac{\partial u}{\partial y} + \frac{\partial v}{\partial x}. \tag{1.25a}$$

Similarly,

$$\gamma_{yz} = \gamma_{zy} = \frac{\partial v}{\partial z} + \frac{\partial w}{\partial y} \quad \text{and} \tag{1.25b}$$

$$\gamma_{zx} = \gamma_{xz} = \frac{\partial w}{\partial x} + \frac{\partial u}{\partial z}. \tag{1.25c}$$

This definition of shear strain, γ, is equivalent to the simple shear measured in a torsion of shear test.

1.7 THE STRAIN TENSOR

If tensor shear strains ε_{ij} are defined as

$$\varepsilon_{ij} = (1/2)\gamma_{ij}, \tag{1.26}$$

small shear strains form a tensor,

$$\varepsilon_{ij} = \begin{vmatrix} \varepsilon_{xx} & \varepsilon_{yx} & \varepsilon_{zx} \\ \varepsilon_{xy} & \varepsilon_{yy} & \varepsilon_{zy} \\ \varepsilon_{xz} & \varepsilon_{yz} & \varepsilon_{zz} \end{vmatrix}. \tag{1.27}$$

Because small strains form a tensor, they can be transformed from one set of axes to another in a way identical to the transformation of stresses. Mohr's circle relations can be used. It must be remembered, however, that $\varepsilon_{ij} = \gamma_{ij}/2$ and that the transformations hold only for small strains. If $\gamma_{yz} = \gamma_{zx} = 0$,

$$\varepsilon_{x'} = \varepsilon_x \ell_{x'x}^2 + \varepsilon_y \ell_{x'y}^2 + \gamma_{xy} \ell_{x'x} \ell_{x'y} \tag{1.28}$$

and

$$\gamma_{x'y'} = 2\varepsilon_x \ell_{x'x} \ell_{y'x} + 2\varepsilon_y \ell_{x'y} \ell_{y'y} + \gamma_{xy}(\ell_{x'x} \ell_{y'y} + \ell_{y'x} \ell_{x'y}). \tag{1.29}$$

The principal strains can be found from the Mohr's circle equations for strains,

$$\varepsilon_{1,2} = \frac{\varepsilon_x + \varepsilon_y}{2} \pm (1/2)\left[(\varepsilon_x - \varepsilon_y)^2 + \gamma_{xy}^2\right]^{1/2}. \tag{1.30}$$

Strains on other planes are given by

$$\varepsilon_{x,y} = (1/2)(\varepsilon_1 + \varepsilon_2) \pm (1/2)(\varepsilon_1 - \varepsilon_2)\cos 2\theta \tag{1.31}$$

and

$$\gamma_{xy} = (\varepsilon_1 - \varepsilon_2)\sin 2\theta. \tag{1.32}$$

1.8 ISOTROPIC ELASTICITY

Although the thrust of this book is on plastic deformation, a short treatment of elasticity is necessary to understand springback and residual stresses in forming processes.

Hooke's laws can be expressed as

$$\begin{aligned} e_x &= (1/E)[\sigma_x - \nu(\sigma_y + \sigma_z)], \\ e_y &= (1/E)[\sigma_y - \nu(\sigma_z + \sigma_x)], \\ e_z &= (1/E)[\sigma_z - \nu(\sigma_x + \sigma_y)], \end{aligned} \tag{1.33}$$

and

$$\begin{aligned} \gamma_{yz} &= (1/G)\tau_{yz}, \\ \gamma_{zx} &= (1/G)\tau_{zx}, \\ \gamma_{xy} &= (1/G)\tau_{xy}, \end{aligned} \tag{1.34}$$

where E is Young's modulus, ν is Poisson's ratio, and G is the shear modulus. For an isotropic material, E, ν, and G are interrelated by

$$E = 2G(1 + \nu), \text{ or} \tag{1.35}$$

$$G = E/[2(1 + \nu)]. \tag{1.36}$$

EXAMPLE 1.8: In Example 1.2 with $\sigma_x = 70\,\text{MPa}$, $\sigma_y = 35\,\text{MPa}$, $\tau_{xy} = 20$, $\sigma_z = \tau_{zx} = \tau_{yz} = 0$, it was found that $\sigma_1 = 79.9\,\text{MPa}$ and $\sigma_2 = 25.9\,\text{MPa}$. Using $E = 61$ GPa and $\nu = 0.3$ for aluminum, calculate ε_1 and ε_1 by

(a) First calculating ε_x, ε_y, and γ_{xy} using equations 1.33 and then transforming these strains to the 1, 2 axes with the Mohr's circle equations.

(b) By using equations 1.33 with σ_1 and σ_2.

SOLUTION:

(a)

$$\begin{aligned} e_x &= (1/61 \times 10^9)[70 \times 10^6 - 0.30(35 \times 10^6 + 0)] = 0.9754 \times 10^{-3}. \\ e_y &= (1/61 \times 10^9)[35 \times 10^6 - 0.30(70 \times 10^6 + 0)] = 0.2295 \times 10^{-3}. \\ y_{xy} &= [2(1.3)/61 \times 10^9](20 \times 10^6) = 0.853 \times 10^{-3}. \end{aligned}$$

Now using the Mohr's strain circle equations.

$$\begin{aligned} e_{1,2} &= (e_x + e_y)/2 \pm (1/2)\left[(e_x - e_y)^2 + \gamma_{xy}^2\right]^{1/2} \\ &= 0.603 \times 10^{-3} \pm (1/2)[(0.7459 \times 10^{-3})^2 + (0.856 \times 10^{-3})^2]^{1/2} \\ &= 1.169 \times 10^{-3}, 0.0361 \times 10^{-3} \end{aligned}$$

(b)

$$\begin{aligned} e_1 &= (1/61 \times 10^9)[79.9 \times 10^6 - 0.30(25.9 \times 10^6)] = 1.169, \\ e_2 &= (1/61 \times 10^9)[25.9 \times 10^6 - 0.30(79.9 \times 10^6)] = 0.0361. \end{aligned}$$

1.9 STRAIN ENERGY

If a bar of length x and cross-sectional area A is subjected to a tensile force F_x, which caused an increase in length dx, the incremental work dW is

$$\mathrm{d}W = F_x\,\mathrm{d}x \tag{1.37}$$

The work per volume, dw, is

$$\mathrm{d}w = \mathrm{d}W/(Ax) = F_x\,\mathrm{d}x/(Ax) = \sigma_x\,\mathrm{d}e_x \tag{1.38}$$

For elastic loading, substituting $\sigma_x = Ee_x$ into equation 1.38 and integrating,

$$w = \sigma_x e_x/2 = Ee_x^2/2. \tag{1.39}$$

For multiaxial loading.

$$\mathrm{d}w = \sigma_x\,\mathrm{d}e_x + \sigma_y\,\mathrm{d}e_y + \sigma_z\,\mathrm{d}e_z + \tau_{yz}\,\mathrm{d}\gamma_{yz} + \tau_{zx}\,\mathrm{d}\gamma_{zx} + \tau_{xy}\,\mathrm{d}\gamma_{xy}. \tag{1.40}$$

and if the deformation is elastic,

$$\mathrm{d}w = (1/2)(\sigma_1\,\mathrm{d}e_1 + \sigma_2\,\mathrm{d}e_2 + \sigma_3\,\mathrm{d}e_3). \tag{1.41}$$

1.10 FORCE AND MOMENT BALANCES

Many analyses of metal forming operations involve force or moment balances. The net force acting on any portion of a body must be zero. External forces on a portion of a body are balanced by internal forces acting on the arbitrary cut through the body. Let the tube length be L, its diameter D, and its wall thickness t and let the pressure be P (Figure 1.11a). The axial stress, σ_y, can be found from a force balance on a cross section of the tube. Since $P\pi D^2/4 = \pi Dt\sigma_y$,

$$\sigma_y = PD/(4t). \tag{1.42}$$

The hoop stress σ_x can be found from a force balance on a longitudinal section of the tube (Figure 1.11b). $PDL = 2\sigma_x tL$ or

$$\sigma_x = \frac{1}{2}PD/t. \tag{1.43}$$

A moment balance can be made about any axis through a material. The internal moment must balance the external moment. Consider a cylindrical rod under torsion. A moment balance relates the torque T to the distribution of shear stress, τ_{xy} (Figure 1.12). Consider an annular element of thickness dr at a distance r from the axis. The shear force on this element is the shear stress times the area of the element, $(2\pi r)\tau_{xy}\mathrm{d}r$. The moment caused by this element is the shear force times the distance r from the axis so $\mathrm{d}T = (2\pi r)\tau_{xy}(r)\,\mathrm{d}r$.

$$T = 2\pi\int_0^R \tau_{xy}r^2\,\mathrm{d}r. \tag{1.44}$$

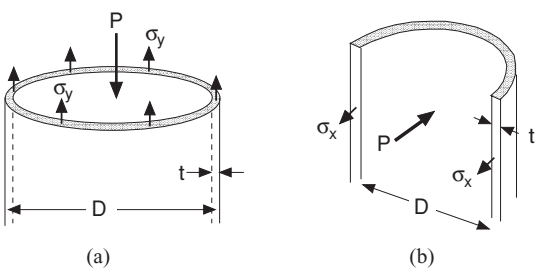

1.11. Forces acting on cuts through a tube under pressure.

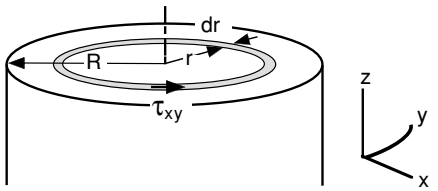

1.12. Moment balance on an annular element.

An explicit solution requires knowledge of how τ_{xy} varies with r for integration.

1.11 BOUNDARY CONDITIONS

In analyzing metal forming problems, it is important to be able to recognize boundary conditions. Often these are not stated explicitly. Some of these are listed below:

1. A stress, σ_z, normal to a free surface and the two shear stresses in the surface are zero.
2. Likewise there are no shear stresses in surfaces that are assumed to be frictionless.
3. Constraints from neighboring regions: The strains in a region are often controlled by the deformation in a neighboring region. Consider a long narrow groove in a plate (Figure 1.13). The strain ε_x in the groove must be the same as the strain in the region outside the groove. However, the strains ε_y and ε_z need not be the same.
4. St.-Venant's principle states that the constraint from discontinuity will disappear within one characteristic distance of the discontinuity. For example, the shoulder on a tensile bar tends to suppress the contraction of the adjacent region of the gauge section. However this effect is very small at a distance equal to the diameter away from the shoulder. Figure 1.14 illustrates this on as sheet specimen.

Bending of a sheet (Figure 1.15) illustrates another example of St.-Venant's principle. The plane-strain condition $\varepsilon_y = 0$ prevails over most of the material because the bottom and top surfaces are so close. However the edges are not in plane strain because $\sigma_y = 0$. However, there is appreciable deviation from plane strain only in a region within a distance equal to the sheet thickness from the edge.

EXAMPLE 1.9: A metal sheet, 1 m wide, 3 m long, and 1 mm thick is bent as shown in Figure 1.15. Find the state of stress in the surface in terms of the elastic constants and the bend radius, ρ.

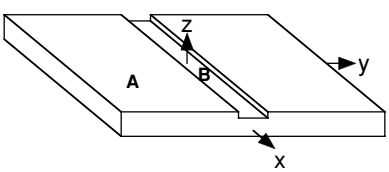

1.13. Grooved plate. The material outside the groove affects the material inside the groove. $\varepsilon_{xA} = \varepsilon_{xB}$.

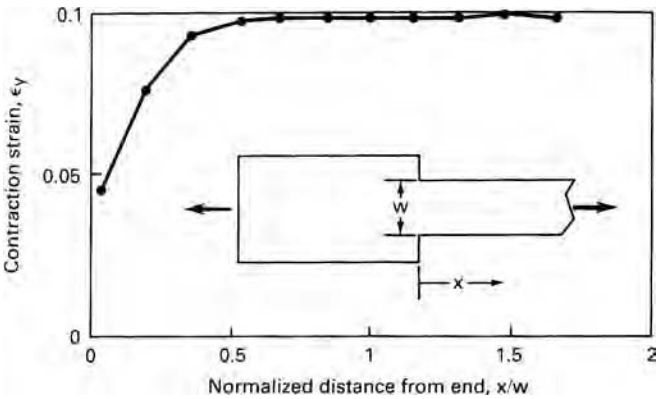

1.14. The lateral contraction strain of a sheet tensile specimen of copper as a function of the distance from the shoulder. The strain was measured when the elongation was 27.6%.

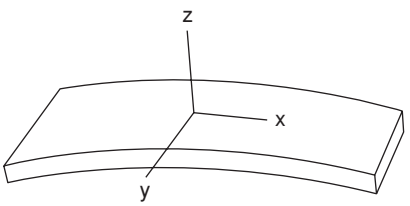

1.15. In bending of a sheet, plane strain ($\varepsilon_y = 0$) prevails except within a distance equal to the thickness from the edges where $\sigma_y = 0$.

SOLUTION: $e_y = (1/E)[\sigma_y - \nu(\sigma_z + \sigma_x)] = 0$ and $\sigma_z = 0$, so $\sigma_y = \nu\sigma_x$. Neglecting any shift of the neutral plane, $e_x = t/(2\rho)$. Substituting into Hooke's law,

$$e_x = t/(2\rho) = (1/E)[\sigma_x - \nu(\sigma_y + \sigma_z)] \quad \text{or} \quad t/(2\rho) = (\sigma_x/E)(1 - \nu^2).$$

Solving for σ

$$\sigma_x = \frac{Et}{2\rho(1-\nu^2)} \quad \text{and} \quad \sigma_y = \frac{\nu Et}{2\rho(1-\nu^2)}.$$

NOTES OF INTEREST

Otto Mohr (1835–1918) made popular the graphical representation of stress at a point (*Zivilingeneur*, 1882, p. 113.) even though it had previously been suggested by Culman (*Graphische Statik*, 1866, p. 226.)

Barré de Saint-Venant was born 1797. In 1813 at the age of 16 he entered l'École Polytechnique. He was a sergeant on a student detachment as the allies were attacking Paris in 1814. Because he stepped out of ranks and declared that he could not in good conscience fight for an usurper (Napoleon), he was prevented from taking further classes at l'École Polytechnique. He later graduated from l'École des Ponts et Chaussées where he taught through his career.

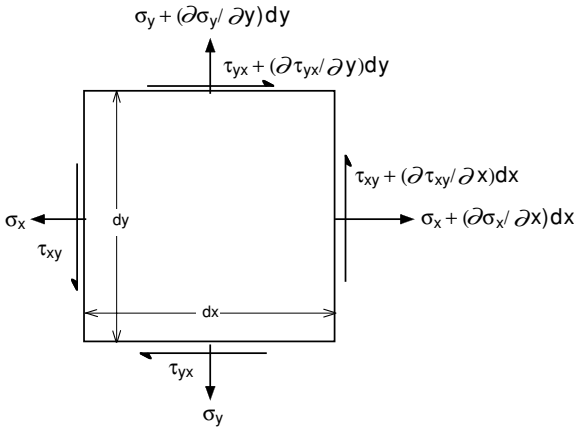

1.16. Variation of a stress state in space.

REFERENCES

R. M. Caddell, *Deformation and Fracture of Solids*, Prentice-Hall, 1980.
H. Ford, *Advanced Mechanics of Materials*, Wiley, 1963.
W. F. Hosford, *Mechanical Behavior of Materials*, Cambridge University Press, 2004.
W. Johnson and P. B. Mellor, *Engineering Plasticity*, Van Nostrand-Reinhold, 1973.
N. H. Polokowski and E. J. Ripling, *Strength and Stucture of Engineering Materials*, Prentice-Hall, 1966.

APPENDIX – EQUILIBRIUM EQUATIONS

As the stress state varies form one place to another, there are equilibrium conditions that must be met. Consider Figure 1.16.

An x-direction force balance gives

$$\partial\tau_{xy}/\partial x + \partial\sigma_y/\partial y + \partial\tau_{yz}/\partial z = 0$$
$$\sigma_x + \tau_{yx} = \sigma_x + \frac{\partial\sigma_x}{\partial x}\mathrm{d}x + \tau_{yx} + \frac{\partial\tau_{yx}}{\partial y}\mathrm{d}y$$

or simply

$$\partial\sigma_x/\partial x + \partial\tau_{xy}/\partial y = 0. \tag{1.45}$$

In three dimensions

$$\begin{aligned}\partial\sigma_x/\partial x + \partial\tau_{xy}/\partial y + \partial\tau_{yz}/\partial z &= 0\\ \partial\tau_{xy}/\partial x + \partial\sigma_y/\partial y + \partial\tau_{yz}/\partial z &= 0\\ \partial\tau_{xz}/\partial x + \partial\tau_{yz}/\partial y + \partial\sigma_z/\partial z &= 0.\end{aligned} \tag{1.46}$$

These equations are used in Chapter 9.

PROBLEMS

1.1. Determine the principal stresses for the stress state

$$\sigma_{ij} = \begin{vmatrix} 10 & -3 & 4 \\ -3 & 5 & 2 \\ 4 & 2 & 7 \end{vmatrix}.$$

1.2. A 5-cm diameter solid shaft is simultaneously subjected to an axial load of 80 kN and a torque of 400 Nm.
a) Determine the principal stresses at the surface assuming elastic behavior.
b) Find the largest shear stress.

1.3. A long thin-wall tube, capped on both ends, is subjected to internal pressure. During elastic loading, does the tube length increase, decrease, or remain constant?

1.4. A solid 2-cm diameter rod is subjected to a tensile force of 40 kN. An identical rod is subjected to a fluid pressure of 35 MPa and then to a tensile force of 40 kN. Which rod experiences the largest shear stress?

1.5. Consider a long thin-wall, 5 cm in diameter tube, with a wall thickness of 0.25 mm that is capped on both ends. Find the three principal stresses when it is loaded under a tensile force of 400 kN and an internal pressure of 200 kPa.

1.6. Three strain gauges are mounted on the surface of a part. Gauge A is parallel to the x-axis and gauge C is parallel to the y-axis. The third gauge, B, is at 30° to gauge A. When the part is loaded the gauges read

Gauge A	3000×10^{-6}
Gauge B	3500×10^{-6}
Gauge C	1000×10^{-6}

a) Find the value of γ_{xy}.
b) Find the principal strains in the plane of the surface.
c) Sketch the Mohr's circle diagram.

1.7. Find the principal stresses in the part of Problem 1.6 if the elastic modulus of the part is 205 GPa and Poissons's ratio is 0.29.

1.8. Show that the true strain after elongation may be expressed as $\varepsilon = \ln\left(\frac{1}{1-r}\right)$ where r is the reduction of area.

1.9. A thin sheet of steel, 1 mm thick, is bent as described in Example 1.9 and Figure 1.15. Assume that $E = 205$ GPa and $\nu = 0.29$, and that the neutral axis doesn't shift.
a) Find the state of stress on most of the outer surface.
b) Find the state of stress at the edge of the outer surface.

1.10. For an aluminum sheet under plane stress loading $\varepsilon_x = 0.003$ and $\varepsilon_y = 0.001$. Assuming that $E = 68$ GPa and $\nu = 0.30$, find ε_z.

1.11. A piece of steel is elastically loaded under principal stresses $\sigma_1 = 300$ MPa, $\sigma_2 = 250$ MPa and, $\sigma_3 = -200$ MPa. Assuming that $E = 205$ GPa and $\nu = 0.29$ find the stored elastic energy per volume.

1.12. A slab of metal is subjected to plane-strain deformation ($e_2 = 0$) such that $\sigma_1 = 40$ ksi and $\sigma_3 = 0$. Assume that the loading is elastic and that $E = 205$ GPa and $\nu = 0.29$ (note the mixed units).
a) Find the three normal strains.
b) Find the strain energy per volume.

2 Plasticity

With elastic deformation, a body returns to its original shape when the stress is removed and the stress and strain under elastic loading are related through Hooke's laws. Any stress will cause some strain. In contrast, no plastic deformation occurs until the stress reaches the *yield strength*. For ductile metals large amounts of plastic deformation can occur under continually increasing stress.

In this text experimental observations are linked with mathematical expressions. *Yield criteria* are mathematical descriptions of the combination of stresses necessary to cause yielding.

2.1 YIELD CRITERIA

A yield criterion is a postulated mathematical expression of the states of stress that will cause yielding. The most general form is

$$f(\sigma_x, \sigma_y, \sigma_z, \tau_{yz}, \tau_{zx}, \tau_{xy}) = C. \tag{2.1}$$

For isotropic materials, this can be expressed in terms of principal stresses as

$$f(\sigma_1, \sigma_2, \sigma_3) = C. \tag{2.2}$$

For most isotropic ductile metals the following assumptions are commonly made:

1. The yield strengths in tension and compression are the same. That is, any Bauschinger* effect is small enough so it can be ignored.
2. The volume remains constant during plastic deformation.
3. The magnitude of the mean normal stress,

$$\sigma_{\mathrm{m}} = \frac{\sigma_1 + \sigma_2 + \sigma_3}{3} \tag{2.3}$$

does not affect yielding.

* J. Bauschinger, *Zivilingenieur*, 27 (1881), p. 289.

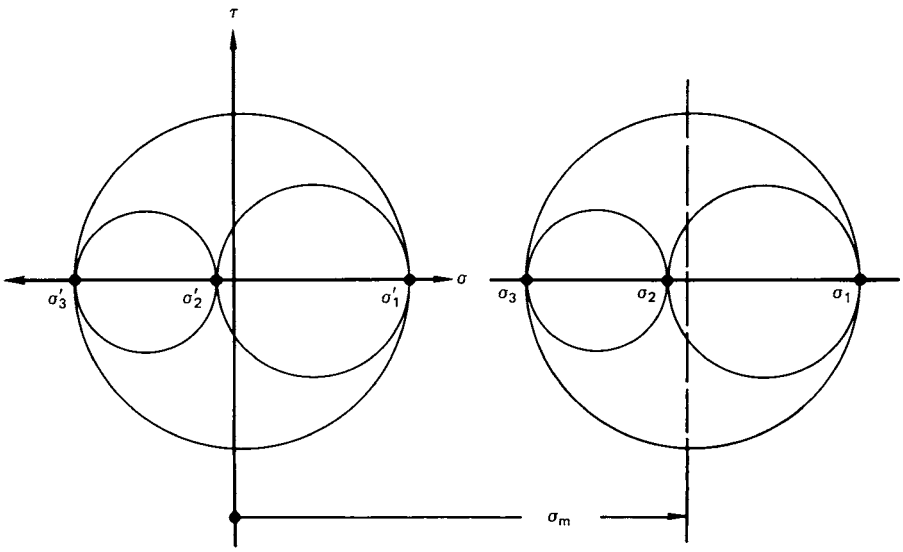

2.1. Mohr's circles for two stress states that differ only by a hydrostatic stress, σ_m, and are therefore equivalent in terms of yielding.

The yield criteria to be discussed involve these assumptions. Effects of temperature, prior straining, and strain rate will be discussed in later chapters.

The assumption that yielding is independent of σ_m is reasonable because deformation usually occurs by slip or twining, which are shear mechanisms. Therefore the yield criteria for isotropic materials have the form

$$f[(\sigma_2 - \sigma_3), (\sigma_3 - \sigma_1), (\sigma_1 - \sigma_2)] = C. \tag{2.4}$$

This is equivalent to stating that yielding depends only on the size of the Mohr's circles and not on their positions. Figure 2.1 shows this. If a stress state $\sigma_1, \sigma_2, \sigma_3$ will cause yielding, another stress state, $\sigma_1' = \sigma_1 - \sigma_m$, $\sigma_2' = \sigma_2 - \sigma_m$, $\sigma_3' = \sigma_3 - \sigma_m$ that differs only by σ_m, will also cause yielding. The stresses $\sigma_1', \sigma_2', \sigma_3'$ are called the *deviatoric stresses*.

2.2 TRESCA CRITERION

The Tresca criterion postulates that yielding depends on the largest shear stress in the body. With the convention $\sigma_1 \geq \sigma_2 \geq \sigma_3$, this can be expressed as $\sigma_1 - \sigma_3 = C$. The constant C can be found by considering a tension test. In this case $\sigma_3 = 0$ and $\sigma_1 = Y$, the yield strength at yielding, so $C = Y$. Therefore this criterion can be expressed as

$$\sigma_1 - \sigma_3 = Y. \tag{2.5}$$

Yielding in pure shear occurs when the largest shear stress $\sigma_1 = k$ and $\sigma_3 = -\sigma_1 = -k$, where k is the yield strength in shear.

$$\sigma_1 - \sigma_3 = 2k. \tag{2.6}$$

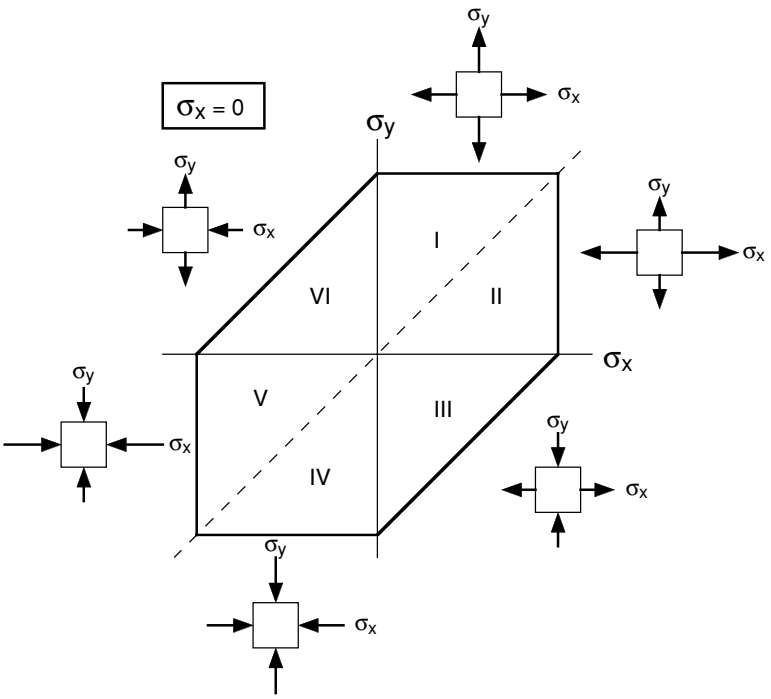

2.2. The Tresca criterion. In the six sectors the following conditions apply:
I $\sigma_y > \sigma_x > 0$, so $\sigma_y = Y$
II $\sigma_x > \sigma_y > 0$, so $\sigma_x = Y$
III $\sigma_x > 0 > \sigma_y$, so $\sigma_x - \sigma_y = Y$
IV $0 > \sigma_x > \sigma_y$, so $\sigma_y = -Y$
V $0 > \sigma_y > \sigma_x$, so $\sigma_x = -Y$
VI $\sigma_y > 0 > \sigma_x$, so $\sigma_y - \sigma_x = Y$

A yield locus is a plot of a yield criterion. Figure 2.2 is a plot of the Tresca yield locus, σ_x vs. σ_y, for $\sigma_z = 0$, where σ_x, σ_y, and σ_z are principal stresses.

EXAMPLE 2.1: A thin-wall tube with closed ends is subjected to a maximum internal pressure of 35 MPa in service. The mean radius of the tube is 30 cm.

(a) If the tensile yield strength is 700 MPa, what minimum thickness must be specified to prevent yielding?

(b) If the material has a yield strength in shear of $k = 280$ MPa, what minimum thickness must be specified to prevent yielding?

SOLUTION:

(a) Hoop stress, $\sigma_1 = Pr/t = 35(30\,\text{cm})/t = \sigma_{\max}$, longitudinal stress $= \sigma_2 = Pr/(2t) = (35\,\text{MPa})(30\,\text{cm})/(2t)$, $\sigma_{\max}$ = thickness stress, $\sigma_3 \approx 0$. Yielding occurs when $\sigma_1 = 700$, or $t = (35\,\text{MPa})(30\,\text{cm})/(700\,\text{MPa}) = 1.5\,\text{cm}$.

(b) $\sigma_1 - \sigma_3 = 2k = 560$ MPa at yielding, so yielding occurs when $t = (35\,\text{MPa})(30\,\text{cm})/(560\,\text{MPa}) = 1.875$ cm.

2.3 VON MISES CRITERION

The von Mises criterion postulates that yielding will occur when the value of the root-mean-square shear stress reaches a critical value. Expressed mathematically,

$$\left[\frac{(\sigma_2 - \sigma_3)^2 + (\sigma_3 - \sigma_1)^2 + (\sigma_1 - \sigma_2)^2}{3}\right] = C_1$$

or equivalently

$$(\sigma_2 - \sigma_3)^2 + (\sigma_3 - \sigma_1)^2 + (\sigma_1 - \sigma_2)^2 = C_2.$$

Again, C_2 may be found by considering a uniaxial tension test in the 1-direction. Substituting $\sigma_1 = Y$, $\sigma_2 = \sigma_3 = 0$ at yielding, the von Mises criterion may be expressed as

$$(\sigma_2 - \sigma_3)^2 + (\sigma_3 - \sigma_1)^2 + (\sigma_1 - \sigma_2)^2 = 2Y^2 = 6k^2. \tag{2.7}$$

Figure 2.3 is the yield locus with $\sigma_2 = 0$.

In a more general form equation 2.7 may be written as

$$(\sigma_y - \sigma_z)^2 + (\sigma_z - \sigma x)^2 + (\sigma_x - \sigma_y)^2 + 6(\tau_{yz} + \tau_{zx} + \tau_{xy}) = 2Y^2 = 6k^2. \tag{2.8}$$

The Tresca and von Mises yield loci are plotted together in Figure 2.4 for the same values of Y. Note that the greatest differences occur for $\alpha = \sigma_3/\sigma_1 = -1, \frac{1}{2}$, and 2.

Three-dimensional plots of the Tresca and von Mises yield criteria are shown in Figure 2.5. The Tresca criterion is a regular hexagonal prism and the von Mises criterion

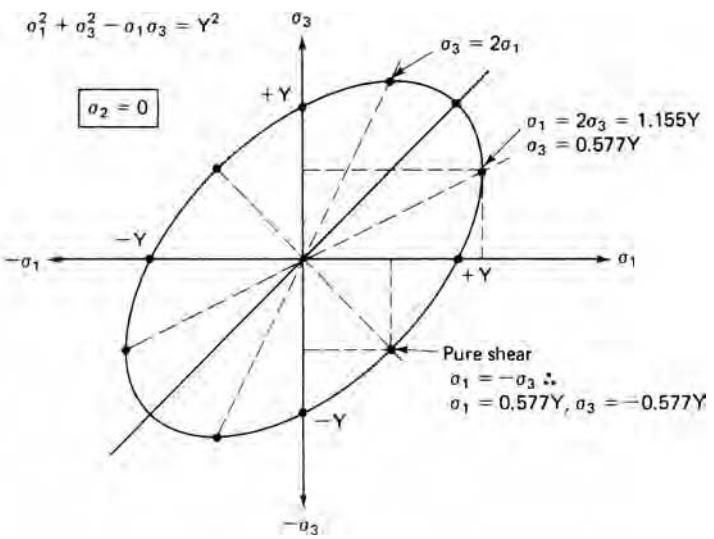

2.3. The von Mises yield locus.

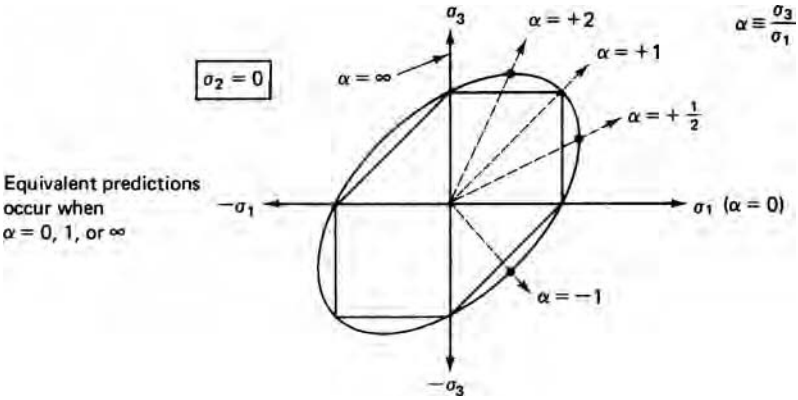

2.4. Tresca and von Mises loci showing certain loading paths.

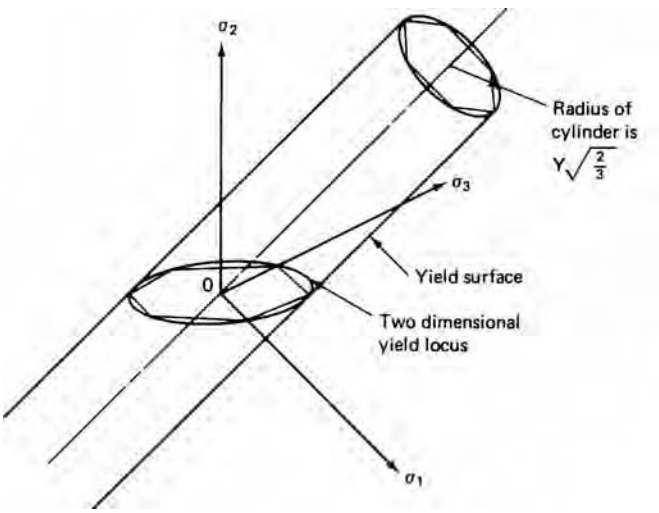

2.5. Three-dimensional plots of the Tresca and von Mises yield criteria.

is a cylinder. Both are centered on a line $\sigma_1 = \sigma_2 = \sigma_3$. The projection of these on a plane $\sigma_1 + \sigma_2 + \sigma_3 =$ constant is shown in Figure 2.6.

EXAMPLE 2.2: Reconsider the capped tube in Example 2.1 except let $t = 1.5$ cm. Use both the Tresca and von Mises criteria to determine the necessary yield strength to prevent yielding.

SOLUTION:
Tresca: $\sigma_1 = Y =$ (700 MPa) (30 cm)/1.5 cm = 14,000 MPa.
Von Mises: $\sigma_1 = (2/\sqrt{3})\ Y$. $Y = (\sqrt{3}/2)$ (700 MPa) (30 cm)/(1.5 cm) = 1212 MPa.

2.4 PLASTIC WORK

The differential amount of plastic work per volume associated with tensile strain $d\varepsilon$ of a bar of length ℓ_0, subjected to a force acting on an area is

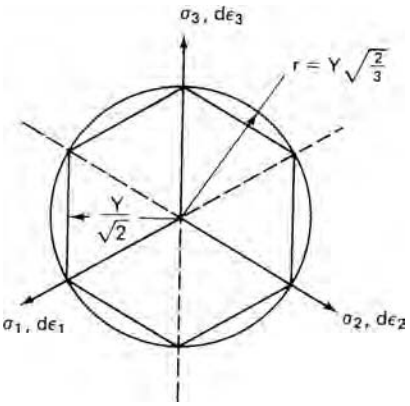

2.6. Projection of the Tresca and von Mises yield criteria onto a plane $\sigma_1 + \sigma_2 + \sigma_3 =$ constant.

$$dw = \frac{F d\ell}{A\ell_0} = \sigma d\varepsilon. \tag{2.9}$$

In the most general case where there are three normal stresses and three shear stresses the plastic work per volume is

$$dw = \sigma_x d\varepsilon_x + \sigma_y d\varepsilon_y + \sigma_z d\varepsilon_z + \tau_{yz} d\gamma_{yz} + \tau_{zx} d\gamma_{zx} + \tau_{xy} d\gamma_{xy}. \tag{2.10}$$

In term of principal stresses and strains,

$$dw = \sigma_1 d\varepsilon_1 + \sigma_2 d\varepsilon_2 + \sigma_3 d\varepsilon_3. \tag{2.11}$$

2.5 EFFECTIVE STRESS

It is useful to define an *effective stress*, $\bar{\sigma}$, for a yield criterion such that yielding occurs when the magnitude of $\bar{\sigma}$ reaches a critical value. For the von Mises criterion,

$$\bar{\sigma} = \sqrt{(1/2)[(\sigma_2 - \sigma_3)^2 + (\sigma_3 - \sigma_1)^2 + (\sigma_1 - \sigma_2)^2]}. \tag{2.12}$$

This can also be expressed as

$$\bar{\sigma} = \sqrt{(1/2)[\alpha^2 + 1 + (1 - \alpha)^2]}\sigma_1 = \sqrt{1 - \alpha + \alpha^2}\sigma_1 \tag{2.13}$$

where $\alpha = \frac{\sigma_2}{\sigma_1}$ and $\sigma_3 = 0$.

For the Tresca criterion,

$$\bar{\sigma} = \sigma_1 - \sigma_3 \tag{2.14}$$

where

$$\sigma_1 \geq \sigma_2 \geq \sigma_3.$$

2.6 EFFECTIVE STRAIN

The *effective strain*, $\bar{\varepsilon}$, is defined such that the incremental plastic work per volume is

$$dw = \sigma_1 d\varepsilon_1 + \sigma_2 d\varepsilon_2 + \sigma_3 d\varepsilon_3 = \bar{\sigma} d\bar{\varepsilon}. \tag{2.15}$$

The von Mises effective strain may be expressed as

$$d\bar{\varepsilon} = \sqrt{[(d\varepsilon_2 - d\varepsilon_3)^2 + (d\varepsilon_3 - d\varepsilon_1)^2 + (d\varepsilon_1 - d\varepsilon_2)^2]}/3, \tag{2.16}$$

or more simply as

$$d\bar{\varepsilon} = \sqrt{(2/3)\left(d\varepsilon_1^2 + d\varepsilon_2^2 + d\varepsilon_3^2\right)} \tag{2.17}$$

For proportional straining with a constant ratio of $d\varepsilon_1$:$d\varepsilon_2$:$d\varepsilon_3$, the total effective strain is

$$\bar{\varepsilon} = \sqrt{(2/3)\left(\varepsilon_1^2 + \varepsilon_2^2 + \varepsilon_3^2\right)}. \tag{2.18}$$

For the Tresca criterion the effective strain is

$$d\bar{\varepsilon} = |d\varepsilon_i|_{\max}, \tag{2.19}$$

where the subscript i refers the principal strains. Thus for Tresca, the effective strain is the absolutely largest principal strain. The relation

$$|\varepsilon_i|_{\max} \leq \bar{\varepsilon}_{\text{Mises}} \leq 1.15|\varepsilon_i|_{\max} \tag{2.20}$$

provides a simple check when evaluating $\bar{\varepsilon}$ for the von Mises criterion.

When the von Mises criterion and effective stress are used, the von Mises effective strain must be used. Conversely if the Tresca criterion and effective stress are used, the Tresca effective strain must be used.

It should be realized that in both cases the $\sigma - \varepsilon$ curve in a tension test is the $\bar{\sigma} - \bar{\varepsilon}$ curve, since $\bar{\sigma}$ reduces to σ and $\bar{\varepsilon}$ reduces to ε in a tension test. It is often assumed that strain hardening is described by the $\bar{\sigma} - \bar{\varepsilon}$ curve found in a tension test. However, at large strains there may be deviations from this because of the different changes in crystallographic texture that occur during straining along different paths.

2.7 FLOW RULES

The strains that result from elastic deformation are described by Hooke's law. There are similar relations for plastic deformation, called the *flow rules*. In the most general form the flow rule may be written

$$d\varepsilon_{ij} = d\lambda(\partial f/\partial \sigma_{ij}), \tag{2.21}$$

where f is the function of σ_{ij} that describes yielding (i.e., the yield criterion.) It is related to what has been called the *plastic potential*. For the von Mises criterion, differentiation results in

$$\begin{aligned} d\varepsilon_1 &= d\lambda[\sigma_1 - (1/2)(\sigma_2 + \sigma_3)] \\ d\varepsilon_2 &= d\lambda[\sigma_2 - (1/2)(\sigma_3 + \sigma_1)] \\ d\varepsilon_3 &= d\lambda[\sigma_3 - (1/2)(\sigma_1 + \sigma_2)]. \end{aligned} \tag{2.22}$$

In these expressions $d\lambda = d\bar{\varepsilon}/\bar{\sigma}$, which varies with position on the $\bar{\sigma} - \bar{\varepsilon}$ curve. However, the ratio of the plastic strains remains constant.

$$d\varepsilon_1 : d\varepsilon_2 : d\varepsilon_3 = [\sigma_1 - (1/2)(\sigma_2 + \sigma_3)] : [\sigma_2 - (1/2)(\sigma_3 + \sigma_1)] : [\sigma_3 - (1/2)(\sigma_1 + \sigma_2)]. \tag{2.23}$$

For Tresca, $f = \sigma_1 - \sigma_3$, so the flow rules are simply

$$d\varepsilon_1 = dl, \quad d\varepsilon_2 = 0, \quad \text{and} \quad d\varepsilon_3 = -dl. \tag{2.24}$$

EXAMPLE 2.4: Show that for plastic deformation in (a) uniaxial tension and (b) plane-strain compression ($\varepsilon_2 = 0$, $\sigma_3 = 0$), the incremental work per volume, dw, found from $dw = \bar{\sigma}\, d\bar{\varepsilon}$, is the same as $dw = \sigma_1 d\varepsilon_1 + \sigma_2 d\varepsilon_2 + \sigma_3 d\varepsilon_3 \cdots$.

SOLUTION:

(a) Substituting $\sigma_2 = \sigma_3 = 0$ into equation 2.12, $\bar{\sigma} = \sigma_1$; substituting $d\varepsilon_2 = d\varepsilon_3 = (-1/2)d\varepsilon_1$ into equation 2.16, $\bar{\sigma}\, d\bar{\varepsilon} = \sigma_1 d\varepsilon_1$.

(b) Substituting $\varepsilon_2 = 0$, $\sigma_3 = 0$ into $dw = \sigma_1 d\varepsilon_1 + \sigma_2 d\varepsilon_2 + \sigma_3 d\varepsilon_3 = \sigma_1 d\varepsilon_1$.

Substituting $d\varepsilon_2 = 0$ and $d\varepsilon_3 = -d\varepsilon_1$ into equation 2.16, $d\bar{\varepsilon} = \sqrt{(2/3)(\varepsilon_1^2 + 0 + (-\varepsilon_1)^2)} = (2/\sqrt{3})\varepsilon_1$. From the flow rules with $\varepsilon_2 = 0$ and $\sigma_3 = 0$, into $\sigma_2 = \sigma_1$. Substituting into equation 2.12, $\bar{\sigma} = (1/\sqrt{2})[(\sigma_1 - \sigma_1/2)^2 + (\sigma_1/2 - 0)^2 + (0 - \sigma_1)^2]^{1/2} = (\sqrt{3}/2)\sigma_1$. Therefore $dw = \bar{\sigma}\, d\bar{e} = [(2/\sqrt{3})d\varepsilon_1](\sqrt{3}/2)\sigma_1 = \sigma_1 d\varepsilon_1$.

EXAMPLE 2.5: A circle 1 cm diameter was printed on a sheet of metal prior to a complex stamping operation. After the stamping, it was found that the circle had become an ellipse with major and minor diameters of 1.300 and 1.100 cm.

(a) Determine the effective strain.

(b) If a condition of plane stress ($\sigma_3 = 0$) existed during the stamping, and the ratio $\alpha = \sigma_2/\sigma_1$ remained constant, what ratio $\sigma_1/\bar{\sigma}$ must have existed?

SOLUTION:

(a) $\varepsilon_1 = \ln(1.3/1) = 0.2624$, $\varepsilon_2 = \ln(1.1) = 0.0953$, $\varepsilon_3 = -\varepsilon_1 - \varepsilon_2 = -0.358$. $\bar{\varepsilon} = \sqrt{(2/3)(\varepsilon_1^2 + \varepsilon_2^2 + \varepsilon_3^2)} = [(2/3)(0.262^2 + 0.0953^2 + 0.358^2)]^{1/2} = 0.3705$. Note that this is larger than 0.358 but not 15% larger.

(b) From the flow rules (equation 2.22) with $\sigma_3 = 0$, $\varepsilon_2/\varepsilon_1 = (2\sigma_2 - \sigma_1)/(2\sigma_1 - \sigma_2)$.

Solving for $\alpha = \sigma_2/\sigma_1 = (2\varepsilon_2/\varepsilon_1 + 1)/(\varepsilon_2/\varepsilon_1 + 2) = [2(0.0953)/(0.2624) + 1]/[0.0953/0.2624 + 2] = 0.946$. Now substituting into equation 2.13, $\bar{\sigma} = \sigma_1\sqrt{1 - 0.946 + 0.946^2}$, $\sigma_1/\bar{\sigma} = 1.027$.

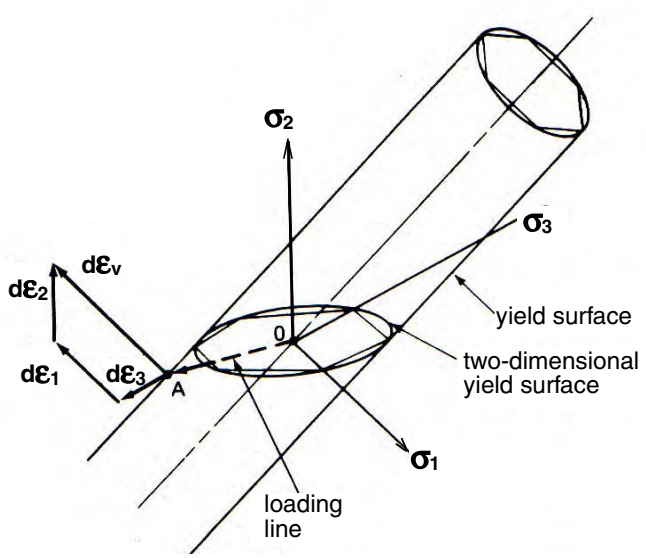

2.7. Three-dimensional yield surfaces. If a material is loaded to yielding at A, the resulting plastic strain is represented by a vector $d\varepsilon_v$ normal to the yield surface, which is the vector sum of $d\varepsilon_1$, $d\varepsilon_2$, and $d\varepsilon_3$.

2.8 NORMALITY PRINCIPLE

One interpretation of the flow rules is that the vector sum of the plastic strains is normal to the yield surface.* This is illustrated in three dimensions in Figure 2.7 and in two dimensions in Figure 2.8. With isotropic solids, the directions of principal strain and principal stress coincide. As a result we obtain the relation

$$\frac{d\varepsilon_2}{d\varepsilon_1} = -\frac{\partial\sigma_1}{\partial\sigma_2}. \tag{2.25}$$

EXAMPLE 2.7: A thin sheet is subjected to biaxial tension $\sigma_1 \neq \sigma_2 \neq 0, \sigma_3 = 0$. The principal strains in the sheet were $\varepsilon_2 = -(1/4)\,\varepsilon_1$.

(a) Using the principle of normality, determine the stress ratio, $\alpha = \sigma_2/\sigma_1$, for the von Mises and the Tresca criteria.

(b) Show that the normal to the yield locus in both cases corresponds to the answers to (a).

SOLUTION:

(a) $\varepsilon_2/\varepsilon_1 = -0.25 = (\sigma_2 - 0.5\sigma_1)/(\sigma_1 - 0.5\sigma_2)$. Solving for $\sigma_2/\sigma_1, \alpha = 2/7$. With the Tresca criterion, $\varepsilon_2 = -(1/4)\,\varepsilon_1$ can occur only at the uniaxial tension corner, so $\alpha = 0$.

(b) See Figure 2.9.

* See D. C. Drucker, *Proc. 1st U.S. Nat. Congr. Appl. Mech.* (1951), p. 487.

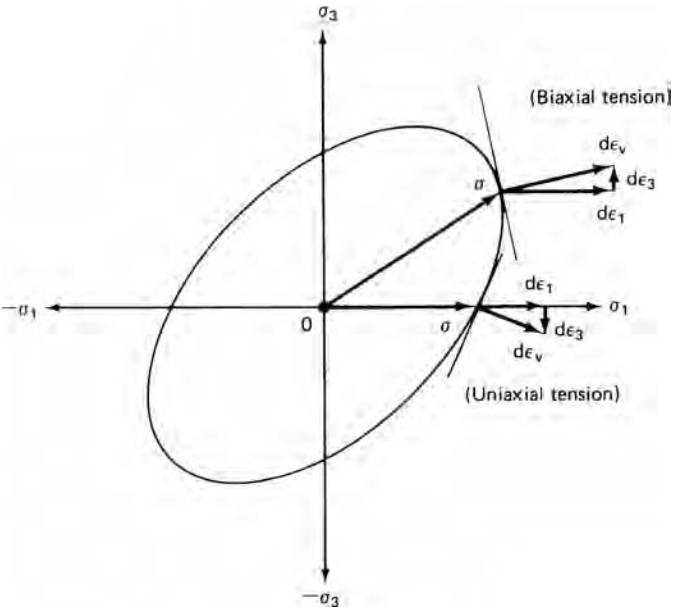

2.8. Illustration of normality. Note that the ratio of $d\varepsilon_3/d\varepsilon_1$ is given by the normal to the yield surface at the point of yielding.

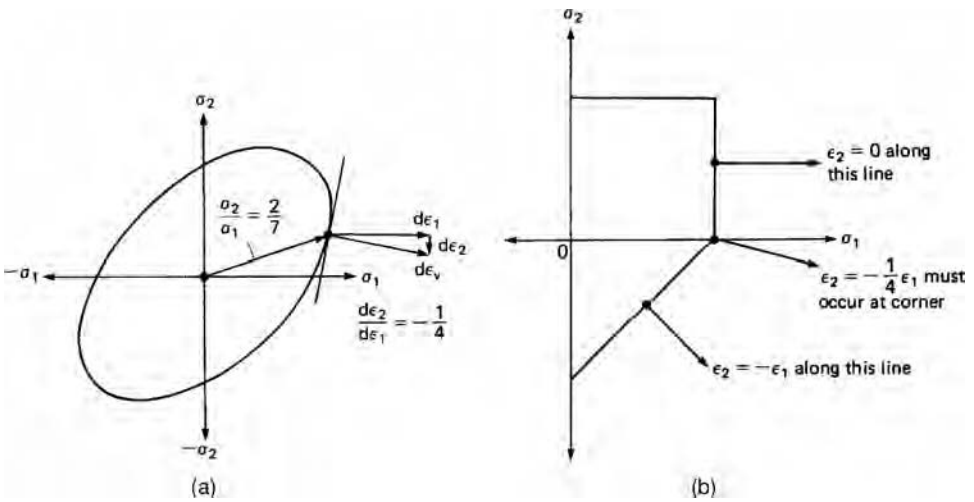

2.9. Normals to yield loci for $\varepsilon_2/\varepsilon_1 = -0.25$. (a) With von Mises criterion, the normal to the yield locus for $d\varepsilon_2/d\varepsilon_1 = -0.25$ predicts $\sigma_2/\sigma_1 = 2/7$. (b) With the Tresca criterion, a range of stress states cause the same ratio of strains. Specific strain ratios, such as $\varepsilon_2/\varepsilon_1 = -0.25$, occur only at corners.

2.9 DERIVATION OF THE VON MISES EFFECTIVE STRAIN

The effective stress-strain function is defined such that the incremental work per volume is $dw = \sigma_1 d\varepsilon_1 + \sigma_2 d\varepsilon_2 + \sigma_3 d\varepsilon_3 = \bar{\sigma}\, d\bar{\varepsilon}$. For simplicity consider a stress state with $\sigma_3 = 0$. Then

$$\bar{\sigma}\, d\bar{\varepsilon} = \sigma_1 d\varepsilon_1 + \sigma_2 d\varepsilon_2 = \sigma_1 d\varepsilon_1 (1 + \alpha\rho), \tag{2.26}$$

where $\alpha = \sigma_2/\sigma_1$ and $\rho = \mathrm{d}\varepsilon_2/\mathrm{d}\varepsilon_1$. Then

$$\mathrm{d}\bar{\varepsilon} = \mathrm{d}\varepsilon_1(\sigma_1/\bar{\sigma})(1 + \alpha\rho). \tag{2.27}$$

From the flow rules, $\rho = \mathrm{d}\varepsilon_2\mathrm{d}\varepsilon_1 = [\sigma_2 - (1/2)\sigma_1]/[\sigma_1 - (1/2)\sigma_2] = (2\alpha - 1)/(2 - \alpha)$ or

$$\alpha = (2\rho + 1)/(2 + \rho). \tag{2.28}$$

Combining equations 2.27 and 2.28,

$$\mathrm{d}\bar{\varepsilon} = \mathrm{d}\varepsilon_1(\sigma_1/\bar{\sigma})[2(1 + \rho + \rho^2)/(2 + \rho)]. \tag{2.29}$$

With $\sigma_3 = 0$, the von Mises expression for $\bar{\sigma}$ is

$$\bar{\sigma} = \left[\left(\sigma_1^2 + \sigma_2^2 - \sigma_1\sigma_2\right)\right]^{1/2} = (1 - \alpha + \alpha^2)^{1/2}\sigma_1. \tag{2.30}$$

Combining equations 2.28 and 2.29,

$$\frac{\sigma_1}{\bar{\sigma}} = \left(\frac{2 + \rho}{\sqrt{3}}\right)\Big/(1 + \rho + \rho^2)^{1/2}. \tag{2.31}$$

Since $\rho = \mathrm{d}\varepsilon_2/\mathrm{d}\varepsilon_1$,

$$\mathrm{d}\bar{\varepsilon} = \left(\frac{2}{\sqrt{3}}\right)\left(\mathrm{d}\varepsilon_1^2 + \mathrm{d}\varepsilon_1\mathrm{d}\varepsilon_2 + \mathrm{d}\varepsilon_2^2\right)^{1/2}. \tag{2.32}$$

Now since with constant value

$$\mathrm{d}\varepsilon_1^2 + \mathrm{d}\varepsilon_2^2 + \mathrm{d}\varepsilon_3^2 = 0 \quad \mathrm{d}\varepsilon_1^2 + \mathrm{d}\varepsilon_2^2 + (-\mathrm{d}\varepsilon_1 - \mathrm{d}\varepsilon_2)^2 = 2\left(\mathrm{d}\varepsilon_1^2 + \mathrm{d}\varepsilon_2\mathrm{d}\varepsilon_1 + \mathrm{d}\varepsilon_2^2\right), \tag{2.33}$$

equation 2.32 becomes

$$\mathrm{d}\bar{\varepsilon} = \left[(2/3)\left(\mathrm{d}\varepsilon_1^2 + \mathrm{d}\varepsilon_2^2 + \mathrm{d}\varepsilon_3^2\right)\right]^{1/2}. \tag{2.34}$$

This derivation also holds where $\sigma_3 \neq 0$, since this is equivalent to a stress state

$$\sigma_1' = \sigma_1 - \sigma_3, \quad \sigma_2' = \sigma_2 - \sigma_3, \quad \sigma_3' = \sigma_3 - \sigma_3 = 0.$$

NOTES OF INTEREST

Otto Z. Mohr (1835–1918) worked as a civil engineer, designing bridges. At 32, he was appointed a professor of engineering mechanics at Stuttgart Polytechnikum. Among other contributions, he also devised the graphical method of analyzing the stress at a point. He then extended Coulomb's idea that failure is caused by shear stresses into a failure criterion based on maximum shear stress, or diameter of the largest circle. He proposed the different failure stresses in tension, shear, and compression could be combined into a single diagram, in which the tangents form an envelope of safe stress combinations.

This is essentially the Tresca yield criterion. It may be noted that early workers used the term "failure criteria," which failed to distinguish between fracture and yielding.

In 1868, Tresca presented two notes to the French Academy.* From these, Saint-Venant established the first theory of plasticity based on the assumptions that

1. plastic deformation does not change the volume of a material,
2. directions of principal stresses and principal strains coincide,
3. the maximum shear stress at a point is a constant.

The Tresca criterion is also called the *Guest* or the "*maximum shear stress*" criterion.

In letters to William Thompson, John Clerk Maxwell (1831–1879) proposed that "strain energy of distortion" was critical, but he never published this idea and it was forgotten. M. T. Huber, in 1904, first formulated the expression for "distortional strain energy." The same idea was independently developed by von Mises† for whom the criterion is generally called. It is also referred to by the names of several people who independently proposed it: Huber, Hencky, as well as Maxwell. It is also known as the "maximum distortional energy" theory and the "octahedral shear stress" theory. The first name reflects that the elastic energy in an isotropic material, associated with shear (in contrast to dilatation), is proportional to $(\sigma_2 - \sigma_3)^2 + (\sigma_3 - \sigma_1)^2 + (\sigma_1 - \sigma_2)^2$. The second name reflects that the shear terms, $(\sigma_2 - \sigma_3)$, $(\sigma_3 - \sigma_1)$, and $(\sigma_1 - \sigma_2)$, can be represented as the edges of an octahedron in principal stress space.

REFERENCES

W. F. Hosford, *Mechanical Behavior of Materials*, Cambridge University Press, 2005.

F. A. McClintock and A. S. Argon, *Mechanical Behavior of Materials*, Addison-Wesley, 1966.

PROBLEMS

2.1. **a)** If the principal stresses on a material with a yield stress in shear are $\sigma_1 = 175$ MPa and $\sigma_2 = 350$ MPa what tensile stress σ_3 must be applied to cause yielding according to the Tresca criterion?

b) If the stresses in (a) were compressive, what tensile stress σ_3 must be applied to cause yielding according to the Tresca criterion?

2.2. Consider a 6-cm diameter tube with 1-mm thick wall with closed ends made from a metal with a tensile yield strength of 25 MPa. Apply a compressive load of 2000 N to the ends. What internal pressure is required to cause yielding according to (a) the Tresca criterion and (B) the von Mises criterion?

2.3. Consider a 0.5 m-diameter cylindrical pressure vessel with hemispherical ends made from a metal for which $k = 500$ MPa. If no section of the pressure vessel is to yield under an internal pressure of 35 MPa, what is the minimum wall thickness according to (a) the Tresca criterion? (b) the von Mises criterion?

2.4. A thin-wall tube is subjected to combined tensile and torsional loading. Find the relationship between the axial stress σ, the shear stress τ, and the tensile

* Tresca, *Comptes Rendus Acad. Sci. Paris* (1864), p. 754.

† von Mises, *Göttinger Nachr. Math. Phys.* (1913), p. 582.

yield strength Y to cause yielding according to (a) the Tresca criterion, (b) the von Mises criterion.

2.5. Consider a plane-strain compression test with a compressive load F_y, a strip width w, an indenter width b, and a strip thickness t. Using the von Mises criterion, find

a) $\bar{\varepsilon}$ as a function of ε_y,
b) $\bar{\sigma}$ as a function of σ_y,
c) an expression for the work per volume in terms of ε_y and σ_y,
d) an expression in the form of $\sigma_y = f(K, \varepsilon_y, n)$ assuming $\bar{\sigma} = K\bar{\varepsilon}^n$.

2.6. The following yield criterion has been proposed: "Yielding will occur when the sum of the two largest shear stresses reaches a critical value." Stated mathematically

$$(\sigma_1 - \sigma_3) + (\sigma_1 - \sigma_2) = C \quad \text{if} \quad (\sigma_1 - \sigma_2) > (\sigma_2 - \sigma_3) \quad \text{or}$$
$$(\sigma_2 - \sigma_3) + (\sigma_1 - \sigma_2) = C \quad \text{if} \quad (\sigma_1 - \sigma_2) \leq (\sigma_2 - \sigma_3)$$

where $\sigma_1 > \sigma_2 > \sigma_3$, $C = 2Y$, and $Y =$ tensile yield strength.

2.7. Consider the stress states

$$\begin{vmatrix} 15 & 3 & 0 \\ 3 & 10 & 0 \\ 0 & 0 & 5 \end{vmatrix} \quad \text{and} \quad \begin{vmatrix} 10 & 3 & 0 \\ 3 & 5 & 0 \\ 0 & 0 & 0 \end{vmatrix}.$$

a) Find σ_m for each.
b) Find the deviatoric stress in the normal directions for each
c) What is the sum of the deviatoric stresses for each?

2.8. A thin wall tube with closed ends is made from steel with a yield strength of 250 MPa. The tube is 2 m long with a wall thickness of 2 mm and a diameter of 8 cm. In service it will experience an axial load of 8 kN and a torque of 2.7 Nm. What is the maximum internal pressure it can withstand without yielding according to (a) the Tresca criterion and (b) the von Mises criterion?

2.9. Calculate the ratio of $\bar{\sigma}/\tau_{max}$ for (a) pure shear, (b) uniaxial tension, and (c) plane-strain tension. Assume the von Mises criterion.

2.10. A material yields under a biaxial stress state, $\sigma_3 = -(1/2)\sigma_1$.

a) Assuming the von Mises criterion, find $d\varepsilon_1/d\varepsilon_2$.
b) What is the ratio of τ_{max}/Y at yielding?

2.11. A material is subjected to stresses in the ratio σ_1, $\sigma_2 = 0.3\sigma_1$, and $\sigma_3 = -0.5\sigma_1$. Find the ratio of σ_1/Y at yielding using (a) the Tresca criterion and (b) the von Mises criterion.

2.12. A proposed yield criterion is that yielding will occur when the diameter of the largest Mohr's circle plus half the diameter of the second largest Mohr's circle reaches a critical value. Plot the yield locus in σ_1 vs. σ_2 in $\sigma_3 = 0$ space.

2.13. Make plot of ε_1 versus ε_2 for a constant level of $\bar{\varepsilon} = 0.10$ according to (a) von Mises and (b) Tresca.

3 Strain Hardening

When metals are deformed plastically at temperatures lower than would cause recrystallization, they are said to be *cold worked*. Cold working increases the strength and hardness. The terms *work hardening* and *strain hardening* are used to describe this. Cold working usually decreases the ductility.

Tension tests are used to measure the effect of strain on strength. Sometimes other tests, such as torsion, compression, and bulge testing are used, but the tension test is simpler and most commonly used. The major emphasis in this chapter is the dependence of yield (or flow) stress on strain.

3.1 THE TENSION TEST

The temperature and strain rate influence test results. Generally the strain rate is in the order of 10^{-2} to 10^{-3}/s and the temperature is between 18 and 25°C. These effects are discussed in Chapter 5. Measurements are made in a gauge section that is under uniaxial tension during the test.

Initially the deformation is elastic and the tensile force is proportional to the elongation. Elastic deformation is recoverable. It disappears when the tensile force is removed. At higher forces the deformation is plastic, or nonrecoverable. In a ductile material, the force reaches a maximum and then decreases until fracture. Figure 3.1 is a schematic tensile load-extension curve.

Stress and strain are computed from measurements in a tension test of the tensile force, F, and the elongation, $\Delta\ell$. The *nominal* or *engineering stress, S*, and *strain, e*, are defined as

$$S = F/A_0 \tag{3.1}$$

and

$$e = \Delta\ell/\ell_0. \tag{3.2}$$

where A_0 is the initial cross sectional area and ℓ_0 is the initial gauge length. Since A_0 and ℓ_0 are constants, the shapes of the S–e and F–$\Delta\ell$ curves are identical. That is why the axes of Figure 3.1 have double notation. The stress at which plastic flow

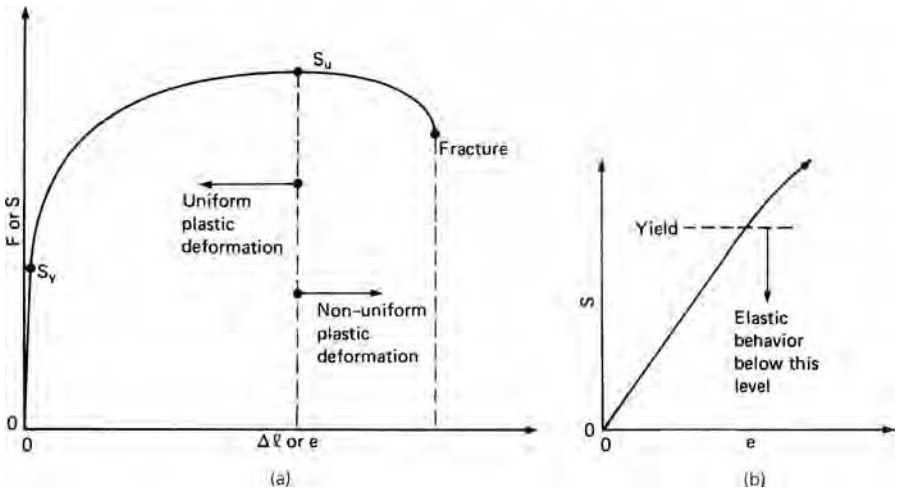

3.1. (a) Load–extension and engineering stress–strain curve of a ductile metal. (b) Expansion of initial part of the curve.

begins, S_y, is called the yield strength, Y, and is defined in terms of the yield force, F_y, as

$$Y = F_y/A_0 = S_y. \tag{3.3}$$

The tensile strength or ultimate tensile strength, S_u, is defined as

$$S_u = F_{max}/A_0. \tag{3.4}$$

Ductility is a measure of the amount that a material can be deformed before failure. There are two common parameters: % elongation and % reduction of area.

$$\%\ \text{elongation} = 100\frac{(\ell_f - \ell_0)}{\ell_0} \tag{3.5}$$

$$\%\ \text{reduction of area} = 100\frac{(A_0 - A_f)}{A_0}, \tag{3.6}$$

where A_f and ℓ_f are the cross-sectional area and gauge length at fracture. Although standard values of A_f and ℓ_f are usually used, the % elongation depends on the ratio of the gauge length-to-diameter because the elongation after necking depends on the diameter and the uniform elongation depends on the gauge length. The % reduction of area is much less dependent on specimen dimensions. The % reduction of area in a tension test should not be confused with the reduction of area, r, in a metal working process,

$$r = \frac{(A_0 - A)}{A_0}, \tag{3.7}$$

where A is the cross-sectional area after forming.

Figure 3.2 shows the yielding behavior of an annealed brass and a low-carbon steel. Brass is typical of most ductile metals. Yielding is so gradual that it is difficult

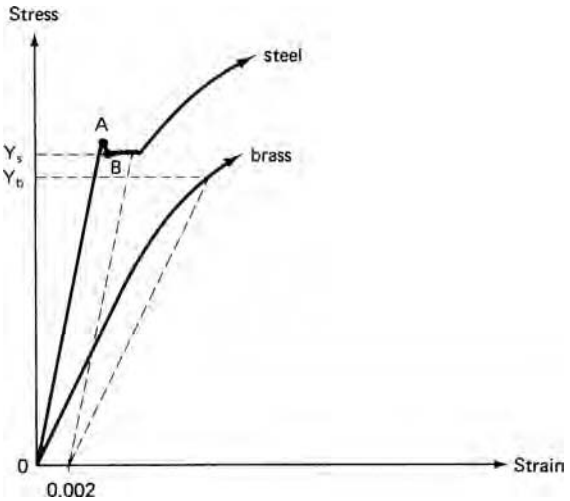

3.2. Offset method for determining the yield strength.

to define the point at which plastic deformation begins. Therefore the yield strength is usually defined as the stress at which the plastic strain is 0.002 or 0.2%. This can be found as the intersection of a line parallel to the elastic portion of the curve with the stress–strain curve. This 0.2% offset yield strength is shown in Figure 3.2 as Y_b. Low carbon steels typically have an upper yield stress (point A) and a lower yield stress (B). Because the upper yield strength is very sensitive to the alignment of the tensile specimen, the lower yield stress (Y_B in Figure 3.2) is defined as the yield strength.

3.2 ELASTIC–PLASTIC TRANSITION

The transition from elastic to plastic flow is gradual as illustrated in Figure 3.3 for plane-strain deformation with $\varepsilon_y = 0$ and $\sigma_z = 0$. For elastic deformation, $\alpha = \nu$, and for fully plastic deformation, $\alpha = 0.5$, where $\alpha = \sigma_y/\sigma_x$. In this figure the ε_x is normalized by the ratio of the yield strength to the modulus. Note that 95% of the change from elastic to plastic deformation occurs when the plastic strain is 3 times the elastic strain.

For a material that strain hardens, there is additional elastic deformation after yielding. The total strain is the sum of the elastic and plastic parts, $\varepsilon = \varepsilon_e + \varepsilon_p$. Even though the elastic strain may be very small relative to the plastic strain, elastic recovery on unloading controls residual stresses and springback.

3.3 ENGINEERING VS. TRUE STRESS AND STRAIN

Figure 3.1 shows that after initial yielding, further deformation requires an increased stress. Although the material strain hardens as it is extended, its cross-sectional area decreases. These two factors control the shape of the load-extension curve. Eventually there is a maximum at which the rate of reduction of load carrying capacity caused by reduction of area equals the rate of strain hardening. Up to this point the deformation along the gauge section is uniform. However, after the maximum load is reached, the

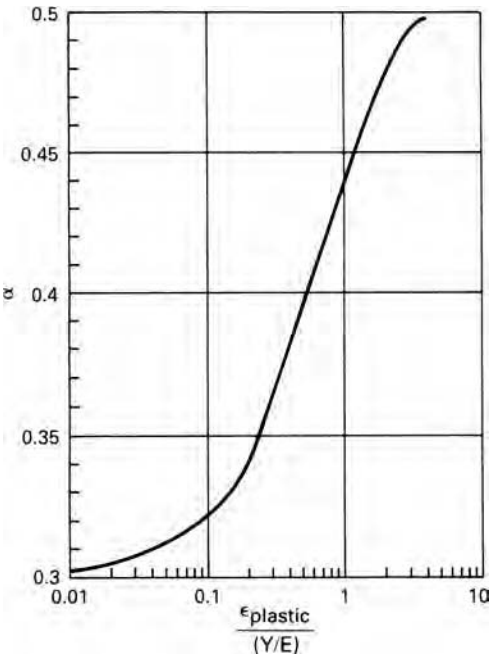

3.3. Change in the stress ratio, $\alpha = \sigma_y/\sigma_x$, for plane strain, $\varepsilon_y = 0$, as a function of strain.

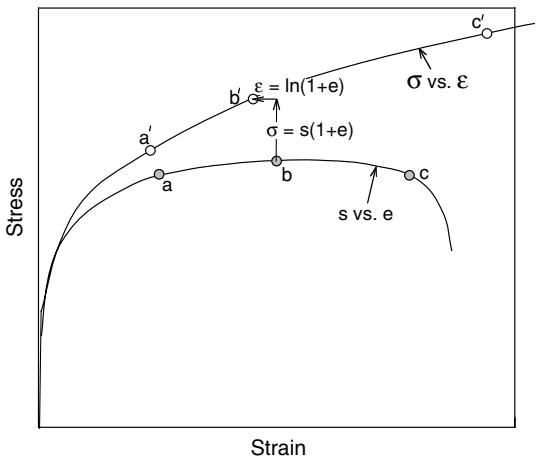

3.4. Comparison of engineering (lower) and true (upper) stress–strain curves.

deformation will localize and a *neck* will form. With continued extension almost all of the deformation is restricted to the neck region.

Figure 3.4 shows the engineering stress–strain curve lower and the corresponding true stress–strain curve (uper).

The true strain is defined by $d\varepsilon = d\ell/\ell$. Before necking occurs

$$\varepsilon = \ln(1 + e). \tag{3.8}$$

After necking the true strain must be based on the area; $d\varepsilon = -dA/A$ or

$$\varepsilon = \ln(A_0/A). \tag{3.9}$$

The true stress $\sigma = F/A$ can be found before necking as $\sigma = S(A_0/A)$ or

$$\sigma = S(1 + e). \tag{3.10}$$

EXAMPLE 3.1: When a tensile specimen with a diameter of 0.505 in and a gauge length of 2.0 in was loaded to 10,000 lb, it was found that the gauge length was 2.519 in. Assuming that the deformation was uniform,

(a) compute the true stress and true strain.
(b) find the diameter.

SOLUTION:

(a) With $d_0 = 0.505$ in, $A_0 = 0.200$ in^2, $S = 10{,}000/0.2 = 50{,}000$ psi. $e = (2.519 - 2.000)/2.000 = 0.259$, $\sigma = S(1+ e) = 50{,}000(1.259) = 62{,}950$, $\varepsilon = \ln(1+ 0.259) = 0.23$.

After necking the actual measured areas must be used to find the average stress in the necked region. Furthermore the stress state is actually triaxial as discussed further in Section 3.7 so $\bar{\sigma} \neq \sigma$.

3.4 A POWER-LAW EXPRESSION

The curve a′b′c′ in Figure 3.4 is the true stress–true strain curve. Often this curve can be approximated by a power-law expression*

$$\sigma = K\varepsilon^n. \tag{3.11}$$

Here σ can be interpreted as the new yield strength after a cold reduction, corresponding to $\varepsilon = \ln[1/(1 - r)]$. Because the tensile true stress, σ, and true tensile strain, ε, in a tension test are the effective stress and strain,

$$\bar{\sigma} = K\bar{\varepsilon}^n. \tag{3.12}$$

EXAMPLE 3.2: The plastic behavior of a metal can be expressed as $\bar{\sigma} = 500\bar{\varepsilon}^{0.50}$ MPa. Estimate the yield strength if a bar of this material is uniformly cold worked to a reduction of $r = 0.3$.

SOLUTION: Substituting $\varepsilon = \ln[1/(1 - 0.3)] = 0.357$, $\bar{\sigma} = 500(0.357)^{0.50} = 299$ MPa.

The values of K and n can be found plotting the true stress–strain curve on log–log coordinates. Noting that $\log \sigma = \log K + n\log \varepsilon$, so the slope equals n and K is the intercept at $\varepsilon = 1$. Figure 3.5 shows such a plot for an aluminum alloy. Note that there are three zones. Zone I is the elastic region where $\sigma = E\varepsilon$. Zone II is the region of transition between elastic and fully plastic behavior and the material in Zone III is fully

* The power-law hardening expression is sometimes called the Hollomon equation because it was first made popular by John H. Hollomon in *Ferrous Metallurgical Design* by John H. Hollomon and Leonard D. Jaffe (New York: J. Wiley).

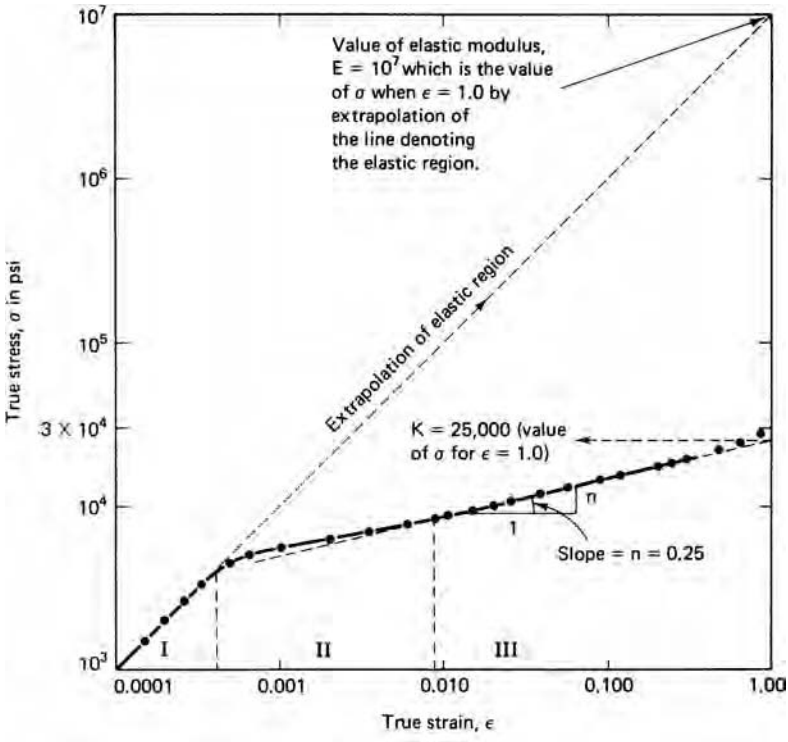

3.5. True stress–strain curve of aluminum 1100-O plotted on logarithmic coordinates.

plastic. Strictly equations 3.11 and 3.12 apply only to the plastic part of the strain, but since the elastic strain is small relative to the plastic strain after a few percent, that distinction can be ignored.

EXAMPLE 3.3: Show that the maximum load in a tension test starts when $\varepsilon = n$.

SOLUTION: Since $F = \sigma A$, when $\mathrm{d}F = 0, \sigma \mathrm{d}A + A\mathrm{d}\sigma = 0$. Rearranging, $\mathrm{d}\sigma/\sigma = -\mathrm{d}A/A$. Substituting $\mathrm{d}\varepsilon = -\mathrm{d}A/A$, the maximum load corresponds to $\mathrm{d}\sigma/\mathrm{d}\varepsilon = \sigma$. With the power law, $\sigma = K\varepsilon^n$ and $\mathrm{d}\sigma/\mathrm{d}\varepsilon = nK\varepsilon^{n-1}$. Equating and simplifying, $K\varepsilon^n = nK\varepsilon^{n-1}$, $\varepsilon = n$. Thus maximum load and necking start when the strain equals strain-hardening exponent.

The true stress at maximum load can be expressed as

$$\sigma_\mathrm{u} = K\varepsilon_\mathrm{u}^n = Kn^n. \tag{3.13}$$

Since

$$S_\mathrm{u}A_0 = \sigma_\mathrm{u}A_\mathrm{u} = (Kn^n)A_\mathrm{u},\ S_\mathrm{u} = (Kn^n)A_\mathrm{u}/A_0.$$

$$\text{Substituting } A_\mathrm{u}/A_0 = \exp(-e_\mathrm{u}),\ S_\mathrm{u} = K(n/\mathrm{e})^n, \tag{3.14}$$

where e is the base of natural logarithms.

EXAMPLE 3.4: In the tension test for Figure 3.5, the tensile strength was experimentally measured as 28,000 psi. Is this consistent with the values of $n = 0.25$ and $K = 50{,}000$?

SOLUTION: Using equation 3.14, $S_u = 50{,}000\ (0.25/e)^{0.25} = 27{,}500$ psi. This is within 2% so it is reasonable in view of errors in establishing n and K.

EXAMPLE 3.5:

(a) The strain hardening behavior of an annealed low-carbon steel is approximated by $\bar{\sigma} = 700\bar{\varepsilon}^{0.20}$MPa. Estimate the yield strength after the bar is cold worked 50%.

(b) Suppose another bar of this same steel was cold worked an unknown amount and then cold worked 15% more and found to have a yield strength of 525 MPa. What was the unknown amount of cold work?

SOLUTION:

(a) The strain was $\ln[1/(1–0.5)] = 0.693$. $\sigma = 700(0.693)^{0.20} = 650$ MPa.

(b) Solving equation 3.12 for $\bar{\varepsilon}$, $\bar{\varepsilon} = (\bar{\sigma}/K)^{1/n} = (525/700)^5 = 0.237$. The 15% cold work corresponds to a strain of $\ln[(1/1 - .15)] = 0.1625$. Subtracting this known strain, the unknown strain must be $0.237 - 0.1625 = 0.0745$. which corresponds to a cold work of 0.72%.

3.5 OTHER STRAIN HARDENING APPROXIMATIONS

While the power law is often a good approximation to the stress–strain behavior, sometimes other expressions are better approximations or more convenient mathematically. The stress–strain curves of some aluminum alloys seem to approach an asymptote indicating a saturation of strain hardening. In this case a better approximation is

$$\sigma = \sigma_0[1 - \exp(-B\varepsilon)], \tag{3.15}$$

where σ_0 is the level of σ at an infinite strain. If there has been prior cold work an appropriate expression may be

$$\sigma = K(\varepsilon + \varepsilon_0)^n, \tag{3.16}$$

where the amount prior cold work was equivalent to a strain of ε_0. It should be noted that the more constants in an approximation the better the fit that can be achieved, but the less useful the approximation is. Sometimes it is reasonable to assume linear strain hardening. This is very simple mathematically:

$$\sigma = \sigma_0 + C\varepsilon. \tag{3.17}$$

3.6 BEHAVIOR DURING NECKING

It was noted in Section 3.4 that once necking starts, $\bar{\sigma} \neq \sigma$ because the stress state is no longer uniaxial. As the smallest section elongates, its lateral contraction is resisted by adjacent regions that are slightly less stressed. This constraint causes lateral stresses

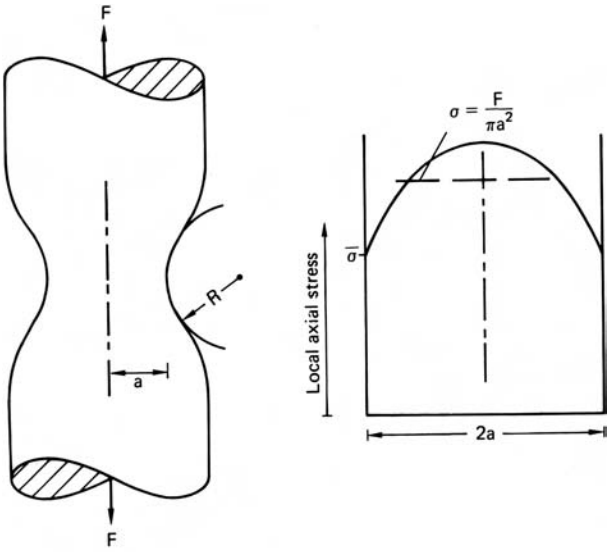

3.6. A neck showing the parameters *a* and *R* (left), and the variation of axial stress σ in the necked region (right).

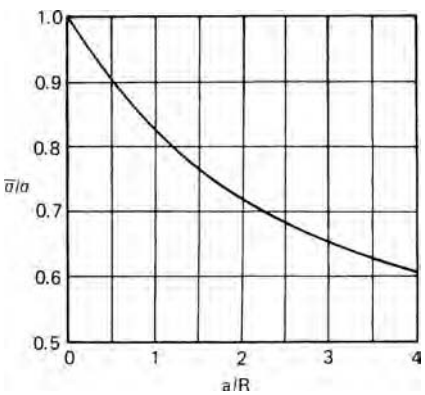

3.7. Ratio of effective stress to average axial stress as a function of neck geometry. After P. W. Bridgman, *Trans. ASM,* 32 (1994), pp. 553–74.

that increase from zero on the outside to a maximum in the center. To maintain plastic flow the axial true stress must become larger than the effective stress.

Bridgman* analyzed this problem and developed an expression for $\bar{\sigma}/\sigma$ as a function of a/R, where $2a$ is the diameter of the minimum section and R is the radius of curvature of the neck as shown in Figure 3.6. He found that

$$\sigma/\bar{\sigma} = (1 + 2R/a)\ln(1 + a/2R), \tag{3.18}$$

where σ is the average value of the axial stress, $\sigma = F/A$. As the neck become sharper the correction becomes greater. Figure 3.7 is a plot of this correction factor.

The use of the Bridgman correction allows effective stress–effective strain data to be collected at large strains. However if a neck becomes too sharp, voids may form at the center of the neck region where the hydrostatic tension is greatest and the voids decrease the load-carrying cross section.

* P. W. Bridgman, *Trans. ASM*, 32 (1944), pp. 553–74.

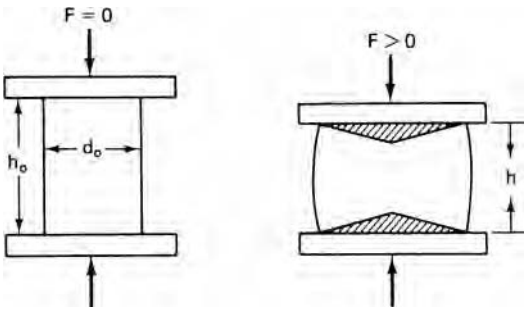

3.8. Barreling and formation of a dead metal zone in compression.

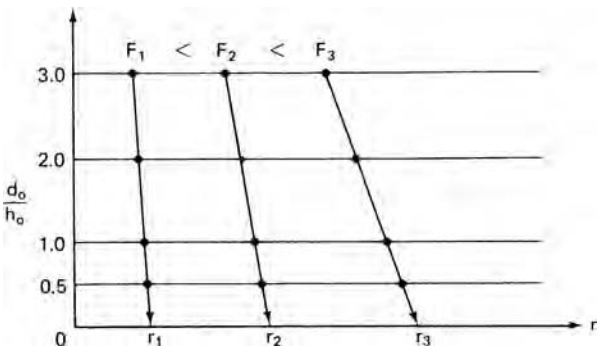

3.9. The Watts and Ford method of finding the true stress strain behavior in compression.

3.7 COMPRESSION TESTING

The compression test is an apparent solution to obtaining data at high strains without the interference of necking. However friction at the interface between the specimen and the platens complicates the stress state and results in *barreling* as shown in Figure 3.8. The friction tends to prevent radial expansion of the material in contact with the platens. This creates a dead-metal zone at the top and bottom. Thus end effects cause nonuniform stresses and strains.

The problem is lessened as the height-to-diameter ratio, h_0/d_0, of the specimen becomes greater. However when h_0/d_0 exceeds about 3, the specimens will buckle. An extrapolation method proposed by Cook and Larke* and improved by Watts and Ford† provides a way to obtain true stress–strain data. They tested well-lubricated specimens of the same initial diameter, but varying heights and measured the radius, r, as a function of load. By plotting d_0/h_0 against r at constant load they could find the value of r corresponding to an infinite h_0/d_0 ratio by extrapolation as shown schematically in Figure 3.9. This value of r was used to find the true strain.

3.8 BULGE TESTING

The hydraulic bulge test is a method of testing a sheet in balanced biaxial tension. A thin disc is clamped around the edges and subjected to increasing fluid pressure on

* M. Cook and E. C. Larke, *J. Inst. Metals,* 71 (1945), pp. 371–90.
† A. B. Watts and H. Ford, *Proc. Inst. Mech. Eng.,* 169 (1955), pp. 114–49.

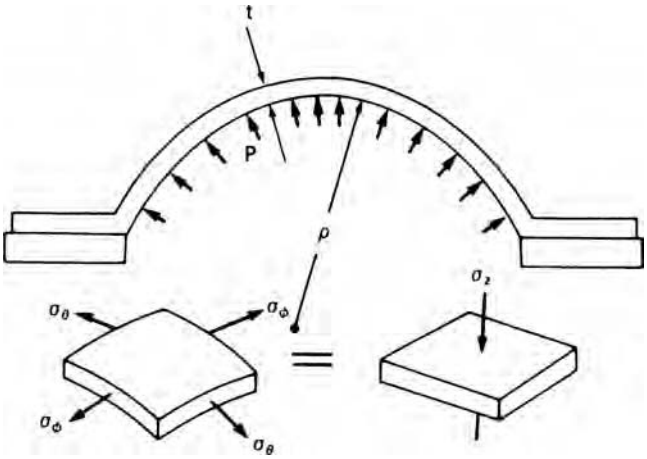

3.10. Schematic of a bulge test.

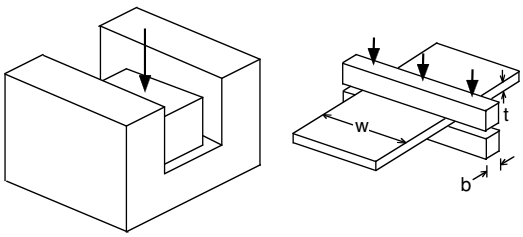

3.11. Two ways of making plane-strain compression tests.

one side as illustrated in Figure 3.10. As the sheet bulges, the region near the dome becomes nearly spherical. The tensile stresses are

$$\bar{\sigma} = \sigma_\theta = \sigma_\phi = P\rho/2t, \tag{3.19}$$

where P is the pressure, ρ is the radius of curvature, and t is the thickness. The effective strain is

$$\bar{\varepsilon} = -2\varepsilon_\theta = 2\varepsilon_\phi = \ln(t/t_0). \tag{3.20}$$

It is necessary to measure the strain to find the thickness t. Duncan* developed a special device for measuring ρ. The advantage of bulge testing is that it can be carried out to much higher strains than in tension testing.

3.9 PLANE-STRAIN COMPRESSION

Figure 3.11 shows two simple ways of making plane-strain compression tests. One is to put a specimen in a well-lubricated channel that prevents lateral spreading. The other is to indent a wide thin specimen with overlapping indenters. The material outside the plastic region will prevent spreading if $w \gg b$. There is friction in both methods. With channel compression there is friction on the sidewalls as well as on the top and bottom.

* J. L. Duncan, *Bulletin of Mechanical Engineering Education*, v. 4 (Pergamon Press, 1965), pp. 29–37. R. F. Young, J. E. Bird, and J. L. Duncan, *J. Applied Metalworking*, 2 (1981), pp. 11–17.

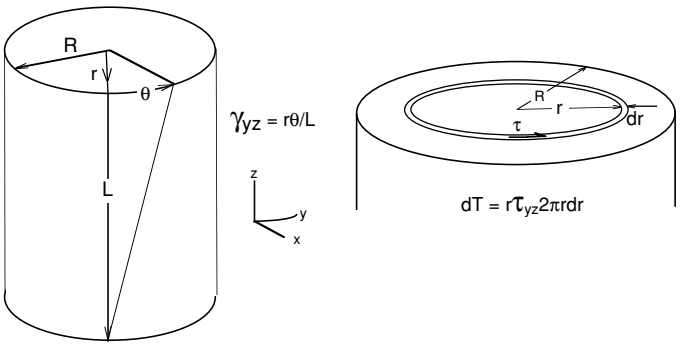

3.12. Schematic of a torsion test.

3.10 TORSION TESTING

Although torsion testing is not widely used, very high strains can be reached without complications from friction or dimensional changes. Figure 3.12 illustrates the essentials. The shear strain in an element is given by

$$\gamma = r\theta/L, \tag{3.21}$$

where r is the radial position of the element.

The torque can be measured and it is related to the shear stress by

$$\mathrm{d}T = 2\pi\,\tau_{yz} r^2 \mathrm{d}r \text{ or } T = 2\pi \int_0^R \tau_{yz} r^2 \mathrm{d}r. \tag{3.22}$$

A difficulty is that τ_{yz} varies with r. The solution to this is to test either very thin-wall tubes, which tend to buckle, or to test two bars of slightly different diameters and take the difference in torques as the torque that would have been measured on a tube whose thickness equals the difference in diameters.*

NOTE OF INTEREST

J. Herbert Hollomon (1919–1985) was born in Norfolk, VA. He studied physics and metallurgy at MIT where he earned a doctorate in 1946. He worked at the Watertown Arsenal during World War II. There he coauthored a book, *Ferrous Metallurgical Design*, with L. D. Jaffe, Wiley, in 1947. Following the war he worked for the General Electric Research Labs where he rose to the position of general manager. In 1962, President Kennedy appointed him the first assistant secretary for science and technology in the department of commerce. In 1960, he had made a speech calling for a national academy of engineering, which was reprinted in *Science*. The academy was established in 1964 and he became a founding member.

REFERENCES

R. M. Caddell, *Deformation and Fracture of Solids*, Prentice-Hall, 1980.
C. R. Calladine, *Engineering Plasticity*, Pergamon Press, 1969.

* D. S. Fields and W. A. Backofen, *Proc. ASTM*, 57 (1957), pp. 1259–72.

P. Han, ed. *Tensile Testing*, ASM International, 1992.
W. F. Hosford, *Mechanical Behavior of Materials*, Cambridge University Press, 2005.
W. Johnson and P. B. Mellor, *Engineering Plasticity*, Van Nostrand Reinhold, 1973.
E. G. Thomsen, C. T. Yang, and S. Kobayashi, *Mechanics of Plastic Deformation in Metal Processing*, Macmillan, 1965.

PROBLEMS

3.1. When a brass tensile specimen, initially 0.505 in in diameter, is tested, the maximum load of 120 ksi was recorded at an elongation of 40%. What would the load be on an identical tensile specimen when the elongation is 20%?

3.2. During a tension test the tensile strength was found to be 340 MPa. This was recorded at an elongation of 30%. Determine n and K if the approximation $\bar{\sigma} = K\bar{\varepsilon}^n$ applies.

3.3. Show that the plastic work is $\sigma_1\varepsilon_1/(n+1)$ for a metal stretched in tension to ε_1 if $\bar{\sigma} = k\bar{\varepsilon}^n$.

3.4. For plane-strain compression (Figure 3.11),

a) Express the incremental work per volume, dw, in terms of $\bar{\sigma}$ and $d\bar{\varepsilon}$ and compare it with $\mathrm{d}w = \sigma_1\mathrm{d}\varepsilon_1 + \sigma_2\mathrm{d}\varepsilon_2 + \sigma_3\mathrm{d}\varepsilon_3$.

b) If $\bar{\sigma} = k\bar{\varepsilon}^n$, express the compressive stress as a function of σ_1, K, and n.

3.5. The following data were obtained from a tension test:

Load (kN)	Min. dia. (mm)	Neck radius (mm)	True strain ε	True stress apparent σ (MPa)	True stress corrected $\bar{\sigma}$ (MPa)
0	8.69	∞	0	0	0
27.0	8.13	∞	0.133	520	520
34.5	7.62	∞			
40.6	6.86	∞			
38.3	5.55	10.3			
29.2	3.81	1.8			

a) Compute the missing values

b) Plot both σ and $\bar{\sigma}$ vs. ε on a logarithmic scale and determine K and n.

c) Calculate the strain energy per volume when $\varepsilon = 0.35$.

3.6. Consider a steel plate with a yield strength of 40 ksi, Young's modulus of 30 $\times 10^6$ psi, and a Poisson's ratio of 0.30 loaded under balanced biaxial tension. What is the volume change, $\Delta V/V$, just before yielding?

3.7. The strain-hardening of a certain alloy is better approximated by $\sigma = A - \exp(1 - B\varepsilon)$ than by $\bar{\sigma} = k\bar{\varepsilon}^n$. Determine the true strain at necking in terms of A and B.

3.8. Express the tensile strength in terms of A and B for the material in Problem 3.7.

3.9. A metal sheet undergoing plane-strain deformation is loaded to a tensile stress of 300 MPa. What is the major strain if the effective stress–strain relationship is $\bar{\sigma} = 650(0.015 + \bar{\varepsilon})^{0.22}$ MPa?

3.10. A metal sheet undergoing plane-strain deformation is loaded to a tensile stress of 300 MPa. What is the strain if the effective stress–strain relation is $\bar{\sigma} = 650(0.015 + \bar{\varepsilon})^{0.20}$?

4 Instability

Different phenomena limit the extent to which a metal may be deformed. Buckling may occur under compressive loading if the ratio of height-to-diameter is too great. Fracture may occur under tension. The thrust in this chapter is with a different type of phenomenon, called plastic instability. When a structure is deformed, there is often a maximum force or maximum pressure after which deformation continues at decreasing loads or pressures. It is assumed throughout this chapter that the strain hardening is described by $\bar{\sigma} = K\bar{\varepsilon}^n$. If other expressions better represent the behavior, they can be used with the same procedures. Solutions for effective strain at instability are functions of n.

4.1 UNIAXIAL TENSION

In a tension test of a ductile metal, the deformation is uniform up to maximum load. After this, localized deformation starts to form a neck. Since $F = \sigma A$, the condition for maximum load can be expressed as

$$\mathrm{d}F = \sigma\,\mathrm{d}A + A\mathrm{d}\sigma = 0. \tag{4.1}$$

Rearranging,

$$\mathrm{d}\sigma/\sigma = -\mathrm{d}A/A = \mathrm{d}\varepsilon, \tag{4.2}$$

or

$$\mathrm{d}\sigma/\mathrm{d}\varepsilon = \sigma. \tag{4.3}$$

This is illustrated in Figure 4.1.

Since $\varepsilon = \ln(1+e)$, $\mathrm{d}\varepsilon = \mathrm{d}e/(1+e)$. Substituting into equation 4.3, the condition for necking can be expressed as $\mathrm{d}\sigma/\mathrm{d}e = \sigma/(1+e)$. This is illustrated by the construction in Figure 4.2, which has been attributed to Considère.* With power-law hardening,

$$\sigma = K\sigma^n,\ \mathrm{d}\sigma/\mathrm{d}\varepsilon = nK\varepsilon^{n-1} = \sigma, \quad \text{or} \quad \varepsilon = n. \tag{4.4}$$

* A. Considère, *Ann. Ponts et Chaussèes*, 9 (1885), pp. 574–775.

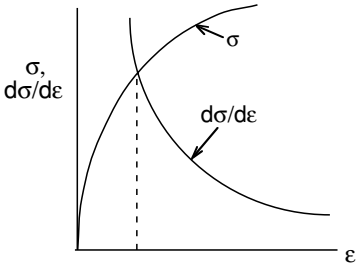

4.1. The maximum load in tension is reached when $d\sigma/d\varepsilon = \sigma$.

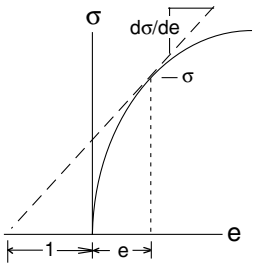

4.2. Considère construction for necking in tension. The critical condition for necking is $d\sigma/de = \sigma/(1 + e)$.

Thus the maximum load, the tensile strength, and the onset of necking occur at a strain equal to the strain-hardening exponent.

4.2 EFFECT OF INHOMOGENEITIES

Material properties and dimensions are usually considered to be uniform in analyses. However real materials are inhomogeneous: the cross-sectional diameter or thickness may vary from one place to another; there may also be variations in grain size, composition, and statistical crystal orientation. These latter inhomogeneities are assumed to influence only K in the expression $\bar{\sigma} = K\bar{\varepsilon}^n$, so they will affect the forces in the same manner as dimensional variations.

The effect of inhomogeneity is illustrated by a tensile specimen having homogeneous properties but two regions of different dimensions, a and b as shown in Figure 4.3.

An inhomogeneity factor f may be defined as

$$f = A_{a0}/A_{b0} \quad \text{where} \quad A_{a0} < A_{b0} \tag{4.5}$$

The two regions, a and b, must support the same force so $F_a = F_b$, or

$$A_a\sigma_a = A_b\sigma_b. \tag{4.6}$$

With power-law hardening, and substituting $A_i = A_{i0}\exp(-\varepsilon_i)$, where A_{i0} is the original cross-sectional area of region i,

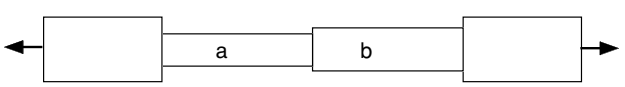

4.3. Stepped tensile specimen.

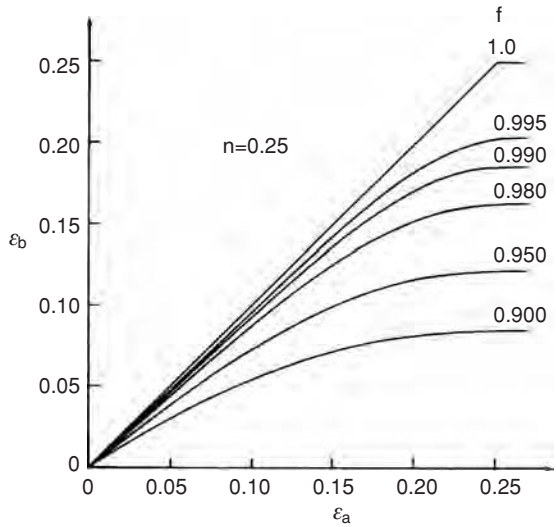

4.4. Strains induced by various inhomogeneity factors.

$$A_{a0}\exp(-\varepsilon_a)K\varepsilon_a^n = A_{b0}\exp(-\varepsilon_b)K\varepsilon_b^n. \tag{4.7}$$

Substituting equation 4.5, equation 4.7 simplifies to

$$f\exp(-\varepsilon_a)\varepsilon_a^n = \exp(-\varepsilon_b)\varepsilon_b^n. \tag{4.8}$$

For given values of f and n, equation 4.8 can be solved numerically to give ε_b as a function of ε_a. Figure 4.4 shows this dependence for several values of f with $n = 0.25$. Note that as $f \to 1$, $\varepsilon_a \to \varepsilon_b$ up to a limiting strain of 0.25 where necking occurs. This implies that the maximum strain outside the neck equals n if $f = 1$. However if $f < 1$, ε_b lags behind ε_a and saturates at ε^* which may be considerably less than n. Figure 4.5 shows such results.

Note that for a typical tensile specimen with a nominal 0.505-in diameter, a diameter variation of 0.001 in, $f = 0.996$ and $\varepsilon_b^* = 0.0208$ instead of 0.25. Figure 4.6 shows the combined effect of f and n on the uniform elongation.

4.3 BALANCED BIAXIAL TENSION

Figure 4.7 illustrates the biaxial stretching of a sheet with $\sigma_1 = \sigma_2$. Instability will occur when $F_1 = F_2$ equals zero. $F_1 = \sigma_1 A_1$,

$$\mathrm{d}F_1 = \sigma_1 \mathrm{d}A_1 + A_1 \mathrm{d}\sigma_1 = 0 \tag{4.9}$$

or

$$\mathrm{d}\sigma_1/\sigma_1 = -\mathrm{d}A_1/A_1 = \mathrm{d}\varepsilon_1. \tag{4.10}$$

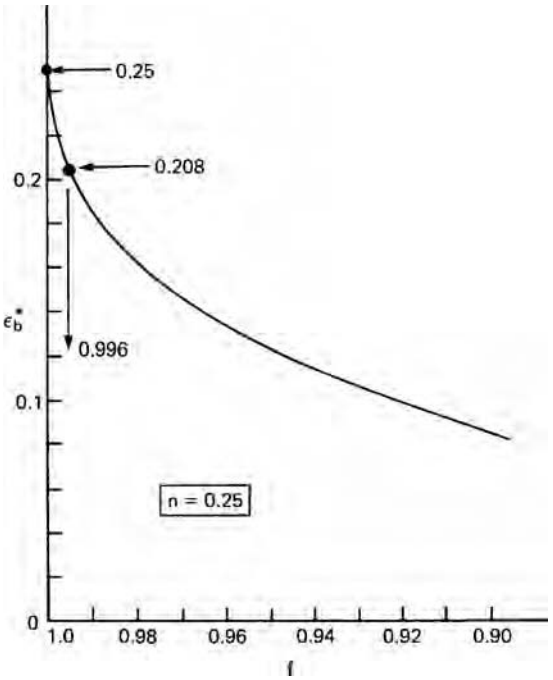

4.5. Effect of the inhomogeneity factor, *f*, on the limit strain, ε_b^*, outside of the neck. A strain-hardening exponent of 0.25 was assumed.

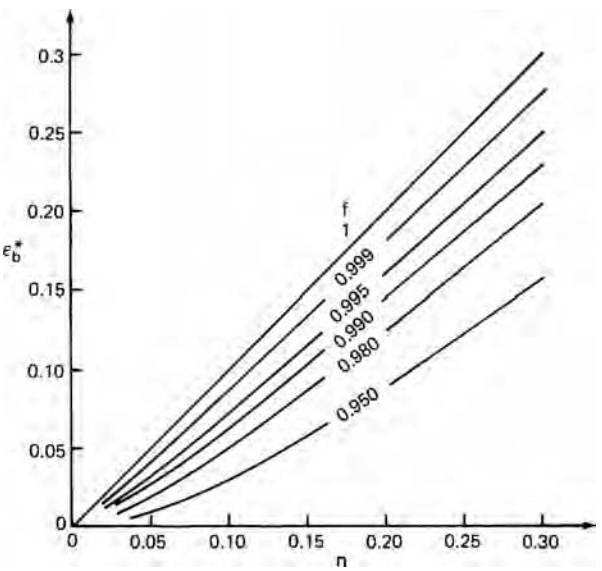

4.6. Effects of *f* and *n* on the uniform elongation, ε_b^*.

With $\sigma_1 = \sigma_2$, the effective stress $\bar{\sigma}$ is

$$\bar{\sigma} = \sigma_1 = \sigma_2 \tag{4.11}$$

According to the flow rules

$$\bar{\varepsilon} = 2\varepsilon_1 = 2\varepsilon_2 = -\varepsilon_3. \tag{4.12}$$

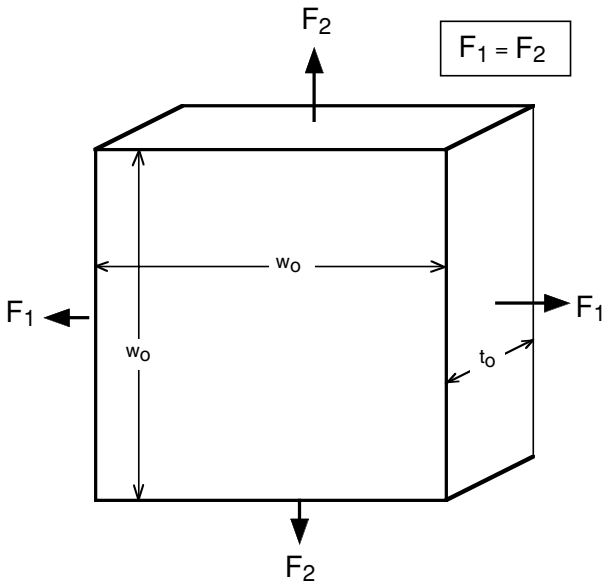

4.7. State of balanced biaxial tension.

Substituting equations 4.7 and 4.6 into equation 4.5

$$\frac{d\bar{\sigma}}{d\bar{\varepsilon}} = \frac{\bar{\sigma}}{2}, \tag{4.13}$$

so

$$\bar{\varepsilon} = 2n \tag{4.14}$$

at instability. Note that this is twice the instability strain for uniaxial tension.

4.4 PRESSURIZED THIN-WALL SPHERE

Figure 4.8 is a free-body diagram of half of a pressurized thin-wall spherical pressure vessel.

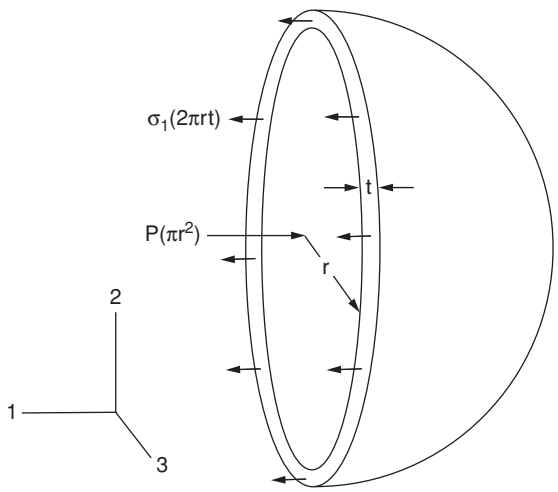

4.8. Free-body diagram of half of a pressurized thin-wall spherical pressure vessel.

A force balance in the 1-direction indicates that $P\pi r^2 = 2\pi r t\sigma_1$, where P is the internal pressure, r and t are the radius and wall thickness, so

$$P = \frac{2t\sigma_1}{r}. \tag{4.15}$$

The maximum pressure corresponds to

$$\mathrm{d}P = 0 = \frac{2t\,\mathrm{d}\sigma_1}{r} + \frac{2\sigma_1\,\mathrm{d}t}{r} - \frac{2t\sigma_1\,\mathrm{d}r}{r^2} \tag{4.16}$$

or

$$\frac{\mathrm{d}\sigma_1}{\sigma_1} = \frac{\mathrm{d}r}{r} - \frac{\mathrm{d}t}{t}. \tag{4.17}$$

Substituting $\mathrm{d}r/r = \mathrm{d}\varepsilon_1$, $\mathrm{d}t/t = \mathrm{d}\varepsilon_3$, and $\mathrm{d}\varepsilon_1 = \mathrm{d}\varepsilon_2 = -\mathrm{d}\varepsilon_3/2$,

$$\frac{\mathrm{d}\sigma_1}{\sigma_1} = -(3/2)\ \mathrm{d}\varepsilon_3. \tag{4.18}$$

Substituting $\mathrm{d}\bar{\varepsilon} = -\mathrm{d}\varepsilon_3$ and $\bar{\sigma} = \sigma_1$, $\mathrm{d}\bar{\sigma}/\bar{\sigma} = (3/2)\ \mathrm{d}\bar{\varepsilon}$ or

$$\mathrm{d}\bar{\sigma}/\mathrm{d}\bar{\varepsilon} = (3/2)\ \bar{\sigma}. \tag{4.19}$$

With power-law hardening, the instability occurs at

$$\bar{\varepsilon} = (2/3)n. \tag{4.20}$$

Substituting $t = t_0 e^{\varepsilon_3} = t_0 e^{-\bar{\varepsilon}}$, $r = r_0 e^{\varepsilon_1} = r_0 e^{-\bar{\varepsilon}/2}$ and $\bar{\sigma} = K\bar{\varepsilon}^n$,

$$P = 2K\bar{\varepsilon}^n \frac{t_0}{r_0} e^{(-1/2)\bar{\varepsilon}}. \tag{4.21}$$

Setting $\mathrm{d}P$ to zero,

$$P_{\max} = 2K(3/2n)^n e^{-n}. \tag{4.22}$$

Figure 4.9 illustrates the variation of pressure with $\bar{\varepsilon}$ and r.

4.5 SIGNIFICANCE OF INSTABILITY

Instability conditions in this chapter relate to a maximum force or pressure. However uniform deformation does not generally cease at a maximum force or pressure as it does in a tension test. Reconsider the case of the thin wall sphere under internal pressure. Although the maximum pressure occurs when $\bar{\varepsilon} = (2/3)n$, strain localization cannot occur, because localization would cause a decrease of the local radius of curvature, which would decrease the stress in that area below that of the rest of the sphere. Instead the sphere will continue to expand uniformly. The walls are in biaxial tension so the maximum wall force will occur when $\bar{\varepsilon} = 2n$. Strain localization still cannot occur because any localization would decrease the radius of curvature. Figure 4.9 shows these points.

Any strain localization under biaxial tension must occur because of local inhomogeneity. The role of inhomogeneity is developed in Chapter 15.

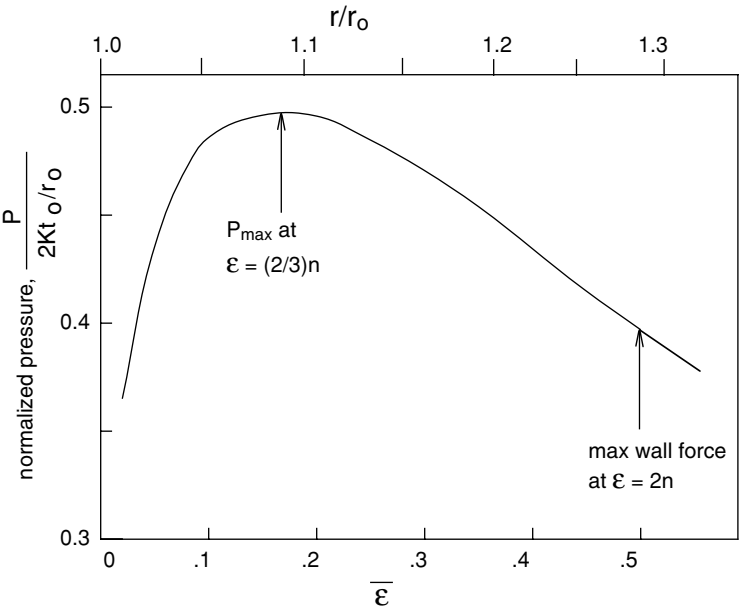

4.9. Variation of pressure with effective strain for $n = 2.25$. Note that the maximum pressure occurs before the maximum wall force.

NOTE OF INTEREST

Professor Zdzislaw Marciniak is a member of the Polish Academy of Sciences and was head of the Faculty of Production Engineering at the Technical University of Warsaw. For some years he was also acting rector of that university. He has published a number of books (mainly in Polish) on scientific aspects of engineering plasticity and on the technology of metal forming. He developed machines for incremental cold forging including the rocking die and rotary forming processes. His inhomogeneity model of local necking in stretch forming of sheet, published with K. Kuczynski in 1967, has had a profound effect on the understanding of forming limits in sheet metal.

REFERENCES

W. A. Backofen, *Deformation Processing*, Addison-Wesley, 1972.
W. F. Hosford, *Mechanical Behavior of Materials*, Cambridge University Press, 2005.

PROBLEMS

4.1. If $\bar{\sigma} = K\bar{\varepsilon}^n$, the onset of tensile instability occurs when $n = \varepsilon_u$. Determine the instability strain as a function of n if

a) $\bar{\sigma} = A(B + \bar{\varepsilon})^n$.

b) $\bar{\sigma} = Ae^n$ where e is the engineering strain.

4.2. Consider a balloon made of a material that shows linear elastic behavior to fracture and has a Poisson's ratio of ½. If the initial diameter is d_0, find the diameter, d, at the highest pressure.

4.3. Determine the instability strain in terms of n for a material loaded in tension while subjected to a hydrostatic pressure P. Assume $\bar{\sigma} = K\bar{\varepsilon}^n$.

4.4. A thin-wall tube with closed ends is pressurized internally. Assume that $\bar{\sigma} = 150\bar{\varepsilon}^{0.25}$MPa.

a) At what value of effective strain will instability occur with respect to pressure?

b) Find the pressure at instability if the tube had an initial diameter of 10 mm, and a wall thickness of 0.5 mm.

4.5. Figure 4.10 shows an aluminum tube fitted over a steel rod. The steel may be considered rigid and the friction between the aluminum and the steel may be neglected. If $\bar{\sigma} = 160\bar{\varepsilon}^{0.25}$MPa for the tube and it is loaded as indicated, calculate the force F at instability.

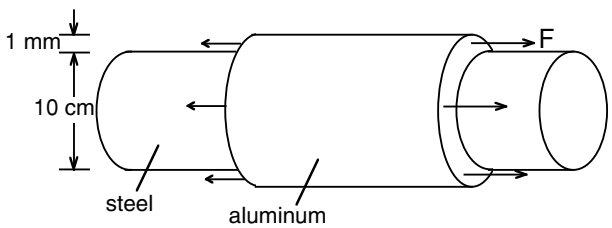

4.10. Sketch for Problem 4.5.

4.6. A thin-wall tube with closed ends is subjected to an ever-increasing internal pressure. Find the dimensions r and t in terms of the original dimensions r_o and t_0 at maximum pressure. Assume $\bar{\sigma} = 500\bar{\varepsilon}^{0.20}$ MPa.

4.7. Consider the internal pressurization of a thin-wall sphere by an ideal gas for which $PV =$ constant. One may envision an instability condition for which the decrease of pressure with volume, $(-dP/dV)_{\text{gas}}$, due to gas expansion is less than the rate of decrease in pressure that the sphere can withstand, $(-dP/dV)_{\text{sph}}$. For such a condition, catastrophic expansion would occur. If $\bar{\sigma} = K\bar{\varepsilon}^n$, find $\bar{\varepsilon}$ as a function of n.

4.8. For rubber stretched under biaxial tension $\sigma_x = \sigma_y = \sigma$, the stress is given by $\sigma = NkT(\lambda^2 - 1/\lambda^4)$ where λ is the stretch ratio, $L_x/L_{x0} = L_y/L_{y0}$. Consider what this equation predicts about how the pressure in a spherical rubber balloon varies during the inflation. For $t_0 = r_0$, plot P vs. λ and determine the strain λ at which the pressure is a maximum.

4.9. For a material that has a stress–strain relationship of the form $\bar{\sigma} = A - B\exp(-C\varepsilon)$ where A, B, and C are constants, find the true strain at the onset of necking and express the tensile strength, S_u in terms of the constants.

4.10. A tensile bar was machined with a stepped guage section. The two diameters were 2.0 and 1.9 cm. After some stretching the diameters were found to be 1.893 and 1.698 cm. Find n in the expression $\bar{\sigma} = K\bar{\varepsilon}^n$ and find $\bar{\varepsilon}$ as a function of n.

4.11. In a rolled sheet, it is not uncommon to find variations of thickness of $\pm 1\%$ from one place to another. Consider a sheet nominally 0.8 mm thick with a $\pm 1\%$ variation of thickness. (Some places are 0.808 mm and others are 0.792 mm thick.) How high would n have to be to ensure that in a tensile specimen every point was strained to at least $\varepsilon = 0.20$ before the thinner section necked?

4.12. A material, which undergoes linear strain hardening so that $\sigma = Y + 1.35Y$, is stretched in tension.

a) At what strain will necking begin?

b) A stepped tensile specimen was made from this material with the diameter of region A being 0.990 times the diameter of region B. What would be the strain in region B when region a reached a strain of 0.20?

5 Temperature and Strain-Rate Dependence

The effects of strain hardening on flow stress were treated in Chapter 3. However, flow stress also depends on strain rate and temperature, usually increasing with strain rate and decreasing with temperature. The effect of strain rate at constant temperature will be considered first.

5.1 STRAIN RATE

Flow stress usually increases with strain rate. The strain-rate effect at constant strain can be approximated by

$$\sigma = C\dot{\varepsilon}^m, \tag{5.1}$$

where C is a strength constant that depends upon strain, temperature, and material, and m is the strain-rate sensitivity of the flow stress. For most metals at room temperature, the magnitude of m is quite low (between 0 and 0.03). The ratio of flow stresses, σ_2 and σ_1, at two strain rates, $\dot{\varepsilon}_2$ and $\dot{\varepsilon}_1$, is

$$\frac{\sigma_2}{\sigma_1} = \left(\frac{\dot{\varepsilon}_2}{\dot{\varepsilon}_1}\right)^m. \tag{5.2}$$

Taking logarithms of both sides, $\ln(\sigma_2/\sigma_1) = m \ln(\dot{\varepsilon}_2/\dot{\varepsilon}_1)$. If, as is likely at low temperatures, σ_2 is not much greater than σ_1, equation 5.2 can be simplified to

$$\frac{\Delta\sigma}{\sigma} \simeq m \ln \frac{\dot{\varepsilon}_2}{\dot{\varepsilon}_1} = 2.3m \log \frac{\dot{\varepsilon}_2}{\dot{\varepsilon}_1}. \tag{5.3}$$

For example, if $m = 0.01$, increasing the strain rate by a factor of 10 would raise the flow stress by only $0.01 \times 2.3 \simeq 2\%$, which explains why rate effects are often ignored.

However, rate effects can be important in some cases. For example, if one wishes to predict forming loads in wire drawing or sheet rolling (where the strain rates may be as high as 10^4/sec) from data obtained in a laboratory tension test, in which the strain rates may be as low as 10^{-4}/sec, the flow stress should be corrected unless m is very small. Ratios of (σ_2/σ_1) calculated from equation 5.2 for various levels of $(\dot{\varepsilon}_2/\dot{\varepsilon}_1)$ and m are shown in Figure 5.1.

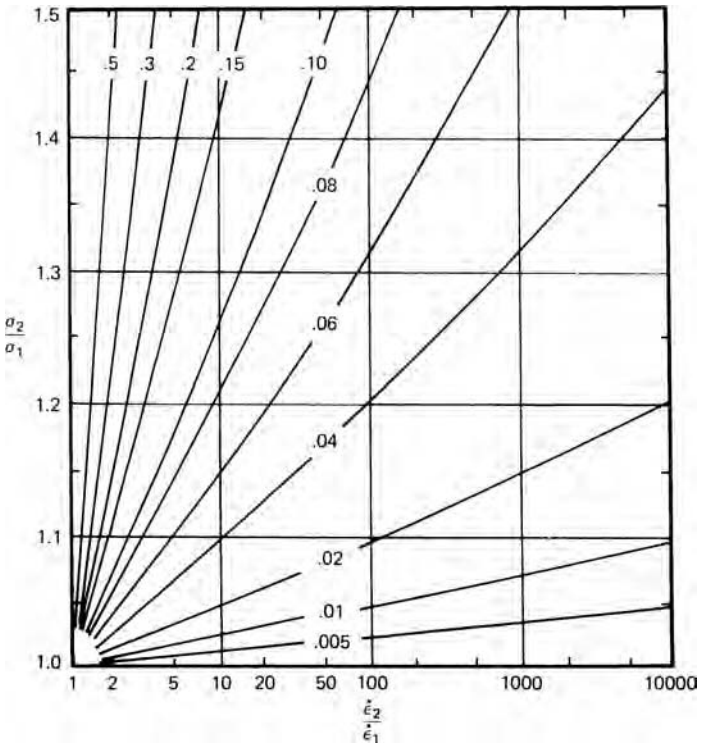

5.1. The influence of strain rate on flow stress for various levels of strain-rate sensitivity, m, indicated on the curves.

There are two commonly used methods of measuring m. One is to obtain continuous stress–strain curves at several different strain rates and compare the levels of stress at a fixed strain using equation 5.2. The other is to make abrupt changes of strain rate during a tension test and use the corresponding level of $\Delta\sigma$ in equation 5.3. These are illustrated in Figure 5.2. Increased strain rates cause slightly greater strain hardening, so the use of continuous stress–strain curves yields larger values of m than the second method, which compares the flow stresses for the same structure. The second method has the advantage that several strain-rate changes can be made on a single specimen, whereas continuous stress–strain curves require a specimen for each strain rate.

A material's strain-rate sensitivity is temperature dependent. At hot-working temperatures, m typically rises to 0.10 or 0.20, so rate effects are much larger than at room temperature. Under certain circumstances, m-values of 0.5 or higher have been observed in various metals. Figure 5.3 shows data for a number of metals obtained from continuous constant strain-rate tests. Below $T/T_m = \frac{1}{2}$, where T/T_m is the ratio of testing temperature to melting point on an absolute scale, the rate sensitivity is low but it climbs rapidly for $T > T_m/2$.

More detailed data for aluminum alloys are given in Figure 5.4. Although the definition of m in this figure is based upon shear stress–strain rate data, it is equivalent to the definition derived from equation 5.1. For alloys of aluminum and many other metals, there is a minimum in m near room temperature and, as indicated, negative m-values are sometimes found. At low strain rates, solutes segregate to dislocations; this lowers

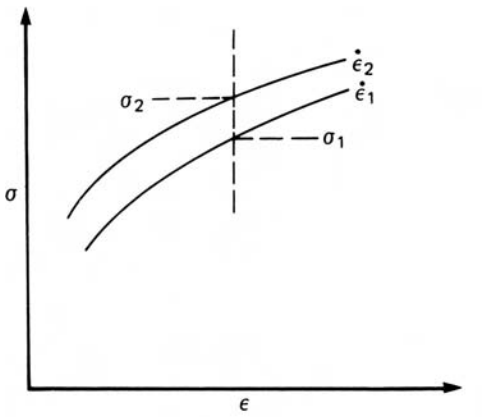

(a)

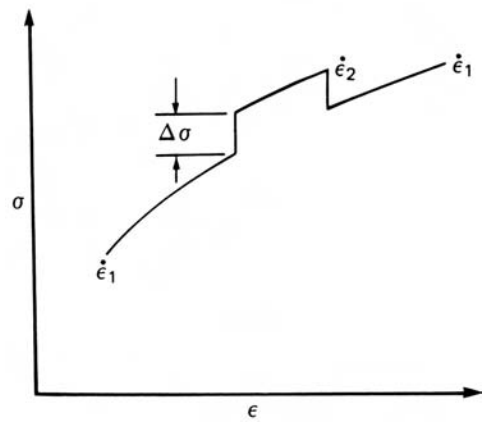

(b)

5.2. Two methods of determining m. (a) Two continuous stress–strain curves at different strain rates are compared at the same strain and $m = \ln(\sigma_2/\sigma_1)/\ln(\dot{\varepsilon}_2/\dot{\varepsilon}_1)$. (b) Abrupt strain-rate changes are made during a tension test and $m = (\Delta\sigma/\sigma)/\ln(\dot{\varepsilon}_2/\dot{\varepsilon}_1)$.

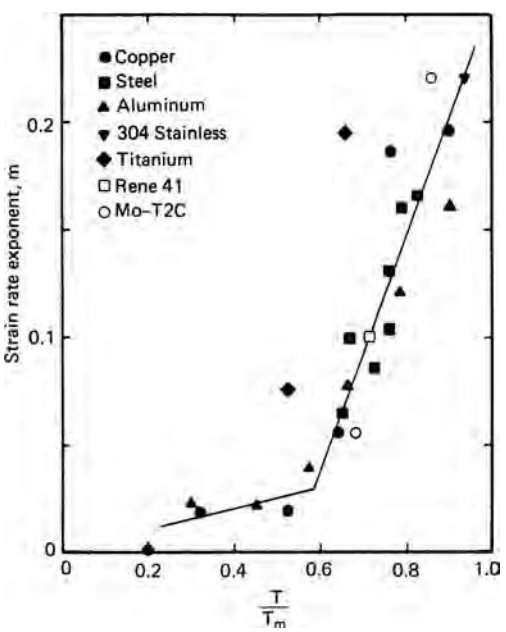

5.3. Variation of the strain-rate sensitivity of different materials with homologous temperature, T/T_m. Adapted from F. W. Boulger, *DMIC Report 226*, Battelle Mem. Inst. (1966), pp. 13–37.

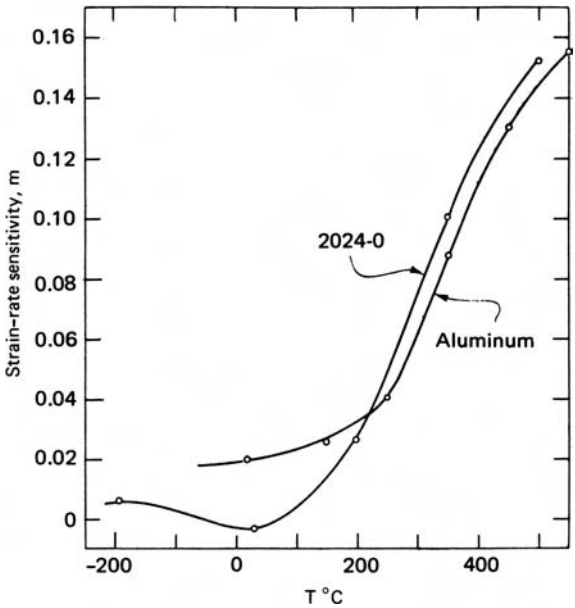

5.4. Temperature dependence of the strain-rate sensitivities of 2024 and pure aluminum. From D. S. Fields and W. A. Backofen, *Trans. ASM*, 51 (1959), pp. 946–60.

their energy so that the forces required to move the dislocations are higher than those required for solute-free dislocations. At increased strain rates or lower temperatures, however, dislocations move faster than solute atoms can diffuse, so the dislocations are relatively solute-free and the drag is minimized. A negative rate sensitivity tends to localize flow in a narrow region which propagates along a tensile specimen as a Lüders band. Localization of flow in a narrow band occurs because it allows the deforming material to experience a higher strain rate and therefore a lower flow stress.

The higher values of rate sensitivity at elevated temperatures are attributed to the increased rate of thermally activated processes such as dislocation climb and grain-boundary sliding.

5.2 SUPERPLASTICITY

As already mentioned, rate sensitivities of 0.5 or greater can sometimes be encountered. The necessary conditions are

1. an extremely fine grain size (a few micrometers or less), with generally uniform and equiaxed grain structure,
2. high temperatures ($T > 0.4\ T_m$), and
3. low strain rates* (10^{-2}/sec or lower).

In addition to the above conditions, the microstructure should be stable, without grain growth, during deformation. Under these conditions, extremely high elongations and very low flow stresses are observed in tension tests, so the term *superplasticity*

* The fact that m itself is rate dependent indicates that equation 5.1 is not a true description of the rate effect. Nevertheless, expressed as $m = (\partial \ln \sigma / \partial \ln \dot{\varepsilon})_{\varepsilon,T}$ it is always a useful index of the strain-rate sensitivity of the flow stress and is a convenient basis for describing and analyzing strain-rate effects.

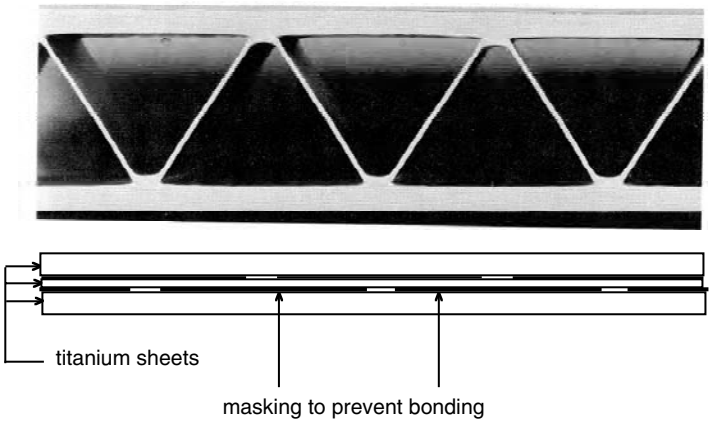

5.5. Aircraft panel made from a titanium alloy by diffusion bonding and superplastic expansion by internal pressure. Photo courtesy of Rockwell International Corp.

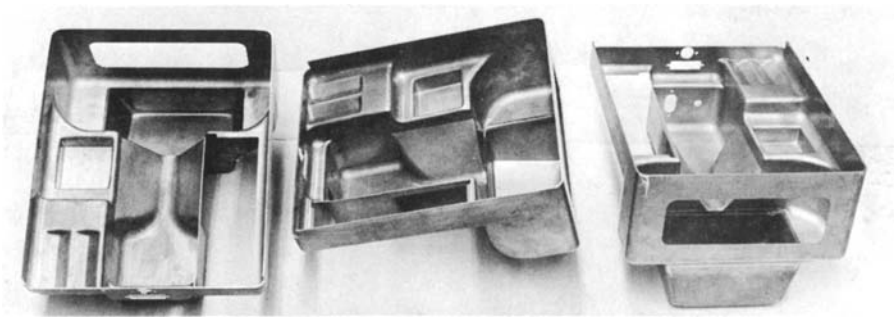

5.6. Complex sheet-metal part of Zn-22% Al made by superplastic forming. Courtesy of D. S. Fields, IBM Corp.

has been used to describe these effects. There have been several excellent reviews of superplasticity and the mechanisms and characteristics.*

There are two useful aspects of superplasticity. One is that superplasticity is usually accompanied by very low flow stresses at useful working temperatures. This permits creep forging of intricately shaped parts and reproduction of fine detail. The other is the extremely high tensile elongations, which permit sheet parts of great depth to be formed with simple tooling.

One application of superplasticity has been in the production of titanium alloy aircraft panels. An example of such a panel in cross section is shown in Figure 5.5. Using superplastic forming with concurrent diffusion bonding (SPF/DB), three sheets are first diffusion bonded at specific locations, bonding elsewhere being prevented by painting the sheets with an inert ceramic. Then the unbonded channels are pressurized internally with argon until the skin pushes against tools that control the outer shape. Superplastic behavior is required to obtain the necessary elongation of the interior core

* J. W. Edington, K. N. Melton, and C. P. Cutler, *Progress in Materials Sci*., 21 (1976), pp. 63–170. O. D. Sherby and J. Wadsworth, *Superplasticity: Recent Advances and Future Directions* (New York: Oxford, 1990). S. Tang, *Mechanics of Superplasticty; Mathematics for Engineering and Science* (Huntington, NY: Krieger, 1979).

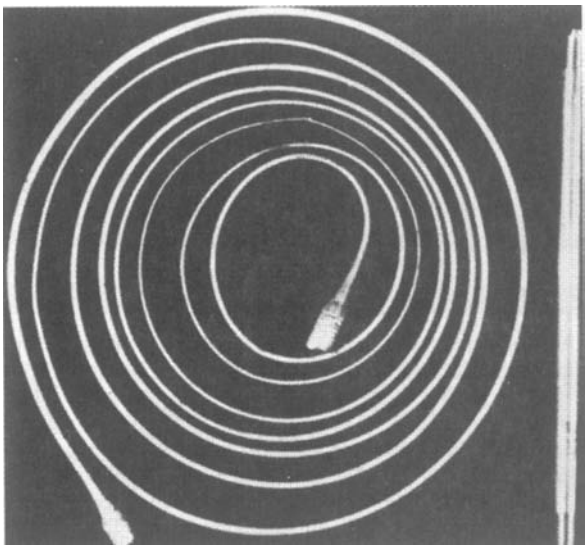

5.7. Superplastically extended tensile bar of Bi-Sn eutectic. From C. E. Pearson, *J. Inst. Metals*, 54 (1934), p. 111.

sheet ligaments, which is over 100% in the example shown. Figure 5.6 shows an example of a deep part made by superplastic forming of Zn-22%Al sheet. A tensile bar elongated 1950% (a 19-fold increase in length!) is illustrated in Figure 5.7. To appreciate this, one must realize that a tensile elongation over 50% is usually considered large.

The tensile elongations for a number of materials are plotted in Figure 5.8 as a function of m. High m-values promote large elongations by preventing localization of the deformation as a sharp neck. This can be seen clearly in the following example.

Consider a bar that starts to neck. If the cross-sectional area in the neck is A_n and outside the neck is A_u, $F = \sigma_u A_u = \sigma_n A_n$ or $\sigma_u / \sigma_n = A_n / A_u$. From equation 5.2,

$$\frac{\dot{\varepsilon}_u}{\dot{\varepsilon}_n} = \left(\frac{\sigma_u}{\sigma_n}\right)^{1/m} = \left(\frac{A_n}{A_u}\right)^{1/m}. \tag{5.4}$$

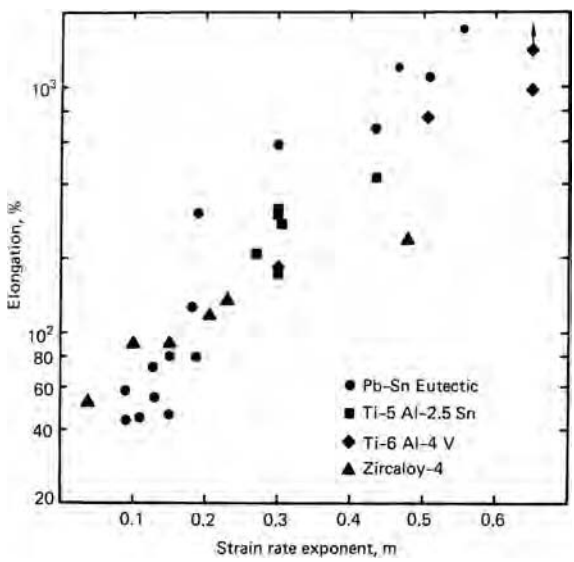

5.8. Correlation of tensile elongation with strain-rate sensitivity. Data from D. Lee and W. A. Backofen, *TMS-AIME*, 239 (1967), p. 1034; and D. H. Avery and W. A. Backofen, *Trans. Q. ASM*, 58 (1965), pp. 551–62.

Since $A_n < A_u$, if m is low, the strain rate outside the neck will become negligibly low. For example, let the neck region have a cross-sectional area of 90% of that outside the neck. If $m = 0.02$, $\dot{\varepsilon}_u/\dot{\varepsilon}_n = (0.9)^{50} = 5 \times 10^{-3}$. If, however, $m = 0.5$, then $\dot{\varepsilon}_u/\dot{\varepsilon}_n = (0.9)^2 = 0.81$, so that although the unnecked region deforms slower than the neck, its rate of straining is still rather large.

5.3 EFFECT OF INHOMOGENEITIES

Reconsider the tension test in Chapter 4 on the stepped bar in Figure 4.3. The bar is divided into two regions, one with an initial cross section of A_{b0} and the other $A_{a0} = fA_{b0}$. Neglect strain hardening and assume that $\sigma = C\dot{\varepsilon}^m$. As before, the forces must balance, so $\sigma_b\, A_b = \sigma_a\, A_a$. Substituting $A_i = A_{i0}\exp(\varepsilon_i)$ and $\sigma_i = C\dot{\varepsilon}_i^m$, the force balance becomes

$$A_{b0}\exp(-\varepsilon_b)\dot{\varepsilon}_b^m = A_{a0}\exp(-\varepsilon_a)\dot{\varepsilon}_a^m, \tag{5.5}$$

where $\dot{\varepsilon}_a$ and $\dot{\varepsilon}_b$ are the strains in the reduced and unreduced sections. Expressing $\dot{\varepsilon}$ as $d\varepsilon/dt$,

$$\exp(-\varepsilon_b)\left(\frac{d\varepsilon_b}{dt}\right)^m = f\exp(-\varepsilon_a)\left(\frac{d\varepsilon_a}{dt}\right)^m. \tag{5.6}$$

Raising both sides to the $(1/m)$ power and canceling dt

$$\int_0^{\varepsilon_b}\exp(-\varepsilon_b/m)\,d\varepsilon_b = \int_0^{\varepsilon_a} f^{1/m}\exp(\varepsilon_a/m)\,d\varepsilon_a. \tag{5.7}$$

Integration gives

$$\exp(-\varepsilon_b/m) - 1 = f^{1/m}[\exp(-\varepsilon_a/m) - 1]. \tag{5.8}$$

Numerical solutions of ε_b as a function of ε_a for $f = 0.98$ and several levels of m are shown in Figure 5.9. At low levels of m (or low values of f), ε_b tends to saturate early and approaches a limiting strain ε_b^* at moderate levels of ε_a, but with higher m-values, saturation of ε_b is much delayed, that is, localization of strain in the reduced section (or the onset of a sharp neck) is postponed. Thus, the conditions that promote high m-values also promote high failure strains in the necked region. Letting $\varepsilon_a \to \infty$ in equation 5.8 will not cause great error and will provide limiting values for ε_b^*. With this condition,

$$\varepsilon_b^* = -m\ln(1 - f^{1/m}). \tag{5.9}$$

In Figure 5.10, values of ε_b^* calculated from equation 5.8 are plotted against m for various levels of f. The values of tensile elongation corresponding to ε_b^* are indicated on the right margin. It is now clear why large elongations are observed under superplastic conditions. The data in Figure 5.8, replotted here, suggest an inhomogeneity factor of about 0.99 to 0.998 (for a round bar 0.250-in diameter, a diameter variation of 0.0005 in corresponds to $f = 0.996$). The general agreement is perhaps fortuitous considering the assumptions and simplifications. The values of ε_b^* are the strains away from the neck, so the total elongation would be even higher than indicated here. On the other hand, strains in the neck, ε_a, are not infinite, so the ε_b^* values corresponding

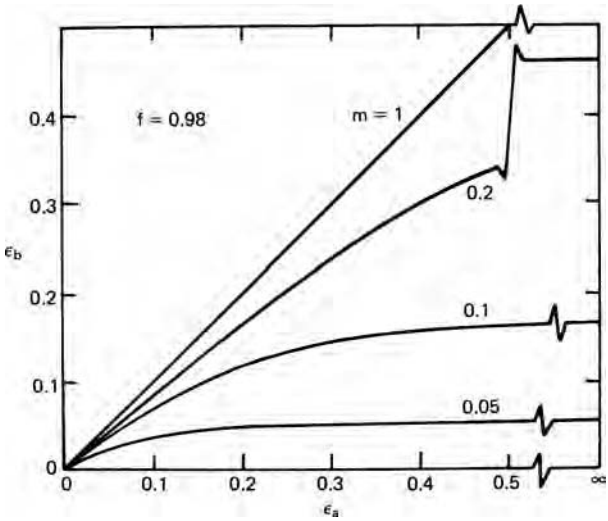

5.9. Relative strains in unreduced, ε_b, and reduced, ε_a, sections of a stepped tensile specimen for various levels of m, assuming no strain hardening.

to realistic maximum values of ε_a will be lower than those used in Figure 5.10. Also, the experimental values are affected by difficulties in maintaining constant temperature over the length of the bar as well as a constant strain rate in the deforming section. Nevertheless, the agreement between theory and experiments is striking.

Figure 5.11 shows the dependence of flow stress of the Al-Cu eutectic alloy at 520°C upon strain rate. The effect of strain is not important here because strain hardening

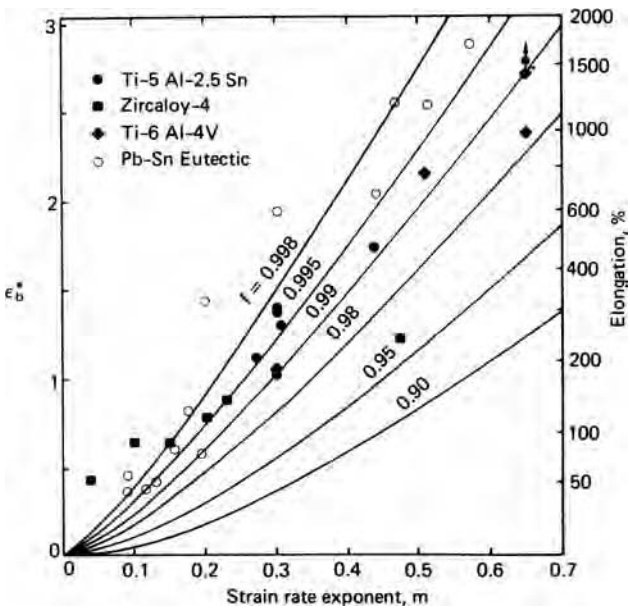

5.10. Limiting strains, ε_b^*, in unreduced sections of stepped tensile specimens as a function of m and f. Values of percent elongation corresponding to ε_b^* are indicated on the right together with data from Figure 5.8.

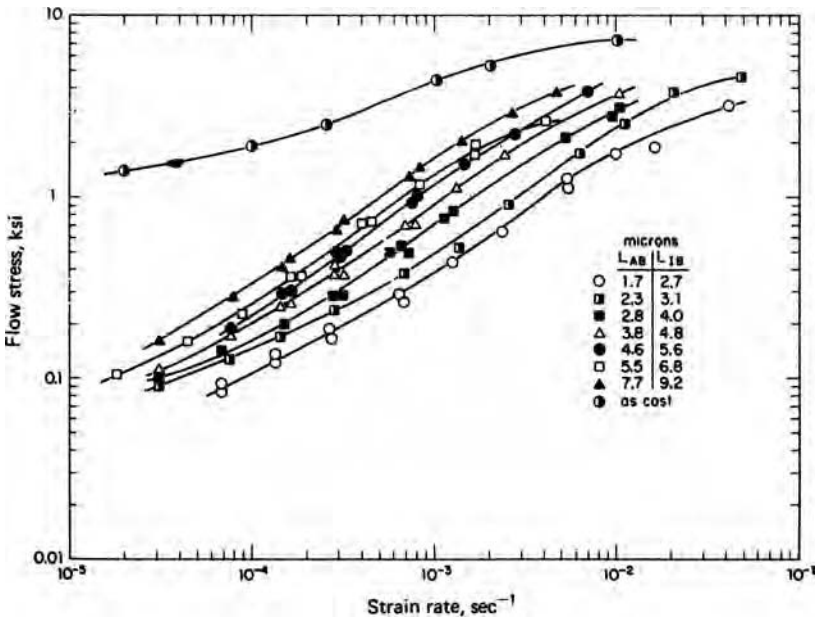

5.11. Dependence of flow stress of hot-worked Al-Cu eutectic alloy on strain rate at 520°C. The curves are for different grain sizes. L_{AB} is mean free path within the grains of κ and $CuAl_2$ phases and L_{IB} the mean free path between interphase boundaries. From D. A. Holt and W. A. Backofen, *Trans. Q. ASM*, 59 (1966), p. 755.

is negligible at this high temperature. Figure 5.12 shows the corresponding value of m as a function of strain rate. At the higher strain rates, m is typical of thermally activated slip. At lower strain rates, deformation mechanisms other than slip prevail. Here there are two schools of thought. One school[*†] maintains that deformation occurs primarily by diffusional creep with *vacancies* migrating from grain boundaries normal to the tensile axis to those parallel to it (i.e., diffusion of *atoms* from boundaries parallel to the tensile axis to boundaries perpendicular to it). Such diffusion causes the grains to elongate in the tensile direction and contract laterally. Whether diffusion is through the lattice or along grain-boundary paths, the strain rate should be proportional to the applied stress and inversely related to the grain size. If diffusion were the only mechanism, m would equal one (Newtonian viscosity) but it is lowered because of the slip contribution to the overall strain. The other school[‡] attributes the high rate sensitivity to the role of grain-boundary sliding (shearing on grain boundaries). Although grain-boundary sliding alone would be viscous ($m = 1$), it must be accompanied by another mechanism to accommodate compatibility at triple points where the grains meet. Either slip or diffusion could serve as the accommodating mechanism. Both models explain the need for a very fine grain size, high temperature, and low strain rate, but the diffusional-creep model does not explain why the grains remain equiaxed after large deformations.

* W. A. Backofen, *Deformation Processing* (Reading, MA: Addison-Wesley, 1972), pp. 217–20.
† A. H. Cottrell, *The Mechanical Properties of Matter* (New York: John Wiley, 1964), p. 202.
‡ M. F. Ashby and R. A. Verrall, *Acta Met.*, 21 (1973), p. 149.

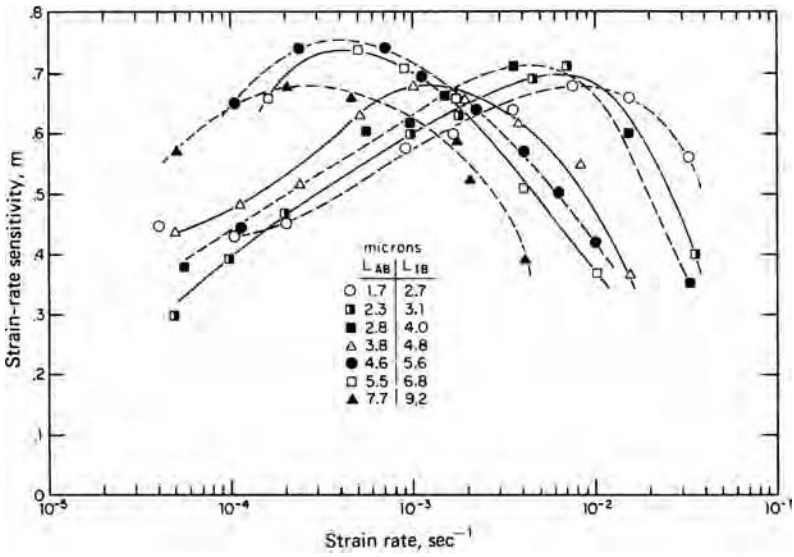

5.12. Variation of strain-rate sensitivity, $m = (\partial \ln \sigma / \partial \ln \dot{\varepsilon})_{\varepsilon,T}$, for the Al-Cu eutectic at 520°C. Compare with Fig. 5.11. Note that the strain rate for peak m increases with decreasing grain size. From D. A. Holt and W. A. Backofen, *op. cit.*

One practical problem is the tendency for grain growth during superplastic deformation because of the high temperature and long times dictated by the slow strain rates and because of the deformation itself.* Such grain growth lowers the m-value,† and increases the flow stress, causing the overall superplastic formability to deteriorate. The effects of grain growth are the most important at very slow strain rates (because of the longer times), and it has been suggested that the decrease in m at low strain rates is caused by such grain growth. Because finely distributed second-phase particles markedly retard grain growth, most superplastic alloys have two-phase microstructures. Among the alloys that exhibit superplasticity are Zn-22% Al and a range of steels (eutectoid) and Sn-40% Pb, Sn-5% Bi, Al-33% Cu (eutectics). Other alloys include Cu-10% Al, Zircaloy, several α-β titanium alloys, and some superalloys ($\gamma - \gamma'$ with carbides.)

Aluminum-base superplastic alloys are of considerable interest in the aerospace industry. It has been found that with controlled size and distribution of inclusions it is possible to generate very fine grain sizes by recrystallization and to prevent excessive grain growth during superplastic forming. Recently it has been found that very fine grain ceramics can be superplastically formed.

Superplasticity of some two-phase ceramics has been studied. These include zirconia-alumina, zirconia-mullite, alumina doped with magnesia, and so forth. These observations suggest that commercial forming of ceramics is a possibility.

* S. P. Agrawal and E. D. Weisert in 7*th North American Metalworking Research Conf.* (Dearborn, MI: Soc. Mfg. Engrs., 1979), pp. 197–204.

† The low m-values often observed at very low strain rates have been attributed in part to grain coarsening during these experiments.

5.4 COMBINED STRAIN AND STRAIN-RATE EFFECTS

Even the low values of m at room temperature can be of importance in determining uniform elongation. In Chapter 4 it was shown that the uniform elongation in a tension test was controlled by the strain-hardening exponent and the inhomogeneity factor f, but strain-rate effects were neglected. Reconsider a tension test on an inhomogeneous specimen with two regions of initial cross-sectional areas A_{b0} and A_{a0} $(= f A_{b0})$. Now assume that the material strain hardens and is also rate sensitive, so that the flow stress is given by

$$\sigma = C' \varepsilon^n \dot{\varepsilon}^m. \tag{5.10}$$

Substituting $A_i = A_{i0} \exp(-\varepsilon_i)$ and $\sigma = C' \varepsilon^n \dot{\varepsilon}^m$ into a force balance, $A_b \sigma_b = A_a \sigma_a$, results in $A_{b0} \exp(-\varepsilon_b) \varepsilon_b^n \dot{\varepsilon}_b^m = A_{a0} \exp(-\varepsilon_a) \varepsilon_a^n \dot{\varepsilon}_a^m$. Following the procedure that produced equation 5.7,

$$\int_0^{\varepsilon_b} \exp(-\varepsilon_b/m) \varepsilon_b^{n/m} \mathrm{d}\varepsilon_b = f^{1/m} \int_0^{\varepsilon_a} \exp(-\varepsilon_a/m) \varepsilon_a^{n/m} \mathrm{d}\varepsilon_a. \tag{5.11}$$

The results of integration and numerical evaluation are shown in Figure 5.13, where ε_b is plotted as a function of ε_a for $n = 0.2$, $f = 0.98$, and several levels of m. It is apparent that even quite low levels of m play a significant role in controlling the strains reached in the unnecked region of the bar.

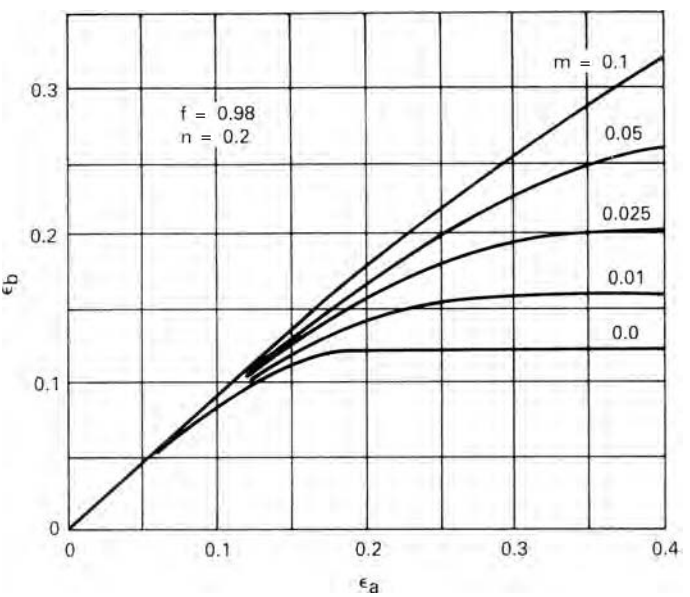

5.13. Comparison of strains in reduced and unreduced regions of a tensile bar calculated with $f = 0.98$ and $n = 0.20$. Note that even relatively low levels of m influence ε_b.

5.5 ALTERNATIVE DESCRIPTION OF STRAIN-RATE DEPENDENCE

For steel and other bcc metals, strain rate sensitivity is better described by

$$\sigma = C + m' \ln \dot{\varepsilon}, \tag{5.12}$$

where C is the flow stress at a reference strain rate and m' is the rate sensitivity. Increasing the strain rate from $\dot{\varepsilon}_1$ to $\dot{\varepsilon}_2$ raises the flow stress by

$$\Delta\sigma = m' \ln(\dot{\varepsilon}_2/\dot{\varepsilon}_1). \tag{5.13}$$

Note the difference between this and equation 5.3, which predicts that $\Delta\sigma = m\sigma \ln(\dot{\varepsilon}_2/\dot{\varepsilon}_1)$. The difference between these two equations is illustrated in Figure 5.14.

Figures 5.15 and 5.16 illustrate this for copper (fcc) and iron (bcc).

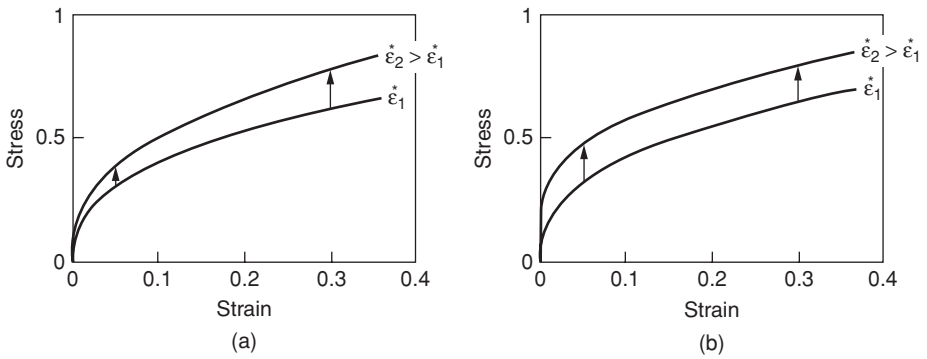

5.14. Two possible effects of strain rate on flow stress. The strain rates for the two curves differ by a factor of 100. (a) Equation 5.3 predicts that $\Delta\sigma$ is proportional to σ while (b) equation 5.13 predicts that $\Delta\sigma$ is independent of σ. From W. F. Hosford, *Mechanical Behavior of Materials*, Cambridge University Press, 2005.

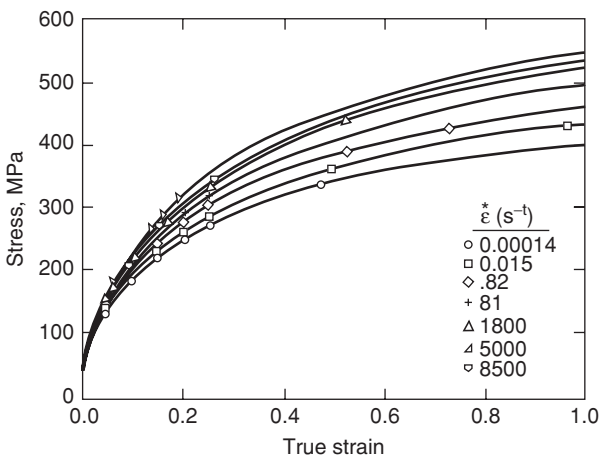

5.15. Stress–strain curves for pure copper at 25°C. Note that $\Delta\sigma$ between curves is proportional to the stress level. From P. S. Follansbee and U. F. Kocks, *Acta Met*., 36 (1988), pp. 81–93.

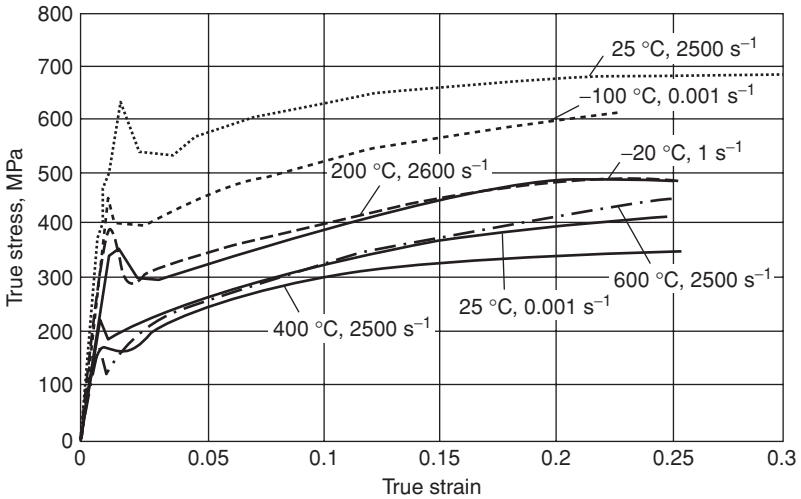

5.16. Stress–strain curves for iron at 25°C. Note that $\Delta\sigma$ between curves is independent of the stress level. From G. T. Gray in *ASM Metals Handbook*, 8, 2000.

For steels the strain-hardening exponent n decreases with increasing strain rates. This is because the combined effects of strain and strain-rate hardening are additive. The C in equation 5.12 is $C = K\varepsilon^n$ so the equation becomes

$$\sigma = K\varepsilon^n + m' \ln \dot{\varepsilon}. \tag{5.14}$$

Figure 5.17 is a plot of equation 5.14 for $K = 520$ MPa, $n = 0.22$, and $m' = 10$ MPa. Figure 5.18 is a logarithmic plot for the same data. Note that the slope n decreases

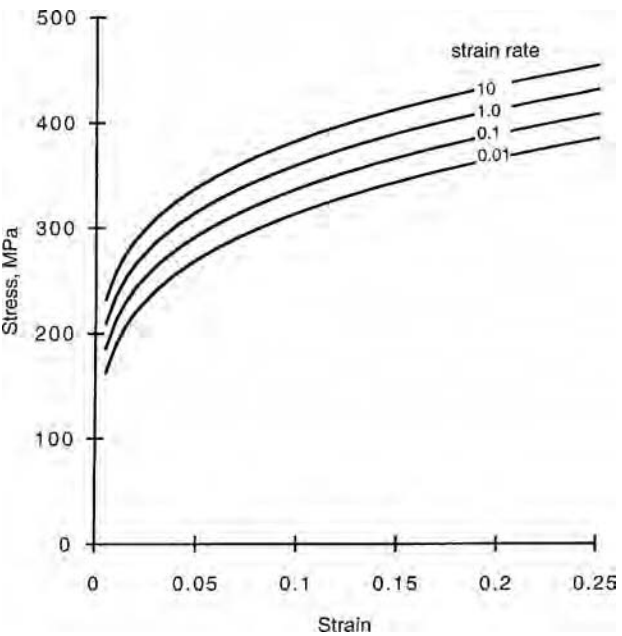

5.17. True stress–strain curves for $\sigma = 520\varepsilon^{0.22} + 10 \ln \dot{\varepsilon}$ with several strain rates. From W. F. Hosford, *op. cit.*

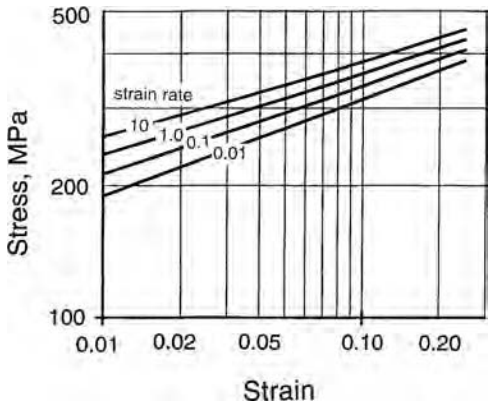

5.18. The same stress–strain curves as in Figure 5.17 plotted logarithmically. Note that the slope decreases at higher strain rates. From W. F. Hosford, *op. cit.*

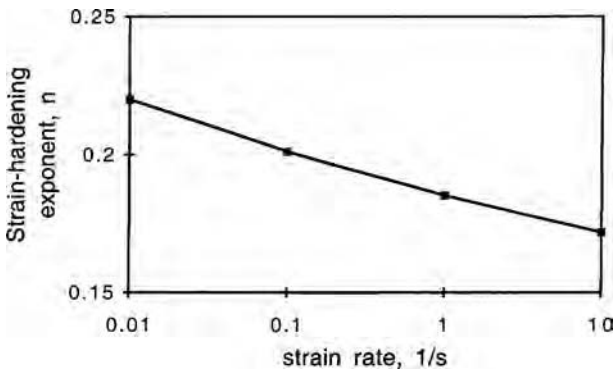

5.19. The decrease of n in $\sigma = K\varepsilon^n$ calculated from Figure 5.18. From W. F. Hosford, *op. cit*.

with increasing strain rate indicating that n decreases. The average slope, n, is plotted against strain rate in Figure 5.19.

5.6 TEMPERATURE DEPENDENCE OF FLOW STRESS

At elevated temperatures, the rate of strain hardening falls rapidly in most metals with an increase in temperature, as shown in Figure 5.20. The flow stress and tensile strength, measured at constant strain and strain rate, also drop with increasing temperature as

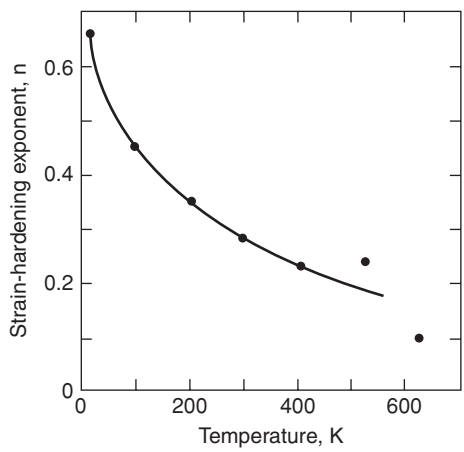

5.20. Decrease of the strain-hardening exponent, n, of pure aluminum with temperature. Adapted from R. P. Carreker and W. R. Hibbard, Jr., *Trans. TMS-AIME*, 209 (1957), pp. 1157– 63.

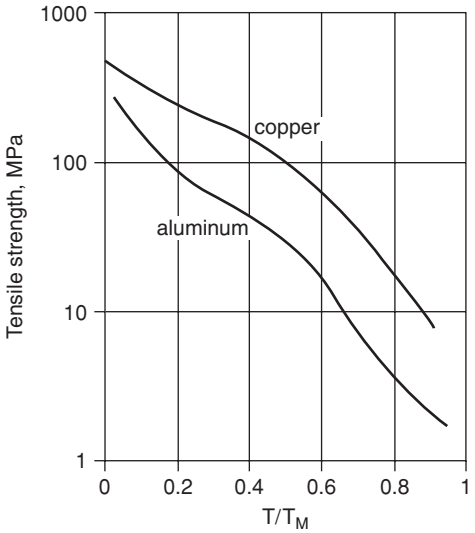

5.21. Decrease of tensile strength of pure copper and aluminum with homologous temperature. Adapted from R. P. Carreker and W. R. Hibbard, Jr., *op. cit.*

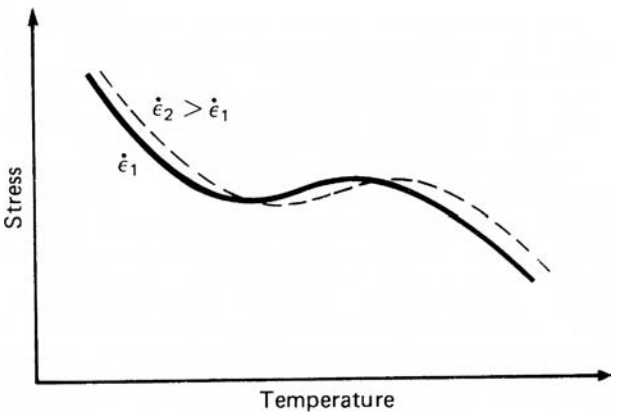

5.22. Schematic plot showing the temperature dependence of flow stress for some alloys. In the temperature region where flow stress increases with temperature, the strain-rate sensitivity is negative.

illustrated in Figure 5.21. However, the drop is not always continuous; often there is a temperature range over which the flow stress is only slightly temperature dependent or in some cases even increases slightly with temperature. The temperature dependence of flow stress is closely related to its strain-rate dependence. Decreasing the strain rate has the same effect on flow stress as raising the temperature, as indicated schematically in Figure 5.22. Here it is clear that at a given temperature the strain-rate dependence is related to the slope of the σ-versus-T curve; where σ increases with T, m must be negative.

The simplest quantitative treatment of temperature dependence is that of Zener and Hollomon* who argued that plastic straining could be treated as a rate process using Arrhenius rate law,† rate $\propto \exp(-Q/RT)$, which has been successfully applied to many rate processes. They proposed that

$$\dot{\varepsilon} = Ae^{-Q/RT} \tag{5.15}$$

* C. Zener and J. H. Hollomon, *J. Appl. Phys*., 15 (1994), pp. 22–32.
† S. Arrhenius, *Z. Phys. Chem*., 4 (1889), p. 226.

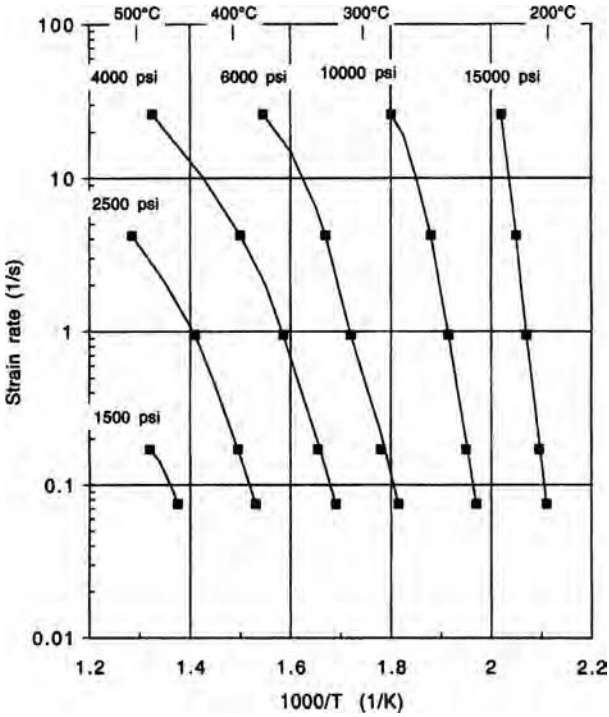

5.23. Strain rate and temperature combinations for various levels of stress. The data are for aluminum alloy 2024 and stresses are taken at an effective strain of 1.0. From D. S. Fields and W. A. Backofen, *op. cit.*

where Q is an activation energy, T the absolute temperature, and R the gas constant. Here the constant of proportionality, A, is both stress and strain dependent. At constant strain, A is a function of stress alone, $A = A(\sigma)$, so equation 5.15 can be written as

$$A(\sigma) = \dot{\varepsilon} e^{Q/RT}, \tag{5.16}$$

or more simply as

$$\sigma = f(z), \tag{5.17}$$

where the Zener–Hollomon parameter $z = \dot{\varepsilon} e^{Q/RT}$. This development predicts that if the strain rate to produce a given stress at a given temperature is plotted on a logarithmic scale against $1/T$, a straight line should result with a slope of $-Q/R$. Figure 5.23 shows such a plot for 2024-O aluminum.

Correlations of this type are very useful in relating temperature and strain-rate effects, particularly in the high-temperature range. However, such correlations may break down if applied over too large a range of temperatures, strains, or strain rates. One reason is that the rate-controlling process, and hence Q, may change with temperature or strain. Another is connected with the original formulation of the Arrhenius rate law in which it was supposed that thermal fluctuations alone overcome an activation barrier, whereas in plastic deformation, the applied stress acts together with thermal fluctuations in overcoming the barriers as indicated in the following development.

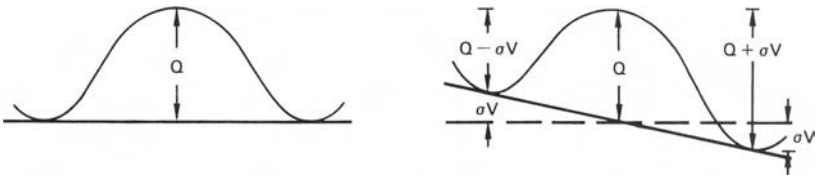

5.24. Schematic illustration of an activation barrier for slip and the effect of applied stress on skewing the barrier.

Consider an activation barrier for the rate-controlling process, as in Figure 5.24. The process may be cross slip, dislocation climb, et cetera. Ignoring the details, assume that the dislocation moves from left to right. In the absence of applied stress, the activation barrier has a height Q and the rate of overcoming this barrier would be proportional to exp $(-Q/RT)$. However, unless the position at the right is more stable—has a lower energy than the position on the left—the rate of overcoming the barrier from right to left would be exactly equal to that in overcoming it from left to right, so there would be no net dislocation movement. With an applied stress, σ, the energy on the left is raised by σV, where V is a constant with dimensions of volume, and on the right the energy is lowered by σV. Thus the rate from left to right is proportional to exp $[-(Q - \sigma V)/RT]$ and from right to left the rate is proportional to exp $[-(Q + \sigma V)/RT]$. The net strain rate then is

$$\begin{aligned}\dot{\varepsilon} &= C\{\exp[-(Q - \sigma V)/RT] - \exp[-(Q + \sigma V)/RT]\} \\ &= C \exp(-Q/RT)[\exp(\sigma V/RT) - \exp(-\sigma V/RT)] \\ &= 2C \exp(-Q/RT) \sinh(\sigma V/RT). \end{aligned} \tag{5.18}$$

To accommodate data better, and for some theoretical reasons, a modification of equation 5.18 has been suggested.*† It is:

$$\dot{\varepsilon} = A[\sinh(\alpha\sigma)]^{1/m} \exp(-Q/RT). \tag{5.19}$$

Steady-state creep data over many orders of magnitude of strain rate correlate very well with equation 5.19, as shown in Figure 5.25.

It should be noted that if $\alpha\sigma \ll 1$, $\sinh(\alpha\sigma) \approx \alpha\sigma$, so equation 5.19 reduces to $\dot{\varepsilon} = A \exp(-Q/RT)(\alpha\sigma)^{1/m}$ or

$$\sigma = A' \dot{\varepsilon}^m \exp(mQ/RT), \tag{5.20}$$

or $\sigma = A' Z^m$, which is consistent with both the Zener–Hollomon development, equation 5.17, and the power-law expression, equation 5.1. Since $\sinh(x) \to e^x/2$ for $x \gg 1$, at low temperatures and high stresses equation 5.19 reduces to

$$\dot{\varepsilon} = C \exp(\alpha'\sigma - Q/RT). \tag{5.21}$$

But now strain hardening becomes important so C and α' are both strain and temperature dependent. Equation 5.21 reduces to

$$\sigma = C + m' \ln \dot{\varepsilon} \tag{5.22}$$

* F. Garofalo, *TMS-AIME*, 227 (1963), p. 251.
† J. J. Jonas, C. M. Sellers, and W. J. McG. Tegart, *Met. Rev.*, 14 (1969), p. 1.

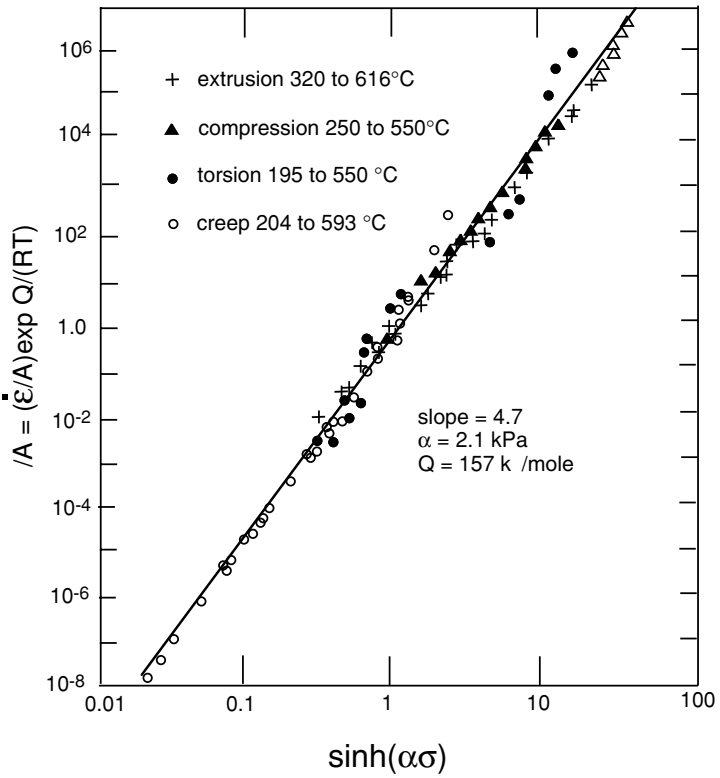

5.25. Plot of the Hollomon–Zener parameter versus flow stress data showing the validity of the hyperbolic sine relation (equation 5.19). Adapted from J. J. Jonas, *Trans. Q. ASM*, 62 (1969), pp. 300–3.

which is consistent with equation 5.12 and explains the often observed breakdown in the power-law strain-rate dependence at low temperatures and high strain rates.

5.7 DEFORMATION MECHANISM MAPS

The controlling mechanisms of deformation change with temperature and strain rate. A typical deformation mechanism map is shown in Figure 5.26. The dominant mechanisms change with temperature and stress. At high stresses slip by dislocation motion predominates. At lower stresses different creep mechanisms are important. The nature of the dominant mechanism shifts with grain size. In particular, with decreased grain size, grain-boundary diffusion (Coble creep) becomes important at higher temperatures.

5.8 HOT WORKING

The decrease in flow stress at high temperatures permits lower tool forces and, consequently, equipment size and power requirements. *Hot working* is often defined as working above the recrystallization temperature so that the work metal recrystallizes as it deforms. However, this is an oversimplified view. The strain rates of many metalworking processes are so high that there is not time for recrystallization to occur during deformation. Rather, recrystallization may occur in the time period between repeated

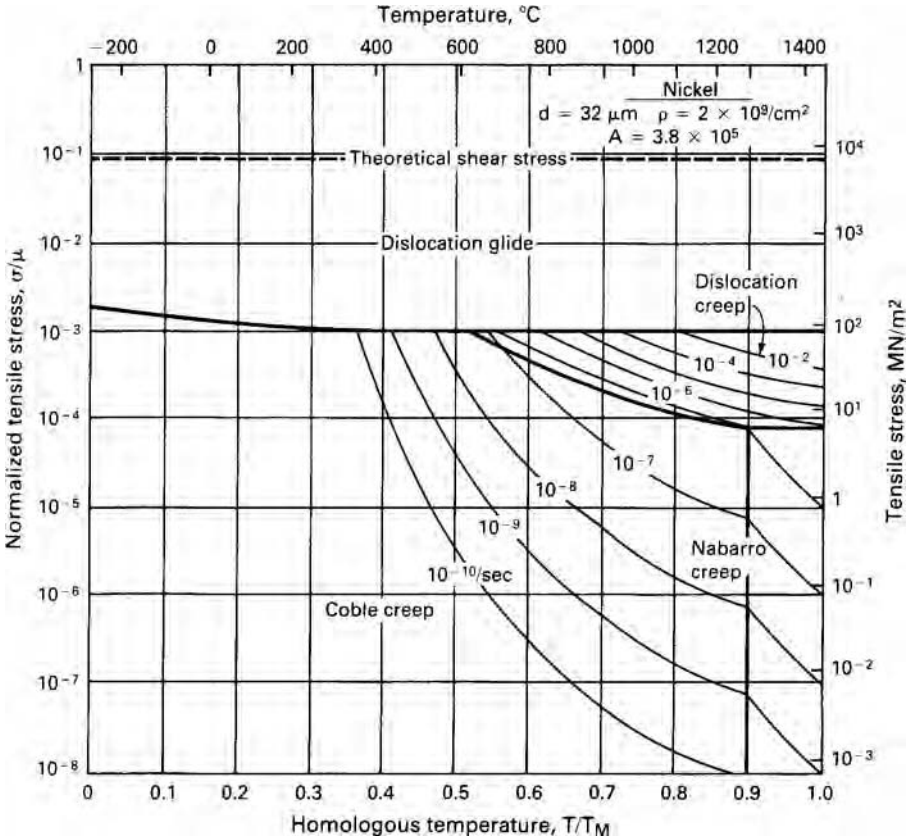

5.26. Deformation mechanism map for pure nickel with a grain diameter $d = 32\ \mu$m, showing the strain rate as a function of stress and temperature. Different mechanisms are dominant in different regimes. Coble creep is controlled by grain-boundary diffusion, and Nabarro creep by lattice diffusion. Reprinted from M. F. Ashby, "A first report on deformation mechanism maps," *Acta Met*. 20 (1972), pp. 887–97, with permission from Pergamon Press Ltd.

operations, as in forging and multiple-stand rolling, or after the deformation is complete, while the material is cooling to room temperature. The high temperature does, however, lower the flow stress whether recrystallization occurs during the deformation or not. Furthermore, the resultant product is in an annealed state.

In addition to lowering the flow stress, the elevated temperature during hot working has several undesirable effects. These include the following:

1. Lubrication is more difficult. Although viscous glasses are often used in hot extrusions, hot working often is done without lubrication.
2. The work metal tends to oxidize. Scaling of steel and copper alloys causes loss of metal and roughened surfaces. While processing under inert atmosphere is possible, it is prohibitively expensive and is avoided except in the case of very reactive metals, such as titanium.
3. Tool life is shortened because of heating, the presence of abrasive scales, and the lack of lubrication. Sometimes scale breakers are employed and rolls are cooled by water spray to minimize tool damage.

4. Poor surface finish and loss of precise gauge control result from the lack of adequate lubrication, oxide scales, and roughened tools.
5. The lack of work hardening is undesirable where the strength level of a cold-worked product is needed.

Because of these limitations, it is common to hot roll steel to about 0.10-in thickness to take advantage of the decreased flow stress at high temperature. The hot-rolled product is then pickled to remove scale, and further rolling is done cold to ensure good surface finish and optimum mechanical properties.

5.9 TEMPERATURE RISE DURING DEFORMATION

The temperature of the metal rises during plastic deformation because of the heat generated by mechanical work. The mechanical energy per volume, w, expended in deformation is equal to the area under the stress–strain curve:

$$w = \int_0^{\bar{\varepsilon}} \bar{\sigma}\, \mathrm{d}\bar{\varepsilon}. \tag{5.23}$$

Only a small fraction of this energy is stored (principally as dislocations and vacancies). This fraction drops from about 5% initially to 1 or 2% at high strains. The rest is released as heat. If the deformation is adiabatic (no heat transfer to the surroundings) the temperature rise is given by

$$\Delta T = \frac{\alpha \int \bar{\sigma}\, \mathrm{d}\bar{\varepsilon}}{\rho C} = \frac{\alpha \bar{\sigma}_a \bar{\varepsilon}}{\rho C}, \tag{5.24}$$

where $\bar{\sigma}_a$ is the average value of σ over the strain interval 0 to ε, ρ is the density, C is the mass heat capacity, and α is the fraction of energy stored as heat (~ 0.98).

EXAMPLE 5.1: Calculate the temperature rise in a high-strength steel that is adiabatically deformed to a strain of 1.0. Pertinent data are $\rho = 7.87 \times 10^3$ kg/m^3, $\sigma_a = 800$ MPa, $C = 0.46 \times 10^3$ J/kg°C.

SOLUTION: Substituting in equation 5.24 and taking $\alpha = 1$,

$$\Delta T = \frac{800 \times 10^6 \times 1.0}{7.87 \times 10^3 \times 0.46 \times 10^3} = 221^\circ\mathrm{C}.$$

Although both σ_a and ε were high in this example, it illustrates the possibility of large temperature rises during plastic deformation. Any temperature increase causes the flow stress to drop. One effect is that at low strain rates, where heat can be transferred to surroundings, there is less thermal softening than at high strain rates. This partially compensates for the strain-rate effect on flow stress and can lead to an apparent decrease in the strain-rate sensitivity at high strains, when m is derived by comparing continuous stress–strain curves.

Another effect of the thermal softening is that it can act to localize flow in narrow bands. If one region or band deforms more than another, the greater heating may lower the flow stress in this region, causing even more concentration of flow and more local heating in this region. An example of this is shown in Figure 5.27,

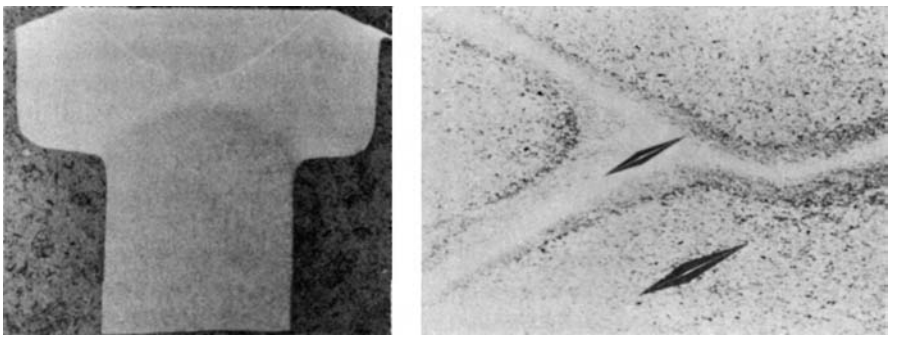

5.27. Flow pattern and microstructure of a bolt head of quenched and tempered 8640 steel after cold upsetting at a high velocity. The light bands of untempered martensite show a higher hardness, as indicated by the Knoop indentations at the right. From F. W. Boulger, *op. cit.*

where in the upsetting of a steel bolt head, localized flow along narrow bands raised the temperature sufficiently to cause the bands to transform to austenite. After the deformation, these bands were quenched to martensite by the surrounding material. Similar localized heating, reported in punching holes in armor plate, can lead to sudden drops in the punching force. Such extreme localization is encouraged by conditions of high flow stresses and strains which increases ΔT, low rates of work hardening and work-piece tool geometry that encourages deformation along certain discrete planes.

NOTES OF INTEREST

Svante August Arrhenius (1859–1927) was a Swedish physical chemist. He studied at Uppsala where he obtained his doctorate in 1884. It is noteworthy that his thesis on electrolytes was given a fourth (lowest) level pass because his committee was skeptical of its validity. From 1886 to 1890 he worked with several noted scientists in Germany who did appreciate his work. In 1887, he suggested that a very wide range of rate processes follow what is now known as the Arrhenius equation. For years his work was recognized throughout the world, except in his native Sweden.

Count Rumford (Benjamin Thompson) was the first person to measure the mechanical equivalent of heat. He was born in Woburn, Massachusetts in 1753, studied at Harvard. At the outbreak of the American Revolution, after been denied a commission by Washington, he was commissioned by the British. When the British evacuated Boston in 1776, he left for England, where he made a number of experiments on heat. After being suspected of selling British naval secrets to the French, he went to Bavaria. In the Bavarian army he eventually became Minister of War and eventually Prime Minister. While inspecting a canon factory, he observed a large increase in temperature during the machining of bronze canons. He measured the temperature rise and, with the known heat capacity of the bronze, he calculated the heat generated by machining. By equating this to the mechanical work done in machining, he was able to deduce the mechanical equivalent of heat.

REFERENCES

W. A. Backofen, *Deformation Processing*, Addison-Wesley, 1972.
W. F. Hosford, *Mechanical Behavior of Materials*, Cambridge University Press, 2005.

PROBLEMS

5.1. Low-carbon steel is being replaced by HSLA steels in automobiles to save weight because the higher strengths of HSLA steels permit use of thinner gauges. In laboratory tests at a strain rate of about 10^{-3} s^{-1}, one grade of HSLA steel has a yield strength of 420 MPa with a strain-rate exponent $m = 0.005$, while for a low-carbon steel, $Y = 240$ MPa and $m = 0.015$. Calculate the percent weight saving possible for the same panel strength assuming

a) a strain rate of 10^{-3} s^{-1},

b) crash conditions with a strain rate of 10^{+4} s^{-1}.

5.2. The thickness of a sheet varies from 8.00 mm to 8.01 mm depending on location so tensile specimens cut from a sheet have different thicknesses.

a) For a material with $n = 0.15$ and $m = 0$, what will be the strain in the thicker region when the thinner region necks?

b) If $n = 0$ and $m = 0.05$, find the strain in the thicker region when the strain in the thinner region is 0.5 and ∞.

5.3. **a)** Find the % elongation in the diagonal ligaments in Figure 5.5, assuming that the ligaments make an angle of 75° with the horizontal.

b) Assuming that $f = 0.98$ and $n = 0$, what value of m is required for the variation of thickness along the ligaments be held to 20%? (The thickness of the thinnest region is 0.80 times the thickness of the thickest region.)

5.4. Find the value of m′ in equation 5.12 that best fits the data in Figure 5.28.

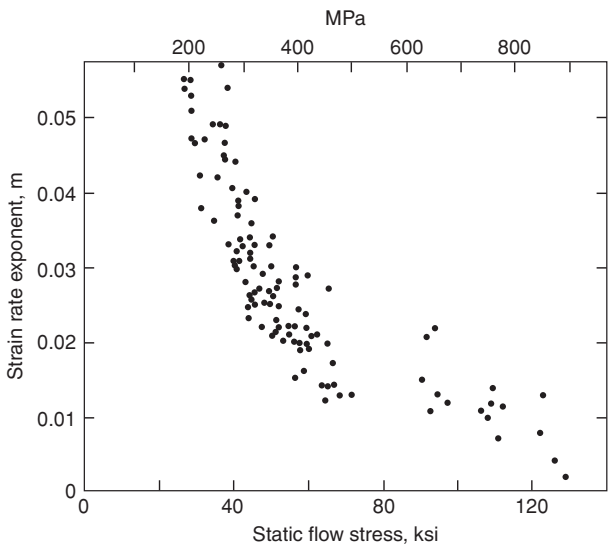

5.28. Effect of stress level on the strain-rate sensitivity of steel. Adapted from A. Saxena and D. A. Chatfield, *SAE Paper 760209* (1976).

5.5. From the data in Figure 5.23, estimate Q in equation 5.15 and m in equation 5.1 for aluminum at 400°C.

5.6. Estimate the total elongation in a tensile bar if
- **a)** $f = 0.98$, $m = 0.5$, and $n = 0$
- **b)** $f = 0.75$, $m = 0.8$, and $n = 0$.

5.7. Estimate the shear strain necessary in the shear bands of Figure 5.27 necessary to explain the formation of untempered martensite if the tensile strength level was 1.75 GPa, $n = 0$, and adiabatic conditions prevailed.

5.8. During superplastic forming it is often necessary to maintain a constant strain rate.
- **a)** Describe qualitatively how the gas pressure should be varied to form a hemispherical dome by bulging a sheet clamped over a circular hole with gas pressure.
- **b)** Compare the gas pressure required to form a hemispherical dome of 5 cm diameter with the pressure for a 0.5-m diameter dome.

5.9. **a)** During a creep experiment under constant stress, the strain rate was found to double when the temperature was suddenly increases from 290°C to 300°C. What is the apparent activation energy for creep?
- **b)** The stress level in a tension test increased by 1.8% when the strain rate was increased by a factor of 8. Find the value of m.

5.10. Figure 5.29 gives data for high-temperature creep of α-zirconium. In this range of temperatures, the strain rate is independent of strain.
- **a)** Determine the value of m that best describes the data at 780°C.

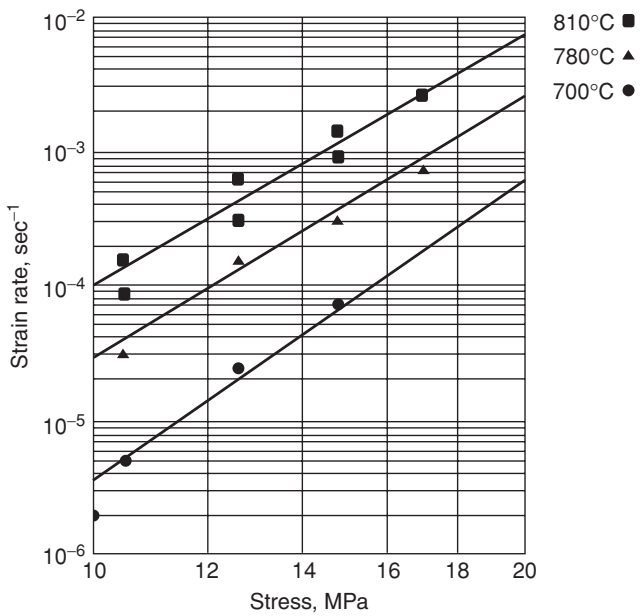

5.29. Strain rate vs. stress for α-zirconium at several temperatures.

b) Determine the activation energy Q in the temperature range 700°C to 810°C at about 14 MPa.

5.11. Tension tests were made in two different labs on two different materials. In both the strain hardening exponent was found to be 0.20, but the post-uniform elongations were quite different. Offer two plausible explanations.

6 Work Balance

This chapter introduces the work or energy balance, which is a very simple method of estimating the forces and energy involved in some metal forming operations. It does not, however, permit predictions of the resulting properties. The energy to complete an operation can be divided into the ideal work, w_i, that would be required for the shape change in the absence of friction and inhomogeneous flow, the work against friction, w_f, and the redundant work, w_r.

6.1 IDEAL WORK

To calculate the ideal work, it is necessary to envision an ideal process for achieving the desired shape change. It is not necessary that the ideal process be physically possible. For example the axially symmetric deformation in the extrusion or wire drawing of an circular rod or wire can be simulated by tension test. The fact that necking would occur in a tension test can be ignored. The ideal work is

$$w_i = \int_0^{\varepsilon} \sigma \, d\varepsilon, \tag{6.1}$$

where $\varepsilon = \ln(A_0/A_f)$. With power-law hardening,

$$w_i = K\varepsilon^{n+1}/(n+1). \tag{6.2}$$

Other expressions of work hardening, if more appropriate, can be used with equation 6.1.

EXAMPLE 6.1: The strain hardening behavior of a metal is approximated by $\bar{\sigma} = 140\bar{\varepsilon}^{0.25}$ MPa. Find the work per volume if a bar of the material is reduced from 12.7 to 11.5 mm diameter in tension.

SOLUTION: This is an ideal process. Using equation 6.2, $\bar{\varepsilon} = 2\ln(12.7/11.5) = 0.199$.

$$w_i = (140 \times 10^6)(0.199)^{1.25}/1.25 = 14.7\,\text{MJ/m}^3.$$

A frictionless compression test could serve as the ideal process for forging. Flat rolling can be simulated by frictionless plane-strain compression.

If a mean flow stress, Y_m, is known, w_i can be taken as

$$w_i = Y_m \bar{\varepsilon}. \tag{6.3}$$

6.2 EXTRUSION AND DRAWING

Figure 6.1 illustrates direct or forward extrusion. A billet of diameter D_0 is extruded through a die of diameter D_1. Except for the very first and last material to be extruded, this is a steady-state operation. The volume of metal exiting the die, $A_1 \Delta \ell_1$, must equal the material entering the die, $A_0 \Delta \ell_0$, so the total external work W_a is

$$W_a = F_e \Delta \ell,$$

where F_e is the extrusion force. Substituting the work per volume as

$$w_a = W_a / (A_0 \Delta \ell),$$

$$w_a = \frac{F_e \Delta \ell}{A_0 \Delta \ell} = \frac{F_e}{A_0}. \tag{6.4}$$

The extrusion pressure P_e must equal w_a, so

$$w_a = P_e. \tag{6.5}$$

Although $w_a = w_i$ for an *ideal* process, for an actual process $w_a > w_i$. Therefore

$$P_e > \int \sigma \, d\varepsilon, \tag{6.6}$$

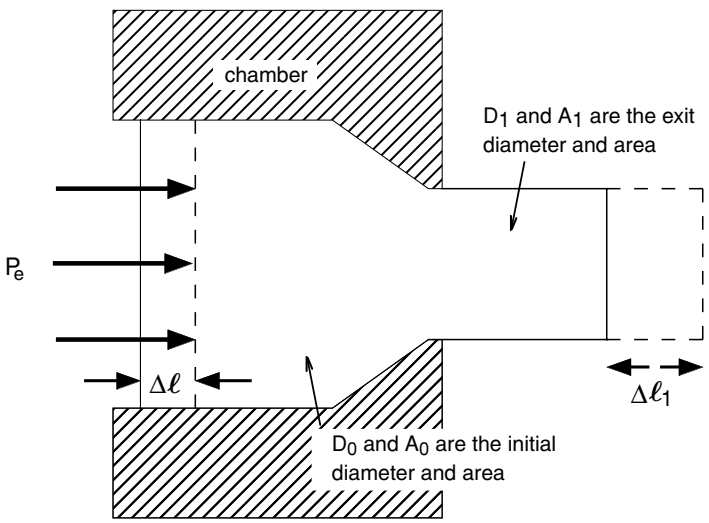

6.1. Direct or forward extrusion.

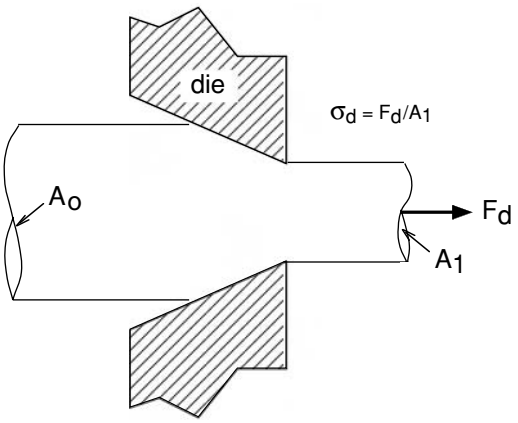

6.2. Rod or wire drawing.

so equation 6.5 underestimates the extrusion work and is a lower bound to the actual value.

Wire and rod drawing (Figure 6.2) can be analyzed in a similar way. The drawing force F_d pulls the metal through the die. The actual work, W_a, in drawing a length $\Delta\ell$ is $W_a = F_d \Delta\ell$, so the work per volume is

$$w_a = F_d / A_1 = \sigma_d, \tag{6.7}$$

where σ_d is the drawing stress. Again because $w_a > w_i$,

$$\sigma_d > \int \sigma \, d\varepsilon. \tag{6.8}$$

EXAMPLE 6.2: Find the drawing stress necessary to reduce the bar in Example 6.1 from 12.7 to 11.5 mm diameter by drawing it through a die assuming an ideal process.

SOLUTION: For an ideal process, $\sigma_d = w_i = 14.7$ MPa.

6.3 DEFORMATION EFFICIENCY

In addition to the ideal work, there is work against friction between work and tools, W_f, and work to do redundant or unwanted deformation, W_r. Expressed on a per volume basis these are w_f and w_r. Figure 6.3 illustrates the redundant work in drawing or extrusion. If the deformation were ideal, plane sections would remain plane. In real processes, the surface layers are sheared relative to the center. The material undergoes more strain than required for the diameter reduction and consequently strain hardens more and is less ductile.

The actual work is the sum of the ideal, frictional, and redundant works:

$$w_a = w_i + w_f + w_r. \tag{6.9}$$

It is often difficult to find w_f and w_r explicitly, but the need to do this can be avoided by lumping the inefficient terms and defining a deformation efficiency, η, where

$$\eta \equiv w_i / w_a. \tag{6.10}$$

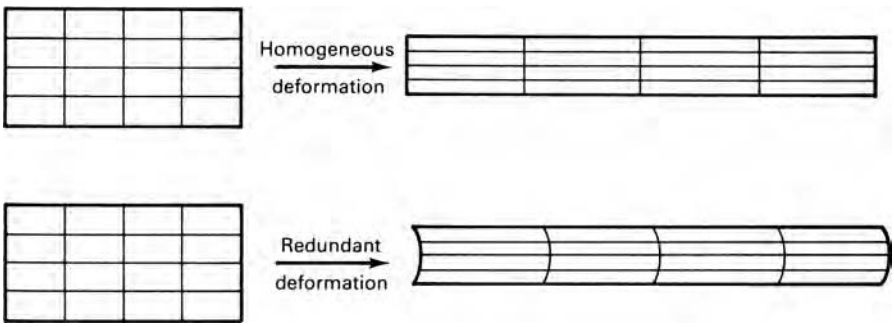

6.3. Comparison of ideal and actual deformation to illustrate the meaning of redundant work.

Experience allows one to make reasonable estimates of η. For wire and rod drawing, it is often between 0.5 and 0.65 depending on lubrication, reduction, and die angle. Using an efficiency, the extrusion pressure or drawing stress can be expressed as

$$P_{\text{ext}} = \frac{1}{\eta} \int \bar{\sigma} \, \mathrm{d}\bar{\varepsilon}. \tag{6.11}$$

If strain hardening is small

$$P_{\text{ext}} = \frac{1}{\eta} \int \bar{\sigma} \, \mathrm{d}\bar{\varepsilon} = \frac{Y_{\text{m}}\varepsilon}{\eta}. \tag{6.12}$$

EXAMPLE 6.3: Calculate the extrusion pressure to extrude the bar in Example 6.1 through a die, reducing its diameter from 12.7 mm to 11.5 mm, if the efficiency is 70%.

SOLUTION: $P_{\text{ext}} = \frac{1}{\eta} \int \bar{\sigma} \mathrm{d}\bar{\varepsilon} = w_{\text{i}}/\eta = 14.7/0.7 = 21\,\text{MPa}.$

6.4 MAXIMUM DRAWING REDUCTION

For drawing, there is a maximum possible reduction per pass because the drawing stress cannot exceed the strength of the dawn wire or rod. Once drawing has started, it is a steady-state process. The maximum reduction corresponds to $\sigma_{\text{d}} = \bar{\sigma}$. If the effect of hardening caused by redundant strain is neglected, the limiting strain, ε^*, can be found by and equating expressions for σ_{d} and $\bar{\sigma}$. For power-law hardening, $\bar{\sigma} = K\varepsilon^{*n}$ and $\sigma_{\text{d}} = K\varepsilon^{*n+1}/(n+1)$ so

$$\varepsilon^* = \eta(n+1). \tag{6.13}$$

For an ideally plastic metal ($n = 0$) and perfect efficiency ($\eta = 1$), the maximum strain would be $\varepsilon^* = 1$ which corresponds to a reduction, r^*, of 63%. With a more reasonable value of $\eta = 0.65$, $\varepsilon^* = 0.65$ and $r^* = 48\%$. In practice, multiple passes are used and after the first or second pass additional strain hardening can be neglected ($n \to 0$).

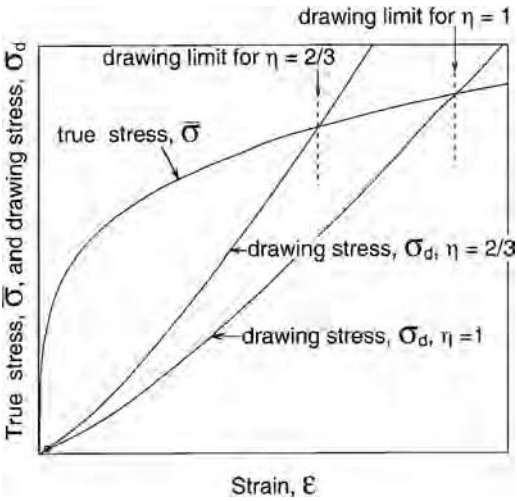

6.4. The drawing limit ε^* corresponds to the intersection of the plots of drawing stress with the stress–strain curve.

For all conditions (strain hardening rules and efficiencies), the maximum drawing strain corresponds to $\sigma_d = \bar{\sigma}/\eta$ as illustrated by Figure 6.4.

The conditions are different in the initial start-up. Undrawn material must be fed through the die. If it is annealed, the maximum drawing force will correspond to the tensile strength, or

$$\sigma_{d(max)} = Kn^n \tag{6.14}$$

and the maximum strain is

$$\varepsilon^* = [\eta(n+1)n^n]^{1/(n+1)}. \tag{6.15}$$

More likely, however, the end of the wire to be fed through the die will be reduced by swaging (see Section 6.6). In this case it will have been strain hardened at least as much as if it had been drawn.

6.5 EFFECTS OF DIE ANGLE AND REDUCTION

Figure 6.5 shows schematically the dependence of the friction and redundant work terms on die angle. For a given reduction, the contact area between the die and material decreases with increasing die angle. The *pressure* the die exerts on the material in the die gap is almost independent of the die angle, so the *force* between the die and workpiece increases with greater area of contact at die angles. With a constant coefficient of friction, w_f increases as α decreases. The redundant work term, w_r, increases with die angle. The ideal work term, w_i, doesn't depend on the die angle. For each reduction, there is an optimum die angle, α^*, for which the work is a minimum.

The efficiency and optimum die angle are functions of the reduction. In general the efficiency increases with reduction. Figures 6.6 and 6.7 are adapted from the measurements of Wistreich*. The optimum die angle increases with reduction.

* J. Wistreich, *Metall. Rev.,* 3 (1958), pp. 97–142.

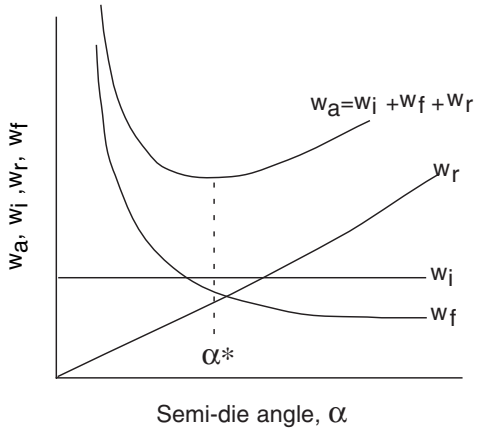

6.5. Dependence of the various work terms on the die angle.

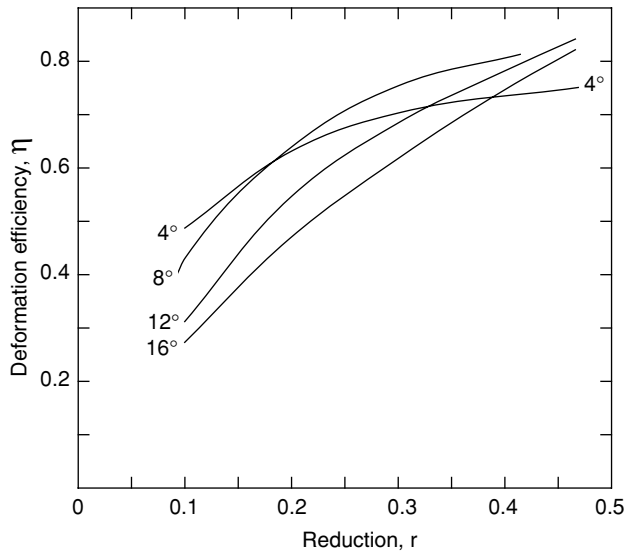

6.6. Wistreich's data show an increase of efficiency with increasing reduction.

In extrusion the same general effects of die angle and reduction on efficiency apply. However, there is no theoretical limit to reduction, though excessive extrusion forces may be beyond the capacity of the extruder. Therefore the reductions and die angles in extrusion tend to be much larger than in drawing. Area reductions of 8:1 ($r = 0.875$) are not uncommon.

6.6 SWAGING

The diameters of wires and tubes may be reduced by rotary swaging. Shaped dies are rotated around the wire or tube and hammer the work piece as they rotate. This causes a swirled microstructure. In a wire drawing plant, swaging is used to reduce the ends of wires so they can be fed through drawing dies in the initial setup. Figure 6.8 is a schematic of the tooling used in swaging.

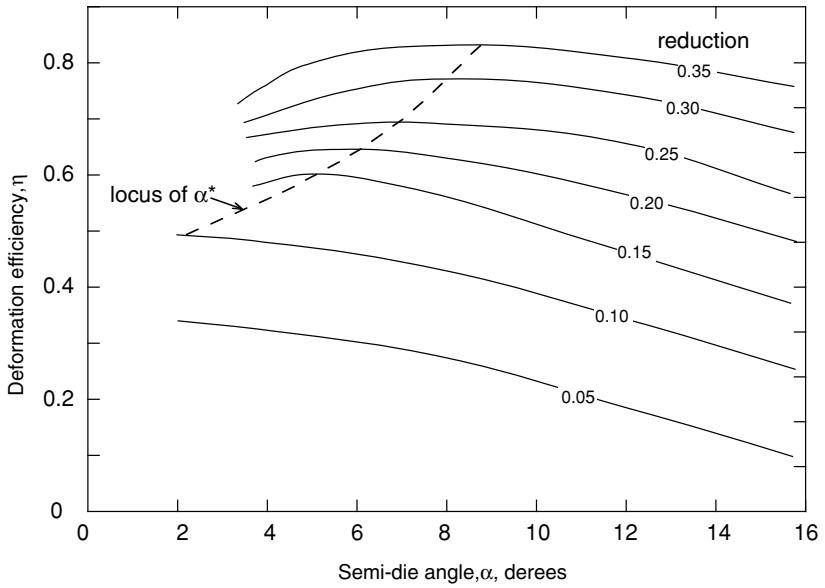

6.7. Replot of data in Figure 6.6 showing the increase of optimum die angle with reduction.

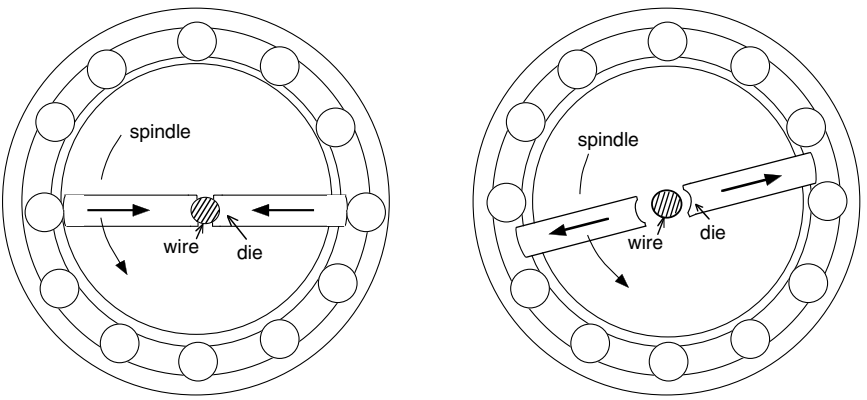

6.8. Tooling for swaging. As the spindle rotates it causes the die to hammer the work at different angles (in this case 30°).

REFERENCES

ASM Metals Handbook: Forging and Forming, vol. 14. 9th ed., ASM 1988.
W. A. Backofen, *Deformation Processing*, Addison-Wesley, 1972.

PROBLEMS

6.1. The diameter, D_0, of a round rod can be reduced to D_1 either by a tensile force of F_1 or by drawing through a die with a force, F_d, as sketched in Figure 6.9. Assuming ideal work in drawing, compare F_1 and F_d (or σ_1 and σ_d) to achieve the same reduction.

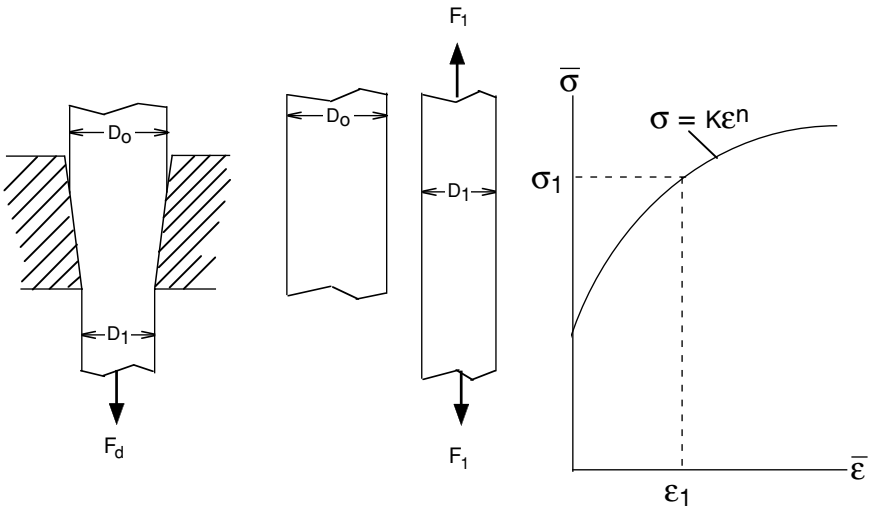

6.9. Sketch for Problem 6.1.

6.2. Calculate the maximum possible reduction, r, in wire drawing for a material whose stress–strain curve is approximated by $\bar{\sigma} = 200\bar{\varepsilon}^{0.18}$ MPa. Assume an efficiency of 65%.

6.3. An aluminum alloy billet is being hot extruded from 20-cm diameter to 5-cm diameter as sketched in Figure 6.10. The flow stress at the extrusion temperature is 40 MPa. Assume $\eta = 0.5$.

a) What extrusion pressure is required?

b) Calculate the lateral pressure on the die walls.

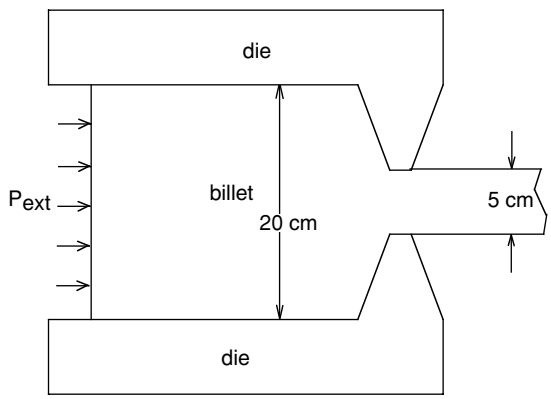

6.10. Aluminum billet being extruded.

6.4. An unsupported extrusion process (Figure 6.11) has been proposed to reduce the diameter of a bar from D_0 to D_1. The material does not strain harden. What is the largest reduction, $\Delta D/D_0$, that can be made without the material yielding before it enters the die? Neglect the possibility of buckling and assume $\eta =$ 60%.

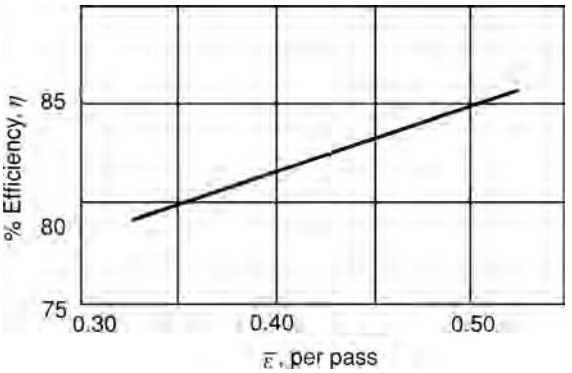

6.11. Unsupported extrusion.

6.5. A sheet, 1 m wide and 8 mm thick, is to be rolled to a thickness of 6 mm in a single pass. The strain-hardening expression for the material is $\bar{\sigma} = 200\bar{\varepsilon}^{0.18}$ MPa. A deformation efficiency of 80% can be assumed. The von Mises yield criterion is applicable. The exit speed from the rolls is 5 m/s. Calculate the power required.

6.6. The strains in a material for which $\bar{\sigma} = 350\bar{\varepsilon}^{0.20}$ MPa are $\varepsilon_1 = 0.200$ and $\varepsilon_2 = -0.125$. Calculate the work per volume.

6.7. You are asked to plan a wire-drawing schedule to reduce copper wire from 1 mm to 0.4 mm in diameter. How many wire drawing passes would be required to be sure of no failures, if the drawing stress never exceeds 80% of the flow stress, and the efficiency is assumed to be 60%?

6.8. Derive an expression for ε^* at the initiation of drawing when the outlet diameter is produced by machining.

6.9. For a material with a stress–strain relation $\sigma = A + B\varepsilon$, find the maximum strain per wire drawing pass if $\mu = 0.75$.

7 Slab Analysis and Friction

Slab analyses are based on making a force balance on a differentially thick slab of material. It is useful in estimating the role of friction on forces required in drawing, extrusion, and rolling. The important assumptions are these:

1. The principal axes are in the directions of the applied loads.
2. The effects of friction do not alter the directions of the principal axes or cause internal distortion. The deformation is homogeneous so plane sections remain plane.

7.1 SHEET DRAWING

Figure 7.1 illustrates *sheet* or *strip drawing*. A force F pulls a strip through a pair of wedges. The strip width w is much greater than the thickness t so the width doesn't change and plane strain prevails. The drawing stress is $\sigma_d = F/wt_e$.

Figure 7.2 shows the differential slab element. Pressure normal to the die, P, acts on two areas of $w\,dx/\cos\alpha$, and the corresponding component of force in the x-direction is $2Pw\,dx(\sin\alpha/\cos\alpha)$. The normal pressure also causes a frictional force on the work metal, $2\mu wP\,dx/\cos\alpha$, with a horizontal component $2\mu wP\,dx(\cos\alpha/\cos\alpha)$, where μ is the coefficient of friction. Both of these forces act in the positive x-direction. The drawing force, $\sigma_x wt$, acts in the negative x-direction, while the force in the positive x-direction is $(\sigma_x + d\sigma_x)(t + dt)w$. An x-direction force balance gives

$$(\sigma_x + d\sigma_x)(t + dt)w + 2w(\tan\alpha)P\,dx + 2\mu Pw\,dx = \sigma_x wt. \tag{7.1}$$

Simplifying and neglecting second order differentials,

$$\sigma_x t + \sigma_x dt + t d\sigma_x + 2(\tan\alpha)P dx + 2\mu P dx = \sigma_x t. \tag{7.2}$$

Substituting $2dx = dt/\tan\alpha$ and $B = \mu\cot\alpha$, $P\,dt + \sigma_x\,dt + t\,d\sigma_x + \mu(\cot\alpha)P\,dt = 0$, or

$$t d\sigma_x + [\sigma_x + P(1 + B)]dt = 0, \text{ or} \tag{7.3}$$

$$\frac{d\sigma_x}{\sigma_x + P(1 + B)} = -\frac{dt}{t}. \tag{7.4}$$

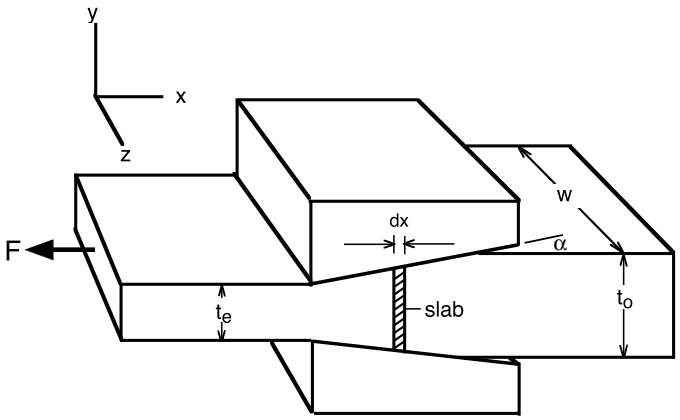

7.1. Plane-strain drawing of a sheet.

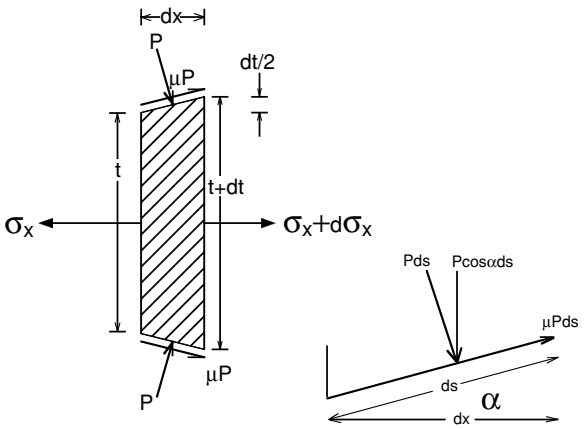

7.2. Slab used for force balance in sheet drawing.

To integrate equation 7.4, the relation between P and σ_x must be found and substituted. The fact that P does not act in a direction normal to x will be ignored and P will be taken as a principal stress, $P = -\sigma_x$. For yielding in plane strain, $\sigma_x - \sigma_y = 2k$, where k is the yield strength in shear. For Tresca $2k = Y$ and for von Mises $2k = (2/\sqrt{3})Y$. Substituting $P = 2k - \sigma_x$ into equation 7.4,

$$\frac{\mathrm{d}\sigma_x}{B\sigma_x - 2k(1+B)} = \frac{\mathrm{d}t}{t}. \tag{7.5}$$

Integrating between $\sigma_x = 0$ and $\sigma_x = \sigma_\mathrm{d}$ and between $t = t_0$ and t_e, and solving for σ_d,

$$\frac{\sigma_\mathrm{d}}{2k} = \frac{(1+B)}{B}\left[1 - \left(\frac{t_\mathrm{e}}{t_0}\right)^B\right]. \tag{7.6}$$

Finally substituting $\varepsilon_h = \ln(t_0/t_e)$ as the homogeneous strains,

$$\frac{\sigma_d}{2k} = \frac{(1+B)}{B}[1 - \exp(-B\varepsilon_h)]. \tag{7.7}$$

Several assumptions are involved in the derivation of equation 7.7. First, it is assumed that $2k$ is constant, which is not true if the material work hardens. The effect of work hardening can be approximated by using an average value of $2k$. Another is that the friction coefficient is constant. The assumption that P is a principal stress is reasonable for low die angles and low coefficients of friction, but the assumption gets progressively worse at high die angles and high friction coefficients.

EXAMPLE 7.1: A 2.5 mm thick metal sheet 25 cm wide is drawn to a thickness of 2.25 mm through a die of included angle 30°. The flow stress is 200 MPa and the friction coefficient is 0.08. Calculate the drawing force using the von Mises criterion.

SOLUTION: Use equation 7.7 and take $B = \mu \cot\alpha = 0.08\cot(15^\circ) = 0.299$ and $\varepsilon_h = \ln(2.5/2.25) = 0.1054$. From equation 7.7, $\sigma_d = 1.15(200)(1.299/0.299)[1 - \exp(-0.299 \times 0.1054)] = 31$ MPa. $F_d = 31\,\text{MPa}\,(0.25\text{m})(0.0225) = 175$ kN.

Note that if $\mu = 0$ (i.e., $B = 0$) were substituted into equation 7.7, with L'Hospital's rule it can be shown that

$$\frac{\sigma_d}{2k} = \varepsilon_h, \tag{7.8}$$

which is exactly what would be predicted by the work balance.

7.2 WIRE AND ROD DRAWING

Sachs* analyzed wire or rod drawing by an analogous procedure. The basic differential equation is

$$\frac{d\sigma}{B\sigma - (1+B)\bar{\sigma}} = 2\frac{dD}{D}, \tag{7.9}$$

where D is the diameter of the rod or wire. Realizing that $2dD/D = -d\varepsilon$,

$$\int_0^{\sigma_d} \frac{d\sigma}{B\sigma - (1+B)\bar{\sigma}} = -\int_0^{\varepsilon_h} d\varepsilon. \tag{7.10}$$

Integrating,

$$\sigma_d = \sigma_a\left(\frac{1+B}{B}\right)[1 - \exp(-B\varepsilon_h)], \tag{7.11}$$

where σ_a is the average flow stress of the material in the die. This analysis neglects redundant strain, has the same limitations as the plane-strain drawing in Section 7.1, and becomes unrealistic at high die angles and low reductions.

* G. Sachs, *Z. Angew. Math. Mech.*, 7 (1927), p. 235.

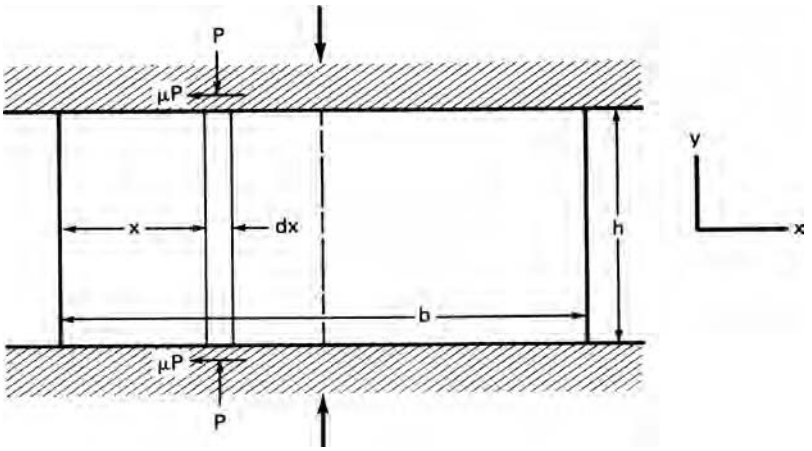

7.3. Essentials for a slab analysis.

7.3 FRICTION IN PLANE-STRAIN COMPRESSION

The slab analysis can also be used for plane-strain compression. Figure 7.3 shows a specimen with $h < b$ being compressed with a constant coefficient of friction, μ. Making a force balance on the differential slab, $\sigma_x h + 2\mu P\,\mathrm{d}x - (\sigma_x + \mathrm{d}\sigma_x)h = 0$. This simplifies to

$$2\mu P\,\mathrm{d}x = h\mathrm{d}\sigma_x. \tag{7.12}$$

Again take $\sigma_y = -P$ and σ_x as principal stresses and realize that for plane strain, $\sigma_x - \sigma_y = 2k$, so $\mathrm{d}\sigma_x = \mathrm{d}P$. Equation 7.12 becomes $2\mu P\,\mathrm{d}x = h\,\mathrm{d}P$ or

$$\frac{\mathrm{d}P}{P} = \frac{2\mu\,\mathrm{d}x}{h}. \tag{7.13}$$

Integrating from $P = 2k$ at $x = 0$ to P at x, $\ln(P/2k) = 2\mu x/h$ or

$$\frac{P}{2k} = \exp\left(\frac{2\mu x}{h}\right). \tag{7.14}$$

This predicts a friction hill, which is illustrated in Figure 7.4.

This is valid from the edge ($x = 0$) to the centerline ($x = b/2$). The average pressure, P_a, can be found by integrating P over half of the block to find the force and dividing that by the area of the half-block.

$$F_y = \int_0^{b/2} P\,\mathrm{d}x = \int_0^{b/2} 2k\exp\left(\frac{2\mu x}{h}\right)\mathrm{d}x = 2k\left(\frac{h}{2\mu}\right)\left[\exp\left(\frac{\mu b}{h}\right) - 1\right], \tag{7.15}$$

$$\frac{P_{av}}{2k} = \left(\frac{h}{\mu b}\right)\left[\exp\left(\frac{\mu b}{h}\right) - 1\right]. \tag{7.16}$$

A simple approximate solution can be found by expanding $\exp(\mu b/h) - 1 = (\mu b/h) + (\mu b/h)^2/2 + \cdots$. For small values of $(\mu b/h)$,

$$\frac{P_{av}}{2k} \approx 1 + \frac{\mu b}{2h}. \tag{7.17}$$

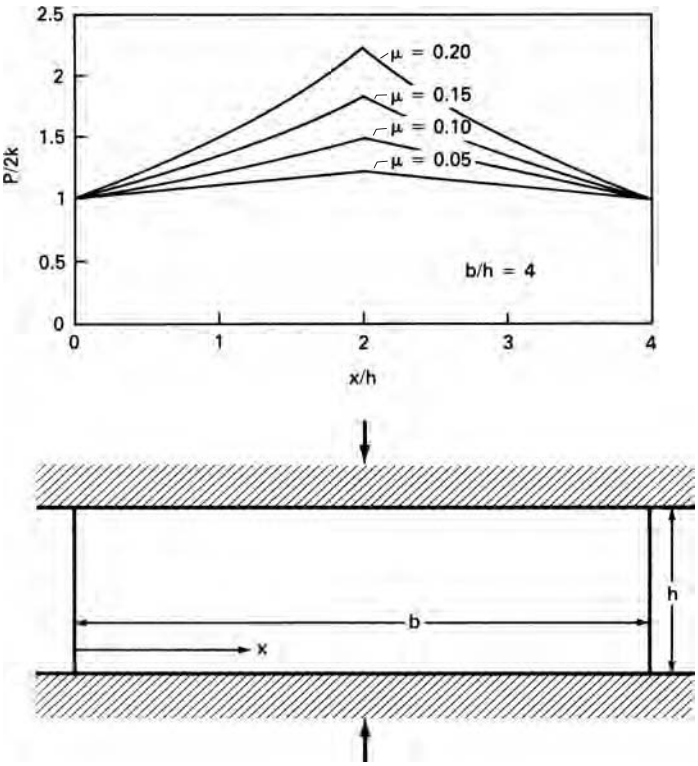

7.4. Friction hill in plane-strain compression with a constant coefficient of friction.

EXAMPLE 7.2: Plane-strain compression is conducted on a slab of metal 20 cm wide and 2.5 cm high, with a yield strength in shear of $k = 100$ MPa. Assuming a coefficient of friction of $\mu = 0.10$,

(a) Estimate the maximum pressure at the onset of plastic flow;
(b) Estimate the average pressure at the onset of plastic flow.

SOLUTION:

(a) From equation 7.14, at $x = b/2$, $P_{\max} = 2k \exp(\mu b/h) = 200 \exp(0.1 \times 20/2.5) = 45$ MPa
(b) Using the exact solution (equation 7.16), $P_{\text{av}} = 200[2.5/(0.1)(20)]\{\exp[(0.10)(0.20)/2.5 - 1]\} = 253$ MPa. The approximate solution (equation 7.17) gives

$$P_{\text{av}} = 200\left[1 + \frac{(0.1)(20)}{2(2.5)}\right] = 280 \text{ MPa}.$$

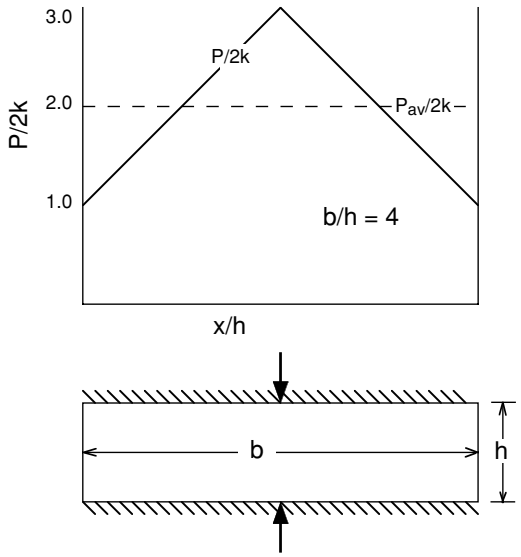

7.5. Friction hill in plain-strain compression with sticking friction.

7.4 STICKING FRICTION

There is an upper limit to the shear stress on the interface. It cannot exceed $2k$. This limits equations 7.16 and 7.17 to

$$x \le \frac{-h}{2\mu}\ln(2\mu) \qquad \text{and} \qquad \frac{b}{h} \le -\ln(2\mu)/\mu. \tag{7.18}$$

Otherwise the tool and work piece will stick at the interface, and the work piece will be sheared. If sticking occurs, the shear stress will be k instead of μP and equation 7.14 will become

$$P/2k = 1 + x/h. \tag{7.19}$$

The pressure distribution is shown in Figure 7.5.

The average pressure is given by

$$\frac{P_{\text{av}}}{2k} = 1 + \frac{b}{4h}. \tag{7.20}$$

EXAMPLE 7.3: Repeat Example 7.2 for sticking friction.

SOLUTION:

(a) Using equation 7.19, $P_{\max} = 200(1 + 20/5) = 1{,}000$ MPa.

(b) Using equation 7.20, $P_{\text{av}} = 200(1 + 20/10) = 600$ MPa.

7.5 MIXED STICKING–SLIDING CONDITIONS

If $b/h \ge -\ln(2\mu)/\mu$, sticking is predicted at the center and sliding at the edges. Equation 7.14 predicts P for $x \le x^*$ where $x^* = -h\ln(2\mu)/(2\mu)$. From x^* to the

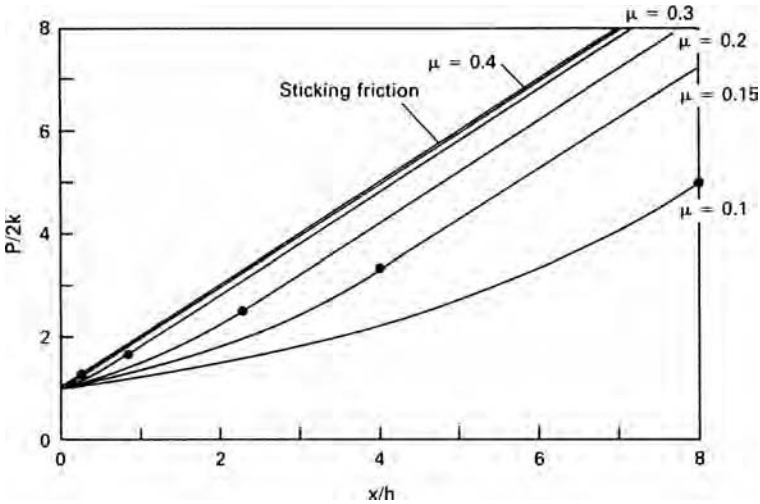

7.6. Pressure distribution with sliding friction near the edges and sticking friction in the center for several values of μ. Points mark the boundaries between sticking and sliding friction.

centerline, $h\,dP = -2k\,dx$. Integrating between $P = 2k\exp(2\mu x^*/h)$ at $x = x^*$ and P at x,

$$\frac{P}{2k} = \frac{x - x^*}{h} + \exp\left(\frac{2\mu x^*}{h}\right). \tag{7.21}$$

This is plotted in Figure 7.6.

The average pressure can be found by integrating $P/2k$ in equation 7.21 over the area of contact:

$$\begin{aligned}\frac{P_{\text{av}}}{2k} &= \left(\frac{2}{b}\right)\int_{x^*}^{b/2}\left[\frac{x - x^*}{h} + \exp\left(\frac{2\mu x^*}{h}\right)\right]\mathrm{d}x + \left(\frac{2}{b}\right)\int_0^{x^*}\exp\left(\frac{2\mu x}{h}\right)\mathrm{d}x \\ &= \frac{b}{4h} - \frac{x^*}{h} + \frac{h}{2b\mu}\exp\left(\frac{\mu b}{h}\right) + \left(1 - \frac{x^*}{2b} - \frac{h}{2b\mu}\right)\exp\left(\frac{2\mu x^*}{h}\right).\end{aligned} \tag{7.22}$$

7.6 CONSTANT SHEAR STRESS INTERFACE

Films of soft materials such as lead or a polymer are sometimes used as lubricants. In this case there will be a constant shear stress, $\tau = mk$, in the interface, where m is the ratio of the shear strength of the film to that of the work piece. The local pressure is now given by

$$P/2k = 1 + mx/h \tag{7.23}$$

and the average pressure by

$$\frac{P_{\text{av}}}{2k} = 1 + \frac{mb}{4h}. \tag{7.24}$$

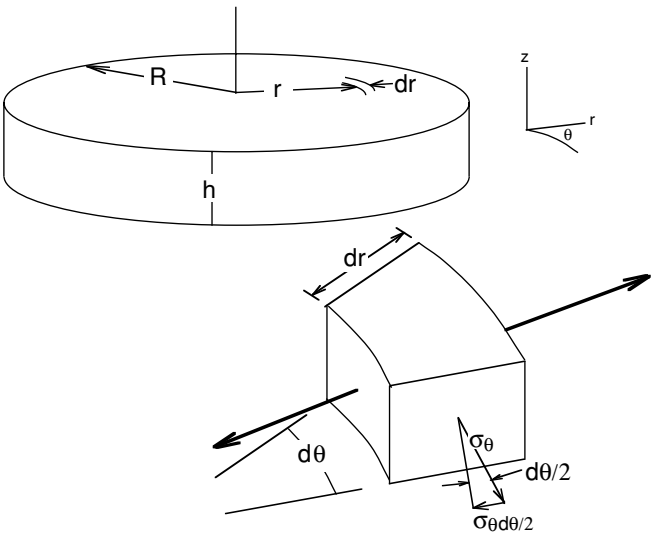

7.7. Differential element for analysis of axially symmetric compression.

7.7 AXIALLY SYMMETRIC COMPRESSION

An analysis similar to that in Section 7.4 can be used for axially symmetric compression. Making a force balance on a differential element (Figure 7.7), $\sigma_r h r\ \mathrm{d}\theta + 2\mu P r\ \mathrm{d}\theta\ \mathrm{d}r + (2\sigma_\theta h\ \mathrm{d}r\ \mathrm{d}\theta)/2 - (\sigma_r + \mathrm{d}\sigma_r)(r + \mathrm{d}r)h\ \mathrm{d}\theta = 0$. Simplifying,

$$2\mu P r\ \mathrm{d}r + h\sigma_\theta\ \mathrm{d}r = h\sigma_r\ \mathrm{d}r + hr\ \mathrm{d}\sigma_r. \tag{7.25}$$

For axially symmetric flow, $\varepsilon_\theta = \varepsilon_r$ so $\sigma_\theta = \sigma_r$. At yielding $\sigma_r + P = Y$ or $\mathrm{d}\sigma_r = -\mathrm{d}P$. Substituting into equation 7.25 gives $2\mu P r\ \mathrm{d}r = -hr\ \mathrm{d}P$ or

$$\int_Y^P \frac{\mathrm{d}P}{P} = -\int_0^R \frac{2\mu}{h}\mathrm{d}r. \tag{7.26}$$

Letting $P = -Y,\ \mathrm{d}\sigma_r = -\mathrm{d}P$ and integrating,

$$P = Y \exp\left[\left(\frac{2\mu}{h}\right)(R - r)\right]. \tag{7.27}$$

The average pressure is $P_{\mathrm{av}} = (1/\pi R^2)\int_0^R 2P\pi r\ \mathrm{d}r$.

$$\begin{aligned} P_{\mathrm{av}} &= \left(\frac{2Y}{R^2}\right)\int_0^R r \exp\left[\left(\frac{2\mu}{h}\right)(R - r)\right]\mathrm{d}r \\ &= \left(\frac{1}{2}\right)\left(\frac{h}{\mu R}\right)^2 Y\left[\exp\left(\frac{2\mu R}{h}\right) - \left(\frac{2\mu R}{h}\right) - 1\right] \end{aligned} \tag{7.28}$$

For small values of $\mu R/h$, this reduces to

$$P_{\mathrm{av}} = Y[1 + (2\mu R/h)/3 + (2\mu R/h)^2/12 + \cdots] \tag{7.29}$$

Here $Y = 2k$ for Tresca and $Y = \sqrt{3}k$ for von Mises. In this analysis, it was tacitly assumed that $\mu P \le k$ so $Y \exp[(2\mu/h)(R - r)] \le k/\mu$. Therefore the limiting radius,

r^*, is $r^* = R - (h/2\mu)\ln(k/\mu Y)$. For sliding to prevail over the entire surface, $R \leq (h/2\mu)\ln(k/\mu Y)$.

For sticking friction over the entire interface, the shear term in equation 7.25 is $2kr\,dr$ instead of $2\mu Pr\,dr$, so $2k\,dr = -h\,dP$ and

$$\int_R^r 2k\,dr = -\int_Y^P h\,dP. \tag{7.30}$$

Integrating

$$P = Y + (2k/h)(R - r). \tag{7.31}$$

The average pressure is

$$P_{av} = Y + 2kR/(3h). \tag{7.32}$$

EXAMPLE 7.4: A solid 10 cm diameter, 2.5 cm high disc is compressed. The tensile and shear yield strengths are 300 and 150 MPa. Estimate the force needed to deform the disc assuming sticking friction.

SOLUTION: Using equation 7.32, $P_{av} = 300 + 5\text{ cm}(150 \times 2)/[3(2.5\text{ cm})] = 500\text{MPa}$.

$$F = \pi(0.05\text{ m})^2(500 \times 10^6\text{ Pa}) = 3.9\text{ MN}.$$

7.8 SAND-PILE ANALOGY

The analyses for axially symmetric and plane-strain compression with sticking friction can be interpreted in terms of the shape of a sand pile. Dry sand piled on a flat surface will form a hill with a constant slope. This slope is analogous to the linear increase of P with distance from the edge of the work piece. The effect of sticking friction can be analyzed using this effect. Sand can be piled onto cardboard or other flat material cut to the shape of the work piece. The volume of sand, found by pouring into a calibrated vessel or by weighing, is proportional to the integral of $(P - Y)$ over the compressed surface, and thus to the total compressive force minus Y times the area. This method can be used to analyze complex shapes.

7.9 FLAT ROLLING

Flat rolling of plates and sheets is essentially a plain-strain compression because the length of contact between rolls and work piece, L, is usually much smaller than the width of the sheet, w (Figure 7.8). As the plastic region is thinned by the compressive stress, σ_z, it is free to expand in the rolling direction, x. However lateral expansion in the y-direction is constrained by the undeforming material on both sides of the roll gap. The net effect is a condition of plane strain, $\varepsilon_y = 0$ and $\varepsilon_z = -\varepsilon_x$, except at the edges.

On the inlet side of the gap, the roll surface is moving faster than the work material, whereas on the outlet side material moves faster than the roll surface (Figure 7.9). This causes friction to act toward the neutral point, N, creating a friction hill.

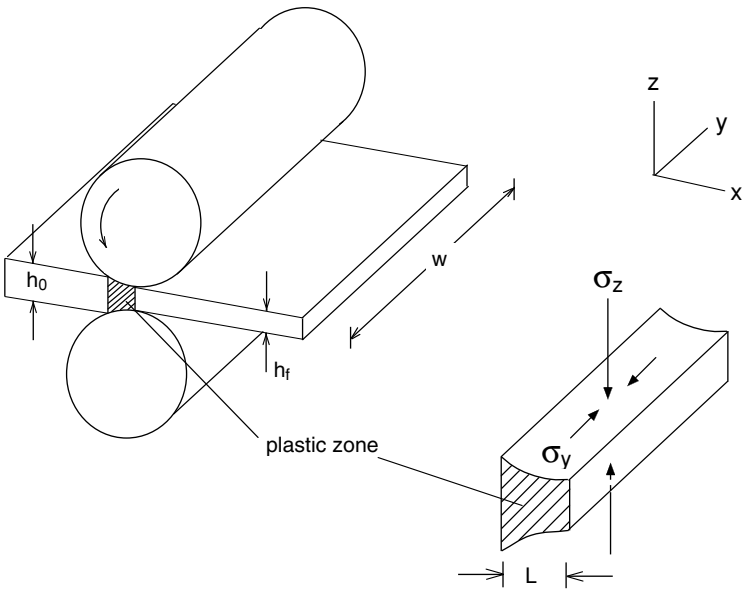

7.8. Schematic of the deformation zone in flat rolling.

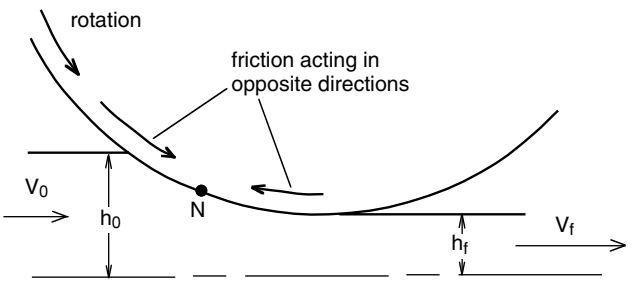

7.9. On the inlet side, the surface of the roll moves faster than the work piece and on the outlet side the work piece moves faster. This causes friction to act on the work piece toward the neutral point, N.

Figure 7.10 shows the roll-gap geometry, where R is the roll radius, $\Delta h = h_0 - h_\mathrm{f}$ and L is the projected contact length. It can be seen that

$$L^2 = R^2 - \left(R - \frac{\Delta h}{2}\right)^2 = R\Delta h - \left(\frac{\Delta h}{2}\right)^2. \tag{7.33}$$

Neglecting the last term,

$$L = \sqrt{R\Delta h} = \sqrt{Rrh_0}, \tag{7.34}$$

where the reduction is $r = \Delta h / h_0$.

The frictional effects are similar to those in plane-strain compression. If the curvature of the roll contact area is neglected, equation 7.16 with L substituted for b and $(h_0 + h_\mathrm{f})/2$ substituted for h can be used to find the average pressure, so

$$P_\mathrm{av} = \frac{h}{\mu L}\left(\exp\frac{\mu L}{h} - 1\right)\sigma_0, \tag{7.35}$$

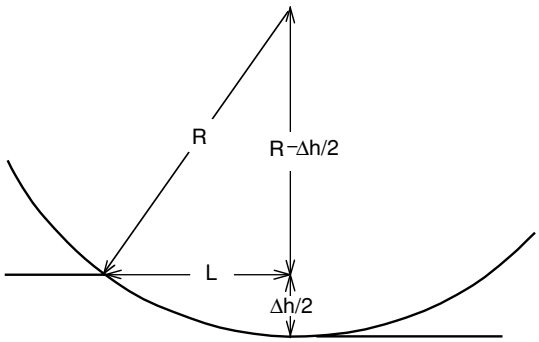

7.10. Geometry of the roll gap.

where σ_0 is the average plane-strain flow stress in the roll gap. If the material strain hardens, a simple approximation is $\sigma_0 = (\sigma_1 + \sigma_2)/2$, where σ_1 and σ_2 are the flow stresses of the material at the entrance and exit if the roll gap.

If front tension or back tension is applied, this has the effect of lowering σ_0 so equation 7.35 becomes

$$P_{av} = \frac{h}{\mu L}\left(\exp\frac{\mu L}{h} - 1\right)[\sigma_0 - (\sigma_{bt} + \sigma_{ft})/2], \tag{7.36}$$

where σ_{bt} and σ_{ft} are the back and front tensile stresses. Figure 7.11 illustrates the effects of back and front tension. The position of the neutral point shifts with front or back tension.

EXAMPLE 7.5: The plane-strain flow stress, σ_0, of a metal is 200 MPa. A sheet 0.60 m wide and 3 mm thick is to be cold rolled to 2.4 mm in a single pass using 30 cm diameter rolls. Assuming a coefficient of friction is 0.075,

(a) Compute the roll pressure.
(b) If front tension of 75 MPa were applied, what would be the average roll pressure?

SOLUTION:

(a) Substituting $h = (3 + 2.4)/2 = 2.7$ mm and $L = \sqrt{(150 \times 0.6)} = 9.487$ mm into equation 7.36, $P_{av} = [2.7/(0.075)(9.487)][\exp(0.075)(9.487)/2.7](200) = 988$ MPa.
(b) $P_{av} = [2.7/(0.075)(9.487)][\exp(0.075)(9.487)/2.7](200 - 37.5) = 803$ MPa.

7.10 ROLL FLATTENING

With thin sheets and large roll diameters, the pressure from the friction hill can be very large, causing P_{av} to be very high. The roll separating force per width, $F_s = P_{av}L$, increases even more rapidly. The high separating force causes the roll surfaces to elastically flatten much as an automobile tire flattens under the weight of a car. The

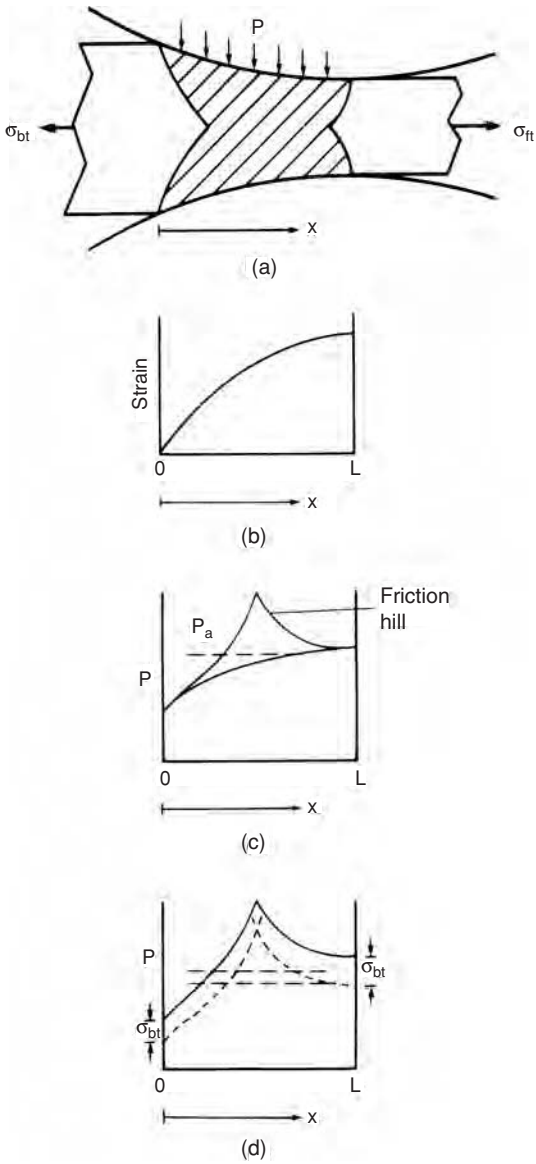

7.11. Roll gap (a) showing how the strain (b) and roll pressure (c) vary across the gap. The effect of front and back tension (d).

actual radius of contact, R', is larger than R as illustrated in Figure 7.12. Hitchcock* derived an approximate expression for R'

$$R' = R\left(1 + \frac{16F_s}{\pi E'\Delta h}\right), \tag{7.37}$$

where $E' = E/(1-\nu^2)$ and ν is Poisson's ratio. With $L = \sqrt{R'\Delta h}$ the roll separating force per unit length becomes

$$F_s = P_{av}\sqrt{R'\Delta h}, \tag{7.38}$$

* J. Hitchcock, "Roll neck bearings," *App. I ASME* (1935), pp. 286–96.

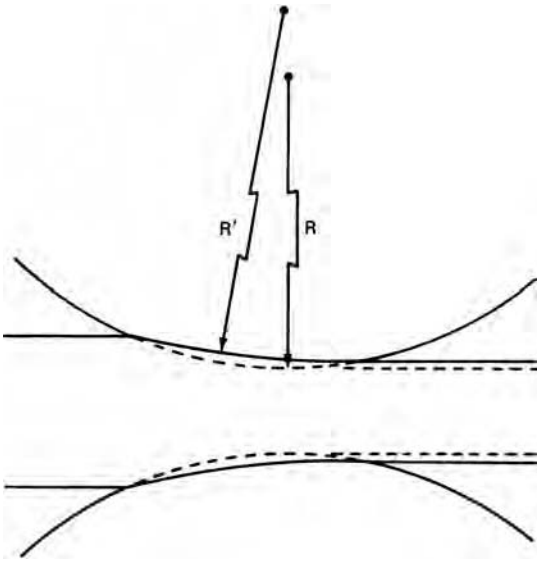

7.12. Roll flattening.

where

$$P_{av} = \frac{h}{\mu\sqrt{R'\Delta h}}[\exp(\mu\sqrt{R'\Delta h}/h) - 1](\sigma_0 - \sigma_t) \tag{7.39}$$

and $\sigma_t = (\sigma_{ft} + \sigma_{bt})/2$. The roll separating force, $F_s = P_{av}L$, may be written

$$F_s = \frac{h}{\mu}[\exp(\mu\sqrt{R'\Delta h}/h) - 1](\sigma_0 - \sigma_t), \text{ and} \tag{7.40}$$

$$P_{av} = \frac{h}{\mu\sqrt{R'\Delta h}}[\exp(\mu\sqrt{R'\Delta h}/h) - 1](\sigma_0 - \sigma_t). \tag{7.41}$$

The effect of roll flattening is to increase the roll separating force because both P_{av} and L increase. Both F_s and R' can be found by solving equations 7.38 and 7.40. Figure 7.13 is a plot of both equations for $\sigma_0 = 100{,}000$ lbs, $E' = 33 \times 10^6$ psi, $r = 5\%$, $R = 5$ in and $\mu = 0.2$. Initial thicknesses of $h_0 = 0.100,\ 0.040,$ and 0.020 in were assumed. The intersections give the appropriate values of F_s and R'. There is no intersection for $h_0 = 0.02$ because the roll flattening is so severe that that thickness cannot be achieved. There is a minimum thickness that can be rolled:

$$h_{min} = \frac{C\mu R}{E'}(\sigma_0 - \sigma_t), \tag{7.42}$$

where C is between 6 and 7.

With $C = 7$, and the conditions cited above, $h_{min} = 0.021$ in, which explains why there is no solution for $h_0 = 0.020$ in Figure 7.13.

Methods of achieving thinner sheets and foils include better lubrication (lower μ), application of back and front tension (σ_{bt} and σ_{ft}), lower σ_0 (achieved by annealing), and use of smaller diameter rolls. Small diameter rolls will bend under high separating forces. The use of back-up rolls lessens this effect. An example is the Sendzimer mill shown in Figure 7.14. Use of carbide rolls instead of steel rolls increases E'.

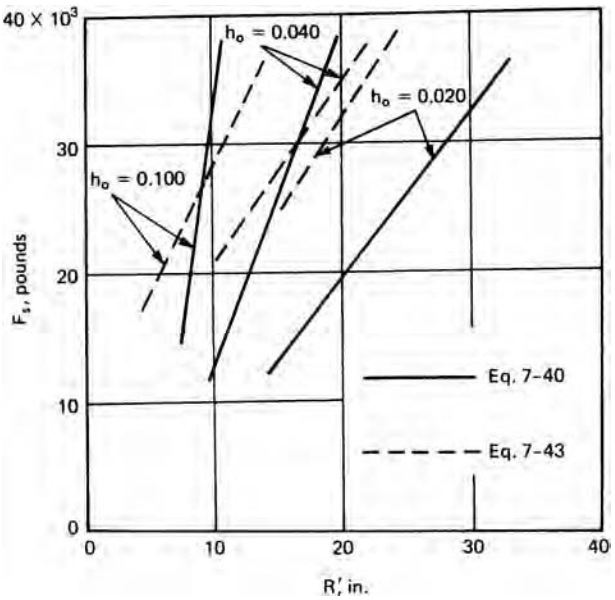

7.13. Variation of roll-separating force vs. R' (solid line) and dependence of flattened radius on roll-separating force (dashed line). A flow stress of 100 ksi was assumed. The intersections satisfy both conditions. Note that there is no solution for $h_0 = 0.02$ in.

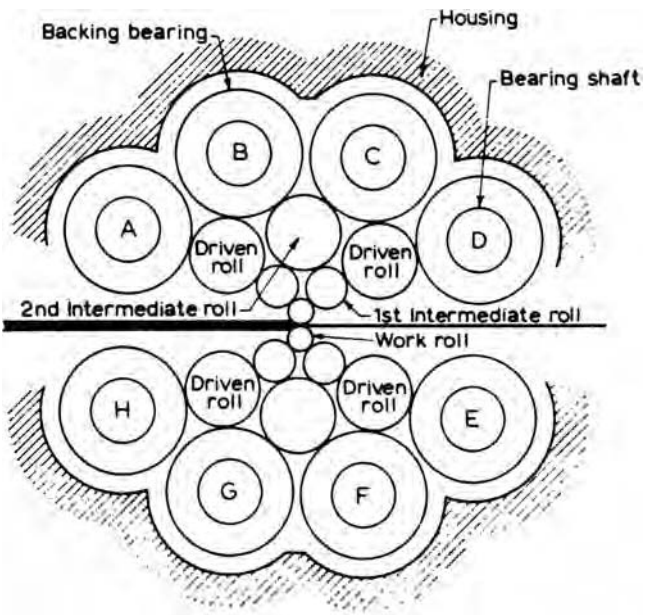

7.14. Sendzimir mill. Courtesy of T. Sendzimir Inc. and Loewy Robertson Engineering Co. Ltd., U.K.

EXAMPLE 7.6: A sheet of steel with a plane-strain yield strength of 500 MPa is cold rolled between 25 cm diameter rolls to a reduction of 5%. The plane-strain modulus $E' = 225$ GPa and the initial sheet thickness is 2.5 mm. The coefficient of friction is 0.15.

(a) Find the roll separating force of length of roll using equation 7.37.
(b) Repeat using equation 7.39.
(c) Compare with Figure 7.13.
(d) If σ_0 were 50 ksi, to what minimum thickness could the sheet be rolled on this mill?

SOLUTION:

(a) $R' = R(1 + \frac{16F_s}{\pi E' \Delta h})$ so $F_s = [(R'/R) - 1]\frac{\pi E' \Delta h}{16}$.

$$F_s = (2 - 1)\pi(33 \times 10^6 \times 0.005)/16 = 32{,}400 \text{ lb}.$$

(b) $F_s = 100{,}000(0.0975/0.15)\{\exp[0.15(10 \times 0.005)^{1/2}/0.975] - 1\} = 27{,}000$ lb.

(c) The left-hand pair of lines in Figure 7.13 intersect at $R' = 9$ in and $F_s = 26{,}000$ lb. Equation 7.34 predicts $F_s = 32{,}000$ lb at $R' = 10$ in as found in (a). Equation 7.37 predicts $F_s = 26{,}000$ lb at $R' = 9$ in as found in (b).

(d) Using equation 7.42 with $C = 7.5$, $h_{\min} = (7.5)(0.15)(9)(500 \times 10^6)/(225 \times 10^9) = 0.02$ in.

One way of circumventing equation 7.42 is to roll two sheets at the same time, artificially increasing $h_{\min}$. Aluminum foil is made by rolling two thin sheets together that are separated after the rolling. The shiny surface was in contact with the rolls and the matte surface was in contact with the other half of the foil.

7.11 ROLL BENDING

Roll bending would produce sheets with varying thickness. To counter this effect, rolls are usually cambered (crowned) as shown in Figure 7.15. The degree of cambering varies with the width of the sheet, the flow stress, and reduction per pass. The results of insufficient camber are shown in Figure 7.16. The thicker center requires the edges to be elongated more. This can cause edge wrinkling or warping of a plate. The center is left in residual tension and center cracking can occur.

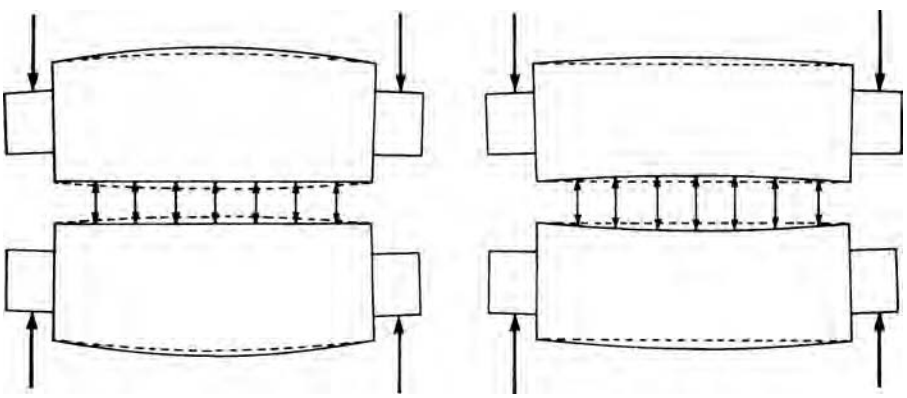

7.15. Use of cambered rolls to compensate for roll bending. Proper camber (left) and no camber (right).

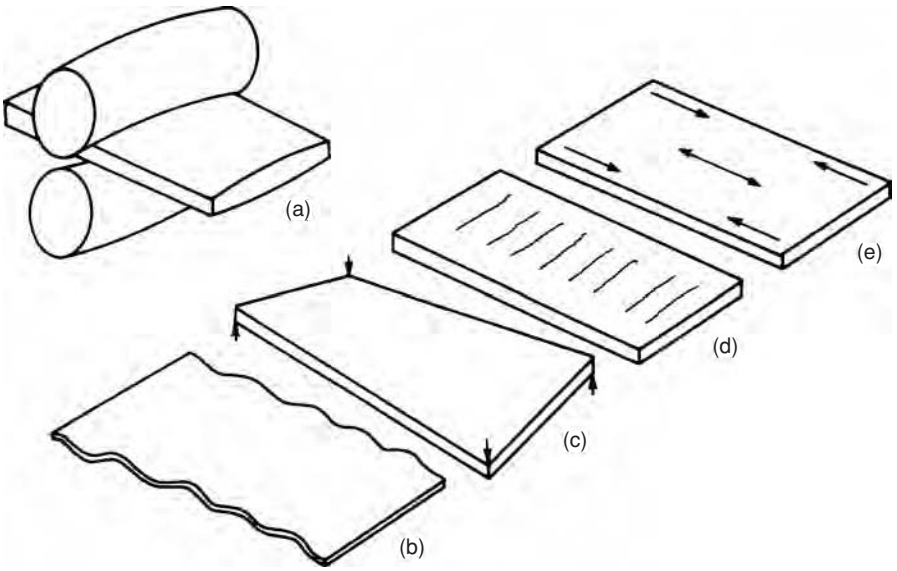

7.16. Possible effects of insufficient camber (a): edge wrinkling (b), warping (c), centerline cracking (d), and residual stresses (e).

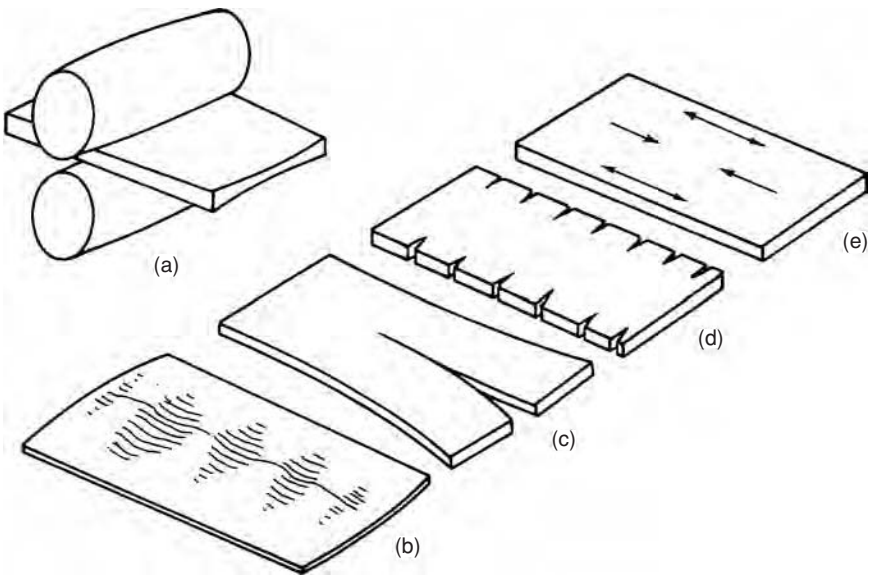

7.17. Effects of over-cambering (a): wavy center (b), centerline splitting (c), edge cracking (d), and residual stresses (e).

If the rolls are over-cambered, as shown in Figure 7.17, the residual stress pattern is the opposite. Centerline compression and edge tension may cause edge cracking, lengthwise splitting, and a wavy center.

There are large economic incentives for proper cambering in addition to assuring flatness and freedom from cracks. A variation of only ± 0.001 in in a sheet of 0.32-in thickness between center and edge is 3%. If a minimum thickness is required, some

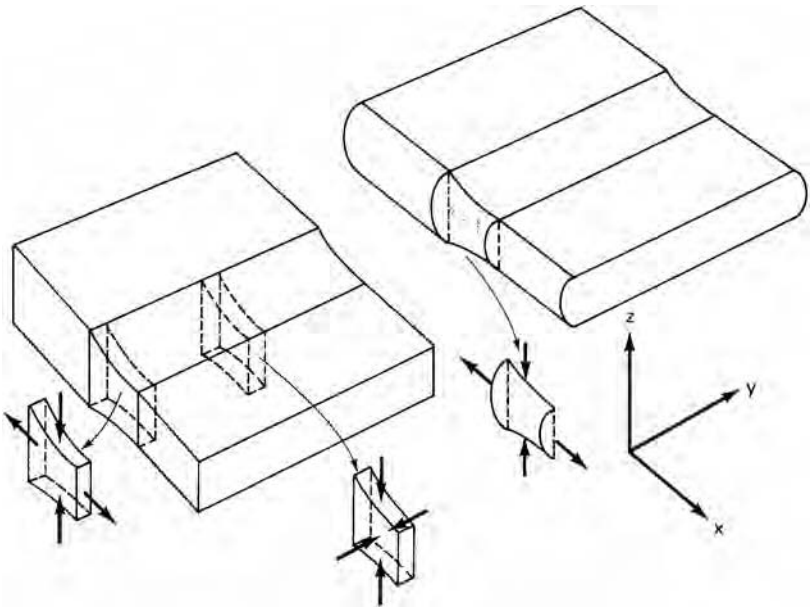

7.18. Stress states at the edge of a rolled strip. Edge cracking is more likely with rounded edges.

of the sheet will be thicker than necessary and either the supplier or the customer (depending on whether the sheet is sold by weight or area) will suffer an economic loss. Furthermore the formability will suffer from variable thickness as discussed in Chapter 15.

Even with proper cambering there is a tendency for edge cracking. Material just outside the roll gap constrains flow to plane-strain ($\varepsilon_y = 0$), except at the edges where plane-stress ($\sigma_y = 0$) prevails. Uniaxial compression at the edge would cause only half as much elongation as in the center but this isn't possible. Instead compatibility with the center requires that the edges experience tension in the rolling direction. This can cause edge cracking. The situation is aggravated if the edges become rounded as in Figure 7.18. With a bulged edge the material at the midplane experiences even less compression so the tensile stresses necessary for compatibility are even larger. In multiple-pass rolling it is common to use small edge rollers to maintain square edges. Figure 11.1 in Chapter 11 illustrates the greater formability when square edges are maintained.

7.12 COINING

Coining is a compression operation that embosses the compressed surface with a design. For the design to be embossed, the entire surface must be at its yield strength although the amount of reduction may be small. The pressure must be at least as high as the predictions of the equations in Section 7.6 with sticking friction. Forming a sharp detail is similar to making a hardness indentation. Since the pressure in hardness indentation is about three times the yield strength, the local pressure near a sharp detail in coining must be that high.

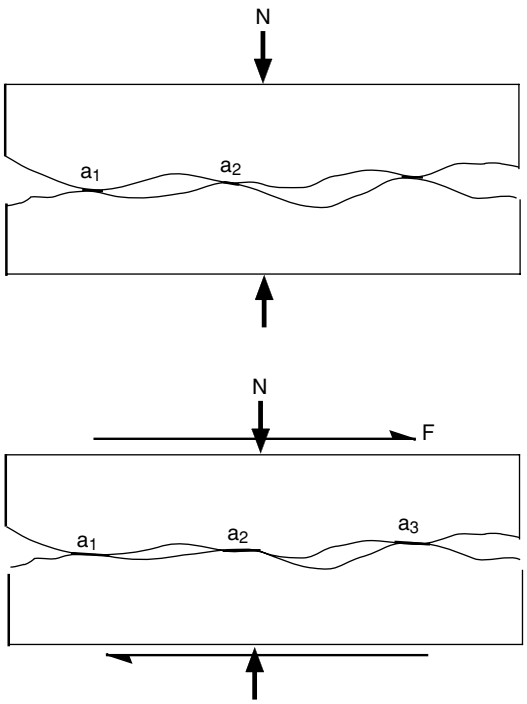

7.19. Under dry conditions, asperities on the opposing surfaces weld and must be sheared for sliding to occur.

7.13 DRY FRICTION

Friction during sliding of two materials depends on their interaction. On a microscopic scale, all surfaces are rough. Figure 7.19 shows two mating surfaces. The normal load, N, is carried by a few small areas of contact. As N increases the area of contact, A, increases:

$$N = HA, \tag{7.43}$$

where H is proportional to the hardness. The frictional force, F, is proportional to A, so

$$F = \tau A, \tag{7.44}$$

where τ is the shear stress strength of the interface. If there is actual welding, τ equals the shear strength of the softer material. Therefore the coefficient of friction, $\mu = F/N$, is given by

$$\mu = \tau / H. \tag{7.45}$$

If there is bulk deformation H must be about 2τ, so $\mu = {}^1/_2$.

7.14 LUBRICANTS

In addition to reducing friction, lubricants should reduce wear and keep metal forming operations cool. There are often other requirements as well. Lubricants for cans and other food containers must be safe. Lubricants for parts to be painted must be either removable or paint compatible. Once removed, lubricants should not pose health or environmental threats. Many lubricants are water based.

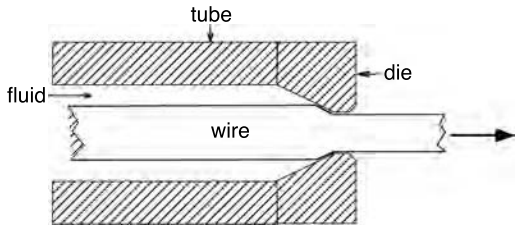

7.20. Hydrodynamic lubrication during wire drawing.

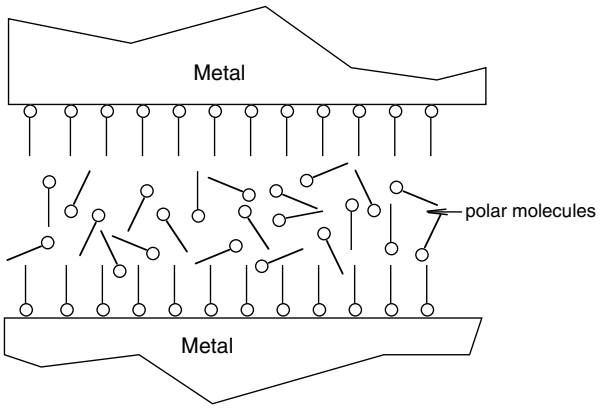

7.21. Boundary lubrication. Polar molecules react with the surface.

There are several types of lubrications. The lowest friction occurs with *hydrodynamic lubrication*. In this case the lubricant completely separates the two surfaces. Complete separation depends on both the sliding velocity and the viscosity. High speeds, high lubricant viscosities, and low normal forces promote hydrodynamic lubrication. Typical viscosities are water 0.01; light mineral oil 0.8; and heavy mineral oil 10 Poise. Figure 7.20 shows the use of hydrodynamic lubrication in wire drawing. The high velocity condition is lost during startup and shut down.

Boundary lubricants contain polar molecules, perhaps 250 nm in length. They are generally fatty acids such as stearic or oleic acid. One end of the molecule reacts with the metal surface to form a soap as shown in Figure 7.21.

Solid lubricants form easily sheared layers between work piece and tools. Soft, ductile solids such as lead, Teflon, or polyethylene between the work piece and tools are easily sheared. Graphite and molybdenum disulfide are other examples. Even tin and polymer coatings can act as solid lubricants.

Extreme pressure lubricants react with the surface of the work piece where other protective films have been broken. Chlorinated and fluorinated hydrocarbons react with the metal surface. However the use of these is severely limited by OSHA.

Steel surfaces may be phosphate coated to provide a better surface for lubricants. Molten glass may be used as a lubricant for hot extrusion.

7.15 EXPERIMENTAL FINDINGS

The experimental findings with respect to disc compression are in direct contrast to the predictions of Sections 7.8 and 7.10. It was predicted that there would be sliding friction at the periphery and sticking friction in the center. Measurements of local pressure made

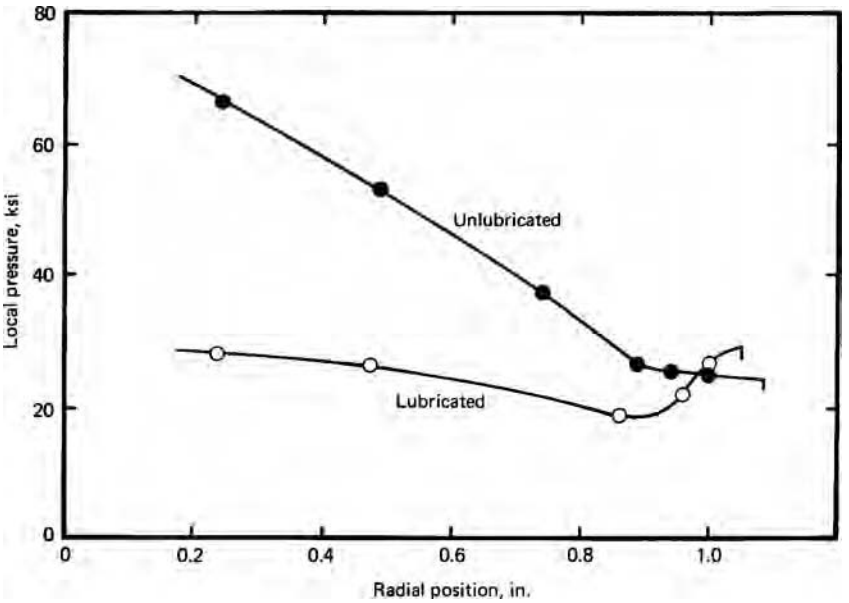

7.22. Variation of local pressure with radial position in disc compression with lubricated and unlubricated conditions at 3% compression. The data were taken from G. W. Pearsall and W. A. Backofen, *Trans. ASME*, 85B (1963), pp. 68–75.

by imbedding pressure-sensitive pins into the compression platens indicate sticking at the edges and sliding in the center. Figure 7.22 shows that P does increase with distance from the edge, but the slope dP/dx decreases, instead of increasing as sliding friction would predict, or remaining constant as sticking friction would predict.

The explanation for this is that early in the compression, lubricant at the edges runs out and the edge of the work piece makes contact with the platen and sticks to it. Lubricant is trapped in the central region so that the frictional shear forces are lower in the center than at the edge. As compression progresses, the side walls fold up onto the compression platen. Figure 7.23 clearly shows this.

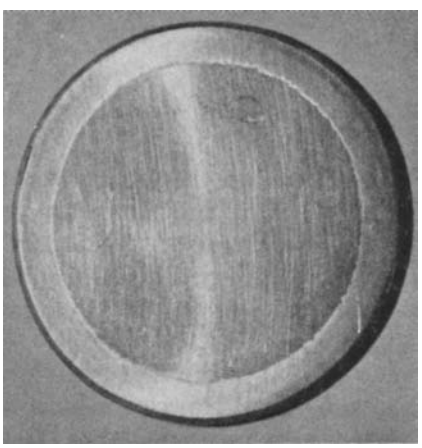

7.23. Surface appearance of an aluminum disc after compression. The outer ring was originally part of the sidewalls. Sticking friction occurred there. From W. Pearsall and W. A. Backofen, *op. cit*.

Even with sheets of plastic or soft metal used to create a low shear-stress interface, the edges of the work piece cut through the film at low strains. Thus for axially symmetric compression neither the assumption of a constant coefficient of friction nor constant shear-stress interface is correct.

7.16 RING FRICTION TEST

A simple test for friction in compression involves compressing a ring as shown in Figure 7.24. If there were no friction the inner diameter would increase by the same percentage as the outer diameter. With high friction, there is a no-slip location between the inner and outer diameters so the inner diameter must decrease during compression.

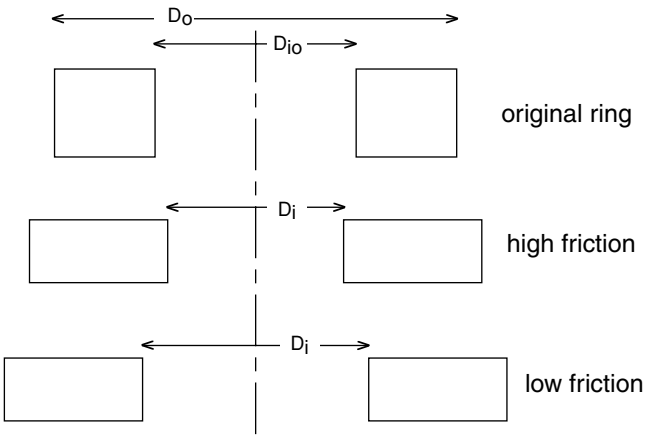

7.24. Ring compression test: original specimen (top); after compression with high friction (middle); and after compression with low friction (bottom).

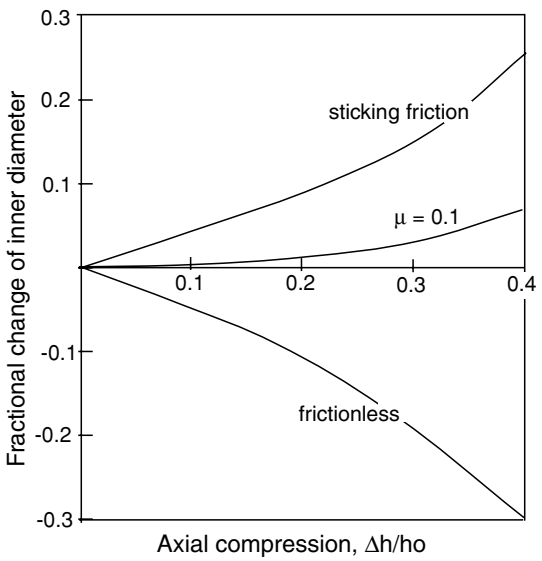

7.25. Inner diameter change calculated for a specimen and with an outer radius twice the inner radius and with a height 1.33 times as high as its inner radius. Data from J. B. Hawkyard and W. Johnson, *Int. J. Mech. Sci*, 17 (1967), pp. 163–182.

Figure 7.25 shows the change of inner diameter as a function of the friction coefficient for a ring with an outer diameter twice the inner diameter.

REFERENCES

W. Johnson and P. B. Mellor, *Plasticity for Mechanical Engineers*, Van Nostrand, 1973.
G. T. van Rooyen and W. A. Backofen, *J. Mech. Phys. Solids,* 7 (1959), pp. 163–68.

PROBLEMS

7.1. A coil of steel, 252 mm wide and 3 mm thick, is drawn though a pair of dies of semi-angle 8° to a final thickness of 2.4 mm in a single pass. The outlet speed is 3.5 m/s. The average yield strength is 700 MPa and the friction coefficient is 0.06. Calculate the power in kW consumed.

7.2. An efficiency of 65% was found in a rod-drawing experiment with a reduction of 0.2 and a semi-die angle of 6°.
- **a)** Using Sachs' analysis, find the coefficient of friction.
- **b)** Using the value of η found in (a), what value of efficiency should be predicted from the Sachs' analysis for $a = 6$ and $r = 0.4$?
- **c)** The actual value of η found for the conditions in (b) was 0.80. Explain.

7.3. Estimate the force required to coin a U.S. 25¢ piece. Assume that the mean flow stress is 30,000 psi, the diameter is 0.95 in, and the thickness after forming is 0.060 in.

7.4. Figure 7.26 shows a billet before and after hot forging from an initial size of 2.5 mm × 2.5 mm × 25 mm to 5 mm × 1.25 mm × 10 mm. This is accomplished by using a flat-face drop hammer. Sticking friction can be assumed. For the rate of deformation and the temperature, a flow stress of 18 MPa can be assumed.
- **a)** Find the *force* necessary.
- **b)** Find the *work* required. (Remember that work $= \int F \mathrm{d}L$ and that F changes with L.)

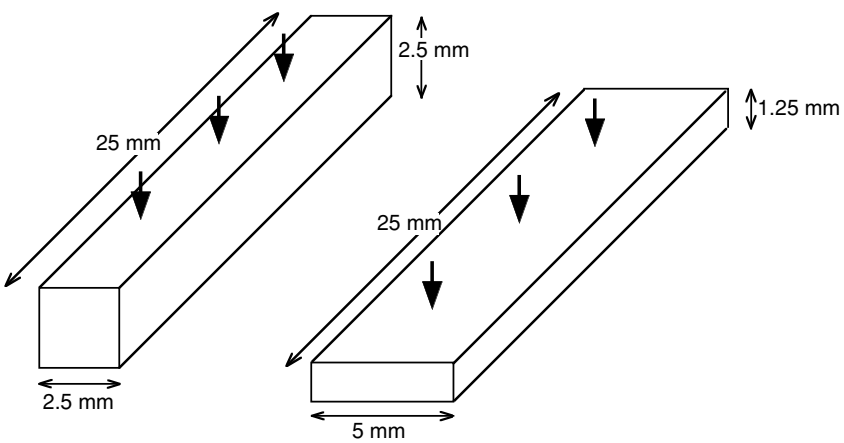

7.26. Compression in Problem 7.4.

c) From what height would the hammer have to be dropped?
d) Compute the efficiency, η.

7.5. Two steel plates are brazed as shown in Figure 7.27. The steel has a tensile yield strength of 70 MPa and the filler material has a tensile yield strength of 7 MPa. Assume that the bonds between the filler and the steel do not break. Determine the force necessary to cause yielding of the joint.

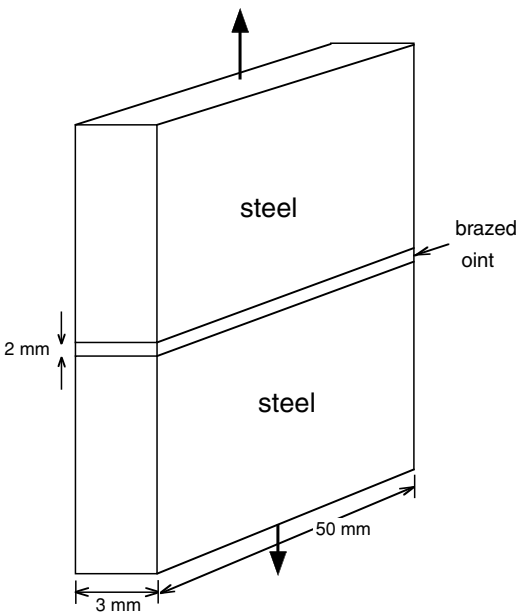

7.27. Brazed joint for Problem 7.5.

7.6. Figure 7.28 shows a thin lead ring being used as a gasket. To insure an acceptable seal the gasket must be compressed to a thickness of 0.25 mm. Assume that the flow stress of lead is 15 MPa and strain hardening is negligible. Find the required force.

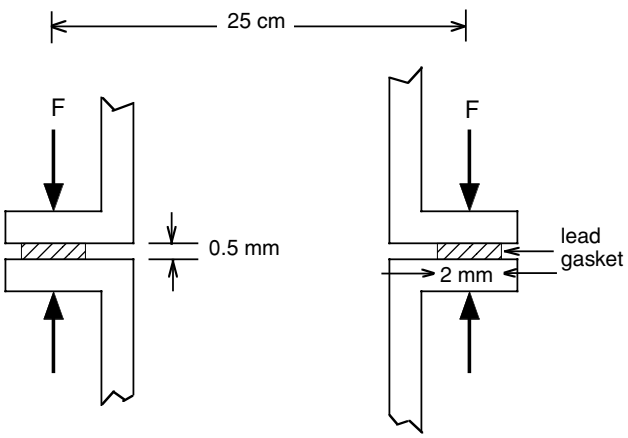

7.28. Lead gasket for Problem 7.6.

7.7. The derivation of equation 7.10 assumed a constant coefficient of friction. Derive an equivalent expression assuming sticking friction.

7.8. Magnetic permalloy tape is produced by roll flattening of drawn wire, as shown in Figure 7.29. The final cross section is 0.2 mm by 0.025 mm. It is physically possible to achieve this cross section with different rolling schedules. However, it has been found that the best magnetic properties result with a maximum amount of lateral spreading. For production the rolling direction must be parallel to the wire axis. Describe how you would vary each of the parameters below to achieve the maximum spreading:

a) roll diameter,
b) reduction per pass,
c) the friction,
d) back and front tension.

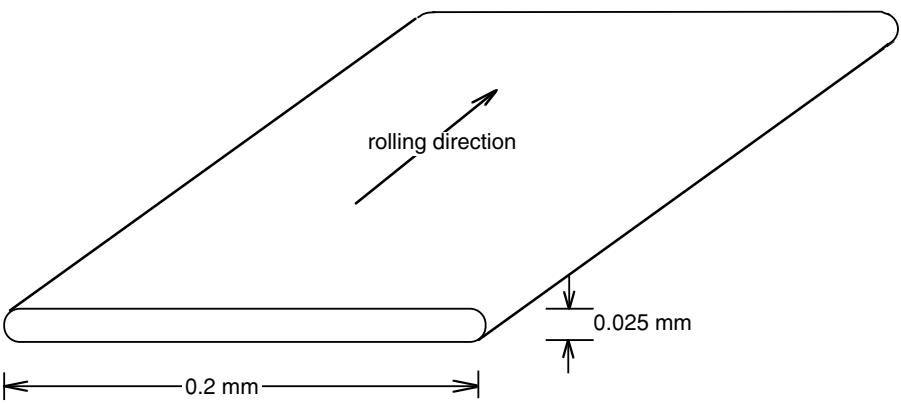

7.29. Permalloy tape (Problem 7.8).

7.9. A metal with a flow stress of 35 MPa is to be drawn from a diameter of 25 mm to 20 mm through a die of 15° semi-angle. Calculate the necessary drawing stress if

a) the conditions are frictionless,
b) there is sticking friction, and
c) $\mu = 0.20$.

7.10. Consider the rolling of a sheet 15 cm wide from a thickness of 1.8 mm to 1.2 mm in a single pass by steel rolls 20 cm in diameter. Assume a friction coefficient of 0.10 and a flow stress of 125 MPa.

a) Calculate the roll pressure if roll flattening is neglected.
b) Calculate the roll pressure taking into account roll flattening.
c) Estimate the minimum thickness that could be achieved.

7.11. Use equation 7.14 to predict how the ratio of w_f/w_i depends on μ, α and ε_h. (Realize that equation 7.14 neglects redundant work. Expand the exponential term after simplifying and assume that ε_h is small enough so higher order terms can be neglected.) Describe in words how w_i depends on μ, α and ε_h.

7.12. In the force balance in the slab analysis for frictional effects in plane-strain compression, P was assumed to be a principal stress, even though with finite friction it can't be. Examine this assumption by assuming a constant shear stress interface with $\tau = mk$, and derive an expression for the angle, θ, between the principal axis, 1, and the x-axis. Express your answer in terms of m, x, h, L, and $2k$. (Not all of these need be in the final expression.) See Figure 7.30.

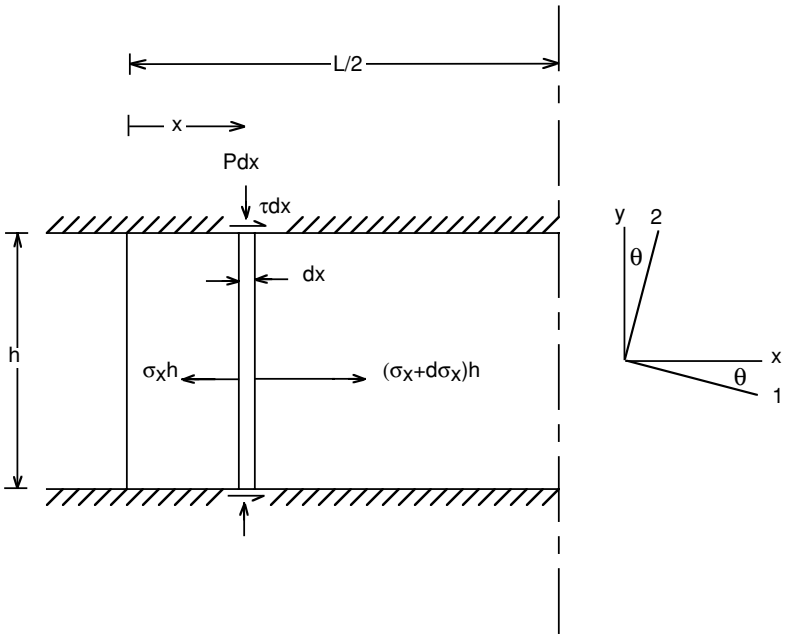

7.30. Sketch for Problem 7.12.

8 Upper-Bound Analysis

Calculation of exact forces to cause plastic deformation in metal forming processes is often difficult. Exact solutions must be both *statically* and *kinematically* admissible. That means they must be geometrically self-consistent as well as satisfying the required stress equilibrium everywhere in the deforming body. Frequently it is simpler to use limit theorems that allow one to make analyses that result in calculated forces that are known to be either correct or higher or lower than the exact solution.

Lower bounds are based on satisfying stress equilibrium, while ignoring geometric self-consistency. They give forces that are known to be either too low or correct. As such they can assure that a structure is "safe." Conditions in which $\eta = 0$ are lower bounds. Upper-bound analyses, on the other hand, predict stress or forces that are known to be too large. These are usually more important in metal forming. Upper bounds are based on satisfying yield criteria and geometric self-consistency. No attention is paid to satisfying equilibrium.

8.1 UPPER BOUNDS

The upper-bound theorem states that any estimate of the forces to deform a body made by equating the rate of internal energy dissipation to the external forces will equal or be greater than the correct force. The method of analysis is to

1. Assume an internal flow field that will produce the shape change;
2. Calculate the rate at which energy is consumed by this flow field; and
3. Calculate the external force by equating the rate of external work with the rate of internal energy consumption.

The flow field can be checked for consistency with a velocity vector diagram or *hodograph*. In the analysis, the following simplifying assumptions are usually made:

1. The material is homogeneous and isotropic.
2. There is no strain hardening.
3. Interfaces are either frictionless or sticking friction prevails.
4. Usually only two-dimensional (plane-strain) cases are considered with deformation occurring by shear on a few discrete planes. Everywhere else the material is rigid.

8.2 ENERGY DISSIPATION ON PLANE OF SHEAR

Figure 8.1(a) shows an element of rigid material, ABCD, moving at a velocity V_1 at an angle θ_1 to the horizontal. AD is parallel to yy'. When it passes through yy' it is forced to change direction and adopt a new velocity V_2 at an angle θ_2 to the horizontal. It is sheared into a new shape A′B′C′D′. The corresponding hodograph is shown in Figure 8.1(b). The absolute velocities V_1 and V_2 are drawn from the origin, O. Because this is a steady-state process, they both have the same horizontal component, V_x. The vector V_{12}^* is the difference between V_1 and V_2 and must be parallel to the line of shear, yy'.

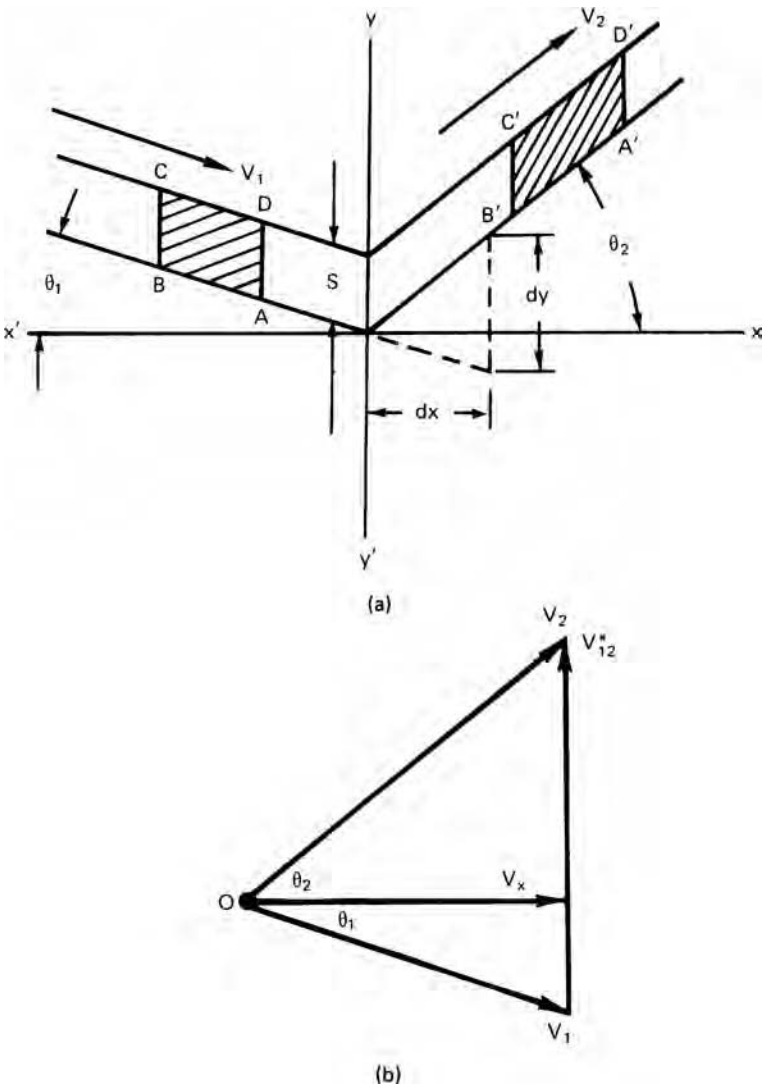

8.1. (a) Drawing for calculating energy dissipation on a velocity discontinuity and (b) the corresponding hodograph.

The rate of energy dissipation along the discontinuity equals the volume of material crossing the discontinuity per time, SV_x times the work per volume. The work per volume is $w = k\,\mathrm{d}y/\mathrm{d}x = kV_{12}^*/V_x$, so the rate of energy dissipation along the discontinuity is

$$\mathrm{d}W/\mathrm{d}t = (kV_{12}^*/V_x)SV_x = kSV_{12}^*. \tag{8.1}$$

For deformation fields with more than one shear discontinuity,

$$\mathrm{d}W/\mathrm{d}t = \sum_i kS_iV_i^*. \tag{8.2}$$

8.3 PLANE-STRAIN FRICTIONLESS EXTRUSION

Consider the plane-strain extrusion through frictionless dies as illustrated in Figure 8.2(a). Only half of the field is shown. There are two planes of discontinuity, AB and BC. The corresponding hodograph, Figure 8.2(b), is constructed by drawing horizontal

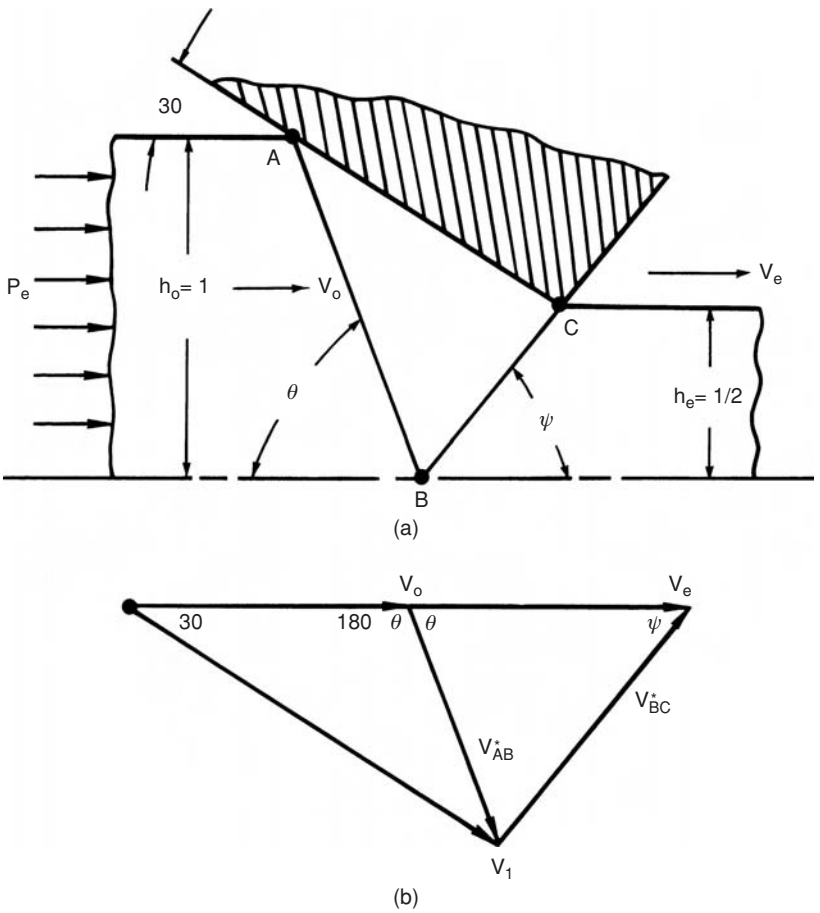

8.2. (a) Top half of an upper-bound field for plane-strain extrusion and (b) the corresponding hodograph.

vectors representing the initial velocity V_0 and the exit velocity V_e. Both start at the origin. The velocity in triangle ABC, V_1, is drawn parallel to AC; it also starts at the origin. The velocity discontinuity, V^*_{AB}, is the difference between V_0 and V_1, and V^*_{BC} is the difference between V_1 and V_e.

The rate of internal work is

$$dw/dt = k(V^*_{AB}\overline{AB} + V^*_{BC}\overline{BC}). \tag{8.3}$$

The rate of external work is $dw/dt = P_e h_0 V_0$. Equating and solving for $P_e/2k$,

$$P_e/2k = \frac{1}{2h_0V_0}(V^*_{AB}\overline{AB} + V^*_{BC}\overline{BC}). \tag{8.4}$$

Equation 8.4 may be evaluated physically by measuring V^*_{AB} and V^*_{BC} relative to V_0 on the hodograph and measuring $\overline{AB}$ and $\overline{BC}$ relative to V_0 on the physical field. However it is easier to evaluate $P_e/2k$ analytically.

$$h_0/\overline{AB} = \sin\theta, \quad h_0/\overline{BC} = \sin\psi.$$

For a 50% reduction with a half die angle of 30°, with the law of sines,

$$V^*_{AB}/\sin 30^\circ = V_0/\sin(\theta - 30^\circ) \quad \text{or} \quad V^*_{AB}/V_0 = \sin 30^\circ/\sin(\theta - 30^\circ) \quad \text{and}$$
$$V^*_{BC}/\sin\theta = V^*_{AB}/\sin\psi \quad \text{so} \quad V^*_{BC}/V_0 = (\sin\theta/\sin\psi)V^*_{AB}/V_0.$$

The magnitude of $P_{ext}/2k$ depends on θ. If $\theta = 90^\circ$, $V^*_{AB}/V_0 = \sin 30^\circ/\sin(90^\circ - 30^\circ) = 0.577$, and $\psi = 30^\circ$. $V^*_{BC}/V_0 = (\sin 90^\circ/\sin 30^\circ)0.577 = 1.154$, $\overline{AB} = \overline{BC} = h_0$. Therefore $P_{ext}/2k = (0.577 + 1.154)/2 = 0.866$.

Figure 8.3 shows the calculated variation of $P_e/2k$ with θ. The lowest value of $P_e/2k \approx 0.78$ occurs when $\theta \approx 72^\circ$. A lower bound can be found as $P_e = \int \sigma\, d\varepsilon = 2k\ln(2)$ so $P_e/2k = 0.693$. The true solution of $P_e/2k = 0.762$ (see Chapter 9) lies between these.

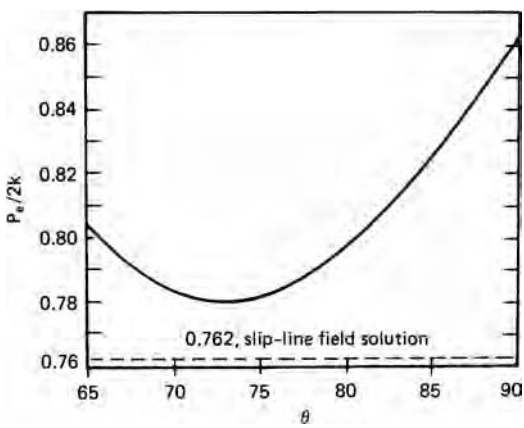

8.3. Variation of calculated extrusion pressure with the angle θ in the upper-bound field of Figure 8.2.

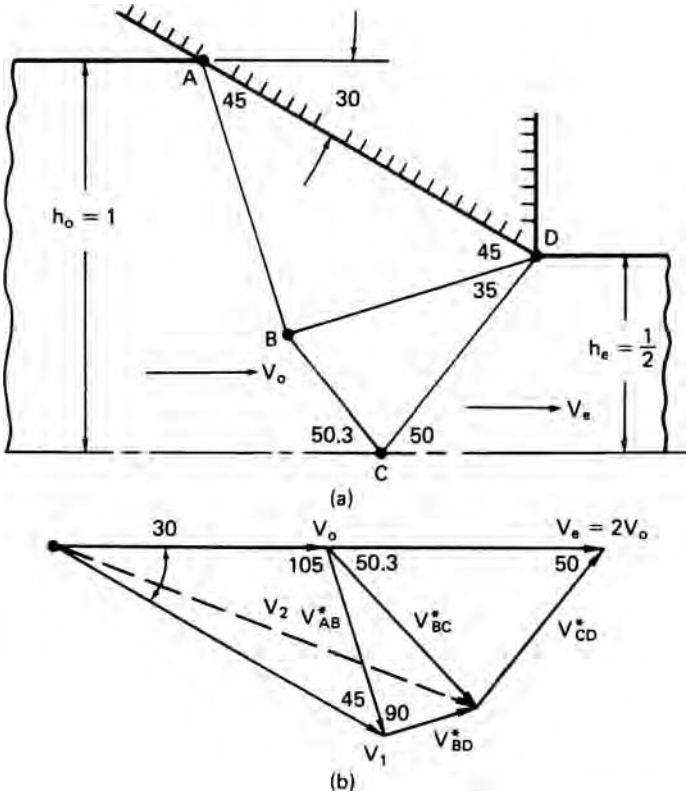

8.4. A two-triangle upper-bound field (a) for plane-strain extrusion and the corresponding hodograph (b).

It is not essential to assume frictionless conditions. If sticking friction is assumed along AC, an additional term, $k(V_1/V_0)(\overline{AC}/h_0)$, must be added to the upper bound so

$$P_e/2k = (1/2)(V_1\overline{AC} + V^*_{AB}\overline{AB} + V^*_{BC}\overline{BC})/(V_0h_0) \quad \text{or}$$
$$P_e/2k = (P_e/2k)_{\text{frictionless}} + (1/2)(V_1/V_0)(\overline{AC}/h_0). \tag{8.5}$$

A plot of $P_e/2k$ vs. θ in equation 8.5 has a minimum of $P_e/2k \approx 1.43$ at $\theta \approx 83^\circ$. If a shear stress mk is assumed along AC, $(1/2)(V_1/V_0)(\overline{AC}/h_0)$ in equation 8.5 is replaced by $m(V_1/V_0)(\overline{AC}/h_0)$.

More complex fields may give lower values of $P_e/2k$. Figure 8.4 shows a field composed of two triangles and the corresponding hodograph. With frictionless conditions on AD, this field gives $P_e/2k = 0.768$, which is close to the exact solution.

The distortion of the extruded slab predicted by a proposed field can be found by following several points through the field.

EXAMPLE 8.1: Construct the distortion of a vertical grid line in Figure 8.5.

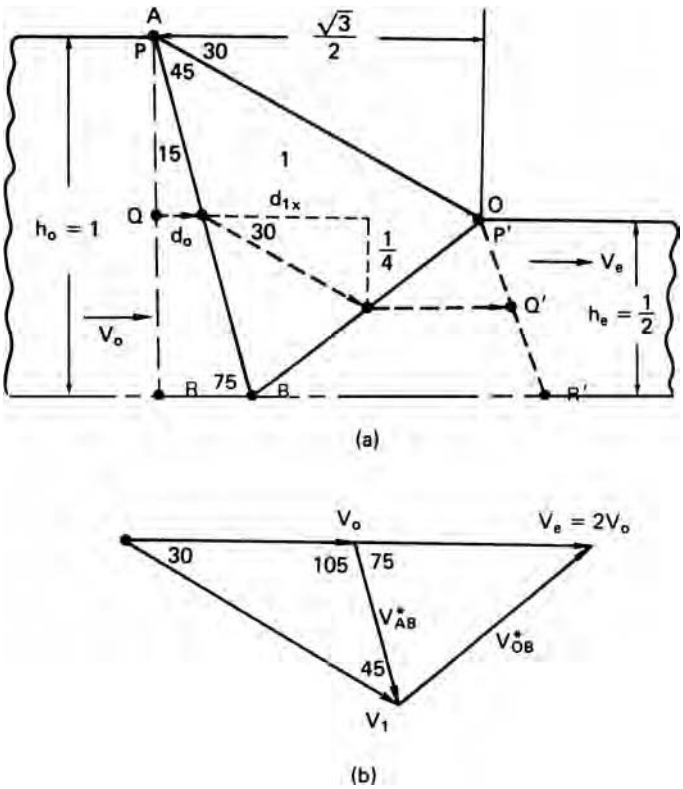

8.5. Single triangle upper-bound field (a) and hodograph (b) used for analyzing grid distortion in extrusion.

SOLUTION: For point P, $d_0 = 0$, $d_{1x} = \sqrt{3}/2 = 0.866$. $V_{1x} = (\cos 30^\circ)(\sin 105^\circ)V_0/\sin 45^\circ = 1.183$. Choosing the time increment t as the time for point P to arrive at P′, $t = 0.866/1.183 = 0.732$.

For point Q, $d_0 = (1/2)\tan 15^\circ = 0.134$. $t_0 = 0.134/1 = 0.134$.

$d_{1x} = (1/2)\sqrt{3}/2 = 0.433$, $t_{1x} = 0.433/1.183 = 0.366$.

$t_e = t - t_0 - t_{1x} = 0.732 - 0.134 - 0.366 = 0.232$.

$d_e = 2(0.232) = 0.464$.

$d_1 = 0.134 + 0.366 + 0.464 = 0.964$.

For point R, $d_0 = \tan 15^\circ = 0.268$, $t_0 = 0.268$, $d_{1x} = 0$.

$t_e = t - t_0 - t_{1x} = 0.732 - 0.268 - 0 = 0.464$.

$d_e = 2(0.464) = 0.928$, $d_1 = 0.268 + 0 + 0.928 = 0.464$.

These points are constructed on Figure 8.5 as points P′, Q′, and R′.

Now consider Figure 8.6, which shows a two-triangle field for the same reduction. Particles crossing AB pass through two constant velocity fields, whereas particles crossing BC pass through only one.

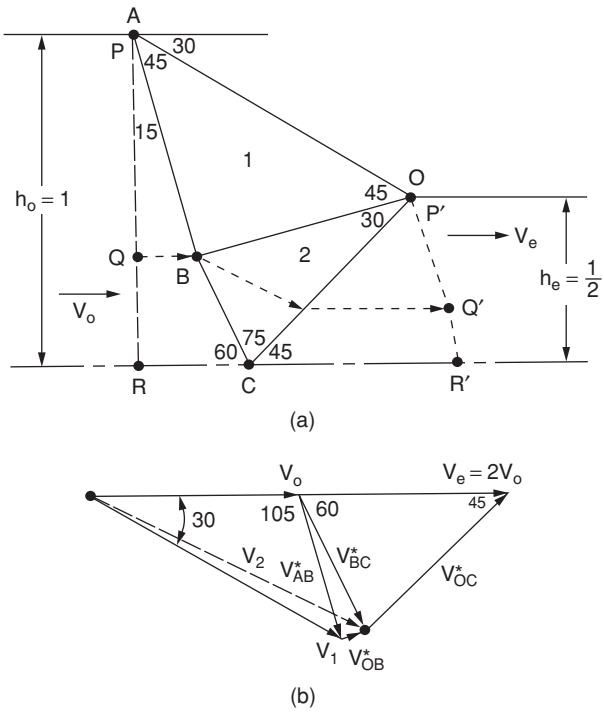

8.6. A two-triangle field (a) and a hodograph (b) for analyzing the distortion of a grid.

8.4 PLANE-STRAIN FRICTIONLESS INDENTATION

Figure 8.7 is a possible upper-bound field and corresponding hodograph for plane-strain frictionless indentation. Considering the right-hand side of the field, we see that shear occurs along AB, BC and CD. The metal outside the triangles is rigid. From the hodograph, the velocity discontinuities $V^*_{OA} = V^*_{AB} = V^*_{AC} = V^*_{BC} = V^*_{CD} = 1/(\cos 30^\circ) = 1.155$. The length of lines $\overline{OA} = \overline{AB} = \overline{AC} = \overline{BC} = \overline{CD} = w/2$, so

$$dW/dt = k(\overline{OA}V^*_{OA} + \overline{AB}V^*_{AB} + \overline{AC}V^*_{AC} + \overline{BC}V^*_{BC} + \overline{CD}V^*_{CD})$$

$$\text{or} \quad dW/dt = 5k(w/2)(2/\sqrt{3}).$$

The rate at which external energy is expended on the right-hand half of the field is

$$P_\perp/2k = 5/\sqrt{3} = 2.89. \tag{8.6}$$

If there is sticking friction along OB, $P_\perp/2k = 6/\sqrt{3} = 3.46 P_\perp/2k = 6/\sqrt{3} = 3.46$.

8.5 PLANE-STRAIN COMPRESSION

An upper-bound analysis of plane strain can be made with the field shown in Figure 8.8. Discrete shear occurs along OA, OB, OC, and OD. The lengths of these discontinuities

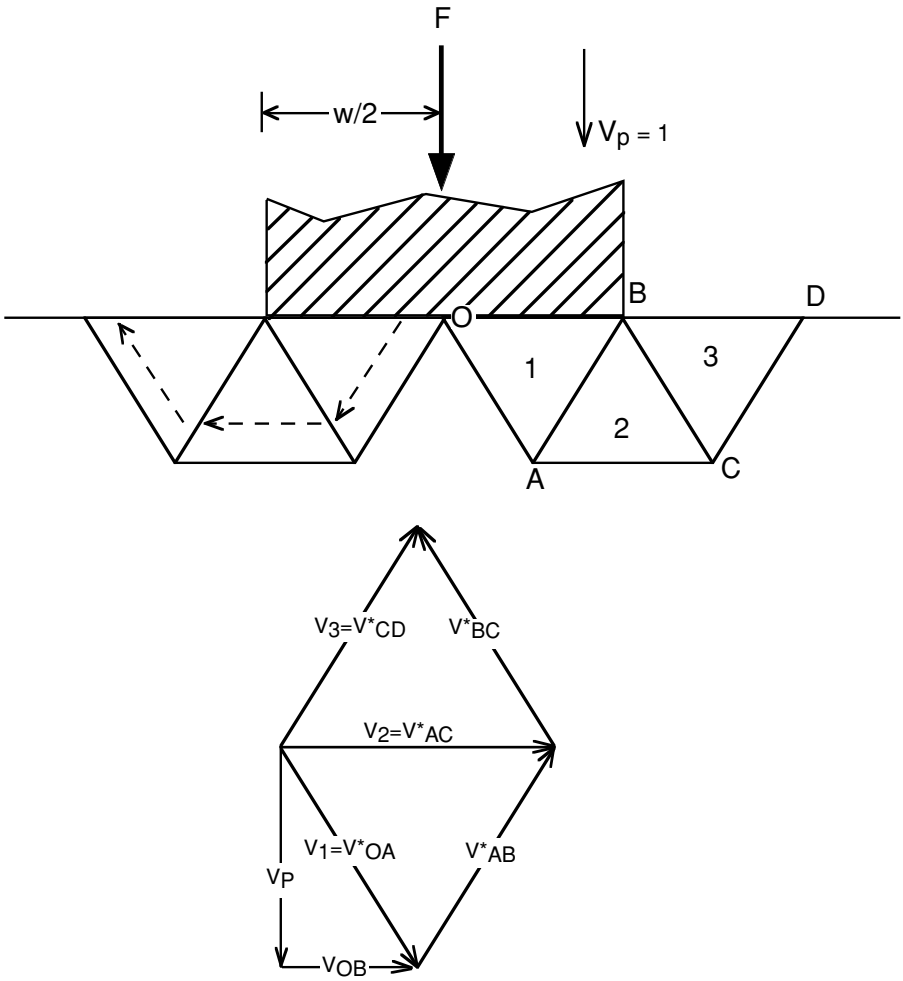

8.7. An upper-bound field for plane-strain, frictionless indentation (a) and the hodograph for the right-hand side of the field (b). The triangles are equilateral so the angles are 60°.

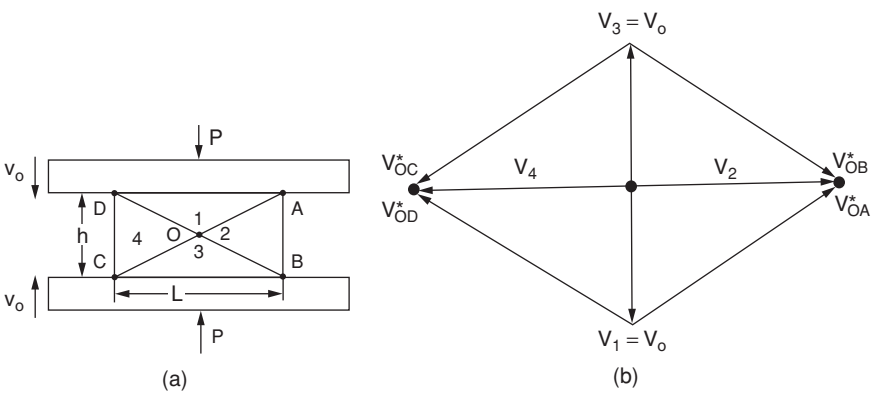

8.8. A possible field for plane-strain compression (a) and the corresponding hodograph (b). From R. M. Caddell and W. F. Hosford, *Int. J. Mech. Eng. Educ.*, 8 (1980). Reprinted by permission of the Council of the Institute for Mechanical Engineers.

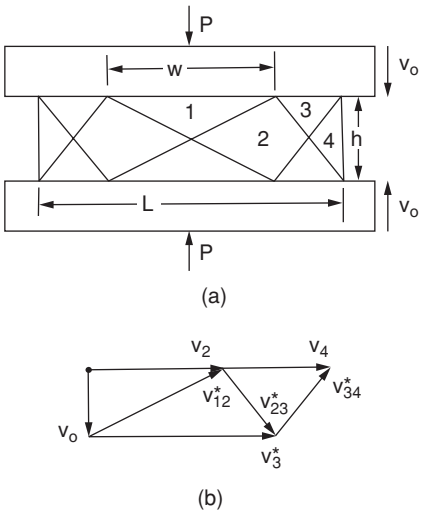

8.9. A different upper-bound field for plane-strain compression (a) and the corresponding hodograph for the upper right-hand quarter (b). From R. M. Caddell and W. F. Hosford, *op. cit.*

equal $2\overline{AO} = (h^2 + L^2)^{1/2}$ and the velocity discontinuity along them is $V^*_{\mathrm{AO}} = V_0(h^2 + L^2)^{1/2}/h$ so $2P_\perp L V_0 = 4k\overline{AO}V^*_{\mathrm{AO}}$. Substituting,

$$P_\perp/2k = (h/L + L/h)/2. \tag{8.7}$$

For large values of L/h, fields consisting of more than one triangle give better solutions. If there is friction, the lowest solutions have an odd number of triangles, because the middle triangle does not slide. The field in Figure 8.9 has three triangles. The general solution for this field is

$$P/2k = 3h/(2L) + L/(2h) + w^2/(2hL) - w/(2h). \tag{8.8}$$

The lowest value of $P/2k$ occurs when $w = L/2$ and is

$$P/2k = 3h/(2L) + 3L/(8h). \tag{8.9}$$

A field consisting of five triangles is shown in Figure 8.10. If $\overline{AB} = \overline{BC}$, the lowest solution occurs when $w = L/3$ and is

$$P/2k = 5h/(2L) + L/(3h). \tag{8.10}$$

A general minimum solution for this class of upper bounds is

$$P/2k = \left(\frac{1}{hL}\right)\left[\frac{nh^2}{2} + C\left(\frac{L}{n+1}\right)^2\right], \tag{8.11}$$

where $C = \frac{3n+1}{2} + \sum_{i=1}^{(n-1)/2}(2i - 1)$ and the number of triangles, n, is an odd integer ≥ 3. The minimum occurs when $w = 2L/(n + 1)$.

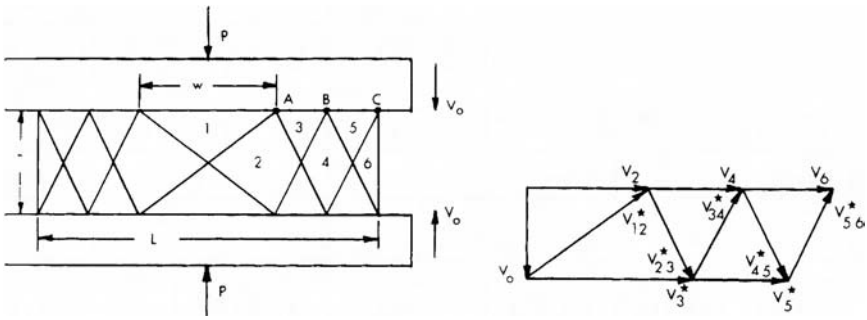

(a) (b)

8.10. A five-triangle upper-bound field for plane-strain compression (a) and the corresponding hodograph (b) for the upper right-hand quarter. From R. M. Caddell and W. F. Hosford, *op. cit.*

8.6 ANOTHER APPROACH TO UPPER BOUNDS

Other deformation fields can be used for upper bounds as long as they are kinematically admissible. An acceptable field may contain regions undergoing homogeneous deformation. For example, consider a slab analysis of plane-strain compression as shown in Figure 8.11. Each element is assumed to deform homogeneously as it slides away from the centerline. The rate of homogeneous work on an element is $2k\dot{\varepsilon}h\,dx$. Substituting $\dot{\varepsilon} = 2V_0/h$, the homogeneous work rate is $\dot{W} = 4kV_0\,dx$.

The velocity of the elements in admissible velocity field is

$$V_x = 2V_0x/h, \tag{8.12}$$

so the rate of energy dissipation on both tool–work-piece interfaces is

$$2kV_x dx = 4kV_0(x/h)\,dx. \tag{8.13}$$

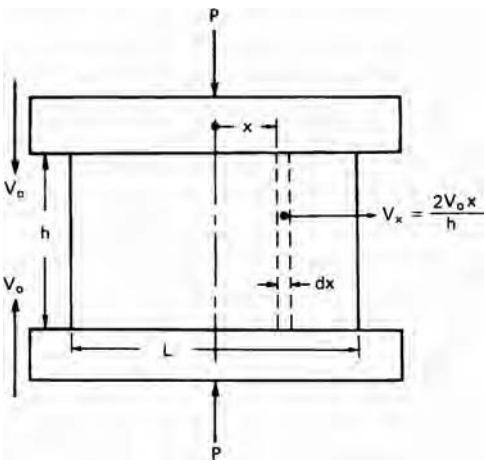

8.11. Drawing for a slab energy-balance upper bound of plane-strain compression.

Equating the external work rate, $2PLV_0$, with the interface and homogeneous work rate,

$$2PLV_0 = 2\int_0^{L/2} 4kV_0(1 + x/h)\,dx,$$

or

$$P/2k = 1 + L/(4h). \tag{8.14}$$

This is identical to the solution obtained by the slab analysis, where b in equation 7.20 is the same as L here. With a constant interfacial stress mk,

$$P/2k = 1 + mL/(4h). \tag{8.15}$$

A similar upper-bound slab analysis for axisymmetric compression with a constant interfacial stress gives

$$P/2k = \sigma_0/2k + mR/(3h), \tag{8.16}$$

which is identical to equation 7.32 if m is taken as unity.

8.7 COMBINED UPPER-BOUND ANALYSIS

The traditional upper-bound and slab-energy analyses can be combined to take advantage of the dead-metal cap. Figure 8.12 shows such a field along with the hodograph for the upper right-hand quarter of the field. The central region is a simple upper-bound field of width w, while the rest of the material undergoes homogeneous deformation. The rate of energy dissipation along OA, OB, OC, and OD is $\dot{W}_c = 2kV_0(h^2 + w^2)/h$.

Energy is also dissipated along AD and GH. The velocity discontinuity here varies with the distance z from the centerline, $V^*_{23} = 2zV_0/h$, so the total rate of energy dissipation on AD and GH is

$$\dot{W}_{23} = 4\int_0^{h/2} kV^*_{23}\,dz = khV_0.$$

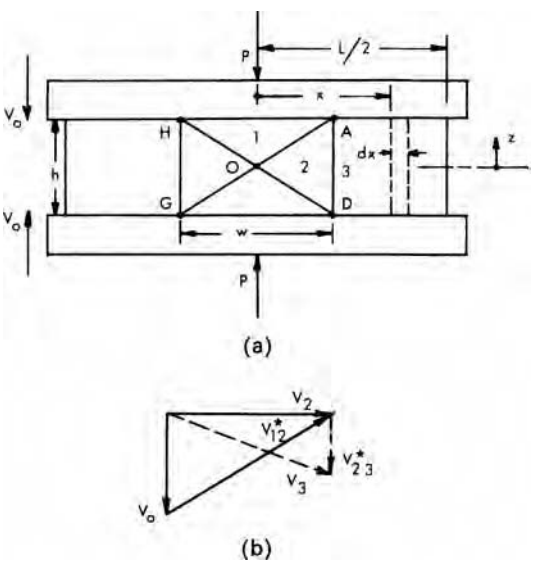

8.12. Combined conventional upper-bound and slab-energy fields for sticking friction (left) and partial hodograph (right). From R. M. Caddell and W. F. Hosford.

In the region $x > w/2$, the velocity V_x equals $2V_0x/h$, so the rate of frictional work is

$$\dot{W}_f = 4\int_{w/2}^{L/2} kV_x\,dx = kV_0(L^2 - w^2)/h. \tag{8.17}$$

The strain rate in the region between $w/2 \le x \le L/2$ is $\dot{\varepsilon} = 2V_0/h$, so the rate of homogeneous work is

$$\dot{W}_h = 2k\dot{\varepsilon}(L - w)h = 4kV_0(L - w). \tag{8.18}$$

Equating the internal work with the rate of external work, $2PLV_0$, $2PLV_0 = \dot{W}_c + \dot{W}_{23} + \dot{W}_f + \dot{W}_h$ or

$$P/2k = 1 + 3h/(4L) + L/(4h) - w/L + w^2/(4hL). \tag{8.19}$$

The minimum occurs if $w = 2h$ so

$$P/2k = 1 + (L/h - h/L)/4. \tag{8.20}$$

8.8 PLANE-STRAIN DRAWING

Figure 8.13 shows the streamlines and hodograph $\dot{W}_a = \dot{W}_h + \dot{W}_f + \dot{W}_r$ for plane-strain drawing of a sheet through a die of semi-angle α. All paths are horizontal before crossing AA′ and after crossing BB′. All particles on a vertical line such as CC′ have the same horizontal component of velocity, V_x, but V_x increases from AA′ to BB′. When a particle crosses AA′ it suffers a velocity discontinuity, V_A^*, which depends on the distance y from the centerline. At the outer surface $(y = t/2)$, $V_A^* = V_0 \tan\alpha$, and at the centerline, $V_A^* = 0$. At other points, $V_A^* = V_0 y \tan\alpha/(t_0/2)$.

The rate of work along this discontinuity is

$$\dot{W}_r = 2\int_0^{t/2} \frac{kV_0 \tan\alpha}{(t_0/2)} y\,dy = kV_0t_0 \tan\alpha/2. \tag{8.21}$$

The rate of sliding along the die is $V_s = V_x/\cos\alpha = V_0t_0/(t\cos\alpha)$. The rate of frictional work is then

$$\dot{W}_f = \int_{t_f}^{t_0} \frac{mkV_0t_0}{\cos\alpha\sin\alpha}(dt/t) = \frac{mkV_0t_0\varepsilon}{\cos\alpha\sin\alpha}, \tag{8.22}$$

where $\varepsilon = \ln(t_0/t_f)$.The external work rate is $\dot{W}_a = \sigma_d V_f t_f = \sigma_d V_0 t_0$. Equating external and internal work rates, $\dot{W}_a = \dot{W}_h + \dot{W}_f + \dot{W}_r$, and simplifying,

$$\sigma_d/2k = (1 + m/\sin 2\alpha)\varepsilon + (1/2)\tan\alpha. \tag{8.23}$$

This can be interpreted as $\sigma_d = w_h + w_f + w_r$ where $w_h/2k = \varepsilon$, $w_f/2k = m\varepsilon/\sin 2\alpha$, and $w_r/2k = (1/2)\tan\alpha$.

The force balance produces equation 8.23 without the $(1/2)\tan\alpha$ term if μP in equation 7.1 is replaced by mk.

8.9 AXISYMMETRIC DRAWING

Consider drawing a rod of diameter D_0 to a diameter D_f through a die of semi-angle α with a constant interface shear stress, mk. For a slab of radius R, the horizontal

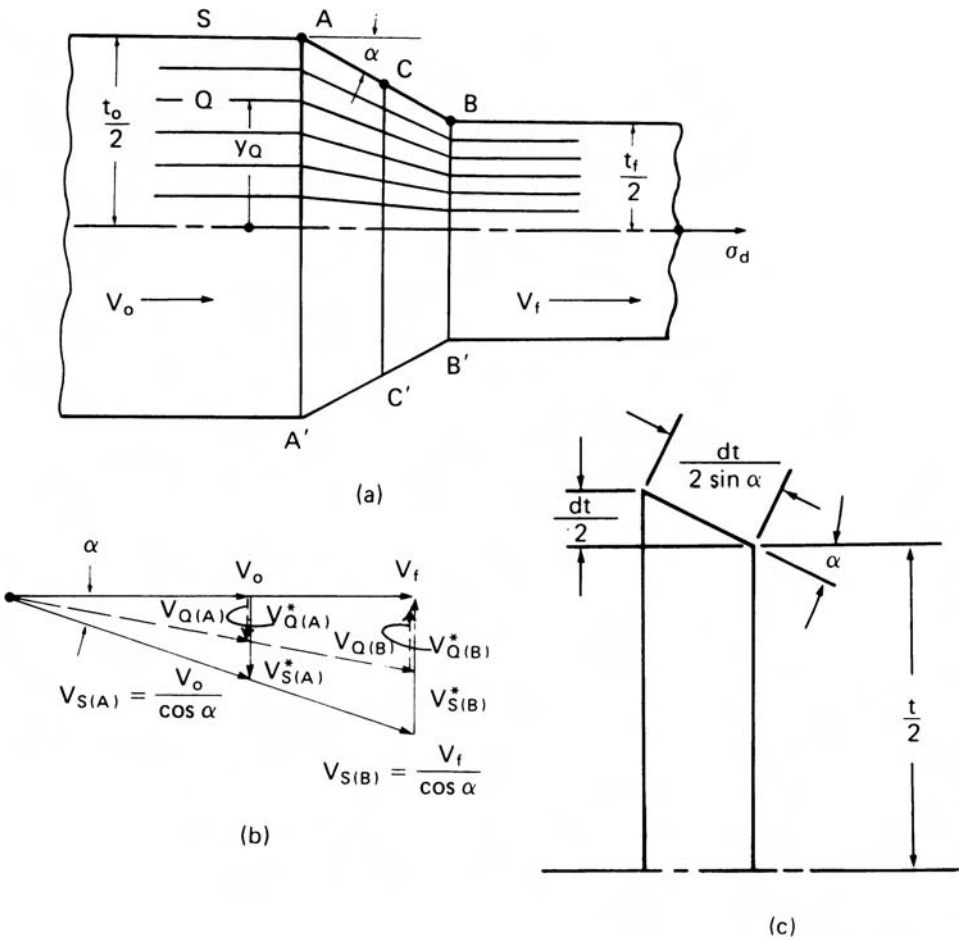

8.13. Plane-strain drawing. (a) Flow lines, (b) partial hodograph, and (c) a differential element.

component of velocity is $V_x = V_0(R_0/R)^2$ so the sliding velocity at the interface is $V_x = V_0(R_0/R)^2/\cos\alpha$. The area of the element in contact with the die is $2\pi R\,\mathrm{d}R/\sin\alpha$ and the interface stress is, substituting $\sin\alpha\cos\alpha = (1/2)\sin 2\alpha$ and $\ln R_0/R_\mathrm{f} = \varepsilon/2$,

$$\dot{W}_\mathrm{f} = \int_{R_\mathrm{f}}^{R_0} \frac{2\pi mkR_0^2V_0}{R\sin\alpha\cos\alpha}\,\mathrm{d}R = 2\pi mkR_0^2V_0\varepsilon/\sin 2\alpha. \tag{8.24}$$

The velocity discontinuity, $V_\mathrm{r}^* = V_0(r/R_0)\tan\alpha$, on entering the field depends on the radial distance, r, so the rate of energy dissipation is

$$\dot{W}_\mathrm{r} = \int_0^{R_0} 2\pi rkV_0(r/R_0)\tan\alpha\,\mathrm{d}r = (2/3)\pi kV_0R_0^2\tan\alpha. \tag{8.25}$$

The homogeneous work rate is

$$\dot{W}_\mathrm{h} = (\sigma_\mathrm{d}/2k)R_\mathrm{f}^2V_\mathrm{f} = (\sigma_\mathrm{d}/2k)R_0^2V_0. \tag{8.26}$$

Equating the rates of external and internal work,

$$\sigma_\mathrm{d}/2k = (\sigma_0/2k + m/\sin 2\alpha)\varepsilon + (2/3)\tan\alpha. \tag{8.27}$$

Again this is equal to the slab analysis that produced equation 8.27 without the redundant work term, (2/3)tan α. Other kinematically admissible fields may be analyzed. Avitzur derived an upper bound for axisymmetric drawing that predicts slightly lower drawing stresses than equation 8.27. His velocity field is more complex and the difference between his prediction and equation 8.27 is small.

REFERENCES

B. Avitzur, *Metal Forming: Processes and Analysis*, McGraw-Hill, 1968.
C. R. Calladine, *Engineering Plasticity*, Pergamon Press, 1969.
W. Johnson and P. B. Mellor, *Engineering Plasticity*, Van Nostrand Reinhold, 1973.

PROBLEMS

8.1. Find $P_e/2k$ for Figure 8.2 if θ is 80° and compare with Figure 8.3.

8.2. Calculate $P_e/2k$ for the plane-strain frictionless extrusion illustrated in Figure 8.14. Triangles ABC and CDE are equilateral.

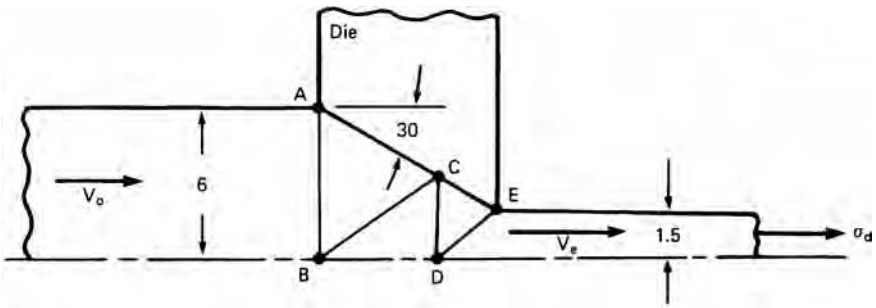

8.14. Upper-bound field for plane-strain drawing for Problem 8.2.

8.3. On which discontinuity in Figure 8.14 is the largest amount of energy expended?

8.4. Draw the hodograph corresponding to the frictionless indentation illustrated in Figure 8.15.

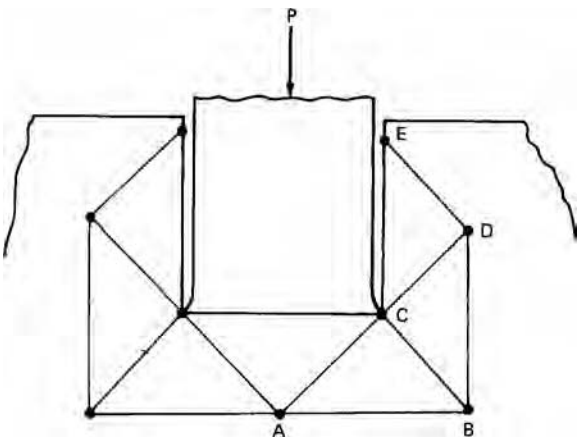

8.15. Upper-bound field for indentation for Problem 8.4.

8.5. For the plane-strain compression illustrated in Figure 8.16, calculate $P_e/2k$ for L/H values of 1, 2, 3, and 4. Assume sticking friction.

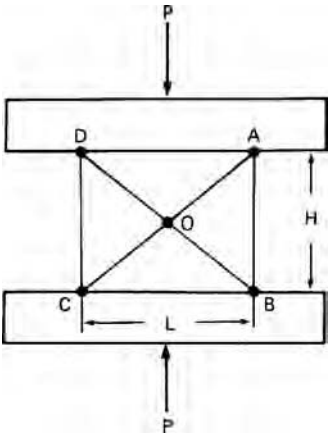

8.16. Upper-bound field for plane-strain compression for Problem 8.5.

8.6. Reanalyze Problem 8.4 if frictionless conditions prevailed.

8.7. For the indentation shown in Figure 8.7, $P_e/2k = 2.89$ if all the angles were 60°. Find $P_e/2k$ if the angles OAB, ABC, and BCD are 90° and the other angles are 45°.

8.8. Figure 8.17 shows an upper-bound field for a plane-strain extrusion. There are two dead metal zones ADB and FEG.

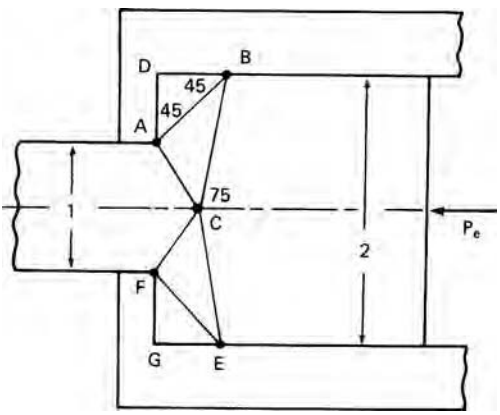

8.17. Upper-bound field for Problem 8.8.

a) Calculate $P_e/2k$ for the field.
b) Determine the velocity inside triangle ABC.
c) Determine V^*_{AC}.
d) Compute the deformation efficiency.

8.9. **a)** Use equation 8.27 to find the drawing stress, σ_d, for an axisymmetric rod drawing (Figure 8.18) with reduction of 30%, a semi-die angle of 10°, and a constant interfacial shear stress of 0.1k. Assume the Tresca criterion.

b) Predict σ_d using the von Mises criterion.

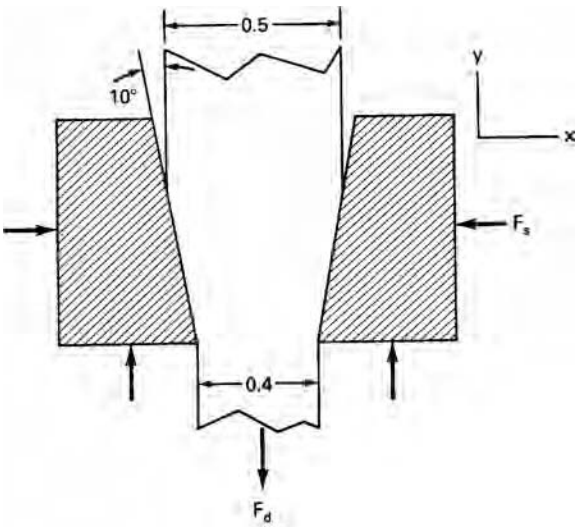

8.18. Illustration of axisymmetric drawing for Problem 8.9.

8.10. Consider the upper-bound field in Figure 8.19 for an asymmetric extrusion.

a) Draw the corresponding hodograph.

b) Determine the angle θ.

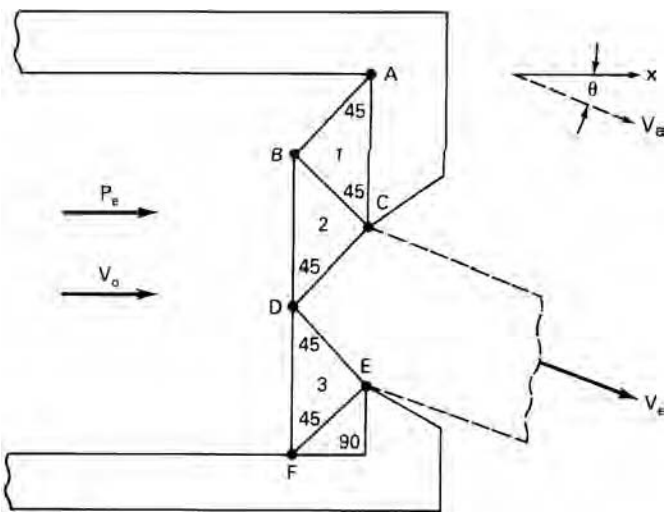

8.19. Illustration of an asymmetric plane-strain drawing for Problem 8.10.

8.11. For the plane-strain compression illustrated in Figure 8.20, calculate $P_e/2k$ for L/h values of 1, 2, 3, and 4. Assume sticking friction.

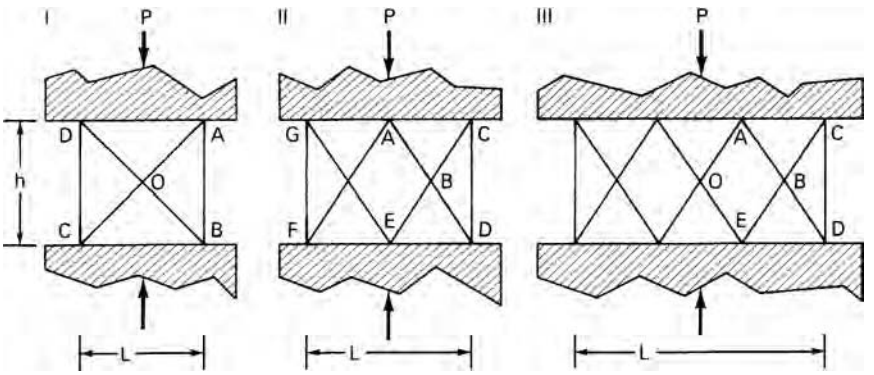

8.20. Upper-bound fields for plane-strain compression in Problem 8.11.

8.12. A proposed upper-bound field for extrusion is shown in Figure 8.21. Draw a hodograph to scale and determine the absolute velocity of particles in the triangle BCD.

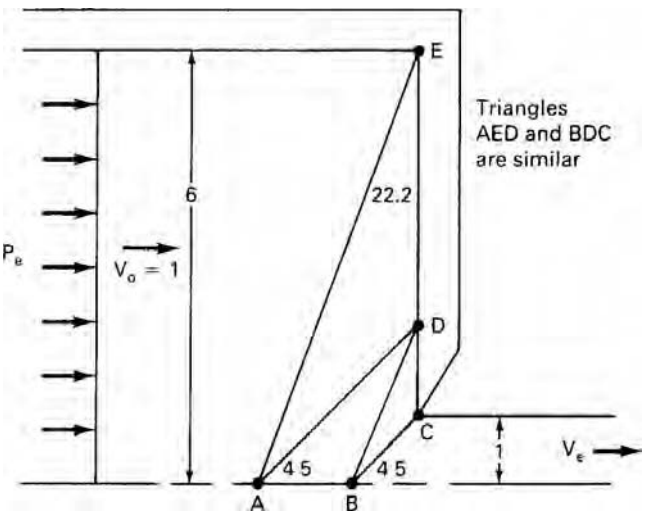

8.21. Upper-bound field for the plane strain extrusion of Problem 8.12.

8.13. Consider the plane-strain indentation illustrated in Figure 8.22. Assume that the deformation in region AA′B′B is homogeneous. There are discontinuities along AA′ and BB′.

a) Write an expression for $V^*_{AA'}$ and $V^*_{BB'}$ in terms of V^0, z, and t.

b) What is the ratio of the energy expended on these discontinuities to the homogeneous work?

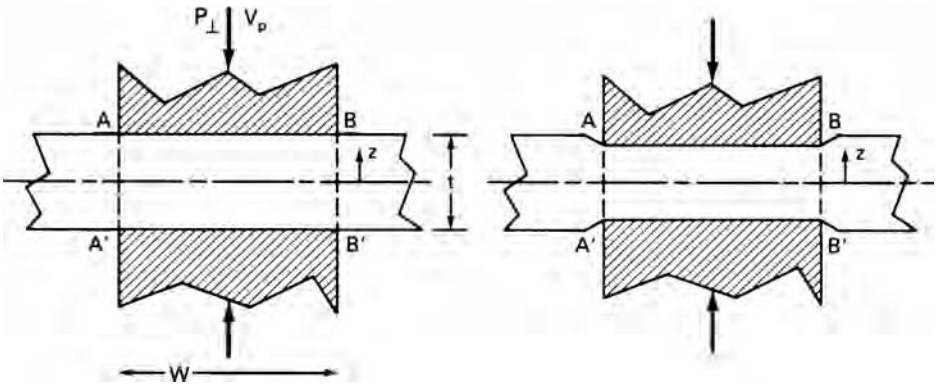

8.22. Figure for Problem 8.13.

8.14. Figure 8.23 shows two different upper-bound fields for a 2:1 reduction by extrusion. Regions ABC and EFG are dead-metal zones.

a) Calculate $P_e/2k$ for both fields.

b) Determine the deformation efficiency, η, for both cases.

c) What is the absolute velocity of a particle in triangle JGH?

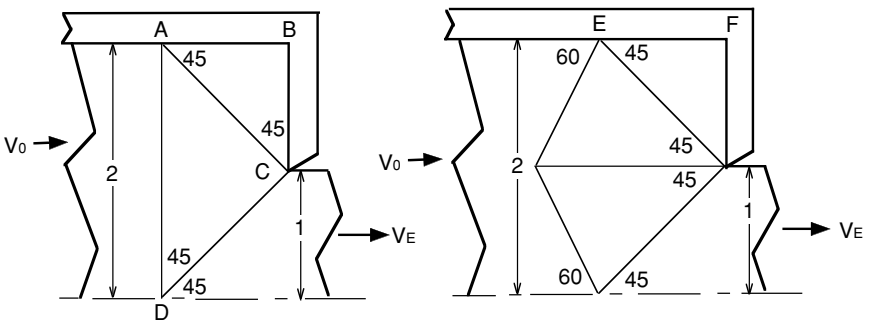

8.23. Two proposed upper-bound fields for a plane-strain extrusion with a 50% reduction for Problem 8.14.

9 Slip-Line Field Analysis

9.1 INTRODUCTION

Slip-line field theory is based on analysis of a deformation field that is both geometrically self-consistent and statically admissible. Slip lines* are planes of maximum shear stress and are therefore oriented at 45° to the axes of principal stress. It is assumed that

1. the material is isotropic and homogeneous,
2. the material is rigid – ideally plastic (i.e., no strain hardening),
3. effects of temperature and strain rate are ignored,
4. plane-strain deformation prevails, and
5. the shear stresses at interfaces are constant: usually frictionless or sticking friction.

Figure 9.1 shows the very simple slip line for indentation where the thickness, t, equals the width of the indenter, b. The maximum shear stress occurs on line DEB and CEA. The material in triangles DAE and CEB is rigid. As the indenters move closer together the field must change. However, for now, we are concerned with calculating the force when the geometry is as shown. The stress σ_y must be zero because there is no restraint to lateral movement. The stress σ_z must be intermediate between σ_x and σ_y. Figure 9.2 shows the Mohr's circle for this condition. The compressive stress necessary for this indentation is $\sigma_x = -2k$. Few slip-line fields are composed of only straight lines. More complicated fields will be considered.

9.2 GOVERNING STRESS EQUATIONS

With plane strain, all of the flow is in the x–y plane. This means that $d\varepsilon_y = -d\varepsilon_x$ and $d\varepsilon_z = 0$ so $\sigma_z = \sigma_2 = (\sigma_x + \sigma_y)/2$. Therefore according to the von Mises criterion, σ_z is always the mean or hydrostatic stress.

$$\sigma_2 = (\sigma_1 + \sigma_2 + \sigma_3)/3 = \sigma_{\text{mean}} \tag{9.1}$$

* The term *slip lines* used here should not be confused with the microscopic slip lines found on the surface of crystals.

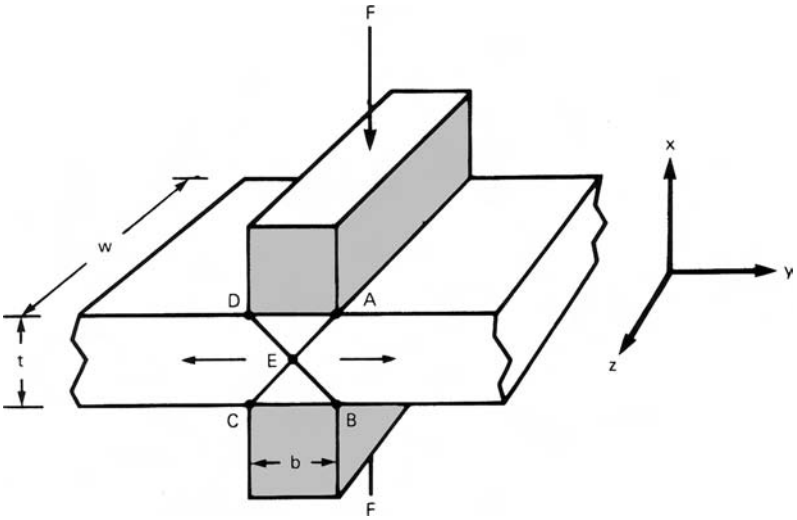

9.1. A slip-line field for frictionless plane-strain indentation.

and

$$\sigma_1 = \sigma_2 + k, \quad \sigma_3 = \sigma_2 - k. \tag{9.2}$$

Thus plane-strain deformation can be considered as pure shear with a superimposed hydrostatic stress, σ_2.

Planes of maximum shear stress are mutually perpendicular. The projections of these planes form a series of orthogonal lines called slip lines. Figure 9.3 illustrates a section of a field of slip lines. The shear stress acting on these lines is k, while the mean stress, σ_2, acts perpendicular to the slip lines. The slip lines are rotated at some angle ϕ to the x and y axes.

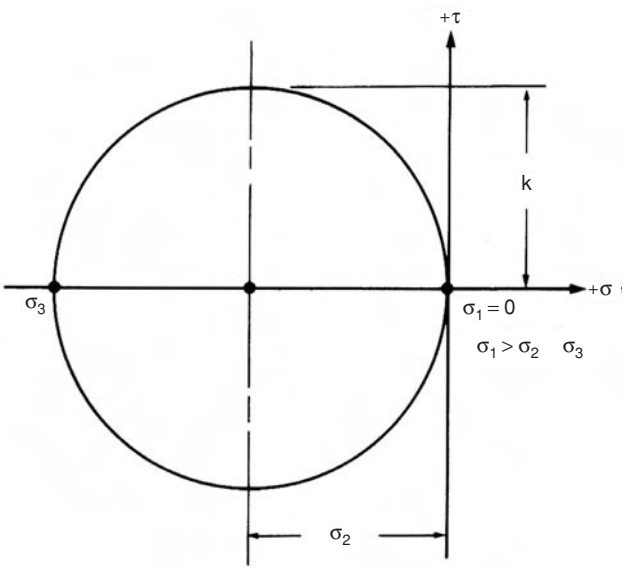

9.2. Mohr's stress circle for frictionless plane-strain indentation in Figure 9.1.

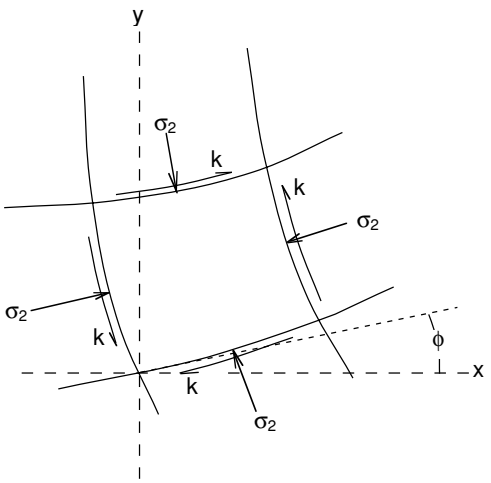

9.3. Stresses acting on a curvilinear element.

To develop the necessary equations it is necessary to adopt a convention for slip-line identification. The families of slip lines are labeled either α and β. The convention is that the largest principal stress (most tensile) lies in the first quadrant formed by α and β lines as illustrated in Figure 9.4. If all of the stresses are compressive, the least negative is σ_1.

For plane strain, τ_{xy} and τ_{zx} are zero, so the equilibrium equations (equation 1.40) reduce to

$$\begin{aligned} \partial\sigma_x/\partial x + \partial\tau_{yx}/\partial y &= 0 \\ \text{and}\quad \partial\sigma_y/\partial y + \partial\tau_{xy}/\partial x &= 0. \end{aligned} \tag{9.3}$$

From the Mohr's stress circle diagram, Figure 9.5,

$$\begin{aligned} \sigma_x &= \sigma_2 - k\sin 2\phi, \\ \sigma_y &= \sigma_2 + k\sin 2\phi, \\ \tau_{xy} &= k\cos 2\phi. \end{aligned} \tag{9.4}$$

Differentiating equations 9.4 and substituting into equations 9.3,

$$\begin{aligned} \partial\sigma_2/\partial x - 2k\cos 2\phi\ \partial\phi/\partial x - 2k\sin 2\phi\ \partial\phi/\partial y &= 0 \\ \partial\sigma_2/\partial y + 2k\cos 2\phi\ \partial\phi/\partial y - 2k\sin 2\phi\ \partial\phi/\partial x &= 0. \end{aligned} \tag{9.5}$$

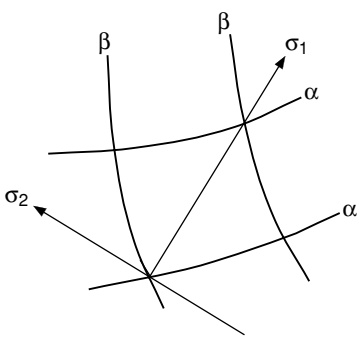

9.4. The 1-axis lies in the first quadrant formed by the α- and β-lines.

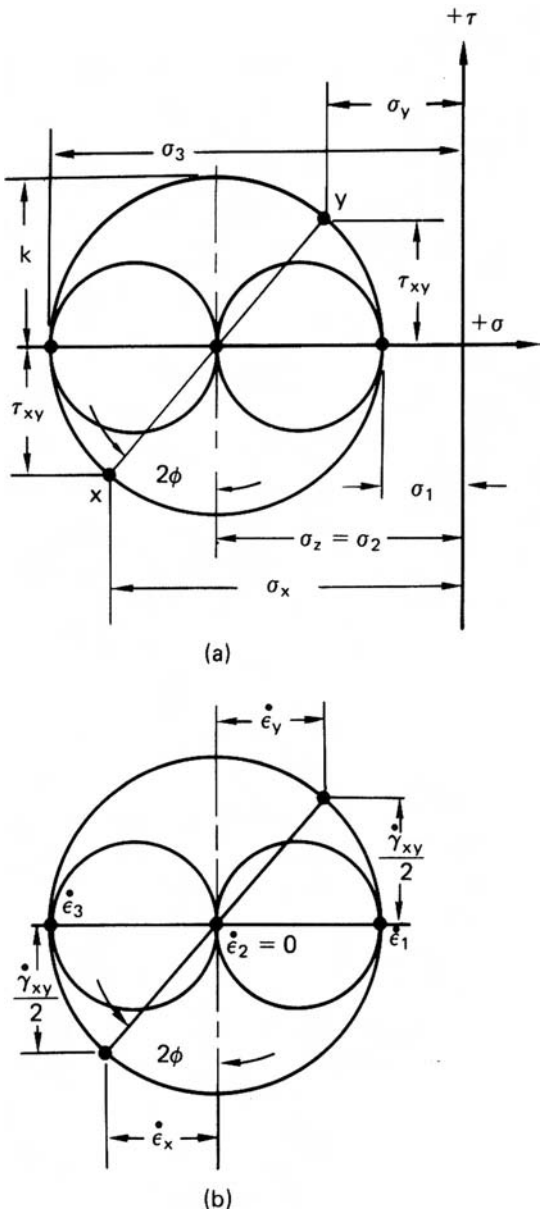

9.5. (a) Mohr's stress and (b) strain-rate circle for plane strain.

A set of axes x' and y' can be oriented so that they are tangent to the α and β lines at the origin. In that case, $\phi = 0$, so equations 9.5 reduce to

$$\begin{aligned} \partial\sigma_2/\partial x' - 2k\partial\phi/\partial x' &= 0 \\ \text{and}\quad \partial\sigma_2/\partial y' + 2k\partial\phi/\partial y' &= 0. \end{aligned} \tag{9.6}$$

Integrating,

$$\begin{aligned} \sigma_2 &= -2k\phi + C_1 \text{ along an } \alpha\text{-line} \\ \text{and}\quad \sigma_2 &= 2k\phi + C_2 \text{ along a } \beta\text{-line.} \end{aligned} \tag{9.7}$$

Physically this means that moving along an α-line or β-line causes σ_2 to change by

$$\begin{aligned} \Delta\sigma_2 &= 2k\Delta\phi \text{ along an } \alpha\text{-line} \\ \text{and } \Delta\sigma_2 &= -2k\Delta\phi \text{ along a } \beta\text{-line} \end{aligned} \tag{9.8}$$

If σ_2 is replaced by $-P$ (pressure), equations 9.8 are written as

$$\begin{aligned} P &= -2k\Delta\phi \text{ along an } \alpha\text{-line} \\ P &= +2k\Delta\phi \text{ along a } \beta\text{-line} \end{aligned} \tag{9.9}$$

9.3 BOUNDARY CONDITIONS

One can always determine the direction of one principal stress at a boundary. The following boundary condition are useful:

1. The force and stress normal to a free surface is a principal stress, so the α- and β-lines must meet the surface at 45°.
2. The α- and β-lines must meet a frictionless surface at 45°.
3. The α- and β-lines meet surfaces of sticking friction at 0 and 90°.

Equations 9.7 establish a restriction on the shape of statically admissible fields. Consider the field in Figure 9.6. The difference between σ_2 at A and C can be found by traversing either of two paths, ABC or ADC. On the path through B, $\sigma_{2B} = \sigma_{2A} - 2k(\phi_B - \phi_A)$ and $\sigma_{2C} = \sigma_{2B} + 2k(\phi_C - \phi_B) = \sigma_{2A} - 2k(2\phi_B - \phi_A - \phi_C)$. On the other hand traversing the path ADC, $\sigma_{2D} = \sigma_{2A} + 2k(\phi_D - \phi_A)$

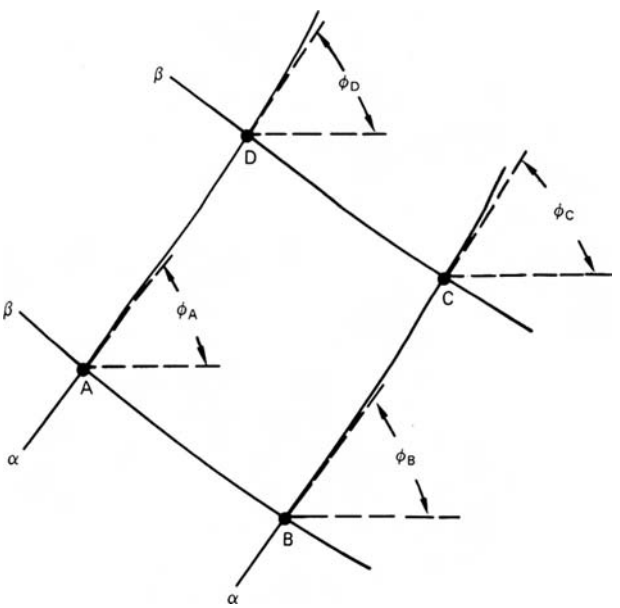

9.6. Two pairs of α- and β-lines for analyzing the change in mean normal stress by traversing two different paths.

and $\sigma_{2C} = \sigma_{2D} - 2k(\phi_C - \phi_D) = \sigma_{2A} + 2k(2\phi_D - \phi_A - \phi_C)$. Comparing these two paths,

$$\begin{aligned} &\phi_A - \phi_B = \phi_D - \phi_C \\ \text{and} \quad &\phi_A - \phi_D = \phi_B - \phi_C. \end{aligned} \tag{9.10}$$

Equation 9.10 implies that the net of α and β lines must be such that the change of ϕ is the same along a family of lines moving from one intersection with the opposite family to the next intersection. This together with the orthogonality requirement indicates that it is the angular change along a line rather than the length of line that is of significance.

9.4 PLANE-STRAIN INDENTATION

There are two simple fields that meet these requirements. One is a set of straight lines and the other is a centered fan (Figure 9.7). σ_2 is the same everywhere in the field of straight lines. It is a constant pressure zone. In the centered-fan field, σ_2 is the same everywhere along a given radius but varies from one radius to another.

A number of problems can be solved with these two fields. Consider plane-strain indentation. A possible field consisting of two centered fans and a constant pressure zone is shown in Figure 9.8. The α and β lines can be identified by realizing that parallel

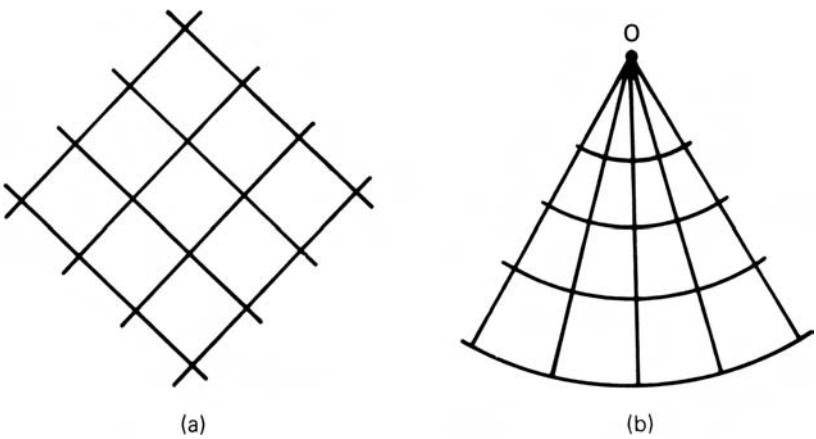

9.7. (a) Net of straight lines and (b) centered fan.

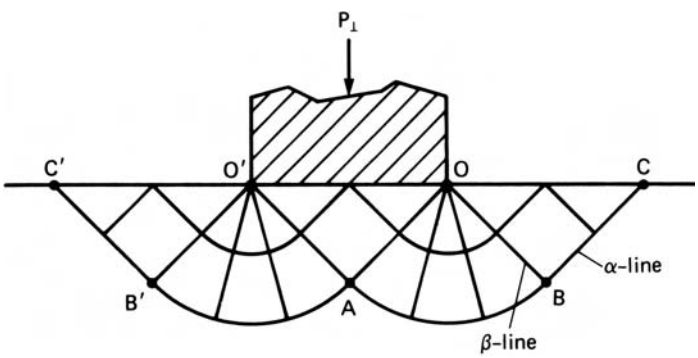

9.8. A possible slip-line field for plane-strain indentation.

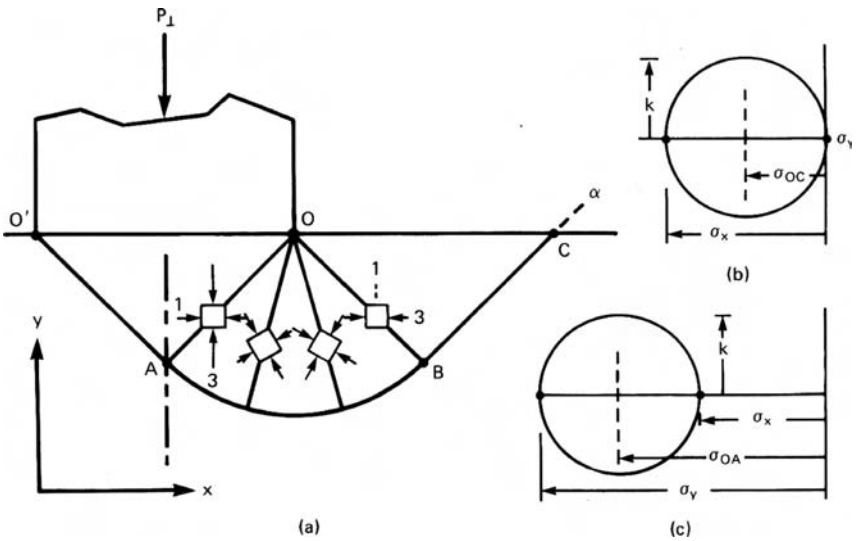

9.9. A detailed view of Figure 9.8 showing the changing stress state (a) and the Mohr's stress circles for triangles OBC (b) and O′OA (c).

to OC the stress is compressive and the stress normal to it is zero. Or alternatively, that under the indenter the most compressive stress is parallel to $P_\perp$

A more detailed illustration of the field is given in Figure 9.9. Along OC, $\sigma_y = \sigma_1 = 0$, $\sigma_2 = -k$, $\sigma_x = \sigma_3 = -2k$. Rotating clockwise along CBAO′ on the α line through $\Delta\phi = -\pi/2$, $\sigma_{2OO'} = \sigma_{2OC} + 2k\,\Delta\phi_\alpha = -k + 2k(-\pi/2)$, $P_\perp/2k = P_O/2k = -\sigma_{2OO}/2k = 1 + \pi/2 = 2.57$.

With the von Mises criterion, $2k = 1.155Y$, so $P_\perp = 2.97Y$. This plane-strain indentation is analogous to a two-dimensional hardness test. It is a frequently used rule of thumb that with consistent units the hardness is 3 times the yield strength. The pressure is constant but different in regions OBC and in O′OA. Although the metal is stressed to its yield stress in these regions, they do not deform.

9.5 HODOGRAPHS FOR SLIP-LINE FIELDS

Construction of hodographs for slip-line fields is necessary to

1. Assure the field is kinematically admissible;
2. Determine where in the field most of the energy is expended; and
3. Predict distortion of material as it passes through the field.

In constructing hodographs it may be noted that

1. The velocity is constant within a constant pressure zone;
2. In leaving a field of changing σ_2 there may or may not be a sudden change of velocity;
3. The magnitude of the velocity everywhere along a given slip line is constant though the direction may change;
4. In a field of curved lines, both the magnitude and direction of the velocity change;

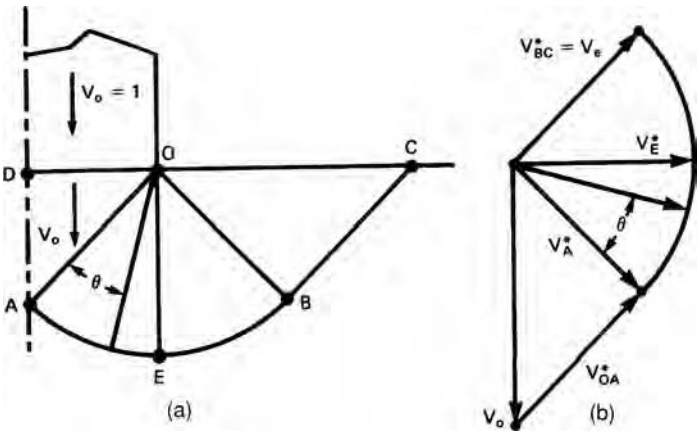

9.10. (a) A partial slip-line field for indentation and (b) the corresponding hodograph.

5. There is always shear on the boundary between the deforming material inside the field and the rigid material outside of it; and
6. The vector representing a velocity discontinuity must be parallel to the discontinuity itself.

Figure 9.10 shows half of the field and the corresponding hodograph. Region OAD moves downward with the velocity, V_0, of the punch. There is a discontinuity V^*_{OA} along OA such that the absolute velocity is parallel to the arc AE at A, and the velocity just to the right of OA differs from that in triangle OAD by a vector parallel to OA. The discontinuity V^*_{A} between the material in the field at A and outside the field is equal to the absolute velocity inside the field at A. This discontinuity between material inside and outside the field has a constant magnitude but changing direction along the arc AEB. There is no abrupt velocity discontinuity along OB.

In this field, there is intense shear along OA (V^*_{OA}), along AEB ($V^*_{\mathrm{A}} = V^*_{\mathrm{E}} = V^*_{\mathrm{B}}$), and along BC ($V^*_{\mathrm{BC}} = V^*_{\mathrm{A}}$). There is also energy dissipated by the gradual deformation in the fan OAB.

9.6 PLANE-STRAIN EXTRUSION

Consider again the frictionless plane stain extrusion treated by upper bounds in Section 8.3 where $r = 50\%$ and $\alpha = 30^\circ$. Figure 9.11(a) is the top half of the slip-line field and Figures 9.11(b) and (c) are Mohr's stress circle diagrams along OB and OC. The force balance on the die wall is shown in Figure 9.11(d).

At the exit the stress $\sigma_1 = \sigma_x = 0$ and the stress σ_y is compressive, so line OC is a β line. On OC, $\sigma_{2\mathrm{OC}} = -k$. Rotating clockwise through $\Delta\phi_\alpha = -\pi/6$ on an α line, $\sigma_{2\mathrm{OB}} = -k + 2k(-\pi/6)$. In triangle ABO, $\sigma_{2\mathrm{ABO}} = -k + 2k(-\pi/6)$ so $P_{\mathrm{ABO}} = k + 2k(\pi/6)$. Acting against the die wall, $P_\perp = P_{\mathrm{ABO}} + k = 2k(1 + \pi/6)$. $F_\perp = P_\perp(\overline{\mathrm{OA}}) = P_\perp r/\sin\alpha = P_\perp$. $P_\perp$ $F_x = F_\perp \sin\alpha = P_{\mathrm{e}}$ (1/2) so P_{ext} $/2k = (0.5)$ $(1 + \pi/6) = 0.762$.

The example above is a special case where the geometry is such that the slip-line field consists of a constant pressure zone and a single centered fan. Figure 9.12 shows

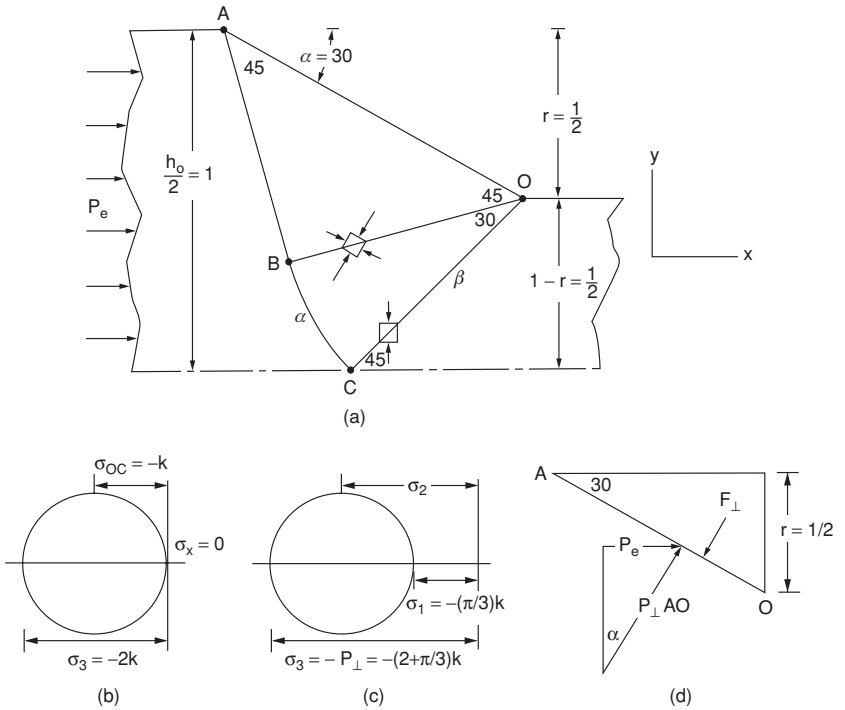

9.11. (a) Slip-line field for a frictionless extrusion, (b) Mohr's stress circle diagram along OB, (c) Mohr's stress circle diagram along OC, and (d) force balance on die wall.

such a field. If the entrance thickness $h_0 = 1$, the exit thickness is $1 - r$. In that case $\sin \alpha = r/2(1 - r)$ or

$$r = 2 \sin \alpha/(1 + 2 \sin \alpha). \tag{9.11}$$

Following the procedure for the 30° die,

$$P_{\text{ext}}/2k = r(1 + \alpha). \tag{9.12}$$

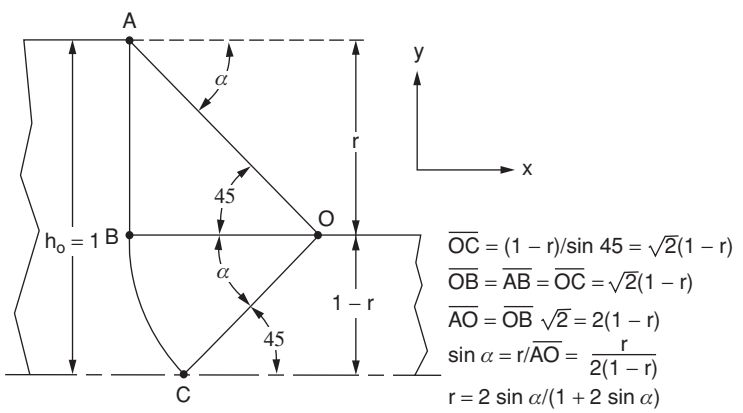

9.12. The geometry of a general field for plane-strain extrusion when $r = (2 \sin \alpha)(1 + 2 \sin \alpha)$.

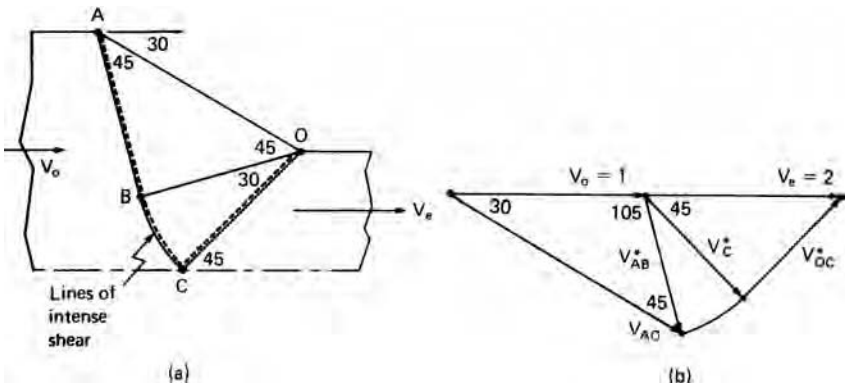

9.13. (a) Slip-line field showing lines of intense shear and (b) hodograph for an extrusion.

The homogeneous work for the reduction is $w_i = \bar{\sigma}\bar{\varepsilon} = 2k \ln[1/(1-r)]$. Since $w_a = P_{ext}$, the efficiency predicted by these fields

$$\eta = w_i/w_a = \ln[1/(1-r)]/[r(1+\alpha)]. \tag{9.13}$$

If the reductions in this section had been made by drawing instead of extrusion, the results would have been the same. To analyze drawing, the exit stress would be σ_d instead of 0, so $\sigma_{2OC} = k + \sigma_d$. $\sigma_{2OAC} = k(\pi/6) + k + \sigma_d$. $P_\perp = k(\pi/6) + 2k + \sigma_d$, $F_x = F_\perp \sin\alpha = rP_\perp = r[k(\pi/6) + 2k + \sigma_d]$, and $F_x = (1-r)\sigma_d$. Equating, we obtain $\sigma_d/2k = r(1+\alpha)$, which is identical to equation 9.12.

9.7 ENERGY DISSIPATION IN A SLIP-LINE FIELD

Consider the plane-strain extrusion in Figure 9.13. There are velocity discontinuities along AB, BC, and CO (Figure 9.13(a)). The hodograph (Figure 9.13(b)) shows that if $V_0 = 1$, $V^*_{AB} = V^*_{BC} = V^*_{CO} = 1/\sqrt{2}$. The lengths are $\overline{AB} = \overline{OC} = 1/\sqrt{2}$ and $\overline{BC} = (\pi/6)/\sqrt{2}$). So the energy dissipation along these lines is $k(\overline{AB}V^*_{AB} + \overline{BC}V^*_{BC} + \overline{OC}V^*_{OC}) = 1.262k$. The extrusion pressure was earlier determined as $P_{ext}/2k = 0.762$, so $P_{ext} = 1.542k$. Thus $1.262/1.542 = 81\%$ of the energy is expended along these lines of discontinuity. The other 17% is expended in the fan OBC.

9.8 METAL DISTORTION

The distortion of the metal in a steady-state process can be determined from a slip-line field and its hodograph. As an example, consider the 2:1 extrusion through a 90° die illustrated in Figure 9.14(a).

Figure 9.14(b) is the hodograph. The triangle to the right of AO is a dead metal zone. A metal entering the field at A suffers a velocity discontinuity V^*_A parallel to the arc at A. A metal entering the field at C suffers a velocity discontinuity V^*_C parallel to the arc at C. All of the velocity discontinuities along the arc have the same magnitude and are parallel to the arc. There is also a velocity discontinuity V^*_{GO} parallel to GO and of magnitude such that V_e is horizontal.

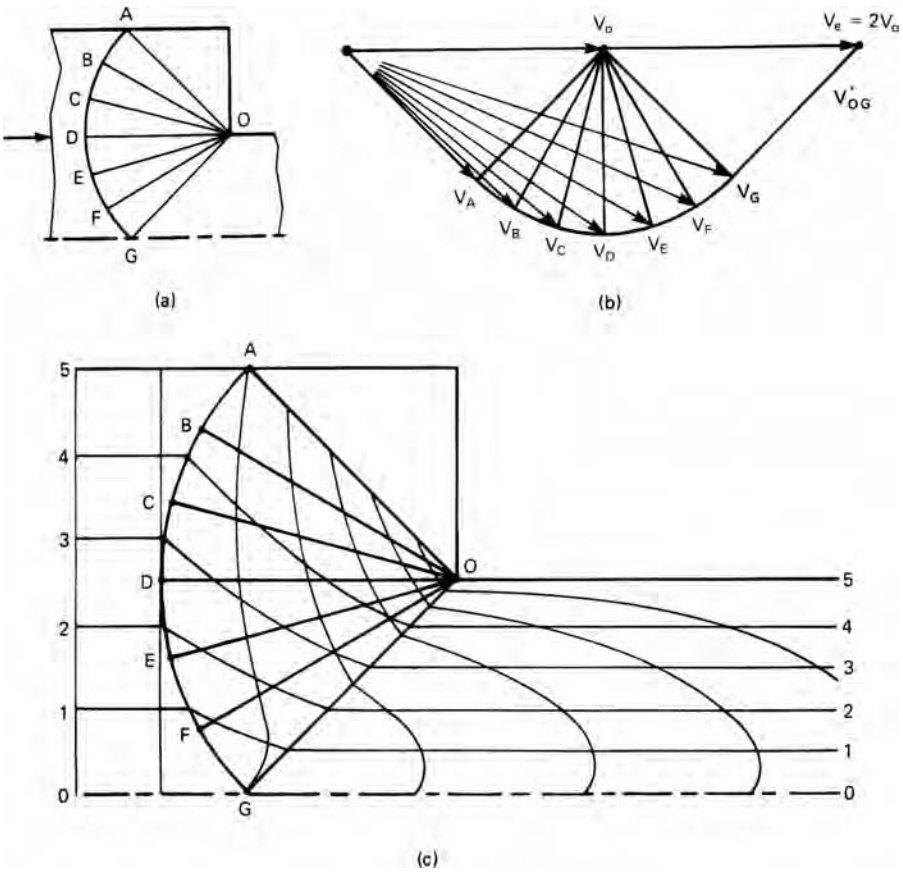

9.14. (a) Slip-line field for a 2:1 extrusion through a 90° die, (b) the hodograph for the field, and (c) the predicted distortion of the metal.

Stream lines can be drawn for particles (Figure 9.14(c)). Consider a particle on line 3, entering the field between C and D. As it enters the field it acquires an absolute velocity midway between V_C and V_D. Its direction gradually changes as it moves through the field. Its velocity equals V_D as it crosses OD, equals V_E as it crosses OE, and equals V_F as it crosses OF. When it crosses OG its velocity must become horizontal. If this construction is made correctly, it emerges on a line 3/5 of the initial thickness.

The distortion of the metal is found by considering the velocity magnitudes at each point along the path. For each time increment Δt, the distance traveled is $\Delta s = V\Delta$t. By following particles that are initially on a vertical grid line, the distortion of that grid line is established. The greatest distortion occurs at the surface because the velocity is least there.

9.9 INDENTATION OF THICK SLABS

The plane-strain indentation of a thick slab by two opposing indenters is shown Figure 9.15. The simple slip-line field in Figure 9.16 is appropriate for special case

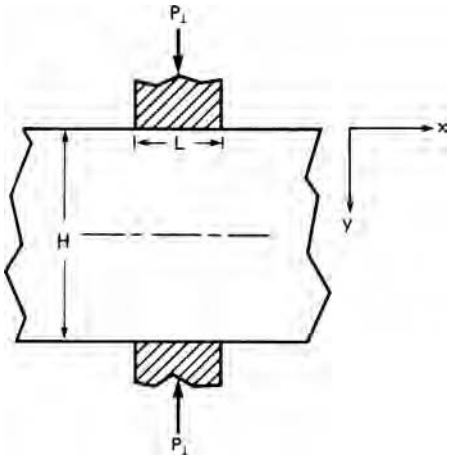

9.15. Plane-strain indentation of a thick slab by two opposing indenters.

where the slab thickness H equals the indenter width L. Along AO, $\sigma_x = 0$ so $\sigma_2 = -k$. The stress is the same everywhere in triangle O′OA so along OO′,

$$\sigma_2 = -k, \quad P_\perp = 2k, \quad \text{and} \quad P_\perp/2k = 1. \tag{9.14}$$

A different field must be used for larger values of H/L. Figure 9.17 shows the field for $H/L = 5.43$. This is a field determined by two centered fans. In triangle O′OA $\sigma_y = -P_\perp$, $\sigma_{2(\mathrm{OA})} = \sigma_y + k = -P_\perp + k$. Moving along an α line to (0, 1) $\sigma_{2(0,1)} = -\sigma_{2(\mathrm{OA})} + 2k\Delta\phi_\alpha$ and moving back along a β line to (1,1), $\sigma_{2(1,1)} = -\sigma_{2(\mathrm{OA})} + 2k(\Delta\phi_\alpha - \Delta\phi_\beta)$. At 1,1, $\sigma_{x(1,1)} = -P_\perp + 2k + 2k(\Delta\phi_\alpha - \Delta\phi_\beta)$ and at every point (n, n) along the centerline $\sigma_{x(n,n)} = -P_\perp + 2k + 2k(\Delta\phi_\alpha - \Delta\phi_\beta)_n$. Since $\Delta\phi_\alpha = -\Delta\phi_\beta$,

$$\sigma_{x(n,n)} = -P_\perp + 2k + 4k\Delta\phi_n, \tag{9.15}$$

where $\Delta\phi_n$ is the absolute value of the rotations.

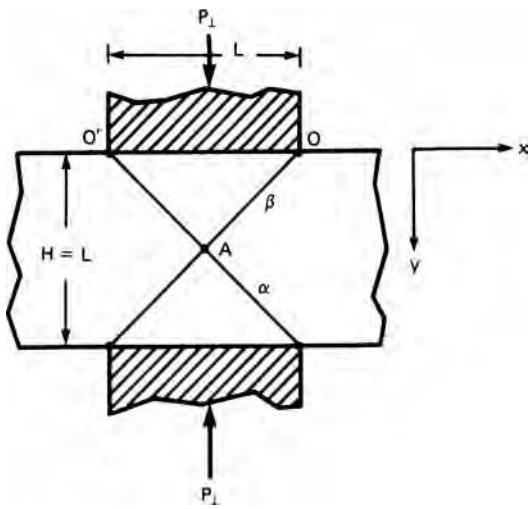

9.16. Special case of plane-strain indentation where the slab thickness H, equals the indenter width L.

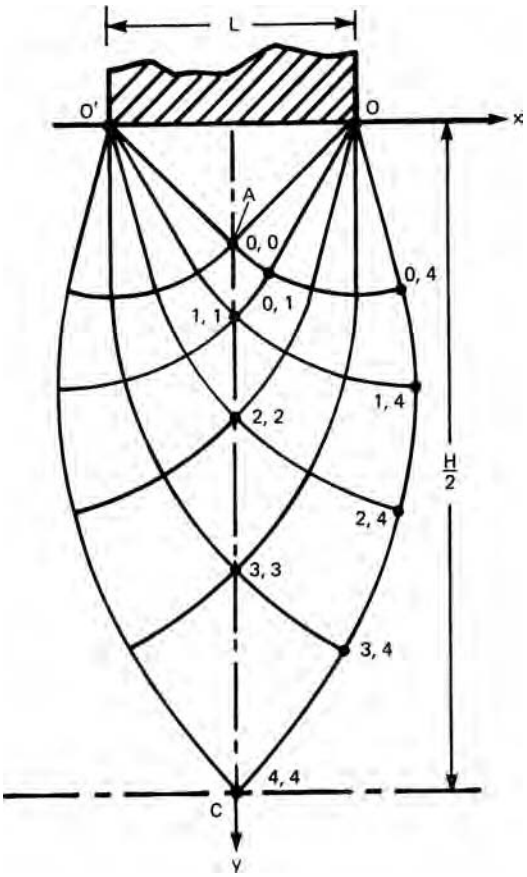

9.17. Slip-line field for mutual indentation with $H/L = 5.43$.

Because there is no x-direction constraint,

$$F_x = 0 = \int_0^{H/2} \sigma_x \, dy. \tag{9.16}$$

Substituting equation 9.15, $\int_0^{H/2} [-P_\perp + 2k(1 + 4\Delta\phi)] \, dy = 0$ or

$$P_\perp = 2k + (4k/H) \int_0^{H/2} 2\Delta\phi \, dy. \tag{9.17}$$

Figure 9.18 gives the values of $\Delta\phi$ as a function of y for nodal points on a 15° net. There is a more detailed net in the appendix. The integration in equation 9.17 can be done numerically using the trapezoidal rule or graphically by plotting $2\Delta\phi$ versus y. The results of such calculations are summarized in a plot of $P_\perp/2k$ versus H/L (Figure 9.19). It should be noted that for $H/L > 8.75$, $P_\perp/2k$ exceeds $1 + \pi/2$ so the field in Figure 9.19 gives a lower value of $P_\perp/2$. Nonpenetrating indentation should be expected for $H/L > 8.75$ and penetrating deformation for $H/L < 8.75$. A corollary is that for valid hardness testing the thickness of the material should be 4 to 5 times as thick as the diameter of the indenter. (Theoretically $H/L < 8.75/2 = 4.37$ for a indentation on a frictionless substrate.)

m, n	$\Delta\phi$	y	x
0, 0	0	1.0	0
0, 1	$\frac{\pi}{12}$	1.225	0.2930
0, 2	$\frac{\pi}{6}$	1.366	0.6380
0, 3	$\frac{\pi}{4}$	1.414	1.000
0, 4	$\frac{\pi}{3}$	1.366	1.366
0, 5	$\frac{5\pi}{12}$	1.225	1.7071
0, 6	$\frac{\pi}{2}$	1.000	2.000
1, 1	0	1.605	0
1, 2	$\frac{\pi}{12}$	1.915	0.404
1, 3	$\frac{\pi}{6}$	2.120	0.904
1, 4	$\frac{\pi}{4}$	2.195	1.471
1, 5	$\frac{\pi}{3}$	2.116	2.070
1, 6	$\frac{5\pi}{12}$	1.873	2.659
2, 2	0	2.440	0
2, 3	$\frac{\pi}{12}$	2.885	0.584
2, 4	$\frac{\pi}{6}$	3.195	1.335
2, 5	$\frac{\pi}{4}$	3.311	2.222
2, 6	$\frac{\pi}{3}$	3.185	3.190
3, 3	0	3.640	0
3, 4	$\frac{\pi}{12}$	4.306	0.870
3, 5	$\frac{\pi}{6}$	4.780	2.021
3, 6	$\frac{\pi}{4}$	4.965	3.414
4, 4	0	5.43	0
4, 5	$\frac{\pi}{12}$	6.45	1.325
4, 6	$\frac{\pi}{6}$	7.18	3.118
5, 5	0	8.16	0
5, 6	$\frac{\pi}{12}$	9.73	2.055
6, 6	0	12.37	0

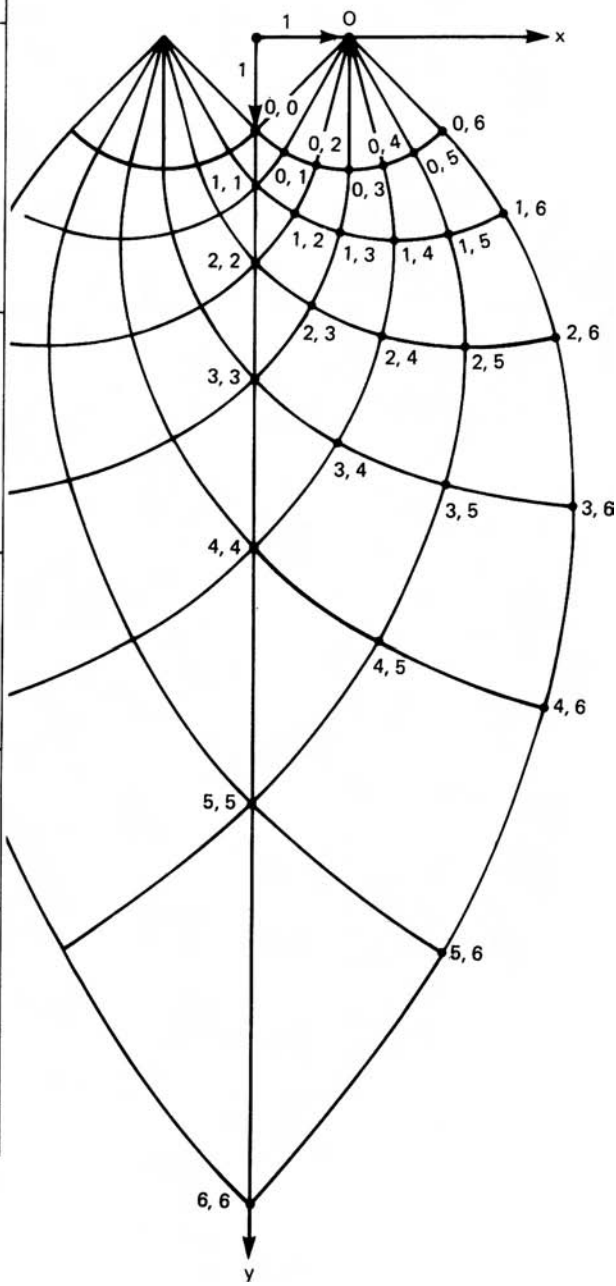

9.18. Slip-line field for two centered fans with x and y values for each node of the 15° net.

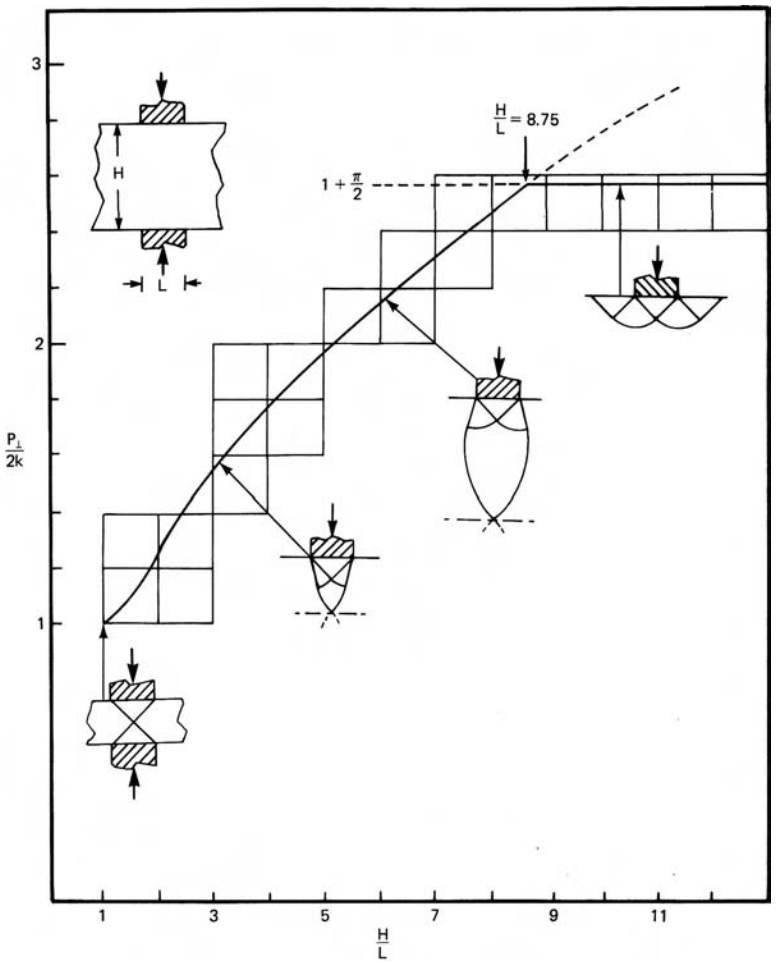

9.19. Normalized indentation pressure as a function of H/L. This type of plot was first suggested by R. Hill.

9.10 PLANE-STRAIN DRAWING

This type of field with two centered fans is useful in analyzing plane-strain drawing or extrusion operations with larger H/L values than are described by equation 9.11 (i.e., $r < 2 \sin \alpha/(1 + 2 \sin \alpha)$). Figure 9.20 shows the field in Figure 9.17, tilted by the die angle α and bounded by α and β lines that meet the centerline at 45°. The appropriate boundary condition for finding σ_d is $F_x = \int \sigma_x dy + \int \tau_{xy} dx$ along a cut from A to $n, n + 1$. Everywhere along the cut A, (0,1), $(n, n + 1)$, $\sigma_x = \sigma_1$, and $\tau_{xy} = 0$, so $F_x = \int \sigma_x dy$. The x and y values of the nodes in Figure 9.18 are now designated as x' and y'. They may be transformed into the coordinates x and y in Figure 9.20 by

$$\begin{aligned} x &= (x' - 1)\cos\alpha - y' \sin\alpha \\ y &= (x' - 1)\sin\alpha + y' \cos\alpha. \end{aligned} \tag{9.18}$$

The stress state at any node point, $(n, n + 1)$, can then be found in terms of $P_\perp$. In triangle AOB, and along the line AO, $P_{AB} = P_\perp - k$. Rotating on an α line through

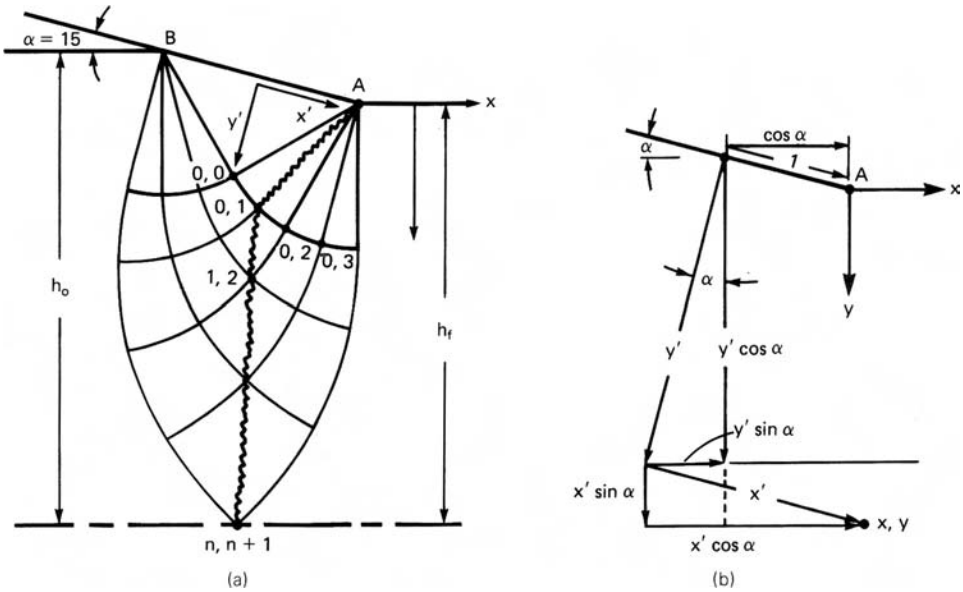

9.20. (a) Slip-line field for drawing with $r < 2\ (\sin\alpha)\ (1 + 2\sin\alpha)$. (b) Coordinate system for analysis along the cut A, (0, 1), (n, n+ 1) where $\sigma_x = \sigma_1$.

$\Delta\phi = +\pi/12$ to (0,1) gives $P_{(0,1)} = P_{\mathrm{OA}} - 2k(\pi/12) = P_\perp - k - 2k(\pi/12)$. Movement to any point $(n, n+1)$ requires an additional rotation of $n(\pi/12)$ on an α line and $-n(\pi/12)$ on a β line so $P_{(\mathrm{n,n+1})} = P_\perp - k - 2k(2n+1)\pi/12$ and

$$\sigma_{x(n,n+1)} = P_\perp - k - 2k[1 + (2n+1)\pi/12]. \tag{9.19}$$

Applying the boundary condition, $F_x = \int_0^{h_\mathrm{f}} \sigma_x dy = 0$, where h_f is the value of y at the centerline,

$$F_x = \int_0^{h_\mathrm{f}} (-P_\perp + 2k[1 + (2n+1)\pi/12]\,\mathrm{d}y = 0. \tag{9.20}$$

Since $P_\perp$ and k are independent of y, equation 9.20 can be written as

$$P_\perp/2k = \frac{\pi}{12h_\mathrm{f}} \int_0^{h_\mathrm{f}} (2n+1)\mathrm{d}y. \tag{9.21}$$

Equation 9.21 may be evaluated either graphically or numerically for any value of h_f. Once $P_\perp$ has been evaluated, a force balance can be used to find P_{ext}.

$$P_{\mathrm{ext}} = \frac{2P_\perp \sin\alpha}{h_\mathrm{f} + 2\sin\alpha}. \tag{9.22}$$

The mechanical efficiency, η, for such frictionless extrusion or drawing may be found by comparing $P_{\mathrm{ext}}/2k$ with the homogeneous work. Figure 9.21 shows how calculated values of η and $P_{\mathrm{ext}}/2k$ vary with reduction, r, and H/L for a 15° die.

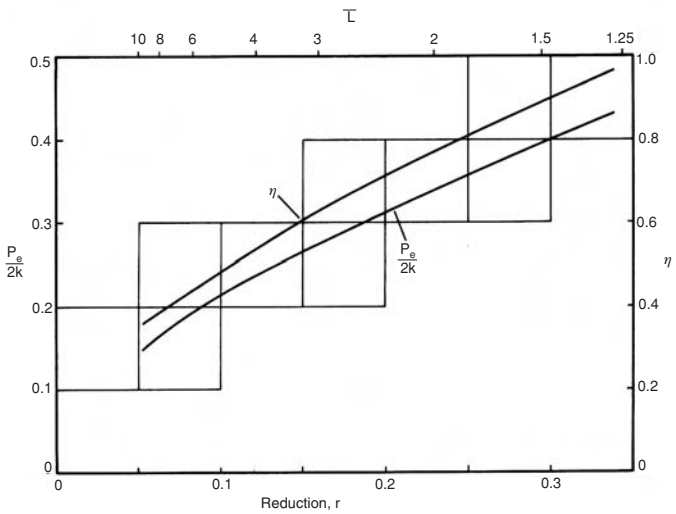

9.21. Variation of η and $P_{ext}/2k$ with r, and H/L for a 15° die.

With very low values r and high die angles, deformation may not be penetrating. The alternate field shown in Figure 9.22 requires less work. This is analogous to a hardness test with a wedge-shaped indenter. This field becomes appropriate when the die pressure reaches a level

$$P_{\perp}/2k = (1 + p/2 - \alpha). \tag{9.23}$$

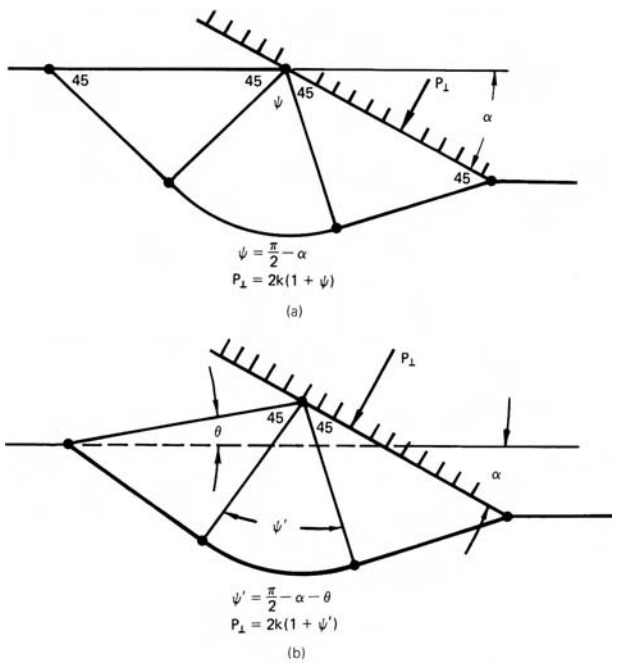

9.22. (a) Slip-line field for initiation of bulging at die entrance with large α and small r. (b) Slip-line field for continued bulging.

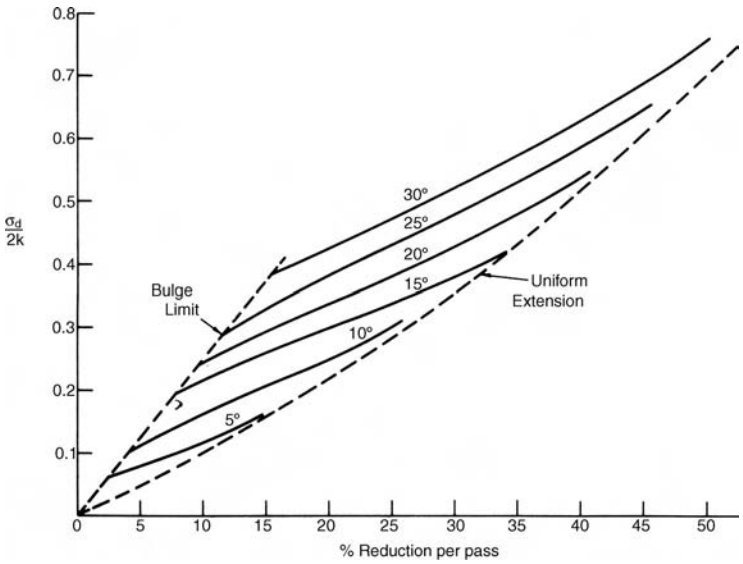

9.23. Dependence of drawing force on reduction and die angle. Bulging occurs at low reductions and high α. From L. F. Coffin and H. C. Rogers *Trans. ASM*, 60 (1967), pp. 672–86.

Material piles up at the die inlet causing the contact length between die and work piece to be great enough make the penetrating field appropriate. Figure 9.23 shows the bulging limit and how the drawing stress increases with reduction.

Figure 9.24 shows the variation of $P = -\sigma_2$ in the deformation zone for plane-strain drawing with $\alpha = 15^\circ$ and $r = 0.085$. Note that σ_2 may become

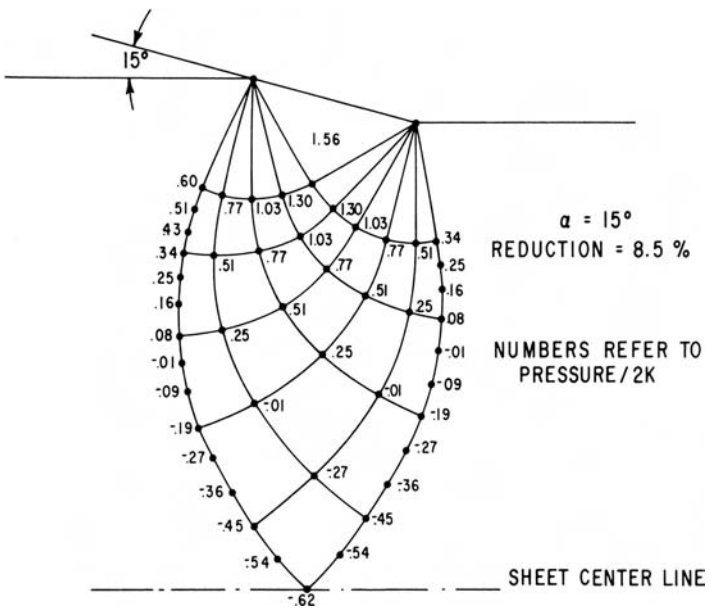

9.24. Variation of $P/2k = -\sigma_2$ over the deformation field for plane-strain drawing with $\alpha = 15^\circ$ and $r = 0.085$. From L. F. Coffin and H. C. Rogers, *op. cit*.

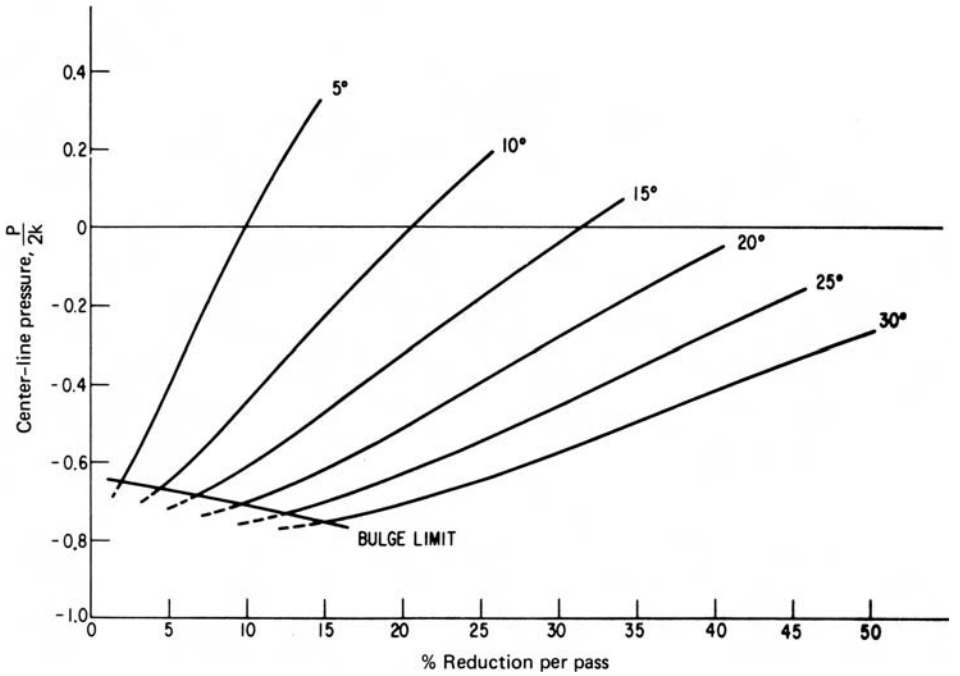

9.25. Centerline pressure as a function of α and r. Negative values of $P/2k$ indicate tension. From L. F. Coffin and H. C. Rogers, *op. cit*.

tensile near the centerline. The hydrostatic tension increases as α increases and r decreases. The centerline pressure for various combinations of α and r is shown in Figure 9.25.

If $r > 2 \sin \alpha/(1 + 2 \sin \alpha)$, a slip-line field different than both Figures 9.11 and 9.20 is required. This is not discussed here but is discussed in W. Johnson and P. B. Mellor, *Engineering Plasticity*, 1973.

9.11 CONSTANT SHEAR-STRESS INTERFACES

Slip-line fields can be used to solve problems with sticking friction or a constant friction interface. One example is the compression between rough platens. This approximates conditions during hot forging. With sticking friction the slip lines are parallel and perpendicular to the platens. There is a dead metal zone where they do not meet the platens. Figure 9.26 shows the appropriate slip-line field. The appropriate boundary condition is $\sigma_x = \sigma_1 = 0$ along the left-hand side of the field. Values of $P_\perp = -\sigma_x$ along the centerline can be found by rotating on α- and β-lines. Then $P_{\perp \text{ave}}$ can be found by numerical integration. How much of this field should be used depends on H/L. Results of calculations for various values of H/L are shown in Figure 9.27. The slab solution of $P_\perp/2k = 1 + (1/4)H/L$ is shown for comparison.

If there shear stress at the tool interface, $\tau = mk$, the α- and β-lines meet the interface at an angle $\theta = (1/2)(\text{arc cos } m)$ and $\theta' = 90 - \theta$. A general Mohr's stress circle plot for this condition is shown in Figure 9.28.

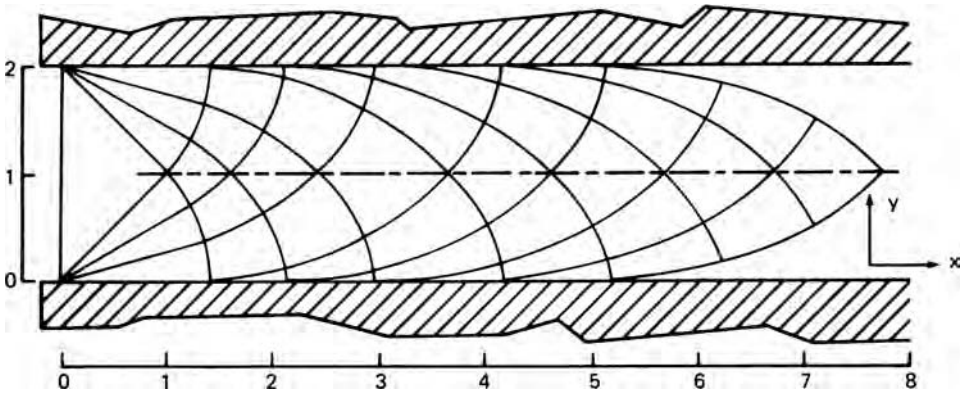

9.26. Slip-line field for compression with sticking friction. Adapted from W. Johnson and P. B. Hellor, *Engineering Plasticity*, Van Nostrand Reinhold, 1973.

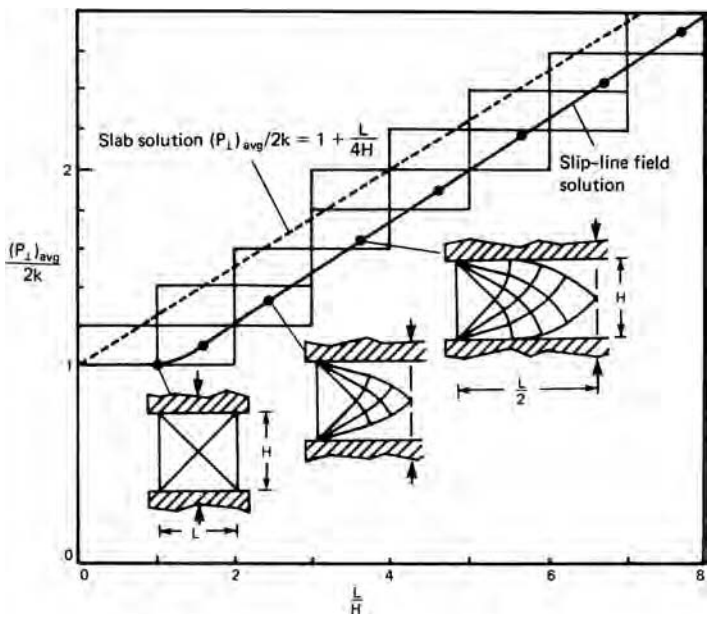

9.27. Average indentation pressure for the slip-line fields in Figure 9.26 and slab force analysis (equation 7.20).

9.12 PIPE FORMATION

The general variation of extrusion force with displacement is sketched in Figure 9.29. For direct or forward extrusion, after an initial rise the force drops because the friction between work material and chamber walls decreases as the amount of material in the chamber decreases. With indirect extrusion there are no chamber walls. As the ram approaches the die, there may be a drop caused by a change of direction of material flow. See Figure 9.30. As material begins to flow along the die wall, a cavity or pipe may be formed. Figure 9.31 shows such a pipe.

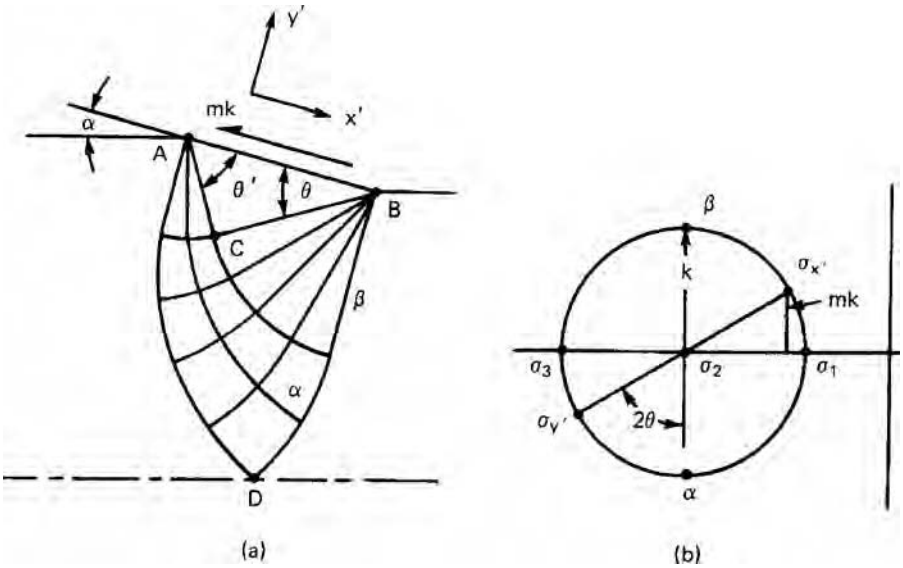

9.28. (a) Slip-line field for interface stress, $\tau = mk$, and (b) corresponding Mohr's stress circle diagram.

NOTES OF INTEREST

W. Lüders first noted the networks of orthogonal lines that appear on soft cast steel specimens after bending and etching in nitric acid in *Dinglers Polytech. J.* Stuttgart, 1860. These correspond to slip lines. An example of slip lines revealed by etching

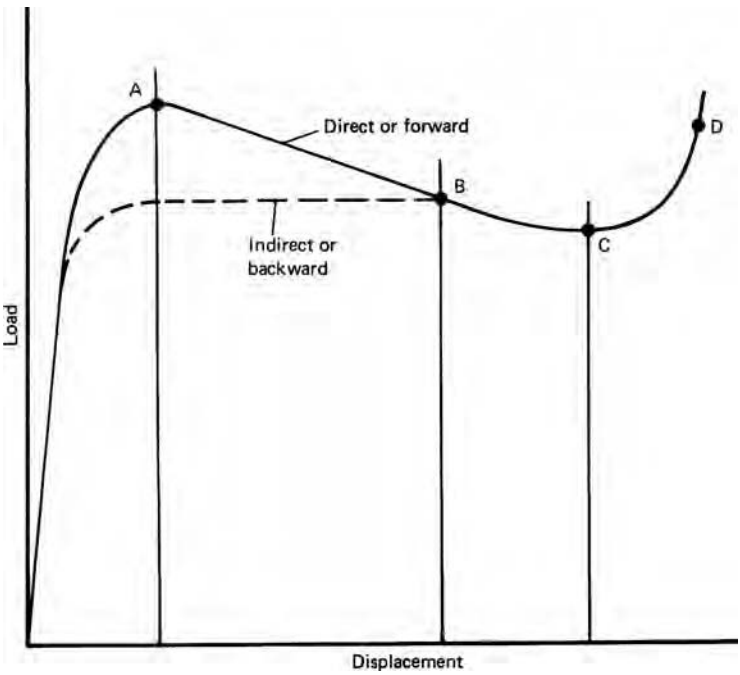

9.29. Schematic of a load-displacement diagram for direct and indirect extrusion.

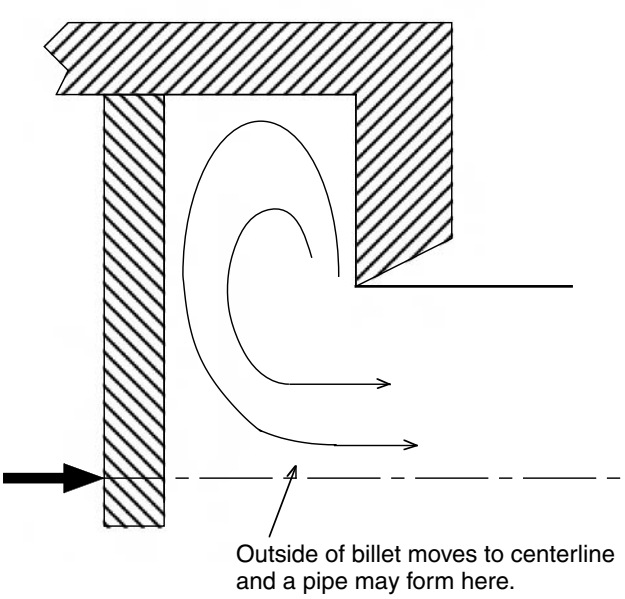

9.30. Flow pattern at the end of an extrusion. This brings material on the outside of the billet to the centerline and leads to formation of pipe.

is given in Figure 9.32. Figure 9.33 shows other examples of slip lines on deformed parts.

There is a simple demonstration of the hydrostatic tension that develops at the center of a lightly compressed strip. If a cylinder of modeling clay is rolled back and forth as it is lightly compressed, a hole will start to develop at the center.

The first systematic presentations of the use of slip-line fields for solving practical problems were the books by Hill and by Prager and Hodge listed in the References.

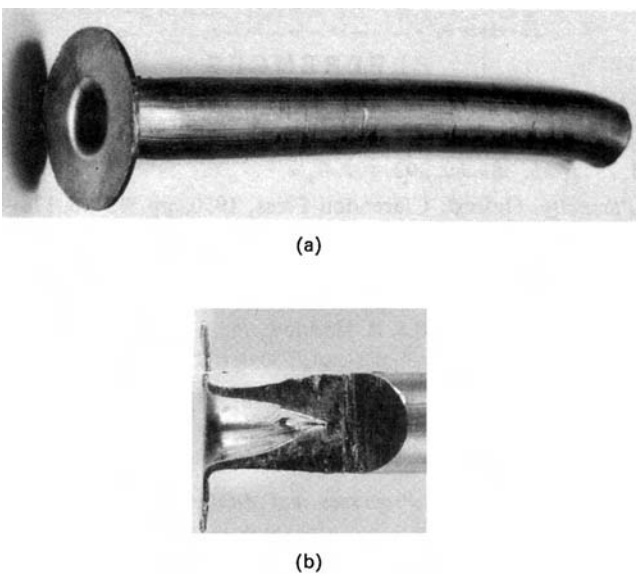

9.31. Billet made by direct extrusion (a) and the pipe at the end (b). Courtesy of W. H. Durrant.

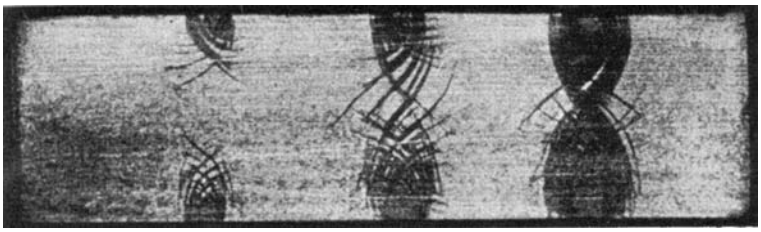

9.32. Network of lines formed by indenting a mild steel. From F. Körber, *J. Inst. Metals*, 48 (1932), p. 317.

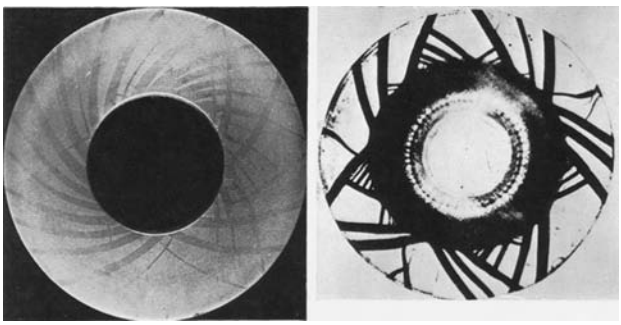

(a) (b)

9.33. (a) Thick wall cylinder deformed under internal pressure and (b) slip lines on the flange of a cup during drawing. From W. Johnson, R. Sowerby, and J. B. Haddow, *Plane-Strain Slip Line Fields*, American Elsevier, 1970.

REFERENCES

B. Avitzur, *Metal Forming: Processes and Analysis*, McGraw-Hill, 1968, pp. 250–74.
L. F. Coffin and H. C. Rogers, *Trans. ASM*, 50 (1967), pp. 672–86.
H. Ford, *Advanced Mechanics of Materials*, Wiley, 1963.
H. Geringer, *Proc 3rd. Int. Congr. Appl. Mech*., 29 (1930), pp. 185–90.
A. P. Green, *Phil. Mag.*, 42 (1951), p. 900.
R. Hill, *Plasticity*, Clarendon Press, 1950.
W. Johnson and P. B. Mellor, *Engineering Plasticity*, Van Nostrand Reinhold, 1973.
W. Johnson, R. Sowerby, and J. B. Haddow, *Plane-Strain Slip Line Fields*, American Elsevier, 1970.
W. Prager and P. G. Hodge Jr., *Theory of Perfectly Plastic Solids*, Wiley, 1951.
E. G. Thomsen, C. T. Yang, and S. Kobayashi, *Mechanics of Plastic Deformation in Metal Processing*, Macmillan, 1965.

APPENDIX

Table 9.1 gives the x and y coordinates of the 5° slip-line field determined by two centered fans. Figure 9.34 shows the slip-line field. These values were calculated from tables* in which a different coordinate system was use to describe the net. Here the fans have a radius of $\sqrt{2}$ and the nodes of the fans are separated by a distance of 2 and the origin is halfway between the nodes.

* E. G. Thomsen, C. T. Yang, and S. Kobayashi, *Mechanics of Plastic Deformation in Metal Processing* (Macmillan, 1965).

Table 9.1. Coordinates of a 5° Net for the Slip-Line Field Determined by Two Centered Fans

$\Delta\phi_\alpha$	n	$m=n$	$m=n+1$	$m=n+2$	$m=n+3$	$m=n+4$	$m=n+5$	$m=n+6$	$m=n+7$	$m=n+8$
0°	0	y = 1.0	1.0833	1.1584	1.2247	1.2817	1.3288	1.3660	1.3926	1.4087
		x = 0.0	0.0910	0.1888	0.2929	0.4023	0.5163	0.6340	0.7544	0.8767
5°	1	1.1826	1.2741	1.3572	1.4312	1.4951	1.5484	1.5907	1.6214	1.6399
		0.0	0.1000	0.2083	0.3243	0.9472	0.5762	0.7101	0.8484	0.9897
10°	2	1.3831	1.4845	1.5770	1.6597	1.7320	1.7925	1.8407	1.8760	1.8975
		0.0	0.1106	0.2312	0.3613	0.4999	0.6463	0.7995	0.9583	1.1218
15°	3	1.6050	1.7177	1.8214	1.9146	1.9963	2.0653	2.1206	2.1611	2.1861
		0.0	0.1232	0.2582	0.4046	0.5617	0.7285	0.9038	1.0868	1.2760
20°	4	1.8519	1.9781	2.0946	2.2001	2.2929	2.3718	2.4351	2.4820	2.5108
		0.0	0.1377	0.2898	0.4554	0.6339	0.8243	1.0257	1.2307	1.4562
25°	5	2.1283	2.2701	2.4018	2.5215	2.6272	2.7176	2.7905	2.8446	2.8781
		0.0	0.1550	0.3267	0.5146	0.7181	0.9364	1.1680	1.4118	1.6665
30°	6	2.4390	2.5991	2.7484	2.8846	3.0056	3.1093	3.1934	3.2560	3.2948
		0.0	0.1749	0.3698	0.5839	0.8166	1.0610	1.3340	1.6162	1.9119
35°	7	2.7897	2.9713	3.1413	3.2968	3.4356	3.5549	3.6519	3.7245	3.7696
		0.0	0.1984	0.4200	0.6647	0.9314	1.2196	1.5278	1.8547	2.1985
40°	8	3.1874	3.3940	3.5879	3.7662	3.9257	4.0632	4.1755	4.2595	4.3121
		0.0	0.2257	0.4787	0.7589	1.0655	1.3977	1.7540	2.1332	2.5331
45°	9	3.6394	3.8755	4.0976	4.3023	4.4859	4.6447	4.7747	4.8732	4.9335
		0.0	0.2575	0.5472	0.8688	1.2219	1.6054	2.0182	2.4586	2.9243
50°	10	4.1561	4.4259	4.6808	4.9162	5.1281	5.3117	5.4626	5.5760	5.6472
		0.0	0.2947	0.6272	0.9973	1.4046	1.8482	2.3269	2.8389	3.3828
55°	11	4.7470	5.0565	5.3496	5.6211	5.8659	6.0786	6.2537	6.3856	
		0.0	0.3380	07205	1.1472	1.6179	2.1318	2.6873	3.2831	
60°	12	5.4248	5.7807	6.1185	6.4321	6.7154	6.9622	7.1657		
		0.0	0.3886	0.8296	1.3223	1.8670	2.4631	3.1091		
65°	13	6.2043	6.6144	7.0043	7.3671	7.6955	7.9820			
		0.0	0.4982	0.9573	1.5269	2.1584	2.8505			
70°	14	7.1023	7.5758	8.0267	8.4470	8.8281				
		0.0	0.5172	1.1055	1.7658	2.4986				
75°	15	8.1290	8.6864	9.2085	9.6961					
		0.0	0.5981	0.5981	1.2794	2.0455				
80°	16	9.3375	9.9715	10.5771						
		0.0	0.6925	1.4827						
85°	17	10.726	11.460							
		0.0	0.8031							
90°	18	12.334								
		0.0								

(Continued)

Table 9.2. (Continued)

$\Delta\phi_\alpha$	n	$n+9$	$n+10$	$n+11$	$n+12$	$n+13$	$n=14$	$n+15$	$n+16$	$n+17$	$n+18$
0°	0	1.4141	1.4087	1.3926	1.3629	1.3288	1.2816	1.2246	1.1584	1.0833	1.000
		1.0000	1.1233	1.2456	1.3660	1.4837	1.5977	1.7071	1.8112	1.9090	2.000
5°	1	1.6463	1.6399	1.6068	1.5892	1.5449	1.4879	1.4189	1.3379	1.2455	
		1.1334	1.2718	1.4222	1.5653	1.7061	1.8434	1.9765	2.1036	2.2240	
10°	2	1.9048	1.8975	1.8751	1.8375	1.7846	1.7163	1.6330	1.5347		
		1.2891	1.4582	1.6282	1.7979	1.9658	2.1305	2.2909	2.4452		
15°	3	2.1946	2.1860	2.1595	2.1151	2.0522	1.9707	1.8707			
		1.4708	1.6686	1.8688	2.0694	2.2690	2.4658	2.6583			
20°	4	2.5207	2.5107	2.4797	2.4272	2.3527	2.2555				
		1.6828	1.9141	2.1497	2.3865	2.6233	2.8574				
25°	5	2.8895	2.8778	2.8414	2.7795	2.6913					
		1.9304	2.2014	2.4777	2.7580	3.0372					
30°	6	3.3083	3.2944	3.2519	3.1789						
		2.2196	2.5366	2.8610	3.1901						
35°	7	3.7853	3.7692	3.7191							
		2.5573	2.9281	3.3089							
40°	8	4.3303	4.3114								
		2.9158	3.3859								
45°	9	4.9584									
		3.4129									

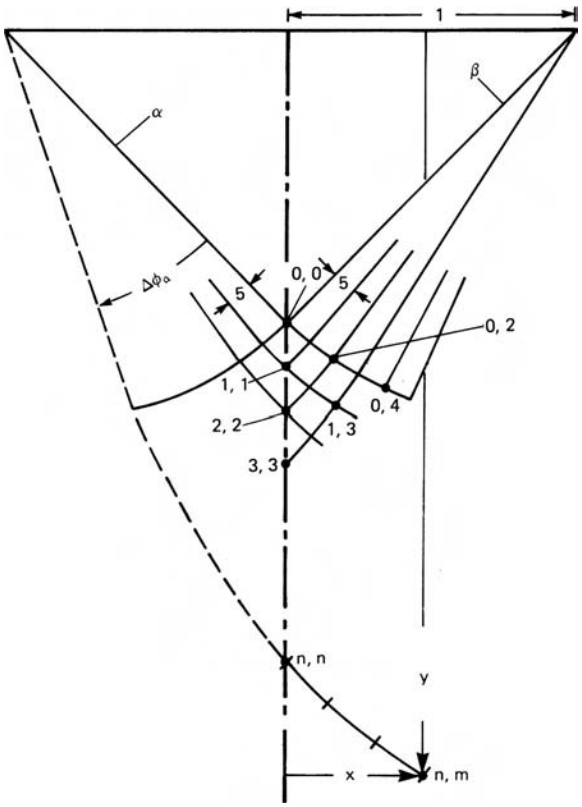

9.34. Slip-line field for Table 9.1.

PROBLEMS

9.1. Using the slip-line field in Figure 9.8 for frictionless indentation it was found that $P_\perp/2k = 2.57$. Figure 9.35 shows an alternate field for the same problem proposed by Hill.

a) Find $P_\perp/2k$ for this field.

b) Construct the hodograph.

c) What percent of the energy is expended along lines of intense shear?

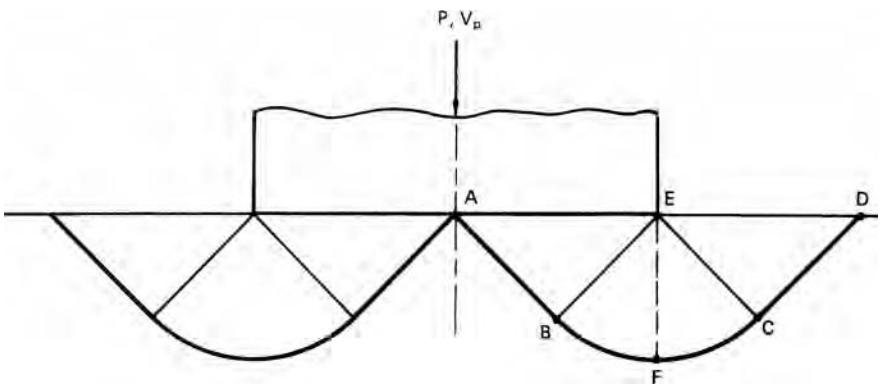

9.35. Slip-line field for plane-strain indentation.

9.2. Figure 9.36 shows a slip-line field with a frictionless punch. Construct the hodograph and find $P_\perp/2k$ for this field.

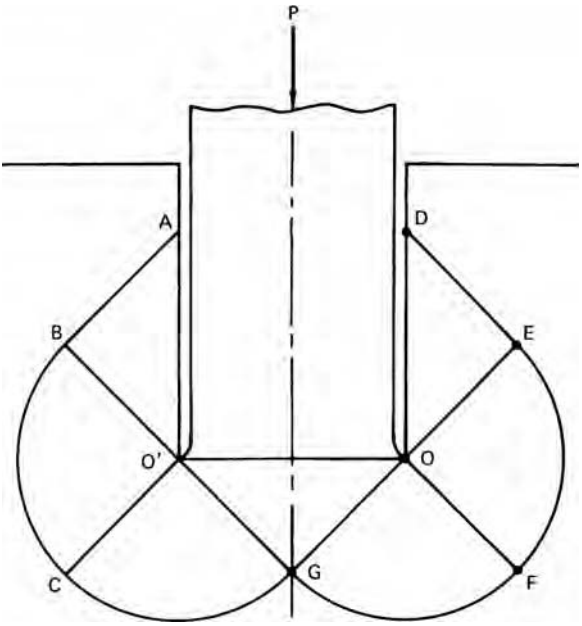

9.36. Slip-line field for Problem 9.2.

9.3. Plane-strain compression of a hexagonal rod is shown in Figure 9.37 together with a possible slip-line field.

a) Determine whether this field or penetrating deformation will occur.

b) Find $P_\perp/2k$.

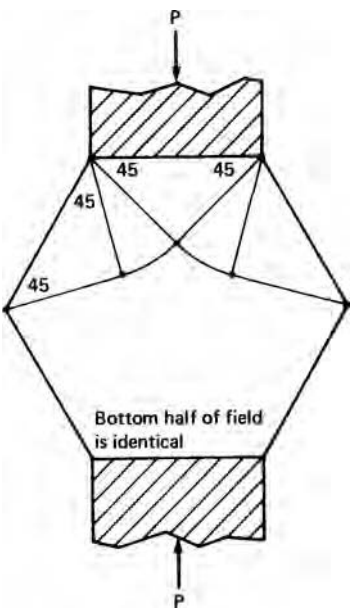

9.37. Possible slip-line field for Problem 9.3.

9.4. Figure 9.38 is the slip-line field for plane-strain wedge indentation. For the volume of the side mounds to equal the volume displaced, the angle ψ must be related to θ by $\cos(2\theta - \psi) = \cos\psi/(1 + \sin\psi)$. Determine F/x in terms of $2k$ for $\theta = 120^\circ$.

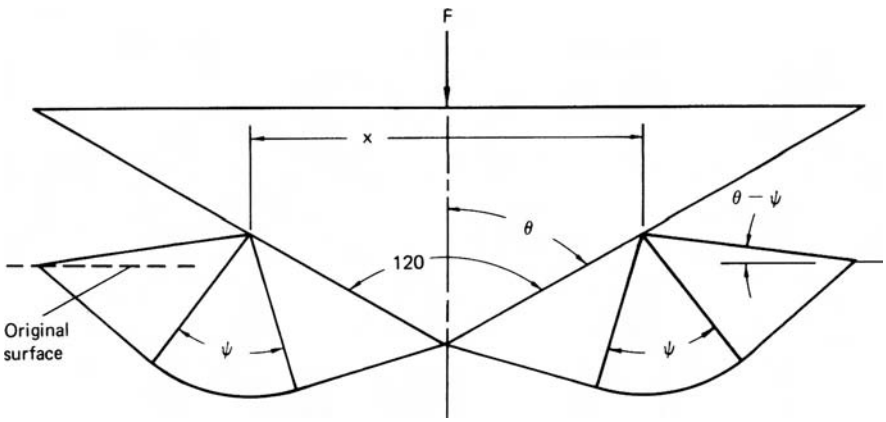

9.38. Slip-line field for plane-strain wedge indentation.

9.5. Figure 9.39 shows the slip-line field for a 2:1 reduction by indirect or backward frictionless extrusion.

a) Determine $P_\perp/2k$.

b) Construct a hodograph for the lower half of the field.

c) Find V^*_{AD}/V_0.

d) What percent of the energy is expended by the gradual deformation in the centered fans?

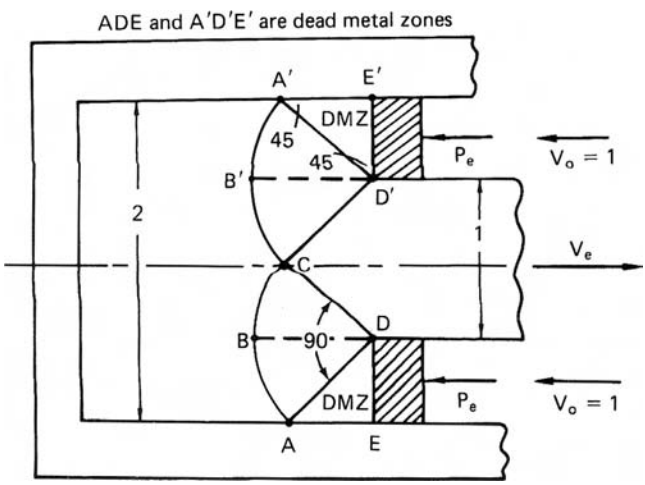

9.39. Slip-line field for the indirect extrusion of Problem 9.5.

9.6. Figure 9.40 shows the slip-line field for the 3:1 frictionless extrusion. Find $P_\perp/2k$ and η.

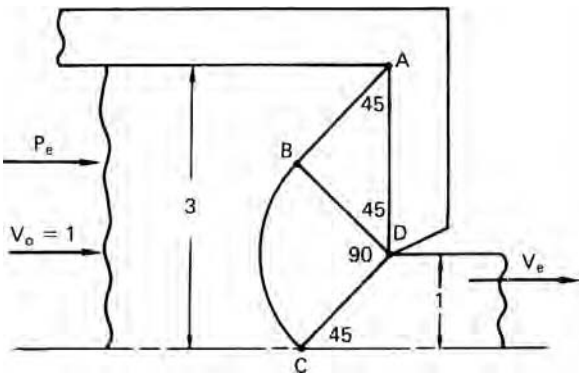

9.40. The slip-line field for the 3:1 frictionless extrusion in Problem 9.6.

9.7. Indentation of a step on a semi-infinite hill is shown in Figure 9.41. Show that this field is not possible and draw a correct field.

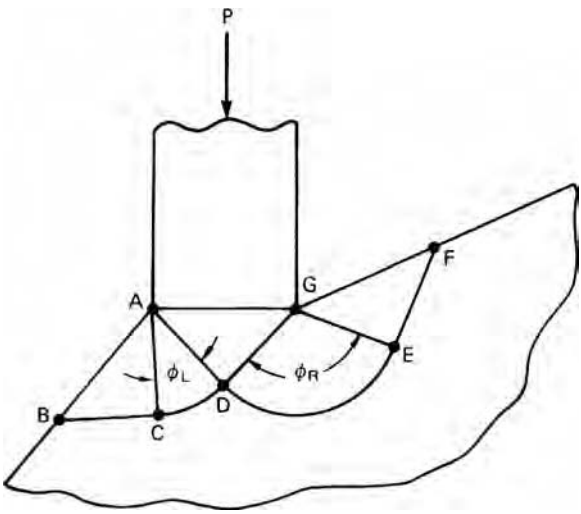

9.41. An incorrect field for indentation on a semi-infinite hill.

9.8. What is the highest level of hydrostatic tension, expressed as $\sigma_2/2k$, that can be induced by two opposing flat indenters as shown in Figure 9.42?

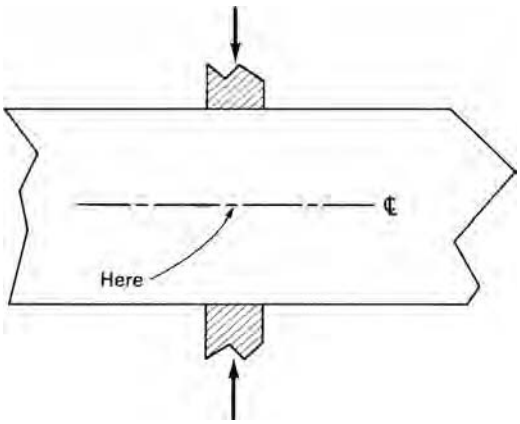

9.42. Indentation by two opposing flat indenters.

9.9. Consider the back extrusion in Figure 9.43. Assume frictionless conditions.

a) Find $P_\perp/2k$.

b) Construct the hodograph.

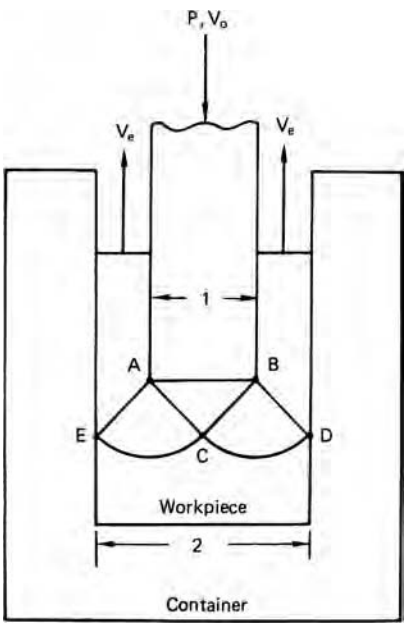

9.43. Back extrusion in Problem 9.9.

9.10. Consider punching a long, thin slot as shown in Figure 9.44. For punching, shear must occur along AB and CD.

a) Find $P_\perp/2k$ as a function of t.

b) If the ratio of t/w is too great, an attempt to punch will result in a plane-strain hardness indentation. What is the largest ratio of t/w for which a slot can be punched?

c) Consider punching a circular hole of diameter, d. Assume a hardness of $P/2k = 3$. What is the lowest ratio of hole diameter to sheet thickness that can be punched?

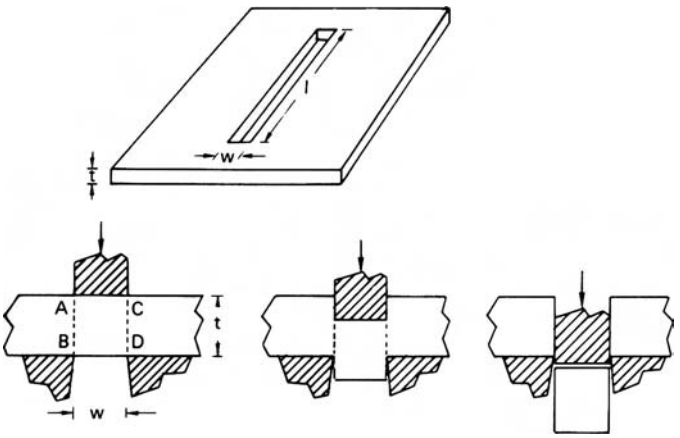

9.44. Slot punching.

9.11. A deeply notched tensile specimen much longer than its width and very deep in the direction normal to the drawing is shown in Figure 9.45. Calculate $\sigma_x/2k$ for the field where $\sigma_x = F_x/t_n$.

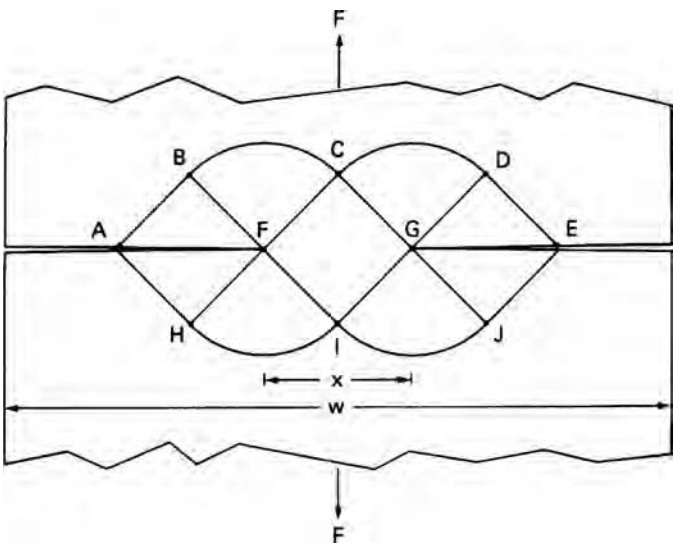

9.45. Deeply notched tensile specimen for Problem 9.11.

9.12. Consider a plane-strain tension test on the notched specimen in Figure 9.46(a). The notch angle is 90° and $w \gg y_0$. Using the slip-line field in Figure 9.46(b), calculate $\sigma_x/2k$ where $\sigma_x = F_x/t_n$.

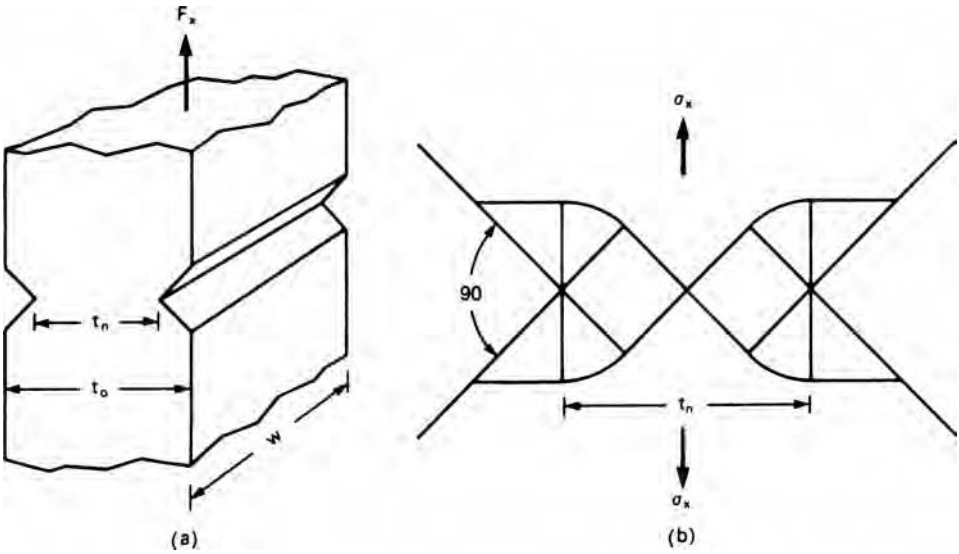

9.46. Notched tensile specimen for Problem 9.12.

9.13. If the notches in Problem 9.12 are too shallow (i.e., t_0/t_n is too small) the specimen may deform by shear between the base of one notch and the opposite side as shown in Figure 9.47. What ratio of t_0/t_n is needed to prevent this?

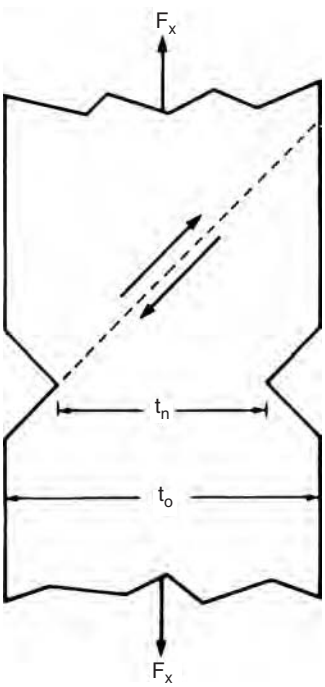

9.47. Alternate mode of failure for a notched tensile bar if t_0/t_n isn't large enough. See Problem 9.13.

9.14. Figure 9.48 shows the appropriate slip-line field for either frictionless plane-strain drawing or extrusion where $r = 0.0760$ and $\alpha = 15°$.

a) Find the level of σ_2 at point (4, 5) for extrusion.

b) Find the level of σ_2 at point (4, 5) for drawing.

c) How might the product depend on whether this is an extrusion or a drawing?

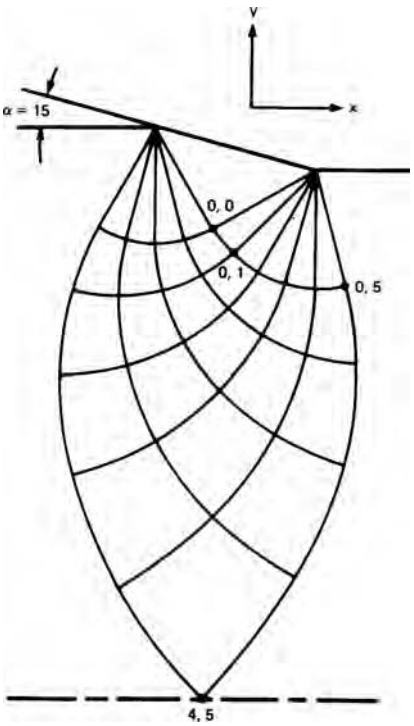

9.48. Slip-line field for Problem 9.14.

9.15. Figure 9.49 shows two slip-line fields for the compression of a long bar with an octagonal cross section. Which field is appropriate? Justify your answer.

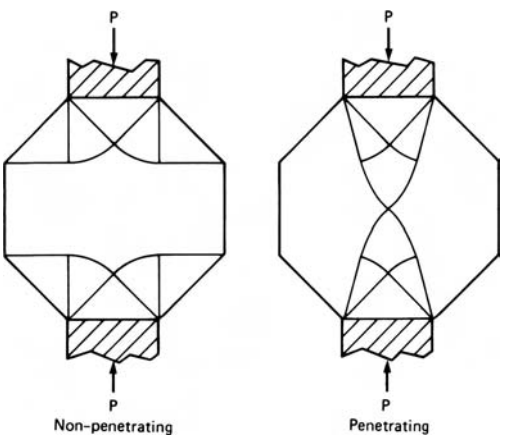

9.49. Two possible slip-line fields for plane-strain compression of an octagonal rod. See Problem 9.15.

9.16. Consider an extrusion in a frictionless die with $\alpha = 30^\circ$ and such that point (2, 4) in Figure 9.18 is on the centerline.

a) What is the reduction?

b) Calculate $P_{ext}/2k$.

c) Calculate η.

d) Find the hydrostatic stress, σ_2, at the centerline.

9.17. Consider the slip-line field for an extrusion with a constant shear stress along the die wall as shown in Figure 9.50.

a) Label the α- and β-lines.

b) Draw the Mohr's circle diagram for the state of stress in triangle ACD showing $P_\perp$, $\tau_f = mk$, α, and β.

c) Calculate the value of m.

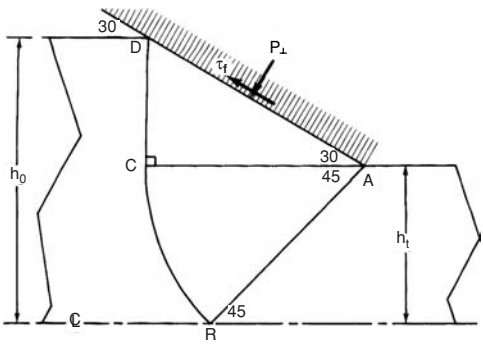

9.50. Slip-line field for extrusion with a constant shear stress die interface. See Problem 9.17.

9.18. At the end of an extrusion in a 90° die, a nonsteady-state condition develops. The field in Figure 9.51(a) is no longer appropriate. Figure 9.51(b) is an

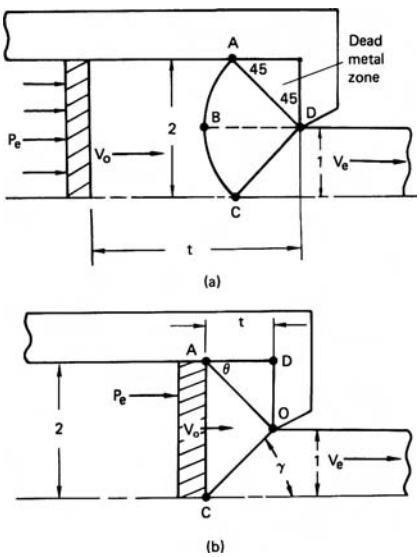

9.51. (a) Slip-line field for a 2:1 extrusion. (b) Upper-bound field for the end of a 2:1 extrusion. See Problem 9.18.

upper-bound field for $t < 1$. Calculate and plot $P_{ext}/2k$ as a function of t for $0.25 \leq t \leq 5$ for the upper-bound field. Include on your plot the value of $P_{ext}/2k$ for the slip-line field.

9.19. In Problem 9.17, either the slip-line field or the upper bound gives a lower solution. However, as discussed in Section 9.12, a pipe may form at the end of an extrusion. Figure 9.52 gives an upper-bound field that leads to pipe formation. Calculate $P_{ext}/2k$ as a function of t for $0.25 \leq t \leq 5$ and compare with the solution to Problem 9.17.

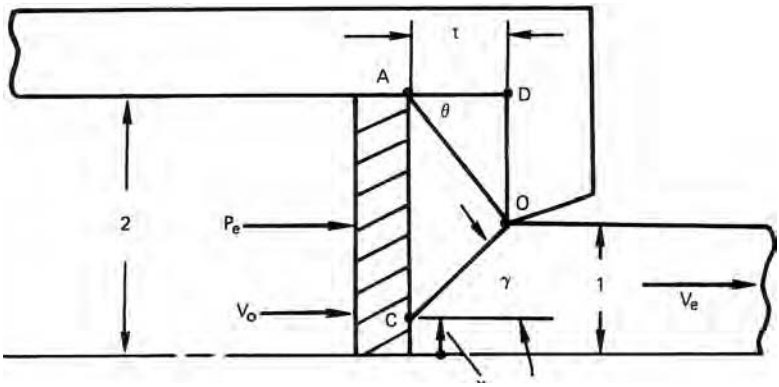

9.52. An upper-bound field for pipe formation. See Problem 9.18.

10 Deformation-Zone Geometry

10.1 THE Δ PARAMETER

The shape of the deformation zone has a strong influence on the redundant work, the frictional work, and the forming forces. It also influences the properties of the product material. The homogeneity, the tendency to crack, the pattern of residual stresses, and the porosity are all affected by the deformation-zone geometry. The parameter Δ, defined as the ratio of the thickness or diameter, H, to the contact length between work piece and die, L, has a large effect on these properties:

$$\Delta = H/L. \tag{10.1}$$

For plane-strain extrusion and drawing, the contact length $L = (H_0 - H_1)/(2 \sin \alpha)$ and the mean thickness $H = (H_0 + H_1)/2$, so

$$\Delta = \frac{(H_0 + H_1)}{(H_0 - H_1)} \sin \alpha. \tag{10.2}$$

Substituting the reduction $r = (H_0 - H_1)/H_0$,

$$\Delta = \frac{2 - r}{r} \sin \alpha. \tag{10.3}$$

Equation 10.2 holds for axisymmetric extrusion and drawing, where H is the diameter, so $r = ({H_0}^2 - {H_1}^2)/{H_0}^2$, so

$$\Delta = \frac{1 + \sqrt{1 - r}}{1 - \sqrt{1 - r}} \sin \alpha = \left(1 + \sqrt{1 - r}\right)^2 \sin \alpha / r. \tag{10.4}$$

Note that for the same α and r, equation 10.3 gives a Δ value for axisymmetric deformation about twice that for plane strain (equation 10.2).

For flat rolling, Δ is simply the mean height $(H_0 + H_1)/2 = H_0(2 - r)/2$ divided by the contact length $L = \sqrt{R \Delta H} = \sqrt{r R H_0}$ (equation 7.34), or

$$\Delta = \frac{2 - r}{2} \sqrt{\frac{H_0}{rR}}. \tag{10.5}$$

Slightly different definitions of Δ are used elsewhere.* In all of the equations, Δ increases with die angle and decreases with reduction.

10.2 FRICTION

The frictional contribution to the total work, w_f/w_a, increases with decreasing Δ because the contact area between the die and work piece increases as Δ decreases. In both plane-strain and axisymmetric drawing, the ratio of contact area to mean cross-sectional area is

$$\text{Area ratio} = \frac{2r}{(2-r)\sin\alpha}. \tag{10.6}$$

The upper-bound analysis for constant friction interface in plane-strain drawing (equation 8.22) predicts that

$$w_f/w_h = m/\sin(2\alpha). \tag{10.7}$$

For small values of α, $\sin 2\alpha \approx 2\sin\alpha$, so at constant friction w_f/w_a is proportional to Δ.

With a constant coefficient of friction, equation 7.11 for axisymmetry and equation 7.7 for plane strain both give

$$\frac{\sigma_d}{\sigma_0} = \frac{1+B}{B}[1-\exp(-B\varepsilon_h)], \tag{10.8}$$

where $B = m\cot\alpha$. Substituting these into the series expansion $\exp(-x) = 1 - x + x^2/2 + \cdots$, $\sigma_d/\sigma_0 = \varepsilon(1 + B - B^2\varepsilon/2 + \cdots)$. Now substituting $w_h = \sigma_0\varepsilon$ and $w_f = \sigma_d - w_h$,

$$w_f/w_h = B(1-\varepsilon/2+\cdots) \approx \mu\cot\alpha(1-\varepsilon/2). \tag{10.9}$$

10.3 REDUNDANT DEFORMATION

It is convenient to describe the redundant strain ε_r by a parameter $\phi = (\varepsilon_r - \varepsilon_h)/\varepsilon_h)$, where ε_h is the homogeneous strain. In the absence of strain hardening, $(w_r + w_h)/w_h = (\varepsilon_r - \varepsilon_h)/\varepsilon_h) = \phi$. In this case

$$\phi = (\sigma_d - w_f)/(\sigma_0\varepsilon_h). \tag{10.10}$$

Equations 8.21 and 8.27 from the upper-bound analysis can be used to predict ϕ for plane-strain and axisymmetric drawing. Comparing with equation 10.10,

$$\phi = 1 + (1/2)\tan\alpha/\varepsilon_h \tag{10.11}$$

for plane strain and

$$\phi = 1 + (2/3)\tan\alpha/\varepsilon_h \tag{10.12}$$

* Backofen defined the mean height, H, as the arc length drawn through the middle of the deformation zone, so that his expressions are identical to equations 10.2, 10.3, and 10.4 except that $\sin\alpha$ is replaced by α.

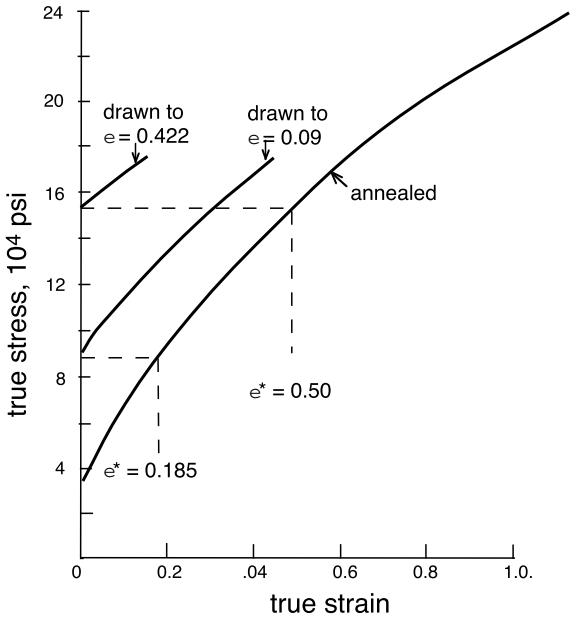

10.1. Stress–strain curves of 303 stainless before and after wire drawing. Adapted from R. M. Caddell and A. G. Atkins, *op. cit.*

for axisymmetry. Numerical evaluation of equations 10.11 and 10.12 for various combinations of $\alpha < 30^\circ$ and $r < 0.5$ result in approximations

$$\phi \approx 1 + \Delta/4 \tag{10.13}$$

for plane strain, and for axisymmetric flow

$$\phi \approx 1 + \Delta/6. \tag{10.14}$$

The slip-line solutions for plane-strain indentation (Figure 9.19) can be approximated by

$$\phi \approx 1 + 0.23(\Delta - 1) \quad \text{for } 1 \leq \Delta \leq 8.8. \tag{10.15}$$

There is no corresponding solution for axisymmetric flow.

Figure 10.1 from Caddell and Atkins* shows the true tensile stress–strain curves for a 303 stainless steel in the annealed condition and after two wire-drawing reductions. Comparing the yield strengths after drawing with the annealed stress strain curve, the value of ϕ could be deduced. The results with other die angles and reductions (Figure 10.2) could be approximated by

$$\phi = C_1 + C_2\Delta. \tag{10.16}$$

where C_1 and C_2 are constants.

* R. M. Caddell and A. G. Atkins, *J. Eng. Ind. Trans ASME*, Series B (1968).

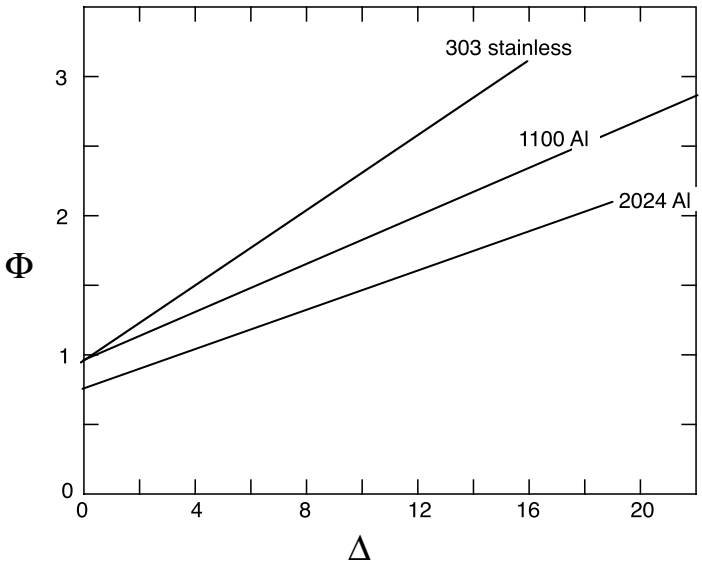

10.2. The influence of Δ on the redundant strain factor ϕ. From R. M. Caddell and A. G. Atkins, *op. cit*.

Similar results were obtained by Backofen* using hardness measurements. By comparing hardness measurements on homogeneously strained material with those after various cold forming operations, he found results very similar to those of Caddell and Atkins (Figure 10.3). For physical reasons ϕ can never be less than unity so Backofen suggested

$$\phi = 1 + C(\Delta - 1) \quad \text{for } \Delta \geq 1 \quad \text{and} \quad \phi = 1 \quad \text{for } \Delta \leq 1, \tag{10.17}$$

where $C = 0.21$ for plane strain and $C = 0.12$ for axisymmetric drawing. Note that the value of $C = 0.21$ is similar to the value 0.23 from slip-line theory. The results for axisymmetric and plain-strain drawing would be much closer if ϕ had been plotted against the ratio of mean cross-sectional area to contact area between work piece and die. This ratio is $\Delta/4$ for axisymmetry and $\Delta/2$ for plane strain.

10.4 INHOMOGENEITY

The redundant strain is not evenly distributed throughout the cross section. Figure 10.4 shows the distortion of gridlines predicted by slip-line field theory for three levels of Δ and Figure 10.5 shows the actual distortion of extruded billets. The effect of Δ on inhomogeneity is also demonstrated by the hardness profiles after flat rolling (Figure 10.6). Backofen characterized the hardness gradients with an inhomogeneity factor

$$\text{I.F.} = (H_s - H_c)/H_c, \tag{10.18}$$

* W. A. Backofen, *Deformation Processing* (Addison-Wesley, 1972) and J. J. Burke, doctoral thesis, MIT (1968).

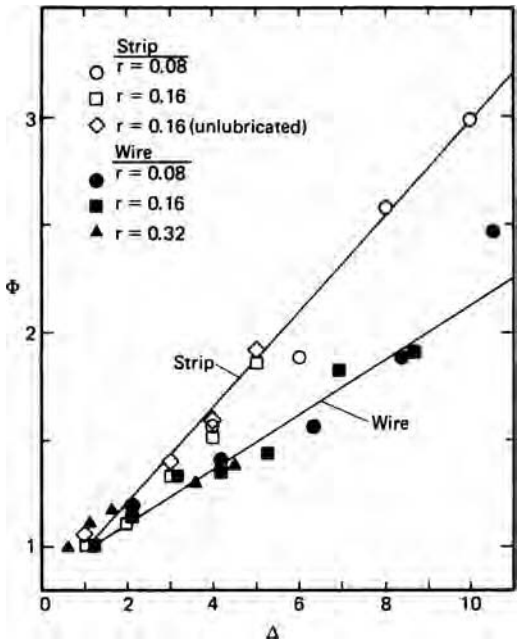

10.3. The influence of Δ on the inhomogeneity factor ϕ for axisymmetric and plane-strain drawing. Adapted form W. A. Backofen and J. J. Burke, *op. cit*.

where H_s and H_c are the Vickers hardnesses at the surface and the center. Plots of I.F. vs. Δ indicate that I.F. increases with Δ but is also dependent on r. If these data are plotted as I.F. versus α (Figure 10.7) there is much less dependence on r and little difference between axisymmetry and plane strain.

Hardness variations after much larger reductions were studied in hydrostatic extrusion experiments by Muira et al.* Figure 10.8 shows that the difference between surface and centerline hardness increases with both increasing die angle and decreasing reduction. At these higher reductions the results correlate roughly with Δ.

Inhomogeneity of flow also affects how crystallographic texture changes between surface and centerline.† If Δ is high, the usual rolling texture will be found only near the centerline. The grain size after recrystallization depends on the amount of deformation prior to annealing. With high Δ the recrystallized grain size at the surface is finer than at the center. Furthermore, if the deformation is rapid enough to be adiabatic, heating will depend on the amount of deformation. This can affect the residual stresses.

EXAMPLE 10.1:

(a) Using the upper-bound field from Sections 8.9 and 8.10, derive an expression for the redundant strain, realizing that it arises from the shear discontinuities at the entrance and exit of the deformation zone.

(b) Find the ratio of the total strain at the surface to that at the center.

(c) The Vickers hardness can be expressed as $H = C\varepsilon^n$, where n is much lower than the strain-hardening exponent in tension. Derive an expression for the inhomogeneity factor in terms of α and r.

* S. Miura, Y. Saeki, and T. Matushita, *Metals and Materials*, 7 (1973), pp. 441–47.
† P. S. Mathur and W. A. Backofen, *Met. Trans*., 4 (1973), pp. 643–51.

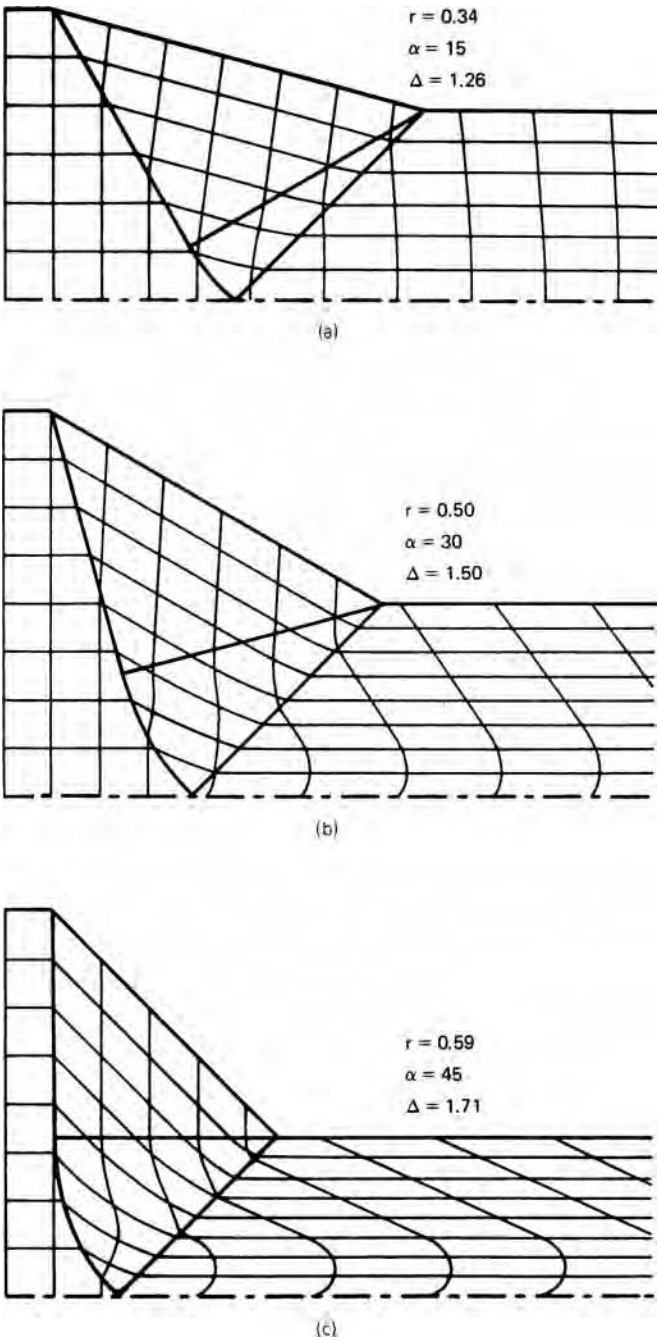

10.4. Grid distortions predicted by slip-line field theory for strip drawing. Note that the distortion increases with increasing Δ.

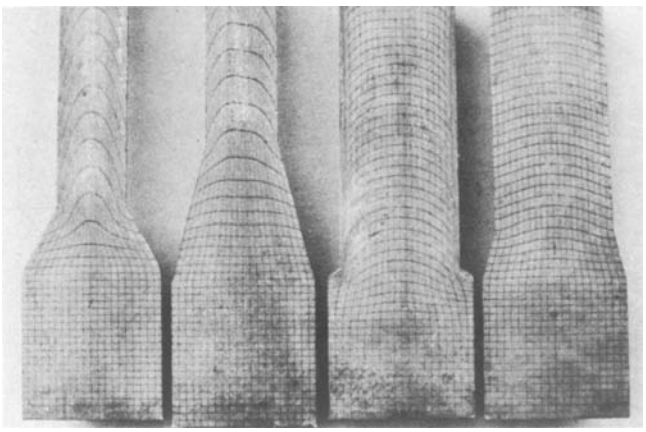

10.5. Grid distortion of cold extruded billets. From D. J. Blickwede. *Metals Progress*, 97 (May 1970), pp. 76–80.

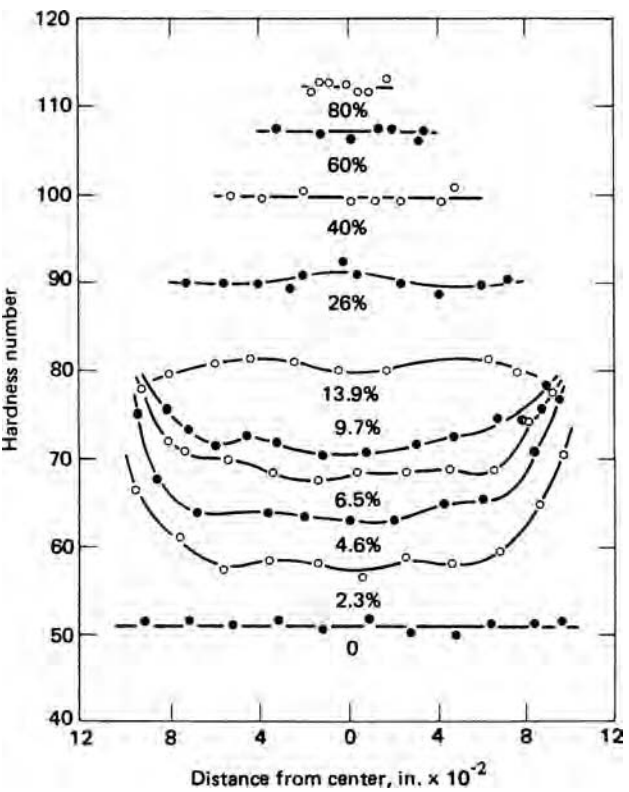

10.6. Hardness gradients in copper after rolling in a single pass to the indicated reduction. Initial thickness was 0.2 in and the roll diameter was 10 in. Note that the inhomogeneity is largest for small reductions. From B. B. Hundy and A. R. E. Singer, *J. Inst. Metals*, 83 (1954–5).

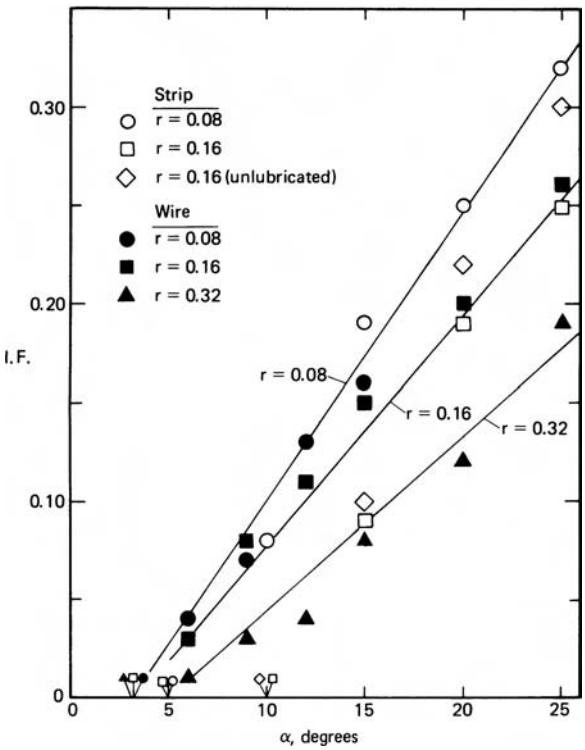

10.7. Dependence of the inhomogeneity factor on die angle. Data from W. A. Backofen and J. J. Burke, *op. cit*.

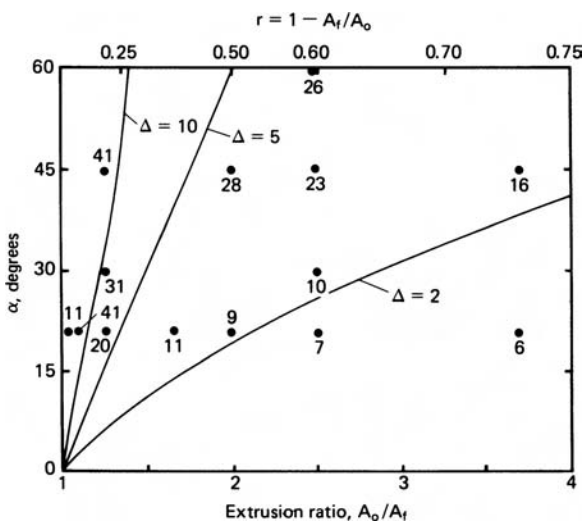

10.8. Effect of die angle and reduction on the inhomogeneity of steel extrusions. Numbers are the difference between the surface and centerline hardnesses. Lines of constant Δ were calculated from equation 10.4. Data from S. Muira et al., *op. cit.*

(d) The reference on which Figure 10.7 is based gives $H = 134\varepsilon^{0.15}$. Using this make a plot of I.F. versus α for $r = 0.08$, 0.16, and 0.32 and compare with Figure 10.7.

SOLUTION:

(a) The hodograph (Fig. 8.13b) shows that the velocity discontinuity at the surface at the entrance and exit is $V_0 \tan\alpha$. This corresponds to a work rate of $kV_0 \tan\alpha \, dy$ in an element of thickness dy. For both the entrance and exits, the redundant work rate is $2kV_0 \tan\alpha \, dy$ and the work per volume is $2k \tan\alpha$. Therefore the redundant strain is $\varepsilon_r = (2k/\sigma_0)\tan\alpha$. Taking $2k = \sigma_0$, $\varepsilon_r = \tan\alpha$ at the surface.

(b) The strain at the centerline is the homogeneous strain, ε_h, so the total strain at the surface is $\tan\alpha + \varepsilon_h$. Therefore, $\varepsilon_s/\varepsilon_c = 1 + (\tan\alpha)/\varepsilon_h$.

(c) I.F. $= H_s/H_c - 1 = (\varepsilon_s/\varepsilon_c)^n - 1 = [1 + \tan\alpha/\varepsilon_h)]^n - 1$.

(d) Taking $\varepsilon_h = -\ln(1-r)$ and evaluating, we obtain the following:

		I.F.			
r	ε	$\alpha = 5°$	$\alpha = 10°$	$\alpha = 20°$	$\alpha = 30°$
0.08	0.0834	0.114	0.186	0.287	0.364
0.16	0.1743	0.063	0.111	0.184	0.245
0.32	0.3857	0.031	0.058	0.105	0.147

This shows that the simple theory is in good agreement with the experimental data for $r = 0.16$ and 0.32 but overestimates I.F. for $r = 0.08$.

All of the previous analyses have assumed dies that are conical or wedge-shaped. However, Devenpeck and Richmond* designed plane-strain dies using slip-line theory and axisymmetric dies using numerical analysis that, in principle, produce no redundant strain and therefore no surface-to-center property gradients. Figure 10.10 shows two such profiles and Figure 10.11 compares experimental and theoretical grid distortion through such dies. Although the agreement is good, it should be noted that low Δ characterizes the dies.

10.5 INTERNAL DAMAGE

The high hydrostatic tension at the centerline that occurs under high Δ conditions can lead to internal porosity and under extreme conditions to internal cracks. This is evident in Figure 9.24, where $\Delta = 5.83$ and there is mid-plane hydrostatic tension of $\sigma_2 = 0.62(2k)$. Mid-plane hydrostatic tension can exist even for extrusion. Coffin and Rogers† found significant losses of density after slab drawing as indicated in Figure 10.12. Note that the density loss increases with die angle and is cumulative, increasing from pass to pass.

The loss in density is caused by microscopic porosity being formed at hard inclusions. There is much less density loss in clean single-phase materials than in dirtier

* M. L. Devenpeck and O. Richmond, *J. Engr. Ind. Trans. ASME*, 87 (1965), p. 425.
† L. F. Coffin Jr. and H. C. Rogers, *Trans. ASM*, 60 (1967), pp. 672–86.

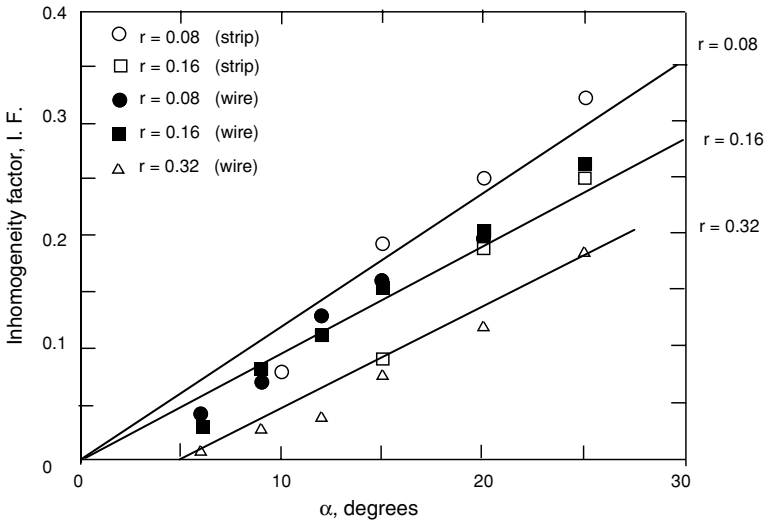

10.9. Calculated α dependence of I.F. (solid lines) and experimental values (symbols) for various reductions.

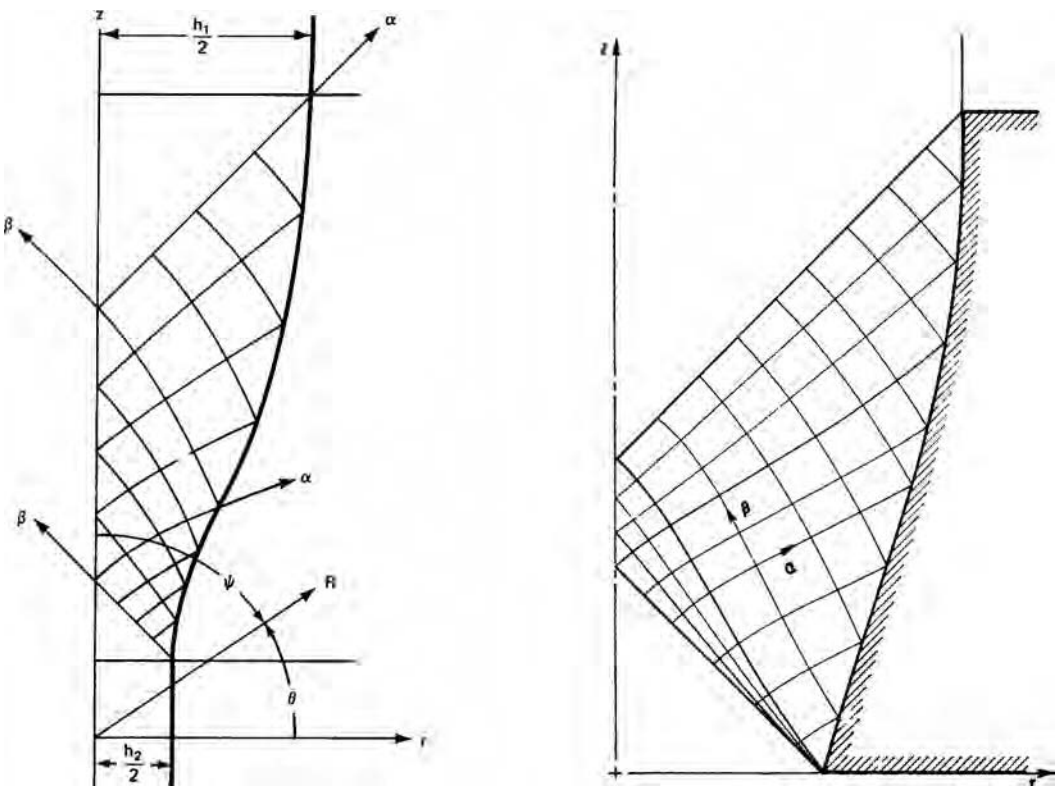

10.10. Two die profiles designed to give zero redundant strain for frictionless conditions. From (left) O. Richmond in *Mechanics of the Solid State*, F. P. J. Rimrott and J. Schwaighofer, eds. (University of Toronto Press, 1968) and O. Richmond and M. L. Devenpeck. *Proc. 4th U. S. Nat. Cong. Appl. Mech*. (1962), and (right) O. Richmond and H. L. Morrison, *J. Mech. Phys*. Solids, 15 (1967).

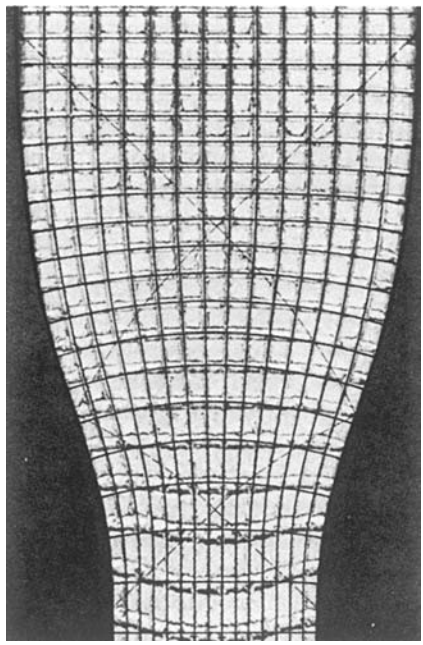

10.11. Overlay of theoretical grid distortions on actual distortions from a die like that in Figure 10.10 (left). From O. Richmond and M. L. Devenpeck, *J. Engr. Ind. Trans. ASME*, 87 (1965).

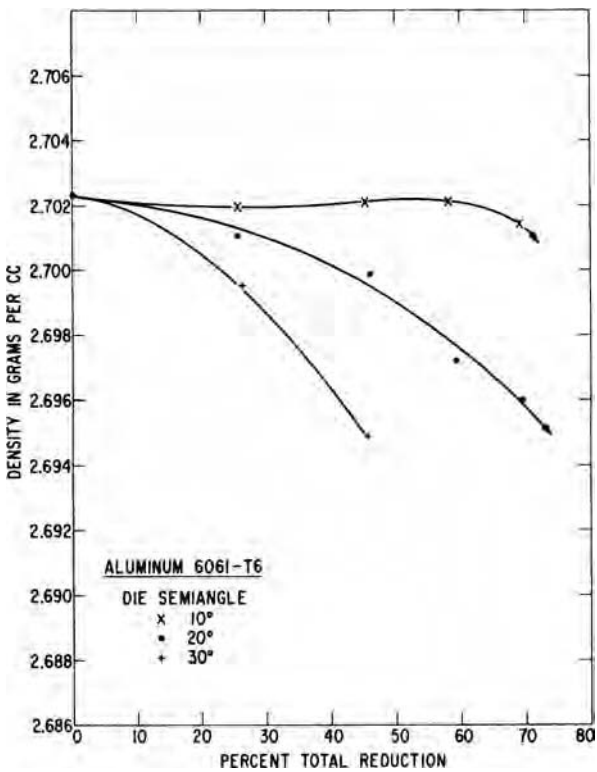

10.12. Density changes after plane-strain drawing in 6061-T6 aluminum. From H. C. Rogers, General Electric Co. Report No. 69-C-260 (July 1969).

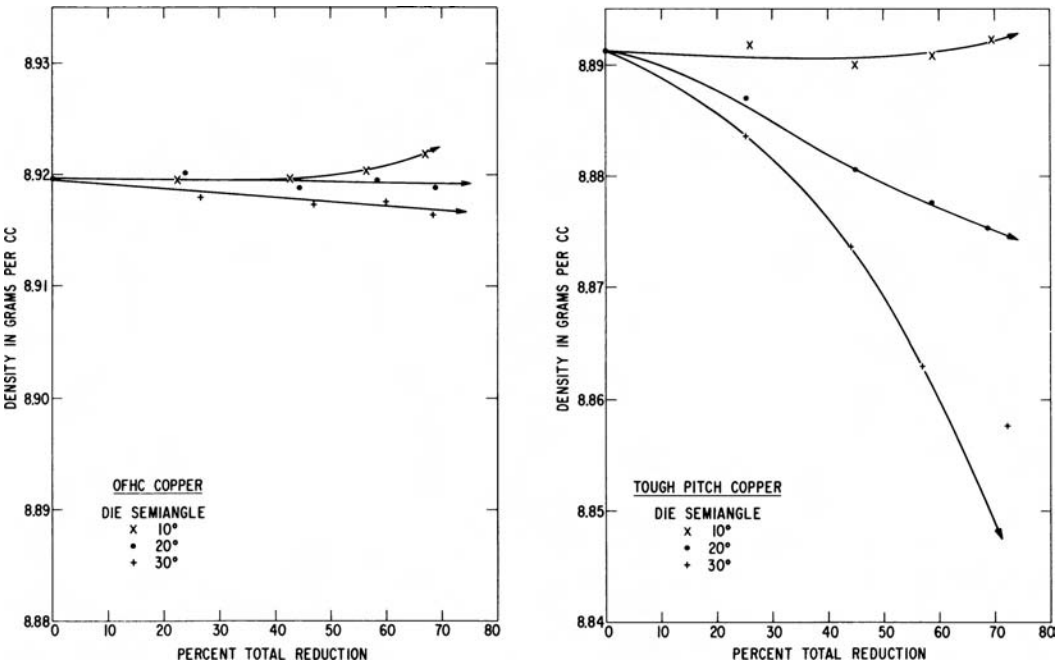

10.13. Density changes in OFHC copper (left) and tough-pitch copper (right) caused by drawing. Note that the density loss is much greater in the tough pitch copper, which contains many hard Cu_2O particles. From H. C. Rogers, *op. cit.*

material with two phases. Figure 10.13 compares the density loss in tough-pitch copper with a high content of Cu_2O particles with that in oxygen-free high-conductivity (OFHC) copper. They also found that the loss of density could be decreased or eliminated by drawing under external hydrostatic pressure.

Under severe conditions pores may link up forming internal cracks. Figure 10.14 shows an early stage of such linking up and Figure 10.15 shows chevron cracks formed

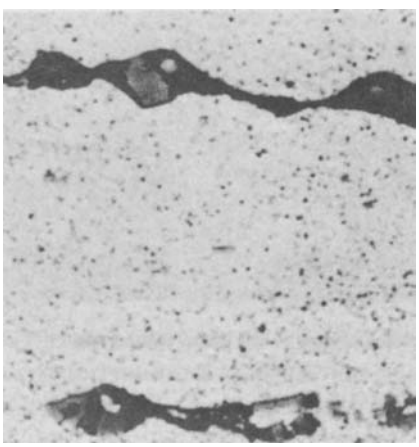

10.14. Voids formed in 6061-T6 aluminum after plane-strain drawing through a 30° die to a total reduction of 75%. From H. C. Rogers, R. C. Leech, and L. F. Coffin Jr., *Final Report, Contract NOw-65-0097-f*, Bureau of Naval Weapons (1965).

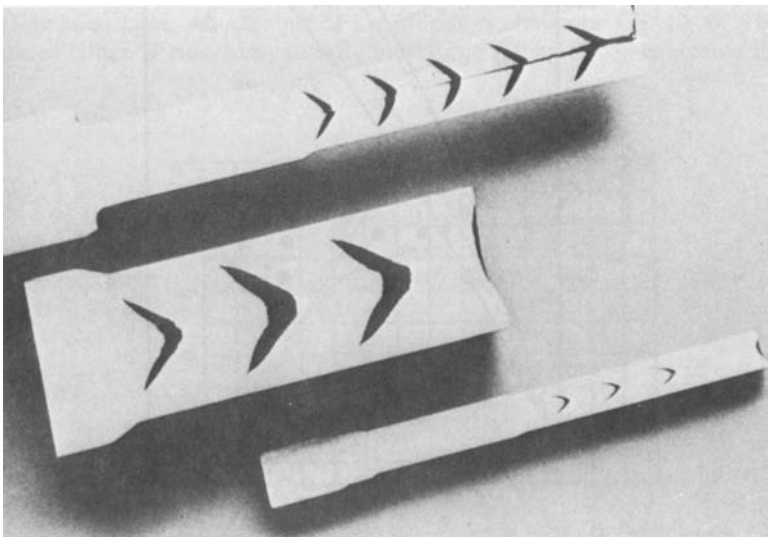

10.15. Chevron cracks formed during extrusion of steel rods. Note the very low reduction and high die angle. From D. J. Blickwede, *op. cit*.

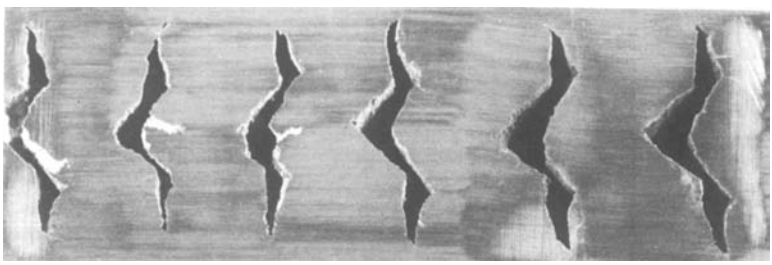

10.16. Cracks formed in a molybdenum bar during rolling under high Δ conditions.

at very high Δ conditions in extrusion. The terms "arrowhead cracks," "centerline burst," and "cuppy core" have been applied to this phenomenon. Figure 10.16 shows similar cracks formed during rod-rolling.

Avitzur* has studied the problem of centerline bursts with an upper-bound analysis and found conditions under which formation of central holes lowers the deformation energy. Figure 10.17 shows the results of his analysis and experimental results for several work-hardened steels. It is interesting to note that the conditions that produce centerline bursts can be described by $\Delta > 2$.

10.6 RESIDUAL STRESSES

The magnitude and nature of residual stresses caused by mechanical processing depend on the shape of the deformation zone. With Δ-values of one or less (high reductions and low die angles) the deformation is relatively uniform and there are only minor residual stresses. With high Δ-values the surface is left under residual tension with residual compression at the centerline. The magnitude of the stresses increases with Δ as shown in Figure 10.18 for rolling, Figure 10.19 for drawing and Figure 10.20 for extrusion.

* B. Avitzur, *Metal Forming: Processes and Analysis* (McGraw-Hill, 1969), pp. 172–6.

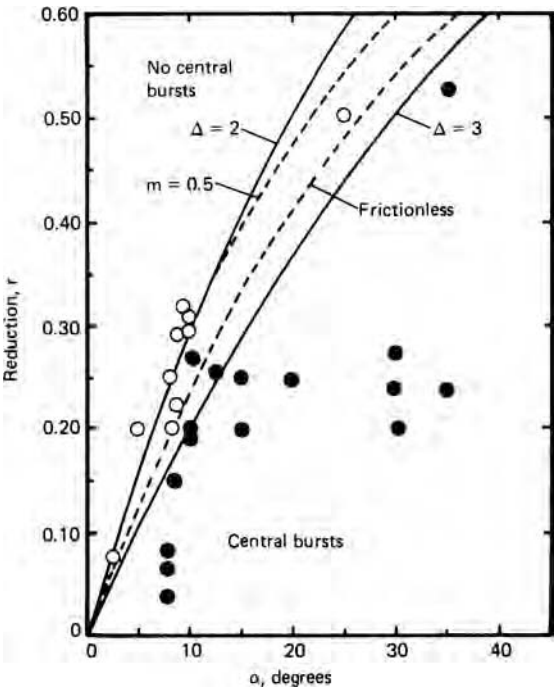

10.17. Occurrence of centerline bursts in three steels during extrusion. Filled circles indicate bursts and open circles indicate no bursts. The dashed lines are Avitzur's analysis for no friction and for interface shear stress, $mk = 0.5k$. The solid lines are for constant Δ. Data from Z. Zimmerman and B. Avitzur, *J. Eng. Ind., Trans. ASME*, 92 (1970), p. 135.

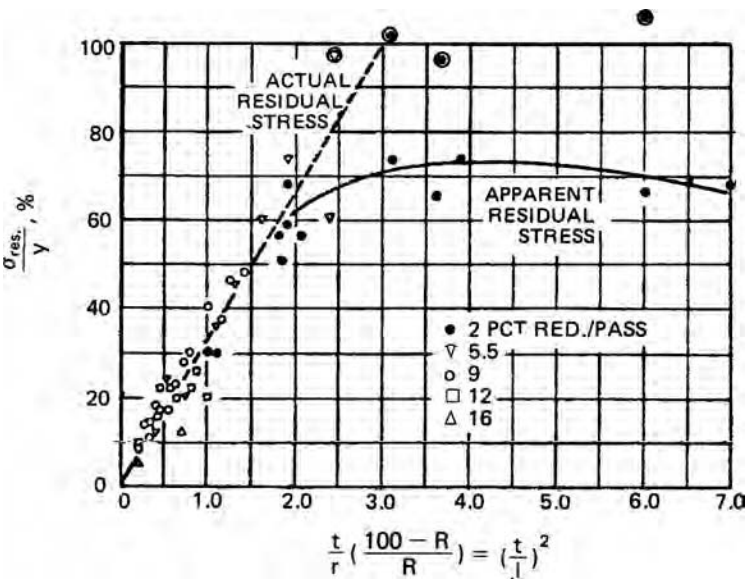

10.18. Residual stresses at the surface of cold rolled strips. The stresses are normalized by the yield strength. Note that $(t/l)^2 = \Delta^2$. From W. M. Baldwin, *Proc. ASTM*, 49 (1949), pp. 539–83.

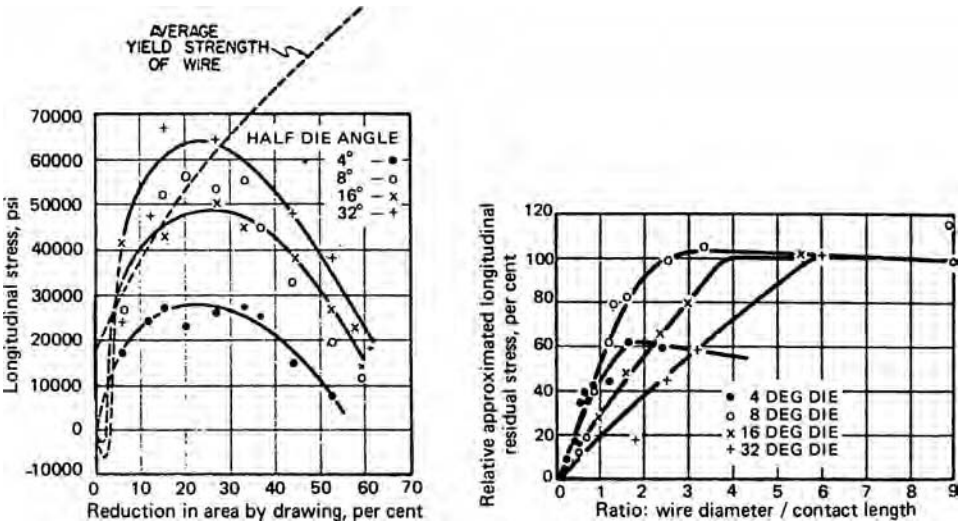

10.19. Residual stresses at the surface of cold-drawn brass wire (left) and the same data replotted as the ratio of residual stress to yield strength versus Δ (right). From W. M. Baldwin, *op. cit*. Original data were from W. Linius and G. Sachs, *Mitt. Dtsch. Materialprüfunsanst*, 16 (1932), pp. 38–67.

High residual stresses coupled with centerline damage may cause spontaneous splitting or "alligatoring" of the work piece as it leaves the deformation zone. Figure 10.21 shows an example. In rolling, this type of failure is most likely in early breakdown of ingots because the section thickness is usually large relative to the roll

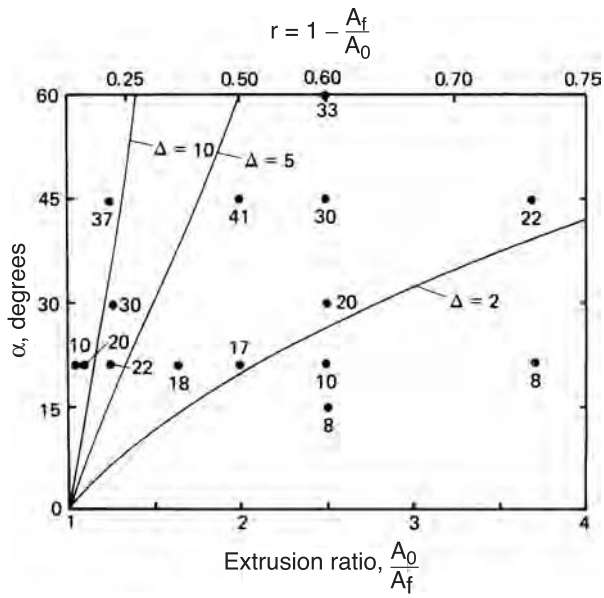

10.20. Effect of die angle and reduction on the residual stresses in extruded steel rods. The numbers are the residual stress on the surface in kg/mm^2. The lines of constant Δ fit the data well. Data from S. Miura et al., *op. cit*.

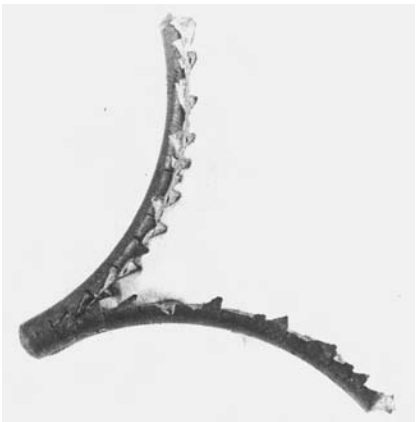

10.21. Molybdenum rod that alligatored during rolling under high Δ conditions. The "teeth" formed by edge cracking are not common in alligatored bars.

diameter. Furthermore, ingots often have porosity and second phases concentrated near the centerline. Hot rolling under favorable Δ conditions tends to close such porosity. Residual tension at the surface is particularly undesirable because it leads to increased susceptibility to fatigue and stress-corrosion cracking.

Despite the general usefulness of slip-line field theory in metal forming, it does not adequately explain the observed patterns of residual stress. For deformation under high Δ conditions, the theory predicts that during deformation, the level of hydrostatic stress is highest at the centerline and most compressive at the surface. The theory allows for no plastic deformation once the material leaves the deformation zone, so unloading must be perfectly elastic. The normal stress must go to zero and the horizontal force must go to zero. It is difficult to rationalize how there can be complete reversal of stresses on unloading.

If the deformation is rapid enough to be nearly adiabatic, the surface will be hotter than the interior. The surface and interior must undergo the same contraction on cooling so the surface will be left under residual tension.

Very low reductions lead to an opposite pattern of residual stress with the surface being left in residual compression. Figure 10.22 illustrates this. Note, however, that as soon as the reduction reaches 0.8% the normal pattern of residual tension on the surface is observed.

10.7 COMPARISON OF PLANE-STRAIN AND AXISYMMETRIC DEFORMATION

Friction, redundant strain, and inhomogeneity effects on plane-strain and axisymmetric forming are summarized in Table 10.1. A general conclusion is that frictional effects depend primarily on die angle. In plane-strain and axisymmetric forming the effects are the same for the same values of α and r. These are the same for Δ in axisymmetric forming half as large as the Δ in plane strain.

Similarly, the inhomogeneity at low α and r is the same in both types of operations. At larger reductions the data of Miura et al., *op. cit.*, indicate a Δ-dependence for axisymmetry. Redundant strain correlates best with Δ. For equal values of Δ, plane-strain operations are characterized by much higher ϕ than for axisymmetry. However,

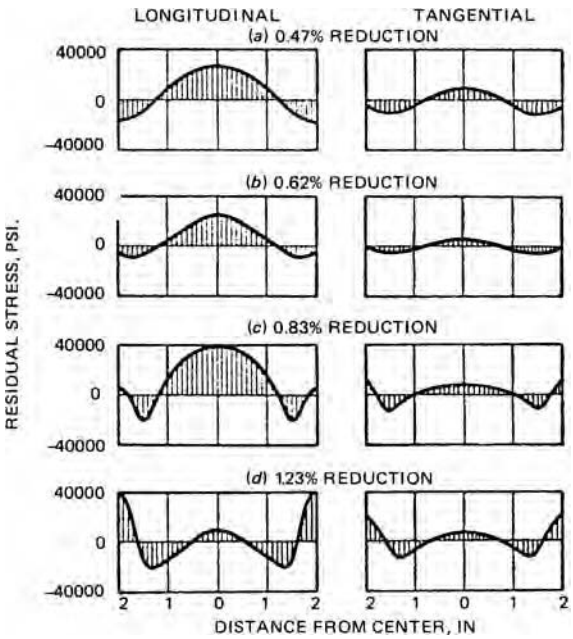

10.22. Residual stresses in lightly drawn steel rods. From W. M. Baldwin, *op. cit.* after H. Bühler and H. Buchholtz, *Archiv. für des Eisenhüttenwesen*, 7 (1933–4), pp. 427–30.

Table 10.1. Comparison of plane-strain and axisymmetric drawing

	Plane strain	Axisymmetry	Comment
Ratio of mean cross-sectional area to tool–workpiece contact area	$\Delta/2$	$\Delta/4$	Equal for same r and α.
Frictional contribution to $\sigma_d/2k$ according to slab analysis with shear stress	$m/\sin 2\alpha$	$m/\sin 2\alpha$	Equal for same r and α, but with same Δ, axisymmetry constant has twice the effect.
Frictional contribution to $\sigma_d/2k$ according to slab analysis with friction coefficient	$\approx\mu \cot\alpha(1-\varepsilon/2)$	$\approx\mu \cot\alpha(1-\varepsilon/2)$	Equal for same r and α, but with same Δ, axisymmetry constant has twice the effect.
Redundant strain contribution to $\sigma_d/2k$ according to upper-bound slab analysis	$\approx\Delta/4$	$\approx\Delta/6$	For same r and α, less redundant strain in plane strain but for same Δ less for axisymmetry.
Redundant strain according to slip-line field theory	$\approx 0.23(\Delta-1)$	no solution for axismmetry	
Redundant strain from Burke and Backofen experiments†	$\approx 0.21(\Delta-1)$	$\approx 0.12(\Delta-1)$	For same Δ, nearly twice as much for plane strain but for same α and r, roughly equal.
Inhomogeneity factor	$[1 + (\tan\alpha)/\varepsilon_h]^n - 1$		Approximately equal for axisymmetry and plane strain at the same α.

†Source: W. A. Backofen, *op. cit.*

if comparisons are made at equal ratios of mean cross-sectional area to contact area, the values of ϕ are slightly higher for axisymmetry.

NOTE OF INTEREST

W. A. Backofen was born December 8, 1928, in Rockville, Connecticut. He studied at MIT from 1943 to 1950, which he received his doctorate and was appointed as an assistant professor. He did much innovative research in his 25 years at MIT. He introduced the basic concepts of superplasticity and of texture strengthening and made clear the importance of deformation-zone geometry. He retired in 1975 to a farm in New Hampshire where he raised Christmas trees, apples, and blueberries. Backofen died in 2007.

REFERENCES

B. Avitzur, *Metal Forming: Processes and Analysis*, McGraw-Hill, 1968.
W. A. Backofen, *Deformation Processing*, Addison-Wesley, 1972.
E. M. Meilnik, *Metalworking Science and Engineering*, McGraw-Hill, 1991.

PROBLEMS

10.1. The XYZ Special Alloy Fabrication Company has an order to roll a $4 \times 4 \times 15$ in billet of a nickel-base superalloy to $\frac{1}{2}$ in thickness. They tried rolling it with a 5% reduction per pass, but it split on the fourth pass. At a meeting the process engineer suggested using a lower reduction per pass, the consultant suggested applying forward and backward tension, and the shop foreman was in favor of heavier reductions per pass. With whom, if anyone, do you agree? Defend your position.

10.2. The Mannesmann process for making tubes from cylindrical billets is illustrated in Figure 10.23. It involves passing the billet between two nonparallel rolls adjusted for a very small reduction onto a mandrel positioned in the middle. Explain why the axial force on the mandrel is low and why the mandrel, which is long and elastically flexible, follows the center of the billet.

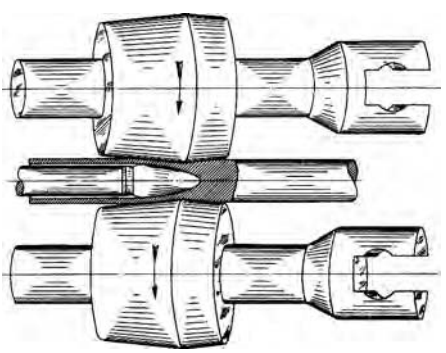

10.23. The Mannesman process for making tubes.

10.3. **a)** Show that as r and α approach zero equations 10.11 and 10.12 reduce to $\phi = 1 + \Delta/4$ for plane strain and $\phi = 1 + \Delta/6$ for axisymmetry.
b) What percent error does this simplification introduce at $r = 0.5$ and $\alpha = 30^\circ$?

10.4. Consider wire drawing with a reduction of $r = 0.25$ and $\alpha = 6^\circ$.

a) Calculate the ratio of average cross-sectional area to the contact area between wire and die.

b) What is the value of Δ?

c) For strip drawing with $\alpha = 6^\circ$, what reduction would give the same value of Δ?

d) For the reduction in (c), calculate the ratio of of average cross-sectional area to the contact area and compare with your answer to (a).

e) Explain why, for the same Δ, the frictional drag is greater for axisymmetric drawing.

10.5. Some authorities define Δ as the ratio of the length of an arc through the middle of the deformation zone, centered at the apex of the cone or wedge formed by extrapolating the die, to the contact length.

a) Show that for wire drawing with this definition $\Delta = \alpha(1 + \sqrt{1 - r})^2/r$.

b) Calculate the ratio of Δ from this definition to the value of Δ from equation 10.4 for (i) $\alpha = 10^\circ$, $r = 0.25$; (ii) $\alpha = 10^\circ$, $r = 0.50$; (iii) $\alpha = 45^\circ$, $r = 0.50$; (iv) $\alpha = 90^\circ$, $r = 0.50$.

10.6. Backofen developed the following equation for the mechanical efficiency, η, during wire drawing: $\eta = [1 + C(\Delta - 1) + \mu \tan\alpha]^{-1}$ for $\Delta > 1$, where C is an empirical constant equal to about 0.12 and μ is the friction coefficient. Note that the term $C(\Delta - 1)$ represents w_r/w_i and the term $\mu/\sin\alpha$ represents w_f/w_i, so $\eta = (1 + w_r/w_i + w_f/w_i)^{-1} = (w_a/w_i)^{-1}$.

a) Evaluate this expression for $\mu = 0.05$ and $\alpha = 0.3$ for $2 \leq \alpha \leq 20^\circ$. Note that for small angles $\Delta < 1$ so the redundant strain term $C(\Delta - 1)$ is zero.

b) Plot η vs. α and find the optimum die angle, α^*.

c) Derive an expression for α^* as a function of μ and r. Does α^* increase or decrease with μ? with r?

10.7. A slab of annealed copper with dimensions 2.5 cm × 1.5 cm × 8 cm is to be compressed between rough platens until the 2.5 cm dimension is reduced to 2.2 cm. With a sketch, describe, as fully as possible the resulting inhomogeneity of hardness.

10.8. A high-strength steel bar must be cold reduced from a diameter of 2 cm to 1.2 cm by drawing. A number of schedules have been proposed. Which schedule would you choose to avoid drawing failure and minimize the likelihood of centerline bursts? Assume $\eta = 0.5$ and give your reasoning.

a) A single pass through a die of semi-angle 8°.

b) Two passes (2.0 cm to 1.6 cm and 1.6 to 1.2 cm) through a die of semi-angle 8°.

c) Three passes (2.0 cm to 1.72 cm, 1.72 cm to 1.44 cm, and 1.44 cm to 1.2 cm) through a die of semi-angle 8°.

d) Four passes (2.0 cm to 1.8 cm, 1.8 cm to 1.6 cm, 1.6 cm to 1.4 cm, and 1.4 cm to 1.2 cm) through a die of semi-angle 8°.

(**e**, **f**, **g**, **h**) Same reductions as in schedules a, b, c, and d except through a die of semi-angle 16°.

10.9. Determine Δ from the data of Hundy and Singer (Figure 10.6) for reductions of 2.3%, 6.5%, 13.9%, and 26%. Make a plot of I.F. versus Δ.

11 Formability

An important concern in forming is whether a desired process can be accomplished without failure of the work material. Forming limits vary with material for any given process and deformation-zone shape. As indicated in Chapter 10, central bursts may occur at a given level of Δ in some materials and not in others. Failure strains for a given process depend on the material.

11.1 DUCTILITY

In most bulk forming operations, formability is limited by ductile fracture.* Forming limits correlate quite well with the reduction of area as measured in a tension test. Figure 11.1 shows the strains at which edge cracking occurs in rolling as a function of the tensile reduction in area. The fact that the limiting strains for strips with square edges are much higher than those with rounded edges indicates that process variables are also important. Similar results are reported for other processes.

11.2 METALLURGY

The ductility of a metal is strongly influenced both by the properties of the matrix and by the presence of inclusions. Factors that increase the strength generally decrease ductility. Solid solution strengthening, precipitation, cold work, and decreased temperatures all lower fracture strains. The reason is that with higher strengths, the stresses necessary for fracture will be encountered sooner.

Inclusions play a dominant role in ductile fracture. The volume fraction, nature, shape, and distribution of inclusions are important. In Figure 11.2, the tensile ductility is seen to decrease with increased amounts of artificial inclusions. Despite the scatter, it appears that some second-phase particles are more deleterious than others. Figure 11.3 shows similar trends for oxides, sulfides, and carbides in steel.

Mechanical working tends to elongate and align inclusions in the direction of extension. This mechanical fibering reduces the fracture strength and ductility normal

* Wire drawing is an exception; the maximum reduction per pass is limited by the ability of the drawn section to carry the required drawing force without yielding and necking. Once the drawn wire necks, it can no longer support the required load, so the subsequent fracture strain is of little concern. It is also possible, though not common, that brittle fracture limits formability.

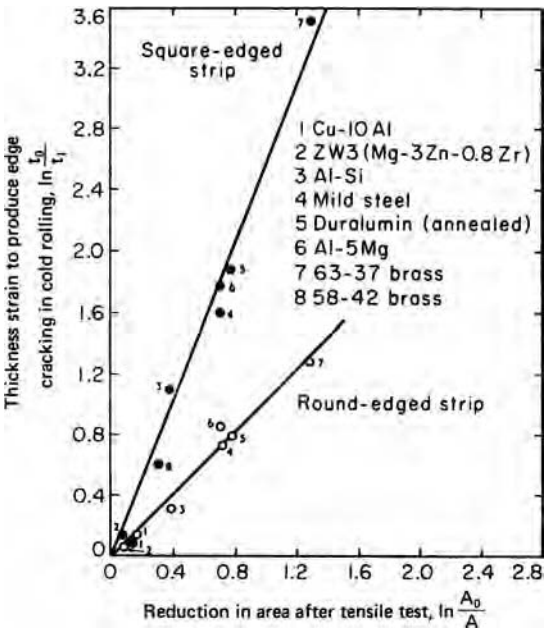

11.1. Correlation of the strain at which edge cracks were first observed in flat rolling with the reduction of area in a tension test. From M. G. Cockcroft and D. J. Latham, *J. Inst. Metals*, 96 (1968), pp. 33–39.

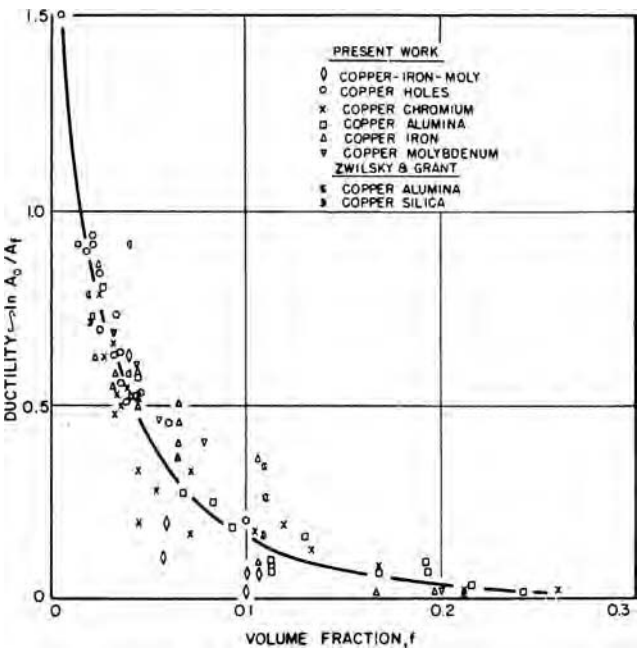

11.2. Effect of volume fraction of second-phase particles in copper on tensile ductility. From B. I. Edelson and W. M. Baldwin, *Trans. Q. ASM*, 55 (1962), pp. 230–50.

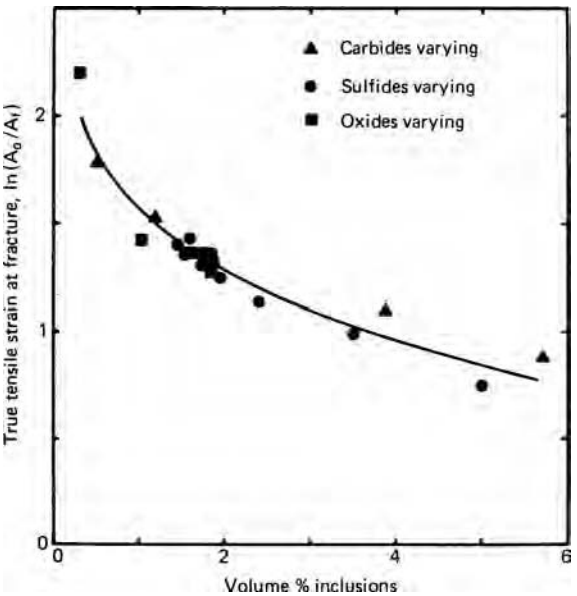

11.3. Effect of volume fraction of natural inclusions on the tensile ductility of steel. Data from F. B. Pickering, *Physical Metallurgy and Design of Steels* (London: Applied Science Pub., 1978), p. 51.

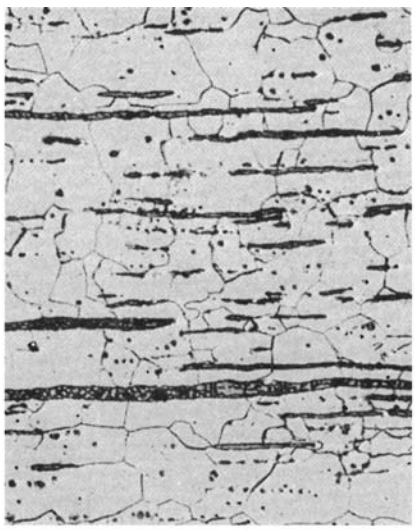

11.4. Microstructure of wrought iron (top) showing elongated glassy silicate inclusions and the woody fracture (bottom) caused by cracking along the inclusions. From J. Aston and E. B. Story, *Wrought Iron and Its Manufacture, Characteristics and Applications* (Pittsburgh: Byer Co., 1939), pp. 49, 92.

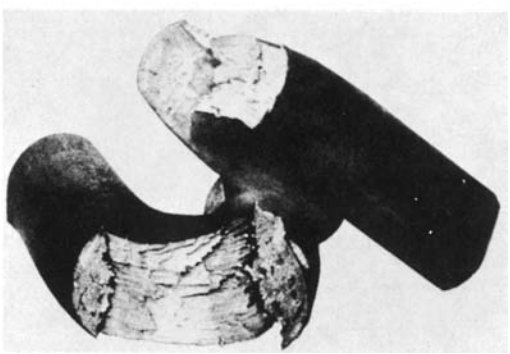

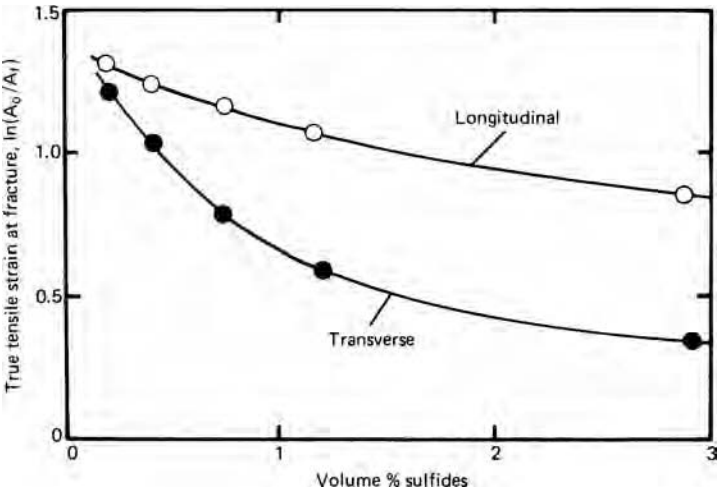

11.5. Effect of sulfides on the ductility of steel. The lower ductility in the transverse direction is caused by the inclusions being elongated during hot rolling. Data from F. B. Pickering, *op. cit.*, p. 82.

to the working direction. Wrought iron, though no longer a commercial product, is an extreme example. Crack paths follow glassy silicate inclusions, producing woody fractures (see Figure 11.4).

In steels, MnS inclusions, elongated during hot working, are a major cause of fracture anisotropy as illustrated in Figure 11.5. Transverse ductility can be markedly improved by *inclusion shape control* (Figure 11.6). This is a practice of adding small amounts of Ca, Ce, Ti, or rare earth elements to react with the sulfur to form hard inclusions that remain spherical during working. If the added cost is justified, the inclusion content can be reduced by desulfurization or vacuum remelting.

The formability of medium and high carbon steels can be improved by spheroidizing the carbides. For example, the manufacture of bolts requires upsetting their ends.

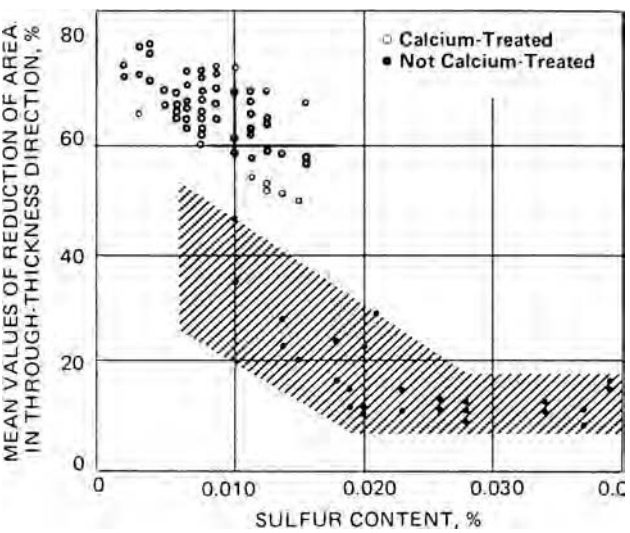

11.6. Effect of inclusion shape control in raising the through-thickness ductility of an HSLA steel. From H. Pircher and W. Klapner in *Micro Alloying* 75 (Union Carbide, 1977), pp. 232–40.

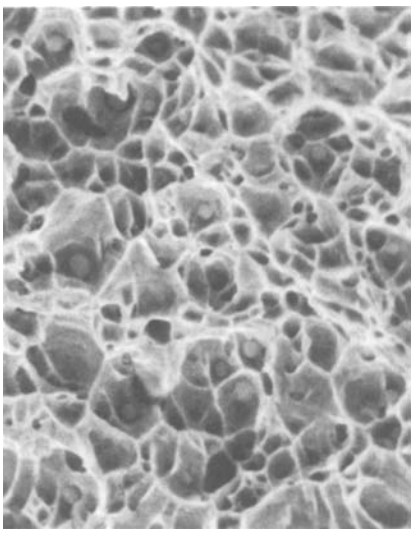

11.7. Dimpled fracture surface of steel. Note that the microvoids are associated with inclusions. Courtesy of J. W. Jones.

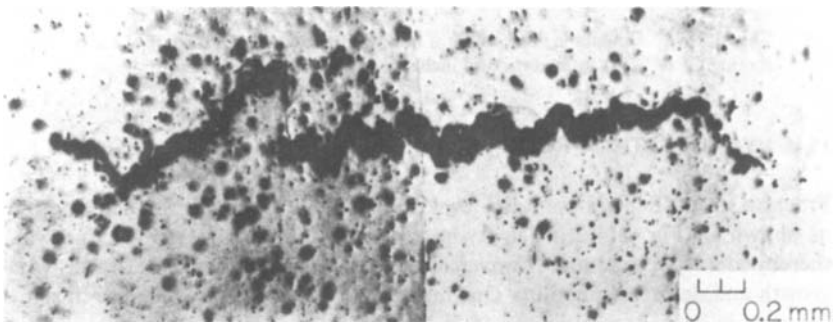

11.8. Crack in the center of a neck in a tensile specimen of 1018 steel. Oil stain from diamond polishing exaggerates the hole size. From F. McClintock in *Ductility* (ASM, 1968), pp. 255–77.

Bolts made from medium carbon steels must be spheroidized to withstand the circumferential strains in upsetting. Although spheroidization of hypoeutectoid steels is often accomplished by heating the steel above the lower critical temperature into the $\alpha + \gamma$ phase region and then slowly cooling just below the critical into the α + carbide region, spheroidizing occurs much quicker if the steel is simply heated to just below the lower critical.*

11.3 DUCTILE FRACTURE

Scanning electron microscope pictures of ductile fracture (e.g., Figure 11.7) are characterized by dimples that are associated with inclusions. They suggests that fractures initiate by opening of holes around the inclusions. These holes grow by plastic deformation until they link up to form macroscopic cracks. Figure 11.8 shows a crack

* J. O'Brien and W. Hosford, *Met. Mat. Trans*., 33 (2002), pp. 1255–61.

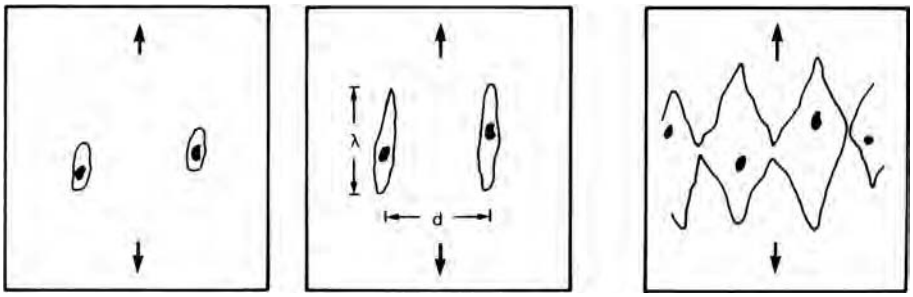

11.9. Schematic sketch showing how a ductile crack can form by necking between elongated voids around inclusions.

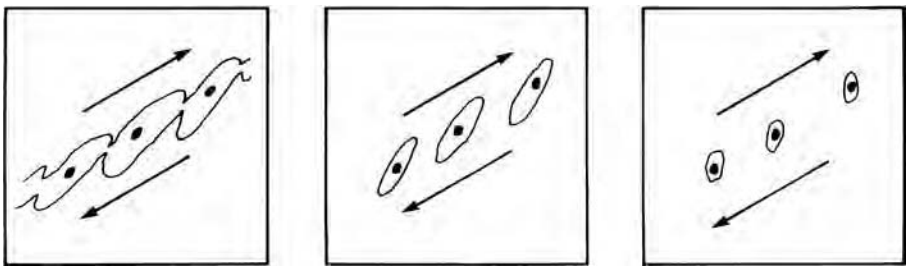

11.10. Schematic sketch showing how a ductile crack can form in shear by linking of voids around inclusions.

near the center of the neck in a tensile bar of cold-rolled 1018 steel prior to final fracture.

Voids may join by preferential growth parallel to the direction of highest principal stress until their length λ approximately equals their separation distance d. Then the ligaments between them may neck on a microscopic scale as suggested in Figure 11.9.

Ductile failure may also occur by localized shear. One example is the shear lip formed on cup-and-cone fractures in tension tests of ductile metals. Shear fracture may also occur in rolling and other forming processes. Void formation around inclusions also plays a dominant role in shear fractures as indicated in Figures 11.10 and 11.11.

11.4 HYDROSTATIC STRESS

Fracture strains depend on the level of hydrostatic stress during deformation as shown in Figure 11.12. High hydrostatic pressure suppresses void growth, thereby delaying fracture. Conversely, hydrostatic tension accelerates void growth.

Bridgman* made a series of tension tests on a mild steel under superimposed pressure. He found that the pressure suppressed final fracture, greatly increasing the reductions of area. Figure 11.13 shows his specimens.

* P. W. Bridgman, *Studies in Large Plastic Flow and Fracture* (Wiley, 1952), pp. 76–78.

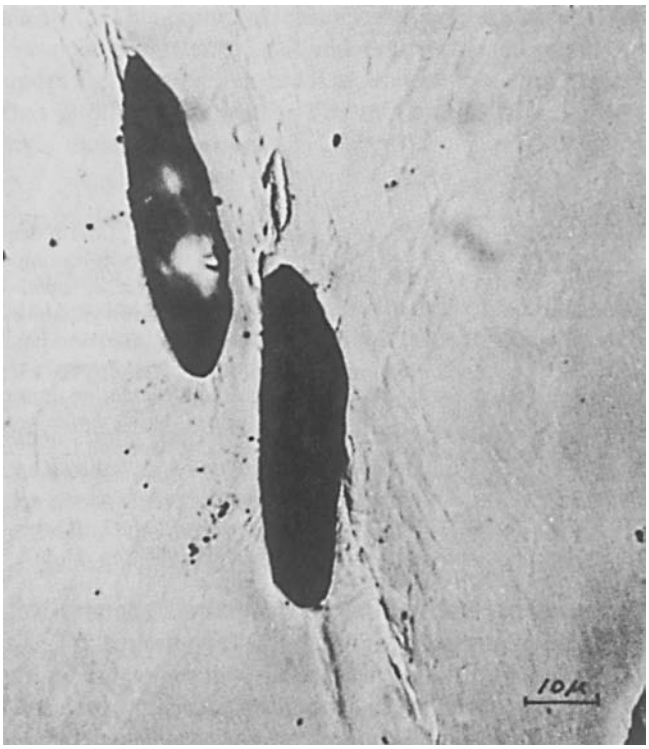

11.11. Photomicrograph of localized shear with large voids in OFHC copper. From H. C. Rogers, *Trans. TMS-AIME*, 218 (1960), pp. 498–506.

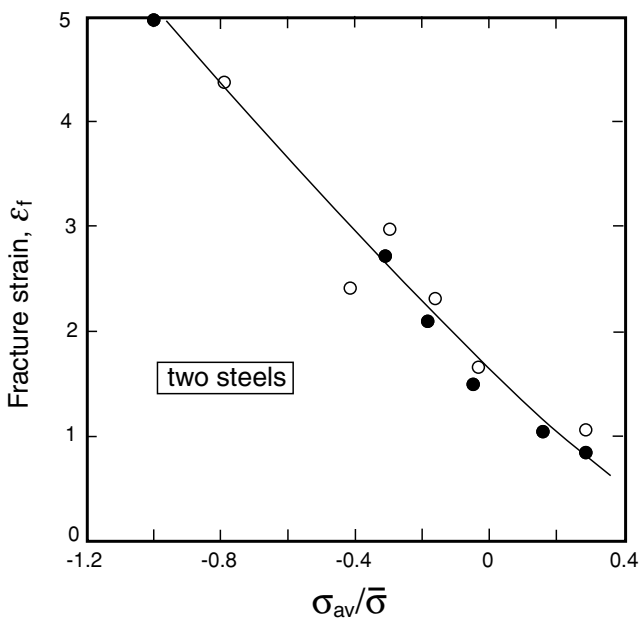

11.12. Correlation of fracture strain with the ratio of hydrostatic stress to effective stress for two steels. Adapted from A. L. Hoffmanner, *Interim Report, Air Force Contract F 33615-67-1466* (TRW, 1967).

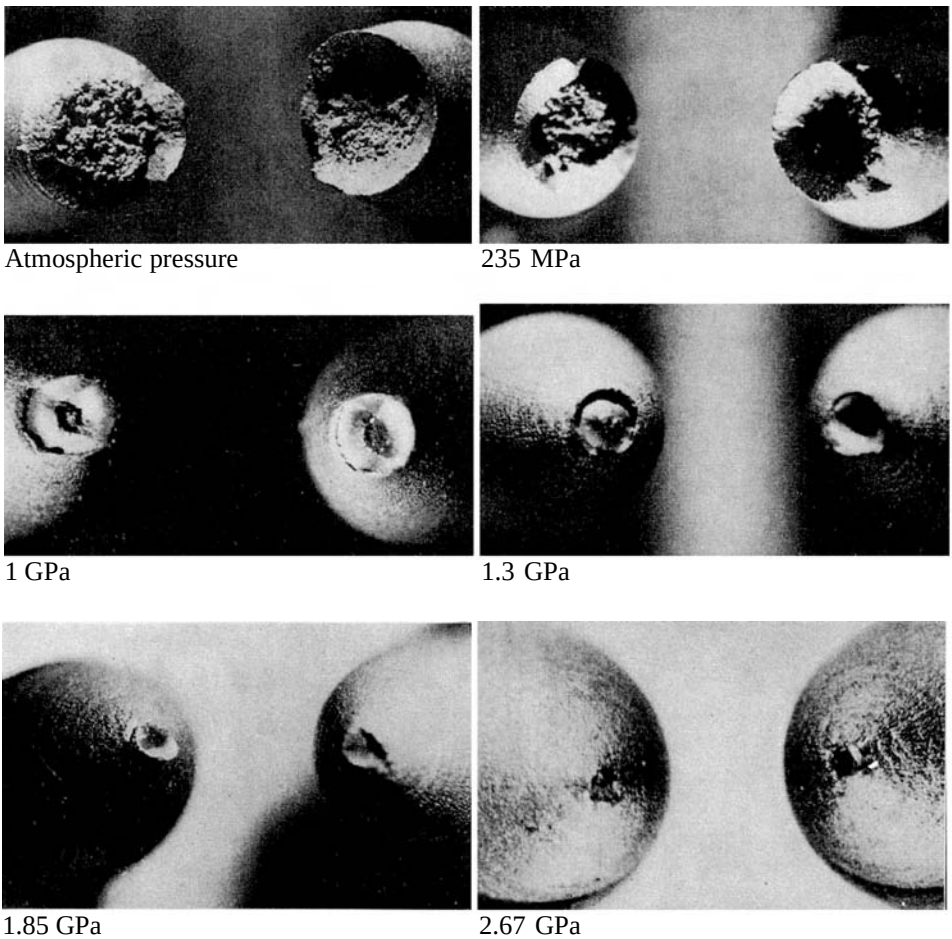

11.13. Reduction of area with increased pressure. From P. W. Bridgman, *Studies in Large Plastic Flow and Fracture* (Wiley, 1952), pp. 76–78.

One measure of the extent of void growth is the decrease in density discussed in Chapter 10. Figure 11.14 shows the effect of hydrostatic pressure on density changes during strip drawing of 6011-T6 aluminum.

Formability problems would be minimized if all stress components could be maintained compressive. Materials of very limited ductility can be extruded if the exit region is under high hydrostatic pressure. Without such special conditions, tensile stresses are apt to arise in processes that are nominally compressive. Edge cracking during rolling and formation of center bursts in extrusion are examples. During upset forging, barreling causes hoop tensile stresses.

Although it has been suggested that failure strains depend on the level of the largest principal stress, σ_1, rather than on the hydrostatic stress, σ_m, the distinction is not great, as can be seen from the extreme possibilities of axisymmetric elongation, $\sigma_m = \sigma_1 - (2/3)\bar{\sigma}$, and axisymmetric compression, $\sigma_m = \sigma_1 - (1/3)\bar{\sigma}$. All other conditions

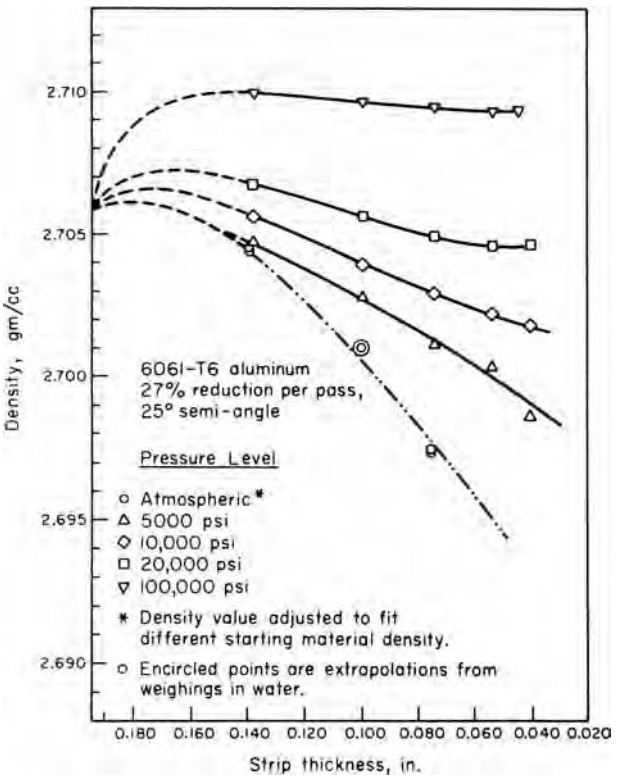

11.14. Loss of density during strip drawing with superimposed hydrostatic pressure. Note that drawing at the highest pressure increased the density by closing up preexisting pores. From H. C. Rogers and L. F. Coffin Jr., *Final Rept. Contract NOw-66-0546-d* (June 1996), Naval Air Systems Command. See also H. C. Rogers in *Ductility* (ASM, 1968), pp. 31–61.

are intermediate so

$$\sigma_m + (1/3)\bar{\sigma} \leq \sigma_1 \leq \sigma_m + (2/3)\bar{\sigma}. \tag{11.1}$$

Cockdroft and Latham* suggested a fracture criterion

$$\int_0^{\bar{\varepsilon}_f} \sigma_1 \, d\bar{\varepsilon} = C. \tag{11.2}$$

The concept is that damage accumulates during processing until the integral reaches a critical value, C. This criterion recognizes the dependence of the fracture strain on σ_1 (or almost equivalently on σ_m). However, if σ_1 is even temporarily compressive, it suggests an accumulation of negative damage. Other criteria have been proposed.†

Gurson‡ has quantitatively treated the role of porosity in ductile fracture. He developed a yield criterion for porous materials that is sensitive to hydrostatic pressure and can be used to predict void growth.

* M. G. Cockroft and D. J. Latham, *J. Inst. Metals*, 96 (1968), pp. 33–39.

† See for example A. G. Atkins, *Metal Sci*. (Feb. 1981), pp. 81–83; A. K. Ghosh, *Met. Trans*., 7A (1976), pp. 523–33; F. A. McClintock, *J. Appl. Mech., Trans. ASME*, 35 (1968), pp. 363–71.

‡ A. L. Gurson, *J. Engr. Mater. Tech*., 99 (1977), pp. 2–15.

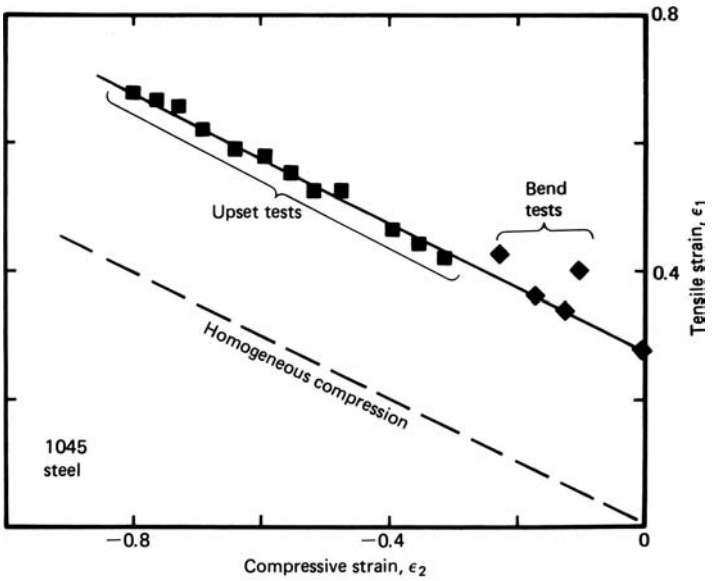

11.15. Forming limits defined by strains at fracture during upsetting. Data from H. A. Kuhn, *Formability Topics—Metallic Materials* (ASTM STP, 647, 1978), pp. 206–19.

11.5 BULK FORMABILITY TESTS

Formability does not always correlate with tensile ductility, especially if cracking starts on the surface. For this reason, other tests are often used. Kuhn* proposed a simple procedure for evaluating formability with upset compression tests. Barreling during upsetting causes hoop tensile stresses that may lead to cracking. He plotted the hoop strain when the first cracks were observed, ε_1, as a function of the compressive strain, ε_2. The ratio of ε_1 to ε_2 was varied by changing the lubrication and height-to-diameter ratio of the specimens. Figure 11.15 is a plot for a 1045 steel. Additional points were obtained from bend tests on wide specimens. The straight line indicates that

$$\varepsilon_{1f} = C - (1/2)\varepsilon_{2f} \tag{11.3}$$

where C is the value of ε_{1f} for plane strain. This line parallels $\varepsilon_1 = -(1/2)\,\varepsilon_2$ for homogeneous compression. Fracture strains vary with orientation as shown in Figure 11.16.

A simple test to measure the effect of spheroidization involves measuring the circumferential expansion when a hollowed tube of the work material is expanded by pushing it onto a conical tool as shown in Figure 11.17.†

* H. A. Kuhn, *Formability Topics—Metallic Materials*, ASTM STP 647 (1978).
† J. O'Brien and W. Hosford, *op. cit*.

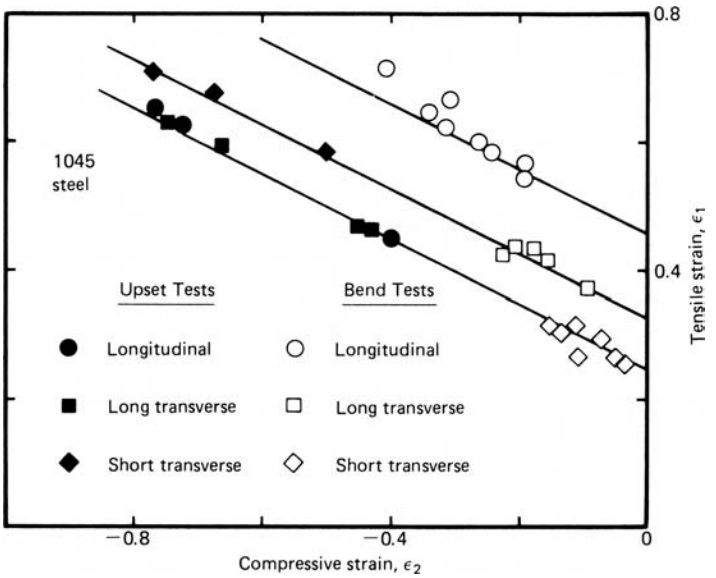

11.16. Effect of specimen orientation on forming limits. Data from A. Kuhn, *op. cit*.

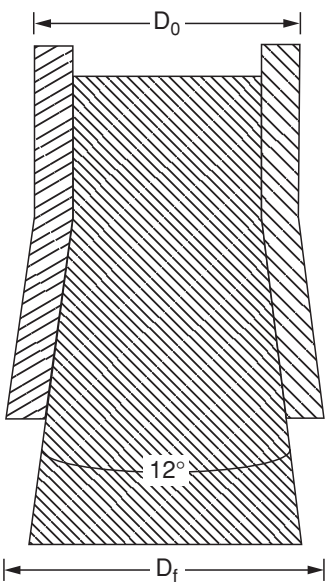

11.17. Tool for testing critical hoop expansion strain, $\varepsilon_h = \ln(D_0/D_f)$, when the bottom of the tubular specimen splits.

11.6 FORMABILITY IN HOT WORKING

Formability in hot working is usually better than in cold working because of the lower stresses. However, sometimes failures occur at very low strains during hot working. This is called *hot shortness*. The usual cause is the presence of a liquid phase. The hot-working temperatures for aluminum alloys are very close to the eutectic

temperature. Sometimes the liquid phase is nonmetallic. In the absence of manganese, sulfur would react with iron to form iron sulfide, which has a low melting temperature and wets the grain boundaries. Fortunately, if manganese is added to the steel, the sulfur preferentially combines with the manganese to form MnS, which is solid at hot working temperatures and does not wet the grain boundaries.

Small amounts of copper or tin picked up by melting scrap can cause surface cracks during hot rolling of steel. These "tramp" elements don't oxidize easily, so as the iron at the surface is oxidized their concentrations at the surface may reach a point where they form a liquid phase, which wets the grain boundaries.

NOTE OF INTEREST

Percy W. Bridgman (1882–1961) was born in Cambridge, Massachusetts. He studied at Harvard where he received a doctorate in 1908. He joined the faculty there in 1910. His research was mainly on the physics of high pressure, for which he received the Nobel Prize in Physics in 1946.

REFERENCES

W. F. Hosford, *Mechanical Behavior of Materials*, Cambridge University Press, 2005.
E. M. Meilnik, *Metalworking Science and Engineering*, McGraw-Hill, 1991.

PROBLEMS

11.1. **a)** Explain why inclusion-shape control is of much greater importance in high-strength steels than in low-carbon steels.
b) Explain why inclusion-shape control improves the transverse and through-thickness properties, but has little effect on the longitudinal properties.

11.2. Figure 11.1 shows that for a given sheet material, greater reductions are possible before edge cracking if square edges are maintained than if the edges are round. Explain why.

11.3. **a)** Wrought iron has high toughness when stressed parallel to the prior working direction, but very low toughness when stressed perpendicular to the prior working direction. Explain why.
b) When wrought iron was a commercial product, producers claimed its corrosion resistance was superior to that of steel. What is the basis of this claim?

11.4. **a)** With the same material, die angle and reduction central bursts may occur in drawing but not in extrusion. Explain why this may be so.
b) Why may a given material be rolled to strains much higher than the fracture strain in a tension test?

11.5. Figure 11.18 is a Kuhn-type forming limit diagram for upsetting a certain grade of steel. The line gives the combination of strains that cause cracking.

a) Superimpose on this diagram the strain path that leads to failure at point *P*.
b) What differences in test variables would lead to cracking at point *S*?

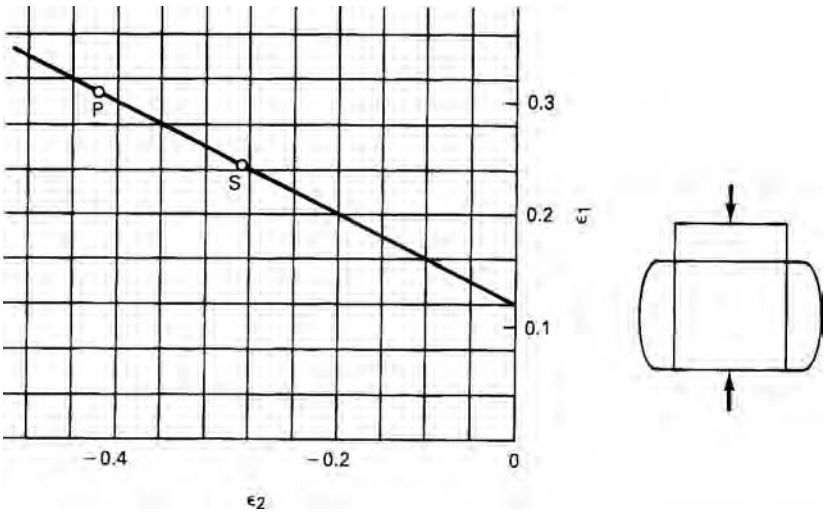

11.18. Figure for Problem 11.5.

12 Bending

All sheet-forming operations involve some bending. Often it is a major feature. Springback occurs after the bending forces are removed and the material contains residual stresses. If the bend radius is too sharp, there may be tensile failure on the outside of the bend or buckling on the inside. A very simple case is considered initially to illustrate the mechanics involved.

12.1 SHEET BENDING

Consider the bending of a flat sheet of a non–strain-hardening material subjected to a pure bending moment. Figure 12.1 shows the coordinate system. Let r be the radius of curvature measured at the mid-plane and let z be the distance of an element from the mid-plane. The engineering strain at z can be derived by considering the arc length L, measured parallel to the surfaces of the sheet in the x-direction. The arc length at the mid-plane, L_0, doesn't change during bending and may be expressed as $L_0 = r\theta$, where θ is the bend angle. At z, the arc length is $L = (r + z)\,\theta$. Before bending, both arc lengths were equal so the engineering strain, e, is

$$e_x = (L - L_0)/L_0 = z\theta/r\theta = z/r. \tag{12.1}$$

The true strain, ε_x, is

$$\varepsilon_x = \ln(1 + z/r). \tag{12.2a}$$

For many bends the strains are low enough so we can approximate

$$\varepsilon_x = z/r. \tag{12.2b}$$

With wide sheets ($w \gg t$) the width strain, ε_y, is negligible. Therefore sheet bending can be considered to be a plane-strain operation, $\varepsilon_z = -\varepsilon_x$. The value of e_x varies from $-t/(2r)$ on the inside ($z = -t/2$) to zero at the mid-plane and $+t/(2r)$ on the outside surface. For small strains, $\varepsilon_x \approx e_x$. The internal stress distribution can be found from the strain distribution and the stress–strain curve. Assume that the material is elastic—ideally plastic (no strain hardening). Let the tensile yield strength in plane strain be Y.

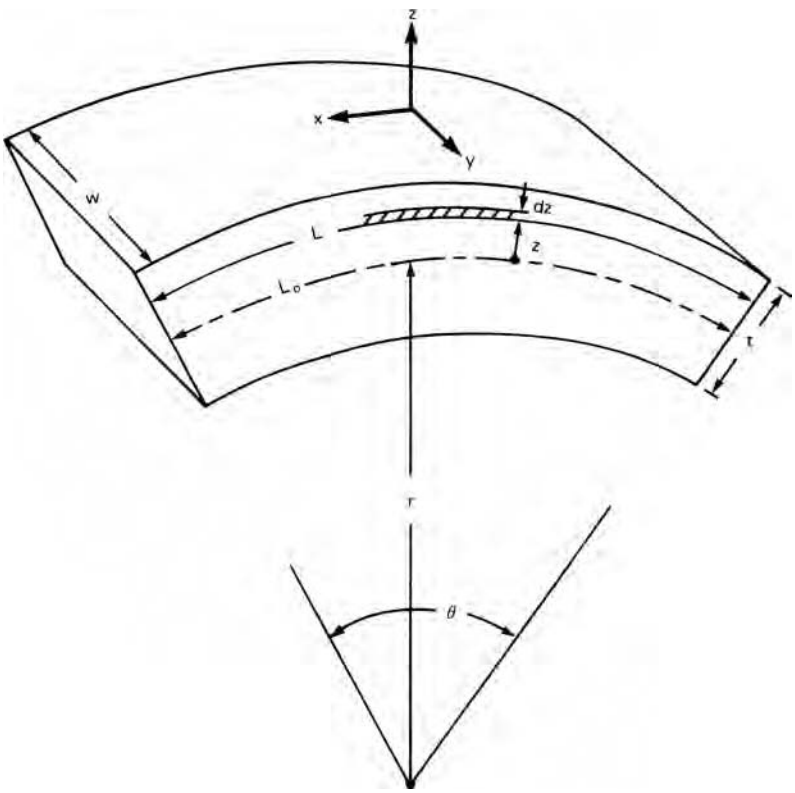

12.1. Coordinate system for analyzing sheet bending.

Figure 12.2 shows the strain and stress distribution. The entire cross section will at a stress $\sigma_x = Y$ or $-Y$ except for an elastic core near the mid-plane. For most bending operations this elastic core can be neglected.

The bending moment can be calculated assuming that there is no net external force, F_x. However, there are internal forces, $\mathrm{d}F_x = \sigma_x w\,\mathrm{d}z$, acting on incremental elements of the cross section. The contribution of stress on every element to the bending moment

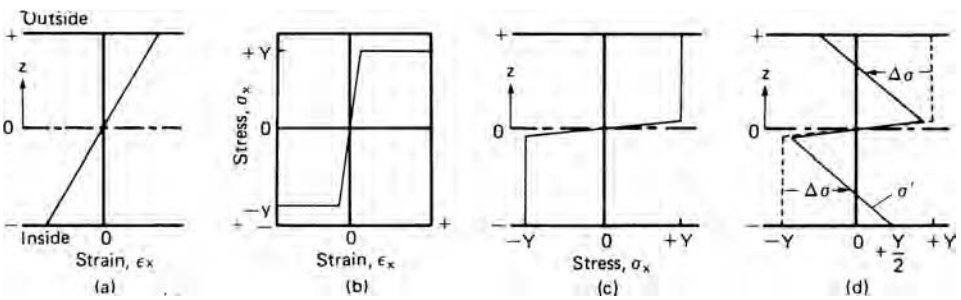

12.2. Stress and strain distribution across a sheet thickness. During bending the strain varies linearly across section (a). With a non–strain-hardening material (b) the bending causes the stress distribution in (c). Elastic unloading results in the residual stresses in (d).

is the product of this incremental force times its lever arm, so $dM = z\sigma_x w\, dz$. The total bending moment is then

$$M = \int_{-t/2}^{+t/2} w\sigma_x z\, dz = 2\int_{0}^{+t/2} w\sigma_x z\, dz. \tag{12.3}$$

It is simpler to take twice the integral between 0 and $t/2$ because the sign of σ_x changes at the mid-plane. For an ideally plastic material

$$M = 2wY\int_{0}^{t/2} z\, dz = wYt^2/4. \tag{12.4}$$

EXAMPLE 12.1: A steel sheet, 1 mm thick, is bent to a radius of curvature of 12 cm. The flow stress in plane strain is 210 MPa and $E' = 224$ GPa.

(a) What fraction of the cross section doesn't yield?

(b) In calculating the bending moment, what percent error would be caused by neglecting the fact that the center hadn't yielded?

SOLUTION:

(a) The yielding strain $= Y/E' = (210\text{ MPa})/(224\text{ GPa}) = 0.00094$. This strain occurs at a position $z = \rho\varepsilon = (0.00094)(120) = \pm 0.11$ mm. The fraction not yielding $= 0.11/0.5 = 22\%$.

(b) To calculate the exact moment, divide the integral in equation 12.3 into two parts,

$$M/w = 2\int_{0}^{0.00012} \frac{E'}{r} z^2 dz + 2\int_{0.00012}^{0.0005} w\sigma_0 z\, dz$$
$$= (2/3)\frac{224\times 10^9}{0.12} 0.00012^3 + 210\times 10^6(0.0005^2 - 0.00012^2) = 51.6\text{ Nm}.$$

An approximate solution, neglecting the elastic core, is $M/w = 2\int_0^{0.0005} \sigma_0 z\, dz = +(210\times 10^6)(0.0005^2 - 0) = 52.5$ Nm. The error is $0.9/51.6 = 1.7\%$.

The bending moment applied by the tools must equal the internal bending moment. When the external forces are removed, the bending moment must vanish, $M = 0$, as the material unloads elastically. The unloading is elastic so

$$\Delta\sigma_x = E'\Delta\varepsilon_x \tag{12.5}$$

where $E' = E/(1+\nu^2)$ and the change of strain, $\Delta\varepsilon_x$, is given by

$$\Delta\varepsilon_x = z/r - z/r' \tag{12.6}$$

where r' is the radius after springback. The change of bending moment is then

$$\Delta M = 2w \int_0^{t/2} \Delta\sigma_x z \, dz = 2w \int_0^{t/2} E(1/r - 1/r')z^2 \, dz. \tag{12.7}$$

Integrating,

$$\Delta M = (wE't^3/12)(1/r - 1/r'). \tag{12.8}$$

After springback the bending moment must be zero so $M - \Delta M = 0$. Combining equations 12.4 and 12.8, $(wE't^3/12)(1/r - 1/r') = wYt^2/4$ so

$$1/r - 1/r' = 3Y/(tE'). \tag{12.9}$$

The residual stress is

$$\sigma_x' = \sigma_x - \Delta\sigma_x = Y - \Delta\sigma_x = Y - E'\Delta e_x = Y - E'z(1/r - 1/r') = Y - E'z[3Y/(tE')],$$

so

$$\sigma_x'/Y = 1 - (3z/t). \tag{12.10}$$

Figure 12.2d shows that on the inside surface $\sigma_x = +Y/2$ and on the outside surface

$$\sigma_x = -Y/2.$$

A similar treatment for work hardening, $\sigma_x = K'\varepsilon_x^n$, results in the moment under load being

$$M = \left(\frac{2}{2+n}\right)(wK'/r^n)(t/2)^{2+n}. \tag{12.11}$$

Substituting ΔM from equation 12.8 and M from equation 12.3 into $M - \Delta M = 0$,

$$\left(\frac{1}{r} - \frac{1}{r'}\right) = \left(\frac{6}{2+n}\right)\left(\frac{K'}{E'}\right)\left(\frac{t}{2r}\right)^n\left(\frac{1}{t}\right). \tag{12.12}$$

The magnitude of the springback predicted by equation 12.12 can be very large. The residual stress pattern can be found by combining equations 12.5, 12.6, and 12.11.

$$\sigma_x' = K'\left(\frac{z}{r}\right)^n\left[1 - \left(\frac{3}{2+n}\right)\left(\frac{2z}{t}\right)^{1-n}\right].$$

Figure 12.3 shows how σ_x and σ_x' vary through the thickness of the sheet.

EXAMPLE 12.2: Find the tool radius that will produce a part of final radius $r' = 25$ cm in a steel of thickness 1.2 mm. Assume a flow stress of 300 MPa and a plane-strain modulus of 224 GPa.

SOLUTION: Substituting $r' = 250$ mm, $t = 0.0012$ m, and $Y = 300$ MPa into equation 12.9, $r = 136$ mm or 13.6 cm. If this were part of a complex stamping, it would be impossible to build this correction into the tooling of a complex part.

12.2 BENDING WITH SUPERIMPOSED TENSION

The springbacks predicted by equation 12.12 are so large that they cannot be compensated for by die design. The solution is to apply tension while bending. This greatly reduces springback. Tension shifts the neutral plane toward the inside of the

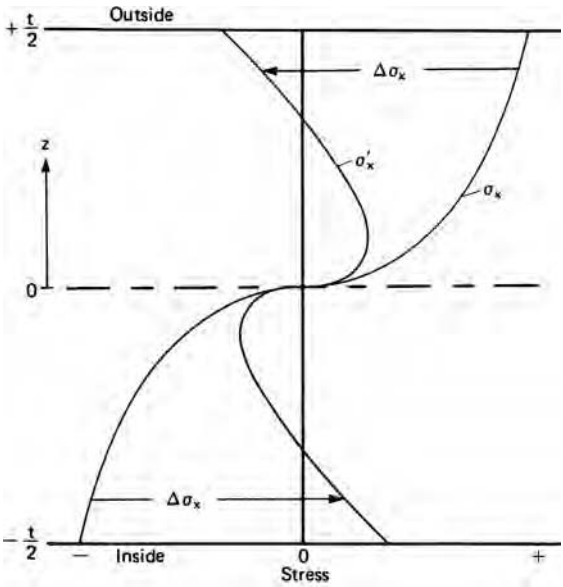

12.3. Stress distribution during bending and after unloading for a strain-hardening material.

bend and, if sufficient, shifts it completely out of the sheet. In this case the entire cross section yields in tension. This is illustrated in Figure 12.4. In an ideally plastic material there would be no springback because the stress, $\sigma_x = Y$, is the same throughout the cross section. However if the material strain hardens, the springback won't completely vanish.

Consider a simple case in which the stress–strain curve is approximated by $\sigma_x = Y + (\mathrm{d}\sigma_x/\mathrm{d}\varepsilon_x)\varepsilon_x$ where $\mathrm{d}\sigma_x/\mathrm{d}\varepsilon_x$ is constant. The stress can be divided into two parts: a bending stress, $\sigma_{x\mathrm{b}} = \varepsilon_{x\mathrm{b}}(\mathrm{d}\sigma_{x\mathrm{b}}/\mathrm{d}\varepsilon_{x\mathrm{b}}) = (z/r)(\mathrm{d}\sigma_{x\mathrm{b}}/\mathrm{d}\varepsilon_{x\mathrm{b}})$, and a uniform tensile stress, $\sigma_{x\mathrm{u}}$. The springback is entirely caused by changes of $\sigma_{x\mathrm{b}}$ on unloading. Relaxation will cause a change of the bending strain, $\Delta\varepsilon_{x\mathrm{b}} = \sigma_{x\mathrm{b}}/E' = (z/r)(\mathrm{d}\sigma_{x\mathrm{b}}/\mathrm{d}\varepsilon_{x\mathrm{b}})/E'$. The relaxed bending strain is then $\varepsilon'_{x\mathrm{b}} = \varepsilon_{x\mathrm{b}} - \Delta\varepsilon_{x\mathrm{b}} = (z/r)[1 - (\mathrm{d}\sigma_{x\mathrm{b}}/\mathrm{d}\varepsilon_{x\mathrm{b}})/E']$. Since

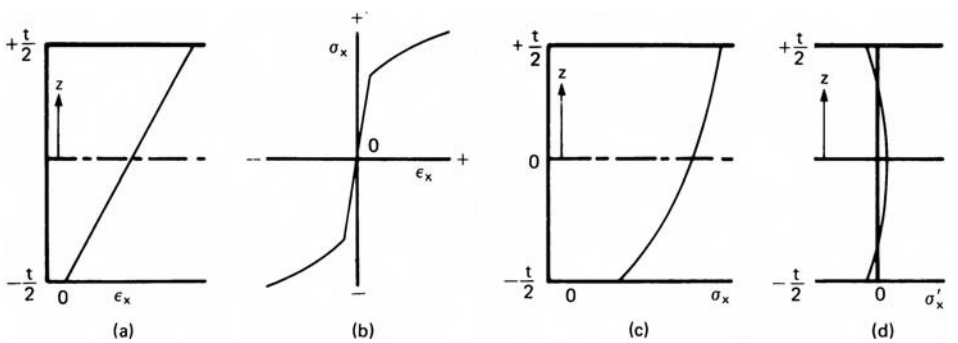

12.4. Bending with superimposed tension. With sufficient tension, the neutral axis moves out of the sheet so the entire thickness is strained in tension (a). With the stress–strain curve shown in (b) the stress distribution in (c) results. On unloading there are only minor residual stresses (d).

$\varepsilon'_{x\mathrm{b}} = z/r'$, the relaxed bending radius, r', is given by $z/r' = (z/r)[1 - (\mathrm{d}\sigma_x/\mathrm{d}\varepsilon_x)/E']$ so

$$r'/r = \left[1 - \frac{(\mathrm{d}\sigma_x/\mathrm{d}\varepsilon_x)}{E'}\right]^{-1} \tag{12.13}$$

Springback is very much reduced by applied tension because $\mathrm{d}\sigma_x/\mathrm{d}\varepsilon_x$ is much lower than E'.*

EXAMPLE 12.3: Reconsider Example 12.2 with sufficient tension to cause a net tensile strain of 0.02 at the centerline. Let the stress–strain curve be approximated by $\sigma = 656\varepsilon^{0.2}$. (This corresponds to a flow stress of 300 MPa at the centerline.)

SOLUTION: Substituting $\mathrm{d}\sigma/\mathrm{d}\varepsilon = nK\varepsilon^{n-1} = 0.2(300)0.02^{-0.8} = 1372$ MPa and $E' = 224$ GPa into equation 12.13, $r = (25\text{ cm})(1-1372/224{,}000) = 24.85$ cm. Compare this with 13.6 cm found in Example 12.2. For the small predicted springback (24.85 cm vs. 25 cm), it is possible to correct for the springback in the tooling design.

12.3 NEUTRAL AXIS SHIFT

The analyses above are based on the neutral plane remaining at the mid-plane of the sheet. Actually the neutral plane moves toward the inside of the bend. There are two reasons for this: On the inside of the bend, elements thicken. Also, the true compressive strains on the inside are greater in magnitude than the strains on the outside.

The thickness of element i is $t_i = t_0/(1 + e_i) = t_0/(1 + z_i/\rho)$ and the true strain, ε_i, at element i is $\ln(1+ z_i /\rho)$. If e_i is positive, the true stress, σ_i, on element i is $\sigma_i = K\varepsilon_i^n = K[\ln(1 + z_i/\rho)]^n$. If e_i is negative, the true stress, σ_i on element i is $\sigma_i = -K(\ln(1 + z_i/\rho)|^n$. The force on element i, on the tensile side of the bend is then

$$F_i = [wt_0/(1 + z_i/\rho)]K[\ln(1 + z_i/\rho)]^n \tag{12.14}$$

and on the compressive side

$$F_i = -[wt_0/(1 + z_i/\rho)]K|\ln(1 + z_i/\rho)|^n. \tag{12.15}$$

where z_i is negative on the inside of the bend and positive on the outside. The ratio of the two at equal displacements from the original centerline is

$$F_\mathrm{O}/F_\mathrm{I} = \left[\frac{\ln(1 + z_{i\mathrm{O}}/\rho)}{|\ln(1 + z_{i\mathrm{I}}/\rho)|}\right]^n \frac{(1 + z_{i\mathrm{I}}/\rho)}{(1 + z_{i\mathrm{O}}/\rho)}, \tag{12.16}$$

where $z_{i\mathrm{O}}$ refers to an element on the outside of the bend and $z_{i\mathrm{I}}$ refers to an element on the inside of the bend. Figure 12.5 is a plot of equation 12.16.

EXAMPLE 12.4: Consider bending of a 1.0 mm thick sheet to a radius of 2.5 cm. Calculate the ratio of the forces on elements at the outside and inside surfaces.

* See J. L. Duncan and J. E. Bird, *Sheet Metal Industries* (Sept. 1978), p. 1015.

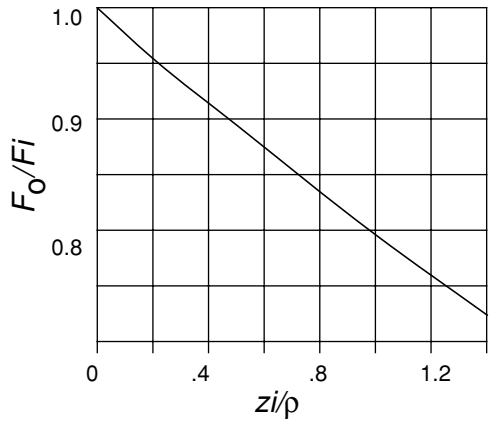

12.5. The ratio of the forces on elements on the outside and inside of the bend, both initially displaced by z from the middle of the sheet.

SOLUTION: Substituting $z/\rho = 0.02$ into equation 12.16, $F_O/F_I = 0.96$. The average ratio for elements on the outside of the bend ($z/\rho = 0.01$) is 0.98. This illustrates that the shift of the neutral plane can be neglected for most bends.

12.4 BENDABILITY

Cracking can occur if the tensile strains on the outside of a bend are great enough. The limiting values of r/t depend on the material (see Figure 12.6). The bend radius, R, in this figure (as is usual in tables of permissible bend radii) is the radius on the inside of the bend rather than at the mid-plane. Therefore $R/t = r/t - 1/2$. The solid lines in Figures 12.6(a) and (b) approximate failure when the tensile strain is equal to that in a tension test.

$$R/t = 2\mathrm{EL} - 1 \tag{12.17}$$

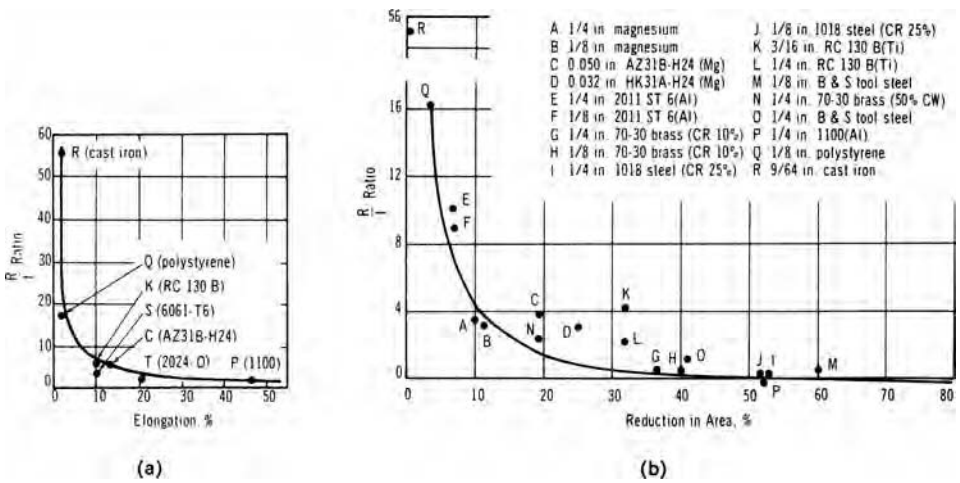

12.6. Correlation of the limiting bending severity (= R/t) with tensile ductility. Note that here R is the inside radius. From J. Datsko, *Material Properties and Manufacturing Processes* (John Wiley, 1966), P. 318.

for Figure 12.6a where EL is the tensile elongation. For Figure 12.6b, where A_r is the reduction in area in a tension test,

$$R/t = 1/(2A_r) - 1. \tag{12.18}$$

These approximations are reasonable for materials with a low ductility (low R/t), but are not accurate for sharp bends (high R/t) because the neutral axis shifts with sharp bends and the shift depends on the friction and applied tension. Furthermore, strains are not limited to the nominally bent region, but spread out. With low bend angles the maximum strains is less than predicted by equation 12.1.

12.5 SHAPE BENDING

The bending of various shapes such as T-, L-, and I-sections and square and circular tubes, as illustrated in Figure 12.7, can be analyzed in a similar manner. Again it is assumed for simplicity that there is no strain hardening, and there is no net x-direction force. It will be assumed that the condition in each element is uniaxial tension or compression in the x-direction rather than plane strain. Unlike the analysis for sheet bending, the width w is a function of z. For shapes symmetrical about the mid-plane, (Figures 12.7a and 12.7b), $M = 2Y \int_0^{h/2} wz\,dz$ and $\Delta M = 2E(\frac{1}{r} - \frac{1}{r'}) \int_0^{h/2} wz^2\,dz$ so the springback is given by

$$\left(\frac{1}{r} - \frac{1}{r'}\right) = \left(\frac{Y}{E}\right)\left(\frac{2Q}{h}\right), \tag{12.19}$$

where $Q = [(h/2) \int_0^{h/2} wz\,dz]/[\int_0^{h/2} wz^2\,dz]$.

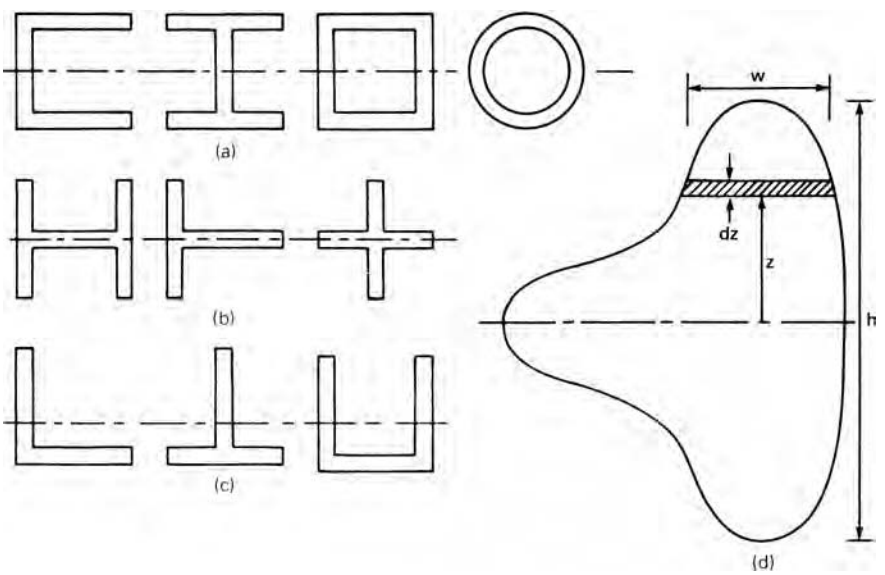

12.7. Cross sections of various shapes.

The residual stress distribution is given by

$$\sigma_x' = Y\left(1 - \frac{2Qz}{h}\right). \tag{12.20}$$

For a flat sheet in which w is not a function of z, equation 12.20 reduces to $Q = 3/2$. For cross sections in which w increases with z, $Q < 3/2$ so there is less springback than with flat sheets with the same value of h, whereas if w decreases with z, $Q > 3/2$ so there is more springback. As with flat sheets, the amount of springback decreases with applied tension.

There may be appreciable movement of the neutral plane during bending if the bends are tight (if r/h is small). The neutral plane moves to the inside of the bend because the cross-sectional area on the outside decreases and the cross-sectional area on the inside increases. With nonsymmetric cross sections, yielding will start on one side before the other and this will cause a shift of the neutral plane.

12.6 FORMING LIMITS IN BENDING

There are two possible failure modes in bending of shapes: There may be a tensile failure on the outside of the bend or buckling on the inside. If the movement of the neutral axis is neglected, the tensile strain on the outside of the bend is $h/(2r)$ and failure occurs when this strain reaches a critical value. For brittle materials, this strain is approximately the percent elongation in a tension test. For ductile materials, necking will occur at a strain a little greater than the uniform elongation in a tension test because of support from elements nearer the neutral plane. This support varies with the section shape, which can be characterized by h/t, where t is the thickness of the section. In slender sections (h/t is large) there is less support to the outer sections than if h/t is small. Therefore the critical value of h/r decreases with h/t.

The tendency to buckling on the inside of the bend depends primarily on h/t but it also increases with bend severity. Wood* determined the forming limits for many materials and shapes in stretch forming. Figure 12.8 is a schematic forming limit diagram for shape bending.

In the bending of tubes the outer fibers tend to move inward, distorting the cross section or even causing a collapse of the tube. In low production items, this tendency can be lessened by filling the tube with sand or a low melting point metal. In high production items, a ball or plug mandrel can be used to preserve the cross section. This internal support will, however, lower the forming limits by causing greater tensile strains in the outside fibers. Figure 12.9 illustrates the use of a mandrel in the bending of a square tube.

NOTE OF INTEREST

If a strip of a low-carbon steel with a yield point is bent the bend tends to concentrate at one point because once one region yields it is softer than other regions. In contrast, a strip of a strain-hardening metal will spread the bend gradually over the entire surface. See Figure 12.10.

* W. W. Wood, *Final Report on Sheet Metal Forming Technology*, Vol. II, ASD-TDR-63-7-871 (July 1963).

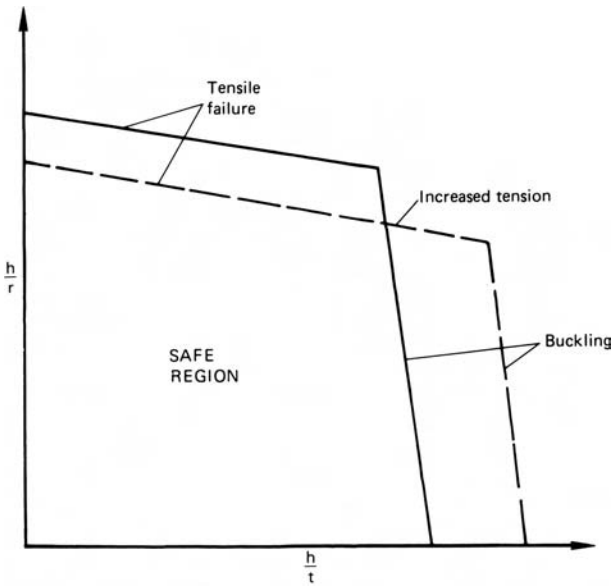

12.8. Schematic of forming limits for shape bending. Critical levels of values of *h/r* and *h/t* depend on the shape and the material. Increasing axial tension lowers the critical *h/r* values and raises the critical *h/t* values.

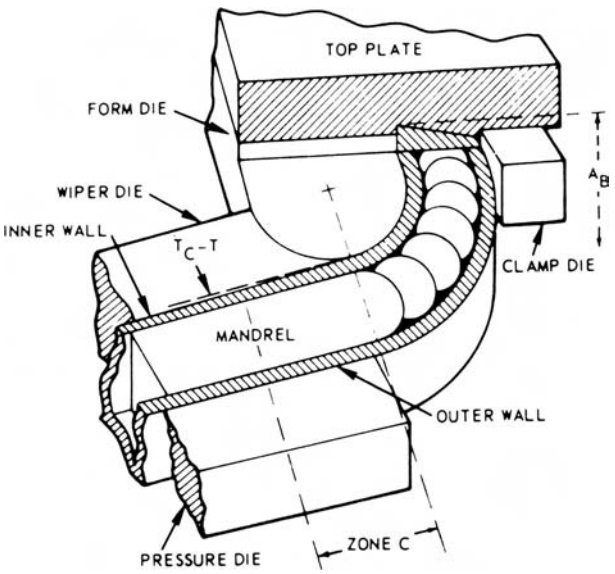

12.9. Use of ball mandrels to prevent collapse of walls during bending of a square tube. From *Cold Bending and Forming Tube and Other Sections* (ASTME, 1966).

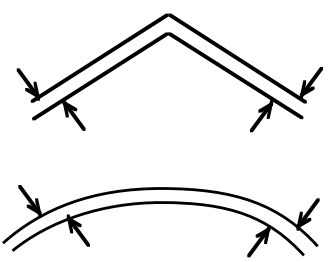

12.10. Bent strips of low-carbon steel (upper) and a strain-hardening material (lower).

REFERENCES

R. J. Kervick and R. K. Springborn, eds., *Cold Bending and Forming Tube and Other Sections*, *ASTME*, 1966.

Z. Marciniak, J. L. Duncan, and S. J. Hu, *Mechanics of Sheet Metal Forming*, Butterworth Heinemann, 2002.

PROBLEMS

12.1. An old shop-hand has developed a simple method of estimating the yield strength of steel. He carefully bends the strip with his hands to a given radius, releases it, and notes whether it has taken a permanent set. He repeats the process until it does take a permanent set. A strip 0.25 in thick, 1 in wide, and 10 in long first takes a permanent set at a radius of 10 in. Estimate the yield strength.

12.2. A coiler is being designed for a cold-rolling line of a steel mill. The coil diameter should be large enough so that coiling involves only elastic deformation. The sheet to be coiled is 1 mm thick, 2 m wide, and has a yield strength of 275 MPa.

a) What is the minimum diameter of the coiler?

b) For this diameter find the horsepower consumed by coiling at 30 m/s.

12.3. In many applications the minimum thickness of a sheet is determined by its stiffness in bending. If aluminum is substituted for steel to save weight, its thickness must be greater.

a) By what factor must the thickness increased?

b) What weight saving would be achieved?

c) Would the weight saving be greater, less, or unchanged if both sheets were corrugated instead of being flat?

Hint: For elastic bending, the deflection δ is given by $\delta = A(FL^3/Ewt)$, where F is the force, L is the span length, E' is the plane-strain modulus, w the sheet width, and t the sheet thickness. For steel $E' = 220$ GPa and $\rho = 7.9$ Mg/m^3. For aluminum $E' = 73$ GPa and $\rho = 2.7$ Mg/m^3.

12.4. For some designs, the minimum sheet thickness is controlled by the ability to absorb energy elastically in bending without any plastic deformation. In this case, what weight saving can be achieved by substituting aluminum for steel? Use the data in Problem 12.3.

12.5. An aluminum sheet 1 mm thick is to be bent to a final radius of curvature of 75 mm. The plastic portion of the stress–strain curve is approximated by $175 + 175\varepsilon$ MPa. Accounting for springback, what radius of curvature must be designed into the tools if the loading is

a) pure bending?

b) tensile enough so that the mid-plane is stretched 2% in tension?

12.6. What fraction of the cross section remains elastic in Problem 12.5a?

12.7. It has been suggested that the residual hoop stress in a tube can be found by slitting a short length of tube longitudinally and measuring the diameter, d, after slitting and comparing this with the original diameter, d_0. A stress distribution

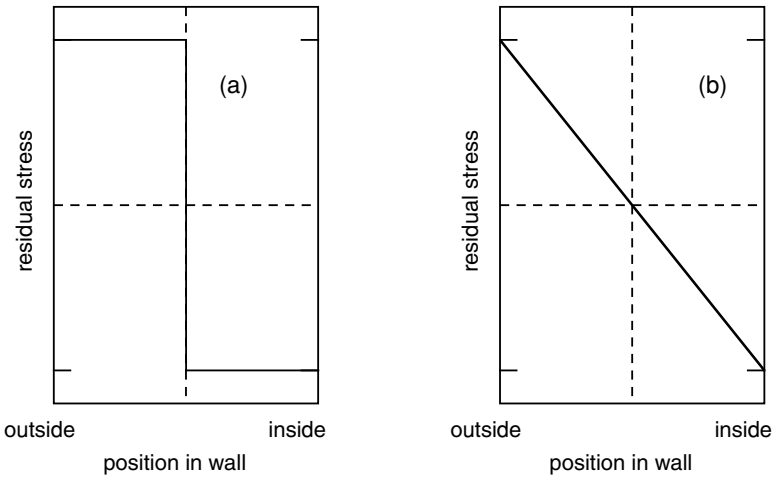

12.11. Assumed stress distributions for Problem 12.7.

must be assumed. Two simple stress distributions are suggested by Figure 12.11. For a copper tube, $d_0 = 25$ mm and $d = 25.12$ mm, $t = 0.5$ mm. Assume $E = 110$ GPA and $\nu = 0.30$. Find the residual stress at the surface using both assumptions about the stress distribution.

12.8. A round bar (radius R and length L) was plastically deformed in torsion until the entire cross section has yielded. Assume an ideally plastic material with a shear strength k and a shear modulus G. When unloaded it untwisted by an amount $\Delta\theta$ (radians).

a) Derive an expression for the level of residual stress, τ', as a function of the radial position r, R, G, and k.

b) Find the relative springback, $\Delta\theta/L$, in terms of G, k, and R.

12.9. A plate was bent to a radius of curvature R. After springback the radius was R'. Later the plate was etched, removing the outer surface. How would you expect the last radius R' to compare with R and R'?

12.10. Consider bending of a strip 80 mm wide and 1.0 mm thick. The stress–strain relation in the elastic region is $\sigma = 210\varepsilon$ GPa and in the plastic region it is $\sigma = 250\varepsilon$ MPa.

a) What is the limiting curvature to which the strip can be bent without yielding.

b) If the strip is bent to a radius of curvature of 500 mm, what is the radius when it is released? Assume bending by a pure bending moment.

12.11. A steel sheet 1.5 m wide and 1.0 mm thick is bent to a radius of 100 mm. Assume no strain hardening, no friction, and no tension. The effective stress–strain relation is $\bar{\sigma} = 650(0.015 + \bar{\varepsilon})^{0.20}$. $E = 210$ GPa and $\nu = 0.29$. Find the radius of curvature after unloading.

13 Plastic Anisotropy

13.1 CRYSTALLOGRAPHIC BASIS

The primary cause of anisotropy of plastic properties is preferred orientation of grains (i.e., statistical tendency for grains to have certain orientations).* Mechanical working of metals produces preferred orientations or crystallographic textures. Recrystallization during annealing usually changes the crystallographic texture but doesn't cause randomness. (Repeated heating and cooling through the $\alpha \rightarrow \gamma \rightarrow \alpha$ transformation may be a possible exception.) How crystallographic textures develop and how texture influences the anisotropy are not treated in this text. The anisotropy of textured titanium sheet will be considered, however, because of the insight it gives to the problem.

Alpha-titanium alloys have a hexagonal close-packed crystal structure. Deformation occurs primarily by slip in close-packed $<11\bar{2}0>$ directions, which lie in the basal plane parallel to the edges of the hexagonal cell as shown in Figure 13.1. Whether slip occurs on the (0001) basal planes or on the $\{10\bar{1}0\}$ prism planes, there is no strain parallel to the *c*-axis because the slip direction is normal to the *c*-axis. Not even slip on the $\{10\bar{1}1\}$ pyramidal planes will cause *c*-axis strain.

Rolled sheets of α-titanium alloys develop strong textures that are most easily described in terms of an ideal texture with the *c*-axis of most grains aligned with the normal to the rolling plane. There is some spread from this ideal orientation, particularly with a rocking of the *c*-axis up to $\pm 40^\circ$ from the sheet normal toward the transverse direction.

When a tensile specimen cut from a sheet is extended, slip can easily occur on the $\{10\bar{1}0\}$ prism planes. Even though the yield strength may be almost unchanged with the orientation of the tensile specimen relative to the rolling direction, the material is not isotropic. Slip on the $\{10\bar{1}0\}$ prism planes causes contraction in the plane of the sheet, but no thinning. A useful parameter to describe this sort of anisotropy is the ratio *R* of the plastic strain in the width direction to that in the thickness direction,

$$R = \frac{\varepsilon_w}{\varepsilon_t}, \tag{13.1}$$

* In contrast, anisotropy of fracture behavior is largely governed by mechanical alignment of inclusions, voids, and grain boundaries.

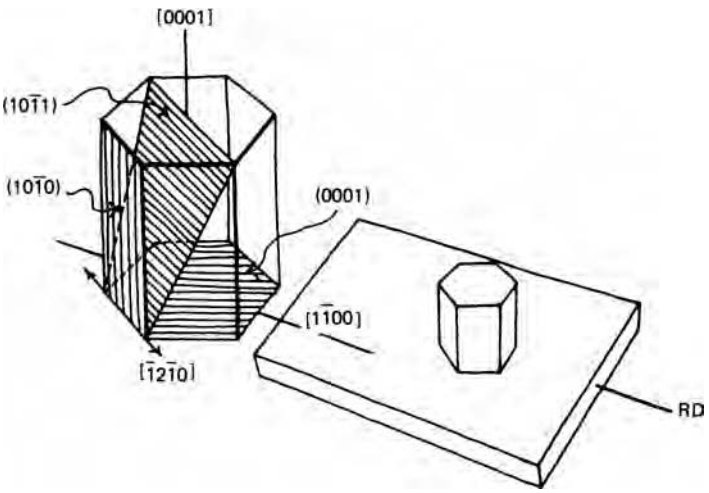

13.1. Idealized texture of an α-titanium sheet with the (0001) plane parallel to the plane of the sheet. Although there are several possible slip planes, slip is restricted to the $<11\bar{2}0>$ family of slip directions, all of which lie in the (0001) plane, so slip can cause no thickening or thinning of the sheet. From W. F. Hosford and W. A. Backofen in *Fundamentals of Deformation Processing* (Syracuse University Press, 1964) p. 262.

where ε_w and ε_t are the contractile trains in the width and thickness directions as illustrated in Figure 13.2. For an isotopic material, $R = 1$, but for ideally textured titanium, $\varepsilon_t = 0$, so $R = \infty$. In commercial titanium sheets, R-values of 3 to 7 are typical. A high R-value suggests that there is a high resistance to thinning and therefore a high strength in biaxial tension in the plane of the sheet and in through-thickness compression. Figure 13.3 illustrates schematically how the R-value affects the shape of the yield locus.

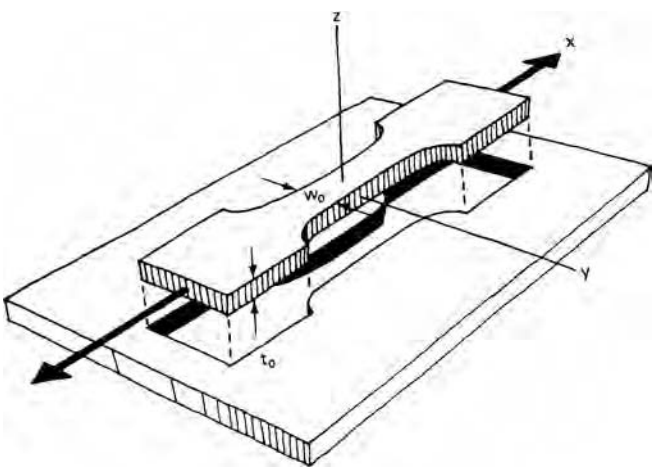

13.2. Strip tensile specimens cut from a sheet. The R-value is defined as the ratio of width-to-thickness strains, $\varepsilon_w/\varepsilon_t$ or $\varepsilon_y/\varepsilon_z$. From W. F. Hosford and W. A. Backofen, *op. cit.*, p. 276.

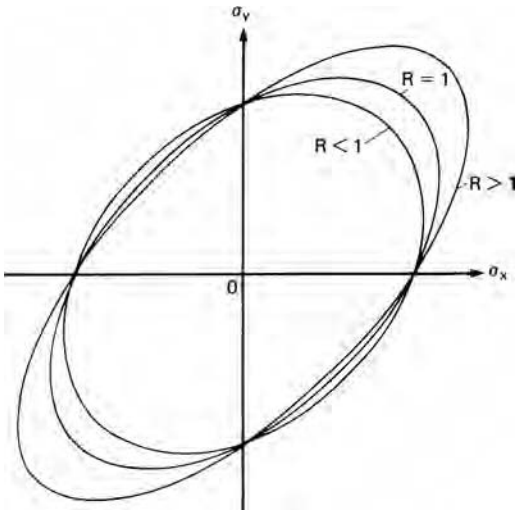

13.3. Schematic yield loci for textured materials with rotational symmetry. A high R-value implies resistance to thinning and hence a high yield strength under biaxial tension, while a low R-value indicates easy thinning and therefore a low yield strength under biaxial tension.

13.2 MEASUREMENT OF *R*

Although the R-value is defined as the ratio of width-to-thickness strains, the thickness strain of a thin sheet cannot be measured accurately. Instead the thickness strain is found from the width and length strains, $\varepsilon_t = -(\varepsilon_w + \varepsilon_l)$. The reduced section of the tensile specimen should be long so the measurements can be made well away from the constraint of the shoulders. The R-value often varies somewhat with the strain, so the length strain at which the measurements are made should be specified. Often 15% elongation is used.

The R-values vary with the test direction in the plane of the sheet. It is customary to define an average value as

$$\bar{R} = \frac{R_0 + 2R_{45} + R_{90}}{4}. \tag{13.2}$$

For steels, the variations of the elastic modulus E and the R-value with texture are usually similar. This correlation is neither exact nor fundamental, but is the basis for a commercial instrument. The instrument measures the velocity of sound in thin strips and is calibrated to give readings of the corresponding R-value.

13.3 HILL'S ANISOTROPIC PLASTICITY THEORY

In 1948, Hill* advanced a quantitative treatment of plastic anisotropy without regard to its crystallographic basis. He assumed materials with three orthogonal axes of anisotropy, x, y, and z about which the properties have two-fold symmetry. The yz, zx, and xy planes are planes of mirror symmetry. In a rolled sheet it is conventional to take the x-, y-, and z-axes as the rolling direction, the transverse direction, and the

* R. Hill, *Proc. Roy. Soc. London*, 193A (1948), p. 281 and *Mathematical Theory of Plasticity*, Chapt. XII (London: Oxford University Press, 1950). See also W. F. Hosford and W. A. Backofen, "Strength and Plasticity of Textured Metals," *Fundamentals of Deformation Processing* (Syracuse, NY: Syracuse University Press, 1964), p. 259.

sheet-plane normal. The theory also assumes equal the tensile and compressive yield strengths in every direction.

The proposed yield criterion is a generalization of the von Mises criterion,

$$F(\sigma_y - \sigma_z)^2 + G(\sigma_z - \sigma_x)^2 + H(\sigma_x - \sigma_y)^2 + 2L\tau_{yz}^2 + 2M\tau_{zx}^2 + 2N\tau_{xy}^2 = 2f(\sigma_{ij})^2, \tag{13.3}$$

where F, G, H, L, M, and N are constants that describe the anisotropy. Note that if $F = G = H = 1$ and $L = M = N = 3$, this reduces to the von Mises criterion. The constants F, G, and H can be evaluated from simple tension tests. Let the x-direction yield strength be X. At yielding in an x-direction tension test, $\sigma_x = X$ and $\sigma_y = \sigma_z = \tau_{ij} = 0$. Substituting into equation 13.3, $(G + H)X^2 = 1$. Similarly,

$$X^2 = \frac{1}{G+H}, \quad Y^2 = \frac{1}{H+F}, \quad \text{and} \quad Z^2 = \frac{1}{F+G}. \tag{13.4}$$

Solving simultaneously,

$$\begin{aligned} F &= (1/Y^2 + 1/Z^2 - 1/X^2)/2, \\ G &= (1/Z^2 + 1/X^2 - 1/Y^2)/2, \\ H &= (1/X^2 + 1/Y^2 - 1/Z^2)/2, \end{aligned} \tag{13.5}$$

where Y and Z are the y- and z-direction yield strengths. However, measurement of Z is not feasible for sheets.

Using equation 2.21

$$\mathrm{d}\varepsilon_{ij} = \mathrm{d}\lambda \frac{\partial f(\sigma_{ij})}{\partial \sigma_{ij}}, \tag{13.6}$$

the flow rules are

$$\begin{aligned} \mathrm{d}\varepsilon_x &= \mathrm{d}\lambda[H(\sigma_x - \sigma_y) + G(\sigma_x - \sigma_z)], \quad \mathrm{d}\varepsilon_{yz} = \mathrm{d}\varepsilon_{zy} = \mathrm{d}\lambda L\tau_{yz} \\ \mathrm{d}\varepsilon_y &= \mathrm{d}\lambda[F(\sigma_y - \sigma_z) + H(\sigma_y - \sigma_x)], \quad \mathrm{d}\varepsilon_{zx} = \mathrm{d}\varepsilon_{xz} = \mathrm{d}\lambda M\tau_{zx} \\ \mathrm{d}\varepsilon_z &= \mathrm{d}\lambda[G(\sigma_z - \sigma_x) + F(\sigma_z - \sigma_y)], \quad \mathrm{d}\varepsilon_{xy} = \mathrm{d}\varepsilon_{yx} = \mathrm{d}\lambda N\tau_{xy}. \end{aligned} \tag{13.7}$$

To derive these flow rules the yield criterion must be written with the shear stress terms appearing as $L(\tau_{yz}^2 + \tau_{zy}^2) + M(\tau_{zx}^2 + \tau_{xz}^2) + N(\tau_{xy}^2 + \tau_{yx}^2)$.

Note that in equation 13.7, $\mathrm{d}\varepsilon_x + \mathrm{d}\varepsilon_y + \mathrm{d}\varepsilon_z = 0$, which indicates constant volume.

The constant N can be found from a tension test made at an angle θ to the x-axis. In such a test yielding occurs when

$$F\sin^4\theta + G\cos^4\theta + H(\cos^4\theta - 2\cos^2\theta\sin^2\theta + \sin^4\theta) + 2N\sin\theta\cos\theta = Y_\theta^2, \tag{13.8}$$

where is the yield strength in the θ-direction test. For a 45° test this becomes $F/4 + G/4 + N = Y_{45}^2$. Solving for N,

$$N = 2Y_{45}^2 - (F+G)/2. \tag{13.9}$$

By differentiating equation 13.8 it can be shown that there are minima and maxima in the value of Y_θ at $\theta = 0°$, 90°, and at an intermediate angle

$$\theta^* = \arctan[(N - G - 2H)/(N - F - 2H)]^{-1/2}. \tag{13.10}$$

There are four possibilities:

With $N > G + 2H$ and $N > F + 2H$, maxima occur at 0° and 90° and there is a minimum at θ^*;

With $N < G + 2H$ and $N < F + 2H$, minima occur at 0° and 90° and there is a maximum at θ^*;

If $G + 2H > N > F + 2H$, θ^* is imaginary and there is a maximum at 0° and a minimum at 90°;

If $G + 2H < N < F + 2H$, θ^* is imaginary and there is a minimum at 0° and a maximum at 90°.

An alternative way of evaluating N is from the R-values. From the flow rules,

$$\begin{aligned}
\varepsilon_x &= \lambda(\sigma_x'[(H + G)\cos^2\theta - H\sin^2\theta] \\
\varepsilon_y &= \lambda(\sigma_x'[(F + H)\cos^2\theta - H\cos^2\theta] \\
\varepsilon_z &= \lambda(\sigma_x'[-F\sin^2\theta - G\cos^2\theta] \\
\gamma_{xy} &= \lambda(\sigma_x' 2N\cos\theta\sin\theta.
\end{aligned} \tag{13.11}$$

The strain ratio R_θ expressed in terms of the anisotropic parameters becomes $R_\theta = [H + (2N - F - 4H)\sin^2\theta\cos^2\theta]/(F\sin^2\theta + G\cos^2\theta)$. For $\theta = 45^\circ$, $R_{45} = (N - F/2)/(F + G)$. Solving for N, $N = (R_{45} + F/2)/(F + G)$. Substituting $R = H/G$ and $P = H/F$,

$$N = (2R_{45} + 1)(R + P)/[2(R + 1)PX^2]. \tag{13.12}$$

The R-value has a minimum or a maximum at 0° and 90° and there may be one minimum or one maximum between 0° and 90°.

For sheet metals, shear tests are necessary to evaluate L and M in equation 13.3. However, γ_{yz} and γ_{zx} are normally zero in sheet forming so these parameters are not necessary.

13.4 SPECIAL CASES OF HILL'S YIELD CRITERION

For the special case in which x, y, and z are principal axes ($\tau_{yz} = \tau_{zx} = \tau_{xy} = 0$), equation 13.3 can be expressed in terms of R and P. Substituting $(G + H)X^2 = 1$,

$$\left(\frac{F}{G}\right)(\sigma_y - \sigma_z)^2 + \left(\frac{G}{G}\right)(\sigma_z - \sigma_x)^2 + \left(\frac{H}{G}\right)(\sigma_x - \sigma_y)^2 = \left(\left(\frac{G}{G}\right) + \left(\frac{H}{G}\right)\right)X^2. \tag{13.13}$$

Now substituting $R = H/G$ and $R/P = F/G$ and multiplying by P,

$$R(\sigma_y - \sigma_z)^2 + P(\sigma_z - \sigma_x)^2 + RP(\sigma_x - \sigma_y)^2 = P(R + 1)X^2. \tag{13.14}$$

The flow rules become

$$\begin{aligned}
\varepsilon_x{:}\varepsilon_y{:}\varepsilon_z = [R(\sigma_x - \sigma_y) + (\sigma_x - \sigma_z)]{:}[(R/P)(\sigma_y - \sigma_z) + R(\sigma_y - \sigma_x)]{:} \\
[(R/P)(\sigma_z - \sigma_y) + (\sigma_z - \sigma_x)].
\end{aligned} \tag{13.15}$$

Express the effective stress and effective strain for this criterion so that they reduce to σ_x and ε_x in a uniaxial tension test:*

$$\bar{\sigma} = \left(\frac{R(\sigma_y - \sigma_z)^2 + P(\sigma_z - \sigma_x)^2 + RP(\sigma_x - \sigma_y)^2}{P(R+1)} \right)^{1/2}, \tag{13.16}$$

and

$$\bar{\varepsilon} = C[P(\varepsilon_y - R\varepsilon_z)^2 + R(P\varepsilon_z - \varepsilon_x)^2 + (R\varepsilon_x - P\varepsilon_y)^2]^{1/2}, \tag{13.17}$$

where $C = [(R+1)/R]^{1/2}/(R+P+1)$.

With rotational symmetry about the z-direction, $F = G = H = N/3$, $L = M$, and $R = P = R_{45}$. The x and y directions may be chosen to coincide with the principal stress axes so $\tau_{xy} = 0$. Substituting $P = R$ into equation 13.14 and the flow rules, equation 13.11, the yield criterion and flow rules become

$$(\sigma_y - \sigma_z)^2 + (\sigma_z - \sigma_x)^2 + R(\sigma_x - \sigma_y)^2 = (R+1)X^2 \tag{13.18}$$

and

$$\varepsilon_x : \varepsilon_y : \varepsilon_z = [(R+1)\sigma_x - R\sigma_y - \sigma_z] : [(R+1)\sigma_y - R\sigma_x - \sigma_z] : [2\sigma_z - \sigma_x - \sigma_y]. \tag{13.19}$$

Equation 13.18 plots in $\sigma_z = 0$ space as an ellipse as shown in Figure 13.4. The extension of the ellipse into the first quadrant increases with increasing R-value indicating that the strength in biaxial tension increases with R.

Equation 13.18 is often used with an average R in analyses for materials that have properties that are not rotationally symmetric about the sheet normal. While this procedure is not strictly correct, it is often useful in assessing the role of normal anisotropy.

13.5 NONQUADRATIC YIELD CRITERIA

Calculations† of yield loci for textured fcc and bcc metals suggested that a nonquadratic yield criterion of the form

$$F|\sigma_y - \sigma_z|^a + G|\sigma_z - \sigma_x|^a + H|\sigma_x - \sigma_y|^a = 1 \tag{13.20}$$

with an exponent much higher than 2 represents the anisotropy much better. With $a = 2$ this reduces to equation 13.14. Exponents of 8 for fcc metals and 6 for bcc metals were suggested. Although this criterion is a special case of Hill's 1979 criterion, it was suggested independently and is not one that Hill suggested would be useful.

For plane stress conditions, this criterion reduces to

$$P|\sigma_x|^a + R|\sigma_y|^a + RP|\sigma_x - \sigma_y|^a = P(R+1)X^a. \tag{13.21}$$

* In Hill's papers the effective stress and strain functions are defined in a way that $\bar{\sigma}$ and $\bar{\varepsilon}$ do not reduce to σ_x and ε_x in a tension test.

† W. F. Hosford, "On Yield Loci of Anisotropic Cubic Metals," *7th North American Metalworking Res. Conf.*, SME, Dearborn MI (1979), and R. Logan and W. F. Hosford, *Int. J. Mech. Sci.*, 22 (1980), pp. 419–30.

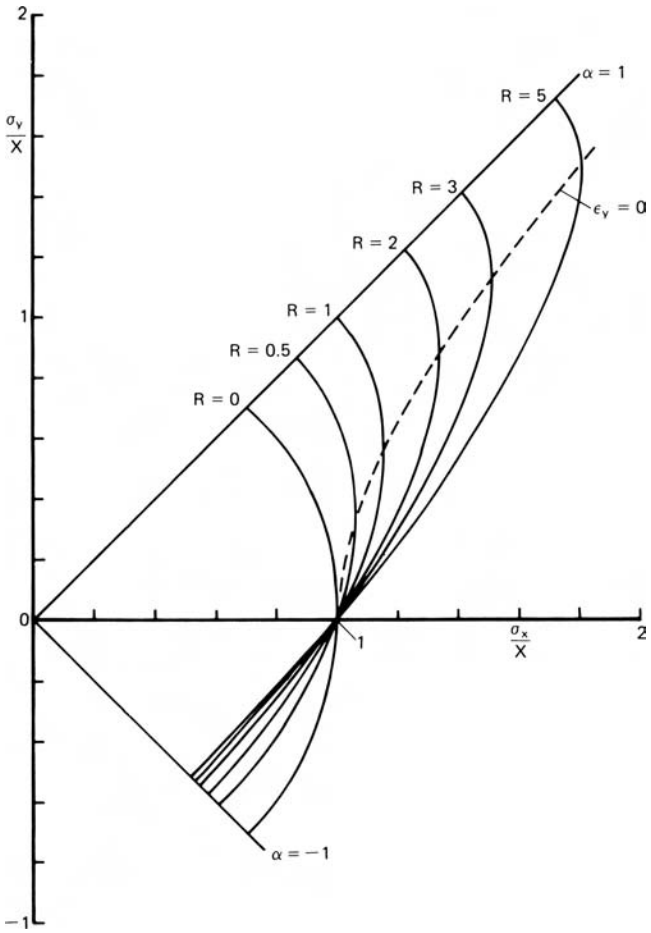

13.4. Plane-stress ($\sigma_z = 0$) yield locus for rotational symmetry about z according to the Hill criterion (equation 13.18). The dashed line indicates the locus of stress states for plane strain, $\varepsilon_y = 0$.

If the exponent is an even integer, the absolute magnitude signs in equation 13.20 are unnecessary. With rotational symmetry about z, $R = P$ and the criterion reduces to

$$\sigma_x^a + \sigma_y^a + R(\sigma_x - \sigma_y)^a = (R+1)X^a. \tag{13.22}$$

The yield locus for equation 13.22 plots between the Tresca and Hill criteria (Figure 13.5).

Note that as a increases, the criterion approaches Tresca. The flow rules for equation 13.20 are

$$\begin{aligned}
\varepsilon_x &= \lambda[P\sigma_x^{a-1} + RP(\sigma_x - \sigma_y)^{a-1}], \\
\varepsilon_y &= \lambda[R\sigma_y^{a-1} + RP(\sigma_y - \sigma_x)^{a-1}], \\
\varepsilon_z &= -\lambda(P\sigma_x^{a-1} + R\sigma_y^{a-1}).
\end{aligned} \tag{13.23}$$

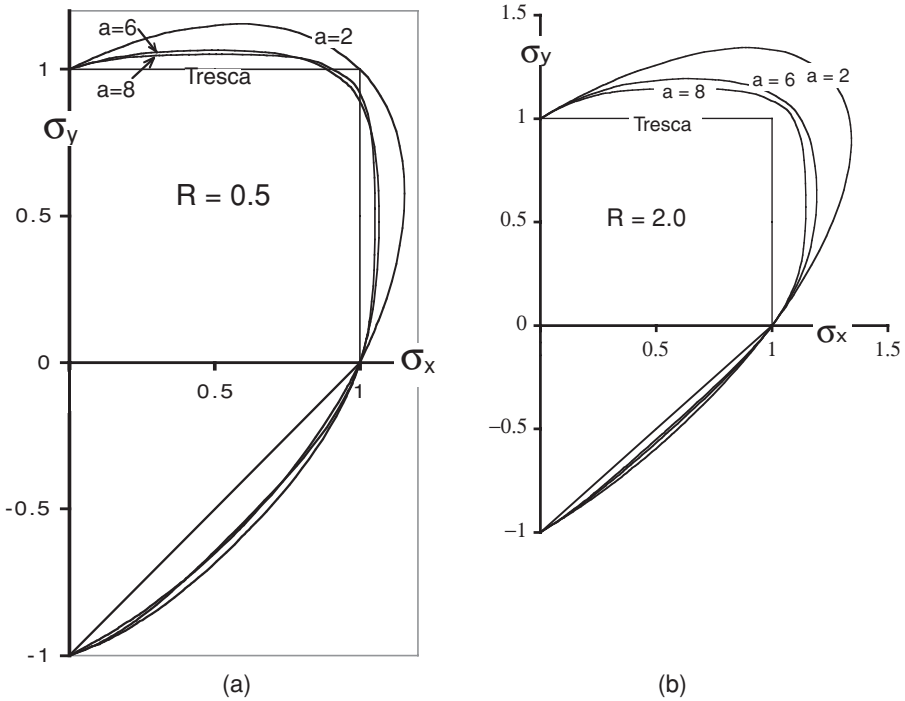

13.5. Plots of the high-exponent criterion given by equation 13.22 for several values of $R = 0.5$ (a) and $R = 2$ (b) with several values of the exponent a. Note as a increases, the loci approach the Tresca locus.

The effective stress and strain functions are

$$\bar{\sigma} = \left(\frac{P|\sigma_x|^a + R|\sigma_y|^a + RP|\sigma_x - \sigma_y|^a}{P(R+1)} \right)^{1/a} \tag{13.24}$$

and

$$\bar{\varepsilon} = \varepsilon_x (1 + \alpha\rho) \frac{\sigma_x}{\bar{\sigma}}, \tag{13.25}$$

where

$$\rho = \frac{\mathrm{d}\varepsilon_y}{\mathrm{d}\varepsilon_x} = \frac{R[\alpha^{a-1} - P(1-\alpha^{a-1})]}{P[1 + R(1-\alpha)^{a-1}]}. \tag{13.26}$$

In 1979, Hill* proposed a generalized nonquadratic criterion to account for an "anomalous" observation that in some aluminum alloys with $R > 1$, $P > 1$, and $R_{45} > 1$, yield strengths in biaxial tension were found to be higher than the yield strength in uniaxial tension. (This is not permitted with Hill's 1948 criterion.) Hill proposed

$$\begin{aligned} f|\sigma_2 - \sigma_3|^m + g|\sigma_3 - \sigma_1|^m + h|\sigma_1 - \sigma_2|^m + a|2\sigma_1 - \sigma_2 - \sigma_3|^m \\ + b|2\sigma_2 - \sigma_3 - \sigma_1|^m + c|2\sigma_3 - \sigma_1 - \sigma_2|^m = 1, \end{aligned} \tag{13.27}$$

* R. Hill, *Math. Proc. Camb. Soc.*, 75 (1979), pp. 179–91.

where the exponent m depends on the material. Hill suggested four special cases with planar isotropy ($a = b$ and $f = g$). Using the corresponding flow rules in these cases to express R

$$R = \frac{2^{m-1}a + h + 2b - c}{2^{m-1}a + g - b + 2c}. \tag{13.28}$$

Of Hill's special cases, only the fourth case, which can be expressed as

$$|\sigma_1 + \sigma_2|^m + (2R + 1)|\sigma_1 - \sigma_2|^m = 2(R + 1)Y^m, \tag{13.29}$$

is free from concavity problems. Values of $1.7 < m < 2.2$ have been required to fit this to experimental data and different exponents are required for different R-values so this criterion cannot be used to predict the effect of R on forming operations. It should be noted that equation 13.20 is a special case of equation 13.27. However, it cannot account for the "anomaly." Equation 13.20 was suggested independently and is not one Hill's special cases.

The high exponent yield criteria, equations 13.20 and 13.29, do not provide any way of treating shear stress terms, τ_{yz}, τ_{zx}, or τ_{xy}. In 1989, Barlat and Lian* proposed a plane-stress criterion that accounts for the in-plane shear stress, σ_{xy}:

$$a|K_1 - K_2|^m + a|K_1 + K_2|^m + (a - 2)|2K_2|^m = 2Y^m, \tag{13.30}$$

where $K_1 = (\sigma_x + h\sigma_y)/2$ and $K_2 = \{[(\sigma_x - h\sigma_y)/2]^2 + p\tau_{xy}^2\}^{1/2}$. Here a, p, h, and m are material constants. The exponent m is approximately 8. It should be noted that this criterion reduces to equation 13.20 for planar isotropy.

Later Barlat and coworkers† proposed a criterion that allows for out-of-plane shear stresses, τ_{yz} and τ_{zx}. However, this criterion requires six constants in addition to m. It will not be discussed further except to state that it does not reduce to equation 13.20 when τ_{yz} and $\tau_{zx} = 0$.

13.6 CALCULATION OF ANISOTROPY FROM CRYSTALLOGRAPHIC CONSIDERATIONS

Taylor‡ analyzed the deformation of a polycrystal by calculating the amount of slip, γ, in each grain necessary to achieve a fixed strain, ε. The ratio $M = \gamma/\varepsilon$ is called the Taylor factor. He assumed that each grain of a polycrystal deforms in such a way that it undergoes the same shape change as the polycrystal as a whole. Later Bishop and Hill,§ using the same assumptions, showed that M can be calculated by considering the stress states capable of activating multiple slip. Taylor further assumed that the strain hardening could be described by

$$\tau = f(\gamma), \tag{13.31}$$

* F. Barlat and J. Lian, *Int. J. Mech. Sci*., 5 (1989), pp. 51–66.
† F. Barlat, D. J. Lege, and J. C. Brem, *Int. J. Plasticity*, 7 (1991), pp. 369–712.
‡ G. I. Taylor, *J. Inst. Met*. 62 (1938), pp. 307–24.
§ J. F. W. Bishop and R. Hill, *Phil. Mag*., 42 (1951), pp. 414–27 and 1298–307.

where τ is the shear stress required to cause slip and γ is the total amount of slip on all slip systems. Using this assumption the stress–strain curve for polycrystals is related to that of a single crystal by

$$\sigma = \bar{M}\tau \quad \text{and} \quad \varepsilon = \gamma/\bar{M}, \tag{13.32}$$

where $\bar{M}$ is the average value of M for all orientations. These approaches have been used to calculate the yield loci for textured metals. Details are given elsewhere.*

NOTE OF INTEREST

Rodney Hill (born 1921 in Leeds) earned his MA (1946), PhD (1948), and ScD (1959) from Cambridge University. He worked in the Armarment Research Dept., Kent, British Iron & Steel Research Association, Bristol University, and Nottingham University before becoming a professor of Mechanics of Solids at Cambridge University. His book, *Mathematical Theory of Plasticity* (Oxford University Press, 1950), is a classic. It contains original work on applications of slip-line fields in addition to introducing the first complete theory of plastic anisotropy.

REFERENCES

R. Hill, *Mathematical Theory of Plasticity*, Oxford University Press, 1950.

W. F. Hosford, *Mechanics of Single Crystals and Textured Polycrystals*, Oxford University Press, 1992.

W. F. Hosford, *Mechanical Behavior of Materials*, Cambridge University Press, 2005.

PROBLEMS

13.1. Show that the 1948 Hill criterion and flow rules predict an angular variation of R as

$$R_\theta = \frac{H + (2N - F - G - 4H)\sin^2\theta\cos^2\theta}{F\sin^2\theta + G\cos^2\theta}.$$

13.2. Using the results of Problem 13.1, derive an expression for N/G in terms of R, $P\ (= R_{90})$ and R_{45}.

13.3. In strip tension tests, the strain ratios $R_0 = 4.0$, $R_{90} = 2.0$, $R_{45} = 2.5$ and yield strengths $Y_0 = 49$, $Y_{90} = 45$ were measured. Using the Hill 1948 criterion calculate $Y_{22.5}$, Y_{45}, and $Y_{67.5}$, and plot Y as a function of θ.

13.4. A thin-wall tube was made from sheet metal by bending the sheet into a cylinder and welding. The prior rolling direction is the axial direction of the tube. The tube has a diameter of 5.0 in and a wall thickness of 0.025 in. The strain ratios are $R_0 = 2.5$, $R_{90} = 0.8$, $R_{45} = 1.8$ and the yield strength in the rolling direction is 350 MPa. Neglect elastic effects.

a) If the tube is capped and loaded under internal pressure, at what pressure will it yield?

* W. F. Hosford, *Mechanics of Single Crystals and Textured Polycrystals* (New York: Oxford University Press, 1992).

b) Will the length increase, decrease, or remain constant?
c) If the tube is extended in tension, will the volume inside the tube increase, decrease, or remain constant?
d) Find the stress in the walls if the tube is capped and filled with water, and pulled in tension to yielding.

13.5. Consider a sheet with planar isotropy (equal properties in all directions in the sheet) loaded under plane stress ($\sigma_z = 0$).
a) Express the ratio $\rho = \varepsilon_y/\varepsilon_x$ as a function of the stress ratio $\alpha = \sigma_y/\sigma_x$.
b) Write an expression for $\bar{\sigma}$ in terms of α, R, and σ_x.
c) Write an expression for $d\bar{\varepsilon}$ in terms of α, R, and $d\varepsilon_x$. Remember that

$$\bar{\sigma}\, d\bar{\varepsilon} = \sigma_x d\varepsilon_x + \sigma_y d\varepsilon_y + \sigma_z d\varepsilon_z.$$

13.6. Using the 1948 Hill criterion for a sheet with planar isotropy,
a) Derive an expression for $\alpha = \sigma_y/\sigma_x$ for plane strain ($\varepsilon_y = 0$) and plane stress ($\sigma_z = 0$).
b) Find the stress for yielding under this form of loading in terms of X, R, and P.
c) For a material loaded such that $d\varepsilon_z = 0$ and $\sigma_z = 0$, calculate σ_x and σ_y at yielding.
d) For a material loaded such that $d\varepsilon_x = d\varepsilon_y$ and $\sigma_z = 0$, calculate σ_x and σ_y at yielding.

13.7. For a sheet with $X = 350$ MPa, $R = 1.6$, and $P = 2.0$, calculate
a) The yield strength in the y-direction.
b) The value of σ_x at yielding with $\varepsilon_z = 0$ and $\varepsilon_y = 0$.
c) The values of σ_x and σ_y at yielding with $\sigma_z = 0$ and $\varepsilon_z = 0$.
d) The values of σ_x and σ_y at yielding with $\sigma_z = 0$ and $\varepsilon_x = \varepsilon_y$.

13.8. Consider a material with planar isotropy and $R = 0.5$. Calculate the stress ratio $\alpha = \sigma_y/\sigma_x$, for plane strain, $\varepsilon_y = 0$, using both the 1948 Hill criterion (equation 13.18) and the high exponent criterion (equation 13.22) for
a) $R = 0.5$
b) $R = 2.0$.

13.9. Using equations 13.22 and 13.23 for planar isotropy with $\sigma_z = 0$, determine the plane strain–to–biaxial strength ratio, $\chi = \sigma_{x(\varepsilon_y = 0)}/\sigma_{x(\varepsilon_y = \varepsilon_x)}$, as a function of R. Plot this ratio as a function of R from $R = 0.5$ to $R = 2$ for both the Hill criterion ($a = 2$) and for $a = 6$.

13.10. Marciniak propose a method of biaxially stretching a sheet by using a cylindrical punch and a spacer sheet with a circular hole as sketched in Figure 13.6. It is often assumed that the stress state is balance biaxial stress ($\sigma_x = \sigma_y$) if there is equal biaxial straining ($\varepsilon_x = \varepsilon_y$), but this isn't true unless $R_0 = R_{90} = R_{45}$. In experiments using this technique, it was found that $\varepsilon_y/\varepsilon_x = 1.035$ for an aluminum sheet with $R_0 = 0.55$ and $R_{90} = 0.89$.
a) Calculate the stress ratio σ_y/σ_x that would produce $\varepsilon_y/\varepsilon_x = 1.035$ using both the Hill criterion ($a = 2$) and for $a = 6$.

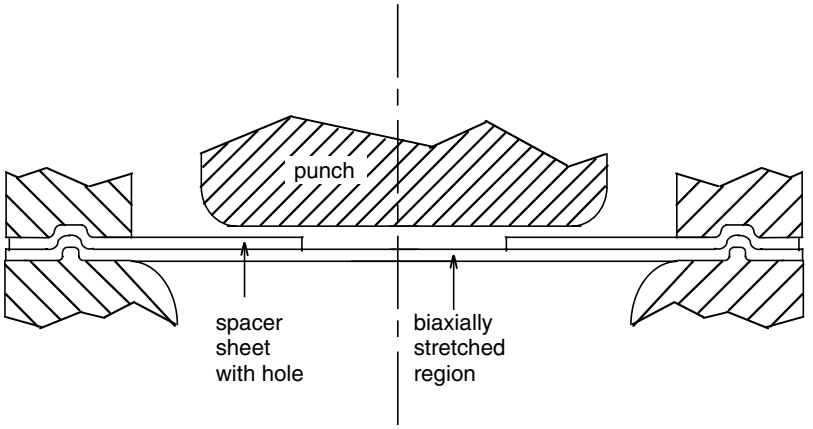

13.6. Setup for biaxial stretching.

b) Calculate the ratio of strains $\varepsilon_y/\varepsilon_x$ that would result from equal biaxial tension, $\sigma_x = \sigma_y$, using both the Hill criterion ($a = 2$) and for $a = 6$.

13.11. W. Lode (*Z. Phys*., 36, 1926, pp. 913–30) proposed two variables for critically testing isotropic yield criteria and their flow rules:

$$\mu = \frac{2(\sigma_2 - \sigma_3)}{(\sigma_1 - \sigma_3)} - 1 \quad \text{and} \quad \nu = \frac{2(\varepsilon_2 - \varepsilon_3)}{(\varepsilon_1 - \varepsilon_3)} - 1.$$

Plot μ vs. ν for the Tresca and von Mises criteria and for equations 13.23 and 13.24 with $R = 1$ and $a = 6$. Compare your plot with Figure 13.7, which is based on experimental data (G. I. Taylor and H. Quinney, *Phil. Trans. Royal Soc., Ser. A,* 203 (1931), pp. 323–62.

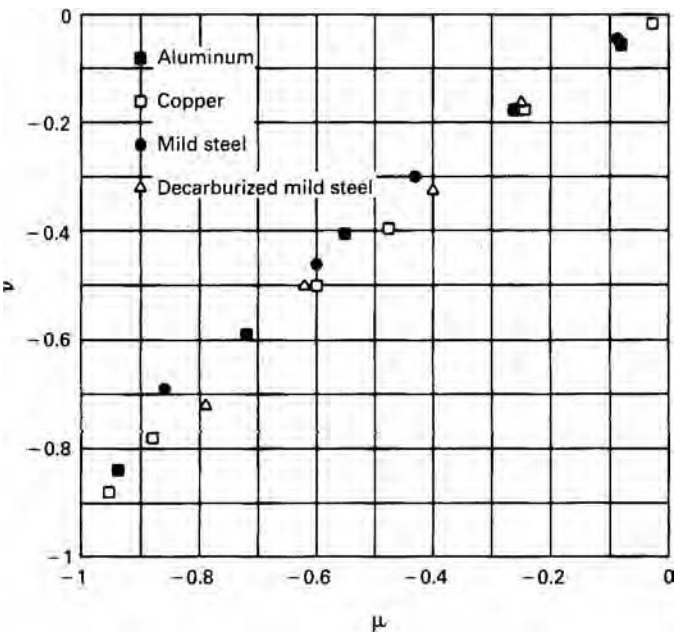

13.7. Plot of Lode's variables for Problem 13.11.

13.12. An automobile part is to be formed from a low-carbon steel. The steel has planar isotropy with $R = 1.8$. During tryouts, circles of 5 mm diameter were marked on the sheet before it was press formed. After forming it was found that circles in a critical region had become ellipses with major and minor diameters of 4.87 and 6.11 mm. Assume that $\sigma_z = 0$.

a) Calculate the strains in the critical area.

b) Find the ratio σ_y/σ_x assuming Hill's 1948 criterion.

c) Find the ratio σ_y/σ_x assuming the high exponent criterion (equation 13.22) with $a = 6$.

14 Cupping, Redrawing, and Ironing

Sheet forming differs from bulk forming in several respects. In sheet forming, tension predominates, whereas bulk forming operations are predominately compressive. In sheet forming operations at least one of the surfaces is free from contact with the tools. Useful formability is normally limited by localized necking rather than by fracture as in bulk forming. There are instances of failure by fracture but these are unusual.

Sheet forming processes may be roughly classified by the state of stress. At one end of the spectrum is the deep drawing of flat-bottom cups. In this case, one of the principal stresses in the flange is tensile and the other is compressive. There is little thinning, but wrinkling is of concern. At the other end of the spectrum are processes, usually called stamping, in which both of the principal stresses are tensile. Thinning must occur. Rarely does the formability in sheet forming processes correlate well with the tensile ductility (either reduction in area or elongation at fracture).

14.1 CUP DRAWING

The deep drawing of flat-bottom cups is a relatively simple process. It is used to produce such items as cartridge cases, zinc dry cells, flashlights, aluminum and steel cans, and steel pressure vessels. The process is illustrated by Figure 14.1. There are two important regions: the flange, where most of the deformation occurs, and the wall, which must support the force necessary to cause the deformation in the flange. If the blank diameter is too large, the force in the wall may exceed its strength, thereby causing failure. Forming limits are described by a *limiting drawing ratio* (LDR), which is the largest ratio of d_0/d_1 that may be successfully drawn. In this respect deep drawing is similar to wire drawing. Indirect compression is induced by tensile forces in the drawn material. Each wedge-shaped element in the flange must undergo enough circumferential compression to permit it to flow over the die lip. A typical drawing failure is shown in Figure 14.2. The flanges must be held down to prevent wrinkling. Figure 14.3 shows what happens when the hold-down force is insufficient.

The following analysis, based on the work of Whiteley,* uses the coordinate system illustrated in Figure 14.4. The following simplifying assumptions are made:

* R. Whiteley, *Trans. ASM*, 52 (1960), p. 154. See also W. F. Hosford in *Formability: Analysis, Modeling and Experimentation*, TMS AIME, NY (1978), p. 78–95.

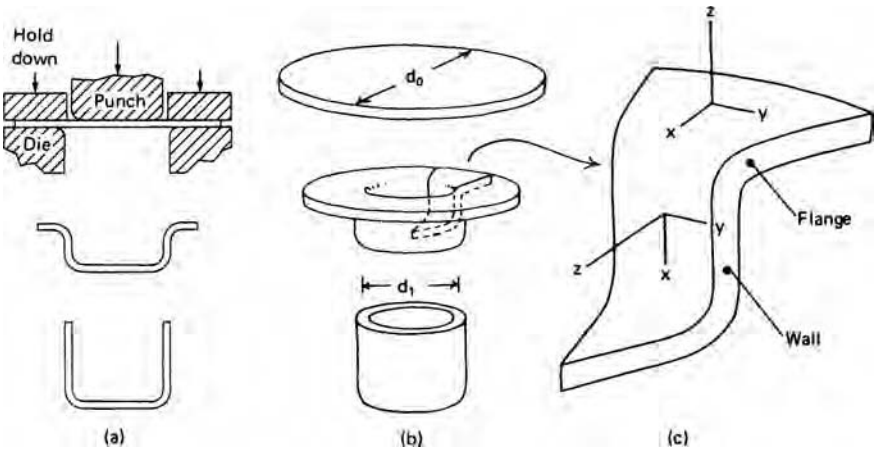

14.1. Illustration of cupping and coordinate axes.

14.2. Drawing failures by necking at the bottom of the cup wall. From D. J. Meuleman, PhD thesis, University of Michigan (1980).

14.3. Wrinkling of partially drawn cups due to insufficient hold-down. From D. J. Meuleman, *op. cit*.

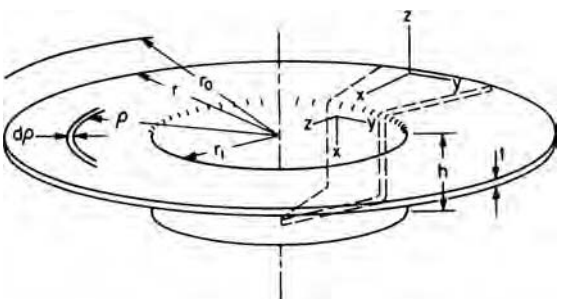

14.4. Schematic illustration of a partially drawn cup showing the coordinate system. From W. F. Hosford in *Formability: Analysis, Modeling and Experimentation*, TMS-AIME (1978), pp. 78–95.

1. All of the energy expended is used to deform the material in the flange. The work against friction and the work to bend and unbend the material as it flows over the die lip are neglected in the initial treatment, but will be accounted for later by an efficiency factor.
2. The material does not strain harden. It will be shown later that n has only a minor effect on the LDR.
3. Flow in the flange is characterized by plane strain, $\varepsilon_z = 0$, so the thickness of the cup wall is the same as the thickness of the blank.

According to the assumption that $\varepsilon_z = 0$ in the flange, the total surface area is constant and the surface area inside an element is also constant. Therefore

$$\pi\rho^2 + 2\pi r_1 h = \pi\rho_0^2 \qquad \text{so} \qquad 2\pi\rho\ \mathrm{d}\rho + 2\pi r_1\ \mathrm{d}h = 0 \qquad \text{or}$$
$$\mathrm{d}\rho = -r_1\ \mathrm{d}h/\rho. \tag{14.1}$$

The circumferential strain is $\mathrm{d}\varepsilon_y = \mathrm{d}\rho/\rho$. Since $\mathrm{d}\varepsilon_z = 0$,

$$\mathrm{d}\varepsilon_x = -\mathrm{d}\varepsilon_y = -\mathrm{d}\rho/\rho = r_1\ \mathrm{d}h/\rho^2, \tag{14.2}$$

where $\mathrm{d}h$ is the incremental movement of the punch. The incremental work done on the annular element between ρ and $\rho + \mathrm{d}\rho$ equals the volume of the element $(2\pi t\rho\ \mathrm{d}\rho)$ times the incremental work per volume, $\sigma_x\ \mathrm{d}\varepsilon_x + \sigma_y\ \mathrm{d}\varepsilon_y + \sigma_z\ \mathrm{d}\varepsilon_z = (\sigma_x - \sigma_y)\,\mathrm{d}\varepsilon_x$, so the total work on the element is $\mathrm{d}W = (2\pi t\rho\ \mathrm{d}\rho)(\sigma_x - \sigma_y)(r_1/\rho^2)\mathrm{d}h$. Although σ_x and σ_y vary throughout the flange the value of $(\sigma_x - \sigma_y)$ is constant and will be designated as σ_f. The total work for all such elements is

$$\frac{\mathrm{d}W}{\mathrm{d}h} = \int_{r_1}^{r} \frac{2\pi r_1 t\sigma_\mathrm{f}\mathrm{d}\rho}{\rho} = 2\pi r_1 t\sigma_\mathrm{f} \ln\left(\frac{r}{r_1}\right). \tag{14.3}$$

The drawing force F_d, which equals $\mathrm{d}W/\mathrm{d}h$, has its largest value at the beginning of the draw when $r = r_0$, so

$$F_{\mathrm{d(max)}} = 2\pi r_1 t\sigma_\mathrm{f} \ln(d_0/d_1), \tag{14.4}$$

where d_0 and d_1 are diameters of the blank and cup.

The axial stress that the wall must carry is then

$$\sigma_x = \frac{F_{\mathrm{d(max)}}}{2\pi r_1 t} = \sigma_\mathrm{f} \ln(d_0/d_1). \tag{14.5}$$

The wall will begin to neck when $\sigma_x = \sigma_\mathrm{w}$, the yield strength of the wall, or

$$\sigma_\mathrm{w} = \sigma_\mathrm{f} \ln(d_0/d_1). \tag{14.6}$$

Both σ_w and σ_f are plane-strain yield strengths. They are equal for an isotropic material, so equation 14.6 predicts that LDR $= \exp(1) = 2.72$. This is much too high. The development should be modified by realizing that the calculated work in the flange and hence the calculated drawing force should be multiplied by $1/\eta$ to account for the work against friction and the work to cause bending. In this case LDR $= \exp(\eta)$. Usually the LDR is about 2, so the efficiency is about 0.70.

14.2 ANISOTROPIC EFFECTS IN DRAWING

It has been found that the LDR increases with R. This is understandable because a high R implies low resistance to in-plane contraction (deformation in the flange) and high resistance to thinning (the failure mode of the wall). If the material is not isotropic, the drawability will be given by

$$\ln(\text{LDR}) = \eta\beta, \tag{14.7}$$

where β is the ratio of the two plane-strain strengths,

$$\beta = \frac{\sigma_{w(\varepsilon_y = 0)}}{\sigma_{f(\varepsilon_z = 0)}}. \tag{14.8}$$

With Hill's 1948 criterion, it can be shown that

$$\beta = \sqrt{(R+1)/2}, \tag{14.9}$$

so

$$\ln(\text{LDR}) = \eta\sqrt{(R+1)/2}. \tag{14.10}$$

Although rotational symmetry about the sheet normal has been assumed in this development, most sheets don't have a single R-value. It has been common to use an average R-value in equation 14.10.

With the high-exponent criterion (equation 13.22), β in equation 14.8 is

$$\beta = (1/2)\left[\frac{2 + 2^a R}{\alpha^a + 1 + R(1-\alpha)^a}\right]^{1/a}, \tag{14.11}$$

where $\alpha = R^{1/(a-1)}/[1 + R^{1/(a-1)}]$.

Figure 14.5 compares the predictions of equation 14.10 (line labeled $a = 2$) with experimental data. It is obvious that equation 14.10 predicts too much dependence of

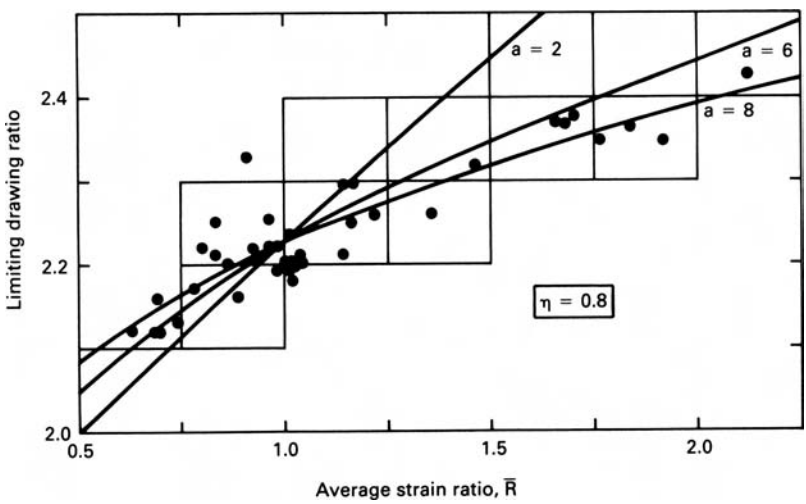

14.5. Dependence of the limiting drawing ratio on R. The line labeled $a = 2$ is the prediction of equation 14.10, while the lines labeled $a = 6$ and $a = 8$ are the predictions of equation 14.7 using the high-exponent criterion. From R. W. Logan, D. J. Meuleman, and W. F. Hosford in *Formability and Metallurgical Structure*, A. K. Sachdev and J. D. Embury, eds. (The Metallurgical Society, 1987).

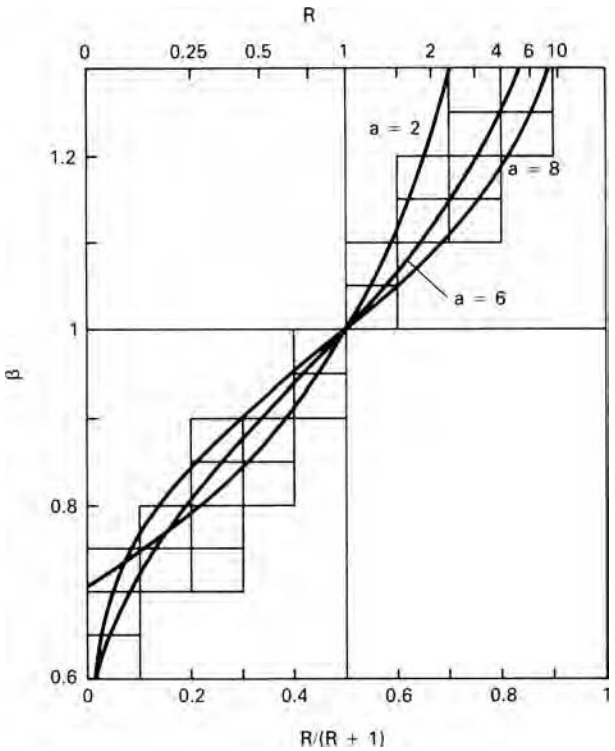

14.6. Relation between the ratio of plane-strain strengths, β, and the average R value.

LDR on R. The lines $a = 6$ and $a = 8$ are the predictions of equation 14.7 with β evaluated using the high exponent criterion and its flow rules. In each case, η was chosen as 0.8. Changing η shifts the level of the curves without affecting their shapes.

Figure 14.6 shows the results of calculations relating β to R. There is much less dependence for $a = 6$ and $a = 8$ than for $a = 2$.

14.3 EFFECTS OF STRAIN HARDENING IN DRAWING

Although work hardening was neglected in the treatment above, it can treated analytically. The calculated effect of the strain-hardening exponent, n, on the LDR of isotropic material is shown in Figure 14.7. The dependence in the range $0.1 \leq n \leq 0.3$ is very small. The results of a more sophisticated analysis that allows for both strain hardening and thickness strains are shown in Figure 14.8 together with the same data as in Figure 14.5. Calculations were made for three values of n and the data are grouped according to the n-value of the material. Figure 14.9 summarizes the effect of n from these experiments and calculations.

Work hardening also controls how the punch force changes during the stroke as shown in Figure 14.10. With increasing n, the maximum is reached later in the stroke. These calculations neglect the bending effect at the die lips early in the stroke. As a consequence, the initial rise of the force is usually less rapid than shown here and the maximum occurs somewhat later.

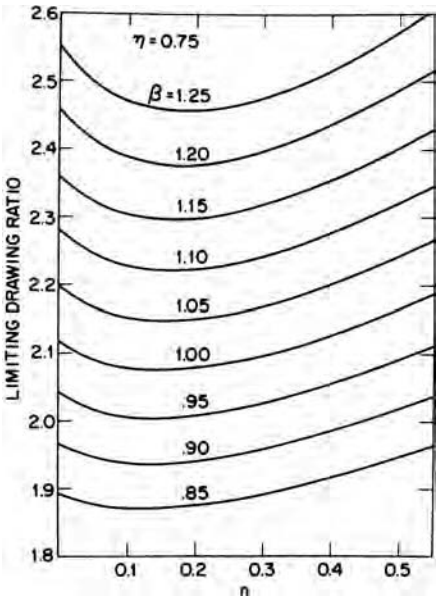

14.7. Calculated values of limiting drawing ratio (LDR) for different strain-hardening exponents. From W. F. Hosford, *op. cit*.

14.4 ANALYSIS OF ASSUMPTIONS

In the previous analyses, plane strain was assumed in the flange so no thickness changes occur. This is not strictly true. The material that becomes the bottom of the wall experiences more tension than compression while it is in the flange, so therefore it thins. In contrast, the material that becomes the top of the wall experiences more compression than tension while it is in the flange, so therefore it thickens.

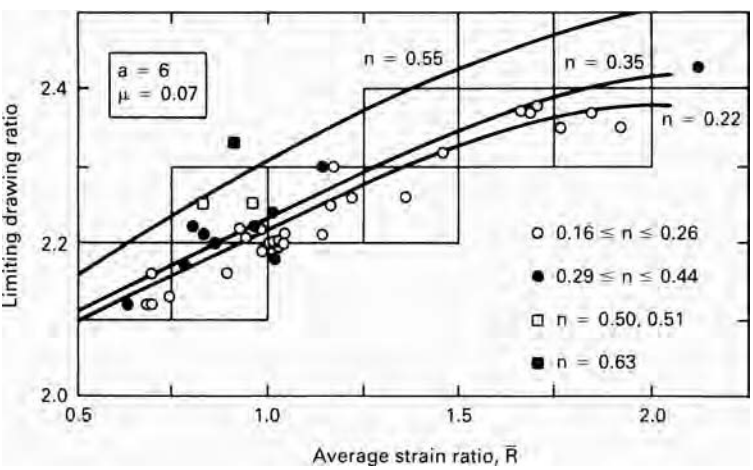

14.8. Effect of R and n on drawability. The solid lines are finite element calculations with $a = 6$. The experimental data are grouped according to their levels of n. From R. W. Logan, D. J. Meuleman, and W. F. Hosford, *op. cit*.

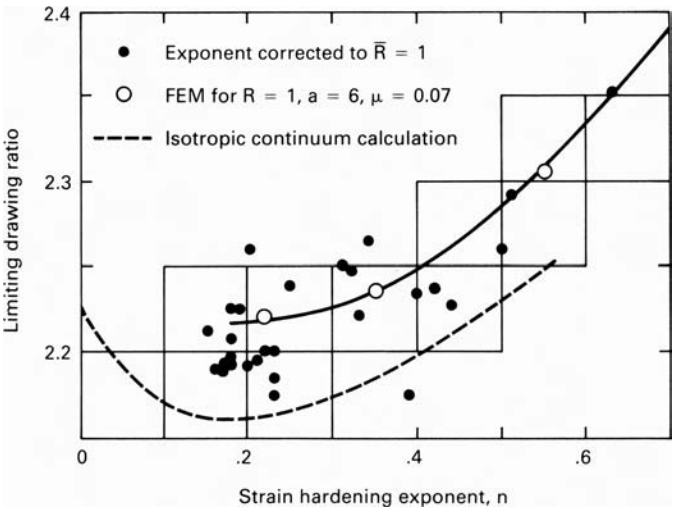

14.9. Summary of the effect of n on LDR, including finite-element (FEM) calculations for $\mu = 0.07$. The experimental data are from Figures 14.5 and 14.8 corrected to $R = 1$. From R. W. Logan, D. J. Meuleman, and W. F. Hosford, *op. cit*.

Figure 14.11(a) shows the calculated thickness changes for an isotropic non–work-hardening material and Figure 14.11(b) shows actual thickness measurements. The effects increase with drawing ratio.

The simplistic assumption of a deformation efficiency is equivalent to assuming that work in bending and unbending, dW_b/dh, and the work against friction, dW_f/dh, are proportional to the deformation work in the flange, dW/dh. For analysis of the LDR, it is important only that this is true at the maximum force. The bending and unbending is in plane strain, $\varepsilon_y = 0$, so this contribution should be proportional to the work in the flange, which also deforms with $\varepsilon_y = 0$. The friction originates in two places. One is

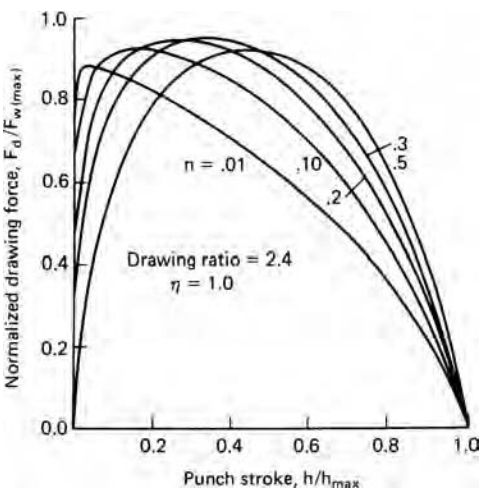

14.10. Calculated variation of punch force with stroke h. From W. F. Hosford, *op. cit*.

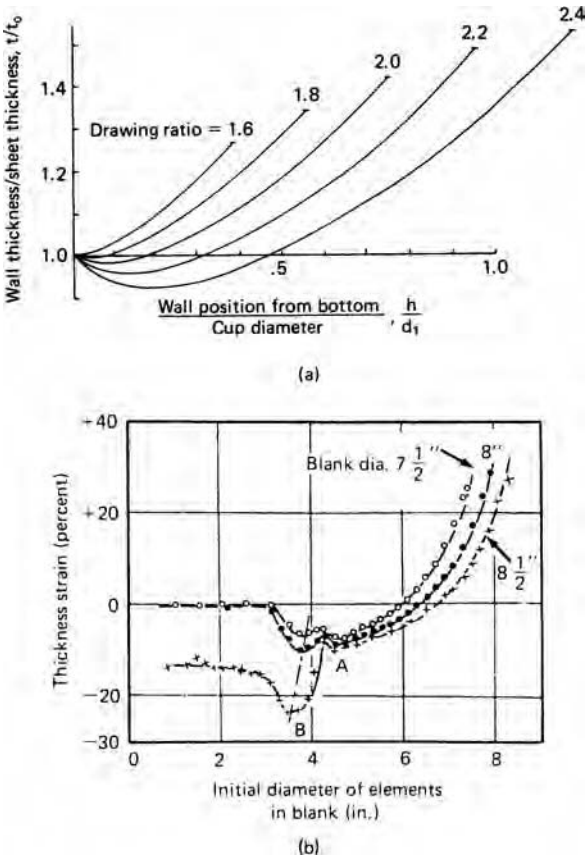

14.11. (a) Calculated variation of wall thickness and (b) experimental measurements. From W. Johnson and P. B. Mellor, *Engineering Plasticity* (Van Nostrand Reinhold, 1973).

at the die lip. Here the normal force is $N \approx \pi F_d/2$, so the frictional contribution to the drawing force should be approximately equal to $\approx \pi \mu F_d/2$ (see Problem 14.4). The other place friction acts is in the flange. If the hold-down force is proportional to the drawing force the frictional force will be also. It has been suggested that the hold-down force be a constant fraction of the tensile strength, which is almost equivalent. Thus the efficiency should not vary significantly with material properties.

Several investigators have considered another possible mode of failure in materials of low n-value. They predict failure in the region between the die lip and punch early in the punch stroke before any wall has formed. Such failures would occur so early in the punch stroke that there would be little expenditure of energy against friction and bending so the efficiency at that point would be much higher than later in the stroke. Therefore these analyses, which are based on 100% efficiency, fail to account for the fact that the drawing force would be higher at a later stage.

14.5 EFFECTS OF TOOLING ON CUP DRAWING

Drawability depends on tooling and lubrication as well as on material properties. The work expended in bending and unbending as the material flows over the die lip increases

with the ratio of the sheet thickness to the radius of the die lip. This causes a higher drawing force and lower LDR. However if the die-lip radius is too large, wrinkling may occur in the unsupported region between the die and punch.

The radius of the punch nose is also important. When failures occur they are usually near the bottom of the wall where the material has not been work hardened. With a generous punch radius, the failure site is moved upward on the wall where the wall has been strengthened by more work hardening.

Lubrication has two opposing effects. Lubrication of the flange and die lip reduces the frictional work. However, high friction between the cup wall and the punch causes shear stresses to move the potential failure site upward into material that has been work hardened more. Abrasion to roughen the punch has been known to increase drawability. However, it is difficult to maintain such roughness in production. A similar increase of drawability has been achieved by drawing into a chamber of pressurized water.* The pressure increases the friction between the punch and the wall. Increased drawability can be achieved by maintaining the punch temperature lower than the flange temperature.† The temperature difference keeps the flange softer than the wall.

Ideally the hold-down force should be adjusted to a level just sufficient to prevent wrinkling. Swift‡ has recommended a hold-down pressure of ½ to 1% of the yield strength but the optimum pressure decreases with increasing sheet thickness. Above $t/d = 0.025$, no hold down is necessary.§

14.6 EARING

The height of the walls of drawn cups usually have peaks and valleys as shown in Figure 14.12. This phenomenon is known as *earing*. There may be two, four, or six ears, but four ears are most common. Earing results from planar anisotropy, and ear height and angular position correlate well with the angular variation of R. For two or four ears, earing is described by the parameter

$$\Delta R = \frac{R_0 + R_{90} - 2R_{45}}{2}. \tag{14.12}$$

If $\Delta R > 0$, there are ears at 0° and 90°, and if $\Delta R < 0$, ears form at 45°. This variation is shown in Figure 14.13. Experimental correlation of earing with ΔR is shown in Figure 14.14.

Earing is undesirable because the walls must be trimmed, creating scrap. With earing, the full benefit of a high R on LDR is not realized.

The angular dependence of earing can be estimated by assuming that the state of stress at the outer edge of the blank is uniaxial compression and that the compressive strain is the same everywhere along the top of the final cup. The thickness strain then is

* W. G. Granzow, Paper No. F-1920, Fabricating Machinery Association, Rockford, IL (1975), pp. 1–18.
† W. G. Granzow, *Sheet Metal Industries*, 55 (1979), p. 561.
‡ Chung and Swift, *Proc. Inst. Mech. Eng.*, 165 (1951), p. 199.
§ D. F. Eary and E. A. Reed, *Techniques of Pressworking of Sheet Metal*, 2nd ed. (Prentice-Hall, 1974).

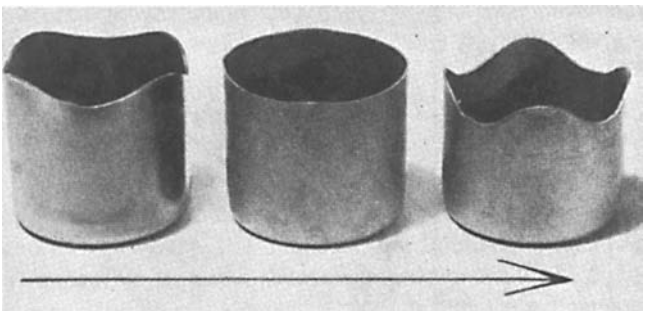

14.12. Ears in cups made from three different copper sheets. The arrow indicates the prior rolling direction. From D. V. Wilson and R. D. Butler, *J. Inst. Met.*, 90 (1961–2), pp. 473–83.

$\varepsilon_{z\theta} = -\varepsilon_y/(R_{\theta+90}+1)$ where $R_{\theta+90}$ is the R-value measured in a tension test normal to θ. The thickness variation along the top of the cup is then described by

$$t_\theta = t_0 \exp \varepsilon_{z\theta} = t_0 \exp\left(\frac{-\varepsilon_y}{R_{\theta+90}+1}\right) = t_0\left(\frac{d_1}{d_0}\right)^{1/(R_{\theta+90}+1)}.$$

It is further assumed that although the wall thickness varies linearly with height the value of

$$h_\theta(t_0 + t_\theta)/2 = h_\theta t_0[1 + (d_1/d_0)^{1/(R_{\theta+90}+1)}]/2, \tag{14.13}$$

is the same everywhere along the top of the wall. Therefore

$$h_{45}\left[1+\left(\frac{d_1}{d_0}\right)^{1/(R_{45}+1)}\right]^{-1} = h_0\left[1+\left(\frac{d_1}{d_0}\right)^{1/(R_{90}+1)}\right]^{-1} = h_{90}\left[1+\left(\frac{d_1}{d_0}\right)^{1/(R_0+1)}\right]^{-1}. \tag{14.14}$$

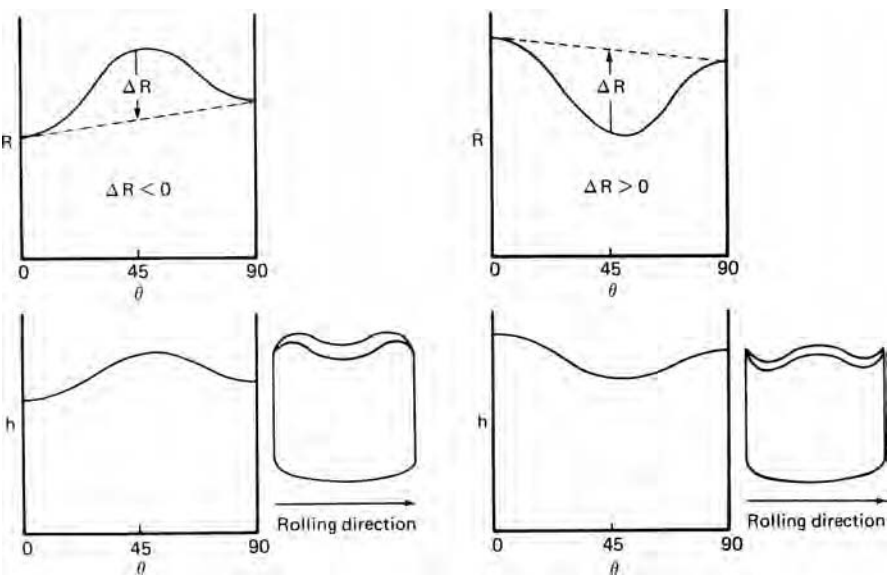

14.13. Relation of earing to angular variation of R.

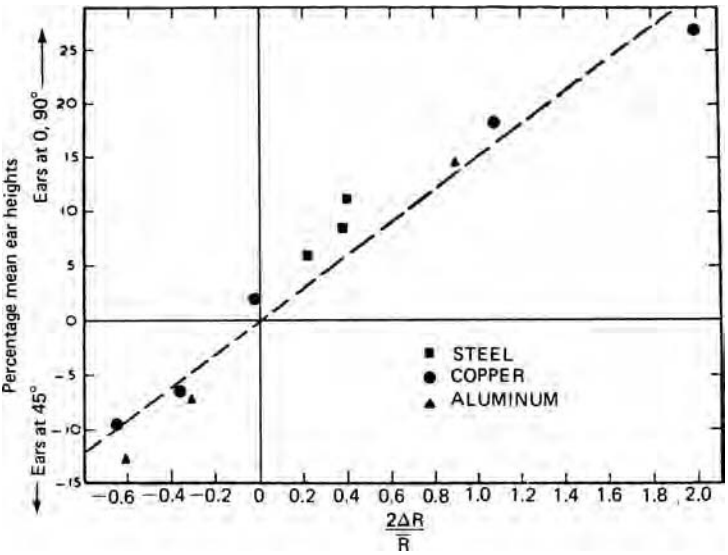

14.14. Correlation of the extent and position of ears with ΔR. From D. V. Wilson and R. D. Butler, *op. cit*.

For a given drawing ratio, the relative ear height $2h_{45}/(h_0 + h_{90})$ can be found from equation 14.14 (see Problem 14.9).

14.7 REDRAWING

Only shallow cups can be made in a single drawing operation. However, redrawing can decrease the diameter and increase wall height. As in drawing, there is little thickness change so the surface area remains constant. Figure 14.15 illustrates direct and reverse redrawing. Hold down is unnecessary in reverse redrawing.

There is a limiting diameter reduction as in drawing. If the redraw ratio is too high, the wall will fail in tension. Redrawing is almost a steady-state process. If the material were non–work-hardening and the wall thickness constant, the drawing force would remain constant except at the start and end. Because the cup walls are thicker at the top

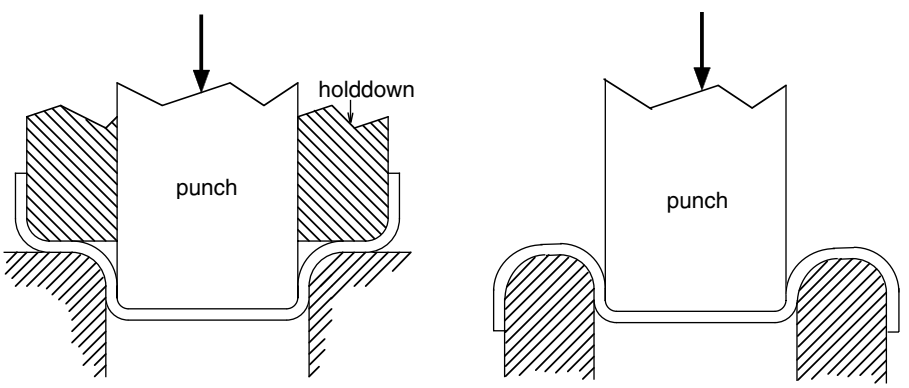

14.15. Direct redrawing (left) and reverse redrawing (right).

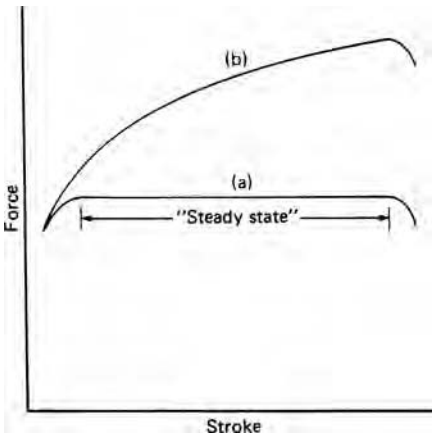

14.16. For a non–strain-hardening material the punch forces during redrawing are constant except at the very start and end (a). The redraw force for a strain-hardening material increases during the stroke because the initial drawing hardens the material at the top of the walls (b).

than the bottom, the redrawing force rises during the punch stroke. Furthermore, with a work-hardening material, the top of the wall will have been strengthened more during the initial draw so the punch force in redrawing must rise with stroke as the harder material is being deformed. This is shown schematically in Figure 14.16. The bottom of the cup wall, which must carry the redrawing force, is not strengthened during the initial draw. The limiting redraw ratio is greater for materials with low n-values (as cold-rolled sheets) than for those with high n-values (annealed sheets). High R-values are beneficial because the flow during the reduction of wall diameter and the potential necking failure of the wall are the same as in the initial cupping.

14.8 IRONING

Ironing is the forced reduction of wall thickness, which increases the wall height. Some ironing of the top of the wall may occur during the initial drawing. In this case the ironing adds to the total punch force as shown in Figure 14.17. Because the ironing occurs late in the draw, it may not affect the drawability.

Ironing is often used as a separate process after drawing and redrawing. In the manufacture of aluminum beverage cans, ironing is used to increase the wall height by a factor of three. Of course, there is a limiting reduction that can be made in a single ironing pass because high reductions may cause the wall strength to be exceeded. As with redrawing, the limiting reduction decreases with work-hardening capacity (higher n-values) because the bottom of the wall is not strengthened as much in the initial drawing. Heavily work-hardened sheets perform better than annealed ones. This is shown in Figure 14.18. Unlike cupping and redrawing, the R-values have no effect on ironability because both the forced deformation and the failure mode involve the same plane strain.

Ironing tends to greatly reduce earring. This is because the valleys are thicker than the ears so are elongated more.

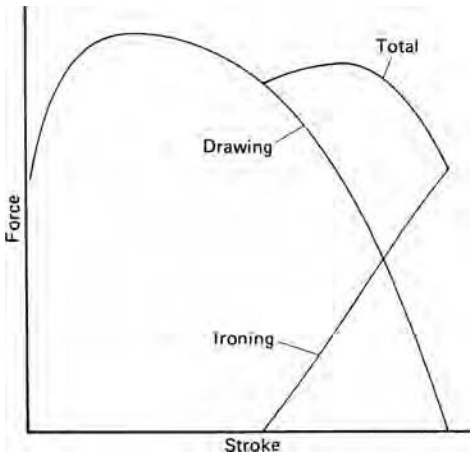

14.17. Any ironing during drawing adds to the drawing force near the end of the draw. The LDR is reduced only if the second peak is higher than the first.

Figure 14.19 shows the forces acting on the deforming metal during ironing. The deformation is much like strip drawing (Chapter 7) except for the action of friction. Friction between the cup wall and deforming material acts to help pull the cup through the die whereas friction between the ironing ring and the deforming material acts in the opposite direction. If friction is neglected, equation 7.7 is applicable.

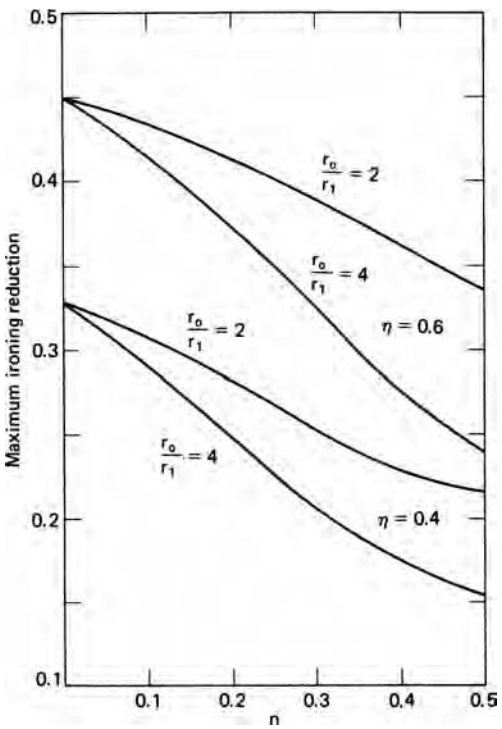

14.18. The calculated dependence of the limiting ironing reduction on the strain-hardening exponent, n, efficiency, η, and prior drawing and redrawing reduction (r_0/r_1). From W. F. Hosford, *op. cit*.

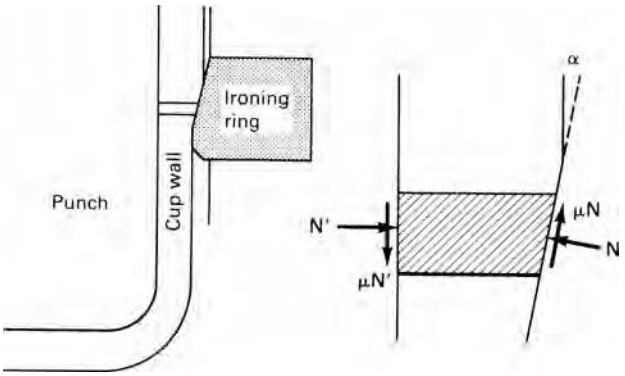

14.19. Frictional forces on opposite sides of the cup wall during ironing act in opposite directions.

It is possible to draw, redraw, and iron in a single stroke of a punch as illustrated schematically in Figure 14.20.

14.9 RESIDUAL STRESSES

The walls have residual stresses after drawing. In the axial direction, there is residual tension in the outside of the walls and residual tension on the inside. These stresses are greatest near the top of the walls because there was little axial tension during the bending and unbending at the die lip. These residual stresses cause a bending moment that is resisted by a hoop tensile stress. Such residual stresses create a sensitivity to stress corrosion in some materials. Figure 14.21 shows cup failures caused by stress corrosion.

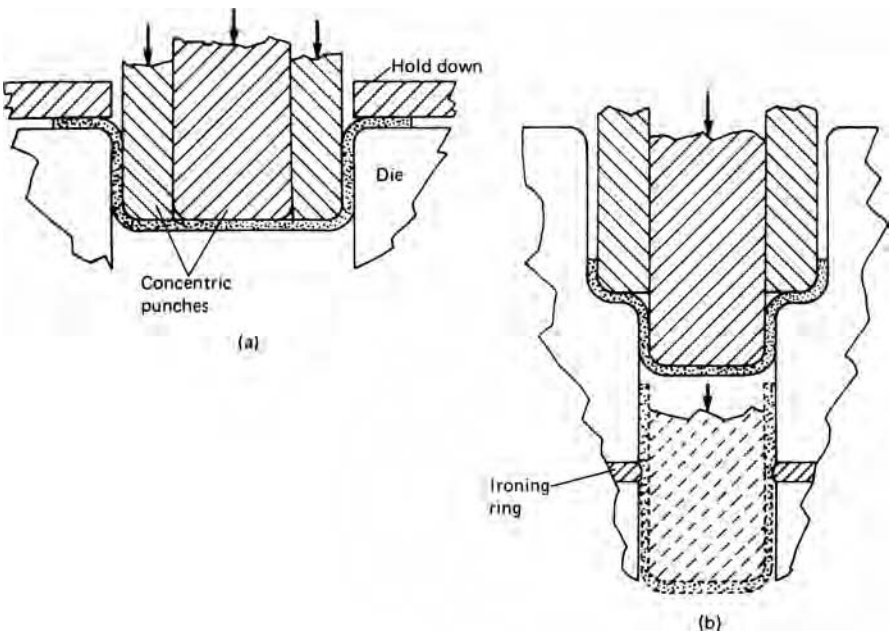

14.20. Illustration of tooling for cupping and redrawing (a) and ironing (b) in one stroke.

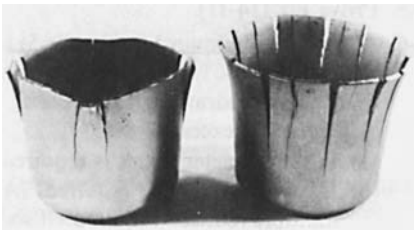

14.21. Stainless steel cups that failed by stress corrosion in a laboratory atmosphere within 24 hours after drawing. The cracks are perpendicular to the hoop tensile stresses. From D. J. Meuleman, *op. cit*.

NOTES OF INTEREST

The first aluminum two-piece beverage cans were produced in about 1963. They replaced the earlier steel cans made from three separate pieces: a bottom, the wall, which was bent into a cylinder and welded, and a top. Today the typical beverage can is made from a circular blank, $5\frac{1}{2}$ inches in diameter, by drawing it into a $3\frac{1}{2}$ inch diameter cup, redrawing to $2\frac{5}{8}$ in. diameter, and then ironing the walls to achieve the desired height. There are about 100 billion made in the United States each year. Beverage cans account for about $\frac{1}{5}$ of the total usage of aluminum. This is enough for every man, woman, and child to consume one beer or soft drink every day.

Cartridge brass (Cu-35 Zn) is susceptible to stress corrosion cracking in atmospheres containing ammonia. Cracks run along grain boundaries under tension. Stress relieving of brass was not common before the 1920s. During World War I, the U.S. Army commandeered barns in France to use as ammunition depots. Unfortunately, the ammonia produced by decomposition of cow urine caused brass cartridge cases to split open. Today, the army requires stress relief of all brass cartridge cases.

REFERENCES

Z. Marciniak, J. L. Duncan, and S. J. Hu, *Mechanics of Sheet Metal Forming*, Butterworth Heinemann, 2002.

Edward M. Meilnik, *Metalworking Science and Engineering*, McGraw-Hill, 1991.

Roger Pierce, *Sheet Metal Forming*, Adam Hilger, 1991.

PROBLEMS

14.1. Calculate the height-to-diameter ratio for drawing ratios of 1.8, 2.0, 2.25, and 2.5. Assume a constant thickness.

14.2. Calculate the slope of LDR vs. R for $R = 1$ and $\eta = 0.75$ according to
- **a)** Whiteley's equation, 14.10;
- **b)** Whiteley's analysis (equation 14.7) using equation 14.11 for β.

14.3. Derive an expression relating R to β from equations 13.27 and 13.28.

14.4. Show that the frictional force acting on the die lip is approximately equal to $\pi \mu F_d/2$.

14.5. Evaluate β for the 1948 Hill yield criterion.

14.6. A typical aluminum beverage can is 5.25 in high and 2.437 in in diameter with a wall thickness of 0.005 in and a bottom thickness of 0.016 in. The starting

material is aluminum alloy 3004-H19 that has already been cold rolled over 80%.

a) What diameter blank is required?

b) Is a redrawing step necessary? (Assume that a safe drawing ratio is 1.8.) If so how many redrawing steps are necessary?

c) How many ironing stages are required? (Assume a deformation efficiency of 50%.)

14.7. In the analysis of deep drawing the work in bending and unbending at the die lip was neglected.

a) Derive an expression for the energy expended in bending and unbending as a function of the strain ratio, R, the yield strength, y, the thickness, t, and the die lip radius r. Assume planar isotropy.

b) What fraction of the total drawing load might come from this source for a sheet with $R = 1$, $t = 1.0$ mm, $r = 0.8$ mm, $d_0 = 50$ mm, and $d_1 = 25$ mm?

14.8. Significant increases in the limiting drawing ratio can be achieved using pressurized water on the punch side of the blank as shown in Figure 14.22. Limiting drawing ratios of three have been achieved for material that with conventional tooling would have an LDR of 2.1.

a) Explain how the pressurized water can increase the drawability.

b) Estimate the level of pressure required to achieve LDR $= 3$ with $\eta = 0.75$ and $Y = 250$ MPa.

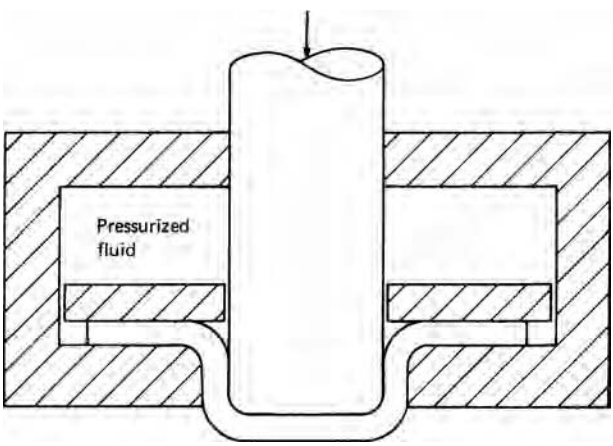

14.22. Cup drawing with pressurized water on the blank.

14.9. Using the procedure in Section 14.6, estimate relative ear height $\Delta h/h_{av} = 2[2h_{45} - (h_0 + h_{90})]/[2h_{45} + (h_0 + h_{90})]$ for a drawing ratio of 1.8 for materials having the following strain ratios:

a) $R_0 = 1.8$, $R_{90} = 2.0$, $R_{45} = 1.4$.

b) $R_0 = 1.2$, $R_{90} = 1.4$, $R_{45} = 1.6$.

c) $R_0 = 0.6$, $R_{90} = 0.4$, $R_{45} = 0.8$.

d) $R_0 = 0.8$, $R_{90} = 0.8$, $R_{45} = 0.5$.

For each material, calculate $2\Delta R/R$ and $\Delta h/h$ and compare with Figure 14.14.

14.10. During the drawing of flat bottom cups, the thickness, t_w, at the top of the wall is usually greater than the original sheet thickness, t_0, as shown in Figure 14.23. Derive an expression for t/t_0 in terms of the blank diameter, d_0, and the cup diameter, d_1. Assume isotropy and neglect the blank holder pressure. Find the ratio of t_w/t_0 for a drawing ratio of 1.8. (*Hint*: Consider the stress state at the outside of the flange.)

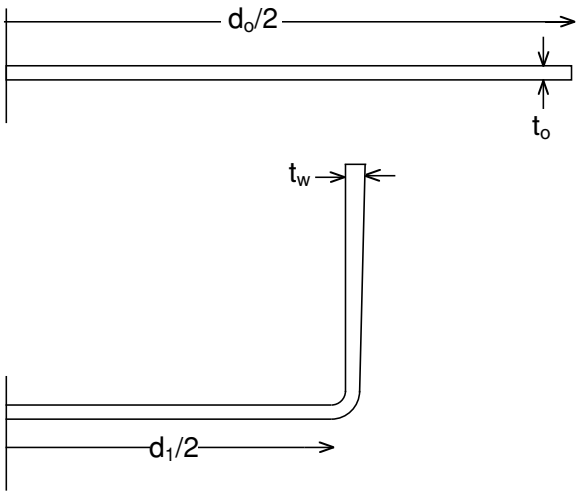

14.23. Wall thickness variation.

15 Forming Limit Diagrams

15.1 LOCALIZED NECKING

Many sheet-forming operations involve biaxial stretching in the plane of the sheet. Failures occur by the formation of a sharp local neck. Localized necking should not be confused with diffuse necking, which precedes failure in round tensile specimens. Diffuse necking of sheet specimens involves contraction in both the lateral and width directions. In sheet specimens, local necking occurs after diffuse necking. During local necking the specimen thins without further width contraction. Figure 15.1 illustrates local necking. At first the specimen elongates uniformly. At maximum load, a diffuse neck forms by contraction of both the width and thickness when $\varepsilon_1 = n$ (Figure 15.1(a)). Finally a local neck develops (Figure 15.1(b)).

In a tension test the strain in the width direction cannot localize easily, but the condition is reached where a sharp local neck can form at some characteristic angle θ to the tensile axis. Typically the width of the neck is roughly equal to the thickness so very little elongation occurs after local necking. The strain parallel to the neck, $d\varepsilon_{2'}$, must be zero, but

$$d\varepsilon_{2'} = d\varepsilon_1 \cos^2\theta + d\varepsilon_2 \sin^2\theta = 0. \tag{15.1}$$

For an isotropic material under uniaxial tension in the 1-direction,

$$d\varepsilon_2 = d\varepsilon_3 = -d\varepsilon_1/2. \tag{15.2}$$

Substituting into equation 15.1, $\cos^2\theta - (\sin^2\theta)/2 = 0$, or

$$\tan\theta = \sqrt{2}, \quad \theta = 54.74^\circ.$$

If the metal is anisotropic,

$$d\varepsilon_2 = -R/(R+1)d\varepsilon_1. \tag{15.3}$$

In this case,

$$\tan\theta = \sqrt{(R+1)/R}. \tag{15.4}$$

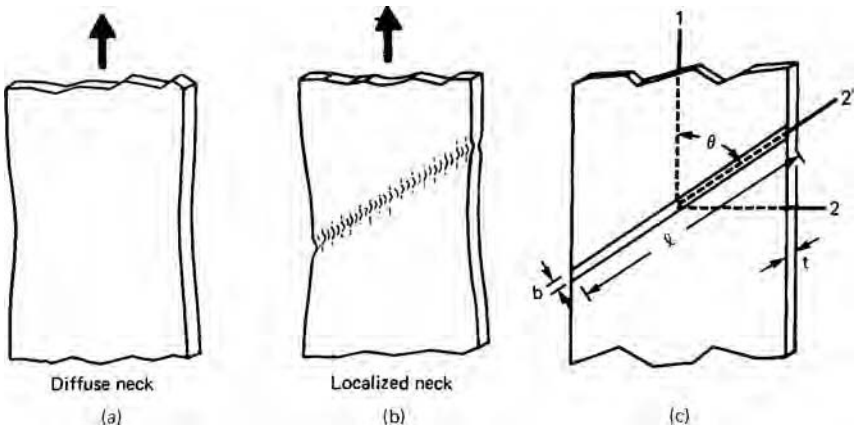

15.1. Diffuse neck (a) and localized neck (b) coordinate system used in analysis (c).

The cross-sectional area of the neck is $A' = \ell t$. Because ℓ is constant, $\mathrm{d}A'/A' = \mathrm{d}t/t = \mathrm{d}\varepsilon_3$, and the area perpendicular to the 1-axis is $A = A' \sin\theta$. However, θ is also constant so a local neck can form only if the load can fall under the constraint $\mathrm{d}\varepsilon_{2'} = 0$. Since $F = \sigma_1 A$,

$$\mathrm{d}F = 0 = \sigma_1 \mathrm{d}A + A\mathrm{d}\sigma_1, \tag{15.5}$$

or $\mathrm{d}\sigma_1/\sigma_1 = -\mathrm{d}A/A = -\mathrm{d}A'/A' = -\mathrm{d}\varepsilon_3$. Since $\mathrm{d}\varepsilon_3 = -\mathrm{d}\varepsilon_1/2$,

$$\mathrm{d}\sigma_1/\sigma_1 = \mathrm{d}\varepsilon_1/2. \tag{15.6}$$

If $\sigma_1 = K\varepsilon_1^n$, $\mathrm{d}\sigma_1 = nK\varepsilon_1^{n-1}\,\mathrm{d}\varepsilon_1$. Therefore the critical strain for localized necking in uniaxial tension is

$$\varepsilon_1^* = 2n. \tag{15.7}$$

In sheet forming, the stress state is rarely uniaxial tension but the same principles can be used to develop the conditions for localized necking under a general stress state of biaxial tension. Assume that the strain ratio $\rho = \varepsilon_2/\varepsilon_1$ remains constant during loading. (This is equivalent to assuming that the stress ratio $\alpha = \sigma_2/\sigma_1$ remains constant.) Substitution of $\varepsilon_2/\varepsilon_1 = \rho$ into equation 15.1 gives $\varepsilon_1 \cos^2\theta + \rho\varepsilon_1 \sin^2\theta = 0$, or

$$\tan\theta = 1/\sqrt{-\rho}. \tag{15.8}$$

The angle θ can have a real value only if ρ is negative (ε_2 is negative). If ρ is positive, there is no angle at which a local neck can form.

The critical strain for localized necking is also influenced by ρ. For constant volume, $\mathrm{d}\varepsilon_3 = -(1+\rho)\,\mathrm{d}\varepsilon_1$. Substituting into $\mathrm{d}\sigma_1/\sigma_1 = -\mathrm{d}\varepsilon_3$,

$$\mathrm{d}\sigma_1/\sigma_1 = (1+\rho)\,\mathrm{d}\varepsilon_1. \tag{15.9}$$

With power-law hardening the condition for local necking is

$$\varepsilon_1^* = \frac{n}{1+\rho}. \tag{15.10}$$

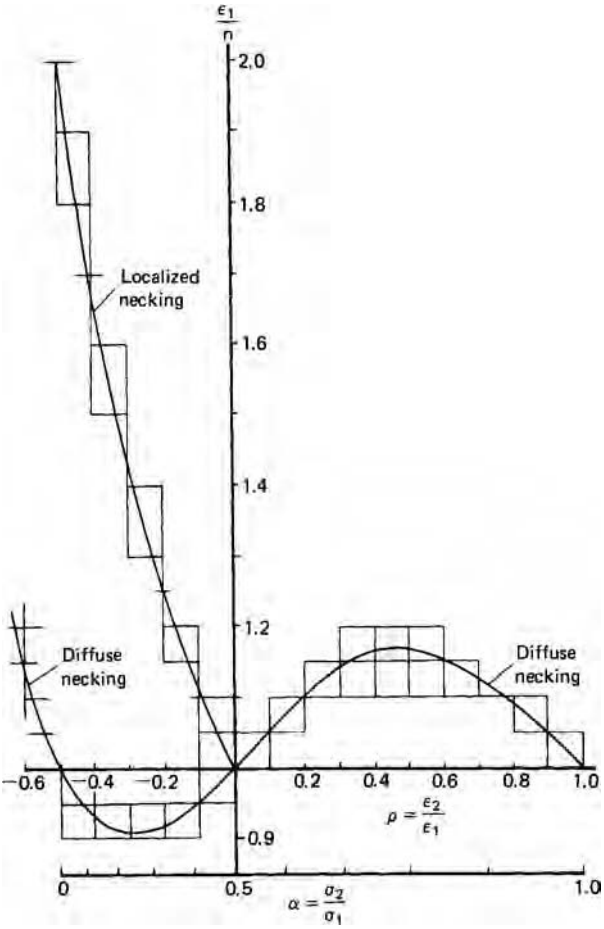

15.2. Critical strains for diffuse and localized necking according to equations 15.10 and 15.11. Loading under constant stress ratio and constant strain ratio is assumed. Note that under these conditions, no localized necking can occur if ε_2 is positive.

Equation 15.10 implies that the critical strain for localized necking, ε_1^*, decreases from $2n$ in uniaxial tension to zero for plane-strain tension.

Swift* showed that diffuse necking can be expected when

$$\varepsilon_1^* = \frac{2n(1+\rho+\rho^2)}{(\rho+1)(2\rho^2-\rho+2)}. \tag{15.11}$$

The criteria for local necking (equation 15.10) and diffuse necking (equation 15.11) are plotted in Figure 15.2.

The previous analysis seems to imply that local necks cannot form if ε_2 is positive. However, this is true only if ρ and α remain constant during loading. If they do change during stretching, local necking can occur even with ε_2 being positive. What is critical

* H. W. Swift, *J. Mech. Phys. Solids*, 1 (1952), pp. 1–18.

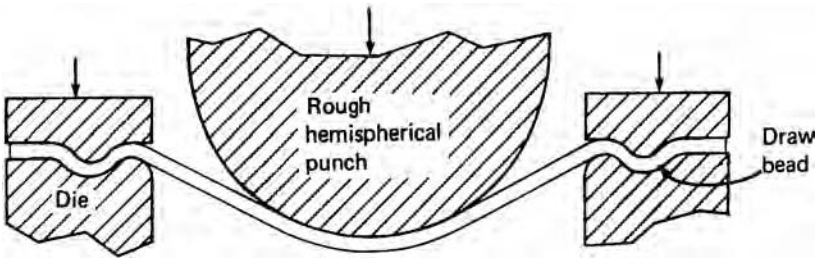

15.3. Sketch of a rough hemispherical punch.

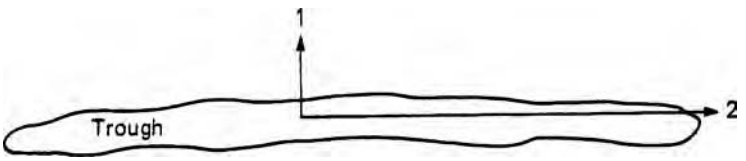

15.4. Sketch of a trough parallel to the 2-axis.

for local necking is that $\rho' = d\varepsilon_2/d\varepsilon_1$ become zero, rather than that the ratio $\rho = \varepsilon_2/\varepsilon_1$ of total strains be zero.

Often, tool geometry causes a change of strain path. Consider a sheet being stretched over a hemispherical dome as shown in Figure 15.3. The flange is locked to prevent drawing. If friction between punch and sheet is high enough to prevent sliding, deformation ceases where the sheet contacts the punch. Elements in the region between the punch and die are free to expand biaxially. However, as the element approaches the punch the circumferential strain is constrained by neighboring material on the punch so $d\varepsilon_2/d\varepsilon_1 \to 0$.

It has been argued* that because of variations of sheet thickness, grain size, texture, or solute concentration, there can exist local troughs that are softer than the surroundings that lie perpendicular to the 1-axis (Figure 15.4). Although such a trough is not a true neck, it can develop into one. The strain ε_1 in the trough will grow faster than outside of it, but the strain ε_2 in the trough can grow only at the same rate as outside the trough. Therefore, the local value of $\rho' = d\varepsilon_2/d\varepsilon_1$ decreases during stretching. Once ρ' reaches zero, a local neck can form. The trough consists of material either thinner or weaker than material outside of it.

As the strain rate $\dot{\varepsilon}_1$ inside the groove accelerates, the ratio $\dot{\varepsilon}_2/\dot{\varepsilon}_1$ approaches zero. Figure 15.5 shows how the strain paths inside and outside of the groove can diverge. The terminal strain outside the groove is the limit strain. Very shallow grooves are sufficient to cause such localization. How rapidly this happens depends on n and to a lesser extent on m.

* Z. Marciniak, *Archiwum Mechanikj Stosowanej*, 4 (1965), p. 579, and Z. Marciniak and K. Kuczynski, *Int. J. Mech. Sci*., 9 (1967), p. 609.

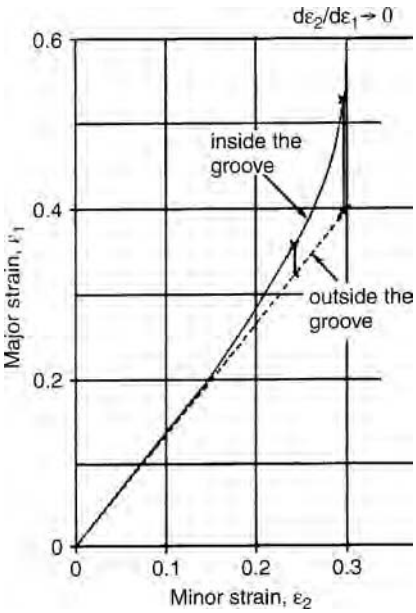

15.5. Strain paths inside and outside a preexisting groove for a linear strain path imposed outside the groove. The forming limit corresponds to the strain outside the groove when $d\varepsilon_2/d\varepsilon_1 \rightarrow 0$.

15.2 FORMING LIMIT DIAGRAMS

The strains ε_1^* at which local necks first form have been experimentally observed for a wide range of sheet materials and loading paths. A widely used technique is to print or etch a grid of small circles of diameter d_0 on the sheet before deformation. As the sheet is deformed, the circles become ellipses. The principal strains can be found by measuring the major and minor diameters after straining. By convention, the engineering strains e_1 and e_2 are reported. These values at the neck or fracture give the failure condition, while the strains away from the failure indicate *safe* conditions as shown in Figure 15.6. A plot of the combination of strains that lead to failure is called a *forming limit diagram* or FLD, also called a Keeler–Goodwin diagram, because of early work by S. P. Keeler* and G. Goodwin.† Figure 15.7 shows a typical FLD for a low-carbon steel. Combinations of $\dot{\varepsilon}_1$ and $\dot{\varepsilon}_2$ below the curve are safe and those above the curve lead to failure. Note that the lowest value of $\dot{\varepsilon}_1$ corresponds to plane strain, $\varepsilon_1 = 0$.

Figure 15.8 is a comparison of this FLD with equations 15.10 and 15.11 for local and diffuse necking. For negative values of e_2, the experimental and theoretical curves are parallel. The fact that the experimental curve is higher reflects the fact that a neck has to be developed before it can be detected.

* S. P. Keeler, SAE paper 680092 (1968).
† G. Goodwin, SAE paper 680093 (1968).

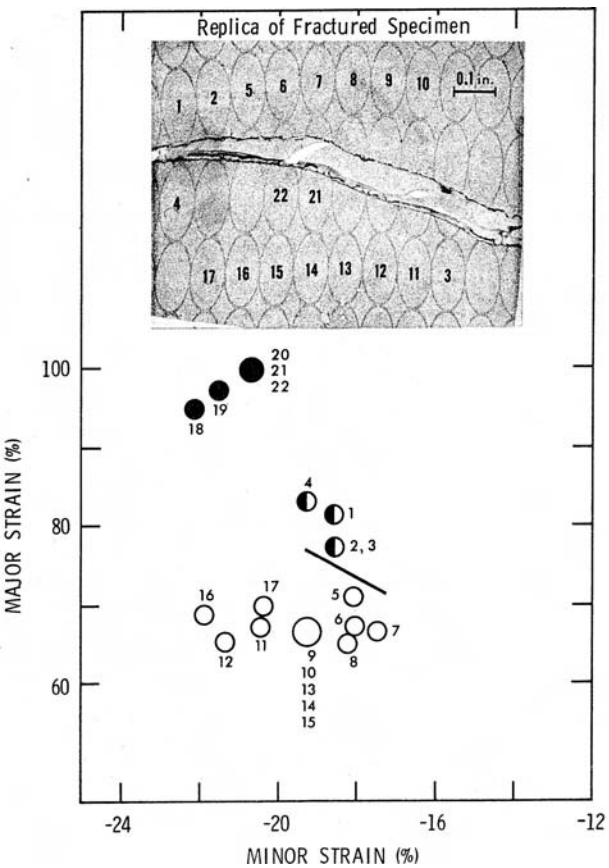

15.6. Distortion of printed circles near a localized neck and a plot of the strains in the circles. Solid points are for grid circles through which the failure occurred. Open points are for grid circles well removed from the failure and partially filled circles are for grid circles very near the failure. From S. S. Hecker, *Sheet Metal Ind*., 52 (1975), pp. 671–75.

15.3 EXPERIMENTAL DETERMINATION OF FLDS

To determine forming limit diagrams experimentally, a grid of circles is printed photographically on a sheet of metal. It is then dyed or lightly etched. Usually the circles are 0.100 in in diameter but smaller ones may be used. The specimens are stretched over a hemispherical dome (usually 4 in in diameter) until a local neck is first observed (Figure 15.9). To achieve various strain paths the lubrication and specimen width are varied. Full-width specimens deform in balanced biaxial tension and very narrow strips are almost in uniaxial tension. Better lubrication moves the failure point toward the dome. Figure 15.10 is a photograph showing the tearing from a localized neck.

Forming limit diagrams determined in different laboratories tend to differ somewhat. The determination of the "first observable neck" is subjective. There is also the question of how far from the center of a neck measurements can be called safe. Some authorities suggested that "safe readings" should be at least 1.5 circle diameters from the center of the neck.

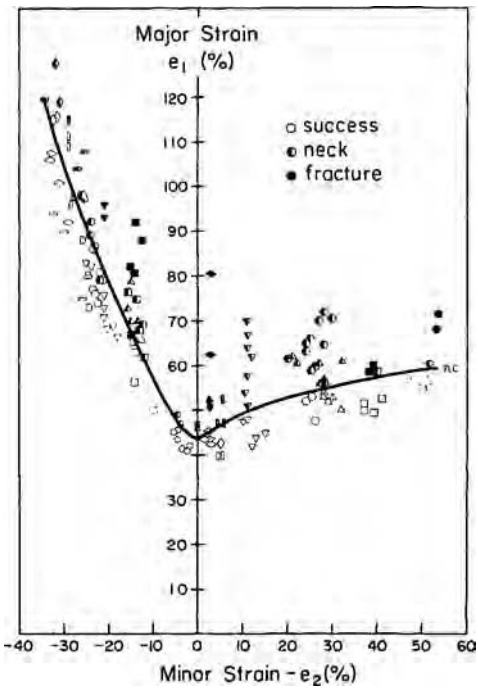

15.7. Forming limit diagram for a low-carbon steel determined from data like that in Figure 15.6. The strains below the curve are acceptable but those above the curve correspond to failure. From S. S. Hecker, *op. cit.*

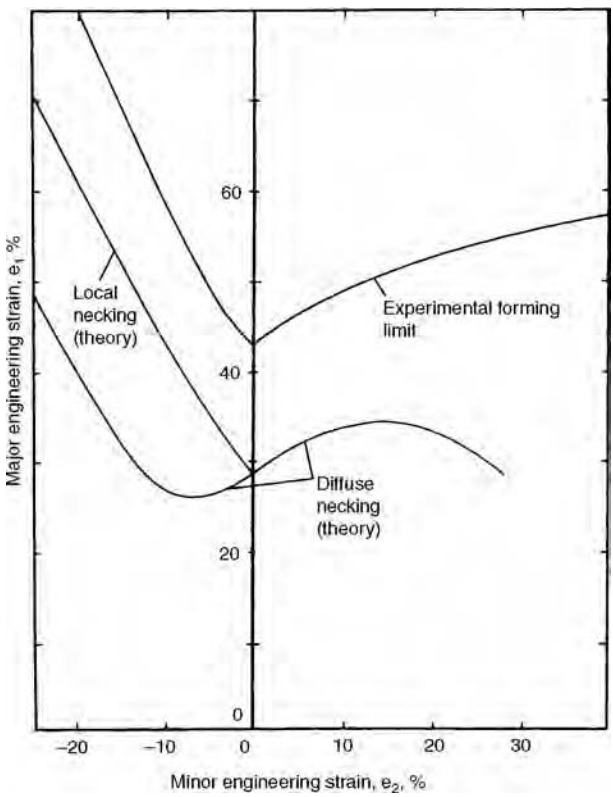

15.8. Comparison of experimental FLD in Figure 15.7 with predictions of equations 15.10 and 15.11.

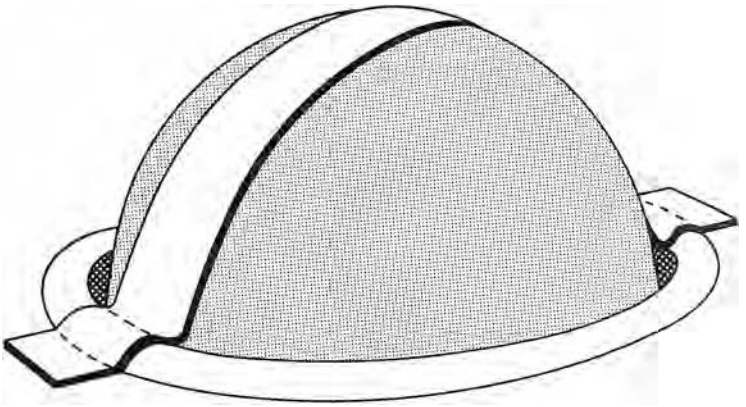

15.9. Schematic drawing of strip being stretched over a dome.

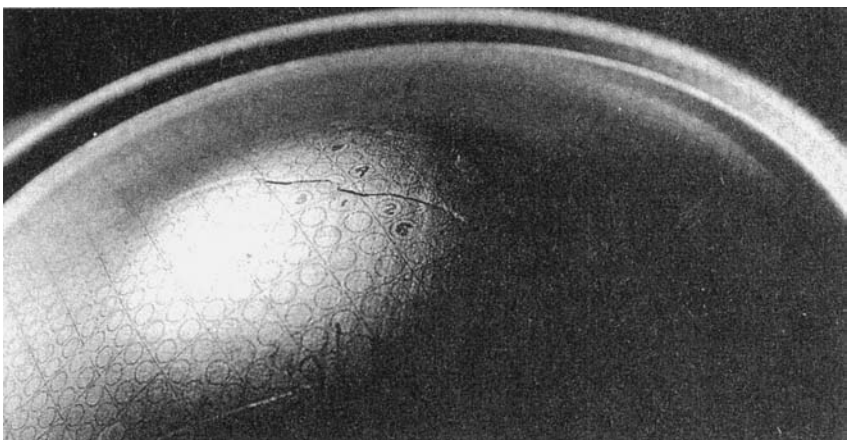

15.10. Failure near the top of a full-width well-lubricated specimen.

15.4 CALCULATION OF FORMING LIMIT DIAGRAMS

Marciniak and Kuczynski* showed that the right-hand side of the forming limit diagram for a material may be calculated by assuming that there is a preexisting defect that lies perpendicular to the major stress axis. For calculation purposes, this defect can be approximated as a region that is thinner than the rest of the sheet. Figure 15.11 illustrates this sort of defect. A ratio of the initial thicknesses inside and outside the defect, $f = t_{b0}/t_{a0}$ is assumed. It is also assumed that the stress ratio α_a outside of the groove remains constant during loading.

The calculations are based on imposing strain increments $\Delta\varepsilon_{b1}$ on the material inside of the defect and finding the corresponding value of $\Delta\varepsilon_{a1}$. This involves an iterative procedure. First a value of $\Delta\varepsilon_{a1}$ must be guessed. (It will be somewhat less

* Z. Marciniak and K. Kuczynski, *Int. J. Mech. Sci*, 9 (1967), pp. 609–20.

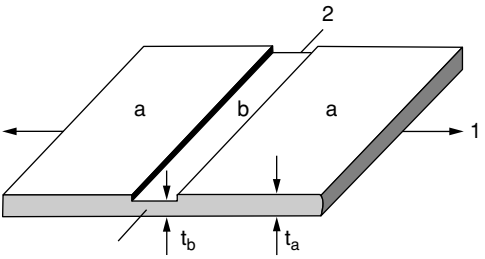

15.11. Schematic illustration of a preexisting defect in a sheet.

than $\Delta\varepsilon_{b1}$.) This value is used to calculate $\Delta\varepsilon_{a2} = \rho_a\ \Delta\varepsilon_{a1}$. Compatibility requires that $\Delta\varepsilon_{b2} = \Delta\varepsilon_{a2}$.

Then

$$\rho_b = \Delta\varepsilon_{b2}/\Delta\varepsilon_{b1} = \dot{\varepsilon}_{b2}/\dot{\varepsilon}_{b1}, \quad \rho_a = \Delta\varepsilon_{a2}/\Delta\varepsilon_{a1} = \dot{\varepsilon}_{a2}/\dot{\varepsilon}_{a1}. \tag{15.12}$$

Then α_a and α_b can be found from the associated flow rule. For Hill's criterion,

$$\alpha = [(R+1)\rho + R]/[(R+1) + R\rho]. \tag{15.13}$$

However, with the high exponent yield criterion, the flow rule

$$\rho = [\alpha^{a-1} - R(1-\alpha)^{a-1}]/[1 + R(1-\alpha)^{a-1}] \tag{15.14}$$

must be solved by iteration.

The ratios $\beta = \varepsilon/\varepsilon_1$ for both regimes can be found using the equation

$$\beta = \Delta\bar{\varepsilon}/\Delta\varepsilon_1 = \dot{\bar{\varepsilon}}/\dot{\varepsilon}_1 = (1 + \alpha\rho)/\varphi, \tag{15.15}$$

where the values of φ_b and φ_a are given by

$$\varphi = \bar{\sigma}/\sigma_1 = \{[\alpha^a + 1 + (1-\alpha)^a]/(R+1)\}^{1/a}. \tag{15.16}$$

The thickness strain rate, $\dot{\varepsilon}_3 = \dot{t}/t$, is also given by

$$\dot{t}/t = -(1+\rho)\dot{\varepsilon} = -(1+\rho)\dot{\varepsilon}_2/\rho. \tag{15.17}$$

The effective stress is given by the effective stress–strain relation

$$\bar{\sigma} = K\dot{\bar{\varepsilon}}^m\bar{\varepsilon}^n. \tag{15.18}$$

In the calculations, the value of $\bar{\varepsilon}$ is incremented by $\Delta\bar{\varepsilon}$, so $\bar{\sigma}$ is calculated as

$$\bar{\sigma} = K\dot{\bar{\varepsilon}}^m(\bar{\varepsilon} + \Delta\bar{\varepsilon})^n. \tag{15.19}$$

Let F_1 be the force per length normal to the groove. The stem per unit width perpendicular to the groove is

$$\sigma_1 = \varphi F_1/t \tag{15.20}$$

$$\dot{\bar{\varepsilon}} = \beta\dot{\varepsilon}_1 = -\beta(\dot{t}/t)/(\rho+1). \tag{15.21}$$

Combining equations 15.17, 15.18, 15.19, and 15.20 results in

$$F_1 = K(t/\varphi)(\bar{\varepsilon} + \Delta\bar{\varepsilon})^n(\beta\dot{\varepsilon}_1)^m. \tag{15.22}$$

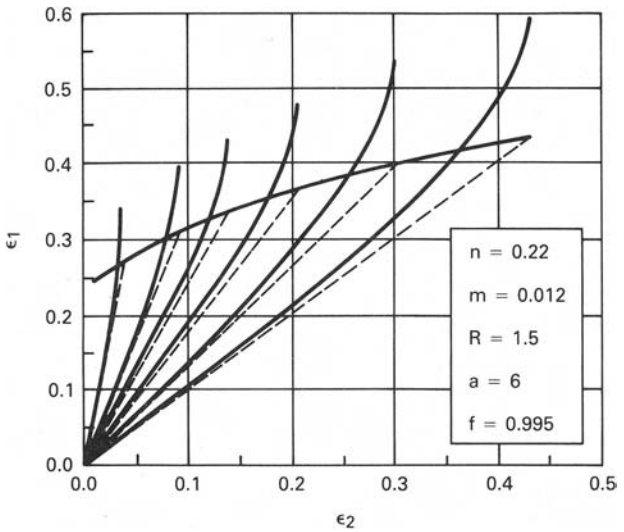

15.12. Calculated forming limit diagram for a hypothetical material using the high exponent yield criterion. From A. Graf and W. F. Hosford, *Met. Trans A*, 21A (1990), pp. 87–94.

The values of F_1 and $\dot{\varepsilon}_2$ must be the same inside and outside of the groove, so

$$(t_a/\varphi_a)(\bar{\varepsilon}_a + \Delta\bar{\varepsilon}_a)^n(\beta_a\varepsilon_{2a}/\rho_a)^m = (t_b/\varphi_b)(\bar{\varepsilon}_b + \Delta\bar{\varepsilon}_b)^n(\beta_b\varepsilon_{2b}/\rho_b)^m. \quad (15.23)$$

Finally, substituting $f = t_{b0}/t_{a0}$ and $t = t_0 \exp(\varepsilon_3)$,

$$(\bar{\varepsilon}_a + \Delta\bar{\varepsilon}_a)^n(\beta_a/\rho_a)^m/\varphi_a = f(\bar{\varepsilon}_b + \Delta\bar{\varepsilon}_b)^n(\beta_b/\rho_b)^m/\varphi_b. \quad (15.24)$$

For each strain increment $\Delta\varepsilon_{b1}$ in the groove there is a corresponding strain increment $\Delta\varepsilon_{a1}$ outside the groove. The procedure is to impose a strain increment $\Delta\bar{\varepsilon}_b$, then guess the resulting value of $\Delta\varepsilon_{a1}$, and use this value together with α_a to calculate β_b, φ_b, ρ_b, and $\bar{\varepsilon}_b$. Then these are substituted into equation 15.23 to find $\Delta\bar{\varepsilon}_a$ and then calculate $\Delta\varepsilon_{a1}$ from the change in $\Delta\bar{\varepsilon}_a$. This value of $\Delta\varepsilon_{a1}$ is then compared to the assumed value. This process is repeated until the difference between the assumed and calculated values becomes negligible.

Additional strain increments $\Delta\varepsilon_{b1}$ are imposed until the $\Delta\varepsilon_{a1} < 0.10\Delta\varepsilon_{b1}$ or some other criterion of approaching plane strain is reached. The values of ε_{a2} and ε_{a1} at this point are taken as points on the FLD. Figure 15.12 shows an example of the calculated strain paths inside and outside of the defect using $\Delta\varepsilon_{a1} < 0.10\Delta\varepsilon_{b1}$, $\varepsilon_{a3} = 0.80\varepsilon_{b3}$ and $\varepsilon_{a3} = 0.90\varepsilon_{b3}$ as criteria for failure.

The calculated forming limit diagrams are very sensitive to the yield criterion used in the calculations. Figure 15.13 shows that the forming limit diagrams calculated with Hill's 1948 yield criterion are very dependent on the *R*-value. This is not in accord with experimental observations. Figure 15.14 shows that with the high exponent criterion, there is virtually no calculated dependence on the *R*-value.

Hill showed that the left-hand side of FLD is easily calculated. Equation 15.10 for localized necking, $\varepsilon_1^* = n/(1 + \rho)$, can be expressed as

$$\varepsilon_3^* = -n, \quad (15.25)$$

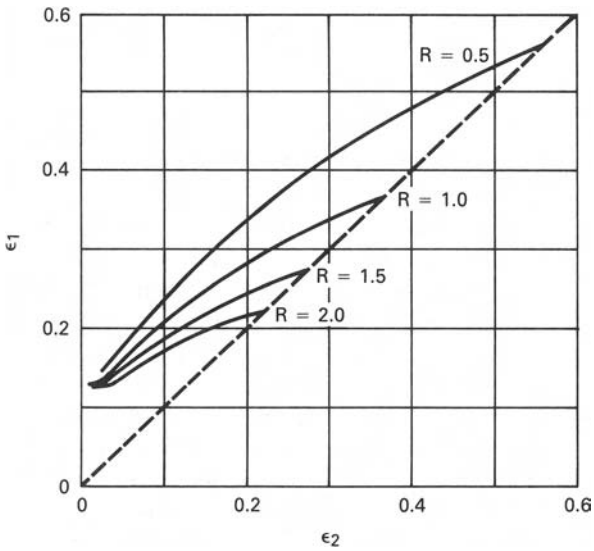

15.13. Forming limit diagrams calculated for several R-values using Hill's 1948 yield criterion. Values of $n = 0.20$, $m = 0$, and $f = 0.98$ were assumed. From A. Graf and W. F. Hosford, *op. cit*.

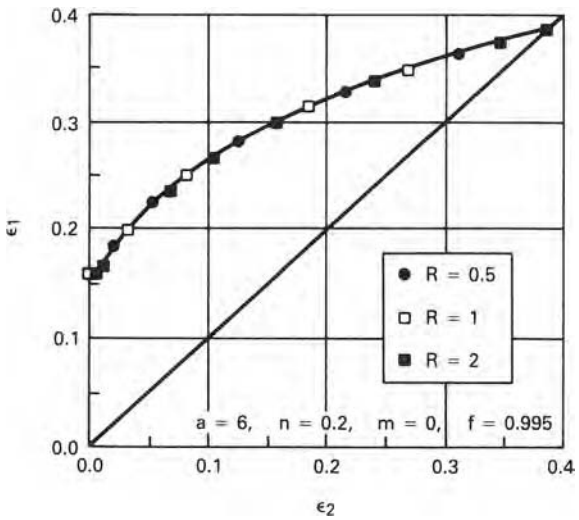

15.14. Forming limit diagrams calculated for several R-values using $a = 6$ in the high exponent yield criterion. Values of $n = 0.20$, $m = 0$, and $f = 0.995$ were assumed. From A. Graf and W. F. Hosford, *op. cit*.

which corresponds to a simple condition of a critical thickness strain.

$$\varepsilon_3^* = -n. \tag{15.26}$$

15.5 FACTORS AFFECTING FORMING LIMITS

The level of the FLD_0 at plane strain, $\varepsilon_2 = 0$, depends primarily on the strain-hardening exponent, n. Theoretically, at plane strain, $\varepsilon_1 = n$. An increased strain-rate exponent m raises the FLD_0 somewhat. Increasing values of n decrease the slope of the right-hand side of the FLD. These effects are illustrated in Figure 15.15.

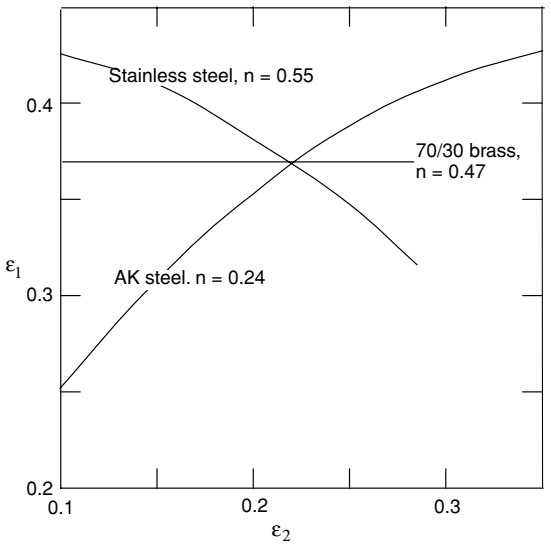

15.15. Increasing values of *n* raise the forming limit for plane strain but lower the slope of the right-hand side of the diagram. Data from M. Azrin and W. A. Backofen, *Met. Trans*, 1 (1970), pp. 2957–65.

Inhomogeneity and defects lower the FLD. These inhomogeneities may be local variations in sheet thickness, composition, grain size, or anything that affects yielding. Anisotropy has almost no effect on the shape or level of the FLD.

In biaxial tension, fracture may occur before local necking. Figures 15.16 and 15.17 show how fracture truncates the FLD caused by local necking.

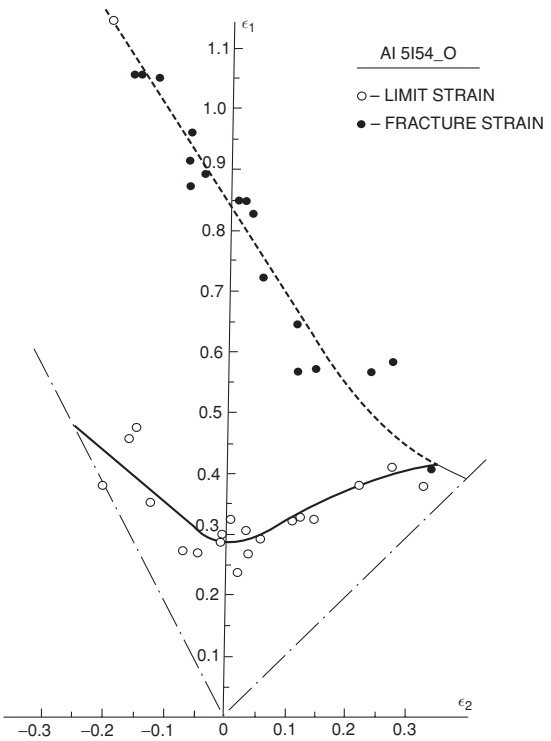

15.16. Forming limit diagram for aluminum alloy 5154–0. From G. H. LeRoy and J. D. Embury in *Formability: Analysis, Modeling and Experimentation*, A. K. Ghosh and H. L. Hecker, eds. (AIME, 1978), pp. 183–207.

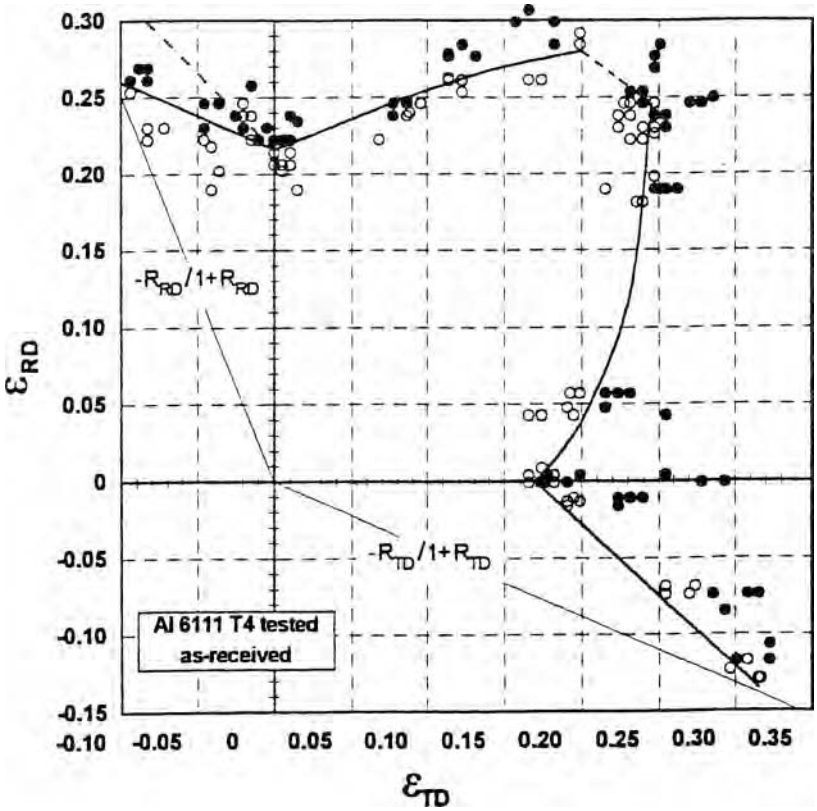

15.17. Forming limit diagram for aluminum alloy 6111-T4. From A. Graf and W. F. Hosford, *I. J. Mech. Sci.*, 36 (1994), pp. 897–910.

It has been found experimentally that the level of the FLD increases with sheet thickness. Keeler and Brazier* have approximated this effect by

$$\begin{aligned} \text{FLD}_0 &= n(1 + 0.72t) \qquad \text{for} \quad n \leq 0.2 \text{ and} \\ \text{FLD}_0 &= 0.2(1 + .72t) \end{aligned} \tag{15.27}$$

where t is the sheet thickness in mm. This is illustrated in Figure 15.18.

Although the thickness effect is well established, the reason for it is still controversial. There is some evidence that the measured forming limits depend on the size of the grid used to measure strains. With thicker sheets, and a constant grid size, the measured strains at the middle of the neck are larger. If this is true, the effect would disappear if the ratio of grid size to thickness were held constant. Finally the level of the FLD may be affected by the method used to detect local necks.

Smith and Lee† have reported that the thickness effect in aluminum alloys is much less than that in steel (Figure 15.19). This can be attributed to the much sharper necks in aluminum alloys.

* S. P. Keeler and W. G. Brazier, in *Micro Alloying 75* (Union Carbide, 1977), pp. 517–30.
† P. E. Smith and D. Lee, *Proc. Intern. Body Eng. Conf.* (SAE Detroit, 1998) (SAE pub. 331, v. 2, pp. 21–28).

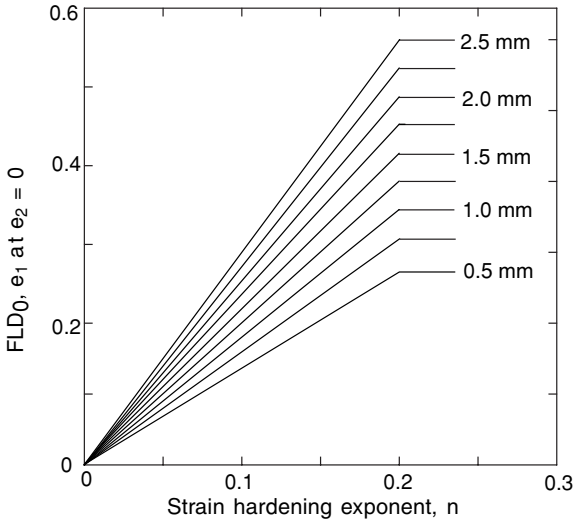

15.18. Effect of sheet thickness on FLDs according to equation 15.27.

Forming limit diagrams have proved useful in diagnosing actual and potential problems in sheet forming. If previously gridded sheets are used in die tryouts, local strains near failures or suspected trouble spots can be measured and compared with the forming limit diagram. This serves two purposes. The severity of strains at potential trouble can be assessed. If the strains are too near the limiting strains, failures are likely to occur in production because of variations in lubrication, tool alignment, tool wear, and material properties and thickness. The second reason is that the nature of the problem can be diagnosed. Because the lowest values of ε_1^* correspond to plane strain, higher levels of ε_1^* can be achieved by either lowering ε_2 with less flange locking or raising ε_2, with better lubrication.

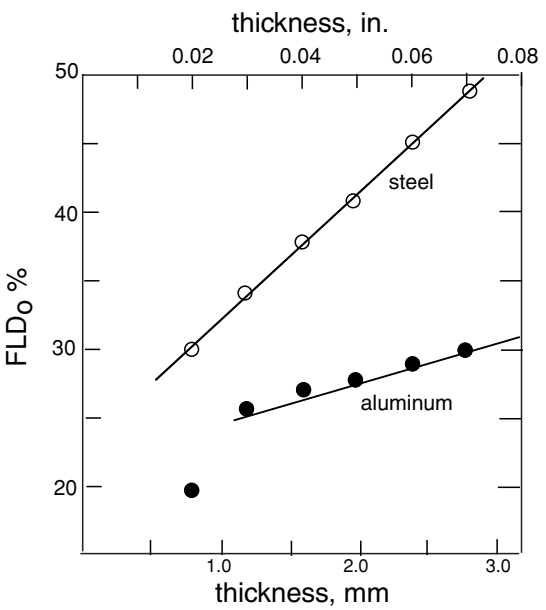

15.19. Effect of thickness on measured forming limits in plane strain. Adapted from P. E. Smith and D. Lee. *op. cit.*

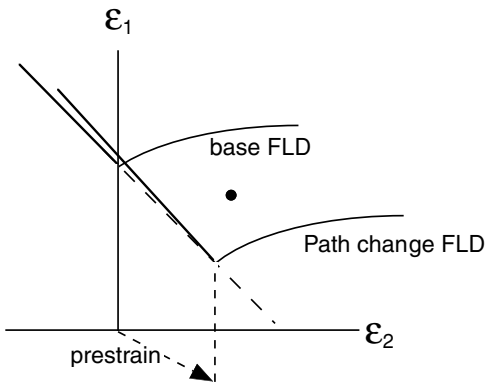

15.20. Tensile prestraining in 2-direction lowers the FLD along a line $\varepsilon_1 + \varepsilon_2 = C$. After the prestraining strains corresponding to the black dot would cause failure.

15.6 CHANGING STRAIN PATHS

Forming limit diagrams are usually determined with experiments that involve nearly linear strain paths (i.e., the ratio of principal stresses to principal strains is nearly constant.) However, in many real stampings, the stain path may vary. Experiments on aluminum alloys using two-stage straining paths have shown that changes in strain path have a very large effect on the forming limits. Prestraining in tension along the 2-direction shifts the FLD downward and to higher values of ε_2, with the minimum following a line $\varepsilon_1 + \varepsilon_2 = C$ where C is a constant equal to the forming limit in plane strain (Figure 15.20). Prestraining intension along the 1-direction raises the FLD curve along the line $\varepsilon_1 + \varepsilon_2 = C$ (Figure 15.21). Prestraining in biaxial tension causes a shift of the FLD to higher values of ε_2 (Figure 15.22). The net effect is that with changing strain paths, combinations of strains are possible well above the standard FLD without failure, or failure may occur with combinations of strains well below the base FLD.

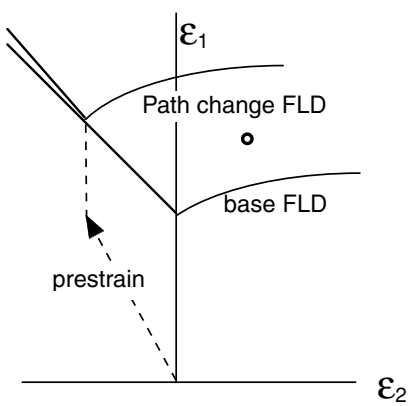

15.21. Tensile prestraining in the 1-direction raises the FLD along a line $\varepsilon_1 + \varepsilon_2 = C$. After the prestraining strains corresponding to the open circle would be possible.

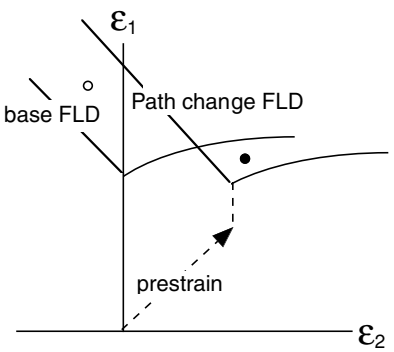

15.22. Prestraining in biaxial tension shifts the FLD to the right. After the prestraining strains corresponding to the open circle would be possible, but those corresponding to the black dot would cause failure.

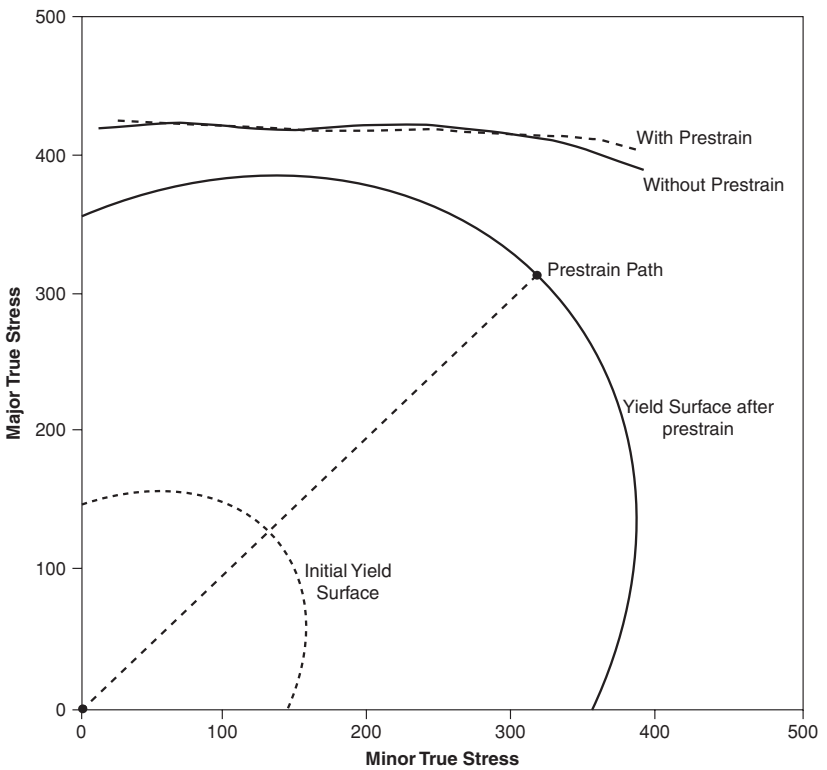

15.23. Stress-based forming limits of aluminum 2008-T4 before and after an equibiaxial prestrain of 0.07.

15.7 STRESS-BASED FORMING LIMITS

Stoughton* proposed that forming limits can be plotted in terms of the stresses at failure instead of the strains. He found that such plots are valid for changing strain paths as well as continuous straining. Figure 15.23 is such a plot for aluminum alloy 2008-T4. Critical forming stresses can be used in finite element codes to check for failure.

NOTE OF INTEREST

Stuart Keeler was born in Wassau, Wisconsin, in 1934. He received a BA from Ripon College and BS and ScD from MIT, where his thesis advisor was W. A. Backofen. His basic research, which led to the development of forming limit diagrams, has transformed sheet metal forming from an art to a science.

REFERENCES

Alejandro Graf and W. F. Hosford, *Met. Trans*., 21A (1990), pp. 87–94.
Alejandro Graf and W. F. Hosford, *Met. Trans*., 24A (1993), pp. 2503–12.
A. Graf and W. Hosfordf, *Int. J. Mech. Sci.*, 36 (1994), pp. 897–910.
S. S. Hecker, A. K. Ghosh, and H. L. Gegel, eds., *Formability Analysis, Modeling and Experimentation,* AIME, 1978.
R. Hill, *J. Mech. Phys. Solids*, 1 (1952), pp. 19–30.
S. P. Keeler and W. A. Backofen, *Trans. ASM*, 56 (1963), pp. 25–48.
S. P. Keeler and W. G. Brazier, in *Microalloying 75*, Union Carbide, 1977, pp. 517–30.
S. L. Semiatin and J. J. Jonas, *Formability and Workability of Metals*, ASM, 1984.
R. H. Wagoner, K. S. Chan, and S. P. Keeler, eds., *Forming Limit Diagrams: Concepts, Methods and Applications*, TMS-AIME, 1989.

PROBLEMS

15.1. Derive an expression for the critical strain, ε_1^*, to produce a diffuse neck as a function of n and the stress ratio α. Assume the von Mises criterion and loading under constant α. [*Hint*: start with equation 15.11.]

15.2. In principle one can determine the R-value by measuring the angle θ of the neck in a strip tension test. How accurately would one have to measure θ to distinguish between two materials having R-values of 1.6 and 1.8?

15.3. It has been suggested that failures in sheets occur when the thickness strain reaches a critical value. Superimpose a plot of e_1 versus e_2 for this criterion on Figure 15.8. Adjust the constant so that the curves coincides for plane strain, $e_2 = 0$. How good is this criterion?

15.4. Repeat Problem 15.3 for a failure criterion that predicts failure when the absolutely largest principal strain, $|e_i|_{max}$, reaches a critical value.

15.5. Ironing of a two-piece beverage can thins the walls from 0.015 to 0.005 in thickness. This strain far exceeds the forming limits. Explain why failure doesn't occur.

* T. B. Stoughton and J. W. Yoon, *Int. J. Mech. Sci.*, 47 (2005), pp. 1972–2002.

15.6. The true minimum of an FLD determined by in-plane stretching (without bending) occurs at plane strain, $\varepsilon_2 = 0$. However, forming limit diagrams are determined by stretching strips over a 4-in diameter dome. Assume that the forming limit is reached when the center of the strip reaches the limit strain for in-plane stretching. If the limit strain is $\varepsilon_1 = 0.30$ for in-plane stretching, what values of ε_1 and ε_2 would be reported for stretching over a 4-in diameter dome?

15.7. The forming limit diagram for a certain steel is shown in Figure 15.24.

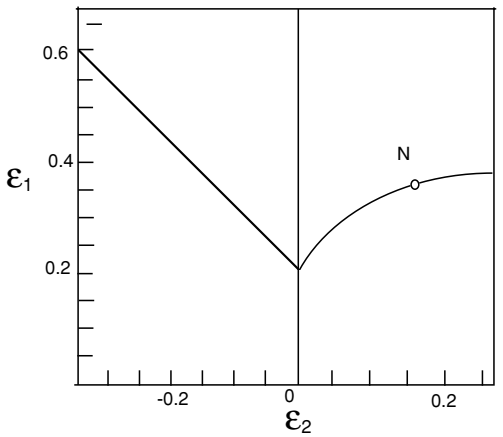

15.24. Schematic forming limit diagram for Problem 15.7.

a) Show the loading path of a specimen that fails at point N.
b) Plot as accurately as possible the locus of points corresponding to uniaxial tension, $\sigma_2 = 0$.
c) Describe qualitatively how the line in (b) would be drawn differently for $R = 2$.

15.8. Frequently the minimum on experimentally determined forming limit diagrams occurs at a slightly positive value of e_2 rather than at $e_2 = 0$. Explain why this might be.

15.9. The following points were taken from the forming limit diagram for aluminum alloy 2008; the strain hardening exponent is 0.265 and $K = 538$ MPa. Plot the forming limits in stress space (i.e., values of σ_1 at failure as a function of σ_2). Assume isotropy.

ε_1	ε_2
0.44	−0.22
0.32	−0.10
0.22	0.0
0.225	0.10
0.23	0.23

16 Stamping

16.1 STAMPING

Operations called stamping, pressing, and sometimes drawing involve clamping a sheet at its edges and forcing it into a die cavity with a punch, as shown in Figure 16.1. The sheet is stretched rather than squeezed between the tools. Pressure on the draw beads controls how much additional material is drawn into the die cavity. In some cases there is a die, which reverses the movement of material after it is stretched over the punch.

16.2 DRAW BEADS

Draw beads (Figure 16.2) are used to create tension in the sheet being formed by preventing excessive drawing. As a sheet moves through a draw bead, it is bent three times and unbent three times. Each bend and each unbend there requires plastic work. Over each radius there is friction. This create resistance to movement of the sheet. If the resistance is sufficiently high, the sheet will be locked by the draw bead. The restraining force of the draw bead can be controlled by the height of the insert.

The restraining force has two components. One is caused by the work necessary to bend and unbend the sheet as it flows over the draw bead and the other is the work to overcome friction. The restraining force F per length resulting from the bending and unbending can be crudely estimated with the following simplifying assumptions: Work

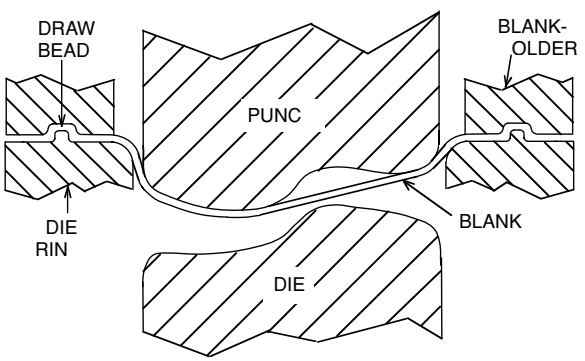

16.1. Schematic punch-and-die set with blank holder.

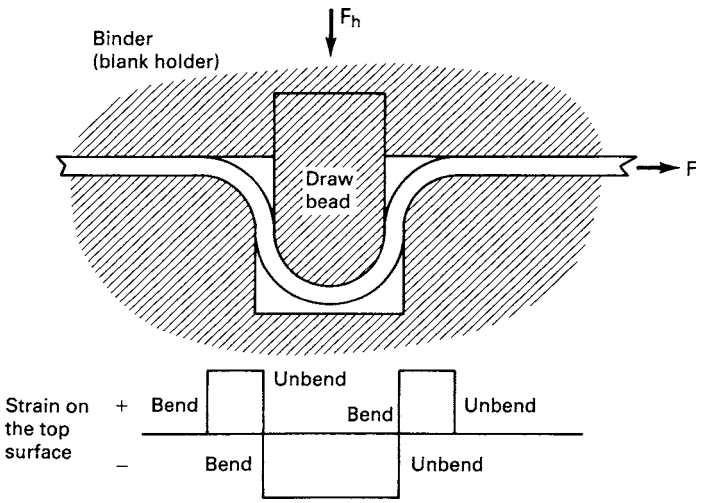

16.2. Sketch of a draw bead. The strains on the top surface are indicated. There is friction wherever the sheet contacts the tooling.

hardening, elastic core, movement of the neutral plane, and the difference between engineering strain and true strain are neglected ($\varepsilon = e$). The strain is given by $e = z/r$, where z is the distance from the neutral plane. In this case the work per volume for an element at z is $Y(z/r)$, where Y is the yield strength and r is the radius of the bend at the neutral axis. The work for all elements then is $\mathrm{d}W/\mathrm{d}L = 2\int_0^{t/2}(Y/r)z\mathrm{d}z = Yt^2/(4r)$. The restraining force cause by bending three times and unbending three times as the sheet moves through the draw bead is then

$$F_\mathrm{b} = 6\mathrm{d}W/\mathrm{d}L = 1.5Yt^2/r. \tag{16.1}$$

This treatment neglects the Bauschinger effect. A more accurate determination of F_b can be obtained by pulling a strip through a fixture in which freely rotating cylinders simulate the draw beads (Figure 16.3).

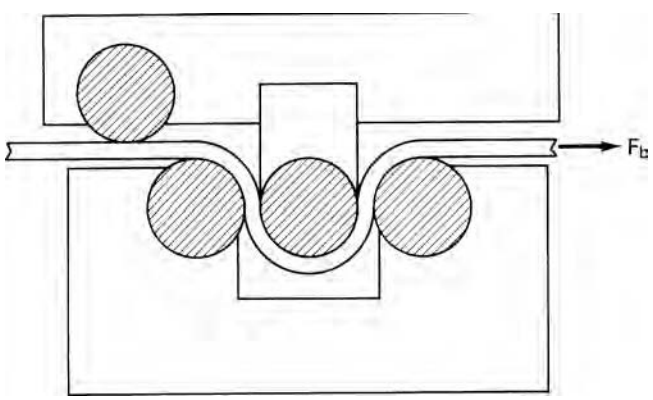

16.3. Determining the bending contribution to the draw bead restraining force.

The position of draw beads is important. They should be placed perpendicular to the direction of metal flow. If they are too close to the trim line, material being drawn over them may become part of the finished product and create a surface defect. If they are too far from the trim line, their effectiveness in preventing drawing will be diminished.

16.3 STRAIN DISTRIBUTION

Forming limit diagrams do not completely describe the forming behavior of different metals. Two materials may have nearly the same forming limits ε_1^*, but differ substantially in formability. For example, consider a symmetric part (Figure 16.4) with a line of length L_0 parallel to the 1-direction. The stress is not uniform along the line so ε_1 will vary from place to place. The total length of line will be given by

$$L = L_0 + \int_0^{L_0} e_x \, dx. \tag{16.2}$$

The height $h_{\max}$ of a hemispherical cup at failure depends on L/L_0 when $\varepsilon_{1\max} = \varepsilon_1^*$. In other words, $h_{\max}$ depends strongly on the distribution of ε_1 on x. The ratio of ε_1 in lightly loaded regions to that in heavily loaded regions depends primarily on the strain-hardening exponent n, but also to some extent on the strain-rate sensitivity, m. Increasing values of n and m distribute the strain so permit deeper parts to be formed. Figure 16.5 illustrates this.

When a sheet that is locked by draw beads is stretched over a hemispherical punch, the failure site depends on the friction between the sheet and the punch. With high friction, the failure usually occurs in the unsupported material near contact with the punch. Just outside of the contact region, the deformation is in plane strain because of the hoop direction constraint from the neighboring material in contact with the punch. With lower friction the failure site moves toward the dome and the depth of cup at failure increases.

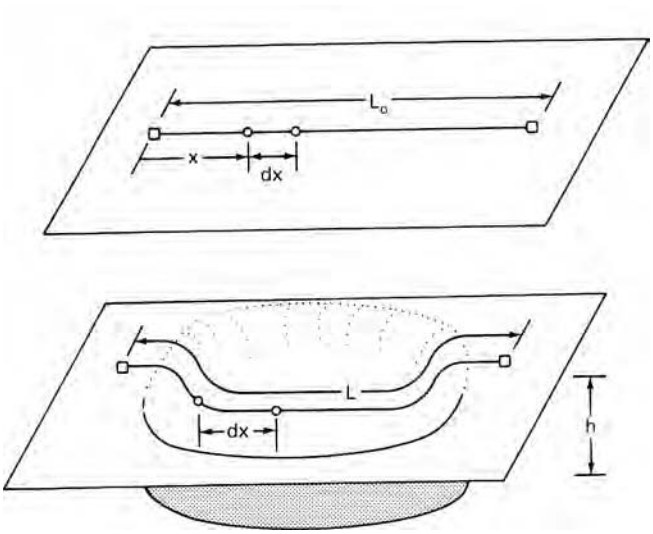

16.4. Increase of line length, L_0.

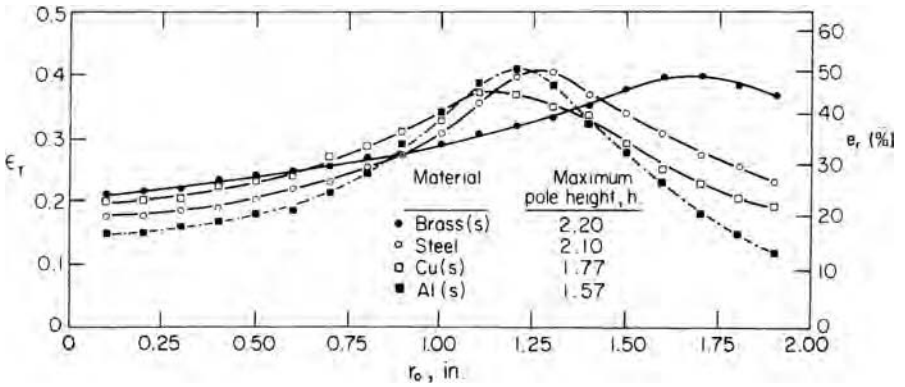

16.5. Distribution of strains during punch stretching of sheets of several metals. The punch was stopped at the same peak strain in each case. Materials with higher values of n had more widely distributed strains and formed deeper cups. From S. P. Keeler and W. A. Backofen, *Trans. Q. ASM*, 56 (1963), pp. 25–48.

16.4 LOOSE METAL AND WRINKLING

When flat sections are not stretched enough, they become loose or floppy. If a potential car buyer puts his hand on the roof of a car and finds that it isn't stiff, he will perceive poor quality. The same is true if the hood of a car vibrates at high speed. Loose metal can be voided by ensuring that all parts of a stamping are deformed to some minimum effective strain (perhaps 4%).

Wrinkling occurs when the stresses in the sheet are compressive. With thin sheets, wrinkling will occur under very low amounts of compressive stress. Figure 16.6 shows the region of wrinkling on a forming limit diagram.

Wrinkling is a potential problem in drawing of many parts. Consider the forming of a flat-bottom cup with conical walls, as shown Figure 16.7. As the punch descends, the shaded element is drawn closer to the punch so its circumference must shrink. Stretching of the wall in tension will reduce the circumference, but if the wall isn't stretched enough it will wrinkle. The amount of stretching can be increased by raising the blank-holder pressure. However, too much restraint by excessive blank-holder pressure or draw beads prevents flange material drawing in and may cause the wall to fail in tension. Therefore the blank-holder pressure must be controlled.*

There is a window of permissible levels of blank-holder force. Too little causes wrinkling; too much force results in wall failure. This is shown in Figure 16.8. Since more circumferential contraction occurs when material with high R-values is stretched, there is more contraction in the plane of the sheet so an increased R widens the left side of the window. With an increased value of n, more stretching can occur before failure. For any given material and required depth of draw, there is a window of permissible blank-holder force. Increasing the depth of draw beads has the same effect as increasing blank-holder force. It is possible to change the blank-holder force during

* J. Havranek, in *Sheet Metal Forming and Energy Conservation, Proc. 9th Bienn. Cong. Int. Deep Drawing Res. Group*, ASM, Ann Arbor, MI (1976), pp. 245–63.

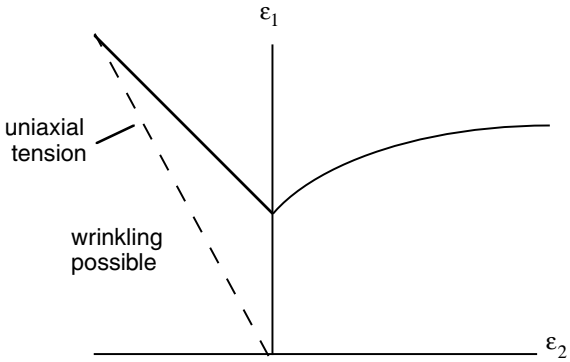

16.6. A forming limit diagram showing the path of a uniaxial tension test (dashed line). To the left of this line, the stress σ_2 is compressive so wrinkling is possible.

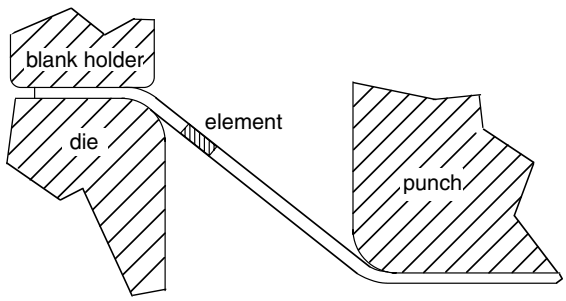

16.7. In drawing of a conical cup, wall wrinkling may occur if there is not enough tensile stretching of the wall.

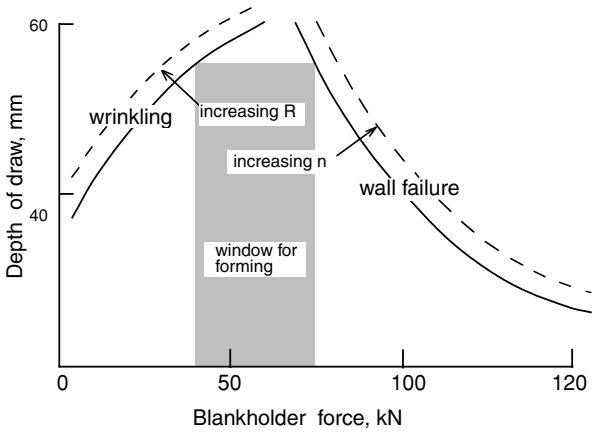

16.8. Forming window for a conical cup. For a draw depth of 55 mm, the blank-holder force must be between 40 and 75 kN.

the draw. Greater depths of draw are possible if the force is low in the early stages of the draw and increases in the later stages.*

16.5 FLANGING

Often edges of sheets are flanged. If the flange is concave, cracking may occur at sheared edges where the edges are elongated in tension. This occurs when a hole is

* D. E. Hardt and R. C. Fenn, *Proc. ASM Symposium on Monitoring and Control of Manufacturing Processes* (1990), pp. 349–72.

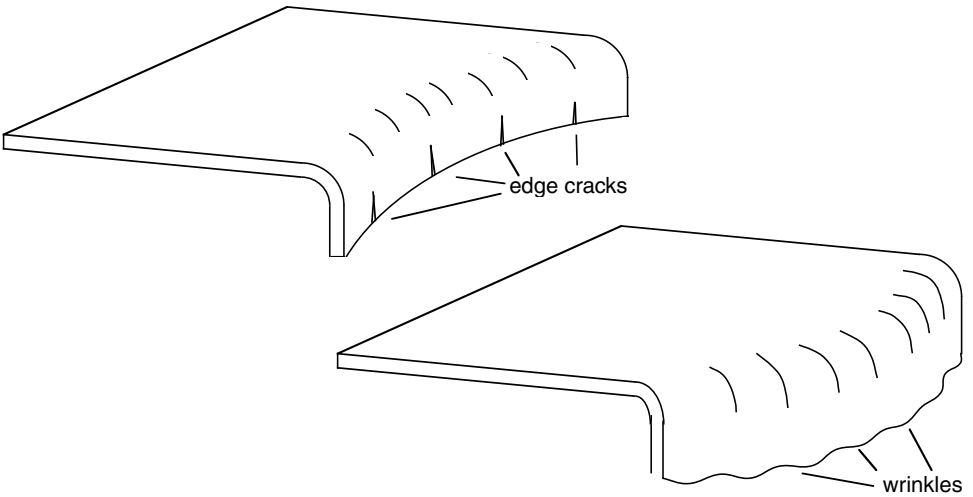

16.9. Edge cracks on a concave flange and wrinkling on a convex flange.

expanded or a concave edge is flared as shown in Figure 16.9. The tensile strain in such a case is

$$\varepsilon_1 = \ln(d_0/d), \tag{16.3}$$

where the diameters before and after flanging are d_0 and d. The tendency is aggravated if shearing has left a burred edge. On the other hand, if the flange is convex, the contraction of the flanged edge may lead to wrinkling.

16.6 SPRINGBACK

Control of springback is very important, especially in lightly curved sections like the bottom of the stamping in Figure 16.10. As indicated in Chapter 12, springback is minimized if tension is sufficient to cause tensile yielding across the whole cross section. Yet the wall force F_2 must not cause a tensile stress that exceeds the tensile strength. The relative magnitudes of F_1 and F_2 can be calculated approximately as follows: A radial force balance on an element in the bend gives the normal force, $\mathrm{d}N = F\,\mathrm{d}\theta$, so the frictional force $\mathrm{d}F$ on the element is $\mu\,\mathrm{d}N = \mu F\,\mathrm{d}\theta$, where μ is the coefficient of friction.

From a force balance in the circumferential direction,

$$F + \mathrm{d}F = F + F\mu\,\mathrm{d}\theta,$$
$$\int_{F_1}^{F_2} \mathrm{d}F/F = \mu \int_0^{\theta} \mathrm{d}\theta \quad \text{so} \quad F_2 = F_1 \exp(\mu\theta). \tag{16.4}$$

Neglecting differences between the plane-strain and uniaxial tensile and yield strengths, $F_2 < (S_\mathrm{u})wt$ and $F_1 > (Y)wt$, where w is the dimension parallel to the bend, t is the sheet thickness, S_u is the tensile strength, and Y is the yield strength. Therefore

$$S_\mathrm{u}/Y > \exp(\mu\theta). \tag{16.5}$$

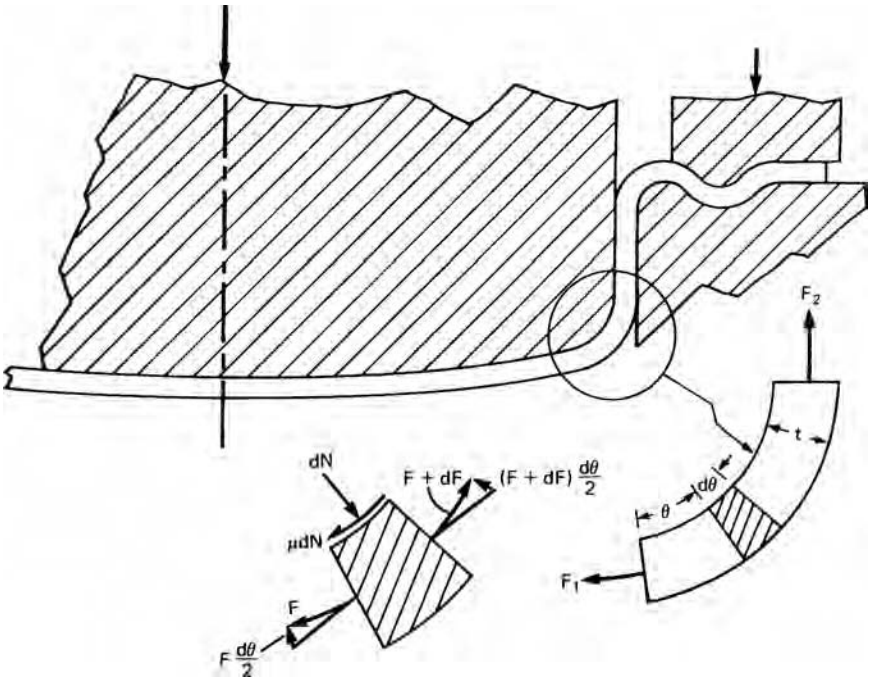

16.10. Sheet being bent over a punch.

Thus the tensile-to-yield strength ratio must exceed a value that depends on both the coefficient of friction and the bend angle. For example, if $\mu = 0.2$ and $\theta = \pi/2$, $S_u/Y > 1.37$.

In springback calculations it should be recognized that when a metal is stretched in tension and unloaded, the unloading is not linear. This is called the *Bauschinger effect*. Figure 16.11 shows typical behavior. Springback is much greater than that calculated by assuming linear elastic unloading.

16.7 STRAIN SIGNATURES

The strain path varies from one place to another in a stamping. The strain path of a particular point is called its strain signature. Figures 16.12 and 16.13 show stampings of a hemispherical cup and a shallow pan with the strain signatures of several locations.

16.8 TAILOR-WELDED BLANKS

In recent years parts are being stamped from blanks made by welding two or more sheets of different thickness or different base materials. The purpose is to save weight by using thinner gauge material where its strength is sufficient and using thicker or stronger material only where necessary. Some difficulties are encountered during forming. Offset blank-holder surfaces are required to assure adequate hold-down. Welding hardens the weld zone, which may reduce the formability and cause cross-weld failures if the direction of major strain is parallel to the weld. The best blank orientation is with the

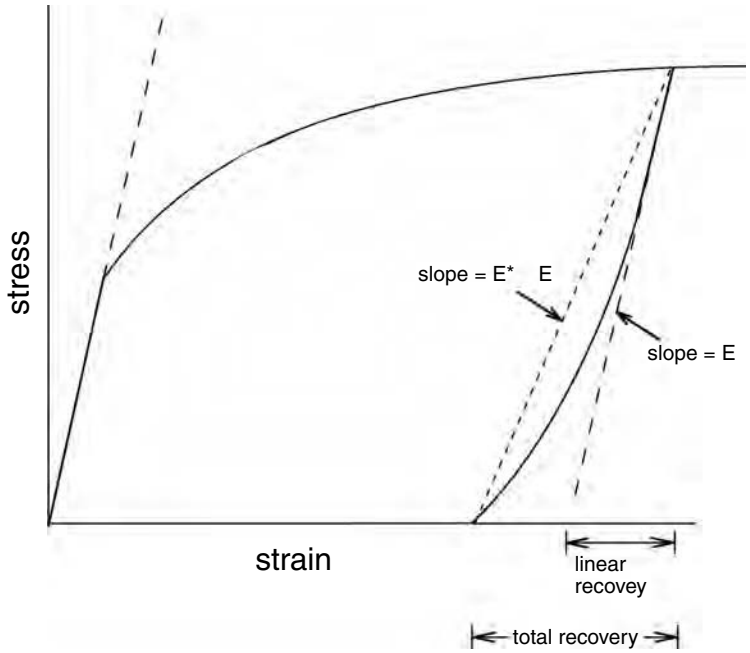

16.11. Nonlinear unloading results in greater springback than calculated assuming linear elasticity.

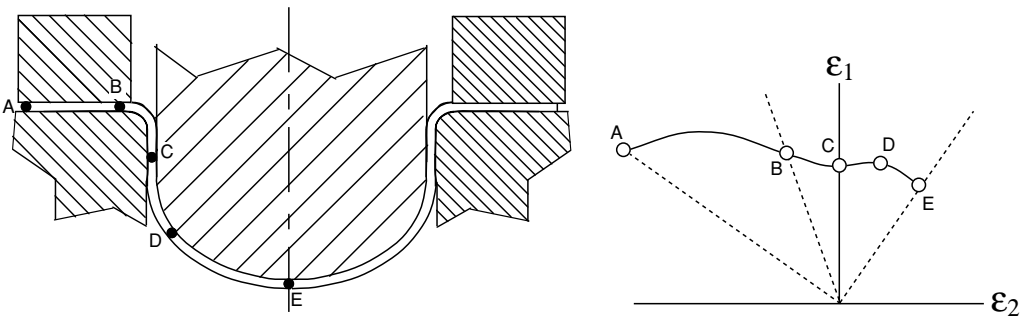

16.12. Strain signature in drawing of a hemispherical cup.

weld perpendicular to the major strain axis. In this case failure is likely to occur by splitting of the thinner material parallel to the weld. This problem can be alleviated to some extent by decreasing the hold-down pressure on the thicker material and allowing more of the thicker metal to flow into the die. The frequency of failures parallel to the weld is reduced by decreasing the movement of the weld in the die.

16.9 DIE DESIGN*

At the center of most sheet stampings a certain effective strain level is necessary to prevent "slack" or "loose" metal and to minimize springback. Otherwise the panel

* This section is a result of private discussions with Edmund Herman, Creative Concepts Company, Shelby Township, MI (2005).

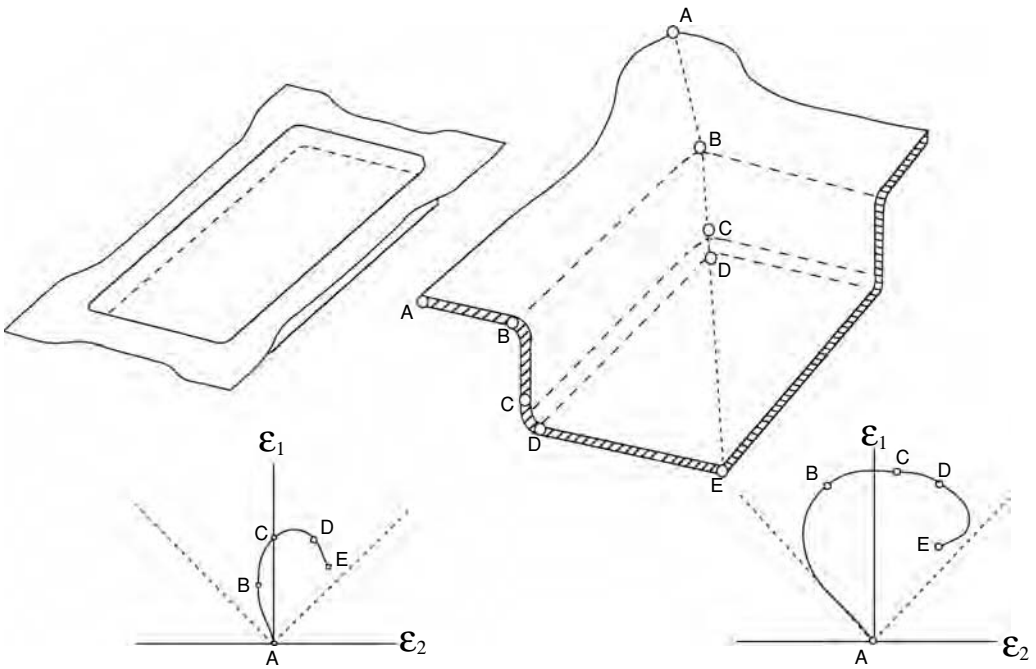

16.13. Strain signatures in a stamping of a shallow pan. The strain path at B is likely to cause wrinkling.

may not retain the desired shape or it may feel floppy to the customer. A target strain at the center of the panel will also ensure enough work hardening to strengthen the panel. To achieve this target strain, there must be sufficient tension in the sheet at that point. Because of friction and bending, the tension at the binder must be much higher. Figure 16.14 illustrates a part being stamped. The final part is actually from A to C. The material between C and the edge of the binder must be stretched in the die to achieve the required stress at point A, but is later trimmed off and discarded. The example

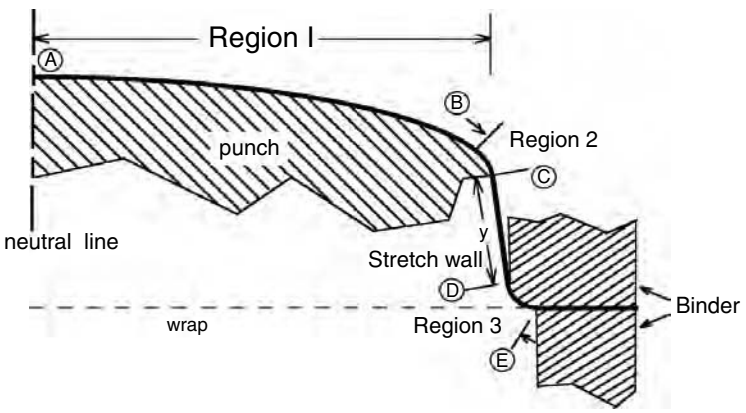

16.14. Schematic of a stamping.

below is in plane strain but real parts are usually stretched in the normal direction as well. The highest stress will occur in the stretch wall between C and D. To determine whether this stamping can be made, it is necessary to fix the strain level required at A and then calculate the stress in this region to determine whether it exceeds the tensile strength of the material.

EXAMPLE 16.1: Determine whether the stamping in Figure 16.14 can be made assuming a target strain at A of $\varepsilon_A = 0.035$. Other data are: the sheet thickness = 1 mm; the stress–strain relation is $\sigma = 520\varepsilon^{0.18}$ MPa; the radii are $r_1 = 8$ m, $r_2 = 0.10$ m, and $r_3 = 0.025$ m; the angles are $\theta_1 = 0.25$, $\theta_2 = 1.05$, and $\theta_3 = 1.30$ radians; and the friction coefficient is $\mu = 0.10$.

For simplicity, assume that this is a plane-strain stamping.

SOLUTION: The thickness at A, $t_A = t_0 \exp(-\varepsilon_A) = (1\text{ mm})\exp(-0.035) = 0.9656$ mm. The tensile force per length at A is $F_A = 520 t_A \varepsilon_A^n = 520(0.9656)(0.035)^{0.18} = 274.6$ kN/m.

The tensile force at B must be enough larger than this to overcome the friction in all the bends.

$$F_B = F_A \exp(\mu\theta) = 274.6\ \exp[(0.10(0.25)] = 275.3\,\text{kN/m},$$
$$F_C = F_A \exp(\mu\theta) = 275.3\ \exp[(0.10)(1.05)] = 305.8\,\text{kN/m} = F_D.$$

The maximum force, F_D, corresponds to the tensile strength time the original thickness $= t_0 K n^n \exp(-n) = (0.001)(520)(0.18^{0.18})\exp(-0.18) = 319.0$ kN/m. The value of F_E is less than this so the stamping can be made.

EXAMPLE 16.2: Find the required length of the stretch wall.

SOLUTION: Guessing that the horizontal component of the stretch wall is 0.04 m, the length of the wrap is $8 \times 0.25 + 0.1 \times 1.05 + 1.3 \times 0.025 + 8 \times 0.25 + 0.04 = 2.178$.

The force per length at B, $F_B = F_A \exp(\mu\theta) = 274.6\,\text{kN/m}\,[(0.10)(0.25)] = 274.6$, but F_B also equals $t_B\sigma_B = t_0 \exp(-\varepsilon_B) K \varepsilon_B^{0.18}$ so $\varepsilon_B^{0.18} \exp(-\varepsilon_B) = F_A/(Kt_0) = 274.6/520 = 0.5281$.

Solving by trial and error, $\varepsilon_B = 0.0521$.

The force per length at C is 305.8 kN/m but F_C also equals $t_C\sigma_C = t_0 \exp(-\varepsilon_C) K \varepsilon_C^{0.18}$ so $\varepsilon_C^{0.18} \exp(-\varepsilon_C) = F_C/(Kt_0) = 305.8/(520) = 0.5881$.

Solving by trial and error, $\varepsilon_C = 0.083$.

Taking the average strain between A and B as $(0.035 + 0.0521)/2 = 0.0436$, the increase in the length of line is $(8 \times 0.25)[\exp(0.0436) - 1] = 0.089$ m.

Taking the average strain between B and C as $(0.0521 + 0.083)/2 = 0.0676$, the increase in the length of line is $(0.1 \times 1.105)[\exp(0.0673) - 1] = 0.0077$ m.

The change of length of the stretch wall is $0.04[\exp(\varepsilon_C) - 1] = 0.0035$ m.

The total change of length is then $0.089 + 0.009 + 0.0035 = 0.10$ m or 100 mm. To this must be added any length of material that comes out of the binder.

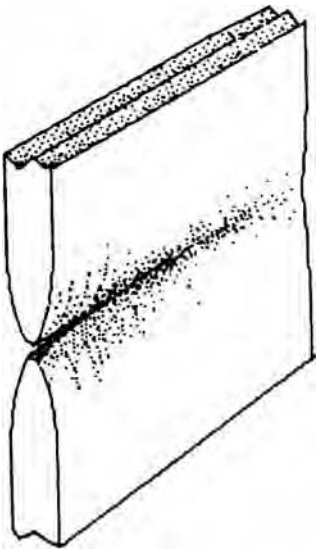

16.15. Sketch of a sheet failure by through-thickness necking.

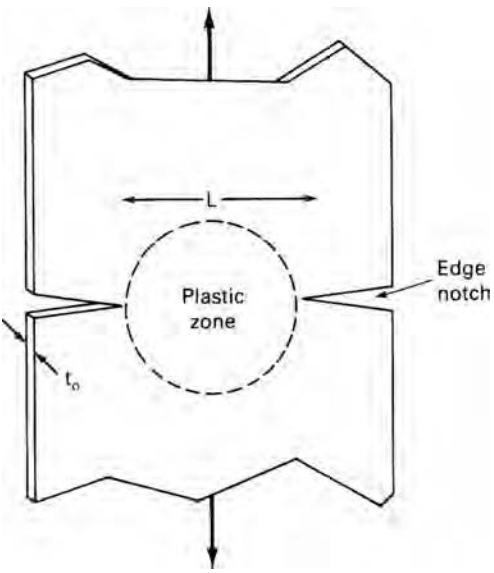

16.16. Plastic zone in a deeply notched tensile specimen.

16.10 TOUGHNESS AND SHEET TEARING

Figure 16.15 is a sketch of a plane-strain neck in a sheet. The volume of the plastic region is proportional to t^2L where t is the specimen thickness and L is the length of the crack. Since the area of the fracture is tL, the plastic work per area is proportional to the thickness t, and the fracture toughness K_C is proportional to $\sqrt{t}$. Very thin sheets tear suddenly at surprisingly low stresses.

A fracture toughness can be associated with the process of localized necking and tearing. A simple way of measuring the toughness is to test a series of deeply edge-notched tensile specimens* like that shown in Figure 16.16. The deep notch confines

* B. Cotterell and J. K. Reddel, *Int. J. Fract.*, 13 (1977), pp. 267–77.

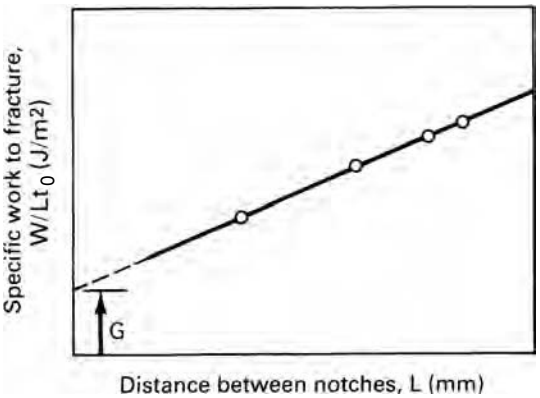

16.17. Schematic plot of the work per area, W/Lt_0, as a function of the distance between notches. G is the value at $L = 0$.

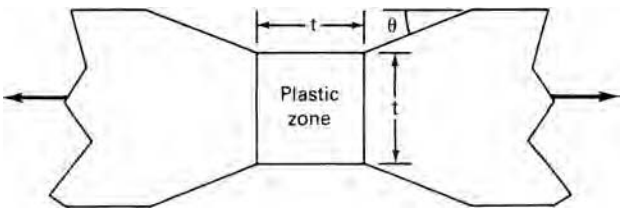

16.18. Shape of plastic zone during local necking of an ideally plastic material.

the plastic deformation to a circular region whose diameter is equal to the distance L between notches. The work is composed of two terms. One is the plastic work in the circular region. The other is the work to propagate the local neck. The total work is

$$W = \alpha L^2 t_0 + GLt_0. \tag{16.6}$$

Here G is the fracture toughness or energy per area to cause the local neck. The constant α reflects the strain distribution in the circular area. G can be determined by plotting $W/(Lt_0)$ as a function of L as shown in Figure 16.17. The intercept at $L = 0$ is G.

At any instant during the necking of an ideally plastic material, plastic deformation is restricted to a region of length t that is equal to the current thickness.* See Figure 16.18. In this case it can be shown that

$$G = t_0 K_{\text{ps}} \int_0^{\varepsilon_f} \varepsilon^n \exp(-2\varepsilon)\, \mathrm{d}\varepsilon. \tag{16.7}$$

Here K_{ps} is the coefficient in the power-law expression for plane strain, $\sigma = K_{\text{ps}}\varepsilon_{\text{ps}}^n$, and is related to K in $\bar{\sigma} = K\bar{\varepsilon}^n$ through the yield criterion. For von Mises, $K_{\text{ps}}/K = (4/3)^{(n+1)/2}$, whereas for equations 13.22 and 13.23 with $R = P$, $K_{\text{ps}}/K = (4/3)^{(n+1)/a}$. The value of the integral is not very dependent on ε_{f} as long as $\varepsilon_{\text{f}} \geq 1$ ($RA = 63\%$). The main problem with this analysis is that the shapes of the necks vary with the material, whereas this analysis predicts $\theta = 26.6°$. Necks are often

* W. F. Hosford and A. G. Atkins, *J. Material Shaping Technol.*, 8 (1990), pp. 107–11.

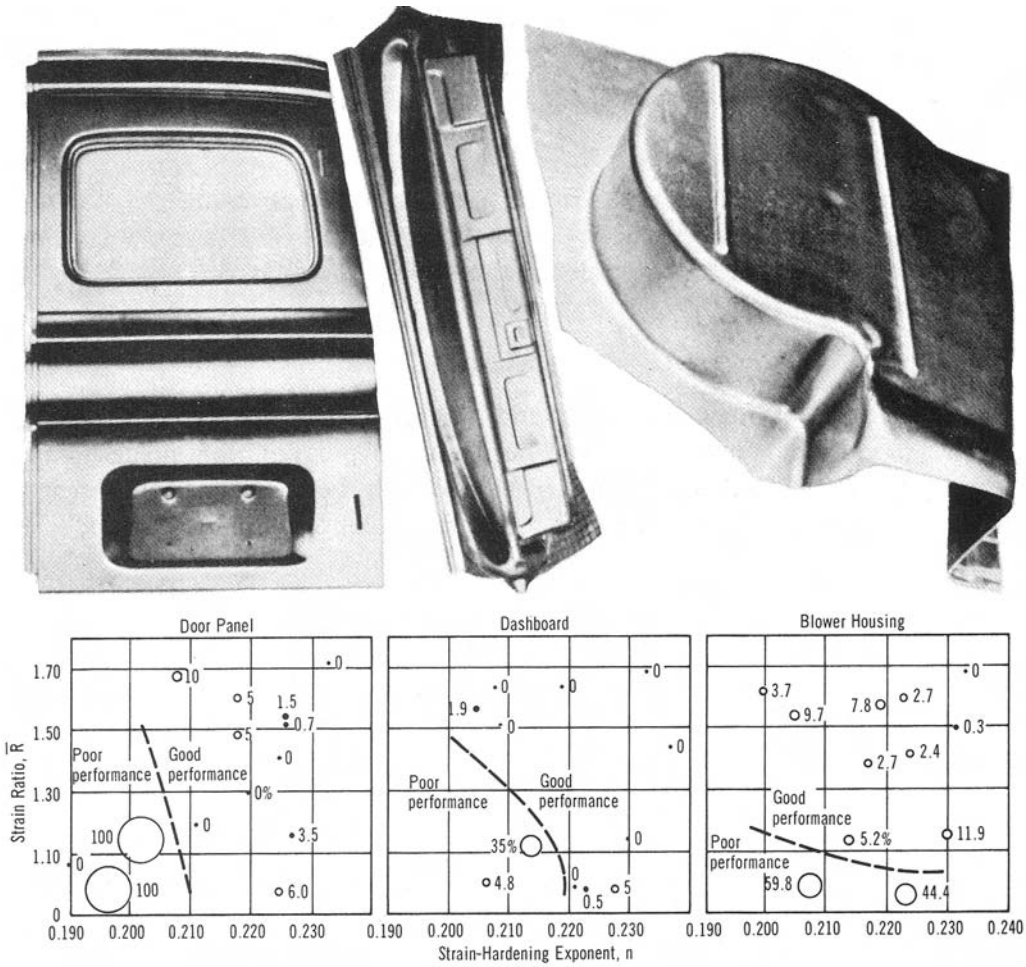

16.19. Dependence of press performance for three parts on n and $\bar{R}$.

more gradual than this prediction, so the plastic zone is longer than t. This is probably the result of a positive rate sensitivity, m, and makes the experimental values of G larger than those predicted by equation 16.7.

16.11 GENERAL OBSERVATIONS

The relative amount of stretching and drawing varies from on part to another. Where stretching predominates, formability depends mainly on n and m, whereas if drawing predominates, $\bar{R}$ is most important. Figure 16.19 relates actual press performance to n and $\bar{R}$.

NOTES OF INTEREST

Johann Bauschinger (1833–1893) was the director of the Polytechnical Institute of Munich. In this position, he installed the largest testing machine of the period and instrumented it with a mirror extensometer so that he could make very accurate strain

measurements. He discovered that prior straining in tension lowered the compressive yield strength and vice versa. Bauschinger also did the original research on the yielding and strain aging of mild steel.

The aluminum pie dish is one of the very few stamped items with wrinkles that consumers accept willingly. The wrinkled sidewalls actually strengthen the pan.

REFERENCES

Z. Marciniak, J. L. Duncan, and S. J. Hu, *Mechanics of Sheet Metal Forming*, Butterworth and Heinemann, 2002.

E. M. Meilnik, *Metalworking Science and Technology*, McGraw-Hill, 1991.

John H. Schey, *Metal Deformation Processes: Friction & Lubrication*, M. Decker, 1970.

PROBLEMS

16.1. Referring to Figure 16.5, determine the values of L/L_0 for brass and aluminum.

16.2. Plot the contour of $\bar{\varepsilon} = 0.04$ on a plot of ε_1 vs. ε_2 (i.e., on a forming limit diagram).

16.3. Show how the dashed line in Figure 16.6 would change for a material having an R-value of 2.

16.4. A sheet of HSLA steel having tensile strength of 450 MPa and yield strength of 350 MPa is to be drawn over a 90° bend. What is the maximum permissible coefficient of friction?

16.5. Consider the deep drawing of a flat-bottom cylindrical cup. Sketch the strain path for an element initially on the flange halfway between the periphery and die lip.

16.6. Calculate the total drag force per length of a draw bead attributable to plastic bending if the bend angle entering and leaving the draw bead is 45° and the bend angle in the middle of the draw bead is 90°. Assume the bend radii are 10 mm and the sheet thickness is 1 mm.

16.7. Calculate the drag force attributable to friction in Problem 16.6, assuming a friction coefficient of 0.10.

16.8. Carefully sketch the strain signature for the conical cup drawing in Figure 16.20.

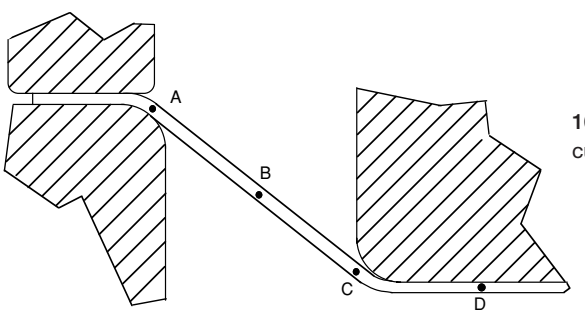

16.20. Drawing of a conical cup.

16.9. Why isn't the bending included in the drag in regions A–B and B–C in Example 16.1?

16.10. It has been noted that when a cup is drawn with a hemispherical punch, greater depths can be achieved before failure when the punch spins. Explain why this might be so.

17 Other Sheet-Forming Operations

17.1 ROLL FORMING

Roll forming transforms a flat sheet into another shape. As the new shape is formed over some distance, its width generally decreases as illustrated in Figure 17.1. During this transformation, the length of the edge must increase. The length must be sufficiently long so that the stretching is elastic. Otherwise, the edge will be longer than the centerline after the forming is complete and caused the formed sheet to warp.* The strain along the edge is

$$\varepsilon = \ln(L_e/L_m), \tag{17.1}$$

but

$$(L_e/L_m) = 1/\cos(\alpha), \tag{17.2}$$

where

$$\alpha = \arctan(W_0 - W)/2L_m. \tag{17.3}$$

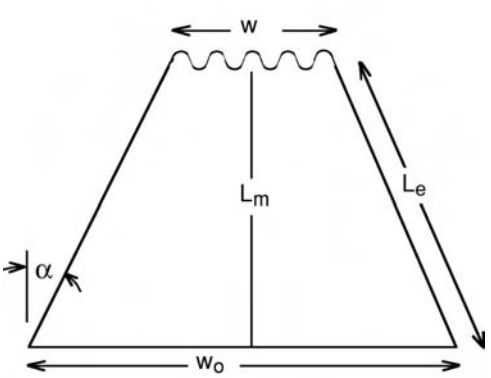

17.1. Stretching of the edge as a sheet is roll formed into a corrugated sheet.

* The author is indebted to J. L. Duncan for this concept.

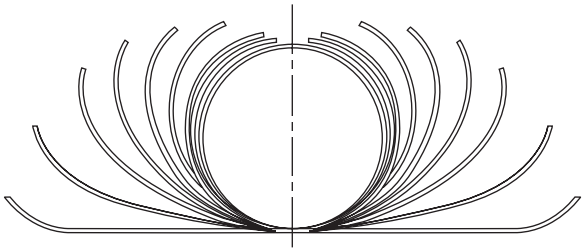

17.2. Progressive shapes in roll forming of a tube from a flat sheet. From H. Singh, *Fundamentals of Hydroforming* (SME, 2003).

EXAMPLE 17.1: How long must L_m be if a sheet 6 feet wide contracts to 4 feet wide? Assume that yielding will occur when the strain reaches 0.002.

SOLUTION: $L_e/L_m = \exp(0.002) = 1.002$.

$\alpha = \arccos(1/1.002) = 3.6^\circ$. $(W_0 - W)/2L_m = \tan\alpha = \tan 3.6^\circ = 0.063$.

$L_m = (W_0 - W)/[2(0.063)] = 15.9$ ft.

Roll forming is used to make welded tubes. Figure 17.2 shows the progressive change of shape.

17.2 SPINNING

Spinning is a sheet-forming process that is suitable for axially symmetric parts. A tool forces the sheet metal disc to conform to a mandrel as shown in Figure 17.3. The tool usually consists of a small wheel. The process should be controlled so that all of the deformation is pure shear under the tool. If the tool causes more thinning than would be produced by shear, the unsupported flange will wrinkle. Even though spinning is slow, it is suitable for low production items because the tooling costs are low.

The reduction r is

$$r = 1 - \sin(\alpha/2). \tag{17.4}$$

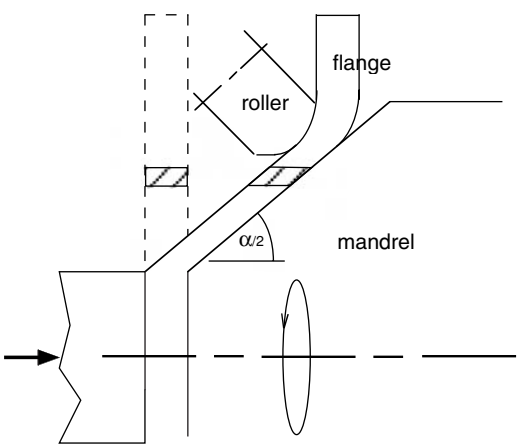

17.3. Sketch of a cup spinning operation. With pure shear, there is no deformation in the flange.

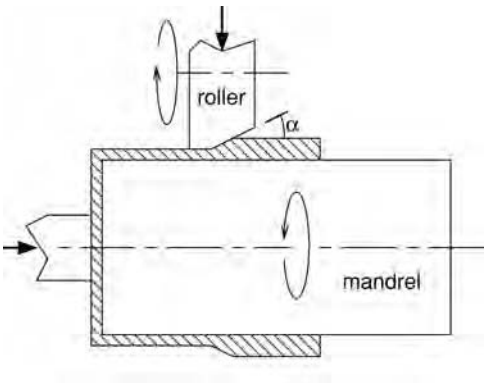

17.4. Reduction of wall thickness by spinning.

Any additional thinning would cause the flange to wrinkle. The shear strain γ is

$$\gamma = \cot(\alpha/2). \tag{17.5}$$

Spinning may also be used to reduce the wall thickness of tubes and cups shown in Figure 17.4.

17.3 HYDROFORMING OF TUBES

In hydroforming of tubes, the tube walls are forced against a die by internal pressure. Hydroforming is used to produce such diverse products as plumbing fittings and vehicle frames. Welded tubes are preferred over seamless tubes because of their more uniform wall thickness. Usually the tubes are subjected to axial compression in addition to the internal pressure. Figure 17.5 shows the production of a plumbing T-fitting. In the case of vehicle frames, the tubes are often bent before hydroforming.

17.4 FREE EXPANSION OF TUBES

A simple balance of forces on the wall (Figure 17.6) results in $p = (t/r)\sigma_\theta$, where p is the internal pressure, r is the tube radius, t the wall thickness, and σ_θ the hoop stress. If

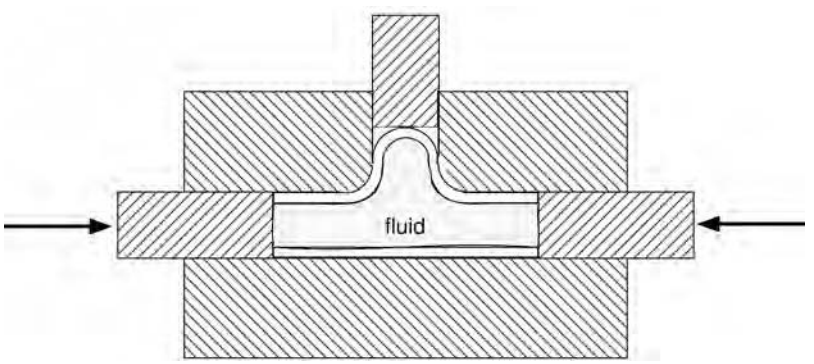

17.5. Production of a T-fitting by internal pressure and axial compression.

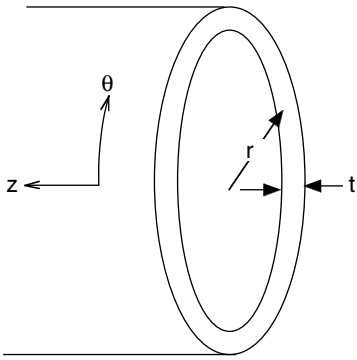

17.6. Force balance on a tube with internal pressure.

the length of the tube is fixed, this is a condition of plane strain where $\sigma_z = \sigma_\theta/2$ and $\sigma_\theta = (2/\sqrt{3})\bar{\sigma}$. Therefore

$$p = (2/\sqrt{3})(t/r)\bar{\sigma} = (2/\sqrt{3})(t/r)K[(2/\sqrt{3})\varepsilon_\theta]^n. \tag{17.6}$$

Substituting $\varepsilon_\theta = \ln(r/r_0)$ and $t = t_0 r_0/r$ into equation 17.6,

$$p = (2/\sqrt{3})\left(t_0 r_0/r^2\right) K[(2/\sqrt{3})\ln(r/r_0)]^n. \tag{17.7}$$

A plot of Equation 17.7 (Figure 17.7) shows that as the tube is expanded, the pressure first rises and then falls. The strain at maximum pressure can be found by differentiating equation 17.7 and setting $\mathrm{d}p/\mathrm{d}r = 0$ as

$$\varepsilon_\theta = n/2. \tag{17.8}$$

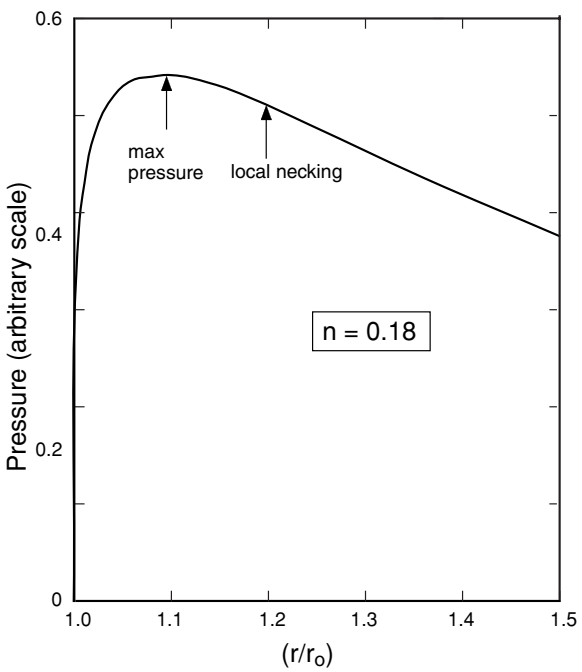

17.7. Variation of pressure with radius as a tube is expanded under plane strain. Under internal pressure, the maximum pressure occurs when $\varepsilon_\theta = n/2$.

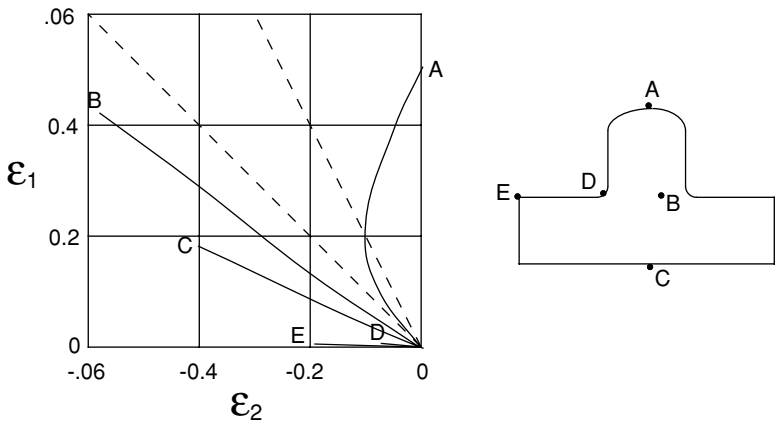

17.8. Strain signatures for several locations on a hydroformed T-joint. After T. Yoshida and Y. Kuriyama, in *Sheet Metal Forming for the New Millennium* (IDDRG, 2000).

The maximum pressure, however, does not represent the condition for failure. Rather failure occurs by plane-strain necking when $\varepsilon_\theta = n$.

The forming limit is increased by enough end pressure to cause the tube to shorten. This shifts the stress state toward uniaxial tension on the left-hand side of the forming limit diagram.

Figure 17.8 shows the strain signatures for several locations on a hydroformed T-joint.

17.5 HYDROFORMING INTO SQUARE CROSS SECTION

Circular tubes are often formed into square or rectangular cross sections to increase their moment of inertia and hence stiffness. As a circular tube is expanded into a square tube, its radius decreases (Figure 17.9). Friction between the tube and die plays an

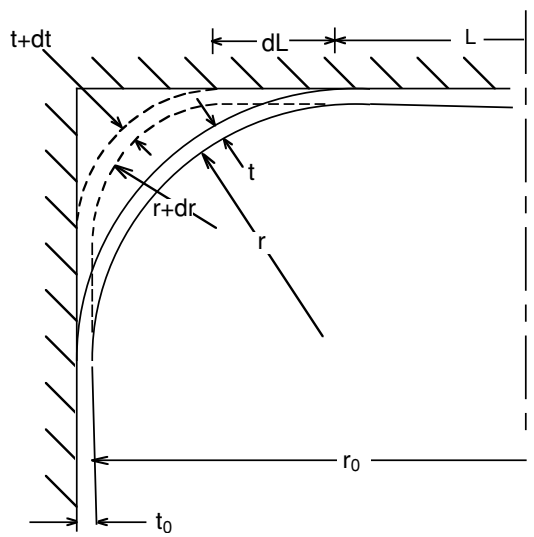

17.9. Incremental expansion of a circular tube into a square.

important role in controlling the strain distribution and limiting radius. Two extreme cases will be considered.

With frictionless conditions, the stress and strain are the same everywhere. If there is no movement along the tube axis,

$$e = \ln[4/\pi + (1 - 4/\pi)(r/r_0)]. \tag{17.9}$$

With sticking friction, only the portion of the tube that is not in contact with the die wall can deform. In this case the strain in the unsupported region is

$$e = (1 - 4/\pi)\ln(r/r_0). \tag{17.10}$$

Figure 17.10 shows how the strain depends on how sharp a radius is formed for these extreme cases. Sliding friction will fall between.

The pressure is given by $P = \sigma t/r$. Substituting $t = t_0 \exp(-\varepsilon)$,

$$P = \sigma t_0 \exp(-\varepsilon)/r. \tag{17.11}$$

For power-law hardening,

$$P = K\varepsilon^n t_0 \exp(-\varepsilon)/r. \tag{17.12}$$

In the *low-pressure* process, the tube is initially filled before being forced into a die cavity that has about the same perimeter as the tube. This avoids stretching of the walls so smaller radii can be achieved. The internal pressure keeps the walls from collapsing.

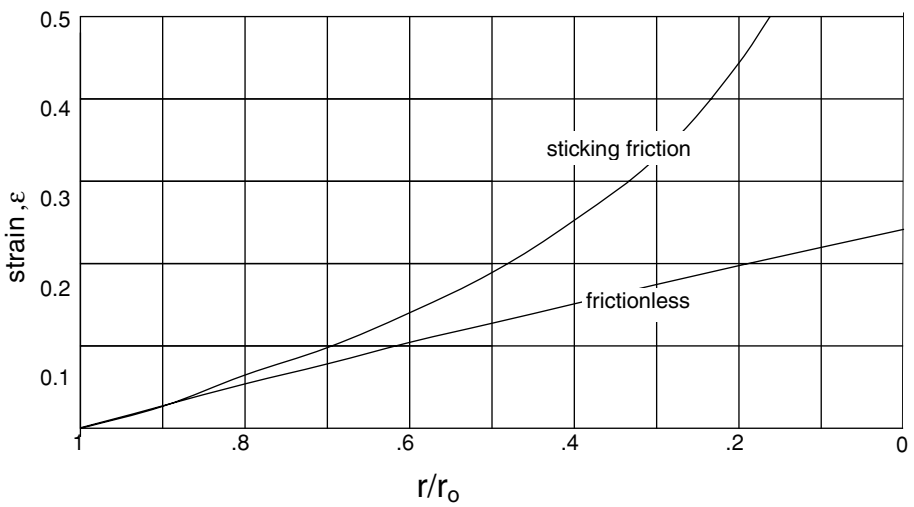

17.10. Strain in unsupported region during filling of a square cross section. With sticking friction, the strains become much higher than with frictionless conditions.

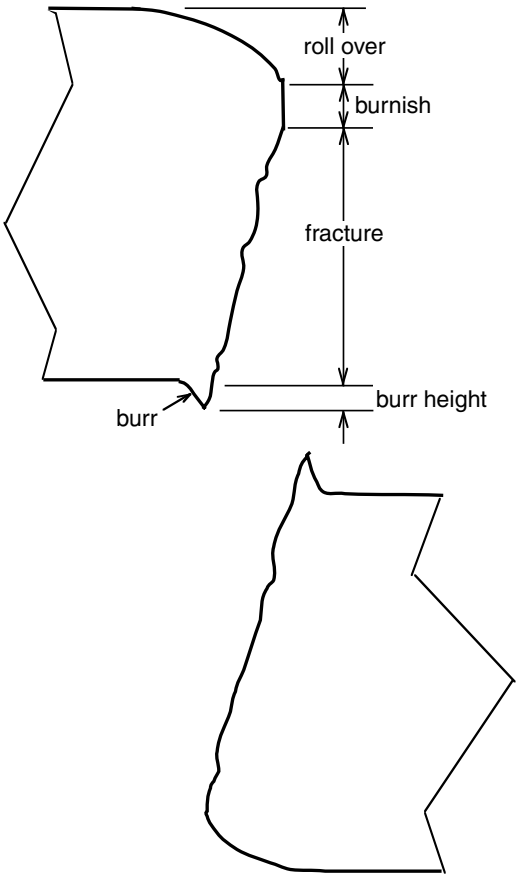

17.11. Sheared edge showing several regions: Rollover is part of original surface; burnish is where tools smeared the shear portion of the fracture; the fracture surface itself; and the burr.

17.6 BENT SECTIONS

Many parts are made from tubes that are bent before hydroforming. Mandrels are used in the bending to keep the tube from collapsing. End feeding by friction or pressure block during bending can induce a net compression during bending. This moves the neutral axis toward the inside of the bend and raises the forming limits during subsequent hydroforming and moves the failure site from the outside of the bend toward the inside. These effects are understandable in terms of how the forming limits are affected by strain-path changes (Section 15.5). Worsick* has found good agreement with stress-based forming limits (Section 15.6).

Tubes formed by welding rolled sheet are preferred for hydroforming of seamless tubes. The reason is that the wall thickness is much more consistent. In the manufacture of seamless tubes, any wandering of the mandrel causes the wall thickness to vary.

17.7 SHEARING

Sheets are sheared in preparing blanks for stamping and in trimming finished stampings. Punching of holes is also a form of shearing. The major concerns in shearing are the

* M. J. Worswick, private communication.

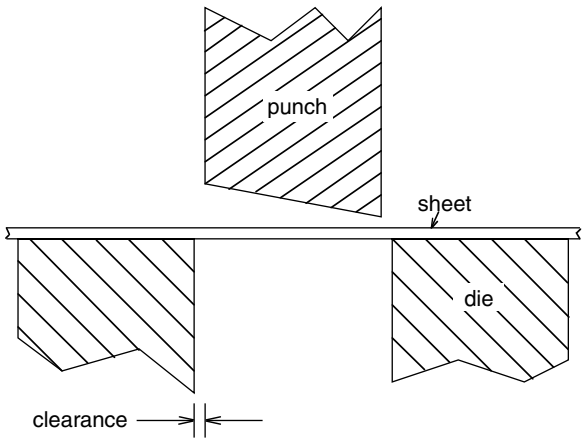

17.12. Tools for hole punching. Note that the cutting edge of the punch is on an angle so the shearing does not occur simultaneously over the entire surface.

nature of the sheared edge, tool wear, and tool forces. The shape of the sheared edge, shown in Figure 17.11, depends on the clearance and the sharpness of the tools. The heights of burr are usually less than 10% of the sheet thickness.

Formability during subsequent hole expansion or flanging depends on the nature of the flanged edges. The presence of burrs decreases forming limits (see Section 18.5). The sharpness of the tools decreases with life as wear occurs. The wear rate is greater in higher strength sheets.

The forces required for shearing depend on the angle of the shearing edge to the sheet. If the cutting edge is parallel to the sheet, all of the shearing will occur simultaneously. By increasing the angle, the amount of material being sheared at any instant decreases. The shearing force is increased with smaller clearances, duller tools, and higher strength sheets. The force also varies during the stroke. Initially the shearing occurs through the entire thickness. As the tool penetrates, the area being sheared decreases.

To avoid excessive shearing forces, the tools for shearing and hole punching are made so that as the tools descend, the shearing progresses from one location to another (Figure 17.12).

REFERENCES

Z. Marciniak, J. D. Duncan, and S. J. Hu, *Mechanics of Sheet Metal Forming*, Butterworth-Heinemann, 2002.

Metals Handbook, 9th ed., v. 14, Forging and Forming, ASM.

H. Singh, *Fundamentals of Hydroforming*, SME, 2003.

PROBLEMS

17.1. Calculate the pressure to expand a tube from a radius r to r_0 if the ends are allowed to move freely. Assume $\sigma = K\varepsilon^n$. Also find the strain at maximum pressure.

17.2. A tube with an external radius of 25 mm and 1.0 mm thickness is to be expanded by internal pressure into a square 50 mm on a side. Assume that

$\sigma = 650\varepsilon^{0.20}$ MPa. Determine the corner radius if the maximum pressure available is 80 MPa, the ends are fixed, and the die is frictionless.

17.3. A cup with 45° walls is to be spun from sheet. What should the thickness of the sheet be if the cup walls are to be 1 mm thick?

17.4. Calculate the percent increase of the moment of inertia when a circular tube of 1 in outside diameter and 0.9 in inside diameter is hydroformed into a square cross section. Assume the wall thickness and tube length are unchanged.

17.5. A thin-wall tube with radius R and wall thickness t is pressurized in a square die. The effective stress–strain curve is $\bar{\sigma} = K(\varepsilon_0 + \bar{\varepsilon})^n$. Assume the length remains constant. Find the relation between the corner radius and the pressure if

a) There is no friction;

b) Sticking friction prevails.

17.6. A steel tube of 50 mm diameter and 1 mm wall thickness is expanded into a square cross section. Assume the effective stress–strain relation is $\bar{\sigma} = 650\bar{\varepsilon}^{0.20}$. Determine the minimum corner radius assuming frictionless conditions.

17.7. Describe the stress state at the edge of a hole during hole expansion.

17.8. Water is used as the pressurized fluid in hydroforming. Why isn't air used?

18 Formability Tests

There are many tests of formability for sheet materials. A given test may correlate well with behavior in one type of forming process and poorly with behavior in another. This is because the relative amounts of drawing and stretching vary from test to test and process to process.

18.1 CUPPING TESTS

The Swift cup test is the determination of the limiting drawing ratio for flat-bottom cups. In the Erichsen and Olsen tests, cups are formed by stretching over a hemispherical tool. The flanges are very large so little drawing occurs. The results depend on stretchability rather than drawability. The Olsen test is used in America and the Erichsen in Europe. Figure 18.1 shows the setup.

The Fukui conical cup test involves both stretching and drawing over a ball. The opening is much larger than the ball so a conical cup is developed. The flanges are allowed to draw in. Figure 18.2 shows the setup. A failed Fukui cup is shown in Figure 18.3.

Figure 18.4 shows comparison of the relative amounts of stretch and draw in these tests.

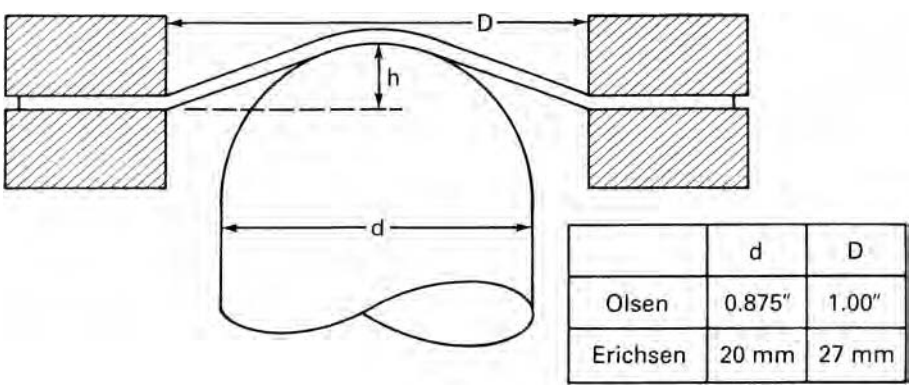

	d	D
Olsen	0.875″	1.00″
Erichsen	20 mm	27 mm

18.1. Olsen and Erichsen tests.

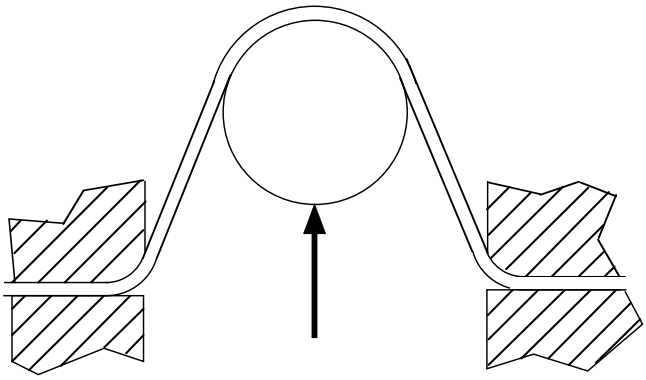

18.2. Fukui test.

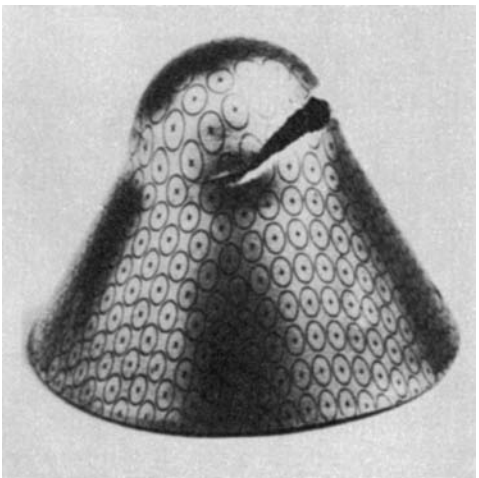

18.3. Failed Fukui cup. Courtesy of *Institut de Recherches de la Sidérurgie Française*.

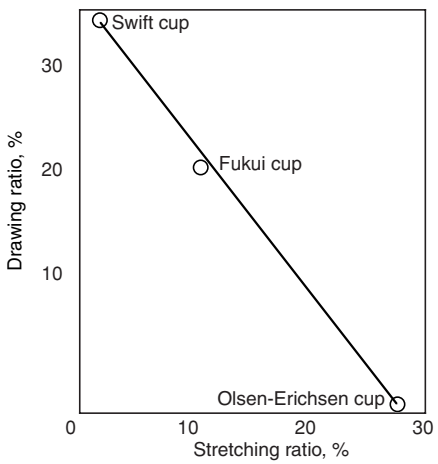

18.4. Relative amounts of stretching and drawing in these cupping tests.

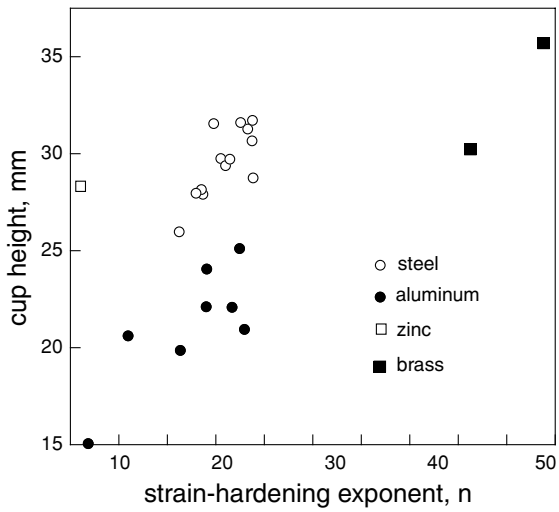

18.5. Failure of cup height to correlate with the strain-hardening exponent, which is the uniform strain before necking. Data from S. S. Hecker, *op. cit*.

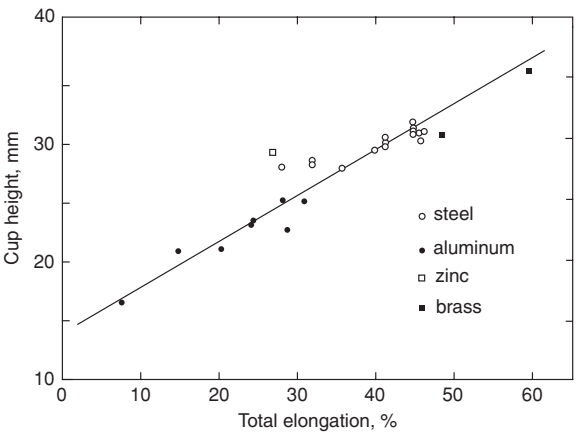

18.6. Correlation of the LDH cup height with the total elongation in a tension test. Data from S. S. Hecker, *op. cit*.

18.2 LDH TEST

The cupping tests discussed above are losing favor because of irreproducibility. Hecker* attributed this to "insufficient size of the penetrator, inability to prevent inadvertent drawing in of the flange, and inconsistent lubrication." He proposed the limiting dome height test (LDH) which uses the same tooling (4 in. diameter punch) as used to determine forming limit diagrams. The specimen width is adjusted to achieve plane strain and the flange is clamped to prevent draw-in. The limiting dome height (LDH) is the greatest depth of cup formed with the flanges clamped. The LDH test results correlate better with the total elongation than with the uniform elongation, as shown in Figures 18.5 and 18.6. The total elongation includes the post-uniform elongation.

* S. S. Hecker, *Met. Engr. Q.*, 14 (1974), pp. 30–36.

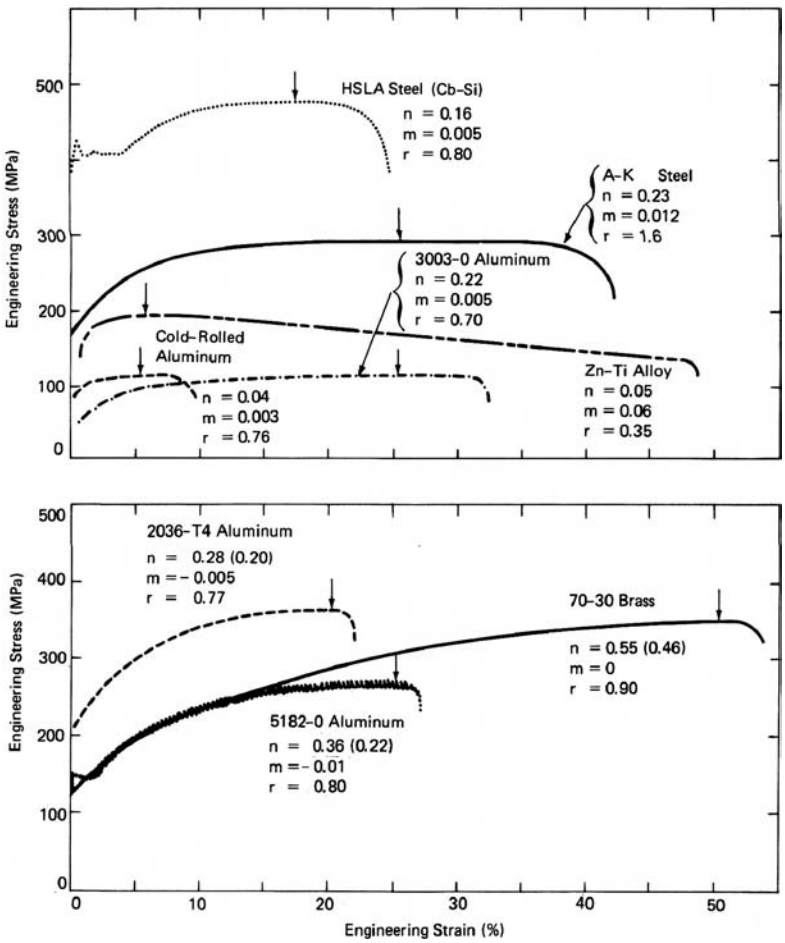

18.7. Engineering stress–strain curves for several metals. The uniform elongation is indicated by an arrow. Note that the post-uniform elongation is greater for materials with higher values of the strain-rate sensitivity, *m*. From A. K. Ghosh, *J. Eng. Matls. Tech. Trans. ASME Series H*, 99 (1977), pp. 264–74.

A major problem with the LDH test is reproducibility within a laboratory and between different laboratories. Part of the problem may be caused by minor variations in details of the clamping.

18.3 POST-UNIFORM ELONGATION

Figure 18.7 shows the engineering stress–strain curves for various sheet metals. It can be seen that the elongation that occurs after necking correlates well with the strain-rate sensitivity. This is plotted in Figure 18.8.

18.4 OSU FORMABILITY TEST

Wagoner and coworkers at Ohio State University have proposed a more reliable test that involves cylindrical punches instead of spherical punches. Three different proposed

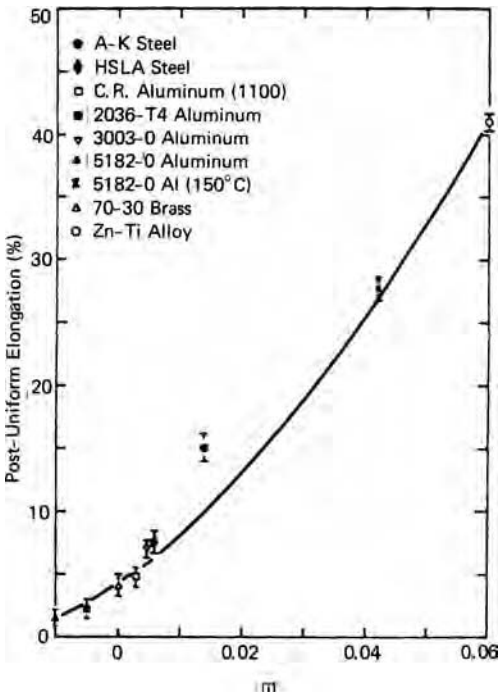

18.8. Post-uniform elongation as a function of the strain-rate sensitivity, m. From A. K. Ghosh, *op. cit.*

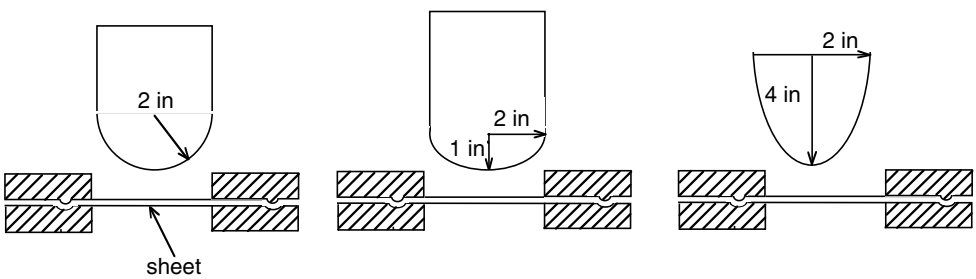

18.9. Tooling for Ohio State University formability test. All three indenters are cylinders.

punch geometries are illustrated in Figure 18.9. The height of the draw at failure is measured.

18.5 HOLE EXPANSION

In the hole expansion test, a punch forces a hole to expand as shown in Figure 18.10, which increases the radius. The engineering strain at which failure occurs is $e = \Delta r / r_0$. The results depend strongly on the height of burrs made when the hole was punched. This dependence is illustrated schematically in Figure 18.11. Failures usually occur

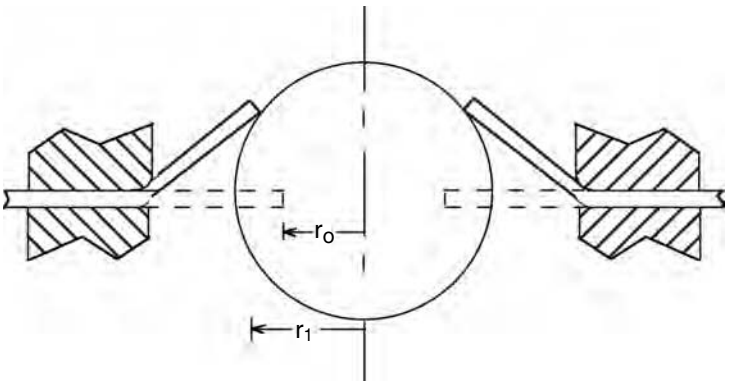

18.10. Hole expansion test.

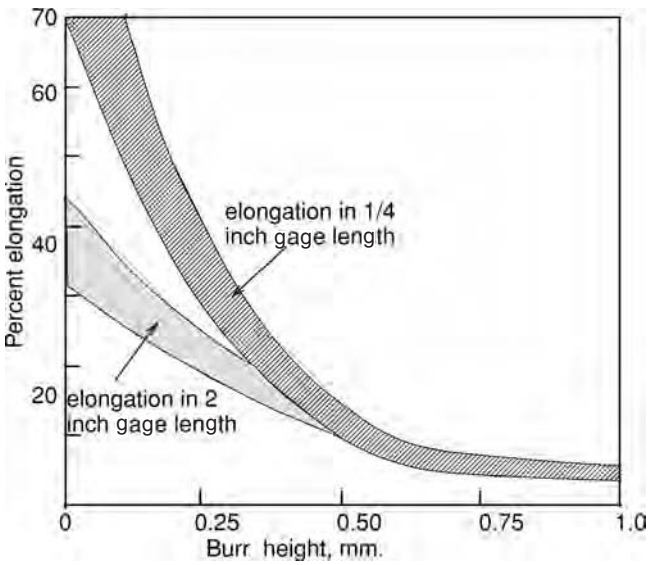

18.11. The amount a hole can be expanded decreases significantly with burr height.

with cracks running parallel to the rolling direction because ductility in the transverse direction is lower than in the longitudinal direction.

18.6 HYDRAULIC BULGE TEST

Much higher strains are possible in a hydraulic bulge test than in a tension test, so the effective stress–strain relations can be evaluated at higher strains. Figure 18.12 shows the setup for a bulge test. The sheet is placed over a circular hole, clamped, and bulged outward by the oil pressure, P.

Consider a force balance on a circular element of radius ρ near the pole (Figure 18.13). The radius r of this element is $r = \rho\Delta\theta$. The vertical component of the force acting on the circumference of this element is $2\pi rt\sigma\,\Delta\theta = 2\pi t\rho\sigma\,\Delta\theta^2$.

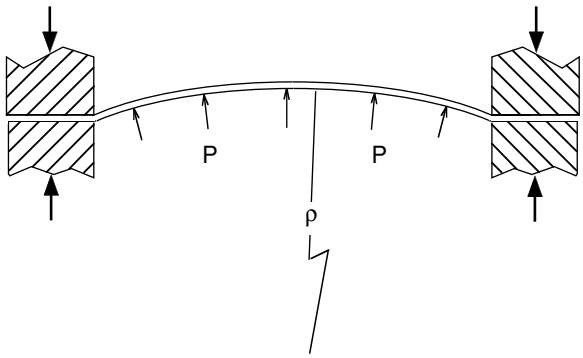

18.12. Hydraulic bulge test.

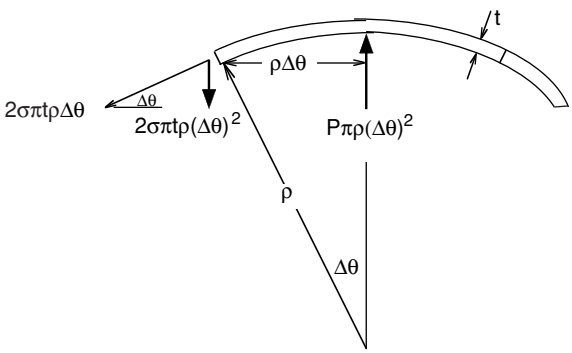

18.13. Force balance in hydraulic bulging.

This is balanced by the force of the oil, $\pi r^2 P = \pi(\rho\Delta\theta)^2 P$. Equating, $2\pi t\rho\sigma\,\Delta\theta^2 = \pi(\rho\Delta\theta)^2 P$ or

$$\sigma = P\rho/(2t). \tag{18.1}$$

The radial strain, ε_r, can be used to find the thickness,

$$t = t_0 \exp(-2\varepsilon_r). \tag{18.2}$$

To obtain the stress–strain relation, there must be simultaneous measurement of ε_r, ρ, and P.

18.7 DUNCAN FRICTION TEST*

This consists of stretching a strip between two fixed cylinders as indicated in Figure 18.14. The strains in sections A and B are measured. From these the stresses, σ_A and σ_B, and the thicknesses, t_A and t_B, can be deduced from $\sigma = K\varepsilon^n$ and $t = t_0 \exp\varepsilon$. Now F_A and F_B can be determined as $F = \sigma tw$ where w is the strip width. Finally, the friction coefficient can be found by solving $F_A/F_B = \exp(\mu\pi/2)$ for μ.

$$\mu = (2/\pi)\ln[(\varepsilon_A/\varepsilon_B)^n \exp(\varepsilon_A - \varepsilon_B)]. \tag{18.3}$$

* J. L. Duncan, B. S. Shabel, and J G. Filho, SAE paper 780391 (1978).

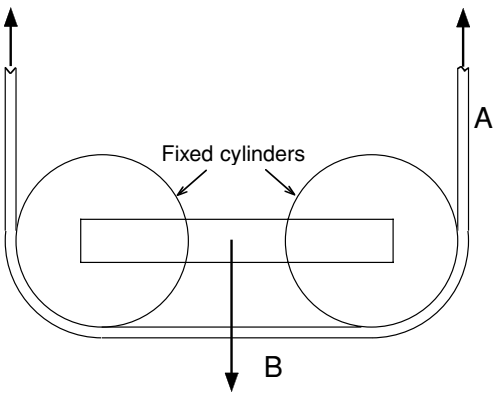

18.14. The Duncan friction test.

REFERENCES

E. M. Mielnik, *Metalworking Science and Engineering*, McGraw-Hill, 1991.

M. P. Miles, J. L. Siles, R. H. Wagoner, and K. Narasimhan, *Met. Trans.*, 24A (1993), pp. 1143–51.

PROBLEMS

18.1. A strip was tested using the friction test in Figure 18.14. Strains of $\varepsilon_A = 0.180$ and $\varepsilon_B = 0.05$ were measured. The tensile stress–strain curve is approximated by $\sigma = 800\varepsilon^{0.20}$ MPa. Calculate the coefficient of friction between the strip and the cylinders.

18.2. Consider a bulge test on a sheet that is clamped at the periphery of a circular hole of radius R (Figure 18.15.) The bulge height is $h = r/2$. Assume for simplicity that the shape of the bulged surface is spherical and that the radial strain is the same everywhere. (Neither of these assumptions is strictly correct.)

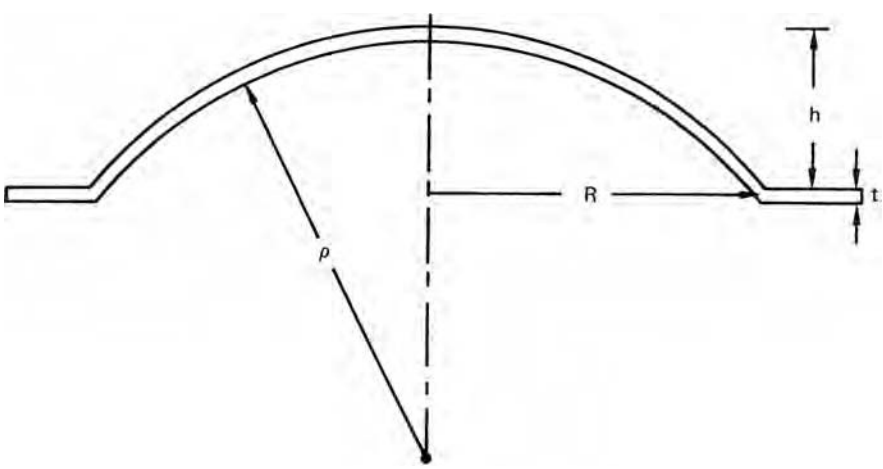

18.15. Bulge test.

a) Calculate the radial strain, ε_r.

b) Calculate the circumferential strain, ε_c, as a function of the initial radial position, r_0.

c) By comparing ε_c and ε_r, deduce how the stress ratio, α, varies with distance from the pole.

18.3. Assume that the bulged surface in a hydraulic bulge test is a section of a sphere. Show that with this assumption the radius of curvature ρ is related to the bulge height h and the die radius R by

$$\rho = \frac{R^2 + h^2}{2h}.$$

18.4. If it is further assumed that the thickness of the bulged surface is the same everywhere (not a particularly good assumption) the thickness can be related to the bulge height h and the die radius R. Derive this relation.

18.5. During a laboratory investigation of springback, strips were bent between three cylinders and unloaded as illustrated in Figure 18.16. It was noted that on unloading, the force dropped abruptly from F_1 to F_2 before noticeable unbending occurred. It was postulated that the drop was associated with the reversal of the direction of friction between the strips and the cylinders. Assuming that this is correct, derive an expression for the coefficient of friction in terms of F_1, F_2, and the bend angle α.

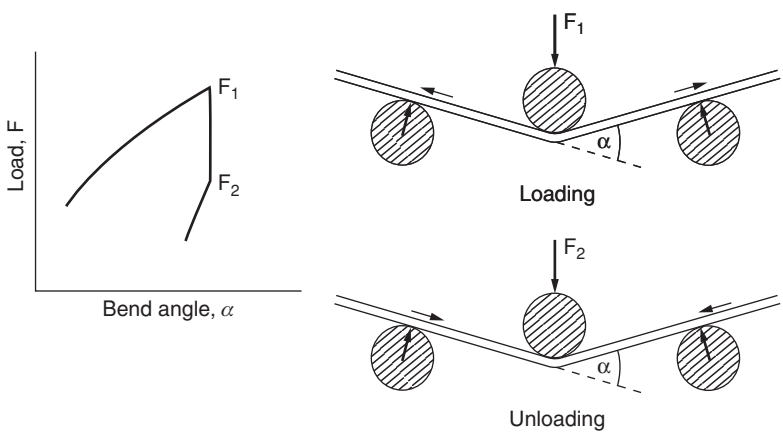

18.16. Change of direction of friction on unloading from bending.

18.6. The apparatus in Figure 18.17 is used to induce balanced biaxial stretching. Draw beads lock the sheet. The amount of stretching is limited by failure of the walls in plane-strain tension. Estimate the maximum biaxial strain that can be achieved in a low-carbon steel with a strain hardening exponent of $n = 0.22$. Neglect any strain-rate dependence and assume that the friction coefficient is 0.12.

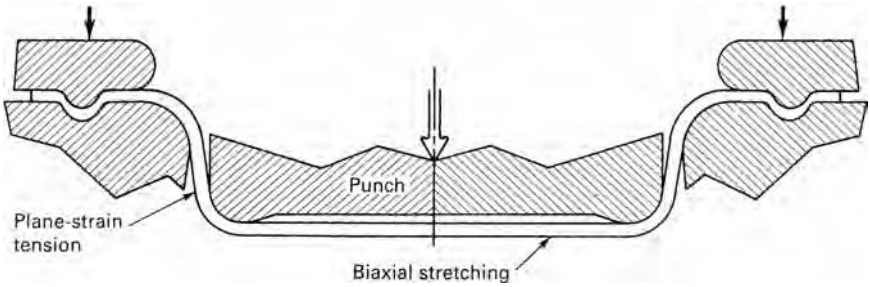

18.17. Apparatus for biaxial stretching.

18.7. Describe the state of stress at the edge of a hole during hole expansion.

19 Sheet Metal Properties

19.1 INTRODUCTION

Properties of sheet metals vary from one class of materials to another. Table 19.1 gives typical ranges of n, m, and $\bar{R}$ within several classes of materials. It should be noted that while these values are typical, higher or lower values may be encountered.

For both fcc and bcc metals, the highest values of $\bar{R}$ correspond to textures with $\{111\}$ planes oriented parallel to the sheet. Grains with $\{100\}$ planes oriented parallel to the sheet tend to have very low $\bar{R}$ values. The recrystallization textures of bcc metals after cold rolling tend to have strong $\{111\}$ textural components parallel to the sheet and the $\bar{R}$-values depend mostly on the amount of the weaker $\{100\}$ component. It has been shown* that pure rotationally symmetric $\{111\}$ textures in bcc metals have a maximum $\bar{R}$-value of about 3. In contrast, cold rolled and recrystallized fcc metals (aluminum, copper, and austenitic stainless steels) usually have very little $\{111\}$ textural component parallel to the surface and consequently have $\bar{R}$-values less than 1.

Table 19.1. Typical sheet metal properties†

Metal	n	$\bar{R}$	m
Low-carbon steel	0.20–0.25	1.4–2.0	0.015
Interstitial-free steel	0.30	1.8–2.5	0.015
HSLA steels	0.10–0.18	0.9–1.2	0.005–0.01
Ferritic stainless steel	0.16–0.23	1.0–1.2	0.010–0.015
Austenitic stainless steel	0.40–0.55	0.9–1.0	0.010–0.015
Copper	0.35–0.45	0.6–0.9	0.005
Brass (70–30)	0.40–0.60	0.8–0.9	0.0–0.005
Aluminum alloys	0.20–0.30	0.6–0.8	–0.005–+0.005
Zinc alloys	0.05–0.15	0.4–0.6	0.05–0.08
α-titanium	0.05	3.0–5.0	0.01–0.02

†Although these values are typical, there is a great deal of variation from one lot to another, depending on the composition and the rolling and annealing practices. In general as the strength levels are increased by cold work, precipitation, or grain-size refinement, the levels of n and m decrease.

* J. O'Brien, R. Logan, and W. Hosford, in *Proceedings of the Sixth International Symposium on Plasticity and Its Current Applications*, A. S. Kahn, ed. (1997).

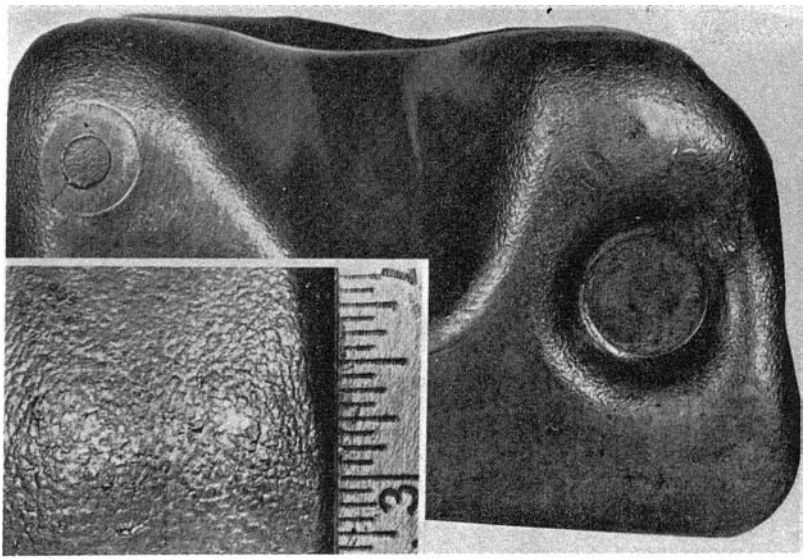

19.1. Example of orange peel. Courtesy of American Iron and Steel Institute.

19.2 SURFACE APPEARANCE

Surface appearance is of great importance for many parts formed from sheet metal. Several types of defects may occur during forming. *Orange peel* (Figure 19.1) is a surface roughening on the scale of the grain size. It occurs because of different orientations of neighboring grains on the surface. During elongation, some grains contract more in the direction normal to the surface and others contact more in a direction in the surface. Orange peel is observed only on free surfaces. The effect can be reduced by using a material with a finer grain size.

A related phenomenon is *roping* or *ridging* of ferritic stainless steels and some aluminum alloys. In this case, whole clusters of grains have two different orientations. These clusters are elongated in the direction of prior working. Figure 19.2 is an example of roping in an automobile hubcap.

Another defect is *stretcher strains*, which are incomplete Lüder's bands. These are very apparent where the overall strain is small. Figure 19.3 shows stretcher strains in a 1008 steel. They occur in low-carbon steels having a yield point and in some nonferrous materials that have a negative strain-rate sensitivity.

19.3 STRAIN AGING

Low carbon steels (%C $\approx$ 0.06 or less) are usually finished by cold rolling and annealing except in heavy gauges ($\gtrsim$2 mm). They are marketed after annealing at 600°C to 700°C. Historically they were produced by casting into ingots and were classified as either *rimmed steel* or *aluminum-killed steel*. A rimmed steel was one that was not deoxidized before ingot casting. During the freezing, dissolved oxygen and carbon react to form CO. Violent evolution of CO bubbles threw sparks into the air. The bubbles stirred the molten metal, breaking up boundary layers. This allowed segregation of carbon to the center of the ingot producing a very pure iron surface. In contrast killed steels

19.2. Ridging in a 430 stainless steel. From *Making, Shaping and Treating of Steel*, 9th ed. (United States Steel Corporation, 1971), p. 1180.

are deoxidized with aluminum so the violent reaction is "killed." The solidification is quiet, so a boundary layer forms and prevents surface-to-center segregation.

Today, continuous casting has almost completely replaced ingot casting. As a result, almost all steels are killed. There has been a trend to casting thinner sections, which require less rolling. This saves money but does not refine the grain structure as much.

Figure 19.4 shows a tensile stress–strain curve of an annealed low-carbon steel. Loading is elastic until yielding occurs (point A). Then the load suddenly drops to a lower yield stress (point B). Continued elongation occurs by propagation of the yielded

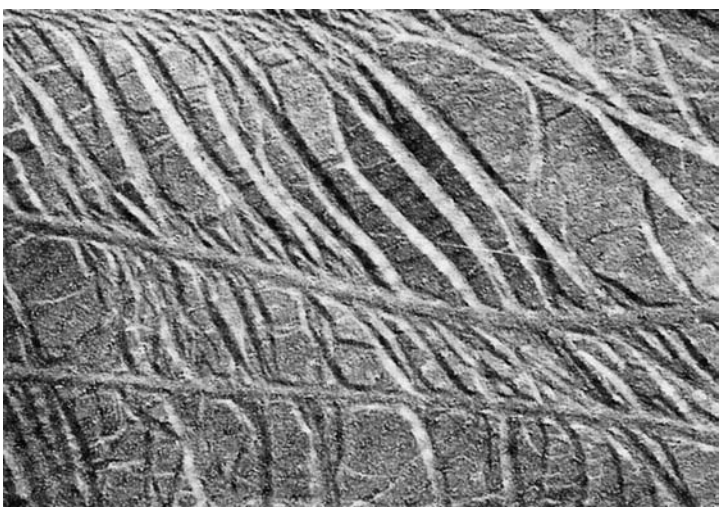

19.3. Stretcher strains in a 1008 steel sheet. From *Metals Handbook*, 8th ed. Vol 7, (*ASM*, 1972), p. 14.

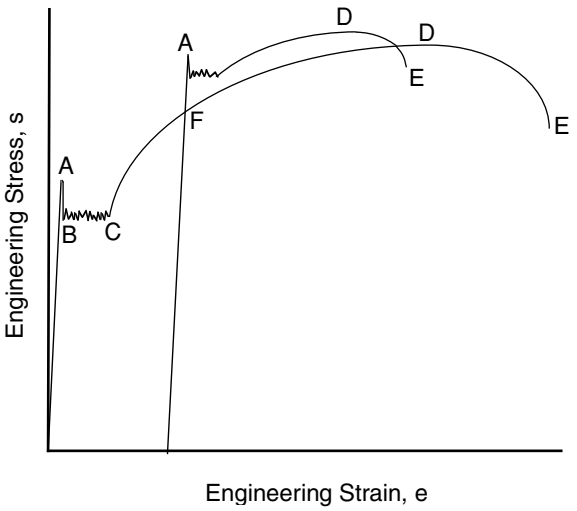

19.4. Engineering stress–strain curve for a low-carbon steel.

region at this lower stress until the entire specimen has yielded (point C). During the extension at the lower stress, there is a sharp boundary or *Lüder's band* between the yielded and unyielded regions as shown in Figure 19.5. Behind this front, all of the material has suffered the same strain. The Lüder's strain or yield point elongation is typically from 1 to 3%. Only after the Lüder's band has traversed the entire specimen does strain hardening occur. Finally at point E the specimen necks.

If the specimen in Figure 19.4 were unloaded at some point D after the lower yield region and immediately reloaded, the stress–strain curve would follow the original curve. However, if the steel were allowed to strain age between unloading and reloading, a new yield point A′ would develop. The tensile strength would be raised to D′ and

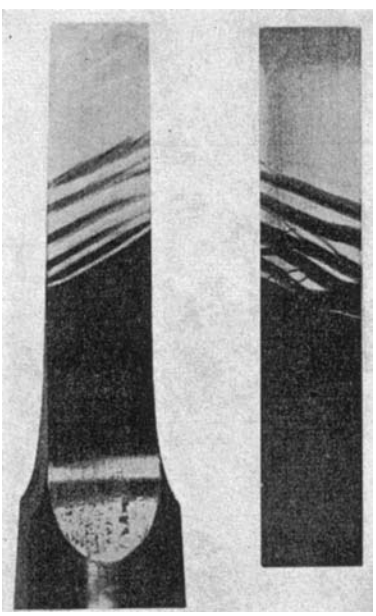

19.5. Tensile specimen of a low-carbon steel during extension. Deformation occurs by movement of a Lüder's band through the specimen. From F. Körber, *J. Inst. Metals*, 48 (1932), pp. 317–342.

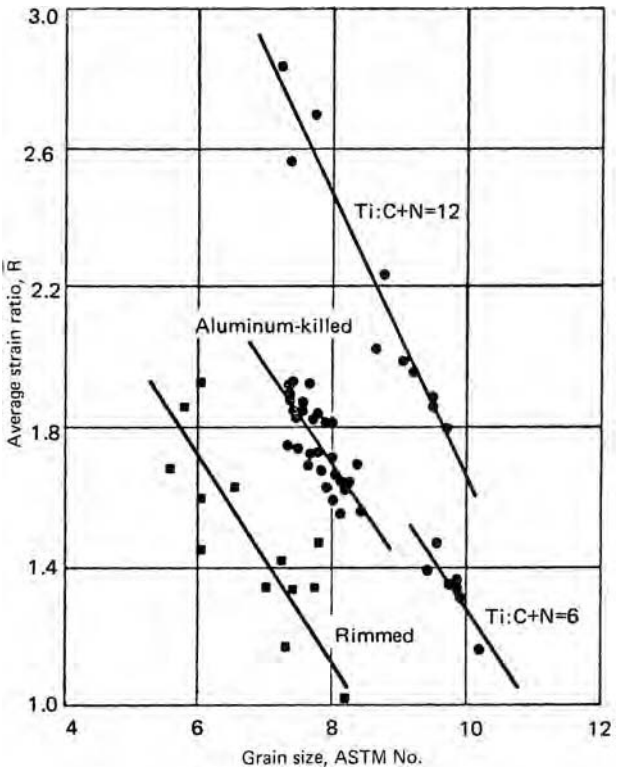

19.6. The average strain ratio increases with grain size. From D. J. Blickwede, *Metals Progress* (April, 1969), p. 90.

the elongation decreased. From the standpoint of forming, the yield point effect and strain aging are undesirable because of the reduction of n and the surface appearance of stretcher strains.

During strain aging, interstitially dissolved nitrogen and carbon segregate to dislocations lowering their energy. A higher stress is required to move the dislocations away from these interstitials than to continue their motion after they have broken free.

In commercial practice, the initial yield point is eliminated by either *roller leveling* or *temper rolling*, both of which impart very small strains (typically $< 0.5\%$) to the sheet.

For killed steels, $\bar{R}$ is usually between 1.4 to 2.0. Much higher values are common in interstitial-free steels as shown in Figure 19.6. The level of $\bar{R}$ increases with grain size, but grain sizes larger than ASTM 7 are usually avoided because of excessive orange peel. The $\bar{R}$-values for hot rolled steels are usually about 1.0.

Properties of sheet steels vary from the interstitial-free steels (IF) with tensile strengths of 150 MPa and tensile elongations of 50% to martensitic steels with tensile strengths of 1400 MPa and tensile elongations of 5%. Table 19.1 lists typical properties of various grades of sheet steels. In general, the strain-hardening exponent and tensile elongation decrease with increased yield strength as shown in Figure 19.7 and Figure 19.8.

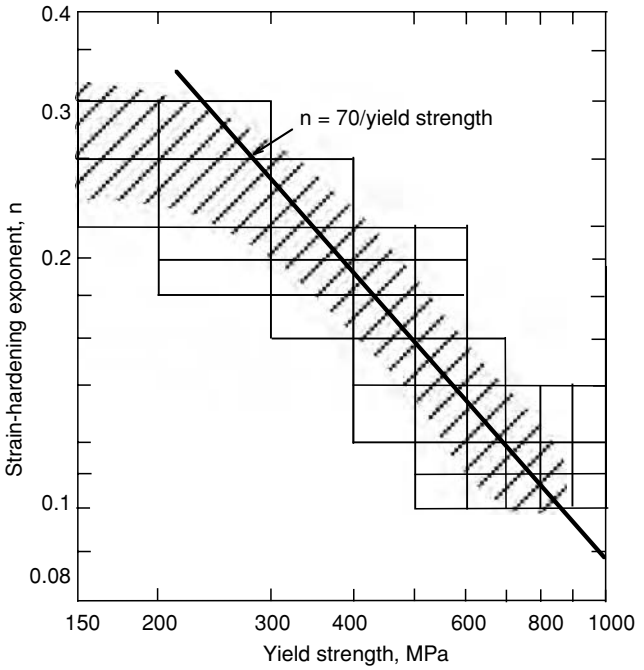

19.7. The strain-hardening exponent decreases with higher yield strengths. Adapted from S. P. Keeler and W. C. Brazier in *Micro Alloying 75* (Union Carbide, 1977), pp. 517–30.

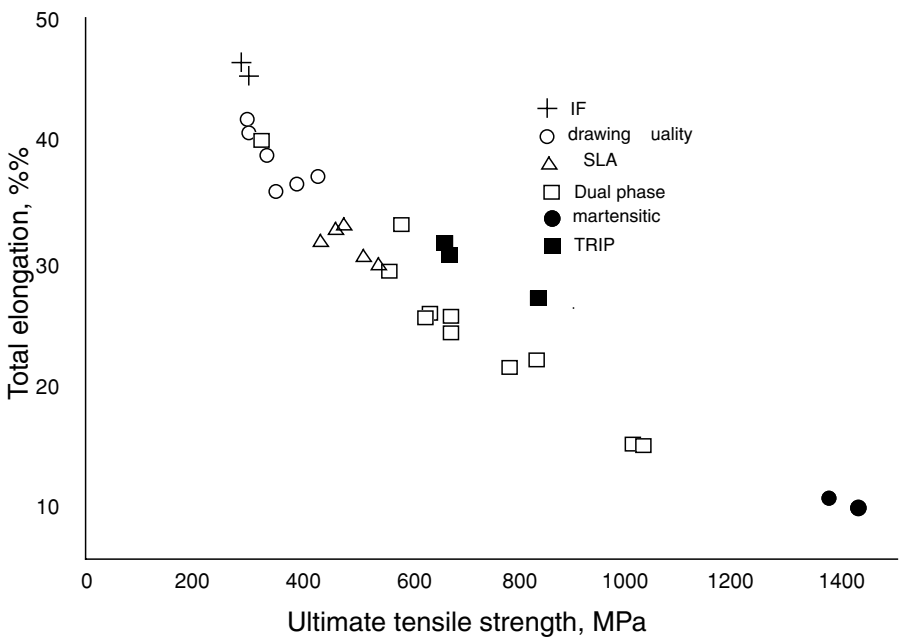

19.8. Decrease of total elongation with increasing strength.

19.4 ALUMINUM-KILLED STEELS

Cold-rolled low-carbon steels are almost always sold in the annealed and temper-rolled condition. They contain 0.06% carbon or less and 0.3 to 0.5% manganese. Aluminum-killed steels will strain age at the temperatures used in baking the paint on car bodies. This adds strength to the final product after forming is complete.

The properties depend on the annealing practice. Today most annealing is done continuously as strip is passed through a furnace. This has largely replaced batch annealing in which large coils were heated for several days. Continuous annealing takes about 10 minutes and results in more uniform properties.

19.5 INTERSTITIAL-FREE STEELS

These are steels from which carbon and nitrogen have been reduced to extremely low levels (less than 0.005%). After vacuum degassing, titanium is added to react with any carbon or nitrogen in solution. Titanium reacts preferentially with sulfur so the stochiometric amount of titanium that must be added to eliminate carbon and nitrogen is

$$\%\text{Ti} = (48/14)(\%\text{N}) + (48/32)(\%\text{S}) + (48/12)(\%\text{C}). \tag{19.1}$$

A typical composition is 0.002% C, 0.0025% N, 0.025% Ti, 0.15% Mn, 0.01% Si, 0.01% P, 0.04% Al, and 0.016% Nb. Niobium may be used instead of titanium but it is more expensive. IF steels typically have very low strengths (YS = 150 MPa and TS = 300 MPa). The advantage of these steels is that they are very formable. Typically $n = 0.28$ and $\bar{R} = 2.0$.

Fine grain sizes and higher strengths can be achieved by alloying with Nb. High-strength IF steels are solution-hardened with small amounts of Mn, Si, and P. The tensile strength is increased 4 MPa by 0.1% Mn, 10 MPa by 0.1% Si, and 100 MPa by 0.1% P in solution. The presence of titanium reduces the phosphorus in solution by forming FeTiP. The increased strength comes at the expense of a somewhat reduced formability. A composition of 0.003% C, 0.003% N, 0.35% Mn, 0.05% P, 0.03% Al, 0.035% Nb, 0.2% Ti, and 0.001% B has the following properties: YS = 220 MPa, TS = 390 MPa, elongation = 37%, $\bar{R} = 1.9$, and $n = 0.21$.

19.6 HSLA STEELS

The term *high-strength low-alloy* (HSLA) is used to describe a range of steels that are stronger than the plain-carbon steels. They are frequently designated by two numbers, which indicate minimum yield and tensile strengths in MPa. Yield strengths vary from 300 to 500 MPa. The increased strength is achieved by the combined effects of solid-solution strengthening, a finer grain size, and precipitation hardening. Somewhat higher than normal carbon and manganese contents as well as intentional phosphorus, silicon, and nitrogen additions cause solid-solution strengthening. Fine ferrite grain sizes are achieved by rapid cooling from hot rolling temperatures. Fine precipitates of carbonitrides of V, Nb, and Ti add to the strength. The increased strength is accompanied by lower formability.

19.7 DUAL-PHASE AND COMPLEX-PHASE STEELS

The microstructures of these consist of islands of martensite in a ferrite matrix. This microstucture is produced by heating the steel slightly into the two-phase ferrite–austenite region and cooling rapidly. The steels contain sufficient manganese, chromium, vanadium, and/or nickel to achieve the necessary hardenability to transform the austenite on cooling. In some there is also bainite. Dual-phase steels have low yield strength (350 MPa) and high tensile strength (600 MPa.) During forming the deformation is largely in the softer ferrite phase. In addition to the work hardening during forming, these steels bake harden.

The microstructures of these consist of very fine-grain ferrite, bainite, and martensite with fine precipitates of niobium, titanium, or vanadium carbonitrides.

19.8 TRANSFORMATION-INDUCED PLASTICITY (TRIP) STEELS

The microstructures of these contain at least 5% austenite, with various amounts of martensite and bainite. During deformation, the austenite transforms to martensite causing hardening. They contain enough carbon to lower the Ms temperature below room temperature. The amount of carbon controls the strain level at which austenite will transform to martensite. In some cases the strain level is high enough so that no additional martensite forms during forming, but will form during crashes absorbing energy. Figure 19.9 shows that in contrast to dual-phase and HSLA steels of comparable yield strength, the strain-hardening exponent maintains a high level to high strains. The result is that the stress–strain curve persists out to higher strains than dual-phase and HSLA steels of comparable yield strength (Figure 19.10).

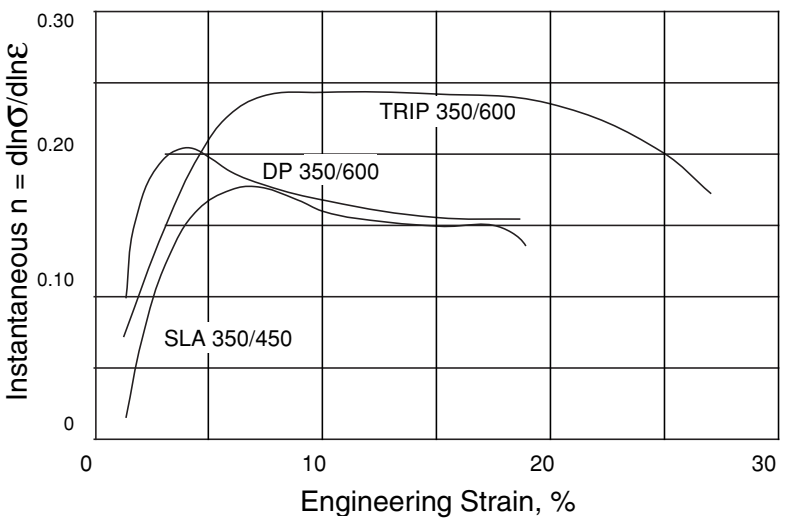

19.9. The change of the instantaneous exponent $n = d(\ln\sigma)/d(\ln\varepsilon)$ with strain.

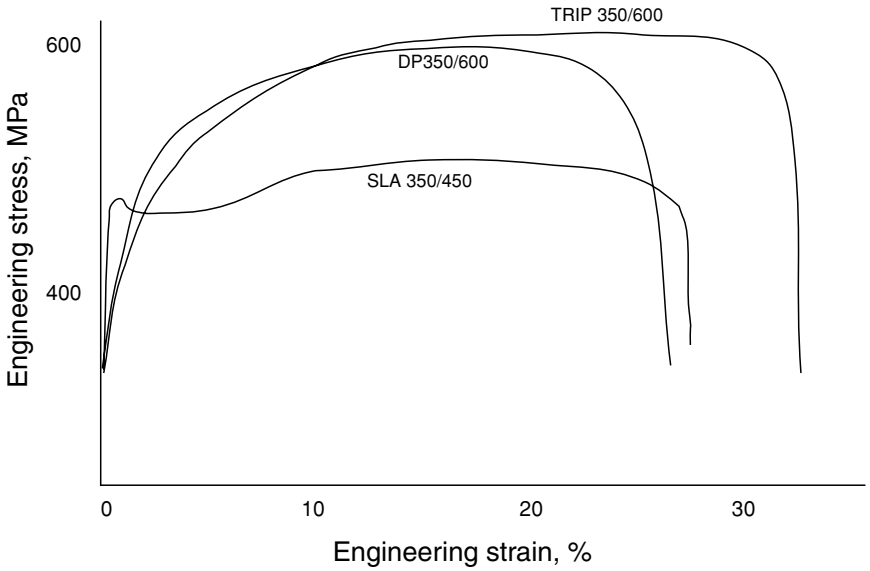

19.10. Stress–strain curves for TRIP, HSLA, and dual-phase steels of comparable yield strengths. Note the higher elongation of the TRIP steel.

19.9 MARTENSITIC STEELS

In these steels, austenite transforms to martensite on cooling from hot rolling. They must contain sufficient amounts of manganese, silicon, chromium, molybdenum, boron, vanadium, and/or nickel to have high enough hardenability. The amount of carbon controls the strength level. The tensile strength in MPa is given by

$$\mathrm{TS} = 900 + 2800(\%\mathrm{C}). \tag{19.2}$$

The formability is limited because of the high strength.

19.10 TRENDS

Until the 1990s, automobile bodies were made almost entirely from low-carbon aluminum-killed steels. The current emphasis on the increased fuel economy of lighter vehicles has led to greatly increased usage of thinner gauges permitted by higher strength steels. Low-carbon steels are rapidly becoming a minor part of auto bodies. The highest strength steels are used mainly for structural parts, rather than for the auto body exterior.

The lower ductility of the higher strength steels (Figure 19.8) results in lower formability. The formability problem is aggravated by the lowering of the forming limit curves by thinner gauges (Figure 15.18). There is much current research aiming to increase the ductility of higher strength steels. One approach is to incorporate more austenite into the microstructures. This together with more martensite and still finer grain sizes also raises the strength level. Most of the higher strength steels are used in structural parts rather than for the auto exterior.

19.11 SPECIAL SHEET STEELS

Sandwich sheets with low-carbon steel on the outside around a polymer are used for sound dampening. For example, their use as the firewall between the engine and passenger compartment lowers engine noise.

Tailor-welded blanks are sheets composed of different thicknesses welded together. Forming parts of these can help reduce weight without the need to weld parts of different thickness after forming.

A pattern can be impressed on the surface of sheets rolled with laser-textured rolls. It has been claimed that this permits better lubrication and better surface appearance after painting.

19.12 SURFACE TREATMENT

Steel mills often sell prelubricated sheets or sheets coated with a polymer coating. Often steel is given a phosphate coating to help lubricants.

Steels are frequently galvanized (plated with zinc) for corrosion protection. Zinc is anodic to iron so it galvanically protects the underlying metal. Steels may be galvanized either by hot dipping or electroplating. In the more common hot dipping process, the thickness of the coating is controlled by wiping the sheet as it emerges from a molten zinc bath. Figure 19.11 shows the surface of a hot-dip galvanized sheet. In electroplating, the plating current and time control the thickness of electroplating. Usually the thickness of the zinc is the same on both sides of the sheet, but sheets can

19.11. Spangles on the surface of a steel sheet that was hot-dip galvanized. From *Making, Shaping and Treating of Steel*, 9th ed. (United States Steel Corporation, 1971), p. 1032.

be produced with the thickness on one side less than the other. Even one-side only plating is possible.

The term *galvanneal* has been applied to hot dip-galvanized sheets that are subsequently annealed to allow the formation of Fe-Zn intermetallic compound.

With the higher strength steels the temperature of the hot dip galvanizing bath causes some loss of strength. Another problem is that in production the heating of the dies caused by the higher forces may lead to transfer of zinc onto the dies.

Other types of plating are sometimes done. Tin plating is an example. However, "tin cans" today have little if any tin on them.

19.13 STAINLESS STEELS

Formable stainless steels fall into two classes: austenitic stainless steels and ferritic stainless steels. The austenitic stainless steels are fcc and contain from 17 to 25% Cr and 2 to 20% Ni with very low carbon. They form the 2xx and 3xx series. They are not magnetic. Austenitic grades are used for high-temperature applications and where superior oxidation resistance is required. Austenitic grades work-harden rapidly and consequentially have very high tensile elongations. The austenite in some grades is metastable and may transform to martensite during deformation. This partially accounts for the very high n-values. Like other fcc metals, the R-values are low.

Ferritic stainless steels are bcc and contain 12 to 18% Cr, less than 0.12% C, and no nickel. They form the 4xx series. The ferritic grades are less expensive and are used widely for decorative trim. The mechanical properties of the ferritic grades are similar to those of low-carbon steel, except the yield and tensile strengths are somewhat higher. Ridging problems, noted in Section 19.2, can be controlled by high-temperature annealing. Both grades may lose their corrosion resistance if welded. Figure 19.12 shows the tensile and yield strengths of typical austenitic and ferritic grades as a function of prior reduction.

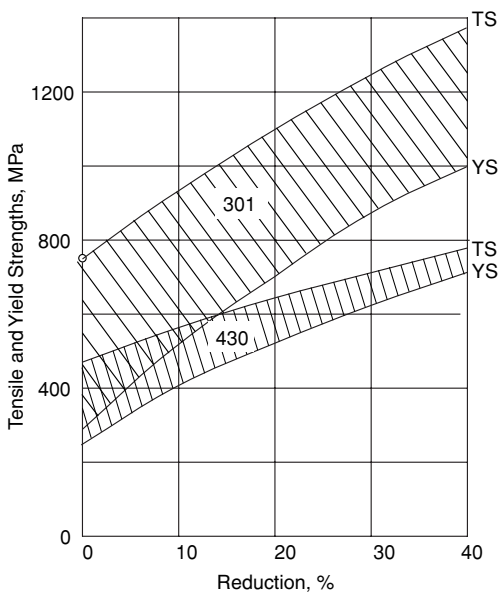

19.12. Tensile and yield strengths of an austenitic (301) and a ferritic (430) stainless steel as a function of cold-rolling reduction. Note the greater strain hardening of the austenitic grade.

19.14 ALUMINUM ALLOYS

There is a wide range of aluminum alloys available in sheet form. The formability varies with grade, but aluminum alloys generally are not as formable as low-carbon steel. Like other fcc metals the *R*-values are less than 1.0. The strain hardening exponents of annealed grades tend to be between 0.2 and 0.3, but the strain rate sensitivity is very low (negative in some cases). Springback is a severe problem in high-strength aluminum alloys as it is in high-strength steels because of the high strength-to-modulus ratio. If the same dies are used when aluminum is substituted for steel, there are often forming problems. However, they can usually be overcome with new dies.

Wrought alloys are designated by four digits. The first indicates the primary alloying element. Copper-containing grades (2xxx), alloys with magnesium and more silicon than required to form Mg_2Si (6xxx) series, and zinc alloys (7xxx) can be strengthened by heat treating. Commercially pure alloys (1xxx), those with manganese as the primary alloying element (3xxx), and those with magnesium as the primary alloy (5xxx) can be strengthened only by cold working.

The condition of aluminum alloys is indicated by a temper designation (Table 19.2).

The 4xxx alloys are those with silicon as the principal alloying element, but none are produced in sheet form. The designation 8xxx is reserved for alloys with other alloying elements (e.g., nickel or lithium)

The 3003 and 3004 alloys are very ductile and have strain-hardening exponents of about 0.25 in the annealed condition. Manganese provides solid solution strengthening. They find use as cooking utensils, roofing, and siding. A special grade of 3004 with very controlled limits on manganese and iron are used as stock for beverage cans. Strong can bottoms are assured by using starting stock that has been very heavily cold rolled (H-19 temper).

The addition of 2 to 5% magnesium (5xxx alloys) achieves greater solid-solution strengthening (see Figure 19.13). The formability and corrosion resistance are good, but these alloys are prone to develop stretcher strains. There are two types of stretcher

Table 19.2. Temper designations for aluminum alloys

Designation	Meaning
F	As fabricated
O	Annealed
H	Strain hardened
H-1x	Strain hardened only
H-2x	Strain hardened and partially annealed
H-3x	Strain hardened and stabilized
The second digit (1 through 9) indicates the degree of strain hardening, 8 indicating a hardness achieved by a 75% reduction.	
W	Solution treated
T-3	Solution treated, strain hardened, and naturally aged
T-4	Solution treated and naturally aged to a stable condition
T-6	Solution treated and artificially aged

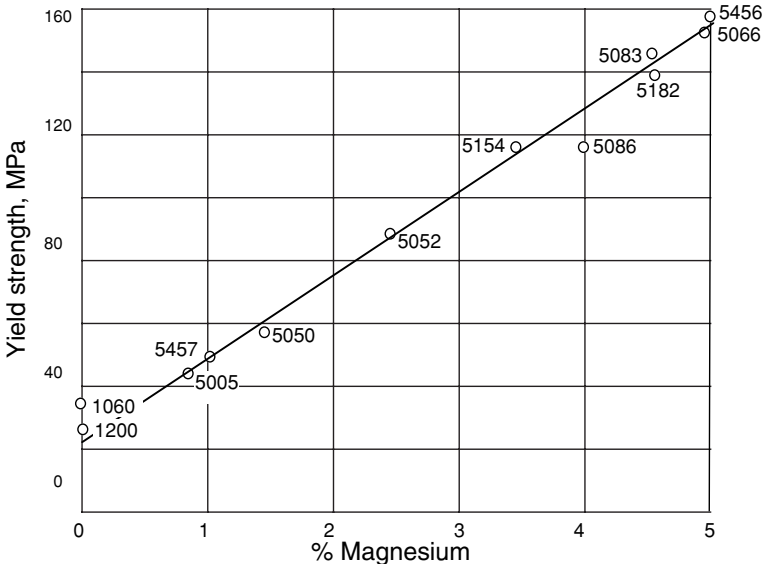

19.13. Annealed yield strength of several aluminum–magnesium alloys. Magnesium has a strong solid solution strengthening effect in aluminum alloys. Data from *Aluminum and Aluminum Alloys, ASM Specialty Handbook* (ASM International, 1993).

strains: Type 1 are coarse like the Lüders strains in low-carbon steel that form at low strains; and Type 2, which are much finer like orange peel. They form at higher strains and are associated with dynamic strain aging that causes serrated stress–strain curves. Cold rolling of these alloys generates even higher strengths. Uses include automobile bodies (not the outer skin), trucks, and trailer parts. Fine-grain 5083 is superplastic and is used in hard-to-form parts for autos and motorcycles (such as motorcycle gasoline tanks). Other applications for 5xxx alloys include canoes and boats. In highly stressed parts, the magnesium content is kept below 3.5% to avoid stress corrosion cracking.

Aluminum alloys containing magnesium may have a negative strain-rate sensitivity. The result may be Lüders lines in formed parts. Figure 19.14 shows an example of Lüders lines on an aluminum–magnesium sheet.

The 2xxx alloys provide higher strengths and are used where the strength-to-weight ratio is important as in aircraft and trucks. However, they have poor corrosion resistance. They may be clad with another aluminum alloy for galvanic protection.

The 6xxx alloys can also be hardened by heat treatment and have better corrosion resistance. They find major usage in automobile bodies. One canoe manufacturer uses the 6061 alloy and heat treats canoe halves before assembly. All automobile outer skins are made from 6xxx alloys. They are formed in the T-4 condition and further aged by the paint-bake cycle.

The highest strengths are achievable with 7xxx alloys containing up to 7% zinc and other elements. They find use in the aerospace industry. They have poor corrosion resistance and are susceptible to stress corrosion cracking. These find applications as automobile bumpers.

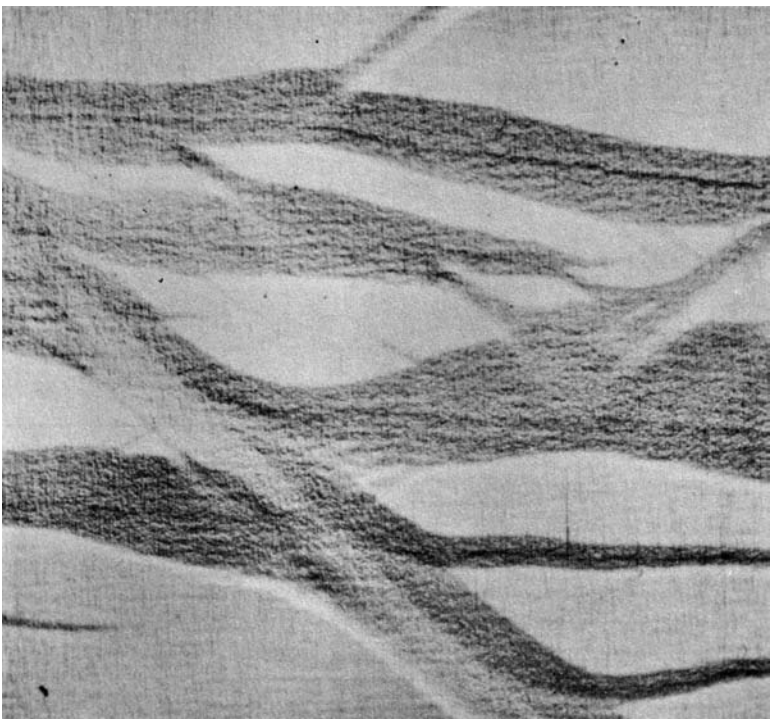

19.14. Lüder lines in aluminum–magnesium alloy sheet, 8×. *Aluminum: Properties and Physical Metallurgy* (ASM, 1984), p. 129. Courtesy of Alcoa.

In North America, the alloys most widely used for automobile bodies are Al-Mg alloys 5052 (O and various H tempers), 5754-O, and 5152-O and in decreasing tonnage Al-Mg-Si alloys containing copper 6111-T4 and 6211-T4. In Europe the most widely used alloys are Al-Mg 5754-O and 5182-O, and Al-Mg-Si alloys 6016-T4, 6181-T4, and 6111-T4. Inner panels are made from 6xxx alloys and 5182. The 5xxx alloys are more formable than the 6xxx alloys. These all have strain hardening exponents between 0.18 and 0.25. The 6xxx alloys are strengthened in the paint baking cycle by precipitation hardening. For all of the aluminum alloys, the combination of possible elongations and strength falls below and to the left of the curve for steels in Figure 19.8. The blank size with aluminum must be larger than with steel because bend radii must be increased. This adds to the cost.

Superplastic forming of aluminum alloys is finding some application in autobody panels. In the United States the interest is currently on fine grain 5083 and in Great Britain on 2004 alloy. The greatest advantage of superplastic forming is in cars produced in low quantities. Superplastic forming of Al 7475 is finding application in the aerospace industry.

19.15 COPPER AND BRASS

Both annealed copper and brass work harden rapidly. The zinc addition in brass increases the yield and tensile strengths as shown in Figure 19.15. The strain-hardening

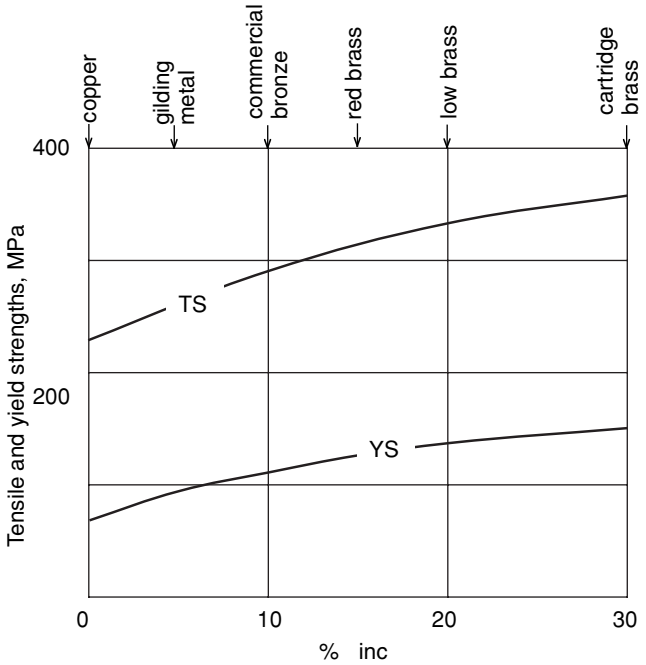

19.15. Increased zinc content raises both the yield and tensile strengths of copper. Note that the difference between yield and tensile strengths increases with zinc content.

exponent (0.35 to 0.5 for copper and 0.45 to 0.6 for cartridge brass) increases with zinc content and larger grain sizes. However, the larger grain size causes the orange peel effect. The strain-rate sensitivities for copper alloys are low (≤ 0.005) and the R-values are less than unity (typically 0.6 to 0.9). Annealing at a very high temperature after a very heavy cold reduction produced a cube texture in which $<100>$ directions are aligned with the rolling, transverse, and thickness directions. The resulting sheet has a low R_{av} and ΔR.

Brasses containing 15% or more zinc under stress are susceptible to stress corrosion cracking in atmospheres containing ammonia. Tensile stresses across grain boundaries cause them to crack as shown in Figure 19.16. The susceptibility increases with zinc content. Unless the parts are stressed in service, the problem can be alleviated by stress-relief anneals. Brasses should be annealed between 200° and 300°C. Higher annealing temperatures are recommended for silicon bronze, aluminum bronze, and cupronickel.

19.16 HEXAGONAL CLOSE-PACKED METALS

The crystallographic textures of hcp metal sheets tend to have the basal (0001) planes aligned with the plane of the sheet. With most, deformation is mainly by $<11\bar{2}0>$ slip, so high R-values are common.

In the past, there was very little forming of magnesium sheets because of limited ductility. Recently, however, there is an increased interest in magnesium because its low density can lead to weight saving. Magnesium sheets have strong crystallographic

19.16. Stress-corrosion cracking in brass. From *Metals Handbook*, 8th ed., Vol. 7 (ASM, 1972), p. 291.

textures with the basal plane aligned with the plane of the sheet. This texture and easy $\{10\bar{1}2\} < \bar{1}011 >$ twinning in tension result in higher in-plane yield strengths in tension than in compression as indicated by Figure 19.17.

Basal slip and twinning are the primary deformation mechanisms. Above about 225°C, other slip modes can be activated. To have the necessary ductility, forming

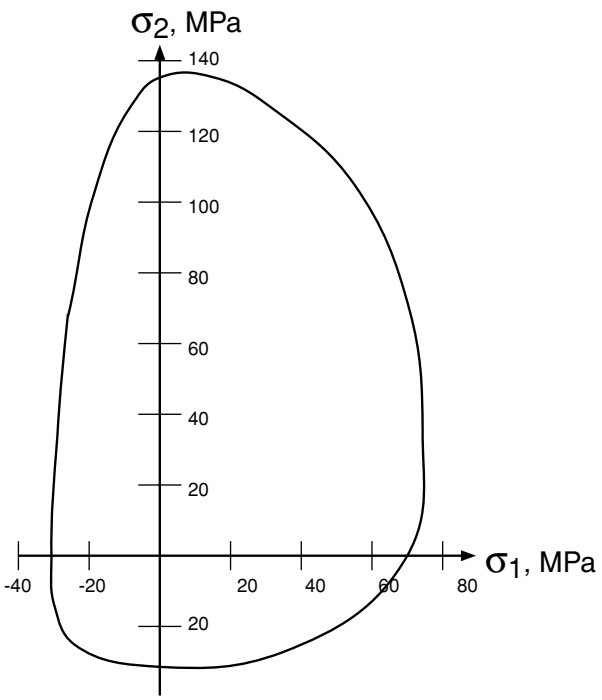

19.17. Yield locus of pure magnesium. Data from E. W. Kelly and W. F. Hosford, *Trans. Met. Soc. AIME*, 242 (1968), pp. 654–661.

of magnesium alloy sheets is generally done at 200°C or higher. The most common sheet alloy, AZ31B, contains about 3% Al and 1% Zn. Rolled sheets have shear bands inclined at about 60° to the sheet normal. These persist even after annealing at 350°C. Rolled sheets of an alloy AE21 (about 2% Al and 1% rare earths) have similar shear bands but these disappear after annealing at 350°C. Rolled ZEK100 (about 1% Zn, and less than ½ % rare earths and zirconium) can be deep drawn at about 150°C.

It has been known for years that repeated roller leveling of AZ31B-O modifies its crystallographic texture and to allows bends of 2 to 3 times sheet thickness instead of the usual 5.5 times sheet thickness. Recently it has been shown that a very fine grain size can be produced by severe deformation. This decreases the anisotropy and decreases the tendency for twinning, so forming can be done at much lower temperatures.*

Zinc alloys have high *m*-values. The high *m*-value is to be expected because room temperature (293 K) is 42% of the melting point (693 K) of zinc. The strain-hardening exponent is very low.

Alpha-titanium alloys (hcp) typically have *R*-values of 3 to 5 and can be drawn into very deep cups. In contrast, β-titanium alloys (bcc) behave more like low-carbon steels. As discussed in Chapter 5, fine-grain titanium alloys may be superplastically formed.

Beryllium is very brittle. Rolled sheets have very high *R*-values. Deformation is limited to $< 11\bar{2}0 >$ slip, so even bending is limited except for very narrow strips.

19.17 TOOLING

Dies for sheet forming are usually made of gray cast iron, Meehanite®, with a fine controlled graphite flake size or an austempered ductile cast iron. High wear locations may be flame hardened. For extreme conditions such as very high production, D2 tool steels with 12% Cr may be used. S7 shock-resistant tool steels are used for flanging and trimming. In all cases it is common to ion nitride or chromium plate the die faces. Various coatings are used on dies for forming of advanced high-strength steels. Initial die tryout may be done on cheaper dies made from a zinc alloy. Thought is being given to using new die materials such as sintered tool steels. One limitation is that the dies must be sturdy and easily repairable.

Flanging and trimming dies are made from tool steels.

19.18 PRODUCT UNIFORMITY

Variations of sheet thickness and properties are undesirable. Subtle changes can cause failures with tooling that has been adjusted to give good parts with a particular batch of steel. Problems may arise from differences from one coil of steel to another or differences between different mills. There may be nothing inherently bad about the steel that performs poorly. There are often differences between the edges and center of a coil. Such property differences may be caused by variations of grain size, texture, or composition.

* Q. Yang and A. K. Ghosh, *Acta Materialia*, 54 (2006), pp. 5159–70.

During casting, impurities segregate toward the center. When the cast slab is rolled, these may cause weakness at the centerline. Curved molds are frequently used in continuous casting. Because the last material to freeze in such molds is displaced somewhat from the centerline, failures may be caused by segregated inclusions not on the exact centerline.

NOTES OF INTEREST

In 1886, both Charles M. Hall in the United States and Paul-Louis-Toussaint Héroult in France independently developed an economical process for producing aluminum. Before this, aluminum was more expensive than platinum, and for that reason it was chosen to cap the Washington Monument. Both men were only 22 years old. Hall was a recent chemistry graduate of Oberlin College and Héroult had studied at the School of Mines in Paris. Within two years, aluminum production was in full swing in Europe and the United States. The American spelling (with "um" instead of the "ium" common to metals) comes from an advertisement of the Pittsburgh Reduction Company, the predecessor of Alcoa. Whether the omission was intended or a mistake is unknown.

In the early 1850s, Henry Bessemer in England and William Kelley in the United States developed a scheme for making cheap steel. Both realized that the carbon content of pig iron could be reduced from about 4% to a low level by blowing air through it. Kelly's family and friends thought he was insane, but he perfected his process by 1851. Six years later, Bessemer received a U.S. patent for essentially the same process. Their steel replaced wrought iron as the strongest material. Although their process was later supplanted first by the open-hearth process and later by the basic oxygen process, the introduction of cheap steel made railroads and later automobiles possible.

W. Lüders first drew attention to the lines that appeared on polished steel specimens as they yielded. *Dinglers Polytech. J.*, Stuttgart, 1860.

REFERENCES

Aluminum: Properties and Physical Metallurgy, ASM, 1984.
W. F. Hosford, *Physical Metallurgy*, Taylor and Francis, 2005.
The Making, Shaping and Treating of Steel, U.S. Steel Corporation, 1971.

PROBLEMS

19.1. The table below from *Making, Shaping and Treating of Steels* gives combinations of aging times and temperatures that result in equal amounts of strain aging in low-carbon steels.

a) From a plot of $\ln(t)$ versus $1/T$, where T is absolute temperature, determine the apparent activation energy for strain aging.

b) Explain the slope change between 0° and 21°C. (Consider how the data were obtained.)

Aging Times and Temperatures That Produce Equal Amounts of Aging

0°C	21°C	100°C	120°C	150°C
I yr	6 mo	4 hr	1 hr	10 min
6 mo	3 mo	2 hr	30 min	5 min
3 mo	6 wk	1 hr	15 min	2.5 min
1 wk	4 d	5 min		
3 d	36 hr	2 min		

19.2. One engineer specified that a part be made from an extra-low-carbon grade of steel. Although it costs more than the usual grade, he thought that with the usual grade there might be an excessive scrap rate.
a) How could you determine whether the cheaper, usual grade could be used?
b) Would the substitution of a cheaper grade result in an inferior product?

19.3. With low-carbon steels, both *n*- and *R*-values can be raised by higher annealing temperatures. Why isn't this practice common?

19.4. The substitution of HSLA steels for aluminum-killed steels to achieve weight saving in automobiles is based on their higher yield strengths.
a) How does this affect the elastic stiffness of the parts?
b) In view of corrosion, how does this affect component life? (HSLA steels have about the same corrosion resistance as aluminum-killed steels.)

19.5. The table below lists properties of several sheet metals at the temperature they will be formed. Choose from these the appropriate material and state the reason for your choice.
a) Greatest LDR in cupping.
b) Most earing in cupping.
c) Greatest uniform elongation in tension.
d) Greatest total elongation in tension.
e) Excluding material E (because of its low yield strength) the material that could be drawn into the deepest cup by stretching over a hemispherical punch.

	Properties						
Material	*E* (MPa)	*Y.S.* (MPa)	R_0	R_{45}	R_{90}	*n*	*m*
A	210	200	1.9	1.2	2.0	0.25	.003
B	210	240	1.2	1.0	1.2	0.22	0.03
C	72	175	07	0.6	0.7	0.22	0.001
D	115	140	0.6	0.9	0.6	0.5	0.001
E	70	7	1.0	1.0	1.0	0.00	0.60

19.6. Explain why with deformation limited to $<11\bar{2}0>$ slip, wide sheets of beryllium can't be bent while narrow strips can.

Index